FLOW PATTERNS, PERFORMANCE AND SCALE-UP OF DISTILLATION TRAYS.

A THESIS SUBMITTED

BY

CHRISTIAN CHIKODILI ANI [M.Sc]

A candidate for the Degree of

Doctor of Philosophy.

The Department of Chemical Engineering

The University of Aston in Birmingham

November 1988

The University of Aston in Birmingham

FLOW PATTERNS, PERFORMANCE AND SCALE UP OF DISTILLATION TRAYS.

A THESIS SUBMITTED BY

CHRISTIAN CHIKODILI ANI

A candidate for the degree of Doctor of Philosophy.

November 1988

ABSTRACT

This work is concerned with the nature of liquid flow across industrial sieve trays operating in the spray, mixed, and the emulsified flow regimes.

In order to overcome the practical difficulties of removing many samples from a commercial tray, the mass transfer process was investigated in an air water simulator column by heat transfer analogy. The temperature of the warm water was measured by many thermocouples as the water flowed across the single pass 1.2 m diameter sieve tray. The thermocouples were linked to a mini computer for the storage of the data. The temperature data were then transferred to a main frame computer to generate temperature profiles - analogous to concentration profiles.

A comprehensive study of the existing tray efficiency models was carried out using computerised numerical solutions. The calculated results were compared with experimental results published by the Fractionation Research Incorporation (FRI) and the existing models did not show any agreement with the experimental results. Only the Porter and Lockett model showed a reasonable agreement with the experimental results for certain tray efficiency values.

A rectangular active section tray was constructed and tested to establish the channelling effect and the result of its effect on circular tray designs. The developed flow patterns showed predominantly flat profiles and some indication of significant liquid flow through the central region of the tray. This comfirms that the rectangular tray configuration might not be a satisfactory solution for liquid maldistribution on sieve trays.

For a typical industrial tray the flow of liquid as it crosses the tray from the inlet to the outlet weir could be affected by the mixing of liquid by the eddy, momentum and the weir shape in the axial or the transverse direction or both.

Conventional U-shape profiles were developed when the operating conditions were such that the froth dispersion was in the mixed regime, with good liquid temperature distribution while in the spray regime.

For the 12.5 mm hole diameter tray the constant temperature profiles were found to be in the axial direction while in the spray regime and in the transverse direction for the 4.5 mm hole tray. It was observed that the extent of the liquid stagnant zones at the sides of the tray depended on the tray hole diameter and was larger for the 4.5 mm hole tray.

The liquid hold-up results show a high liquid hold-up at the areas of the tray with low liquid temperatures, this supports the doubts about the assumptions of constant point efficiency across an operating tray.

Liquid flow over the outlet weir showed more liquid flow at the centre of the tray at high liquid loading with low liquid flow at both ends of the weir.

The calculated results of the point and tray efficiency model showed a general increase in the calculated point and tray efficiencies with an increase in the weir loading, as the flow regime changed from the spray to the mixed regime the point and the tray efficiencies increased from approximately 30 to 80%.Through the mixed flow regime the efficiencies were found to remain fairly constant, and as the operating conditions were changed to maintain an emulsified flow regime there was a decrease in the resulting efficiencies.

The results of the estimated coefficient of mixing for the small and large hole diameter trays show that the extent of liquid mixing on an operating tray generally increased with increasing capacity factor, but decreased with increasing weir loads. This demonstrates that above certain weir loads, the effect of eddy diffusion mechanism on the process of liquid mixing on an operating tray to be negligible.

Key wards :- FLOW PATTERNS, PERFORMANCE, SCALE UP, HEAT AND MASS TRANSFER AND DISTILLATION TRAYS.

LIST OF PUBLICATIONS

[1] Porter,K.E ,Davies,B. ,Enjugu ,B.A, and Ani,C.C.,IChmE. Symp. Series. 1987, No 104, A569 - A588. The Effect of Liquid Flow Patterns on Sieve Tray Performance by Means of the Water Cooling Technique.
Work Based on Chapter 7.

[2] Kler,S. ,Lavin,J.T. ,Ani,C.C ,and Davies,B. ,IChmE. Symp. Series, No 104, B471. The Use of low Voltage Displacement Transducer to measure Tray Deflection.
Based on Contract Work done for B.O.C

[3] Ani,C.C. ,and Davies,B. IChmE. Annual Research Meeting University of Nottingham, 1987. The Effect of Hole Size on Liquid flow Patterns and Scale up of sieve Trays.
Work Based on Chapter 7.

Dedicated to my family and close friends

CERTIFICATE

I hereby certify that the work presented has been done by the candidate except where other wise acknowledged, and that this thesis has not been submitted for a higher degree at any other university.

.....

Dr B . Davies

.....

C . C . ANI

ACKNOWLEDGEMENTS

I am highly indebted to my supervisors, Prof. K.E. Porter, and Dr B. Davies for having benefitted enormously from their deep understanding of both theory and practice.

My sincere thanks also go to all the members of the academic staff and the Engineering workshop of the Department of Chemical Engineering for their excellent support and advice in the design and careful revamping of the equipment.

The author would like to thank Dr Kler, S.C. and Mr Lavin, J.T. , both of B.O.C Cryoplants, UK, for their supply of some of the apparatus and designed trays used to test and improve the new theory and technique developed in the course of this work.

Finally, the author would like to thank the Nigerian Government for the Financial support provided throughout the duration of this work and his friends and members of his family, without whose encouragement and support, this work would never have been completed.

Table of contents

PAGE
MISSING
IN
ORIGINAL

FIGURES

TABLES

Experimental findings are messy and inexact , believed by every one except the man who developed that work.....

Harlow

Chapter 1

INTRODUCTION

The study of flow patterns on commercial scale distillation plates and the subsequent point and plate efficiencies have been reported by many authors. Some progress has been made towards understanding the effect of this phenomena on the performance of commercial scale plates.

In recent years, most of these studies have been carried out on sieve plates which are one of the most simply constructed and widely used devices for gas-liquid contacting in distillation columns.

The operation of cross flow trays for vapour-liquid contacting is characterised by the presence of different hydrodynamic conditions depending on tray design and vapour and liquid loadings.

In 1936, **Lewis** (41) published a mathematical model for distillation efficiency, in which he assumed that the liquid flow across the plate is uniform. Subsequently, there have been a number of important studies by research workers such as **Bell** (8) (1972), **Porter et al** (56), (1972), **Lockett** and **Safekoudi** (58), (1976), **Sohlo** and **Kinnunen** (67), (1977), **Solari** and **Bell** (10), (1978), **Sohlo** and **Kouri** (68), (1979), **Kafarov et al** (32), (1979), **Porter** and **Jenkins** (57), (1979), **Zuiderweg** (78), (1982), **Solari** and **Bell** (71), (1982), **Raper, Pinczewski** and **Fell** (63), (1983), **Kouri** and **Sohlo** (40), (1984) and **Stichlmair et al** (83), (1987). In their work ,these authors have been concerned with the effect of mixing on the tray efficiency and theoretical models have been proposed by some of these authors for the characterisation of liquid mixing and relating the point efficiency to the Murphree tray efficiency and the overall column efficiency .

In the past , most of the models have been developed on the assumptions that the shape of the plate is rectangular and the liquid flows uniformly across the tray with a mixing mechanism superimposed on the models.

In the early 1970's, **Bell** (8) studied the liquid flow patterns on a commercial scale distillation tray and employed a fibre optic technique to obtain residence time distributions for the liquid at various points in the Fractionation Research Inc (F.R.I.) four-foot and eight-foot diameter experimental column. For sieve plates the flow pattern was observed to deviate severely from the idealised flow situation.

Porter et al (56) carried out a photographic study of the froth behaviour in a four-foot diameter (1.2 m) water simulator. Stagnant regions were observed at the sides of the plate with the bulk of the liquid flowing in a channel along the central region of the tray from the inlet downcomer to the outlet downcomer. A two region model was developed by **Porter et**

al for a single-pass cross flow plate in which the flow around the converging edge of the tray is considered stagnant.

Bell and **Solari** (10) (1974) have shown that a simple non-uniform velocity distribution can subsequently reduce the tray efficiency even in those cases where mixing is not an important factor and in cases where retrograde flow is present although the magnitude depends on the intensity of velocity maldistribution, the efficiency is further affected. In their further studies, **Bell** and **Solari** (71) (1980) reported that the residence time distribution is strongly affected by the gas rate and extended residence time near the wall and relatively shorter residence times near the centre line were shown.

Sohlo and **Kinunen** (66) (1977) reported that small gas and liquid rates and high weir heights favoured more nonideal velocity distribution. **Fell et al** (61) (1983) have recently studied the residence time distribution of liquid on sieve trays operating in the spray regime and presented a model for the effect of the concentration profile on the plate efficiency. The model was based on a region of the tray from the inlet weir for which the liquid is only partially backmixed (Plug flow) and well mixed zone near the outlet weir (completely mixed).

Sohlo and **Kouri** (67) (1984) studied the effect of developing liquid flow patterns on plate efficiency as well as ways to simplify the treatment of the two dimensional velocity field by means of a mathematical model based on the concept of mixing by dispersion. To obtain a meaningful prediction of the plate efficiency, sufficient information on transverse liquid flow non-uniformity throughout the flow path length must be available since overestimation of the liquid channelling effect on plate efficiency would be inevitable if based on the previously used assumption of fully developed transverse flow.

From the above work, it has become clear that non-ideal liquid flow is a characteristic of conventional cross flow plates, except for very small diameter columns. Therefore, it is necessary to consider ways of studying the effect of liquid flow distribution and the degree of mixing in the axial and transverse directions. From the calculated results using the existing models and particularly at higher Peclet numbers and hence at larger plate diameters sufficient experimental liquid flow pattern data throughout the flow path length should be available in order to make a quantitative allowance for the effect of flow patterns on plate efficiencies.

In the absence of sufficient experimental data, it will be very difficult to assign any particular liquid flow pattern profile to describe the development of liquid non-uniformity on industrial trays.

The existing velocity and concentration profile data have yielded some useful information but the data are limited in their application to industrial operating columns.

In this research a new experiment has been developed which now permits the effect of the flow patterns on mass transfer to be determined in the laboratory. A technique has been developed where hot water is cooled as it flows across a tray, simulating the mass transfer

process normally encountered in distillation columns. By measuring the temperature of the water at many points, the difficulty of sampling and analysing liquid samples from commercial columns is eliminated.

The experimental liquid temperature data can be used to determine the liquid flow pattern on a tray and U-shaped temperature profiles have been observed on the tray. This method can successfully be applied to industrial scale trays as originally carried out by **Enjugu** (18) who used the water cooling technique to investigate the effect of the liquid flow pattern on tray efficiency for only one design of tray, an 8% sieve tray with 12.5 mm diameter holes. By measuring temperature profiles **Enjugu** (18) demonstrated that the temperature profile experiment is a powerful tool which can be used to investigate the effect of liquid flow pattern on tray efficiency. **Enjugu** (18) has shown that 12.5 mm diameter hole trays are often subjected to the liquid channelling effect described in the theoretical models.

The justification for this work is the comprehensive investigation of the many different phenomena which may be expected to influence the liquid and gas two phase flow pattern and thus the point and tray efficiencies of an operating sieve plate.

A long term objective for tray research is to develope the appropriate theories of tray fundamental two phase flow such that, for any tray design and system, the flow pattern and tray efficiency may be predicted. Before this can be accomplished far more knowledge is required of the behaviour of the mixture crossing the tray. Thus the main objective of this work is to provide a comprehensive experimental investigation of the many different tray phenomena which may be expected to determine (or be a result of) the liquid flow pattern.

Different experiments have been designed for investigating the liquid flow pattern across an operating tray. These are :-

1 A study of the existing efficiency models

2 Measurement of temperature profiles by the water cooling in a channel of uniform width

3 Measurement of circular tray temperature profiles in water cooling for different hole size trays

4 Measurement of liquid hold-up at points all over the tray active area

5 Measurement of the uniformity or variation of liquid flow over the outlet weir and.

6 Measurement of the back mixing in a channel of uniform width.

All the above experiments were carried out in an air water simulation column with the flowrates set to simulate conditions in the spray, mixed and the emulsified flow regimes.

Chapter 2

REVIEW OF PREVIOUS WORK

2.1 INTRODUCTION

It has been noted in the previous chapter that the efficiency of large diameter distillation columns is very much dependent on the liquid flow patterns as the liquid crosses the tray from the inlet to the outlet downcomer.

This work has been reviewed in a recent paper by **Sohlo** (68). Most of the published work is theoretical and very few experimental observations have been made on the effect of the liquid flow pattern on mass transfer on a commercial size tray due to the difficulty in obtaining samples from commercial or large scale distillation columns.

Most of the models are based on the assumption of uniform liquid flow and the models differ only in the particular mechanism used to describe the liquid mixing process.

The most important difference between the assumptions and models is in the shape of the plate (that is, is it rectangular with a constant width or does it have curved walls with changing width of the tray ?).

On a rectangular plate the liquid flows from downcomer to downcomer with uniform and constant velocity profile with mixing sometimes superimposed on the froth. However on plates of conventional construction the liquid flow is far from ideal as has already been established and these deviations from ideal flow cause considerable reductions in the mass transfer efficiency.

This chapter reviews the experimental work which has been published.

2.2 EXPERIMENT TO FIND THE EXTENT OF NON-UNIFORM LIQUID FLOW ON DISTILLATION PLATES

The first attempt to account quantitatively for the effect of liquid mixing on the tray efficiency was made by **Kirschbaum** (36) in 1934, who proposed that the liquid on the tray be divided into a number of pools and that the liquid flowed from one pool into the other until it reached the outlet weir (plug flow of liquid). However **Kirschbaum** failed to indicate how to determine the number of pools. His concept was reviewed by **Gautreax** and **O'Connell** (26) who derived an expression for the Murphree vapour efficiency . No further work was attempted until in the late 1950s the pool concept was further developed by **Marangozis** and **Johnson** (31) who included the effect of a series

of pools containing perfectly mixed liquid in both the vertical and horizontal direction. In addition to mass transfer by the bulk flow of liquid crossing the tray, it was assumed that material was also transfered from one position to another at a rate proportional to the concentration gradient in the direction of the liquid flow.This is simply the analogy to diffusion theory of the kinetic theory of gases and the proportional factor is called the Eddy- diffusion coefficient.

In 1972 **Bell** (8) developed and used a fibre optic technique to measure the residence time distribution on a commercial scale type distillation tray .The method was based on the use of fibre optic probes to detect the presence of a fluorescent tracer which has a very rapid activation and decay time .

Lines of constant residence time were obtained by cross plotting the data from the nine probes on the tray.Their data showed a zone of extended residence time near the walls and relatively shorter residence times near the centre line of the tray.

In two different experiments, **Porter, Lockett** and **Lim** (56) were able to show that liquid flowed directly across the plate from the inlet downcomer to the outlet downcomer without spreading sideways. However the liquid at the edges of the tray remained there for a much longer time without being replenished directly by any of the liquid crossing the plate in the central region of the tray. In their first experiment , **Porter, Lockett** and **Lim** used an air-water simulator containing a sieve plate 1.2 m diameter of 6.35 mm diameter holes with inlet and outlet weir lengths of sixty percent of the column diameter. A coloured tracer (potassium permanganate solution) was used to trace the movement of the water crossing the tray. The tracer was rapidly removed from the central bubbling area between the downcomers, but near the edge of the tray the tracer persisted for several seconds.

2.3 MODELLING OF THE EFFECT OF NON-IDEAL LIQUID FLOW ON PLATE EFFICIENCY.

The design of bubbly tray fractionating towers has been based on the assumption of the theoretical stages where the vapour and liquid are completely mixed with the result that the vapour and liquid leave in equilibrium . This is not a true representation of the conditions on a tray.The first attempt to account quantitatively for the effect of liquid mixing on tray efficiency was made by **Kirschbaum** in 1934 (36). He proposed that the tray be divided in the direction of liquid flow into several equal sized perfectly mixed pools. The liquid was assumed to flow from one pool to the next until the liquid reached the outlet weir. A tray of a single pool corresponded to a perfectly mixed tray and a tray with an infinite number of pools corresponded to a completely unmixed tray (plug flow of liquid). However due to the assumptions and complicated analysis, virtually no

application of **Kirchbaum`s** proposals have been made.

In 1936 **Lewis** (41) assumed that the liquid flowed across the plate unmixed. The **Lewis** equations have been widely used and are the basis for most of the analysis between tray point efficiency (E_{og}) and Murphree tray efficiency (E_{mv}). **Lewis** derived his equation for three cases :

(1) Liquid flowed across the plate unmixed and the vapour entered the plate completely mixed.

(2) Liquid is unmixed and the vapour flowed from plate to plate with out mixing and the liquid flowed in the same direction on all plates.

(3) Liquid is unmixed and the vapours flowed from plate to plate with out mixing and the liquid flowed in opposite directions on alternate plates.

Case 1 has the widest application and for this case the relationship between the overall plate efficiency (E_{mv}) and the point efficiency(E_{og}).

$$E_{mv} = \lambda \, (\exp(E_{og}/\lambda) - 1) \qquad (2.3.1)$$

$\lambda = L / MG$

G = Vapour rate mole/time

L = Liquid flowrate mole/time

m = Slope of the equilibrium curve

Equation 2.3.1 is based upon the assumptions that,

(1) the liquid flows across the tray unmixed,

(2) the vapour enters the plate completely mixed,

(3) the L/V is constant,

(4) the slope of equilibrium curve for the condition of the plate is constant,and

(5) the point efficiency is constant across the plate.

The basic difficulty with equation (2.3.1) is assumption (1). There is a considerable amount of liquid mixing and the degree of mixing is influenced by the diameter of the tray and hence the liquid flow path . The complexity of tray operation and the fact that complete liquid mixing is not obtained have led many research workers in this field to determine the effect of the deviation from ideality on the tray point efficiency, the Murphree tray efficiency and the over column efficiency.

The term efficiency is used to describe the performance of the individual trays and the overall column. The approach to equilibrium at any point on the tray can be represented in terms of the vapour and liquid composition at the immediate vicinity as follows:

$$E_{og} = (Y'_i - Y) / (Y_i^* - Y)$$

$$= (Y'_i - Y) / (m X_i - Y + b) \qquad (2.3.2)$$

where Y'_i and Y are the point vapour compositions leaving and entering the tray respectively and Y_i^* is the vapour composition in equilibrium with the liquid X_i leaving the point on the tray.

while the point efficiency is related to the individual film resistance by **Gerster et al** (13) .

$$- 1/\ln(1-E_{og}) = G / zk_g a + m G / zk_l a \qquad (2.3.3)$$

or in terms of the number of transfer units

$$- 1/\ln(1-E_{og}) = 1/N_g + m V/L N_l \qquad (2.3.3a)$$

Where N_g and N_l are the vapour and the liquid number of transfer units respectively.

The overall plate efficiency or Murphree efficiency is the ratio of the actual change in the (bulk) vapour compositions divided by the change that would occur if the vapour leaving the tray was in equilibrium with the liquid leaving the tray .

$$E_{mv} = (Y_i - Y) / (Y^* - Y) \qquad (2.3.4)$$

where Y_i and Y are the bulk vapour compositions leaving and entering the tray respectively and Y^* is the vapour composition in equilibrium with the liquid leaving the tray.

In 1972 **Porter et al** (56) developed a theoretical model where the liquid flow pattern across a tray was divided into two areas (a) defined as that part of the tray where liquid is not continually replaced by the liquid crossing the plate and (b) an active area in which the path of the flowing liquid is the region between the inlet and outlet downcomer (see figure 2.1a).

Porter et al derived two different mass transfer equations to predict the concentration of the liquid at points on the plate using the following assumptions:

(a) The flow of liquid across the tray is dominated by the momentum of the liquid entering the tray from the inlet downcomer.

(b) On entering the tray at the inlet downcomer , the liquid developes into a diverging flow channel . The liquid flows straight across the tray leaving essentially stagnant regions at the circular sides of the tray and the liquid flow is uniform in the active region of the tray. The liquid term was represented by a ratio of the liquid flowrate (L) to the outlet weir length (W) as shown below :

$$L' = L/W \qquad (2.3.5)$$

(c) The liquid entering a tray is well mixed and the analysis is restricted to one component mass transfer (or a binary mixture). The equilibrium line is straight over the liquid concentration range of a single tray.

$$Y^* = m X + b \qquad (2.3.6)$$

(d) The point efficiency E_{og} is constant over the plate and is defined by

$$E_{og} = (Y_2 - Y_1) / (Y^* - Y_1) = (Y_2 - Y_1) / m (X_2 - X^*) \qquad (2.3.7)$$

(e) The mixing of liquid caused by the gas passing through it may be expressed in terms of an eddy diffusivity coefficient which is equal in all horizontal directions.

(f) Lateral vapour mixing may be described in terms of an eddy diffusion coefficient and axial vapour mixing may be neglected in comparison with bulk flow.

Because the flow pattern on a tray is symmetrical about the centre line, calculations were based on only half of the tray. A material balance on one of the components of a binary mixture will constitute the following terms.

(a) Input by liquid flow through froth = $L'X_n dw$

(b) Input by vapour flow through froth = $G'Y_{n-1} dz'd1$

(c) Input by diffusion (Ficks Law)

Hence the total input after mathematical rearrangements is:

$$D_e\left[\frac{d^2X}{dw^2} + \frac{d^2X}{dz^2}\right] - \frac{L}{h_f\rho_L\rho_f}\frac{dX}{dz} - \frac{G}{h_f\rho_L\rho_f}(Y_1 - Y_2) = 0 \qquad (2.3.8)$$

similarly, the total output is:

$$D_e\left[\frac{d^2X}{dw^2} + \frac{d^2X}{dz^2}\right] + \frac{G}{h_f\rho_f\rho_L}(Y_1 - Y_2) = 0 \qquad (2.3.9)$$

Hence an overall material balance at steady state on an element of the froth (figure(2.1c) in region 1 yields:

Input - output = 0

Note that the liquid flow term is zero in the stagnant zone (region II)

Porter et al introduced the concept of a mixing zone between the active and stagnant regions which they calculated to be approximately 1 to 2ft in width. The value for the mixing zone was obtained by solving equations (2.3.8) and (2.3.9) for unidirectional diffusion into the stagnant region from the active region. The mixing zone is the distance over which any significant amount of materials can be transferred into the stagnant regions. Therefore when the maximum width of the stagnant region is less than about two feet, the mixing action can eliminate the effect of channelling and stagnant regions would not be expected.

Using the **Porter et al** model to predict the concentration profile, it can be shown that starting with small diameter columns the plate efficiency will increase with increasing column diameter due to the cross flow effect. The potential stagnant regions are smaller than the width of the mixing zone and consequently the stagnant zones will be eliminated by the mixing. When the plate diameter increases above about 5ft the plate efficiency increases more slowly due to the cross flow effect and the stagnant zones become greater than the mixing zone. Therefore when cross flow trays are stacked above each other in a column, the stagnant zones are also situated above each other. Thus vapour passes through the stagnant zones and equilibrium is rapidly achieved and no further change in the vapour composition occurs and a form of vapour by-passing is observed. Thus, the plate efficiency falls to approach the result of the limiting solution of E_{og} for a large tray.The dimensionless group E_{og}, influences the relative importance of the cross-flow effect and the opposing effect of vapour by passing.

In 1974 **Bell and Solari** (10) presented a mathematical model to investigate two variations in non uniform liquid flow across a tray. In the first model, non-uniform

velocity distribution across the tray with out retrograde flow was assumed and in the second model the effect of retrograde flow was added to the non-uniform velocity distribution with mass transfer occurring in both the forward and retrograde flow paths .The model was developed for a rectangular plate without liquid mixing and so is valid only for the limiting solution of large diameter plates. If the usual assumption of linear equilibrium data is made the general equation for a mass transfer at any point on the tray was modified to :

$$qVX_n - \lambda E_{og} (X_{n+1} - X_n) = 0 \qquad (2.3.10)$$

The vector q represents the velocity field normalized by the average velocity V in equation (2.3.10) below which will exist in a uniform flow field with the same geometry and average flow rate,

$$qv = V \qquad (2.3.10b)$$

q in equation (2.3.10b) is an arbitrary velocity distribution which may include retrograde flow. E_{og} is taken to be constant but not necessarily the same in the forward and retrograde flow path. **Bell** and **Solari** considered the second mathematical model based on retrograde flow. The model is distinguished from the simple nonuniform flow model by the presence of retrograde flow paths on either side of the forward flow path figure (2.2). The two regions are separated by a line along which the velocity must be zero.

The forward flow path occupies a fraction B of the total tray area, and consequently for a rectangular tray the line of zero flow must be located a distance B from the centre line on normalised half plane co-ordinates . At the outlet a volume of liquid corresponding to a fraction of the liquid coming to the tray is diverted into the retrograde flow paths near the walls. At the tray outlet three models were considered which dealt with the details of how the fluid is diverted at the weir.

In the first model it is assumed that the fluid from the forward flow path is completely mixed at the outlet and then an appropriate amount is introduced into the retrograde channel. Since the fluid entering the retrograde path has uniform composition, the model is referred to as the uniform composition model.

In the second model the flow path is assumed to be rotated off the tray so that the fluid from a flow line near the centre of the tray rotates to a position near the wall. In this case the fluid composition varies across the inlet to the retrograde path, this is referred to as external rotation model.

A variation of this model was considered in which fluid rotation started inside a trap of distance z = B from the inlet, but it shows an identical result to the external rotation model. Methods similar to these employed for the simple non-uniform velocity profile were used to calculate the plate efficiency and the combined effect of the non-uniform liquid flow and the retrograde liquid flow over the plate, as expected, showed that the tray efficiency is substantially reduced . If a uniform velocity distribution is assumed on both sides of the tray, plate efficiency increases with increase in B due to the fact that more of the plate area is used for vapour liquid contacting and the plate will be more closely approximated to the ideal case.The retrograde flow model is similar to the limiting condition of the stagnant region model predicted by **Porter et al** (8). In the latter model the retrograde flow term was assumed to be zero. Therefore, for the same B the efficiency predicted by **Bell and Solari** is less than the efficiency resulting from the stagnant regions model.

Kafarov et al (32) in 1979 suggested that the principles of systematic analysis be used while investigating bubbler plates. In their work a systematic approach to investigating diffusion processes based on the preliminary analysis of approximate information concerning the physics of the process was used.

A mathematical dependence that can serve as the basis of describing the process of mass transfer was examined both for molecular and macromolecular interactions. They determined the structures of flow on the plate which included consequentive parallel connection of complete mixing zones, zones described by diffusion model and also by-passing and recirculating flows .

To determine the structures of flow on the plates and parameters for the mathematical models describing the process **Kafarov et al** carried out a series of experiments using sieve plates, bubble cap plates, valve and tunnel caps trays. The group presented equations to predict the effect of column diameter on tray efficiency based on their experiments with full scale plant.

Their equation for the most commonly occurring case;

$\lambda E_{og} = 1$ to 3 is

$$E_{mv} / E_{og} = 1.0345 + 0.069L - 0.06W + 1.15h_w - 0.25D_{ap} + 0.22\lambda E_{og} \qquad (2.3.11)$$

where,

E_{mv} & E_{og} = plate and point efficiencies respectively

L = total liquid rate (m^3/s m)

W = vapour velocity (m/s)

h_w = weir height (m)

D_{ap} = diameter of the column (m) and

R = M/V

2.4 FLOW REGIMES

In recent years several authors have described the gas-liquid mixture formed on a tray in terms of the following flow regimes ,

(a) The spray regime

(b) The bubbly regime

(c) The emulsion flow regime, and

(d) The free bubbly regime

It is assumed that liquid transport across the tray is by the random movement of liquid elements thrown about on the tray in different directions by the rising jets of vapour. The operating range of sieve trays is defined by the upper boundary which is the flooding limit and the lower boundary which is the weeping limit.

2.4.1 SPRAY REGIME

It is assumed that liquid transport across the tray is by the random movement of liquid. This regime occurs at relatively low liquid loadings and high vapour velocities. The liquid is dispersed almost completely into small droplets by the action of the vapour jet issuing from the tray perforations (figure(2.4a)) and the transport of the liquid across the exit weir is also by a spraying action.

The onset of the spray regime is mainly influenced by the hole velocity , the vapour density, liquid holdup and the sieve tray hole size. A number of correlations have been proposed for the transition into spray regime from the bubbly regime.

Barber and Wijn (6) equation(2.4.1)

From the correlation of their experimental results carried out in a flash vessel they identified the transition from spray to the bubbly (mixed) flow regime by a photograghic study of the dispersed liquid droplets formed in the space above the froth and from the flow parameters and the system variables to predict the transition as follows :

$$\frac{h_L}{d_p} = 1.35\left[\frac{U_g\,(\rho_g/\rho_L)^{0.5}}{F\,(d_n)^{0.5}}\right] - 0.59\left[\frac{\rho}{d_n}\right]^{0.33} \qquad (2.4.1)$$

Hofhuis and Zuiderweg (30) equation (2.4.2a).

The authors used the same light transmision method as in **Porter** and **Wong**(59) experiment and they identified three separate flow regimes and for the first time reported that the transition from the spray to bubbly and vice versa occurs over a range of liquid flowrates for a fixed gas rate. The three main regimes identified are as follows :

(a) spray regime (dominant in vacuum distillation)

(b) mixed (bubbly) regime (dominant atmospheric pressure distillation)

(c) emulsified flow regime (dominant at high liquid/ vapour ratio (ie high pressure systems)).

The correlated equations for the transitions are given below :

(1) transition into the spray regime

$$C_F = U_g \left[\frac{\rho_g}{\rho_L}\right]^{0.5} = 0.85 \left[\frac{\rho_g^{0.5}\, h_L^{1.5}\, F}{d_n}\right] \qquad (2.4.2a)$$

(2) transition into the emulsified flow regime

$$\frac{L}{U_g}\left[\frac{\rho_L}{\rho_g}\right]^{0.5} > 3.0\, b\, h_L \qquad (2.4.2b)$$

The nature of equation (2.4.2b) or the transition can be moved over a range of conditions from atmospheric to high presure distillation by varying the weir height which influences the liquid hold up and by varying the weir length.

Lockett (45) equation (2.4.3)

The author found discrepancies between the transition models predicted by **Hofhuis** and **Zuiderweg** (30) and pointed out that because at high gas velocities tray oscillation occurs and becomes significant to the tray orifice behaviour, thus the relationship between h_l/d_h and U_g as proposed in the model to be misleading particularly at high gas velocities. **Lockett** (45) predicted a model for the transition from the spray to the bubbly (mixed) flow regime.

$$C_F = U_g \left[\frac{\rho_g}{\rho_L}\right]^{0.5} = \frac{0.36\,(h_L F)}{d_n} \qquad (2.4.3)$$

Porter and Wong(59) equation (2.4.4)

The authors derived a correlation for flow regime transition starting from the spray to the bubbly (mixed) flow regime. Their prediction was based on the changes observed by detecting the change in a resistance bridge when light was transmitted through a bed of distributed gas and liquid mixture in a static column (i.e. there was no cross flow of liquid thus eliminating any effect of liquid mumentum). The liquid droplets that make up the spray bed in the space above the tray are distributed in various sizes. Theoretically droplets of similar sizes form a plane above the tray whose height is determined by their terminal velocity U_t. The formation of larger drops increased with increase in the liquid flowrate (and thus increase in the liquid hold up). At the transition multiple coalescence takes place transforming the plane into the surface of a bubbly dispersion. From the experimental results the authors derived the following correlation.

$$\frac{Z_t}{d_n \rho_f} = 4.0 + 9\left[\frac{1 - A_f C_t g^{0.5} (\rho_L / \rho_g)^{0.5} (1 / U_s)}{1 - A_f}\right] \qquad (2.4.4)$$

$$= 4.0 + 9\,[(U_n - U_t) / (U_n - U_s)]$$

$$U_t = 1.04\,(\rho_L / \rho_g)^{0.5}$$

Where

U_s = superficial (or empty column) gas velocity (m/s)

U_n = gas velocity through tray holes (m/s)

U_t = terminal velocity of large drops or equivalent gas velocity (m/s)

Z_t = liquid hold up per unit area at transition from spray to bubbly (m)

ρ_f = density of froth

Porter and Jenkins (57) suggested the use of the flow ratio number (Ψ) defined by **Hofhius** and **Zuiderweg** as the functional parameter for a more close correlation of different flow regimes.

$$\Psi = \frac{q/b}{U_g}\left[\frac{\rho_L - \rho_g}{\rho_g}\right]^{0.5} \qquad (2.4.5)$$

$$U_g\left[\frac{\rho_g}{\rho_L - \rho_g}\right]^{0.5} \text{ against } \frac{q}{b} \qquad (2.4.6)$$

where q/b is the weir load, q is the liquid flow rate and b, the weir length. They also fitted a straight line on a flow ratio group plot of equation (2.4.5) and (2.4.6) above.

2.4.2 Emulsion Flow Regime

This regime is distinguished by vapour jets from the orifice appearing in the form of dispersed bubbles in a liquid medium. Unlike the spray regime, it has a definite surface as an upper boundary (figure 2.4b).The size of the bubbles formed is important for mass transfer and two main types of bubbles have been identified :

(1) The large formation size bubbles (with vapour voids) and
(2) The small size bubbles which come to equilibrium with the liquid

The distribution depends on the gas loading, the gas-liquid behaviour is dominated by the momentum of the liquid flowing across the tray.The flow of liquid over the weir was represented by the Francis Weir equation. **Porter** and **Jenkins** correlated this regime using the flow ratio group.

$$\Psi = \frac{q/b}{U_g}\left[\frac{\rho_L - \rho_g}{\rho_g}\right]^{0.5} > 0.2 \qquad (2.4.7)$$

The above correlations were used by **Hofhius** and **Zuiderweg** (30) to define the transition between the mixed flow regime and the the emulsified flow regime and this was

shown to occur at $\Psi = 0.2$ as shown in equation (2.4.7) above. The above correlations were based on limited experimental data .

2.4.3 Mixed Regime

This regime is defined as that regime between the spray regime and the emulsified flow regime. Although many real trays operate in this regime, very little is known about the nature of this regime. **Porter** and **Jenkins** (57) also suggested the use of the flow ratio number (Ψ) defined by **Hofhius** and **Zuiderweg** (30) to correlate the transition between the spray regime and the mixed regime by the following equation :

$$\Psi = (q/b) / U_g [(\rho_l - \rho_v) / \rho_v]^{0.5} = 0.7 \qquad (2.4.8)$$

2.5 CONCLUSION ON THE LITERATURE SURVEY

A review of the literature in this work clearly points out what has already been established by most of the previous workers who have oversimplified phenomena that existed in the design of distillation columns.

MAIN CONCLUSIONS

(1) Liquid flow across a sieve tray is non uniform.
(2) Mixing zone is approximately 0.6 m.
(3) Stagnant zones occur for trays more than 1.2 metre in diameter.
(4) At least four different flow regimes occur on the tray under different operating conditions.
(5) Conditions listed in 1 to 4 affect the tray and column efficiencies.

(6) The most traditional prediction method (AIChemE) does not allow for most of these conditions.

(7) The greatest problem is that most of the suggested correlations are based on models rather than experimental data because of the difficulties in obtaining experimental data from real operating columns.

(8) Therefore a new simple technique is needed to over come these problems.

(9) To improve tray design with the intension to completely remove non-uniform liquid flow across the tray.

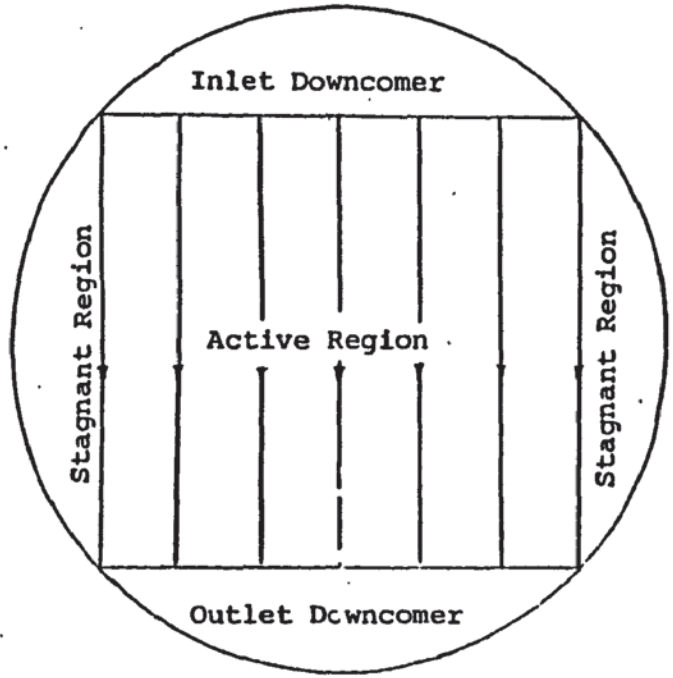

a. A schema of the liquid flow pattern

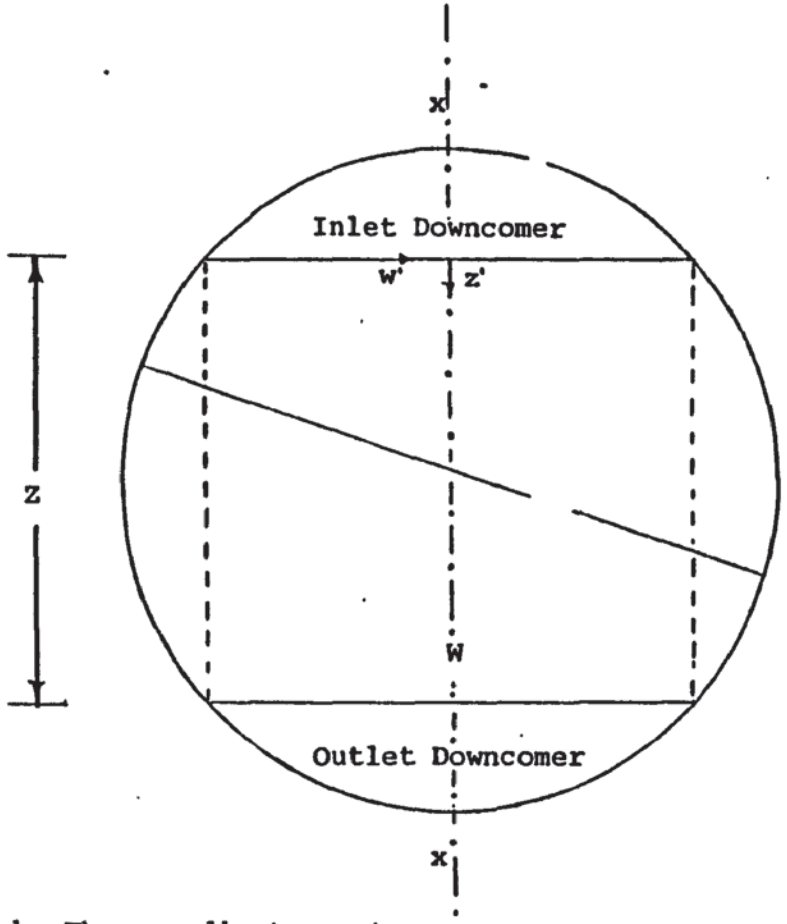

b. The coordinate system

Figure (2.1) Description of the formulation of the channelling model

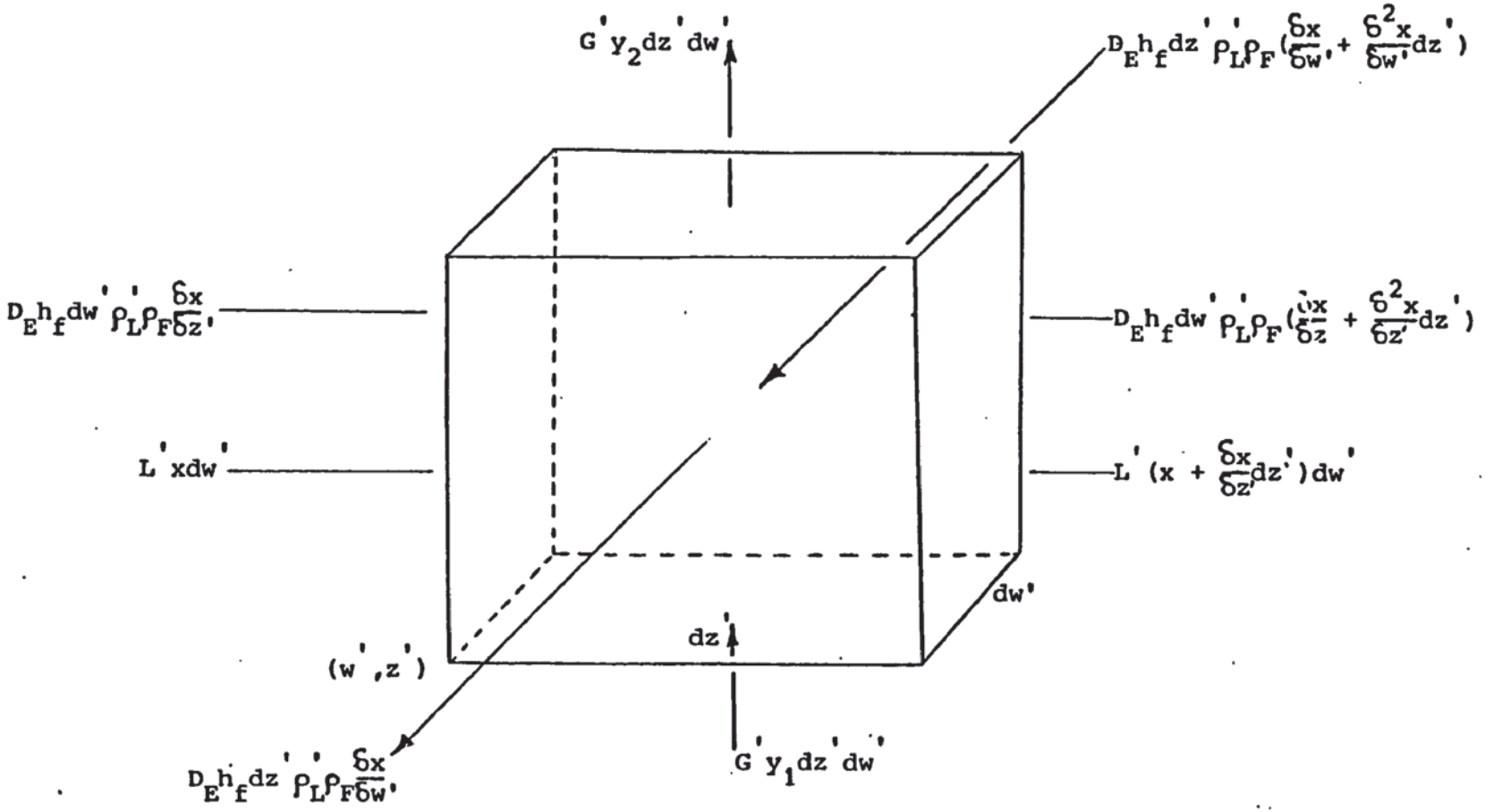

Figure (2.1c) Material balance over an element of froth

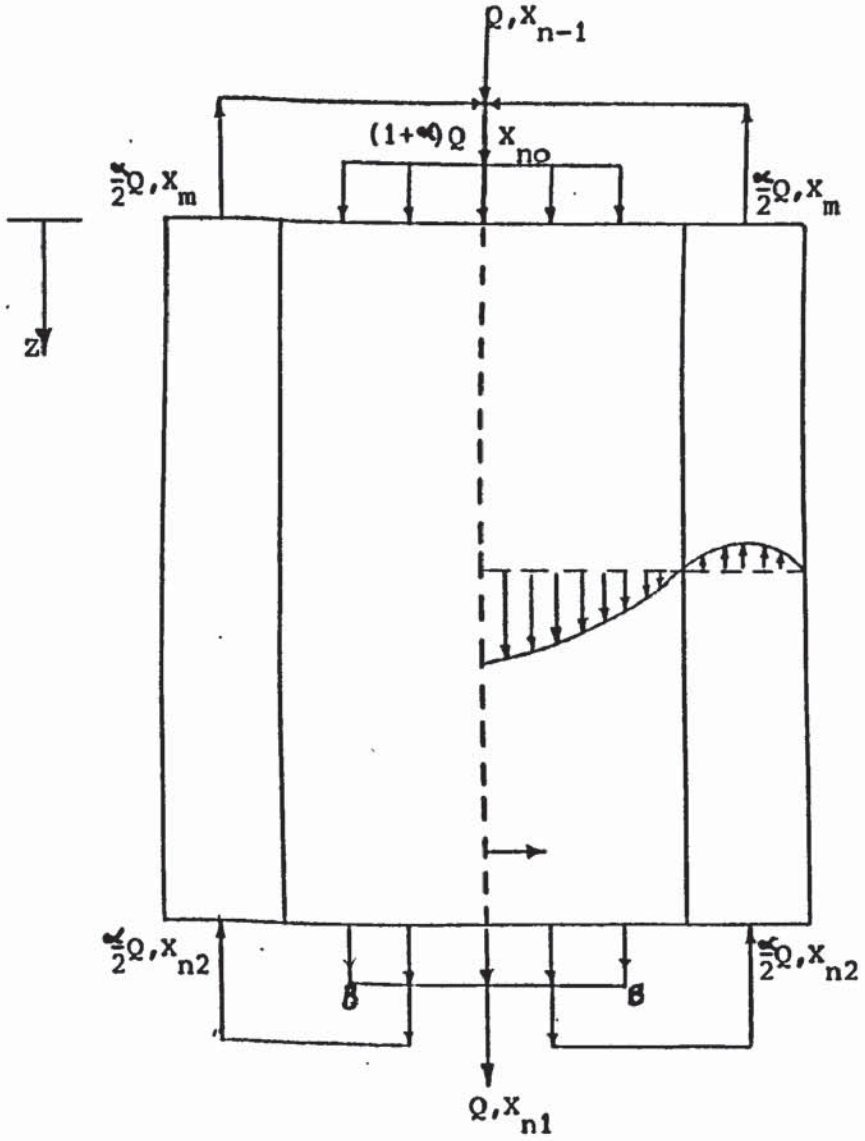

Figure (2.2) Schema for the nonuniform retrograde flow model

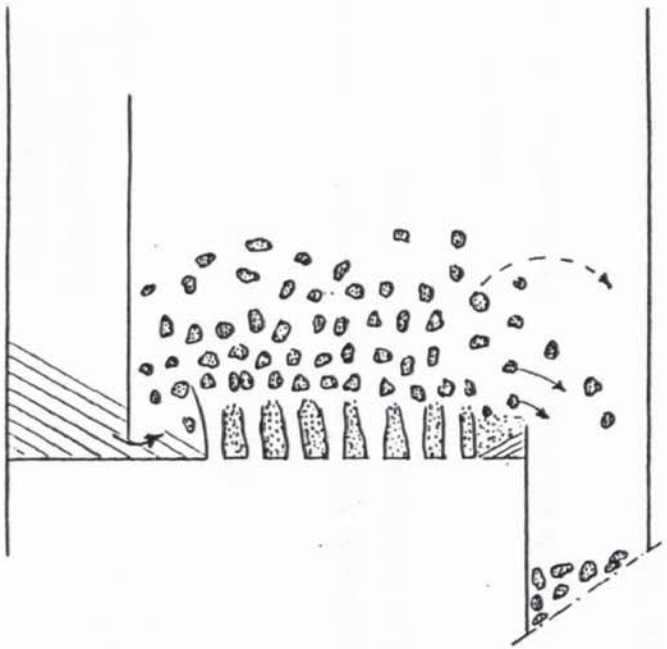

a.Supposed Froth Structure in Spray Regime
A gas continuous phase(comprises liquid droplets)

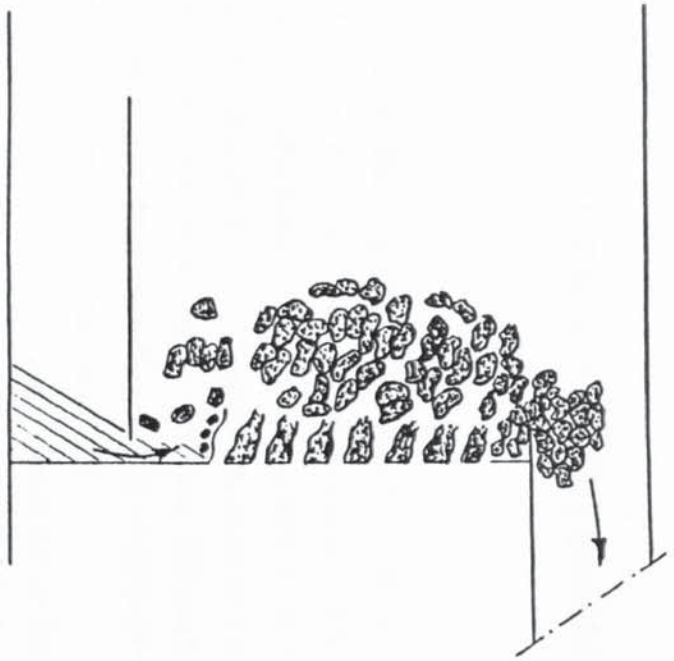

b.Supposed Froth Structure in Emulsified
or Bubbly Regime
A liquid continuous phase

Figure (2.4) Supposed froth structure in flow regimes

Chapter 3

APPROACH TO THE PROBLEM

3.1 INTRODUCTION

A complete understanding of gas-liquid contacting on distillation trays requires a full experimental study of the flow of the phase mixture across the tray. The need to know how liquid flows across and around the tray from the inlet to the outlet downcomer will enable the engineers not only to understand the dynamic situation on industrial trays but also the physics of mass transfer rates (tray efficiency) on the tray. However , there are significant practical difficulties in obtaining data from large scale industrial columns and thus most of the published work concerns small rectangular trays.

Maldistributions are known to be more significant on large diameter plates and a study of this phenomena can only be understood if similar industrial scale equipment is used.

Thus in order to remove the practical difficulty of obtaining and analysing samples from a large diameter column , a new technique (the water cooling technique) has been developed where warm water flows across a tray and the water is cooled by contact with up flowing unsaturated air. Thus, temperature profiles can be obtained from a significant number of temperature measuring devices situated in the water across the tray. It can be shown that the temperature profiles are analogous to the concentration profiles normally encountered on a conventional distillation tray. Thus data concerning flow patterns, liquid maldistribution and efficiencies can be deduced from the temperature profiles. The cooling mechanism is due to

(a) sensible heat transfer between liquid and the air, and
(b) heat of evaporation of water.

It may be shown that for the air-water system the rate of heat transfer may be predicted by using the enthalpy of air water vapour mixture as a driving force in a mass transfer equation.

$$C_p L\, dT = G dH = k_g a (H^* - H_o) \qquad (3.1.1)$$

where ,

L = moles of liquid
G = moles of gas
T = temperature of liquid on the tray

H^*= enthalpy of gas in equilibrium with the liquid at

T =Temperature

H_o= enthalpy of gas leaving the plate

k_g= gas film transfer coefficient

C_p= specific heat of liquid

In the above equation using the analogy between heat and mass transfer the liquid concentration x and vapour concentration y have been replaced by the liquid temperature T and the air enthalpy H respectively.

3.2 SCOPE OF THE PRESENT INVESTIGATION

It has been established by several previous workers that the efficiency of large diameter columns is dependent on the liquid flow pattern as the liquid crosses the tray from the inlet to the outlet downcomer. However , most of this work is theoretical and very few experimental observations have been published concerning the effect of the liquid flow pattern on the mass transfer processes on a commercial size tray. This experiment is too difficult to be practicably possible.

The water cooling technique in this research programme has been used to investigate the following:

(1) The new technique was used to investigate commercial size sieve tray designs and an attempt was made to determine whether the channelling flow pattern is developed at the inlet downcomer or produced by the outlet weir. It was important that the sieve trays and the loadings used in this study were typical of those used in industry so that the information would be applicable to commercial applications.

(2) A rectangular tray was used to investigate the extent of flat uniform channelling flow on a rectangular flow path and the effect of the developed flow patterns on tray efficiencies.

(3) Using a dye tracer of common salt , the extent of liquid back mixing was studied and the coefficient of mixing determined for different air and liquid loadings on a rectangular tray. A rectangular tray was used in order to eliminate the influence of liquid recirculation.

(4) An investigation of non-uniform liquid flow over the outlet weir, as liquid flows across the tray from the inlet to the outlet downcomer was made.

(5) A study was made (by numerical methods) of different theoretical models of tray efficiency (eg Lewis, Diener, and Porter and Lockett) so as to examine the extent of agreement between the models and the experimental reported results from FRI 1.2 m diameter column.

Visual observations were made of the flow patterns. In addition , a video film and still photographs of the progress of a dye tracer injected onto the tray at the inlet downcomer were made and analysed.

3.3 THE THEORETICAL ANALOGY BETWEEN WATER COOLING AND DISTILLATION

3.3.1 GENERAL DESCRIPTION OF THE WATER COOLING TECHNIQUE

The column contained three 1.2 m diameter trays (see tables 6.1 and 7.1 for tray specification) and a section of packing. The packed section and two of the trays were installed to provide uniform air distribution. The function of the tray is to produce the large water surface area required for the best possible air-water contact. Warm water entered the tray through the inlet downcomer and flowed across the tray in cross flow with the air. Air travelled up the column passing through the sieve holes producing jets, which, in passing vertically through the clear liquid, threw the liquid particles upwards in the active section of the tray.

Atomisation of the liquid droplets by the vapour jets is dependent on the surface tension, density and the velocity of the vapour flowing through the holes and the depth of the clear liquid seal.

The column operated on the principle of evaporative cooling as follows :

(1) When the hot water has its surface exposed to cool and unsaturated air , the water temperature falls, and the rate of cooling increases as the amount of exposed water surface increases.

(2) The heat transfer process has two parts,

(a) Heat is lost from the water by the evaporation of a small percentage of the water. (latent heat)

(b) Heat is transferred from the water to the air by convection heat transfer. (sensible heat)

(3) The cooled water leaving the column can not have a temperature less than that of the wet bulb temperature of the entering air but it is possible to cool the water below the entering dry bulb temperature of the air. In this theory , the surface (water) is assumed to be separated from the bulk air stream by a thin air film in which all the resistance to heat and mass transfer lies (ie gas film controlled process).

It is the enthalpy difference across this film which provides the driving force for the cooling process and its value will change across the tray. The assumptions used in the analysis are :

(1) The G and L are both constant .

(2) The process is gas film controlled that is;

(i) $K_g = k_g$

(ii) There is no heat transfer resistance in the water film and hence the water temperature at the water surface equals the adjacent water bulk temperature T_l.

(iii) The air at any point on the air-water interface is saturated and at T_1, the enthalpy of the saturated air is H_g^* .

In mass transfer processes such as distillation, the rate of transfer of the more volatile component, is given by:

$$dN = Gdy = k_y a(Y - Y_i) = Ldx \qquad (3.2)$$

and the point efficiency (E_{OG}) for such a process is given by:

$$E_{OG} = \frac{Y_2 - Y_1}{Y^* - Y_1} \qquad (3.3)$$

Where water cooling is being used to simulate distillation, the enthalpy of the air (H) is analogous to the vapour concentration (y) and the water temperature (T) is analogous to the liquid concentration (x). The equilibrium line relates the enthalpy of air saturated with water vapour (H*) to the water temperature. Thus the above equations may be rewritten as:

$$Q = GdH = k'_y a (H^* - H) = C_p L dT \qquad (3.4)$$

$$E_{OG} = \frac{(H_2 - H_1)}{(H^* - H_1)} \qquad (3.5)$$

$$E_{MV} = \frac{(H_2 - H_1)}{(H^*_{out} - H_1)} \qquad (3.6)$$

where from the overall heat balance:

$$H_2 = L/G\, C_p (T_{in} - T_{out}) + H_1 \qquad (3.7)$$

$$H^* = C_{air} \times T + H^* ([C_w \times T] + H_{fg}) \qquad (3.8)$$

Where $H^*_{av} = 1/A \int H^* . dA$

$$H_1 = C_{air} \times T + H_{air} ([C_w \times T] + H_{fg}) \qquad (3.9)$$

Porter, Lockett et al (56) quoted equations to model the effect of liquid concentration in Region 1 (the central portion of a tray between the inlet and outlet downcomers) and Region 2 (the stagnant zones). In their models, the liquid and vapour concentrations (x and y) have been replaced by the water temperature (T) and the enthalpy of air (H) respectively, as follows:

Active Region 1

$$D_e \frac{d^2T}{dw^2} + \frac{d^2T}{dz^2} - \frac{L}{h_f \rho_L \rho_F} \frac{dT}{dz} + (H_2 - H_1) G / h_f \rho_L \rho_F = 0 \qquad (3.10)$$

Stagnant Region 2

$$D_e \frac{d^2T}{dw^2} + \frac{d^2T}{dz^2} - (H_2 - H_1) G / h_f \rho_L \rho_F = 0 \qquad (3.11)$$

Using the above equations, lines of constant temperature can be predicted for given flow conditions across the tray.

3.4 THE ANALOGY BETWEEN HEAT AND MASS TRANSFER

The calculation of overall column efficiency E_o from the tray efficiencies starts with the knowledge of the mass transfer resistance for the liquid and vapour phase and the operating line (CT/L) gradient.

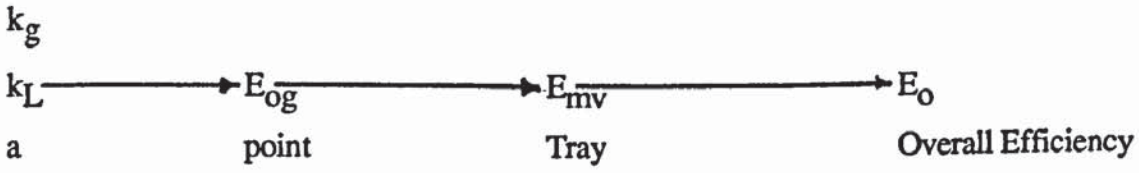

Point efficiency for a complete mixed flow in the vertical direction can be expressed as shown in equation 3.12. It is possible to alter the relative vapour and liquid-phase resistance to mass transfer by altering (G/L). But by changing L for example will also change N_L, as L increases λ decreases and N_L decreases and the system becomes vapour controlled.

$$E_{og} = N_{OG}/(1 + N_{OG}) \quad (3.12)$$

for plug flow,

$$E_{og} = 1 - \text{Exp}(-N_{OG}) \quad (3.13)$$

$$N_{OG} = K_g a\, G\, h_f\, A_f\, (Y^* - Y) \quad (3.14)$$

For water cooling technique

$$N_{OG} = K_g a\, G\, h_f\, A_f\, (H^* - H) \quad (3.15)$$

$$LdT = G\,(H_2 - H_1)\,dz \quad (3.16)$$

$$H_2 - H_1 = E_{og}\,[H^* - H_1] \quad (3.17)$$

$$H^* - H_1 = [(mT_{out} + C) - (mT_{IN} + C)] \quad (3.18)$$

$$H_2 - H_1 = E_{og}\, m\,[T_{IN} - T_{OUT}] \quad (3.19)$$

Substituting (3.16) into (3.19)

$$\frac{dT}{T_{IN} - T_{OUT}} = \frac{mG}{L} E_{og}\, dz \quad (3.20)$$

Integrating and rearranging equation (3.20)

$$\text{Ln}\ \frac{T_{IN}}{T_{OUT}} = \text{Exp}\,(\lambda E_{og}) \quad (3.21)$$

The reistance in heat transfer

Similarly resistance to mass transfer for binary mixture in which mass transfer takes place an expression to heat transfer can be drawn for the resistance to heat transfer taking place in the same binary mixture.

The heat flow through the surface may be represented thus.

$$Q = K_T a h_f A_f\,(H^* - H) = h_w\, a\, h_f\, A_f\,(T - T_1) = K_T a h_f A_f\,(H_1 - H) \quad (3.22)$$

The resistance follows :

$$\frac{1}{K_T a} = \frac{1}{K_T a}\left[\frac{H^* - H}{H_1 - H}\right] = \frac{1}{K_T a}\left[\frac{(H^* - H_1) - (H - H_2)}{(H_1 - H)}\right] = \frac{1}{K_T a}\left[1 + \frac{(H^* - H_2)}{(H_2 - H)}\right] \quad (3.23)$$

$$= \frac{1}{K_T a} + \frac{1}{h_w a}\left[\frac{(H^* - H)}{(T - T_1)}\right] = \frac{1}{K_T a} + \frac{m}{h_w a} \quad (3.24)$$

In practice the task of determining the transfer coefficient $K_G a$ and $K_T a$ is a formidable one, often it suffices to base the determination of the point efficiency on the general equation.

Chapter 4

EFFICIENCY MODELS STUDY

4.1 INTRODUCTION

The understanding of sieve tray performance has been improved in recent years because the different types of liquid and vapour flow have been identified on a tray. The factors that affect tray efficiency include the mass-transfer resistance in the liquid and vapour phases and the entrainment of liquid in the vapour. These factors depend upon the physical properties of the bi-phase system, the tray design and the hydrodynamics of the vapour and liquid in cross flow on the tray.

The separation efficiency of a distillation tray has often been defined in terms of the fractional approach to an equilibrium stage. However, in the past several workers have tried to represent the conditions on an operating tray by the use of empirical relationships and theoretical models.

Lewis developed theoretical equations relating the point efficiency and the plate efficiency for three different cases. **Diener** extended **Lewis**'s theoretical model by describing liquid mixing in terms of an Eddy diffusion coefficient. **Porter, Lockett et al** conducted dye tracer experiments in a 1.2 metre air-water simulator in order to understand the behaviour of the liquid as it crosses the tray from the inlet to the outlet downcomer. They observed that the dye was rapidly removed from the central bubbling area of the tray, whereas the dye persisted for several minutes at the sides of the tray. From their observations a model was proposed for single pass trays. In the model it was assumed that the liquid flowed directly across the tray from the inlet downcomer to the outlet downcomer without spreading sideways. As a result of this, two distinct flow patterns or regions existed on each plate, one where the liquid moves across the plate uniformly (Region 1) figure (2.1a) and another where the liquid is virtually stagnant or recirculating in closed streamlines and is not replenished directly by fresh liquid crossing the plate (Region 2).

The point efficiency can be calculated from the resistances to mass-transfer to the liquid or vapour phases and the major problem concerns the prediction of the resistance .It is possible to make a guess of the mass-transfer coefficients, then to calculate the point and plate efficiencies and mean downcomer liquid compositions and make a comparison between the experimental and calculated values, with further iterations until the experimental and calculated values agree. But, would the optimum values of mass transfer coefficients thus obtained be suitable for designing smaller or larger columns ? If not what would be the best method for predicting tray efficiencies and designing new distillation columns?

Previous workers who have attempted to answer some of these problems, have merely tried to interprete plant data on the basis of:

1. The simple plug flow model , and

2. Models containing a series of well mixed pools

In order to advance beyond the limitations of completely mixed pools and plug flow of liquid, a better understanding of liquid flow or bi-phase flow characteristics must be achieved. In an attempt to find a solution to the problem, **Porter, Lockett et al, Lewis 1, 2 and 3** and **Denier models** have been used to study the effect of each model on prediction of point and tray efficiencies. The scale up effect on the calculated efficiencies has been evaluated by using a statistical optimization technique to interprete experimental results published by the Fractionation Research Incorporated (FRI) for a 1.2 metre diameter column operating at total reflux and 165 kPa pressure on a binary mixture of cyclohexane and n- heptane.

4.2 REVIEW OF EFFICIENCY MODELS

This section will review some of the available methods for predicting the efficiencies and the liquid flow patterns on a distillation tray from published results, which may lead to a better understanding of how accurate or reliable the individual models are under different operating conditions.

The efficiency of a distillation column is based on the efficiency of the trays in the column and the tray efficiency is defined as the ratio of the concentration change achieved to the maximum possible concentration change.

POINT EFFICIENCY (E_{og})

For any particular point on a tray the degree of mass transfer between the liquid and the vapour entering and leaving that point relative to the equilibrium state is defined as the point efficiency, given by :

$$E_{og} = (Y_n - Y_{n-1}) / (Y_n^* - Y_{n-1})$$

Where Y_n and Y_{n-1} are the composition of the vapour leaving and entering the point respectively. Y_n^* is the composition of the vapour in equilibrium with the liquid at the point X_n.

MURPHREE (OR PLATE) EFFICIENCY (E_{mv})

The proportion of liquid and vapour and their physical properties varies up the column and to obtain a better picture of the meaning of the tray efficiency the condition of the liquid flow on the individual tray must be examined. For a single ideal tray, the vapour leaving is (assumed to be) in equilibrium with the liquid leaving and the ratio of the actual change in composition achieved to that which would occur at equilibrium, is referred to as the Murphree or plate efficiency and can be expressed as :

$$E_{mv} = (Y_n - Y_{n-1})/(Y_n^* - Y_{n-1})$$

Where Y_n^* is the composition of the vapour that would be in equilibrium with the liquid average composition X_n actually leaving tray n .

Y_n and Y_{n-1} are the average compositions of the vapour leaving and entering the tray respectively. In terms of the liquid, the efficiency can be represented as:

$$E_{ml} = (X_{n+1} - X_n)/(X_{n+1} - X_n^*)$$

Where X_n is the composition of the liquid that would be in equilibrium with the average composition Y_n of the vapour stream actually leaving the tray. X_n and X_{n+1} are the average compositions of the liquid and entering the tray.

OVERALL COLUMN EFFICIENCY (E_o)

The performance of a distillation colum is based on the overall efficiency of the column. The number of ideal stages required for any desired separation can be calculated from a number of established methods listed below.

(1) McCabe - Thele method.
(2) Analytical methods based on straight equilibrium and operating lines for the gas versus the liquid phase concentration plots.
(3) Analytical method based on the relative volatility (Fenske), and
(4) Tray to tray analysis (by computer programs).

The ratio of the number of the ideal stages (N) to the number of the actual trays (N_p) represents the overall efficiency (E_o) of the column and is given by :

$$E_o = N / N_p$$

Since in real distillation an ideal separation is hardly achieved, many authors have suggested different ways of using the point efficiency to calculate the overall efficiency of the column , most of the theoretical methods have been based on different assumptions of the flow pattern of the bi-phase across the tray from the inlet downcomer to the outlet weir.

THEORETICAL EQUATIONS FOR TRAY EFFICIENCY

It was first assumed that the vapour rising through the liquid on a bubble-cap tray does completely mix the liquid. This assumption implied that the liquid composition would be the same at all points on the tray. However, this assumption was first examined and questioned by **Kirschbaum** (36) who later showed that a liquid concentration gradient does exist across the tray. **Lewis** (41) assumed plug flow of liquid across a rectangular flow area and proposed a model for tray efficiency which was later modified by **Diener** (17) who superimposed on the assumption of liquid plug flow an estimate of back mixing and expressed it in terms of a diffusion coefficient or the liquid Peclet number.

Lewis equation for tray efficiency

Lewis (41) developed his theoretical models for predicting the efficiency of a distillation tray, by making the follow assumptions in all of the three cases:

1.No mixing of liquid across the tray.

2.Rectangular liquid flow path

3. Constant liquid and vapour flowrates

4. Constant point efficiency across each tray

4.2.1 Lewis 1

1. Completely mixed vapour in between the trays, and
2. Liquid cross flow.

$$E_{mv} = 1/\lambda \, [\exp(E_{og} \lambda) - 1] \qquad (4.2.1)$$

4.2.2 **Lewis 2** the changes to the assumption were

1. No mixing of vapour and

2. Parallel liquid flow across the trays.

$$E_{mv} = 2E_{og} / (2 - E_{og}) \qquad (4.2.2)$$

Where $\lambda = [1/E_{og} + 1/(\alpha - 1)] \ln \alpha = 1$

α = Relative volatility

4.2.3 **Lewis 3**

1. No vapour mixing between the trays.
2. Cross flow of liquid across the tray and

$$E_{mv} = (2 - E_{og}) E_{og} / 2(E_{og}^2/3 - E_{og} + 1) \qquad (4.2.3)$$

4.2.4 **Diener**(17) introduced an Eddy diffusion coefficient into the **Lewis** model in order to account for back mixing of the liquid on the tray but still maintained the assumption of a rectangular flow path.

$$E_{mv} = 2E_{og} P_e^2 / 2E_{og} [\exp(P_e) + P_e - 1] + P_e^2 (2 - E_{og}) \qquad (4.2.4)$$

Where $P_e = LD / wh_f \rho_f \rho_L D_e$

4.2.5 The **A.I.Ch.E.**(1) method of estimating tray efficiency follows the procedure developed earlier by **Gerster, Colburn et al** (25), based on a two-resistance concept of mass transfer. The method involves six steps.

(1) The resistance to mass transfer in the vapour phase is estimated from an empirical correlation

$$NTU_G = \frac{0.776 + 0.116W - 0.29F + 0.0217L}{(Sc)^{0.5}} \qquad (4.2.5)$$

where Sc = dimensionless gas-phase Schmidt number

W = height of outlet weir in inches

$F = \text{F-factor} = U_G \rho^{0.5}$

Expressed in $ft^3/s/ft^2$ of the bubbling area

(b) Component liquid hold up on tray Z_c expressed in inches of clear liquid.

$$Z_c = 1.65 + 0.19W + 0.020L - 0.65F \qquad (4.2.6)$$

(c) Compute average liquid contact time t on the tray in seconds

$$t_L = \frac{37.4\, Z_c\, Z_L}{L} \qquad (4.2.7)$$

where Z_L is distance in feet travelled on the tray by liquid and may be taken as the distance between inlet and outlet weir.

(2) The resistance to mass transfer in liquid phase is estimated from the empirical correlation:

$$NTU_L = (1.06\ \ 10\, D_L)^{0.5}\ (0.26F\ \ 0.15)t_L \qquad (4.2.8)$$

where D_L is liquid-phase diffusivity ft^2/h

(3) The vapour and liquid resistance are added to obtain an overall mass transfer resistance

$$\frac{1}{(NTU)_{OG}} = \frac{1}{(NTU)_G} + \frac{1}{(NTU)_L} \qquad (4.2.9)$$

(4) A point efficiency E_{og} is calculated from the overall mass-transfer resistance

$$E_{og} = 1 - \exp\text{-}NTU_{OG} \qquad (4.2.10)$$

(b) computed the value of effective diffusivity in the direction of liquid flow.

$$(D_e)^{0.5} = 0.0124 + 0.017U_g + 0.00250L + 0.015Q_w \qquad (4.2.11)$$

where U_g = gas rate ft^3/s (ft^2 tray bubbling area)

D_e = effective diffusivity (ft^2/s)

The correlation above is suitable for round-cap bubble trays having cap diameter of 3 inches or less; in the case of 6.5in round bubble caps the predicted value should be increased by 33% while for sieve trays it should be multiplied by 1.25 (1)

(c) Compute liquid Peclet number P_e

$$P_e = Z_L^2 / (D_e t_L)$$

(5) The Murphree vapour efficiency E_{mv} is calculated from the point efficiency. This involves the estimation of the degree of liquid mixing on the tray in terms of the liquid Peclet number calculated above and leads to the following expression:

$$\frac{E_{mv}}{E_{og}} = \frac{1 - \exp\text{-}(n\text{-}P_e) + \exp n - 1}{(n+P_e)[1+(n+P_e)/n] + n\{1-[n/n+P_e)]} \qquad (4.2.12)$$

$$\text{where } n = \frac{P_e[(1+4E_{og}/p_e)^{0.5} - 1]}{2}$$

(6) To account for entrainment the murphree vapour efficiency is adjusted accordingly,

$$E_a = \frac{E_{mv}}{1+r_e E_{mv}} \qquad (4.2.13)$$

where r_e is the molar ratio of the liquid entrained in the vapour to the liquid overflowing the weir.

4.2.6 Porter and Lockett Model

Porter Lockett et al eliminated the assumption of a rectangular flowpath and related the tray efficiency to four dimensionless groups which are as follows:

1. point efficiency
2. ratio of slope of equilibrium line to slope of the operating line
3. liquid Peclet number
4. parameter to characterise the circular nature of the trays

By interpreting the effect of liquid channelling on tray efficiency in terms of the "width of the mixing zone" between the active and stagnant region of the tray a model was developed which contributed immensely to the understanding of the effect of liquid maldistribution on scaling up of trays. The equations were solved using boundary conditions and in the form of finite difference equations using numerical solutions.

Two different mass transfer equations were derived to predict the concentration of liquid at different points on the plate based on the following assumptions,

(a) The flow of liquid across the tray is dominated by the momentum of the liquid entering the tray from the inlet downcomer.

(b) On entering the tray at the inlet downcomer , the liquid developes into a diverging flow channel. The liquid flows straight across the tray leaving essentially stagnant regions at the circular sides of the tray . The liquid flow is uniform in the active region of the tray and is represented by the ratio of the liquid flow rate to the outlet weir length as given below :

$$L' = L/W$$

(c) The liquid entering a tray is well mixed and the analysis is restricted to one component mass transfer (for a binary mixture).

The equilibrium line is straight over the liquid concentration range of a single tray.

$$Y^* = mX + b \qquad (4.2.14)$$

(d) The point efficiency E_{og} is constant over the plate and is defined by

$$Eog = \frac{Y_2 - Y_1}{Y^* - Y_1} = \frac{Y_2 - Y_1}{m(X_2 - X_1^*)} \qquad (4.2.15)$$

(e) The mixing of liquid caused by the gas passing through it may be expressed in terms of an eddy diffusivity coefficient which is equal in all horizontal directions.

(f) Lateral vapour mixing may be described in terms of an eddy diffusion coefficient and axial vapour mixing may be neglected in comparison with bulk flow.

Calculations were based on only half of the tray because the flow pattern on a tray is symmetrical about the centre line.

A material balance on one of the components of a binary mixture (figure 4.2.1)) will constitute the following terms.

(a) Input by liquid flow through froth = $L'x_n dw$

(b) Input by vapour flow through froth = $G'y_{n-1}dz'd1$

(c) Input by diffusion (Fick`s Law)

Hence the total input after mathematical rearrangements is:

$$D_e h_f \rho_l \rho_f [d^2x_n/dw^2 - d^2x_n/dz^2] - L dx_n/dz - m G E_{og}(x_n - x^*_{e,n-1}) = 0 \qquad (4.2.16)$$

similarly, the total output is:

$$D_e h_f \rho_l \rho_f [d^2x_n/dw^2 - d^2x_n/dz^2] - m G E_{og}(x_n - x^*_{e,n-1}) = 0 \qquad (4.2.17)$$

Hence an overall material balance at steady state on an element of froth in region 1 yields:

Input - Output = 0

Note that the liquid flow term is zero in the stagnant zone (region II)

Note that $L' = L/W$ $G' = G/A$

Multiplying each term by the factor WD/L and

The distance in the coordinate directions were made dimensionless by the following transformations.

$$Z = Z'/D \qquad W = W'/D$$

$$Z_L = Z/D \qquad W_L = W/2D$$

Where :

Z' = fractional distance along the weir

Z = total weir length

D = tray diameter

The partial derivatives then becomes,

$$d^2x_n/dw^2 = 1/D^2\, d^2x_n/dz^2$$

$$d^2x_n/dw^2 = 1/D^2\, d^2x_n/dz^2$$

$$d\,x_n/dz = 1/D\, dx_n/dz$$

where $\dfrac{LD}{D_e h_f \rho_f \rho_f W} = P_e$ the liquid Peclet number ,

$$\frac{mG}{L} = \lambda \qquad \frac{\text{slope of equilibrium line}}{\text{slope of operating line}} \qquad \text{and}$$

A = bubbling area on the plate

The above equations can be rewritten as:

For region I

$$1/P_e[d^2x_n/dw^2 + d^2x_n/dz^2] - dx_n/dz - E_{og}\lambda\,(WD/A)\,(x_n - x^*_{e,n-1}) = 0 \qquad (4.2.18)$$

For region II

$$1/P_e[\, d^2x_n/dw^2 + d^2x_n/dz^2] - E_{og}\,\lambda\,(WD/A)\,(x_n - x^*_{e,n-1}) \quad = 0 \qquad (4.2.19)$$

Boundary Conditions For The Material Balance

Based on the physical characteristics of the problem the following boundary conditions were used.

(a) By symmetry along the line xx (figure(2.1b))

$$\frac{dx_n}{dw} = 0 \text{ at } w = 0 \text{ for } 0 < z > Z_L$$

(b) At the liquid inlet (Danckwert's)

$$\text{at } Z = 0 \text{ for } 0 < w < W_L$$

(c) At the liquid outlet

$$\frac{dx_n}{dz} = 0 \quad \text{at } z = Z_L \quad \text{for } 0 < w < W_L$$

(d) At the impermeable column walls

$$\frac{dx_n}{dn'} = 0$$

where n' is the dimensionless distance in the radial direction.
After rearranging and substitution the solution became:

$$E_{mv} = mE_{og}/A \int_A (x_n - x^*_{e,n-1})dA / [1/W \int_{-w/2}^{+w/2} x_n\, dw - 1/A \int_A x^*_{e,n-1} dA \qquad (4.2.20)$$

After some algebraic manipulations the above equation becomes:

$$E_{mv} = (E_{og}/A \int_A (x_n - x^*_{e,n-1})dA / [1/W \int_{-w/2}^{+w/2} x_n\, dw - 1/A \int_A x^*_{e,n-1} dA \qquad (4.2.20)$$

Equation (4.2.20) and (4.2.21) show that the concentration profile and therefore the

plate efficiency is a function of dimensionless group P_e, WD/A, and E_{og}.

The term WD/A is the expression which makes **Porter et al** model different from the AIChemE model. The concept of a mixing zone between the active and stagnant regions was introduced by **Porter** and **Lockett** (74) and the zone is typically 1 to 2 feet in width .

The mixing zone is the distance over which materials can be transferred in any significant amount into the stagnant regions. Therefore when the maximum width of the stagnant region is less than about two feet, the mixing action can eliminate the effect of channelling.

The concentration profiles predicted from the **Porter et al** model shows that as the diameter increases from a small value the plate efficiency increases because of the cross flow effect. The stagnant regions are small compared to the width of the mixing zone and have a negligible effect . As the plate diameter increases further above about 5ft the cross flow effect causes a less steep rise in the plate efficiency and the stagnant zone becomes larger than the mixing zone. Vapour by-passing occurs when a number of such cross flow trays are stacked above each other because the vapour and liquid in such stagnant zones rapidly achieve equilibrium causing no or very little mass transfer. Thus, the plate efficiency falls to approach the result of the limiting solution for a large tray.

The dimensionless group E_{og}, influences the relative importance of the cross-flow effect and the opposing effect of vapour by passing.

In spite of the search for improved theoretical models for predicting distillation point and tray efficiencies, it is worth noting that empirical correlations are still good enough for designing columns whose specifications lie within those embraced by these correlations.

4.3 COMPARISON OF THE EFFICIENCY MODELS USING FRI TEST DATA

Test runs using cyclohexane and n-heptane were carried out by **Sakata** and **Yanagi** (65) in a 1.2 metre diameter column operating at total reflux and at a pressure of 165 kPa. The experiments were conducted away from such adverse conditions such as weeping and entrainment were avoided. The following equipment detail and experimental results have been published by **Sakata** and **Yanagi** (65) :

4.4 **Table (4.1) Tray Design Details**

	FRI tray
column diameter (m)	1.2
tray spacing (mm)	610
perforated sheet material	316SS
perforated sheet material thickness (mm)	1.5
edge of hole facing vapour flow	sharp
hole diameter and spacing (mm x mm)	12.7 x 38.1
outlet weir, height x length (mm x mm)	51.0 x 940
clearance under downcomer (mm)	38, 51
effective bubbling area (m^2)	0.859
hole area (m^2)	0.0715

RUN AT TOTAL REFLUX

Table (4.2) Conditions based on tray number 4 and 5 (from bottom)

	Run No 105	Run No 106
Vapour density (kg / m^3)	4.69	4.67
Liquid density (kg / m^3)	565	568
Vapour rate (kg/s)	5.87	5.59
Liquid rate (m^3/h)	32.02	30.43
Entrainment (kg/s)	-	-
Tray pressure drop (kPa)	1.62	1.61
Overall tray efficiency (%)	89.4	91.4
Spray height on tray 4 (mm)	610	610

Table (4.3) Cyclohexane liquid composition

COMPOSITION OF LIQUID	MOLE % CYCLOHEXANE	
	Run No 105	Run No 106
Reflux	93.1	94.8
Tray 10 outlet	93.1	94.8
Tray 8 outlet	90.9	91.8
Tray 7 outlet	87.1	87.9
Tray 6 outlet	81.9	83.2
Tray 5 outlet	75.0	76.7
Tray 4 outlet	73.5	73.6
Tray 3 outlet	57.5	56.6
Tray 2 outlet	46.7	47.9
Tray 1 outlet	38.0	39.0
Reboiler liquid	28.1	28.8

Table (4.4) Vapour mixing models considered

MODELS CONSIDERED	VAPOUR MIXING USED
Lewis 1	TOTAL
Lewis 3	NO
Diener 2	NO
Porter and Lockett	NO

The tables (4.5 and 4.6) show the variation of the N_g, N_l, reboiler hold-up and the point and tray efficiencies from one model to the other. One important feature of these results produced by running the programs in a way which led to the optimisation of the mass transfer coefficents and the reboiler hold-up is the increase in the point efficiencies for all the tested models from the top of the column to the bottom while the tray efficiencies predicted by **Lewis 1, Lewis 2,** and **Porter** and **Lockett** models have increased in the same manner as the point efficiencies the predicted tray efficiency for **Diener 2** model have showed a decrease from the top to the bottom tray of the column.

The program was repeated by starting from FRI plant data for a 1.2 metre diameter column

and using the optimum values thus obtained to design a 2.4 metre diameter column using the data obtained from the FRI 1.2 metre diameter column.

For scale-up design a four-fold increase in reboiler heat input was assumed because of an Equivalent increase in effective bubbling area of the tray, as a result of the diameter and weir length having been doubled.

4.5 RESULTS

Table (4.5) Optimum results of the model from top to bottom tray (Run No 105)

Model	optimum values		reboiler	E_{og}	E_{mv}
	N_g	N_l	hold-up		
Lewis 1	1.486	2.396	59.31	65.7 - 59.2	81.3 - 82.4
Lewis 3	1.552	2.439	59.18	66.5 - 60.0	81.6 - 82.2
Diener 2	2.277	2.997	59.75	78.6 - 71.5	84.0 - 80.1
Porter & Lockett	1.76	2.28	59.43	71.5 - 64.4	79.9 - 85.9

Table (4.6) Optimum results of the model from top to bottom tray (Run No 106)

Model	optimum values		reboiler	E_{og}	E_{mv}
	N_g	N_l	hold-up		
Lewis 1	1.53	2.49	59.93	66.9 - 60.4	83.1 - 84.6
Lewis 3	1.69	1.64	59.9	64.1 - 55.6	75.6 - 79.1
Diener 2	2.3	3.0	59.70	79.4 - 72.7	85.0 - 80.9
Porter Lockett	1.84	2.4	59.59	73.1 - 66.0	81.0 - 85.1

DISCUSSION

The FRI run was conducted at total reflux, 165 kPa pressure on the cyclohexane /n-heptane system. The equated values for the overall column plate efficiency were 89.4% for experimental run number 105 and 91.4 % for run number 106 both at total reflux without entrainment. The calculated values for the individual experiment by the computerised method vary from one theoretical model to another as shown in tables (4.5 and 4.6).

It is remarkable that the optimal reboiler hold-up predicted by all the models is almost the same. However, there is a wide variation in the optimum values of the mass-transfer coefficients and there is a significant difference in the tray efficiency values.

The optimum efficiencies increase from the top to the bottom of the column as opposed to a decrease in the case of the **Diener** 2 model. Note that **Diener** 2 and **Porter** and **Lockett** models both considered backmixing of liquid on the trays so the switch of pattern in the predicted tray efficiency in the case of Diener 2 model may be due to the consideration of liquid channelling by the latter model.

If stagnant liquid zones are situated above each other on the single-pass trays, then the effect of vapour by-passing on tray efficiency becomes more significant from the bottom to the top of the column leading to lower efficiency values at the top and higher ones at the bottom as observed with the **Porter** model.

It is important to note that **Lewis** 1 and Lewis 3 models take no account of scale-up since the same efficiencies were obtained for the 1.2 metre diameter column as for the 2.4 metre diameter column.

However **Porter** and **Lockett** model predicted a considerable decrease in efficiency. It is evident that there is no agreement between experimental and calculated results.

4.7 Conclusions

A comparison between tray efficiencies values predicted by the models show a reasonable agreement between the **Porter** and **Lockett** model and the experimental results.
However, all the theoretical models calculated tray efficiencies from a point efficiency. The point efficiency can easily be calculated if the liquid and vapour phase mass-transfer resistances are known.

The mass transfer coefficients were estimated from empirical correlations, since the tray

efficiency determined from any theoretical model would depend on the point efficiency or the liquid and vapour phase mass-transfer resistance the predicted results using such models would always show no agreement with the real plant results. Thus unless an improved method for calculating mass-transfer resistance is available or a better way of estimating tray efficiency without the need for a knowledge of the tray point efficiency is developed can a better estimate of the tray and the overall column performance be made.

Having established the inadequacy of the existing models the author can now proceed to the proposed technique to over come this difficult problem.

Chapter 5

EQUIPMENT DESCRIPTION

5.1 Air Water Simulator

A 1.2 metre diameter column made of transparent (P.V.C) was used in this work (figure 5.1a). The trays inside the column were supported with vertical stainless steel rods passing through a series of support rings which were located at 2 ft (0.6 m) intervals up the column.

The upper section contained the gas distribution system whilst the lower section contained the hot water sump. The process flow diagram is shown in figure 5.1a, a detailed diagram in figure 5.1b and a photograph in figure 5.1c

Air was introduced into the base of the column through a 0.45 m square duct from the supply fan. The air flowrate was measured by a calibrated Pitot tube which was situated in the longest straight length of the duct. The air passed through a mild steel distributor above which there was a 1.0 m section of 50 mm Pall rings packings. Two more sieve trays, acting as air distributors , were situated above the packing section.

After leaving the test tray, the air passed through a section of "Knitmesh" packing to reduce entrainment losses. A Pitot tube traverse was carried out over a large number of points in the region above the test tray and below the section of Knitmesh packing to ensure that uniform gas flow had been achieved over the column cross sectional area.

Liquid was pumped to the top of the column from the sump through one of three rotameters. Each rotameter had been calibrated for a particular flowrate range. Just before the water entered the top of the simulator, live steam was fed into the water supply line to maintain an inlet temperature of approximately 40^{o}C.

In order to achieve uniform liquid distribution in the inlet downcomer and therefore onto the test tray, the water flowed through a sparge pipe onto the top of a section of 50 mm Pall Ring packing which was contained in the inlet downcomer. The downcomer was 0.915 m high and the packed section commenced approximately 0.28 m above the tray floor in order to leave sufficient clearance for liquid backup in the downcomer. The liquid leaving the tray flowed over the outlet weir and through the downcomer directly back to the sump without

any contact with the incoming air. The sump had a capacity of approximately 2.7 m^3 and its contents could be heated by live steam injection.

Pressure tappings were positioned both above and below the test tray and clear liquid holdups were measured at a number of points across the tray. The liquid temperatures on the test tray were measured by twenty six Nickel/Chrome thermocouples which were placed at the positions on the tray as shown in Figure (5.1d). Each thermocouple tip was situated on a PTFE seat approximately 5 - 10 mm above the tray floor and between the holes in the tray. The outputs from the thermocouples were linked directly to a data-logging system. The thermocouples were calibrated over the experimental temperature range.

The humidity of the inlet air was measured immediately below the test tray by a hygrometer. In order to minimise the risk of the air sample becoming contaminated with water droplets from liquid which might weep through the plate, the sampling probe was shielded and the humidity samples were withdrawn from a number of positions across the tray. Experiments were also carried out in the absence of water cooling when a dye tracer was injected across the test tray at the inlet weir and both still photographs and video recordings were taken of the resulting dye patterns.

5.1.1 Water Supply System

A centrifugal pump capable of delivering 250 cm^3/ s cm against a head of 8.4 metre was used. The pump was close coupled to a 3 kW 1440 RPM TEFC squirrel cage motor. The discharge from the centrifugal pump was delivered to the test tray inlet downcomer through one of three supply pipes (Table 5.1). Each of the supply pipes contained a rotameter which had been calibrated for a particular range of flowrate. The hot water was distributed on to the test tray by passing it through a sparge pipe which distributed the hot water into the inlet downcomer packed with 50 mm Pall rings to a height of 500 mm. The packing was held up at a clearance of 280 mm from the downcomer tray floor to allow sufficient room for liquid backup in the downcomer.

Table (5.1) Water supply pipes specification

Pipe internal diameter (mm)	Orifice (mm)	Flow rate range
76.2 (3.0 in)	38.1 (1.5 in)	0.0 --- 0.0303×10^{-3} m^3/s m
76.2 (3.0 in)	50.8 (2.0 in)	0.0303×10^{-3} -- 1.518×10^{-3} m^3/s m
203.0 (8.0in)	152.4 (4.0in)	0.758 ---- 7.583×10^{-3} m^3/s m

5.1.2 Air fan

A centrifugal fan was used which was capable of delivering about 6 m^3/s m^2 of air to the column from a distance of about 20 m over a height of 5m through a rectangular duct of 45cm x 45 cm cross section. Air was introduced tangentially into the column . To remove swirl and any other maldistribution in the air stream, the air was passed through a 1 metre section of 50 mm Pall rings packing and two redistribution trays located above the packing.

The existence of rectangular elbows in the air duct line from the plant room where the fan was situated created some oscillation of the air stream as it approached the column. A perforated mild steel sheet was placed across the air duct line both to regulate the flow of the air and to dampen the oscillating behaviour. A wooden choke was used to cover the part of the fan suction area to achieve low air flow rates. Further control of the air flow rates was achieved by a simple butterfly valve fitted to the air duct close to the inlet to the base of the column.

5.1.3 Steam supply

The steam used for the experiments was taken from the main steam line in the laboratory and sparged into the sump through 0.7 m long and 12.7mm diameter perforated copper tube.

5.2 Trays

The details of the test trays used in the research programme are given in Tables 6.1 and 7.1. In order to examine the effect of heat losses through the metal trays, a test tray of 12.5mm hole diameter was made from perspex using the same thickness as the metal trays.

All the holes were drilled on a triangular pitch and with sharp edges in accordance with industrial practice. Figure (5.2a and 5.1a) shows the trays used and the air water simulator.

5.3 MEASUREMENTS OF OPERATING SYSTEM VARIABLES

The essential variables required to implement the water cooling technique fall into two separate groups . The air and water flow rates may be called the operating variables while the water temperature and the air enthalpy were grouped as the system variables. It was assumed that under all the operating conditions used for the experiments in this work the other physical properties of the system such as the viscosity and the density did not change significantly. The

procedures used for these variables are described in sections 5.3.1.

5.3.1 Calibration Of The Inclined Manometer

A necessary requirement in the experiment was to make sure that the required air velocity was supplied to the test tray and the air was evenly distributed over the active area of the tray. The air distribution was checked by measuring the air flow pattern above the test tray at the top of the column. These air flow patterns were measured with a Pitot tube.

The air flow rate was found to be almost uniform with some slight deviation at the walls of the column. The Pitot tube located in the air supply duct was then calibrated against the data which had been obtained from the gas distribution flowrate measurements. A calibration was plotted for the air supply duct Pitot tube against the pressure drop measured on an inclined manometer (see figure 5.3a and 5.3b). The calibration tables are given in Appendix ((2) Tables (5.2 & 5.3)).

The Pitot tube was located in the longest straight section of the air supply duct . The change in the liquid head (h) due to the passing air was read from the inclined manometer connected to the pitot tube. The air velocity (U_s) was calculated from the equation:

$$U_s = (2\,g\,h)^{0.5} \qquad (5.1)$$

Where g is the acceleration due to gravity (9.81 m/s^2)

The correct equation for the superficial air velocity through sieve trays is given by :

$$U_s = C_d\,(2\,g\,h)^{0.5} \qquad (5.2)$$

Where C_d is the discharge coefficient for sieve trays (C_d = 0.66), and

$$C_{sb} = U_s\,(\rho_g / (\rho_l - \rho_g))^{0.5} \qquad (5.3)$$

5.4 PERIPHERIAL EXPERIMENTAL APPARATUS

The air-water simulator is capable of being operated at industrial scale gas and liquid loadings.

The temperature of water in cross flow with air on the tray was transmitted as voltages across the cold and hot ends of K-type thermocouples .The voltages were converted to temperatures using an online Commodore micro-computer connected to the apparatus through the peripherial devices shown in fig (5.4).

5.4.1 Details of commodore 4000 and peripherials used

The computer connected to the rig was a series 4000 Commodore system, in conjuction with the peripherials.

The computer had two functions. First it controlled the other devices in the system. Secondly, it performed calculations, manipulated information and displayed the results on a twelve inch green and black video screen

(a) The Isothermal box, which was placed near the tray, was made from die cast aluminum lined with expanded polystyrene insulation. Screw terminals for the thermocouples from the plate leads were mounted on a copper block inside the box. Also mounted on this box was an encapsulated platinum resistance sensor (RTD) which was used to determine the temperature of the copper block which was used as a reference temperature. Each of the boxes was capable of holding up to 16 thermocouples. Therefore two of these boxes were used and 32 way sockets connected them to the TC-16 bus.

(b) The TC-16 provided the elements for temperature monitoring up to 16 thermocouple per card. A module within the microlink mainframe provided multiplexing and amplification of the thermocouple voltages. The module allowed software selection of the thermocouple to be sensed and software control over the gain of the amplifier so that temperatures close to ambient could be resolved with greater precision. The detail of the conversion of voltage to temperature is discussed in (3)

(c) The printer was used to output information onto paper

5.4.2 Calibration of the thermocouples

The thermocouples were calibrated against a standard 9540 digital Platinum resistance thermometer.

The thermocouples were immersed in a hot water bath with a temperature control thermostat and with the tip of the platinum resistance in the same bath at the same depth. The temperature of each thermocouple was recorded at the same time as the platinum resistance thermometer. The values obtained were plotted against the platinum resistance thermometer reading as shown in Appendix 13 .

5.5 Tracing the contours through the temperature grid

The temperature variation over the tray was plotted on the vertical scale of a three dimensional representation of the tray. Although temperatures were measured at known positions on the tray, it is only possible to determine temperatures at intermediate points between the measurement points by some theoretical method.

For the contour height or the defined surface to be smooth, it is necessary for the function T(I,J) to be continuous and also to have a continuous first derivative at every point in the temperature field area. The temperature at a given point will be dependent on the temperature points close to the point rather than those further away from the point.

To obtain the temperature of the surface at a given point only, data which lie within a circle of radius S centred on the given point will be used. The temperature values of the data points used are weighted by a factor W depending on their distance D from the given point.
For the surface to be continuous, weight W must be continuous in D and must tend to zero when D approaches S and as the surface passes through the data points, the weight W must tend to infinity as D approaches zero. For the surface to have a continuous derivative, the derivative of the weight W with respect to D must be continuous and also must approach zero as D approaches S.

$$W = [(S - D)/D]^2 \qquad \text{for } (S>D)$$

Having assigned a weighting to each of the data points in the vicinity of T(I,J), a weighted mean of the surrounding points must be used to determine T(I,J):

$$T(I,J) = \frac{\Sigma\,(\text{weight})_i \times T(X_i,Y_i)}{\Sigma\,(\text{weight})_i} \qquad (5.5.1)$$

where (X_i,Y_i), for $i = 1, 2, 3, \ldots . r$, are the coordinates of the data points lying within a distance S of T(I,J). $T(X_i,Y_i)$ is the given temperature at (X_i,Y_i) and $(\text{weight})_i$ is the

weighting applied to the point (i).

$$(\text{weight})_i = \frac{[\,S - d(i)\,]^2}{d(i)} \qquad (5.5.2)$$

$$d(i)^2 = (X_i - I)^2 + (Y_i - J)^2 \qquad (5.5.3)$$

The above will give maxima and minima of the surface temperature only at the data point temperature. Since the temperature at any point will always lie between the highest and lowest temperature point under consideration, the required temperatures in between are obtained by a least squares fit of a paraboloid surface to the weighted data point..

If the coordinates are changed such that (I,J) becomes the origin:

$$U_i = X_i - I$$

$$V_i = Y_i - J$$

and fitting a paraboloid of the form:

$$T = K(U^2 + V^2) + gU + fV + C \qquad (5.5.4)$$

at $U = 0$ $V = 0$ solving for C

Values of the constants K, g, f and C must be found so that

$$\phi = \sum_{i=1}^{r} (\text{weight})_i \times [K(U_i^2 + V_i^2) + gU_i + fV_i + C - T(U_i,V_i)]^2 \qquad (5.5.5)$$

is a minimum

This is achieved by solving for C in the four simultaneous line equations:

$$\frac{d\phi}{dK} = 0 \qquad \frac{d\phi}{dg} = 0 \qquad \frac{d\phi}{df} = 0 \qquad \frac{d\phi}{dC} = 0$$

we have

$$\sum_{i=1}^{r} = (\text{weight})_i \times [K(U_i^2 + V_i^2) + gU_i + fV_i + C - T(U_i,V_i)]^2 \times (U_i^2 + V_i^2) = 0 \quad (5.5.6)$$

$$\sum_{i=1}^{r} = (\text{weight})_i \times [K(U_i^2 + V_i^2) + gU_i + fV_i + C - T(U_i,V_i)]^2 \times (U_i) = 0 \quad (5.5.7)$$

$$\sum_{i=1}^{r} = (\text{weight})_i \times [K(U_i^2 + V_i^2) + gU_i + fV_i + C - T(U_i,V_i)]^2 \times (V_i) = 0 \quad (5.5.8)$$

$$\sum_{i=1}^{r} = (\text{weight})_i \times [K(U_i^2 + V_i^2) + gU_i + fV_i + C - T(U_i,V_i)]^2 = 0 \quad (5.5.9)$$

The above can be represented in the form

$$C * X = K$$

where X is a column vector containing the unknown constants K, g, f and C.

K is a column vector containing the constant terms of the equation

Determine T(I,J), is determined by a weighted mean of the heights of the surrounding points.

$$T(I,J) = \frac{\sum_{i=1}^{r} (\text{weight})_i * T(X_i,Y_i)}{\sum_{i=1}^{r} (\text{weight})_i} \quad (5.5.10)$$

where (X_i,Y_i) i =1, 2, 3 ... r are the coordinates of the data points lying within S of (I,J), $T(X_i,Y_i)$ is the given temperature at (X_i,Y_i) and $(weight)_i$ is the weighting applied to the point (i).

$$(weight)_i = \frac{[S - d(i)]^2}{[\ d(i)\ ]} \qquad (5.5.11)$$

$$[\ d(i)\ ]^2 = (X_i - I)^2 + (Y_i - J)^2$$

The above will give maxima and minima of the surface temperature only at the data point temperature. Since the temperature at any point will always lie between the highest and the lowest temperature point under consideration, the required temperatures in between are obtained by a least square fit of a paraboloid surface to the weighted data point.
If the coordinates are changed such that (I,J) becomes the origin

$$U_i = X_i - I \quad \text{and} \quad V_i = Y_i - J$$

Fitting a paraboloid of the form,

$$T = K(U^2 + V^2) + gU + fV + C \qquad (5.5.12)$$

At U = 0, V = 0 C is solved where C is the symetric coefficient matrix of the unknowns.

Using the method of solution given by **Wilkinson** and **Reinsch** (8), and **Heap** and **Pink** (9), C is first factorised into the form

$$C = L * D * L^T \qquad (5.5.13)$$

where L is a lower triangular matrix with a unit leading diagonal, L^T is its transpose and D is a diagonal matrix. Thus the vector X is given by

$$X = (L)^{T-1} * D^{-1} * L^{-1} * K \qquad (5.5.14)$$

A computer program was developed to solve the above equations and the output from the program is given in the form of the temperature profile and surface contour plots.

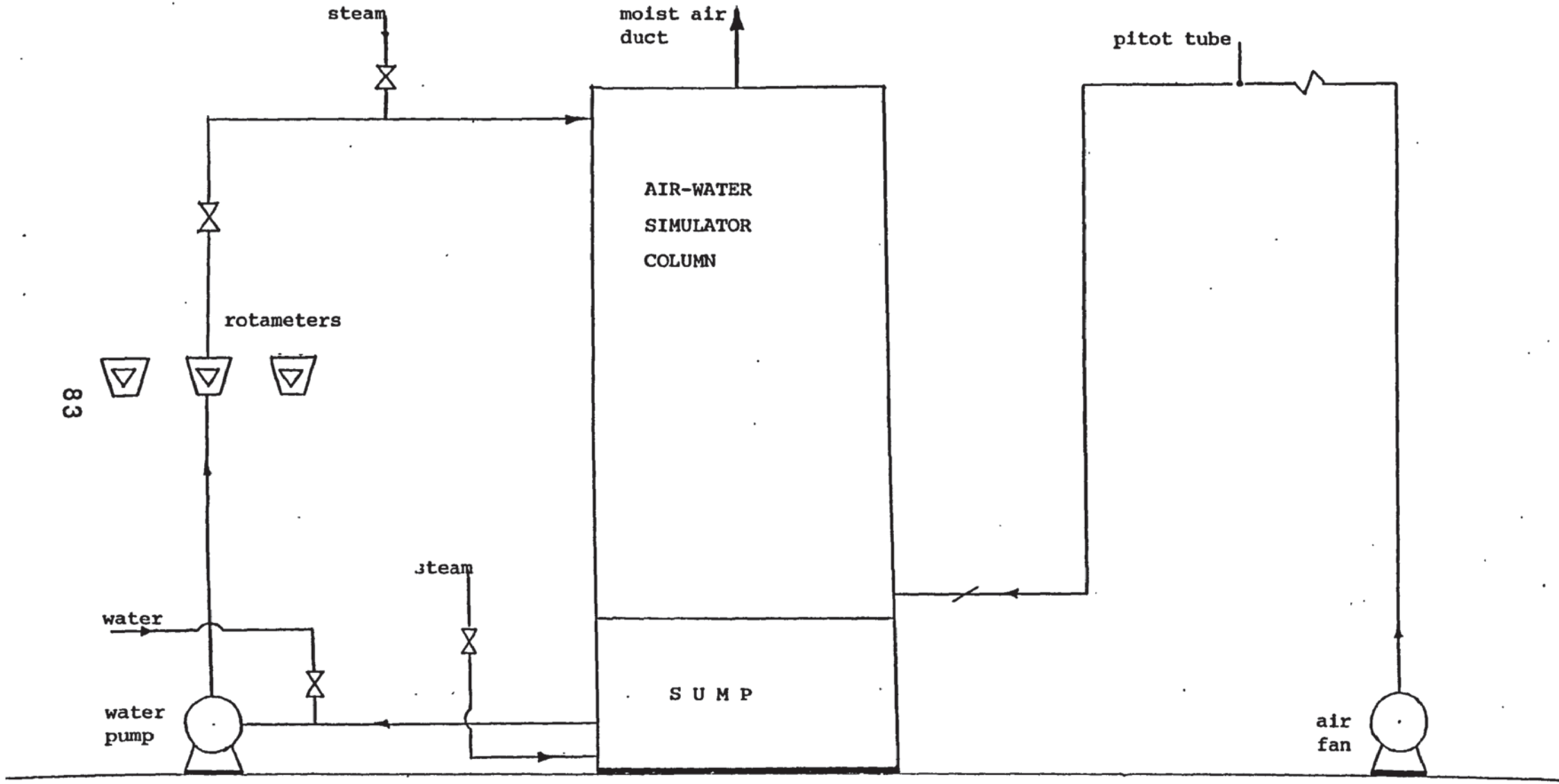

Figure (5.1a) Flowsheet of the rig

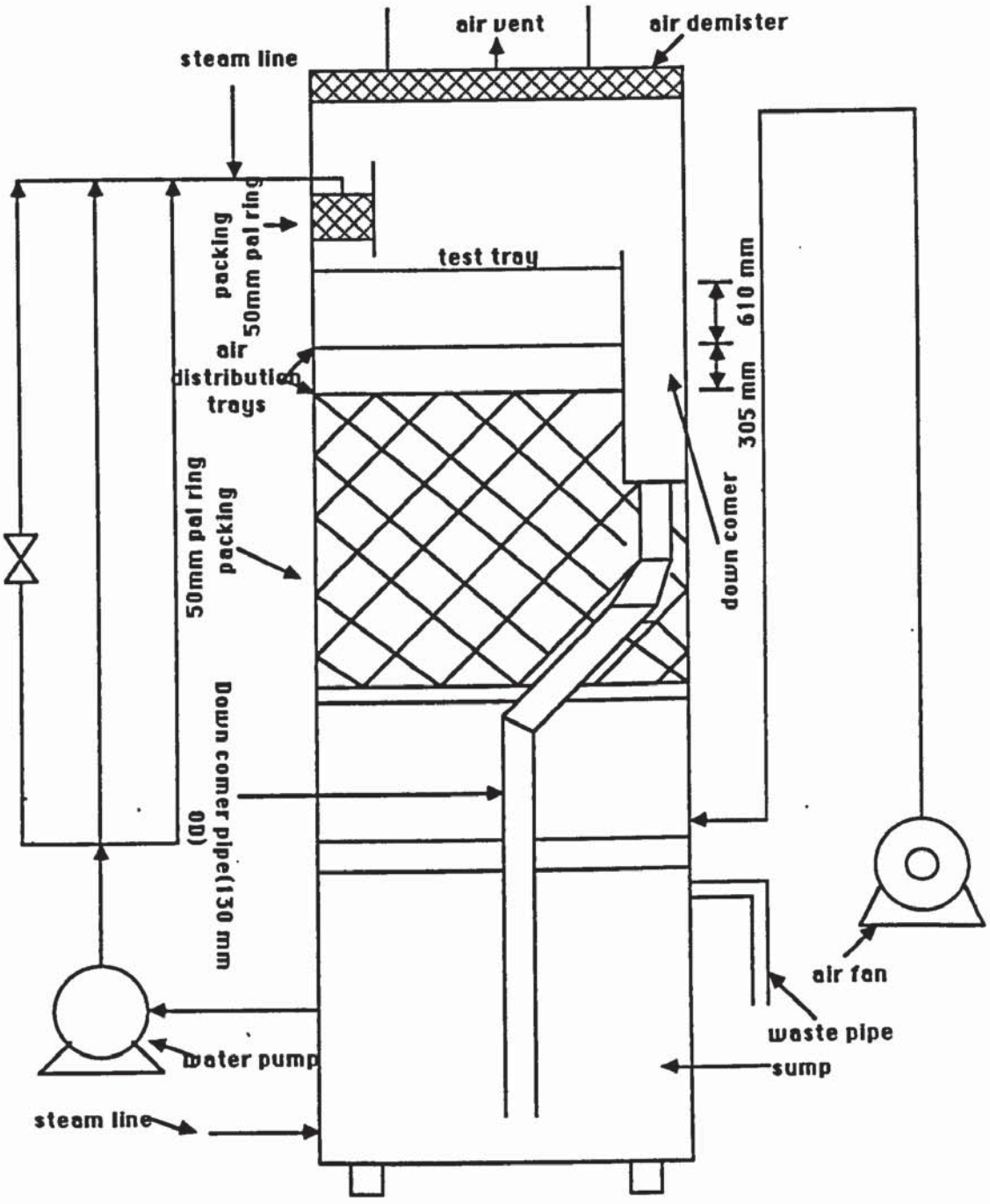

FIGURE (5.1b)AIR-WATER SIMULATOR COLUMN

Figure (5.1c) Photographic view of experimental rig

thermocouple location on the tray (units: mm)

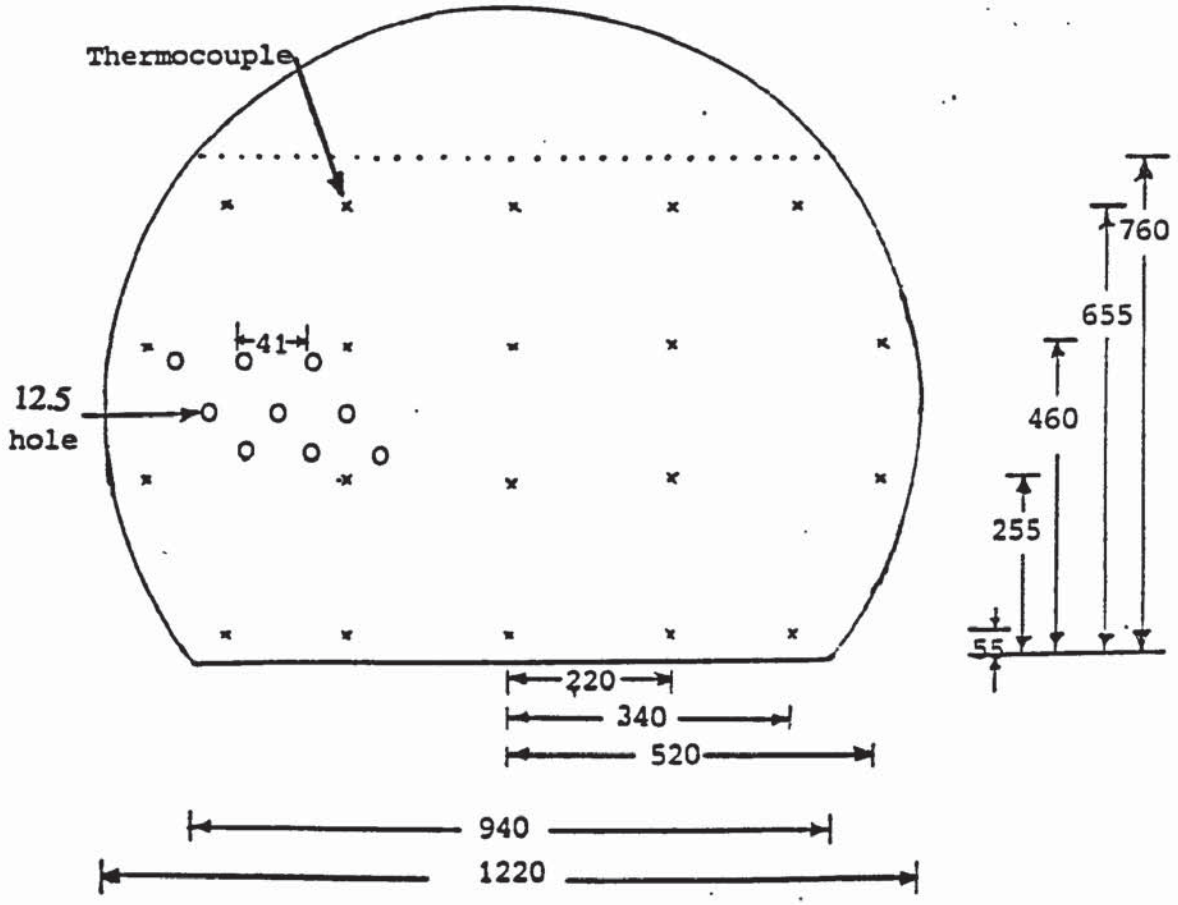

Figure (5.1d) Thermocouples position on test tray

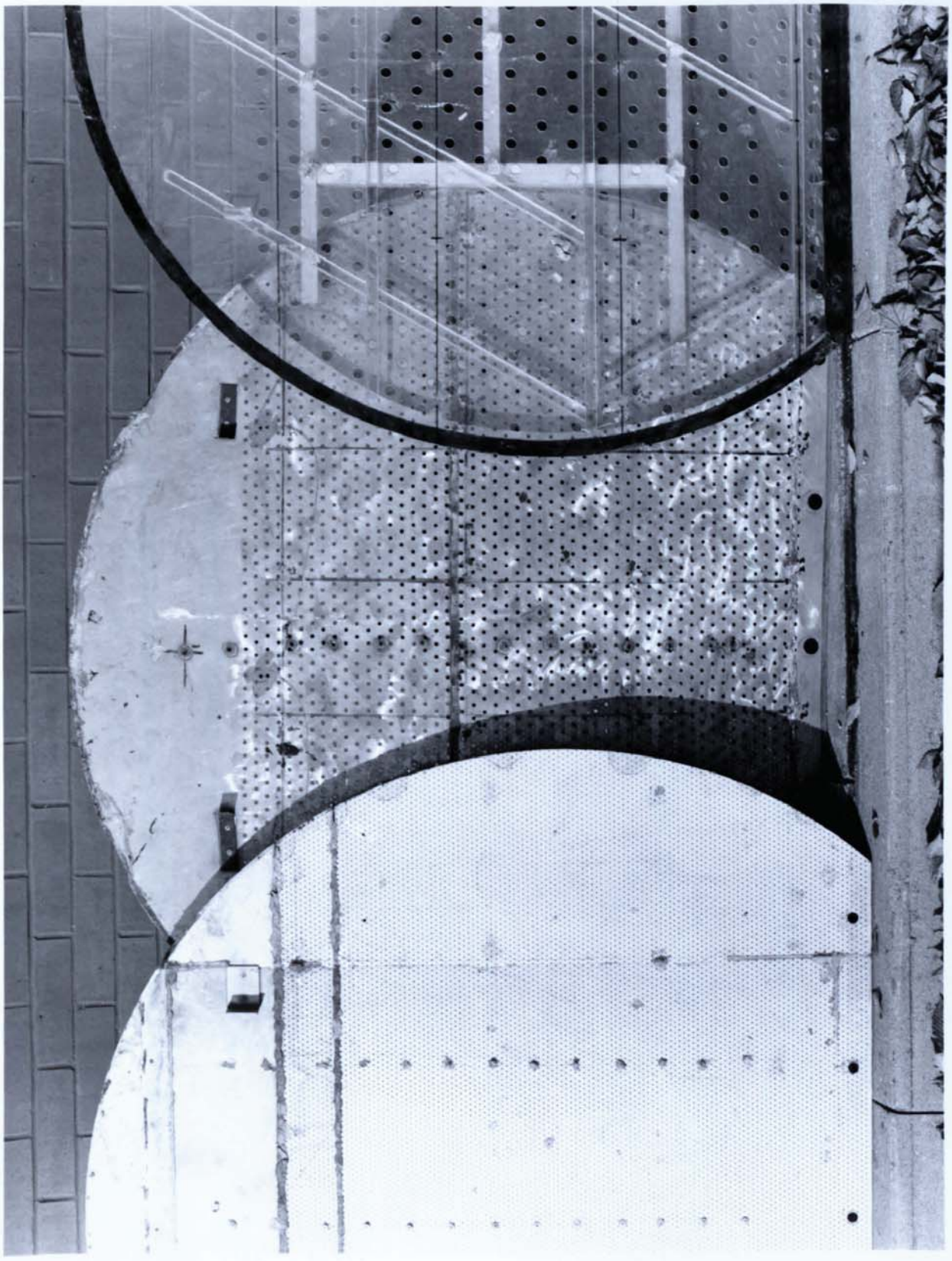

Figure (5.2a) Typical test trays used

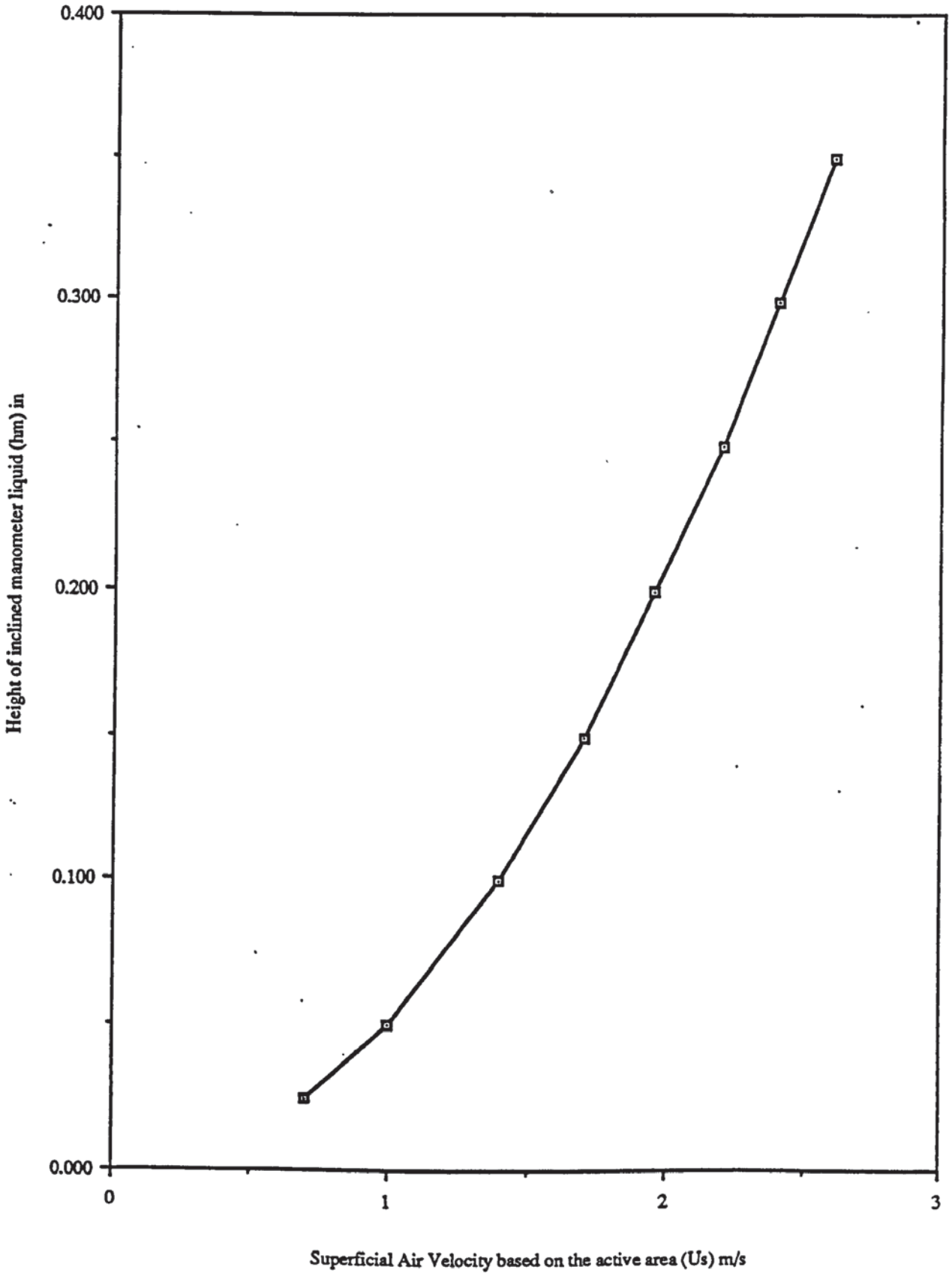

Figure (5.3a) Graph of inclined manometer reading versus Superficial air velocity based on the active area of the tray

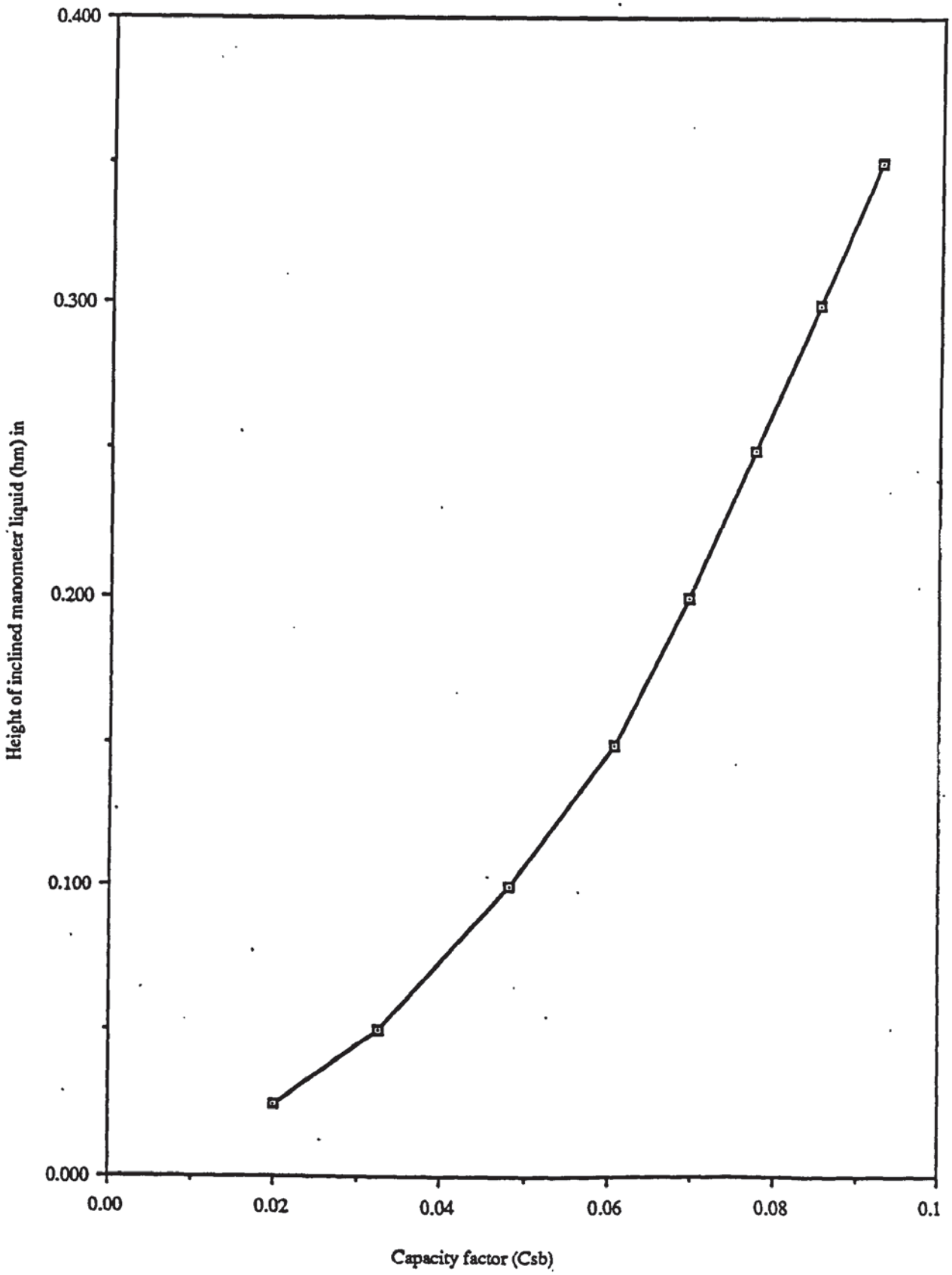

Figure (5.3b) Graph of inclined manometer reading (hm) versus Air Capacity Factor (Csb)

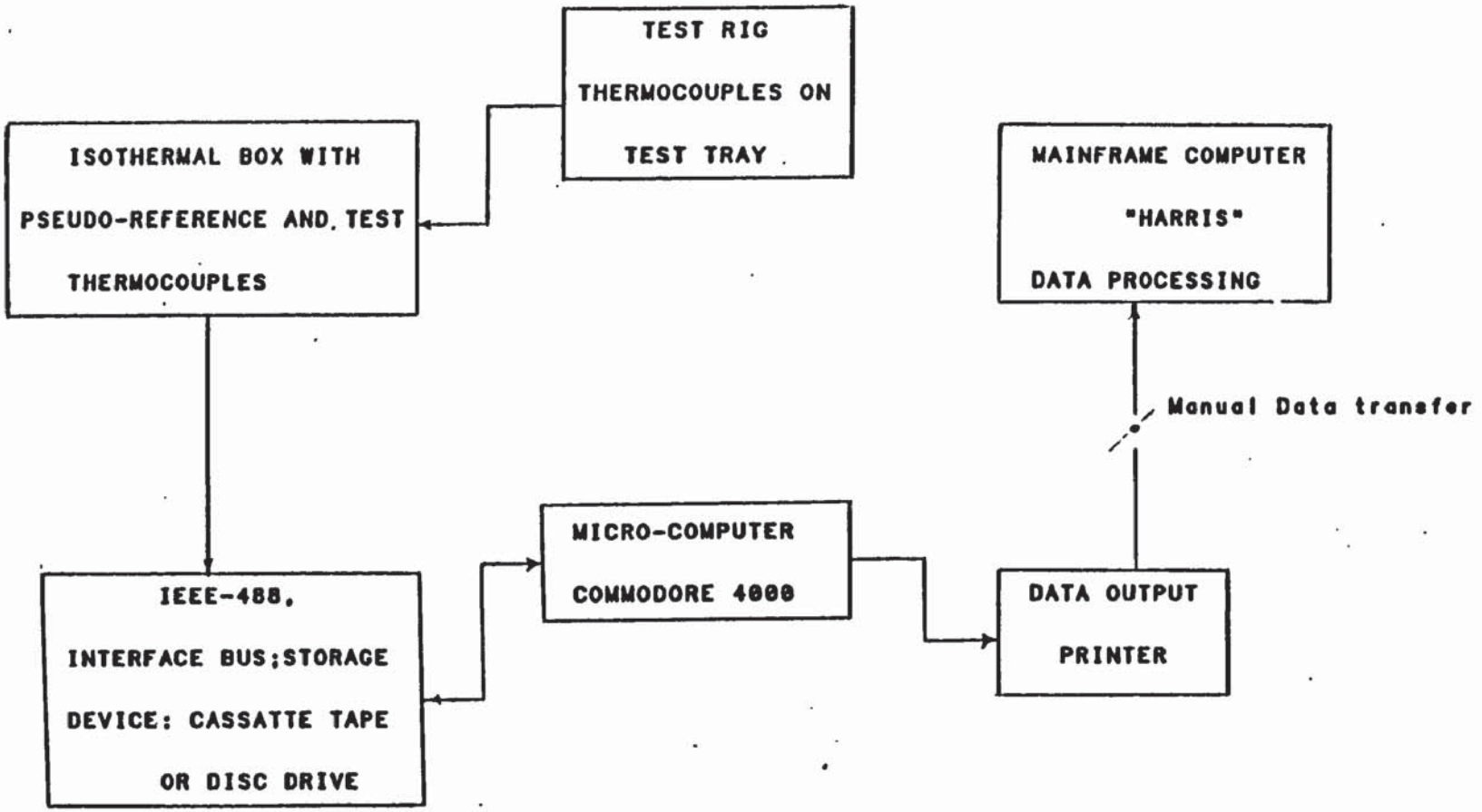

Figure (5.4) Information flow sheet for data logging instruments

Chapter 6

RECTANGULAR TRAY EXPERIMENTS

6.1 INTRODUCTION

Initial research concerning the flow condition on a distillation tray was based on the idealised concept that plug flow of both the vapour and the liquid bi-phase occurred across the tray. It was believed that no significant errors were introduced by representing their flow path as simply rectangular or plug flow.

The information presented in Chapter 4 and the data reported by previous research workers have shown that the discrepancies arising from the use of such simplified models in the design of large trays leads to an error in predicting the efficiency. Such problems are highlighted when considering the extent of the effects of tray hydraulics and liquid flow patterns on the performance of distillation columns.

Initially, many assumptions have been employed in the design and modelling of distillation tray performance. For example, the nature of the liquid flow pattern across a distillation tray while operating in a particular flow regime must be established before the mass transfer processes on such trays can be modelled adequately. Many early models have not considered the effect of flow patterns or flow regimes on a tray.

The flow patterns of flow regimes differ and thus may have different effects on the tray performance. The extent of the effect of the developed flow patterns and the significance of the associated flow regime will be discussed in the results of the research work reported in the next Chapters.

The main purpose of the work in this chapter is to assess whether the widely used assumption of rectangular configuration can be justified in practice.

6.2 REVIEW OF PREVIOUS APPLICATIONS

Kirschbaum (36) quantitatively attempted to account for the effect of liquid maldistribution on tray efficiency by dividing a tray into several equal sized perfectly mixed pools. The liquid was imagined to flow from one pool into the next until it reached the outlet weir. A tray of an infinite number of pools corresponded to an entirely unmixed tray (plug flow). This assumption is complicated by the decision required to decide the number of mixed pools to achieve a perfectly mixed tray or to maintain a plug flow situation on a real operating tray. Nevertheless, a number of authors have applied similar concepts in order to try to achieve an advanced tray design practice.

Gautreaux and O'Connell (26) 1955 revived the pool concept of **Kirschbaum** and derived an expression for the Murphree tray efficiency E_{mv}, assuming that the equilibrium and operating lines were straight over the concentration range of a single tray.Their result was:

$$E_{mv} = \frac{[(1 + (\lambda * E_{og}))^n - 1]}{\lambda} \qquad (6.2.1)$$

where n is the number of pools, λ is the ratio of the slopes of the equilibrium and the operating lines MG/L and E_{og} is the point efficiency. In their model, **Gautreaux and O`Connell** (26) mathematically represented the amount of mixing on a plate with the introduction of a number of pools .

Another approach to the problem of liquid mixing on distillation trays was introduced by **Gilliland et al** (1) and this was based on the assumption that mixing takes place by an eddy-diffusion mechanism in addition to material transport by the bulk flow of liquid across the tray. **Gilliland et al** assumed that material is also transported from one position to another at a rate proportional to the concentration gradient in the direction of the liquid flow. By analogy to diffusion theory of the kinetic theory of gases , the proportionality factor is called an eddy-diffusion coefficient .

In 1953, a paper was published by **Danckwerts** (15) on his study of unified and comprehensive treatment of the residence-time concept in continuous-flow systems. The mixing of liquid on sieve trays in the direction of the liquid flow was studied by **Gerster et al** (28). The work done was restricted to a small rectangular section of the tray with the width and length of the liquid flow path being the most important part of the system. The liquid flow at the periphery of the circular section of the tray was not considered. Based on

the assumption that the gas passes uniformly up through the liquid in plug flow and that the operating and equilibrium lines are straight for a given tray the concentration of a given fluid stream at any location on the tray was expressed as:

$$C(\xi,t) = C^*_{in} + (C_{in} - C^*_{in})\exp(-\lambda E_{og} t\, \xi/\tau) \qquad (6.2.2)$$

By solving equation (6.2.2) for liquid concentrations at the tray exit (ξ =1) and by weighting the concentration of each stream according to the residence time distribution, the Murphree vapour efficiency was determined:

$$E_{mv} = \frac{1 - \int_0^{\infty} \exp(-\lambda E_{og} t/\tau)(t)dt}{[\lambda \exp(-\lambda E_{og} t/\tau)]\, f(t)\, dt} \qquad (6.2.3)$$

The Murphree liquid efficiency was :

$$E_{mL} = \frac{1 - \int_0^{\infty} \exp(-\lambda E_{og} t/\tau)\ (t)\, dt}{1-\lambda^{-1}\ [1 - \int_0^{\infty} \exp(-\lambda E_{og} t/\tau)]\, f(t)\, dt} \qquad (6.2.4)$$

Where :

ξ = operating length of the tray

τ = mean age of fluid element leaving the tray

C^*_{in} & C^*_{out} = mole fractions of volatile components in the liquid that would be in equilibrium with the gas entering and leaving the tray respectively

$C(\xi,t)$ = mole fraction of volatile component in liquid element at point ξ, which is to reside on the tray for time t

$f(t)dt$ = fraction of liquid flow which has ages between t & t + dt at instant of leaving the tray

t = time (s)

In order to predict the Murphree plate efficiency by equation 6.2.4 above , it is necessary to know both the residence-time function and the point efficiency. For a liquid-phase controlling system, $k_l a$ was determined by **Gerster et al** from measurements made in a large pool of froth, 6 inches wide and 24 inches long. The system used was oxygen rich water and liquid samples were taken at several points.

In their study of the oxygen-air-water system, the liquid phase was the controlling

system and the (λE_{og}) product in equation (6.2.4) reduces to,

$$N_L = k_l a Z_f / L \qquad (6.2.5)$$

where ($k_l a$) is the liquid-phase mass transfer coefficient, and Z_f is the height of aerated liquid above the tray floor and L is the liquid flow rate. Under the operating conditions, the rate of supply and removal of oxygen may be equated as:

$$L(C_{in} - C) = k_L a \, Z_f \, (C - C^*_{out}) \qquad (6.2.6)$$

where C and C_{out} are the compositions of the liquid at any point on the tray and the liquid leaving the tray respectively and C_{in} is the composition of the entering liquid.

The value of $k_l a$ was computed by use of experimentally measured values of oxygen concentration and froth height Z_f.

The residence-time distribution functions were determined from the strip-chart records by first averaging random concentration fluctuations in four (some times three) duplicate runs made at each condition. Averages were made at equally spaced values of time by superimposition of the charts. The averaged strip-chart readings were used to calculate the tray response to the unit step input and the residence-time distribution was then computed from the response with respect to time by the use of a 7 point least squares method. Some typical distribution functions for high and low froth velocity were obtained. Gas rates of 6 ft/s and the froth height were maintained at 4in for the runs. The time scales were made dimensionless by dividing by the mean residence time (T)

$$\text{Hence} \quad (\theta = t / T) \qquad (6.2.7)$$

The distribution at high froth velocity was more sharply peaked than those at lower velocity. At the high froth velocity, no liquid leaves the tray until it has resided at a time of at least one half the normal residence time. At lower froth velocity, liquid begins to leave the tray somewhat earlier. In both cases only about 56% of the liquid has left the tray after residing one residence time. At high froth velocity only about 2.5% remains longer than 1.5 residence time, whereas 10.5% remains greater than 1.5 residence time at the low froth velocity.

From these observations, it may be stated that the mixing rate at the low froth velocity is higher than the rate at the higher velocity . The position of the peaks relative to the means shows a distribution that is peaked before the mean implying that there is some vapour by-passing or short-circuiting of the liquid. Also, the distribution functions near the liquid inlet indicate some by-passing.

After determination of both the residence-time distribution for a given operating condition and the mass transfer coefficient applicable at that condition, it is possible to compute the actual tray efficiency by equation (6.2.4). The tray efficiency was computed using a point efficiency which was estimated from the mass transfer coefficients,the error in the point efficiency will be carried forward leading to doubts about the calculated tray efficiency.

Diener (17) introduced an eddy diffusion coefficient into the model developed by **Lewis** (41) in order to account for back mixing of liquid on the tray. However, he still maintained the previous assumption of a rectangular flow path. This assumption was later eliminated after work had been carried out in the study of the liquid hydrodynamics.

Diener obtained equation 6.2.8 for the Murphree plate efficiency in the case of parallel flow of liquid and no mixing of vapour on bubble-cap trays.

$$E_{mv} = \frac{2E_{og} P_e^2}{2(E_{og} (\exp-P_e + P_e - 1) P_e^2 (2-E_{og})} \qquad (6.2.8)$$

In all the experimental work by these authors liquid samples were taken from the test tray while operating at preset vapour and liquid flow rates. The sampling mechanism could be affected by :

(1) Difficulties of liquid entrainment in the vapour phase, vapour entrainment in the liquid phase and vapour condensation, and
(2) location of the sample position due to liquid and vapour maldistribution.

6.3 EXPERIMENTAL CONDITIONS

All experiments were conducted on the 1.2 metre diameter air water simulator described in section 5. The experimental conditions were the same as employed for tests on the 1.2 metre diameter circular trays. All the experiments were carried out by first setting the minimum air flow rate above the incipient weeping point. The liquid and air flowrates were selected to

investigate the temperature profiles in the different flow regimes. The transition between the flow regimes was based on the liquid dispersion observed as in the correlations used by **Porter** and **Jenkins** (57) and **Zuiderweg** (75) for the 12.5 mm diameter hole trays. The gas flowrates were set at C_{sb} values of 0.0605, 0.0695, 0.0775 and 0.0085 m/s.The weir load was varied in increments of 10gall/min (0.0454 m^3/min) between 0.08 and 1.61x 10^{-2} m^3/s m.

6.3.1 TRAY DESIGN SPECIFICATION

The rectangular tray used for this experiment was made out of a 1.2 metre diameter circular tray where both sides of the tray were blanked off to convert the active area to a rectangular cross section.

Table (6.1) Rectangular tray design specification

Hole Diameter(mm)	1
Tray Width (mm)	600
Tray Length(m)	0.74
Tray Spacing (mm)	610
Hole Spacing (mm)	7.0
Outlet Weir Height (mm)	12.5
Effective Bubbling Area (m^2)	0.444
Hole Area (m^2)	0.00925
Gap Under The Apron (mm)	25.4
Material Of Construction	Aluminium
Edge of Hole Facing The Vapour	Sharp

6.3.2 DISCUSSION OF RESULTS

In order to allow for different inlet water temperatures used in the experiments, the temperatures obtained from the tray were normalised by the use of reduced temperatures defined as:

$$T_R = (T - T_{out}) / (T_{in} - T_{out}) \qquad (6.3.1)$$

Thus the normalised inlet temperature for each run will automatically be set to unity and all the temperatures across the tray will be less than one. (see section 7.3).

This investigation was carried out on one tray (1mm diameter hole) and the detailed results are obtained for capacity factors of (0.0605, 0.0775 and 0.0851m/s) and increasing weir loads from 0.0008 to 0.008 m^3/s m in increments of 0.0008 m^3/s m .

Capacity factor (Csb) of 0.0605

At the low liquid loading (see figure 6.3.2a), the temperature profiles were virtually parallel with the weir and only some minor deviations were measured near the outlet weir This flow pattern shows an agreement close to the plug flow concept.

Although some U-shaped profiles were present in the area close to the outlet weir, the tray operation was predominantly plug flow in nature.

Liquid flow over the outlet weir was mainly in the form of liquid sprays thrown across by the momentum of the air through the holes. As the weir load was increased toward the mixed flow regime , the area occupied by the U-shaped profiles increased indicating more rapid movement of the liquid in the central section of the tray. Similar flow patterns were observed throughout the flow conditions covering the mixed flow regime (figure(6.3.2b)).

As the operating condition was changed to the emulsified flow regime Figure(6.3.2c), more severe U-shaped profiles were determined and some liquid recirculation occurred in the centre portion of the tray.

Capacity factor (C_{sb}) of 0.0775 m/s

Flat temperature profiles at low liquid rate were obtained (Plug flow) without any sign of U-shaped profiles in the upper and lower sections of the tray (figure 6.3.2d). As the liquid flowrate was increased to operate in the mixed flow regime, slightly U-shaped temperature profiles were obtained near the exit weir without any form of liquid constant temperature regions on the tray (figure 6.3.2e). A further increase in the liquid flowrate towards the emulsified flow regime caused an increase in the size of the U-shaped profiles.

Figure (6.3.2f) shows the profile while operating in the emulsified flow regime.The temperature profiles were observed to be of three distinct regions. The upper section of the tray contained predominantly flat temperature profiles (Plug flow). The middle section contained a small constant temperature region (recirculation) and the lower section (toward the outlet weir) contained predominantly U-shaped profiles.

Capacity factor (C_{sb}) of 0.0851 m/s

From visual observation of the dispersion over the tray at low liquid rates (q/b = 0.0008 m^3/s m) a very fine spray of liquid was seen over the entire surface of the tray (liquid remained as the dispersed phase) and the tray floor was clearly visible.The temperature profile (figure(6.3.2g))was predominantly in the transverse direction (flat or plug flow) with some recirculation zones in the middle half of the tray.

When the weir load was increased to give a mixed flow regime (figure 6.3.2h) , the small recirculation zones combined to form a large constant temperature zone in the centre half of the tray. The upper and lower sections of the tray still contained flat and U-shaped profiles respectively. As the weir load was increased further to operating conditions corresponding to the emulsified flow regime Figure(6.3.2i) the inlet section of the tray remained in the transverse (ie plug flow) direction and the recirculation zones in the central region increased. The lower section of the tray (towards the outlet weir) was found to be U-shaped.

6.3.3 POINT AND TRAY EFFICIENCY RESULTS

The point and tray efficiencies were calculated and listed in (Appendix 3 tables 6.2 ,6.3 and 6.4). The data have been plotted in (figures 6.3.3a and 6.3.3b) . Low efficiencies at low liquid loadings of (0.00124 m^3/s m -intense spray) were obtained and the point and tray efficiencies increased with increased weir load for the spray regime. The efficiencies remained constant in the spray regime for all the investigated capacity factors and at increasing weir load. The average point efficiency was 55.5 % the average tray efficiency was 64 %.

6.3.4 CONCLUSION

In practical distillation trays, the liquid phase is thought to be well mixed and is even more so for relatively small diameter columns. This was reported by **Stichlmair** and **Weisshuhn** (82) who measured the temperature across an 0.45 m diameter hole tray with a flow path length of 0.27m using a water cooling experiment. The concentration profiles were irregular and compared well with the results reported in this thesis. However the flow path length was too small to be assumed to be a true represention of a real tray behaviour.

At low weir loads and for all the investigated capacity factors, the temperature profiles were predominately in the transverse direction and decreased uniformly from the inlet to the outlet weir demonstrating plug flow.

However, in the mixed regime, U-shaped temperature profiles were found as well as constant temperature lines in the transverse direction and an absence of liquid recirculation zones at the walls of the tray.

The U-shaped profiles observed towards the outlet weir showed that the liquid in the centre line of the U-shaped profiles had a higher momentum than the liquid at the sides of the tray.

The presence of some U-shaped profiles with constant temperatures in the transverse direction raises the following questions.

(1) Can an operating tray be represented by the plug flow model ?

(2) Can flow through a rectangular tray section be a good representation of circular distillation trays ?

(3) At what width of a rectangular tray section can the flow be treated as that through a pipe ?

The combined effect of air flow through the holes and the momentum of the liquid across the tray at the emulsified flow regime created confused flow patterns on the tray.

The point and tray efficiencies increased with increasing weir load and capacity factor while operating in the spray regime. In the mixed flow regime the efficiency values remained approximately constant and decreased in the emulsified regime.

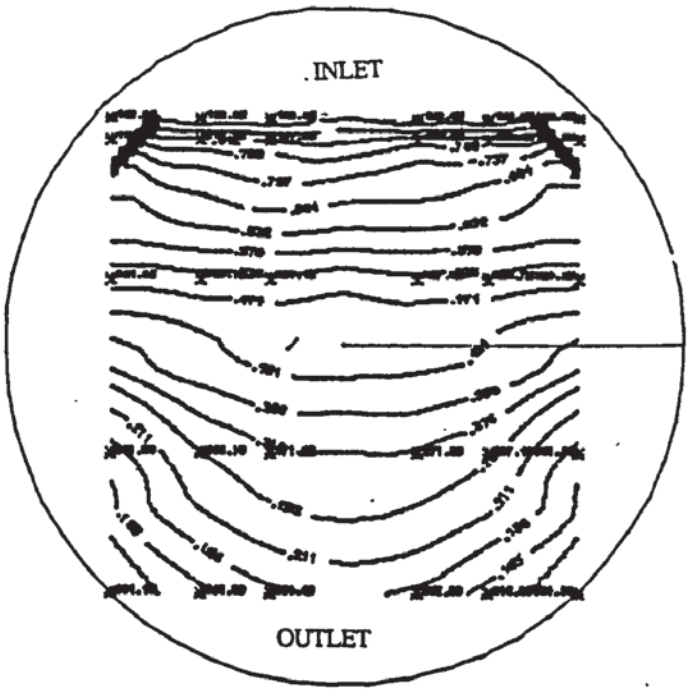

SYMBOL		TR
A	=	0.737
B	=	0.525
C	=	0.421
D	=	0.211
E	=	0.158
F	=	0.105

Figure (6.3.2a) Temperature Profiles for 1 mm diameter holes Rectangular tray.
weir load (q/b) = 0.0008 m^3/s.m : Csb = 0.0605 m/s
Flow regime : Spray

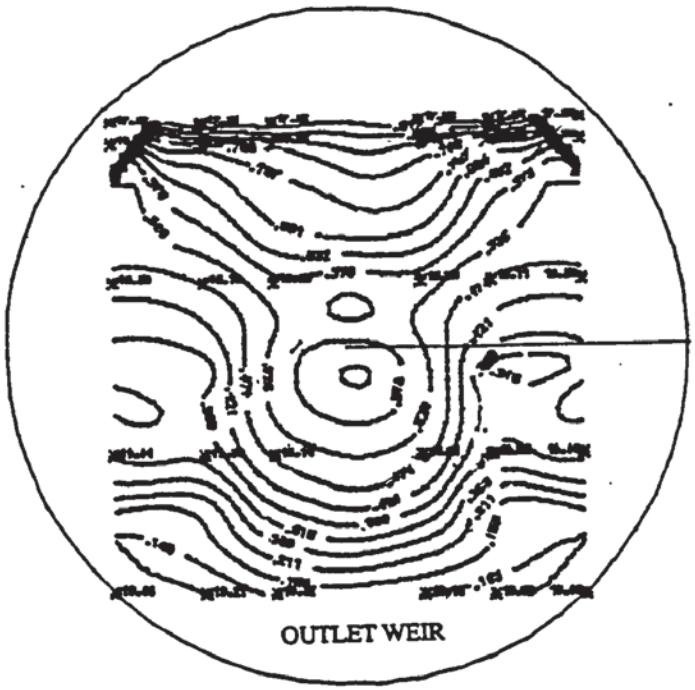

SYMBOL		TR
A	=	0.737
B	=	0.525
C	=	0.421
D	=	0.211
E	=	0.158
F	=	0.105

Figure (6.3.2b) Temperature Profiles for 1 mm diameter holes Rectangular tray.
weir load (q/b) = 0.0048 m^3/s.m : Csb = 0.0605 m/s
Flow regime : Mixed

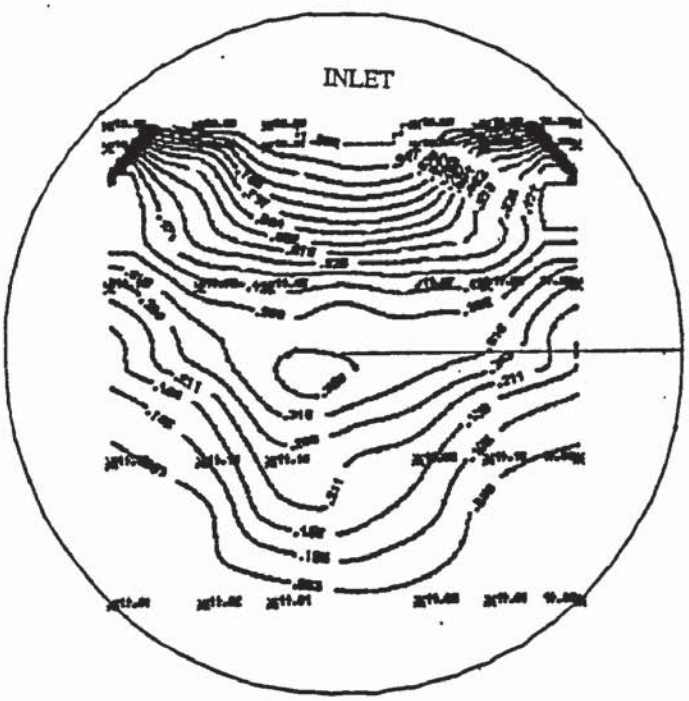

SYMBOL		TR
A	=	0.737
B	=	0.525
C	=	0.421
D	=	0.211
E	=	0.158
F	=	0.105

Figure (6.3.2c) Temperature Profiles for 1 mm diameter holes Rectangular tray.
weir load (q/b) = 0.008 m^3/s.m : Csb = 0.0605 m/s
Flow regime : Emulsified

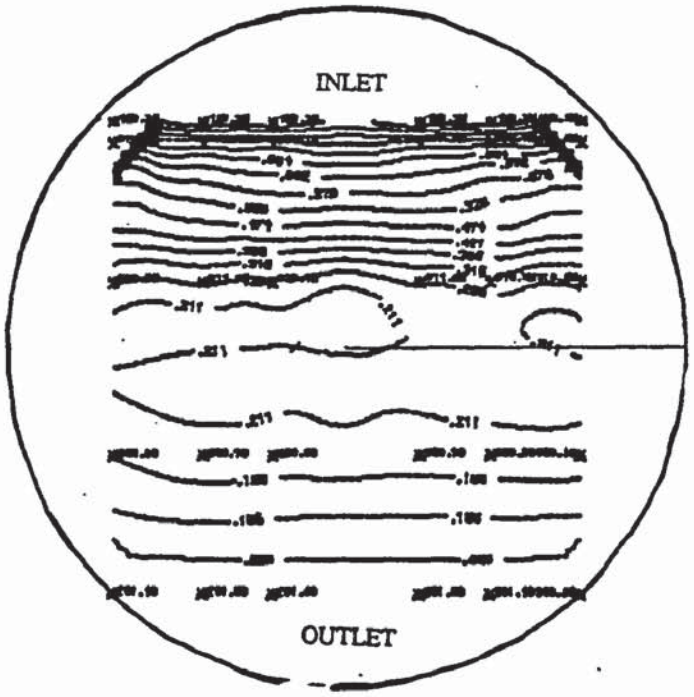

SYMBOL		TR
A	=	0.737
B	=	0.579
C	=	0.474
D	=	0.211
E	=	0.105
F	=	0.053

Figure (6.3.2d) Temperature Profiles for 1 mm diameter holes Rectangular tray.
weir load (q/b) = 0.0008 m^3/s.m : Csb = 0.0775 m/s
Flow regime : Spray

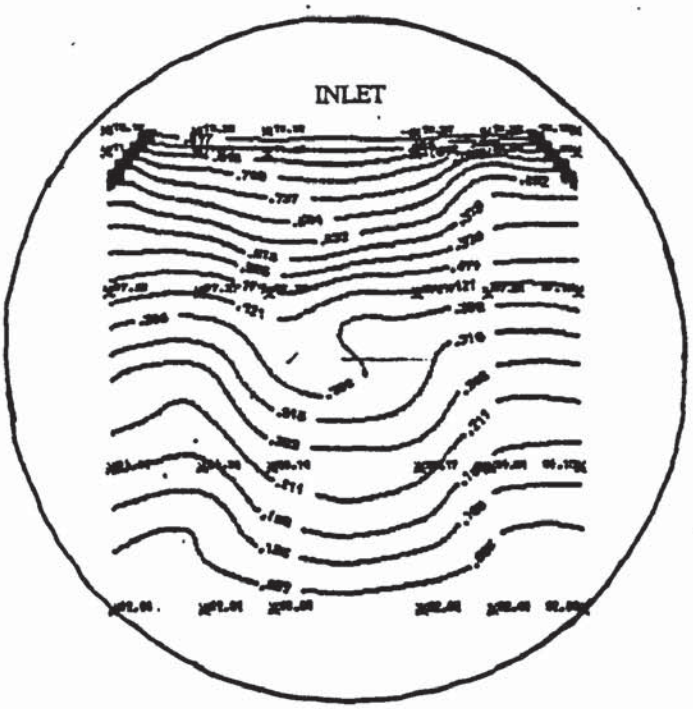

SYMBOL		TR
A	=	0.737
B	=	0.579
C	=	0.474
D	=	0.211
E	=	0.105
F	=	0.053

Figure (6.3.2e) Temperature Profiles for 1 mm diameter holes Rectangular tray.
weir load (q/b) = 0.0048 m^3/s.m : Csb = 0.0775 m/s
Flow regime : Mixed

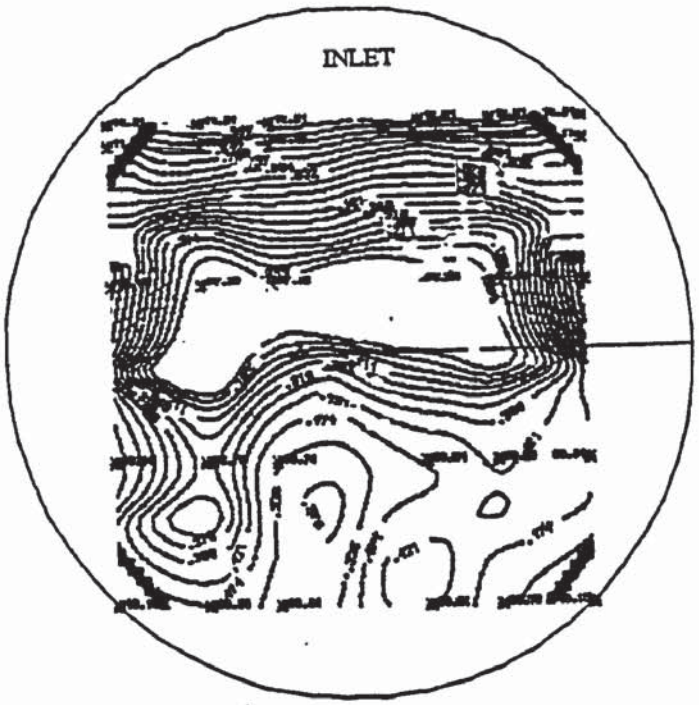

SYMBOL		TR
A	=	0.737
B	=	0.579
C	=	0.474
D	=	0:211
E	=	0.105
F	=	0.053

Figure (6.3.2f) Temperature Profiles for 1 mm diameter holes Rectangular tray.
weir load (q/b) = 0.008 m^3/s.m : Csb = 0.0775 m/s
Flow regime : Emulsified

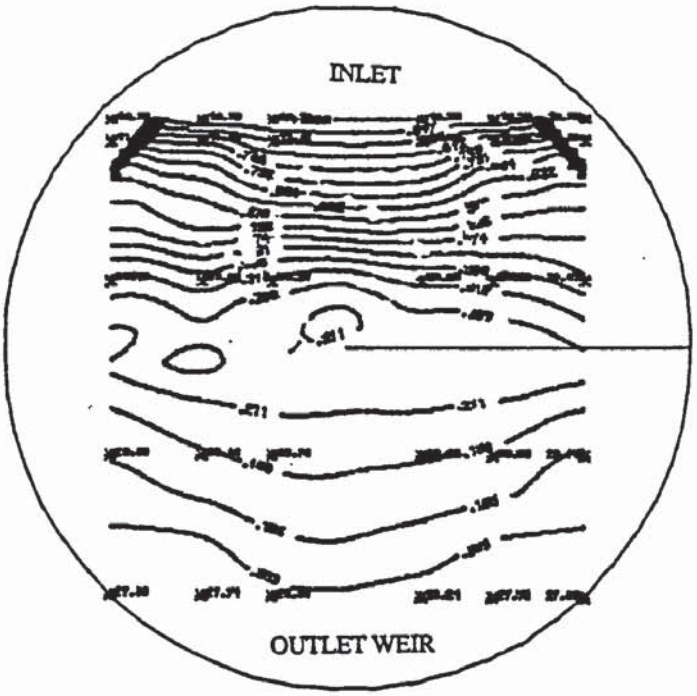

SYMBOL		TR
A	=	0.947
B	=	0.737
C	=	0.525
D	=	0.211
E	=	0.105
F	=	0.053

Figure (6.3.2g) Temperature Profiles for 1 mm diameter holes Rectangular tray.
weir load (q/b) = 0.0008 m^3/s.m : Csb = 0.0851 m/s
Flow regime : Spray

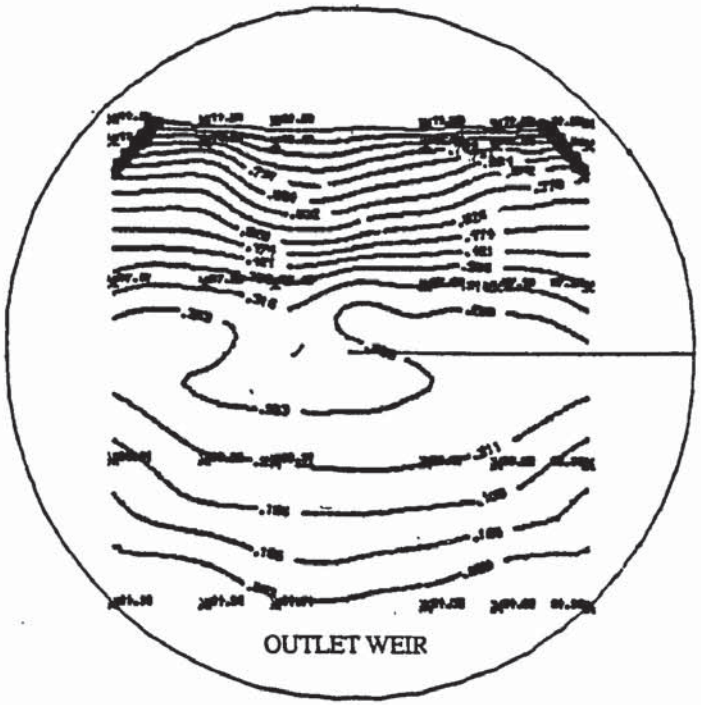

SYMBOL		TR
A	=	0.947
B	=	0.737
C	=	0.525
D	=	0.211
E	=	0.105
F	=	0.053

Figure (6.3.2h) Temperature Profiles for 1 mm diameter holes Rectangular tray
weir load (q/b) = 0.0048 m^3/s.m : Csb = 0.0851 m/s
Flow regime : Mixed

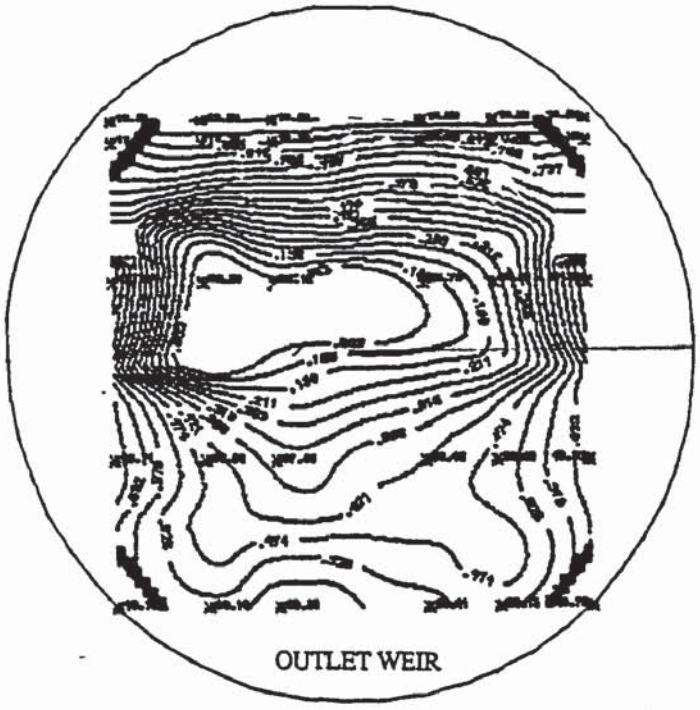

SYMBOL		TR
A	=	0.947
B	=	0.737
C	=	0.525
D	=	0.211
E	=	0.105
F	=	0.053

Figure (6.3.2i) Temperature Profiles for 1 mm diameter holes Rectangular tray.
weir load (q/b) = 0.008 m^3/s.m : Csb = 0.0851 m/s
Flow regime : Emulsified

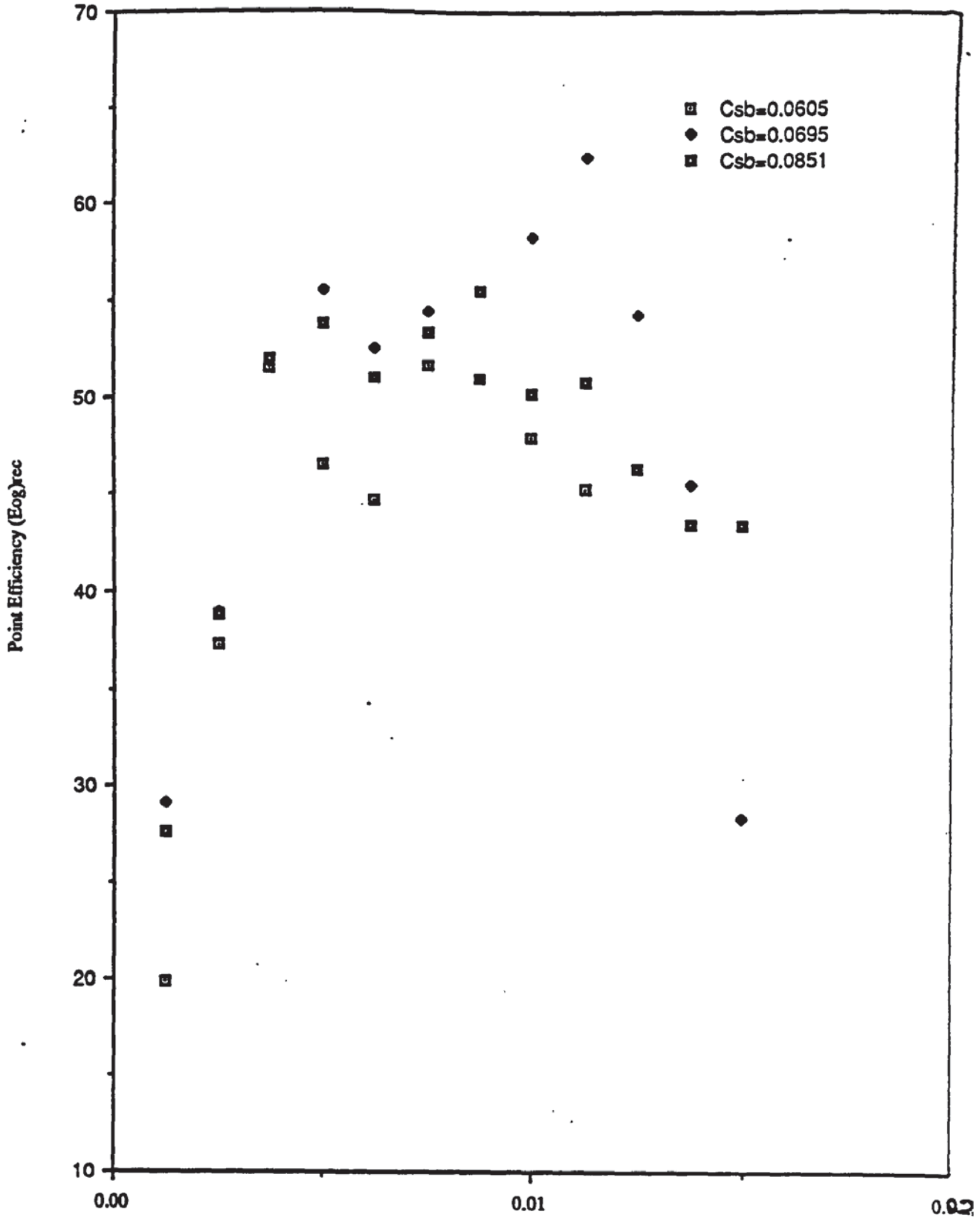

Weir load (q/b): $m^3/s.m$

Figure (6.3.3a) Rectangular Tray Point Efficiency (Eog) versus Weir Load (q/b)

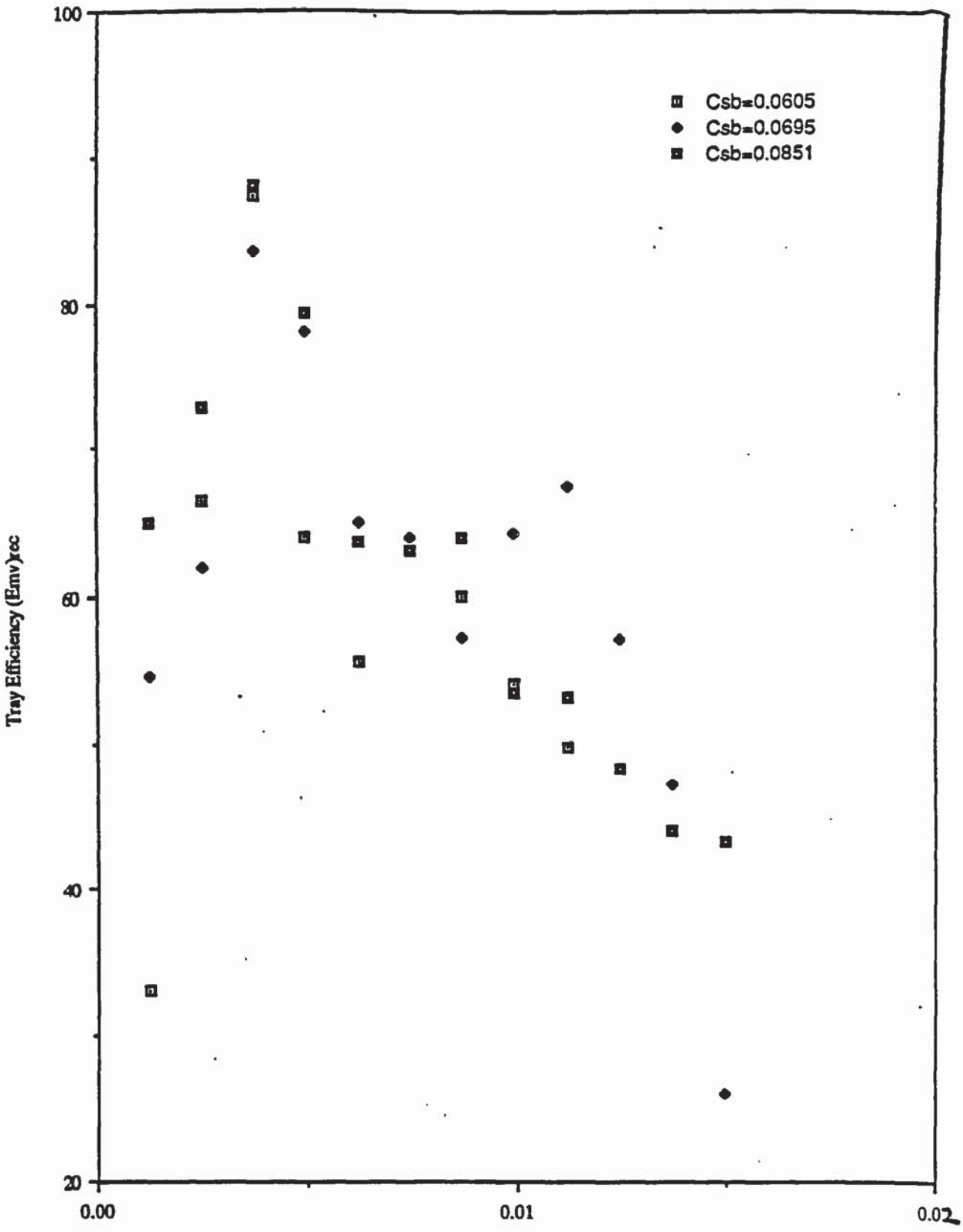

Figure (6.3.3b) Rectangular Tray Efficiency (Emv) versus Weir Load(q/b)

Chapter 7

CONVENTIONAL TRAY EXPERIMENTS

7.1 INTRODUCTION

The flowrates used in the experimental programme enabled flow patterns to be obtained for the spray , mixed and emulsified flow regimes. The maximum allowable delivery of the liquid circulating pump was such that the weir loading could only be set to cover the operating conditions required for the three flow regimes. Each set of experimental results have been presented in terms of temperature profiles and the data have been presented in the form of the three dimensional best surface profile of the temperature differences on the tray.

7.2 EXPERIMENTAL CONDITIONS

In all the experiments the minimum air flowrate was set above the incipient weeping limit. It is known that random weeping occurs from real trays as **Brambilla** (11) has used the water cooling technique to study the effect of weeping. When weeping occurs , the enthalpy of the inlet air could no longer be assumed to be uniform with subsequent effects on the temperature profiles and the calculated efficiencies.

The liquid and air flowrates were selected to obtain temperature profiles in the different flow regimes. The transition between the separate flow regimes was based on the correlations used by **Porter and Jenkins** (57) and **Zuiderweg** (30) (figure 7a). The gas flowrate was set at C_{sb} values of 0.0605, 0.0695, 0.0775 & 0.085 m/s. Since **Porter** and **Jenkins** correlation relates only to 12.5 mm hole tray the transition between the flow regimes for the small hole trays were based on the developed froth dispersions similar to those obtained for the 12.5 mm hole tray. The weir load was varied in increments of $0.0008 m^3/s$ m. The experimental temperature measurements are given in Appendices 4, 5 and 6 for the different hole sizes and operating conditions. In order to account for all the tested operating conditions the temperature profiles graphs have been numbered with respect to the text subsections in which the results have been discussed.

7.2.1 EXPERIMENTAL TRAY DETAILS

Table(7.1): Tray Design Specification

	TRAY A	TRAY B	TRAY C	TRAY D
Hole Diameter (mm)	4.5	12.5	1	12.5
Tray Diameter (m)	1.22	1.22	1.22	1.22
Tray Spacing (mm)	610	610	610	610
Tray Thickness (mm)	1.5	1.5	0.9	1.5
Hole Spacing (mm)	12.7	41	7.0	41
Outlet Weir Height (mm)	38.1	75	12.7	75
Outlet Weir Length (mm)	940	940	940	940
Downcomer Area (%)	13	13	13	13
Effective Bubbling Area (m^2)	0.8554	0.8554	0.8554	0.8554
Hole Area (m^2)	0.021	0.0715	0.00925	0.0715
Gap Under The Inlet Apron (mm)	25.4	25.4	25.4	25.4
Material of Construction	Stainless	Stainless	Aluminium	Perspex

7.3 EXPERIMENTAL RESULTS

With the existing equipment it was possible to keep the inlet water temperature approximately constant during a particular experiment, but it was not possible to set the inlet water temperature at exactly the same particular value for each experiment. Also the inlet air condition (dry bulb [T] and wet bulb temperatures [T_{wb}]) could differ for each experiment. Thus to enable the data from one experiment to be compared with results from another experiment, the temperatures were calculated and plotted as the reduced temperature T_R:

$$T_R = \frac{T - T_{wb}}{T_{in} - T_{wb}} \qquad (7.3.1)$$

or

$$T_R = \frac{T - T_{out}}{T_{in} - T_{out}} \qquad (7.3.2)$$

The time taken to scan all the thermocouples was approximately one minute. The thermocouples were then scanned by the data logging system a further twenty times and the average of the twenty one sets of data was taken to produce the temperature profiles. The standard deviation was calculated and the data was used only if the standard deviation was equal to or less than 0.05. The data was discarded if the standard deviation was greater than the set value. This latter situation could occur if the water inlet temperature had changed significantly during the experiment although in most experiments the inlet water temperature changed by less than $1^{o}C$.

Temperature profiles are shown in Figure(7.4.1a - 7.4.1d) for the 1 mm diameter hole tray, Figure (7.4.2a - 7.4.2d) for 4.5 mm diameter hole and in Figure (7.4.3a - 7.4.3d) for 12.5 mm diameter hole for weir loads which varied from 0.8×10^{-3} m^3/s m to 14.0×10^{-3} m^3/s m and for gas loadings (in terms of C_{sb}) which varied from 0.0605 to 0.0851 m/s. The method for calculating the temperature profiles is given in Chapter (5.5).

7.4 EFFECT OF HOLE SIZES AND TRAY DESIGN ON TEMPERATURE PROFILES

7.4.1 1mm Temperature Profiles

Temperature profiles were obtained for a 1mm diameter hole tray covering the flow regimes starting from intense spray (a) to the emulsified regimes (d) and these are given in figure (7.4.1a - 7.4.1d). The 1mm diameter hole tray had been manufactured commercially and differed from the remaining test trays in that it had an approximately 75mm wide calming zone and the material of construction was 0.9 mm thick aluminium sheet.

In figure 7.4.1a, there was a significant section of the tray area which was occupied by transverse temperature profiles whilst some moderate "U"-shaped profiles occupied the area between the central region of the tray and the outlet weir. Some small recirculation zones emanated from the edge of the tray to the outlet weir. As the liquid loading was increased (Figure 7.4.1b), a similar flow pattern was observed with slightly more "U"-shaped profiles towards the outlet weir region of the tray .

As the weir load was increased causing the bi-phase behaviour to approach that of the emulsified regime (Figure 7.4.1c), a confused flow profile was observed with recirculation zones at the edge of the tray , close to the tray outlet weir and the region close to the inlet downcomer. At the highest liquid loading (Figure 7.4.1d), the recirculation zones were scattered all over the tray active area and some of the smaller zones may have combined to form larger zones.

7.4.2 4.5mm Temperature Profiles

Severe "U"-shaped temperature profiles were obtained at the lowest liquid loading (Figure 7.4.2a) . No transverse temperature profiles were present on the tray. The profiles occupied the central region of the tray from the inlet downcomer region to the outlet weir. Also a significant area at the edge of the tray between the outlet and inlet weir was occupied by the recirculation zones. A very similar flow pattern was obtained for the next liquid loading (Figure 7.4.2b), although the severe "U"-shaped profile in the centre of the tray included a recirculation zone. As the liquid loading was further increased (Figs 7.4.2c & 7.4.2d), the severe "U"-shaped temperature profile was almost totally replaced by large recirculation zones with some recirculation zones at the inlet weir.

7.4.3 12.5mm Temp Profiles

At a very low liquid flowrate Figure (7.4.3a) was obtained . A severe "U"-shaped profile with indications of liquid recirculating region at the edge of the tray. As the liquid loading was increased Figure (7.4.3b), a much less "U"-shaped profile was obtained with constant temperature profiles covering most of the transverse direction (i.e parallel with the weir) and some moderate "U"-shaped profiles were located between the central area of the tray and the outlet weir. With a further increase in the weir load (Figure7.4.3c), some distortion of the profiles became evident with, for example, the commencement of recirculation zones at the edge of the tray, in the central region of the tray and near to the inlet weir. At the highest liquid loading (Figure 7.4.3d), a more confused flow profile was observed with circulating zones at the edge and over the whole tray area .

7.4.4 1mm, 4.5mm & 12.5mm Surface Contours

Three dimensional representations of the tray temperatures are presented as surface contour profiles in Figures (7.4.4a - 7.4.4d) for the 1mm diameter hole tray , in Figures (7.4.4e - 7.4.4h) for the 4.5 mm diameter hole tray and in Figures (7.4.4i -7.4.4l) for the 12.5 mm diameter hole tray. In the surface contour profiles where temperature is plotted as a "height", the areas where the contour of the map is "low" indicate areas of "considerable cooling" and thus correspond to the recirculation or stagnant zones which occurred in the tray temperature profiles . The areas on the contour map where the contour is "high" relate to areas where the liquid is still "hot" and thus continual replenishment of the liquid is occurring with significant mass transfer.

7.5 THE EFFECT OF CAPACITY FACTORS AND INCREASING WEIR LOAD ON LIQUID FLOW PATTERNS

7.5.1 INTRODUCTION

Details of the experimental test trays used in this work were given in section 7.2.1 and photographs of typical trays used in these experiments are shown in figure (5.2a).

One important feature of this work has been the effect of increasing weir load on the mass transfer taking place for a particular capacity factor. In practice distillation columns should be operated with such combined flow rates as to improve the liquid flow patterns there by increasing the mass transfer rate on the tray, but not in such a way as to badly affect the performance of the trays.

The combined effect of the gas and liquid loadings for the three flow regimes (spray , mixed and the emulsified flow regime) will be explained by examining the temperature profiles for the 12.5mm diameter hole tray commencing with the spray regime at high capacity factor of C_{sb} = 0.0851 m/s to the lowest capacity factor applied in this investigation of C_{sb} =0.0605 m/s.

7.5.2 TEMPERATURE PROFILES IN THE SPRAY REGIME

7.5.2.1 Capacity factor (0.0851m/s)

As shown in figures (7.5.1a to 7.5.1e) , severely U-shaped profiles were observed for the first two weir loads of (0.0008 and 0.0016 m^3/s m) . As the liquid rate was increased and the spray regime was obtained, predominantly transverse temperature profiles without any U-shaped profiles both at the upper and the lower half of the tray were obtained, suggesting that liquid was present over all the tray area.

The profiles occupied most of the tray in the transverse direction while the fraction of the tray that was usually occupied by U-shaped profiles was seen to decrease with increasing weir load.

7.5.2.2 Capacity factor (0.0775m/s)

In the upper half of the tray predominantly transverse temperature profiles were obtained (Figure (7.5.2a- 7.5.2c) with some U-shaped profiles in the region near the outlet weir. As the weir loading was increased toward the mixed regime the flow patterns became predominantly flat (transverse temperature profiles) between the inlet downcomer and the central region of the tray with significant U-shaped profiles at the lower part of the tray. recirculation zones and a generally confused flow pattern occurred at the highest weir load.

7.5.2.3 Capacity factor (0.0695m/s)

At an initial weir load of 0.0008 m^3/s m Figure (7.4.3a) the entire tray area was dominated by severe "U"-shaped profiles. As the liquid loading was increased Figure (7.4.3b) the area between the inlet downcomer and the central region of the tray was occupied by transverse flow patterns and this area was greater than that for the runs for capacity factor of 0.0605m/s (Figure (7.5.3a - 7.5.3e)).

The nature of the U-shaped profiles in the lower section of the tray was found also to be less severe than those for 0.0605m/s.

7.5.2.4 Capacity factor (0.0605m/s)

The temperature profiles at low weir loads (figure 7.5.3a - 7.5.3e) were found to have severe channelling of the liquid through the central part of the tray, causing the circular sides of the tray to have liquid of relatively low temperature.Virtually no transverse temperature profiles were observed in the upper section of the tray suggesting a total

domination of the gas passing through the liquid. This phenomena may be described as an intense spray situation on the tray and this was confirmed by visual observation when the tray floor could clearly be seen during the experiment.

It was found that as the weir load was increased thus bringing the condition towards the the spray and the mixed regime transition, transverse temperature profiles were developed in the region of the inlet downcomer,whilst the area between the centre of the tray and the outlet weir was dominated by severe U-shaped profiles.

7.5.7 CONCLUSION ON THE SPRAY REGIME

(1) As the capacity factor and the weir load were increased the temperature profiles were predominantly in the transverse direction indicating non liquid channelling on the tray.

(2) The severe U-shaped profiles between the central part of the tray and the outlet weir suggested that there is a combined effect of the vapour momentum and the outlet weir which slows the velocity of the liquid as it crosses the tray from the inlet downcomer to the outlet weir.

(3) For conditions where the severe U-shaped profiles occupied the lower half of the tray the calculated efficiencies were very low which explains the significance of such profiles on the performance of tray columns.

(4) High capacity factor tend to generally improve the temperature profiles while operating in the spray regime.

7.6 TEMPERATURE PROFILES FOR THE MIXED REGIME

7.6.1 Capacity factor of (0.0851 m/s)

Transverse temperature profiles were mainly obtained (see figures 7.5.1f to 7.5.1h), although some U-shaped profiles were observed and the width of the central channelling region was such that there was no liquid recirculation at the circular sides of the tray. As the liquid flow rate was increased towards the emulsified regime, some liquid recirculating zones were detected in the central region of the tray. This phenomena persisted as the weir load was further increased.

7.6.2 Capacity factor of (0.0775 m/s)

Considerable transverse temperature profiles at these operating conditions were obtained (see figure 7.5.2d to 7.5.2f) . The well developed transverse temperature profiles in the inlet downcomer section of the tray were significantly extended into the outlet half of the tray.

As the weirload was increased to near to the emulsifed flow regime, some recirculating liquid zones were observed at the outlet weir region of the tray. On increasing the weir load futher the recirculation zones increased in size.

7.6.3 Capacity factor of (0.0695 m/s)

As shown in figure (7.4.3c) the temperatures were similar to those for the case of capacity factor of (0.0605 m/s), but the U-shaped profiles in the central region of the tray occupied a larger area of the tray, leaving a very small area on both sides of the tray where low temperature liquids were observed. As the weir load was increased toward the emulsified flow regime, a non uniform recirculating liquid temperature region was found to develop near the outlet weir. As the flow regime moved into the emulsified regime , the area near to the outlet weir was dominated by this recirculating liquid flow patterns.

7.6.4 Capacity factor of (0.0605 m/s)

At this gas flow rate the temperature profiles were observed figure (7.5.3f to 7.5.3g) to be distinctly U-shaped in the central region of the tray with some small transverse profiles near the inlet weir. As the liquid loading was increased the U-shaped profiles were found to increase and low liquid temperatures (recirculation) were observed at the tray circular edge.

With increasing weir load the temperatures at the sides of the tray were found to be decreasing while at the central region of the tray there was an increase in temperature. The higher temperatures at the central region of the tray decreased uniformly towards the outlet weir.

The observed low temperatures at the tray corners can be explained by two major principles.

(1) That the liquid stayed longer on the tray at this area.

(2) The liquid at the circular edge was recirculating.

7.6.5 CONCLUSION

The temperature profiles in this regime were predominantly in the transverse direction signifying a well mixed liquid profile both in the transverse and in the axial direction.

This observation may explain why higher tray efficiencies are obtained for operating conditions in the mixed flow regimes and higher performance in this regime may underline why industrial columns are often operated in the mixed regime.

7.7 TEMPERATURE PROFILES IN THE EMULSIFIED FLOW REGIME

For the increasing weir loads investigated at each of the four air capacity factors a mixture of flow patterns was observed in this regime as shown in figures (7.5.3h & 7.5.3i) for C_{sb} of 0.0605 m/s, (7.4.3d) for C_{sb} of 0.0695 m/s. Initially the tray area was completely covered in small recirculating liquid zones. As the weir load was increased towards the maximum capacity of the delivery pump, more confused flow patterns were observed with recirculating liquid zones scattered over the tray central region and about the inlet downcomer region of the tray.

The predominant recirculation zones and other irregular patterns on the tray suggests that there might be some regions where different flow regimes were occurring. The low temperatures associated with the recirculation zones observed in the central region of the tray could be as a result of any of the following operating conditions or a combination of their effect.

(1) Vapour by passing through the froth.

(2) Liquid sloshing on the tray and

(3) Liquid jetting on to the tray from the inlet downcomer caused by a significant liquid head in the downcomer and the 25mm fixed gap under the apron.

The reduction in the calculated tray efficiencies are also explained by the poor flow patterns observed in this regime.

7.8 DISCUSSION OF TEMPERATURE PROFILES RESULTS

The temperature profiles for the 12.5 mm diameter hole tray had recirculation zones situated towards the outlet weir and very flat transverse profiles between the inlet weir and the central region of the tray and moderate "U"-shaped profiles between the central region of the tray and the outlet weir. However there was a significantly different shaped set of profiles for the 4.5 mm diameter hole tray. On this tray, there was a very significant recirculation zone at the edge of the tray from the inlet weir to the outlet weir. The remaining central region of the tray contained very severe "U"-shaped profiles and it would appear that as the hole diameter decreased the size of the recirculation zone at the edge of the tray increased and occupied more of the area between the inlet and outlet weir. Also the profiles in the remaining central part of the tray between the inlet and outlet weirs became very severe "U"-shaped. The poorer mixing associated with the 4.5 mm diameter hole tray may be explained by the way in which the gas emerged from the hole - in the case of the smaller hole it is thought that the gas tended to emerge in the form of a jet whilst in the case of the larger hole the gas was thought to diverge with a larger cone angle which would give the gas more sideways direction and thus improve the mixing characteristics of the tray.

Visual observations of the dispersion on the tray indicated that the liquid remained as a continuous phase in the case of the 4.5 mm diameter hole tray whilst in the case of the 12.5 mm diameter hole tray, the liquid was more discontinuous with a greater formation of bubbles.

When the temperature profiles were being examined, the effect of the different flow regimes must be considered and the boundaries between the different flow regimes were taken from (Figure 7.a) where the transition from the spray to the mixed regime and the transition from the mixed to the emulsified regime have been calculated from correlations given by **Porter** and **Jenkins** (57) and **Zuiderweg** and **Hofhuis** (30). These correlations are only valid for 12.5 mm hole trays.

The relationship of the temperature profiles and the flow regimes will be discussed in terms of the 12.5 mm diameter hole tray results (Figures 7.4.3a - 7.4.3d). In Figure 7.4.3a severe "U"-shaped profiles were obtained at a very low liquid loading. From the loading diagram, Figure (7.2a), the tray was operating with an intense spray as defined by **Enjugu** (18). A visual observation of the liquid behaviour on the tray indicated that most of the liquid had been dispersed into a cloud of drops above the tray and that the tray floor was visible. The liquid flowed over the weir in the form of a cloud of droplets rather than in the conventional way as indicated by the Francis Weir equation. At these operating conditions,

a baffled or blocked outlet weir would be used in commercial columns.

It was found that as the liquid rate was increased (Figs 7.4.3b & 7.4.3c), the operating conditions changed from the spray regime to the mixed regime , Figure (7.2a) , and the fraction of the active tray area which was occupied by the flat or transverse temperature profiles increased . A mixture of flow patterns was evident in the mixed regime as shown by the temperature profiles. There were few "U"-shaped profiles but more transverse profiles (i.e. parallel to the outlet weir) and the occasional irregular liquid recirculation point . Generally, by increasing the weir load, the shape of the profile was affected and the U-shaped profile moved towards the outlet weir of the tray with increasing recirculation or stagnant zones towards the edges of the tray and the outlet weir. As the weir load was increased further, the operating conditions corresponded to the emulsified regime , Figure (7.4.3d) , and a more confused flow pattern was observed with recirculation zones scattered over the central region of the tray and at the circular edges of the tray The confused shape of the flow pattern may be explained by the relatively high liquid momentum in the central region may be insufficient to overcome the retrograde force (opposite flow) often thought to emanate from the outlet weir.

7.9 Point and Murphree Efficiencies

The point efficiency (E_{og}) was calculated from the experimental data for the12.5 mm diameter hole trays using equations 4.4 - 4.8. In equation 4.7, the equilibrium enthalpy (H^*) was calculated from an average of all the individual enthalpies which were in equilibrium with the liquid at temperatures given by the temperature profiles. The Murphree efficiency (E_{MV}) was also calculated from the experimental results using the inlet and outlet tray conditions. The calculated results are given in Appendix (3.1) and tables (6.2 to 6.4) for the 1 mm diameter hole tray and in Appendix (4.1) and tables (7.2 to 7.5) for the 12.5 mm hole tray.

The individual efficiencies and the ratio of the efficiencies were plotted against weir load for four different gas flowrates in Figures (7.8a - 7.8c) for 1mm diameter hole tray and figures (7.8d -7.8f) for 12.5 mm diameter hole. The Murphree vapour efficiency (E_{MV}) was calculated from the Plug Flow model and plotted in Figures (8.4i & 8.4j) for 1mm diameter hole tray and Figure (8.4k & 8.4l) for 12.5 mm diameter hole. Similar plots are presented in for the Murphree vapour efficiencies (E_{MV}) calculated from the **Porter** and

Lockett model (56) using the experimentally determined values of the point efficiency and the experimental conditions given by λ for the 1 mm diameter hole tray (figures 8.4m and 8.4n) and the 12.5 mm diameter hole tray (figures 8.4o and 8.4p).

The data from the water cooling experiment was used in the calculation of the point efficiencies for each test condition. The calculation procedure which was used to obtain the efficiencies from the data is independent of the flow patterns. The graphical plots in Figures (7.8a) of point efficiency (E_{OG}) against the weir load (q/b) show that in general the point efficiency increased with the weir load. As the flow regime changed from the spray to the mixed regime, so the point efficiency increased from approximately 30% to values between 60 & 80%. For the mixed regime, it was observed that the point efficiency was approximately constant with values between 60 & 80%. As the operating conditions changed to the emulsified flow regime, there was a decrease in the point efficiency.

Maximum point efficiencies were obtained at C_{sb} values of 0.0775 m/s whilst the minimum value was at the lowest value of C_{sb} = 0.0605 m/s showing an increase in the point efficiency with an increase in the vapour load. However, at the highest gas loading (C_{sb} = 0.0851 m/s) the point efficiencies were less than the point efficiencies for gas loadings of C_{sb} = 0.0775 and 0.0695 m/s respectively. This drop in efficiency may be a result of the gas momentum totally dominating over the liquid momentum with such an effect that the vapour residence time was reduced and the liquid was being blown off the tray to form an intense spray and the tray floor could clearly be seen.

In the spray regime, the momentum of the gas dominates over the liquid momentum and combined with the large hole diameter of 12.5 mm discreet droplet formation is favoured which is likely to enhance the structure of the spray in the space above the tray and help increase the point efficiency in this regime. With the increase of liquid loading resulting in the tray operating in the mixed regime, further increases in the point efficiencies were observed and these were attributed to the longer contact time of the air in the froth at the higher liquid flowrates.

The expected trend of increasing point efficiency with increasing weir load was not observed in the emulsified regime. **Zuiderweg** (74) has suggested a possible explanation for real distillation systems operating in the emulsified regime where vapour may be entrained over the outlet weir to the tray below thus reducing the point efficiency.

However in the case of air - water simulators and for this particular experimental rig this would not be the case due to the construction of the equipment. An alternative explanation for the decrease in the point efficiency at high liquid loadings could be that all the experiments were carried out with a fixed clearance gap of 25.4 mm at the inlet weir. At very high liquid loadings corresponding to the emulsified regime causing a significant liquid backup in the inlet downcomer, liquid was observed to jet from the inlet across to the middle of the tray causing some of the liquid to effectively by-pass the active area of the tray and with a subsequent reduction in the contact time of the froth with the vapour.

The decrease in tray efficiencies for real systems has also been reported by **Sakata** and **Yanagi** (64) who presented overall tray efficiency data for systems such as the distillation of iso-butane - butane at high pressure and cyclohexane - n-heptane at atmospheric and reduced pressures over the range of twenty to one hundred percent flood. At very high percent flood, the tray efficiency decreased slightly in the case of the butane system and significantly in the case of the cyclohexane system. It is also worth noting that in the case of the FRI data, at low liquid loadings an inlet downcomer gap of 38 mm was used whilst for the higher liquid loadings an inlet downcomer gap of 51 mm was used thus avoiding the problem encountered in this work of liquid jetting across the tray due to the constant and restricted inlet downcomer gap.

In all the conditions, the calculated tray efficiencies increased in value when there was a reduction in the "U-shaped" profiles and in the size of the recirculating or stagnant regions at the circular edges of the tray. The presence of "U-shaped" profiles is indicative of significant cooling of the water accompanied by poor or zero replenishment of the water leading to the water and the air reaching equilibrium. The presence of such zones stacked up above each other in single pass trays leads to another form of vapour by-passing with a subsequent reduction in tray efficiency. This observation is very much in agreement with the concept that the performance of a distillation tray is highly reduced by the presence of non-uniform flow patterns on the tray.

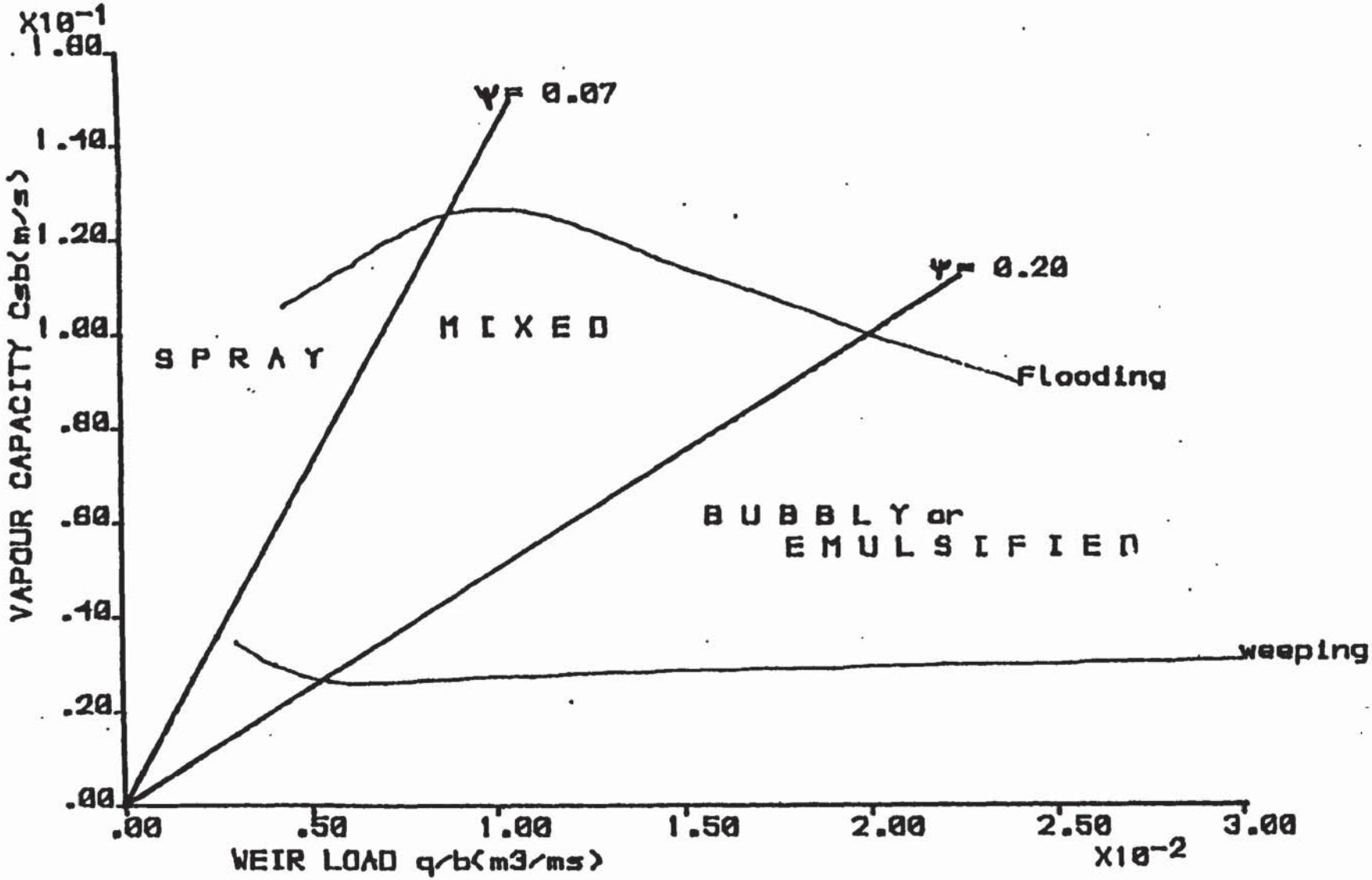

Figure (7a) Flow regimes transition line (Porter / Jenkins)

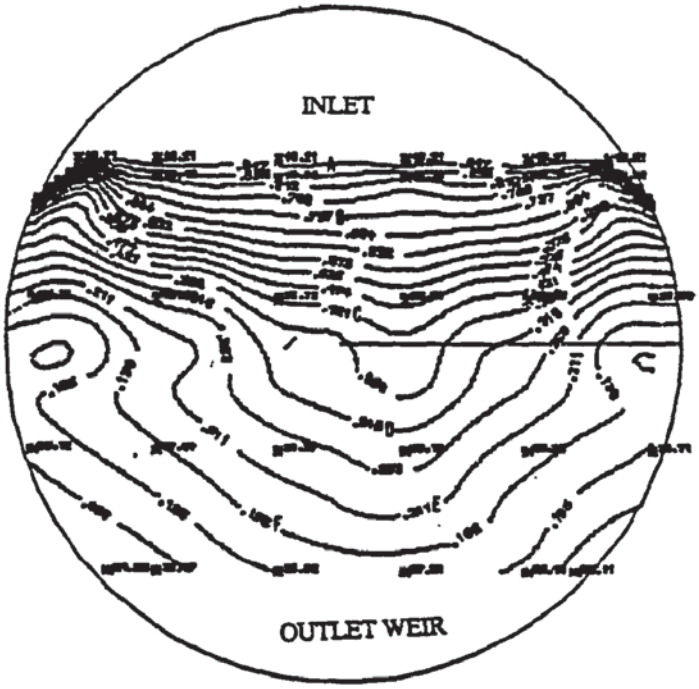

SYMBOL		TR
A	=	0.847
B	=	0.757
C	=	0.421
D	=	0.318
E	=	0.211
F	=	0.158

Figure (7.4.1a) Temperature profiles - 1mm diameter hole tray

Capacity factor (C_{sb}) = 0.0695 m/s

Weir load (q/b) = 0.0008 m^3/s m

Flow regime : Intense spray

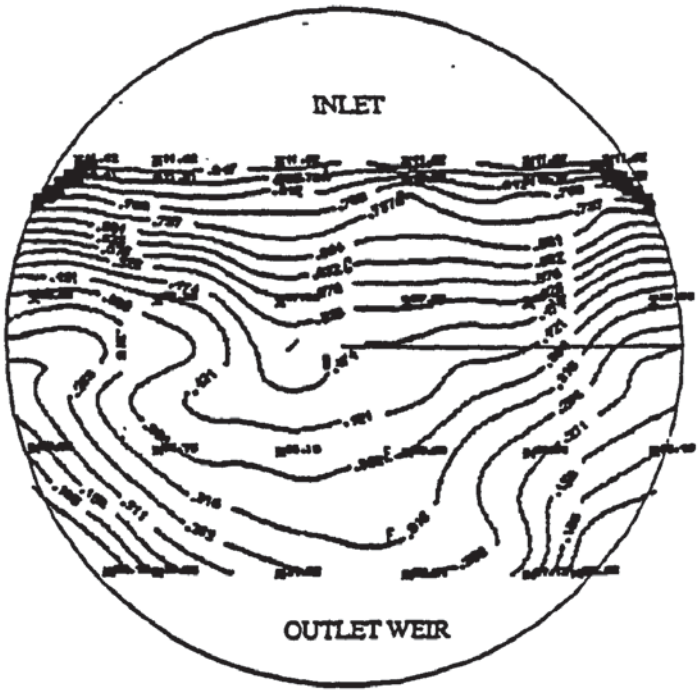

SYMBOL		TR
A	=	0.842
B	=	0.787
C	=	0.532
D	=	0.474
E	=	0.368
F	=	0.316

Figure (7.4.1b) Temperature profiles - 1mm diameter hole tray

Capacity factor (C_{sb}) = 0.0695 m/s

Weir load (q/b) = 0.002 m^3/s m

Flow regime : Spray

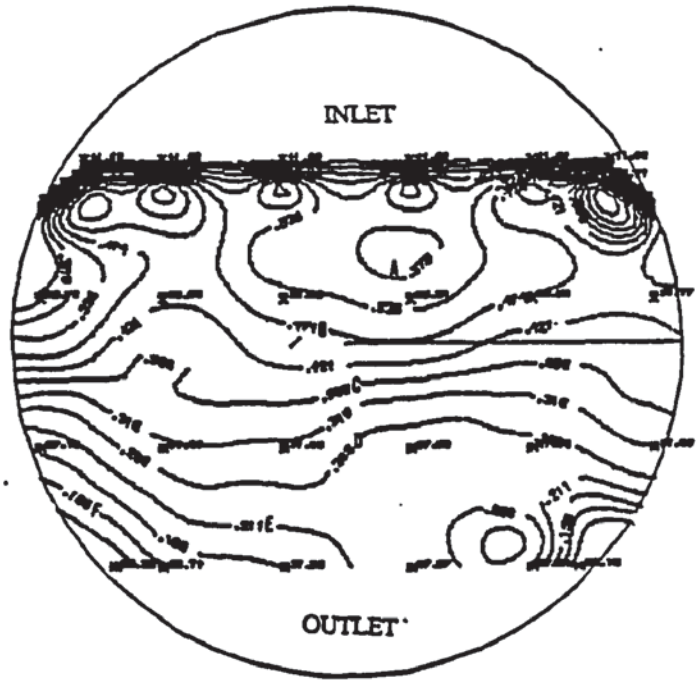

SYMBOL		TR
A	=	0.579
B	=	0.474
C	=	0.357
D	=	0.268
E	=	0.211
F	=	0.105

Figure (7.4.1c) Temperature profiles - 1mm diameter hole tray

Capacity factor (C_{sb}) = 0.0695 m/s

Weir load (q/b) = 0.008 m^3/s m

Flow regime : Mixed

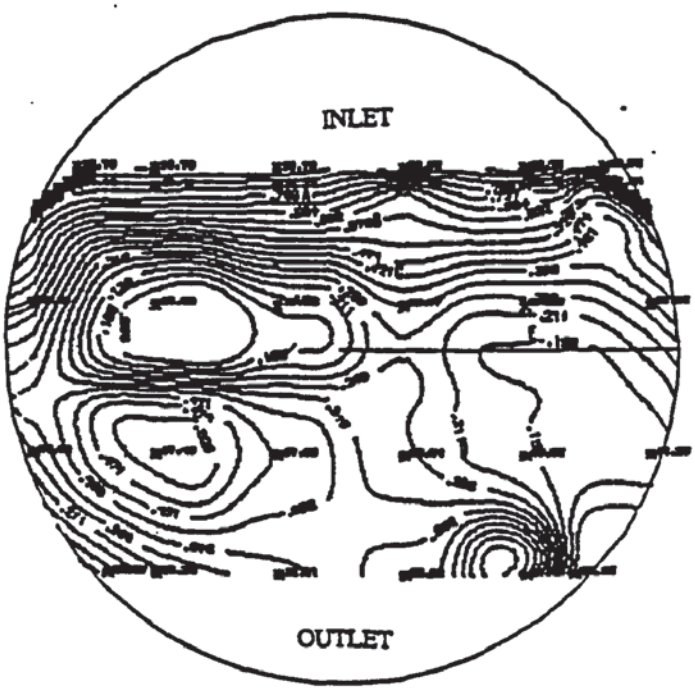

SYMBOL		TR
A	=	0.788
B	=	0.578
C	=	0.421
D	=	0.211
E	=	0.158

Figure (7.4.1d) Temperature profiles - 1mm diameter hole tray

Capacity factor (C_{sb}) = 0.0695 m/s

Weir load (q/b) = 0.015 m^3/s m

Flow regime : Emulsified

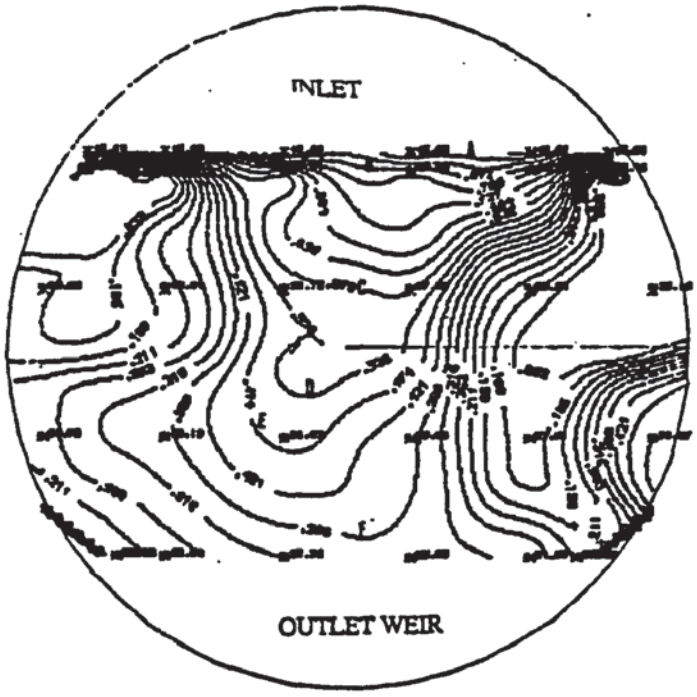

SYMBOL		TR
A	=	0.985
B	=	0.832
C	=	0.578
D	=	0.526
E	=	0.474
F	=	0.388

Figure (7.4.2a) Temperature profiles - 4.5 mm diameter hole tray

Capacity factor (C_{sb}) = 0.0695 m/s

Weir load (q/b) = 0.0008 m^3/s m

Flow regime : Intense spray

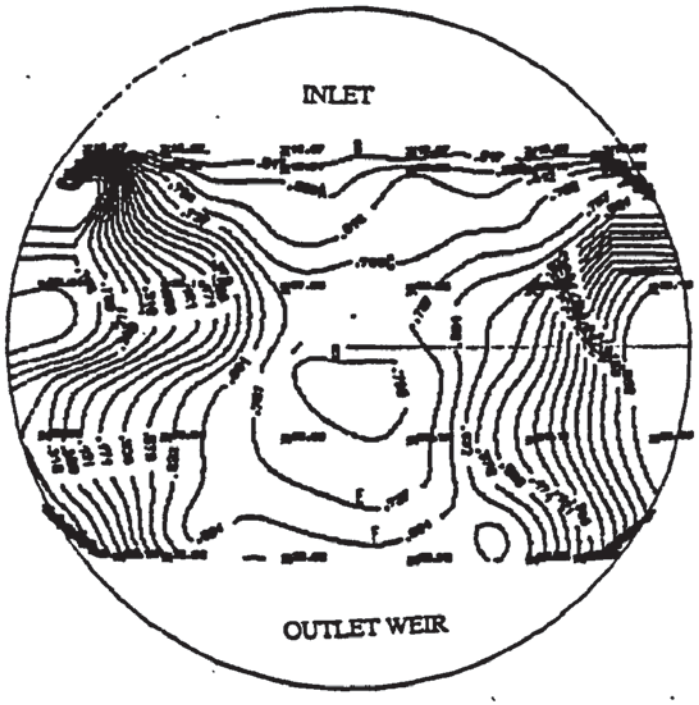

SYMBOL		TR
A	=	0.883
B	=	0.972
C	=	0.789
D	=	0.745
E	=	0.737
F	=	0.684

Figure (7.4.2b) Temperature profiles - 4.5 mm diameter hole tray

Capacity factor (C_{sb}) = 0.0695 m/s

Weir load (q/b) = 0.002 m^3/s m

Flow regime : Spray

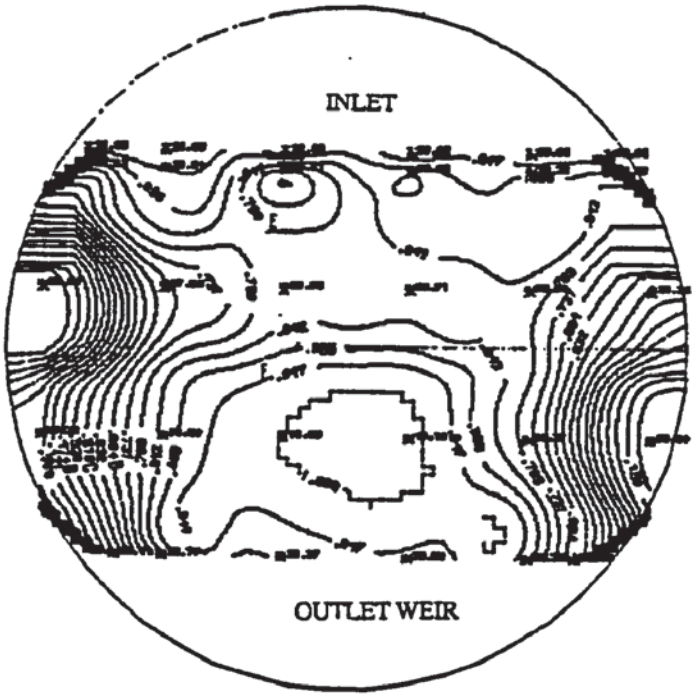

Figure (7.4.2c) Temperature profiles - 4.5 mm diameter hole tray

Capacity factor (C_{sb}) = 0.0695 m/s

Weir load (q/b) = 0.008 m^3/s m

Flow regime : Mixed

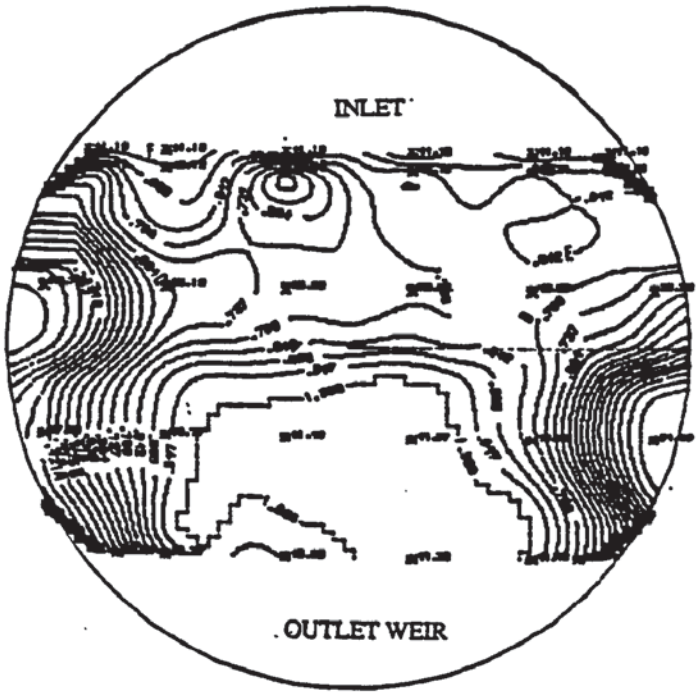

Figure (7.4.2d) Temperature profiles - 4.5 mm diameter hole tray

Capacity factor (C_{sb}) = 0.0695 m/s

Weir load (q/b) = 0.015 m^3/s m

Flow regime : Emulsified

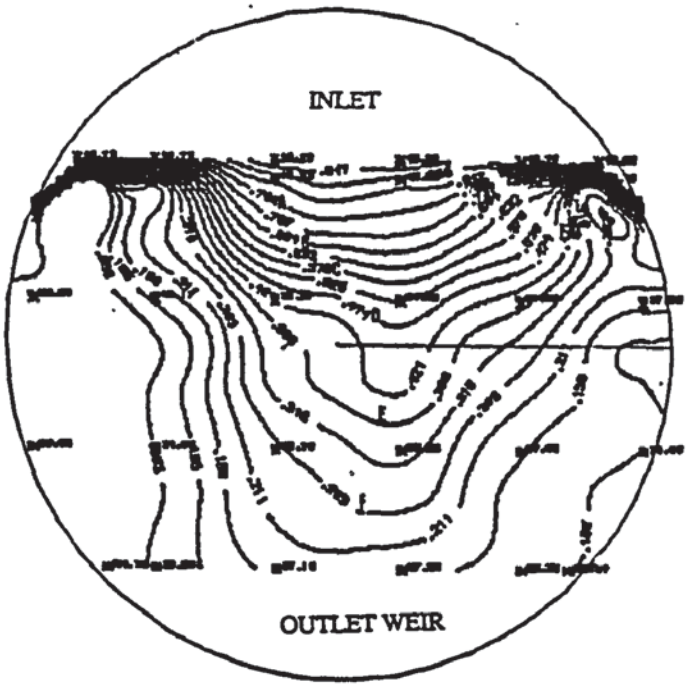

SYMBOL		TR
A	=	0.744
B	=	0.644
C	=	0.574
D	=	0.474
E	=	0.388
F	=	0.289

Figure (7.4.3a) Temperature profiles - 12.5 mm diameter hole tray

Capacity factor (C_{sb}) = 0.0695 m/s

Weir load (q/b) = 0.0008 m^3/s m

Flow regime : Intense spray

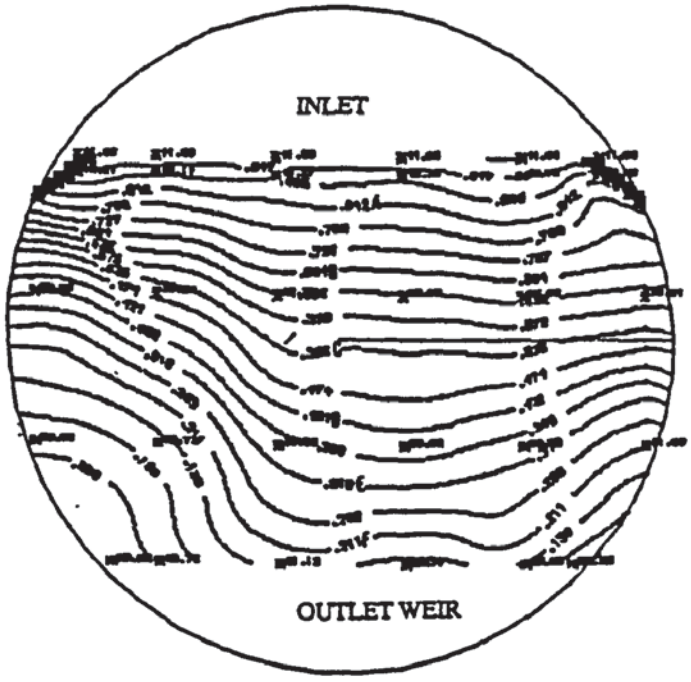

SYMBOL		TR
A	=	0.842
B	=	0.681
C	=	0.525
D	=	0.421
E	=	0.318
F	=	0.211

Figure (7.4.3b) Temperature profiles - 12.5 mm diameter hole tray

Capacity factor (C_{sb}) = 0.0695 m/s

Weir load (q/b) = 0.002 m^3/s m

Flow regime : Spray

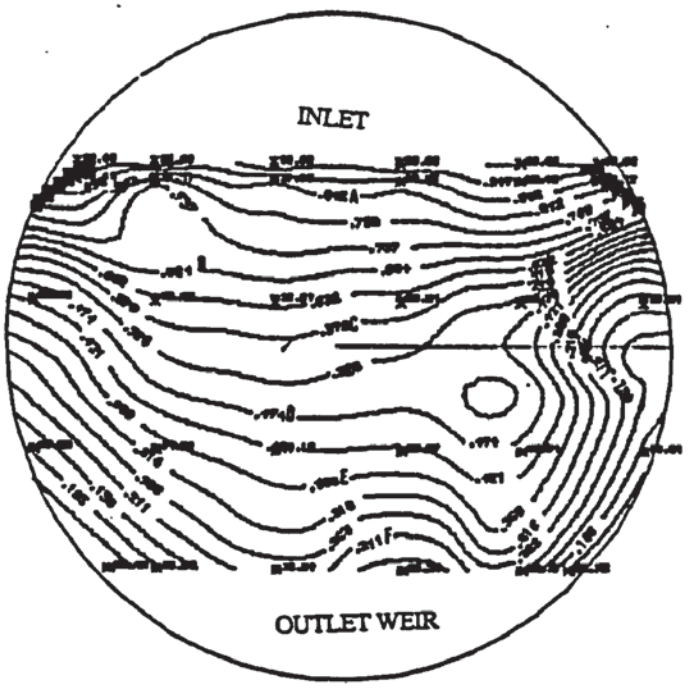

Figure (7.4.3c) Temperature profiles - 12.5 mm diameter hole tray

Capacity factor (C_{sb}) = 0.0695 m/s

Weir load (q/b) = 0.008 m^3/s m

Flow regime : Mixed

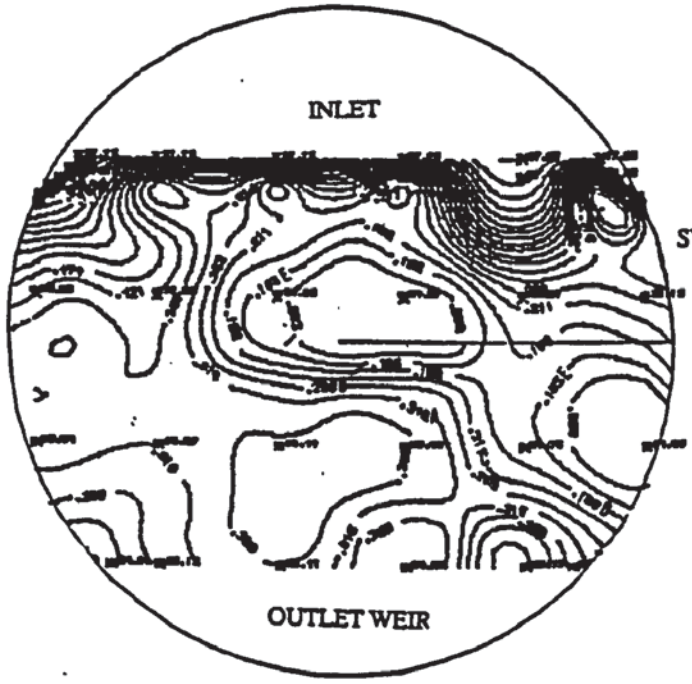

Figure (7.4.3d) Temperature profiles - 12.5 mm diameter hole tray

Capacity factor (C_{sb}) = 0.0695 m/s

Weir load (q/b) = 0.015 m^3/s m

Flow regime : Emulsified

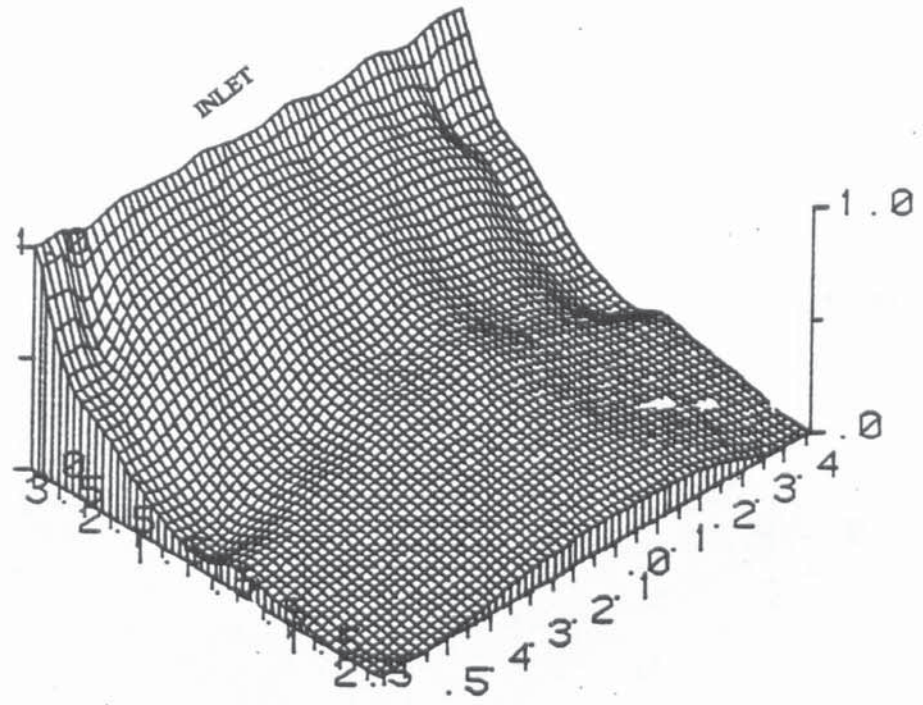

Figure (7.4.4a) Surface contour Profile-1mm Hole Diameter Tray

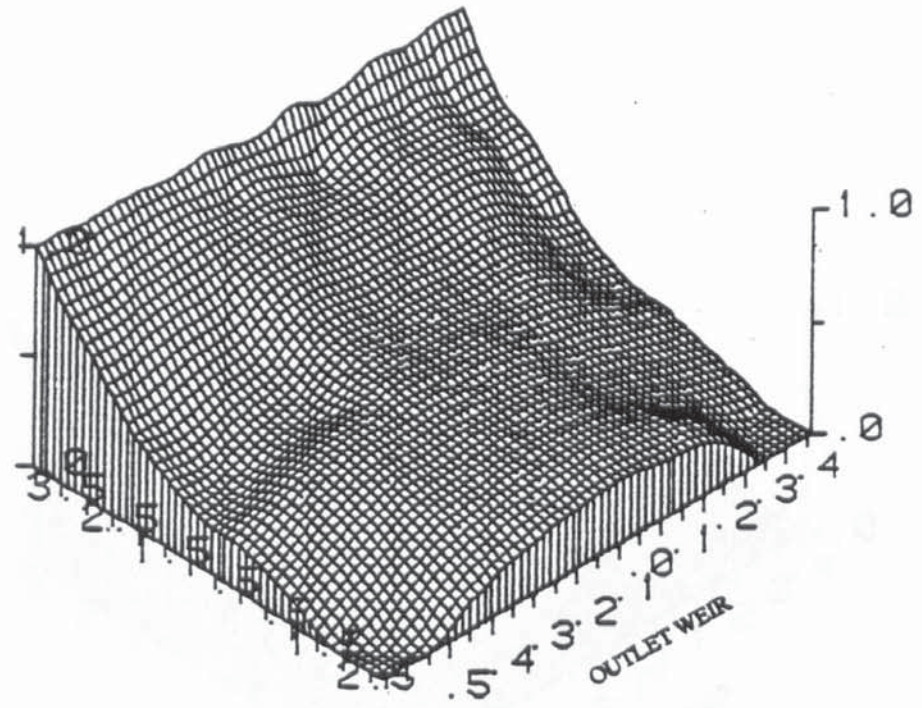

Figure (7.4.4b) Surface contour Profile-1mm Hole Diameter Tray

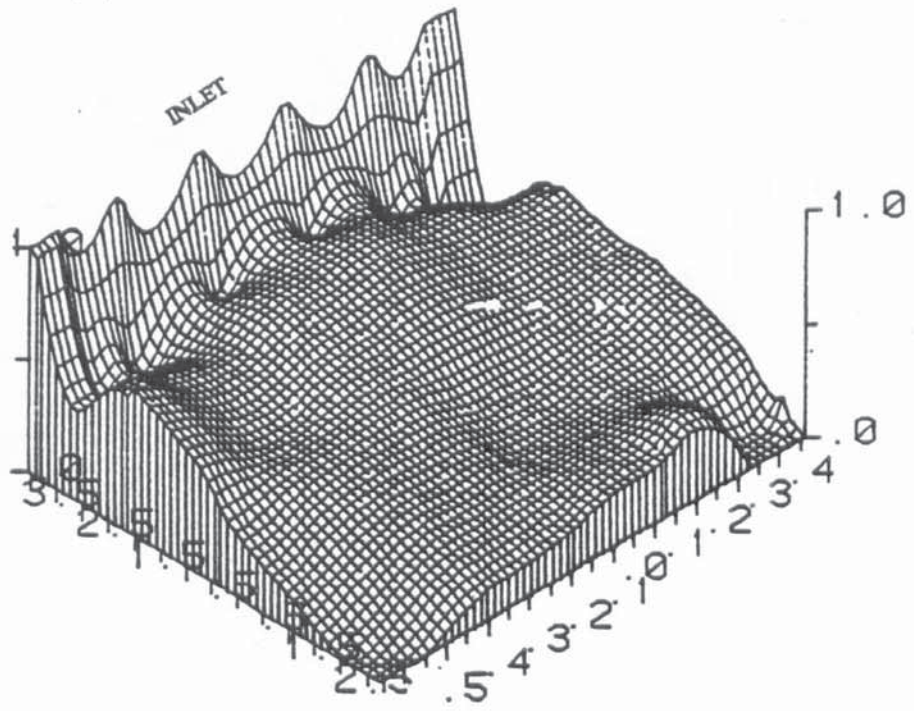

Figure (7.4.4c) Surface contour Profile- 1mm Hole Diameter Tray

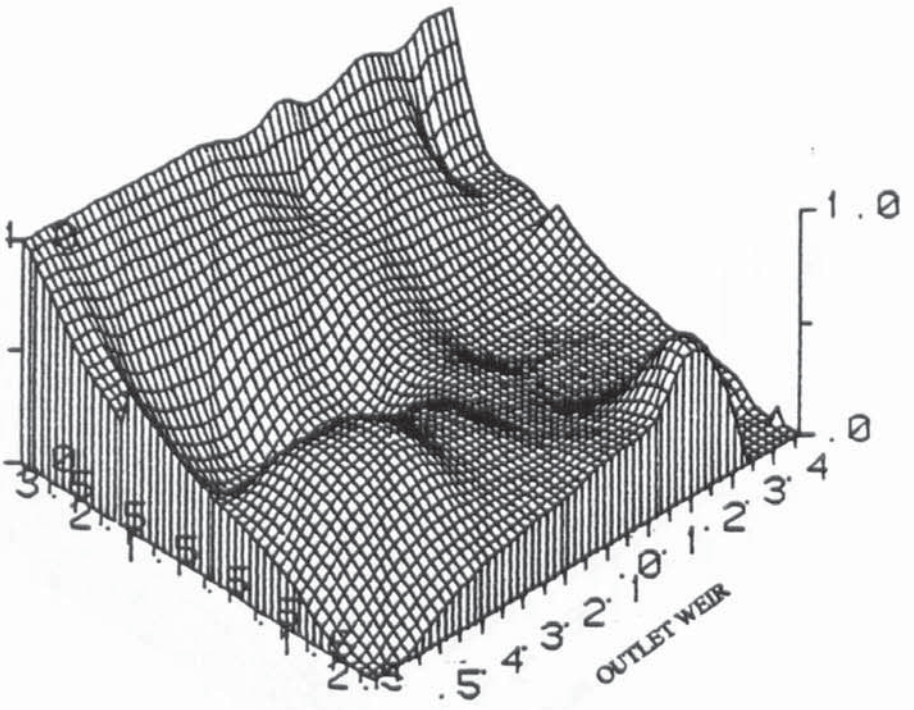

Figure (7.4.4d) Surface contour Profile- 1mm Hole Diameter Tray

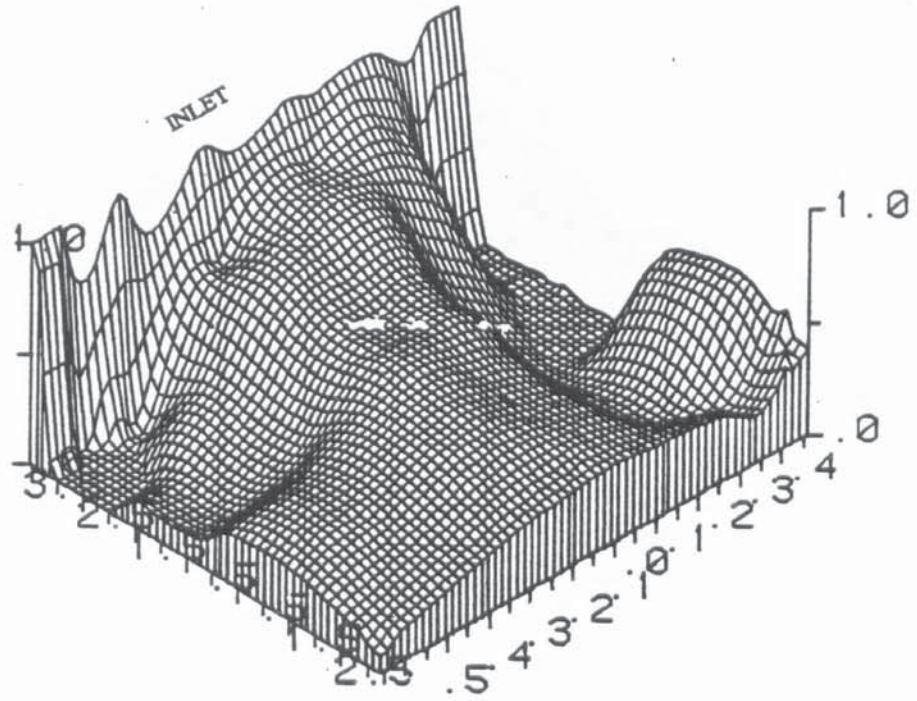

Figure (7.4.4e) Surface contour Profile-4.5mm Hole Diameter Tray

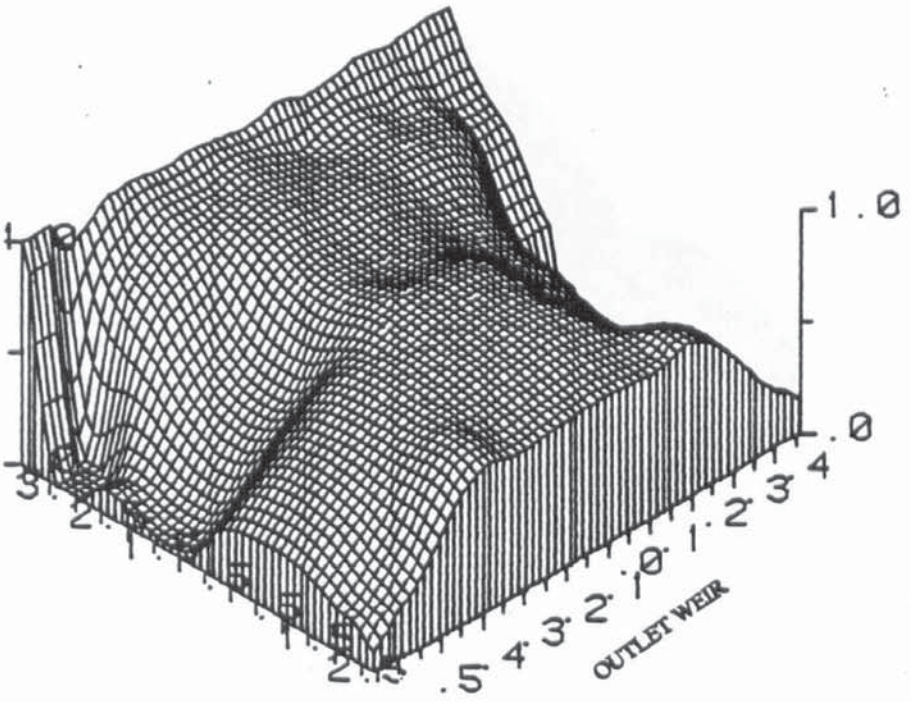

Figure (7.4.4f) Surface contour Profile-4.5mm Hole Diameter Tray

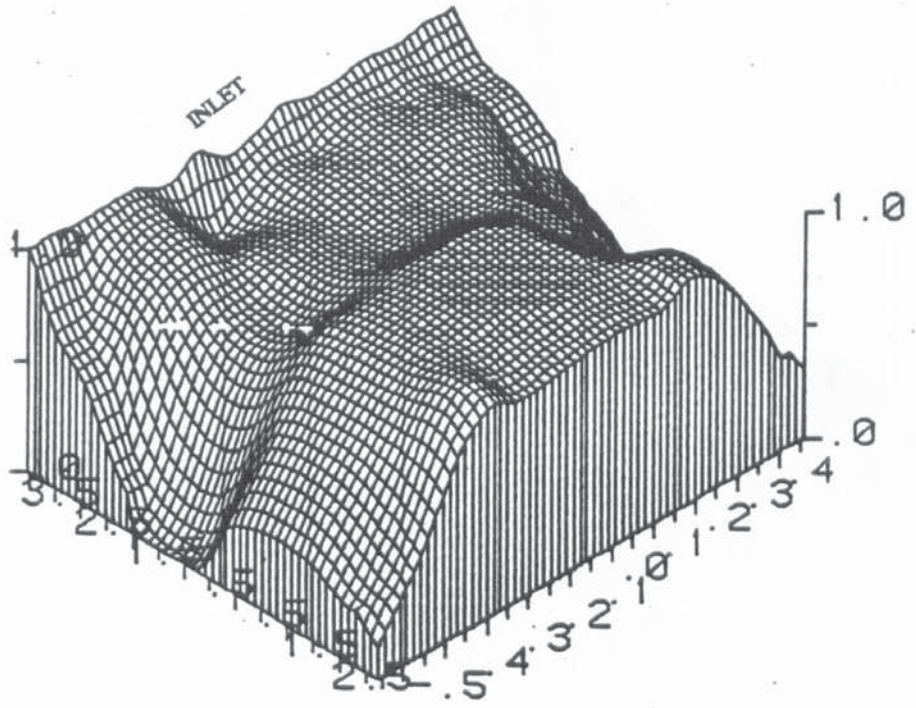

Figure (7.4.4g) Surface contour Profile-4.5mm Hole Diameter Tray

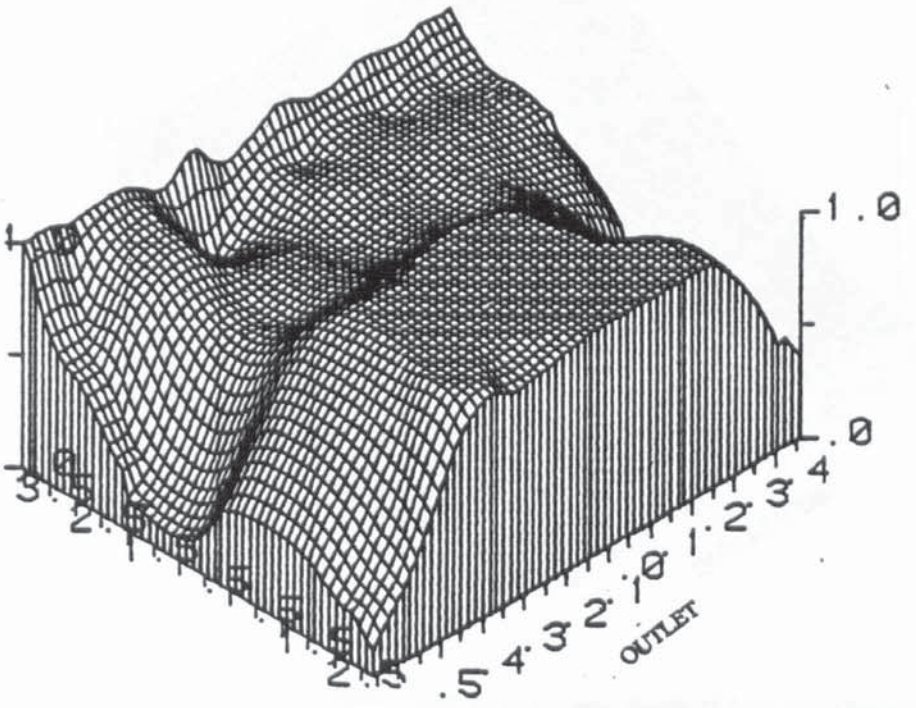

Figure (7.4.4h) Surface contour Profile-4.5mm Hole Diameter Tray

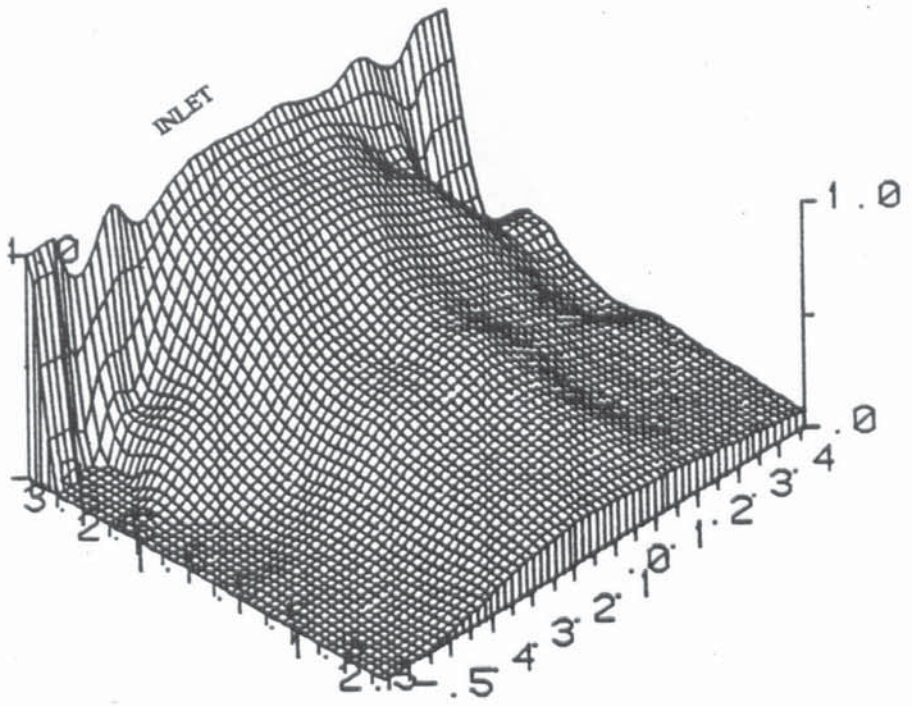

Figure (7.4.4i) Surface contour Profile-12.5mm Hole Diameter Tray

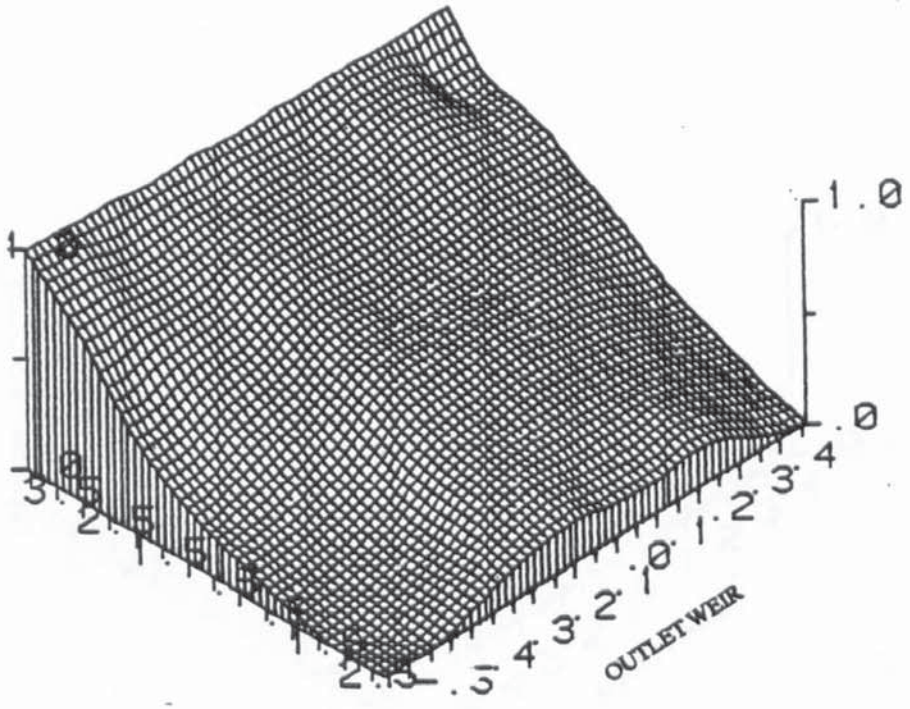

Figure (7.4.4j) Surface contour Profile-12.5mm Hole Diameter Tray

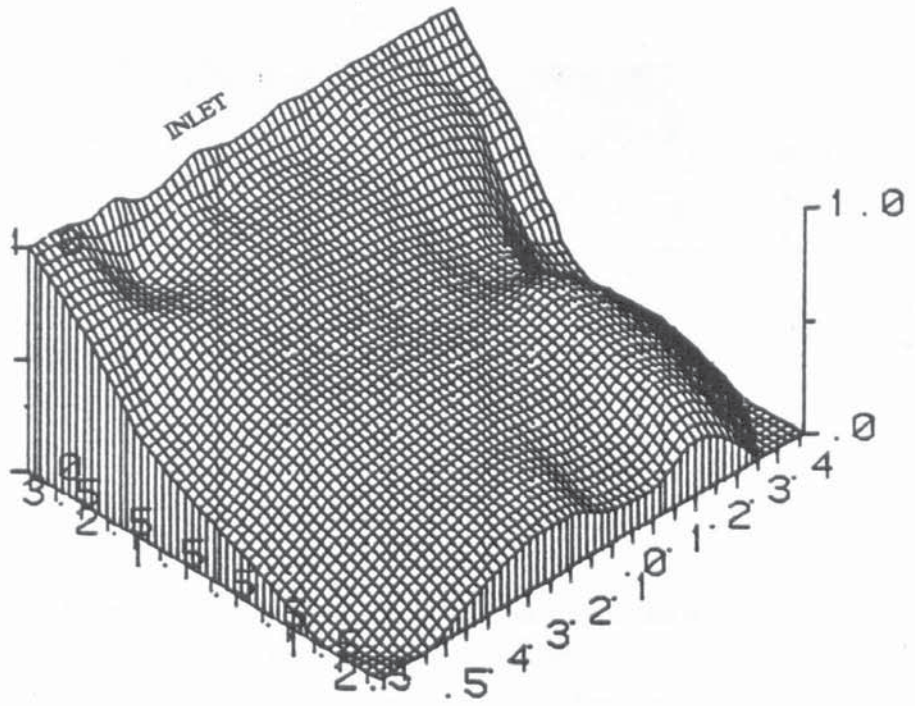

Figure (7.4.4k) Surface contour Profile-12.5mm Hole Diameter Tray

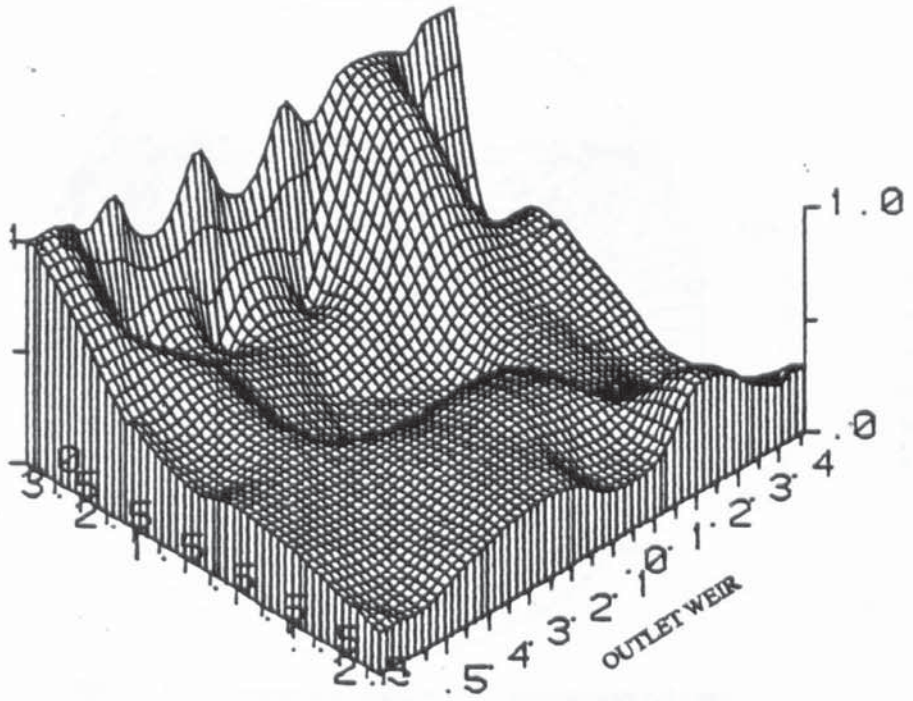

Figure (7.4.4l) Surface contour Profile-12.5mm Hole Diameter Trav

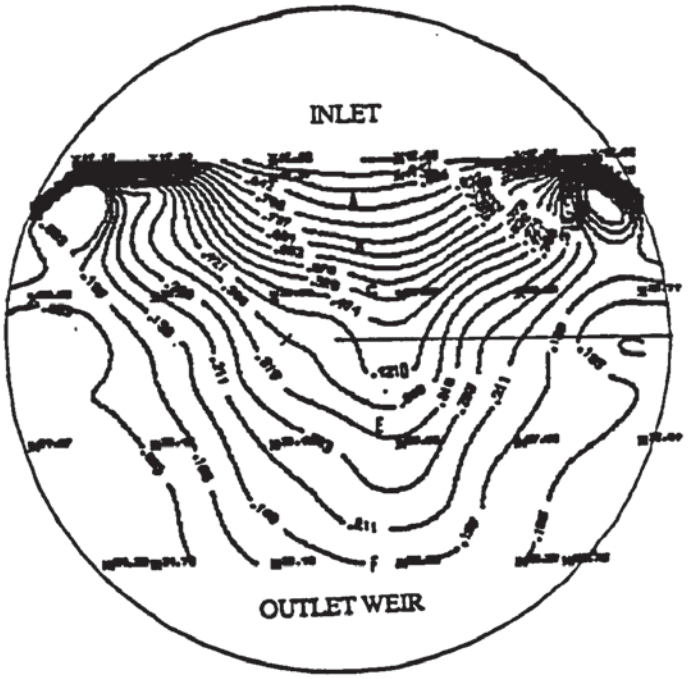

SYMBOL		TR
A	=	0.842
B	=	0.684
C	=	0.526
D	=	0.421
E	=	0.316
F	=	0.158

Figure (7.5.1a) Temperature profile for 12.5 mm diameter hole tray

Capacity factor (C_{sb}) = 0.0851 m/s

Weir load (q/b) = 0.0008 m^3/s m

Flow regime : Intense spray

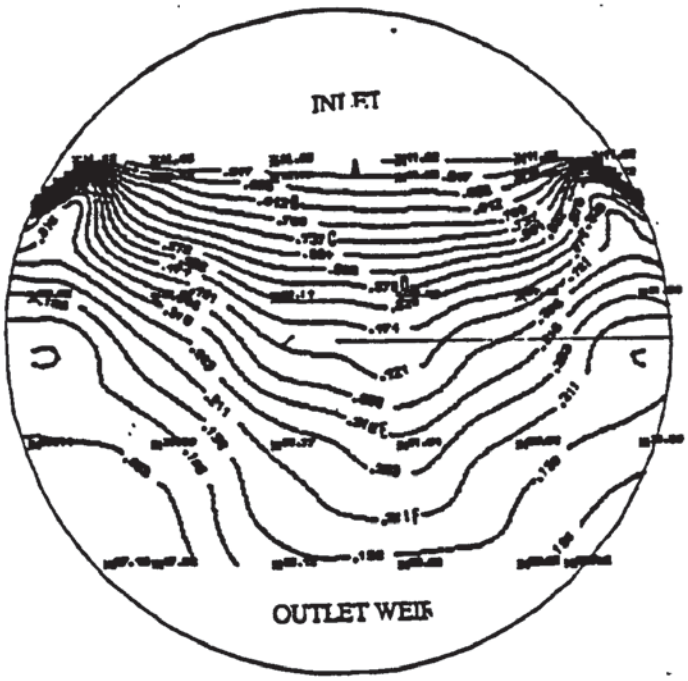

SYMBOL		TR
A	=	0.947
B	=	0.842
C	=	0.737
D	=	0.578
E	=	0.316
F	=	0.211

Figure (7.5.1b) Temperature profile for 12.5 mm diameter hole tray

Capacity factor (C_{sb}) = 0.0851 m/s

Weir load (q/b) = 0.0016 m^3/s m

Flow regime : Spray

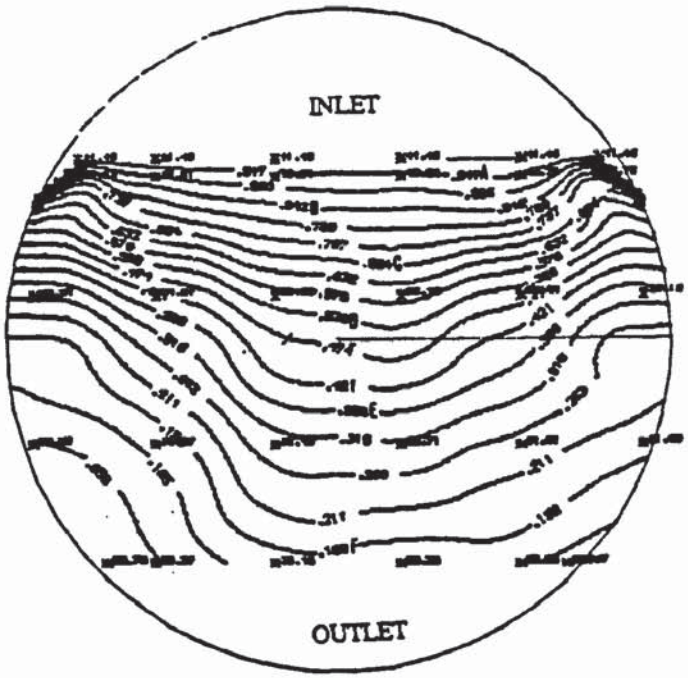

SYMBOL		TR
A	=	0.947
B	=	0.842
C	=	0.684
D	=	0.528
E	=	0.368
F	=	0.158

Figure (7.5.1c) Temperature profile for 12.5 mm diameter hole tray

Capacity factor (C_{sb}) = 0.0851 m/s

Weir load (q/b) = 0.002 m^3/s m

Flow regime : Spray

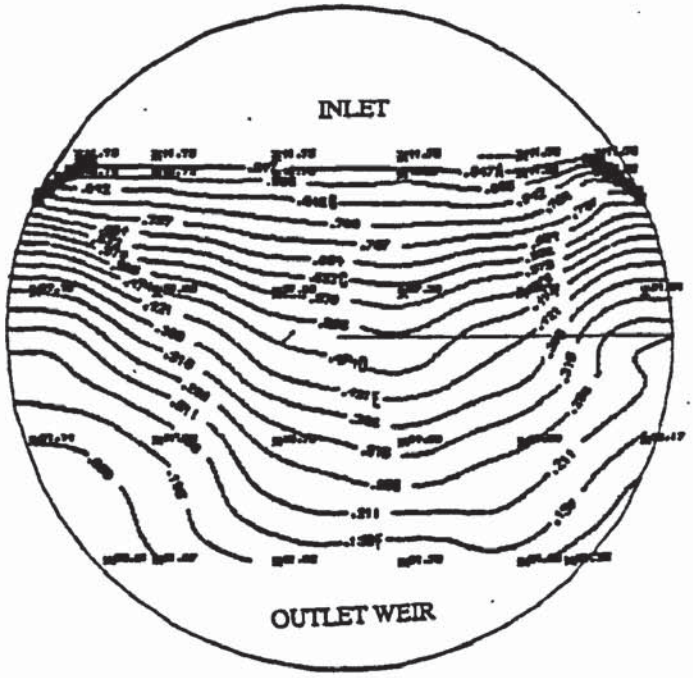

SYMBOL		TR
A	=	0.947
B	=	0.842
C	=	0.632
D	=	0.474
E	=	0.421
F	=	0.158

Figure (7.5.1d) Temperature profile for 12.5 mm diameter hole tray

Capacity factor (C_{sb}) = 0.0851 m/s

Weir load (q/b) = 0.0032m^3/s m

Flow regime : Spray

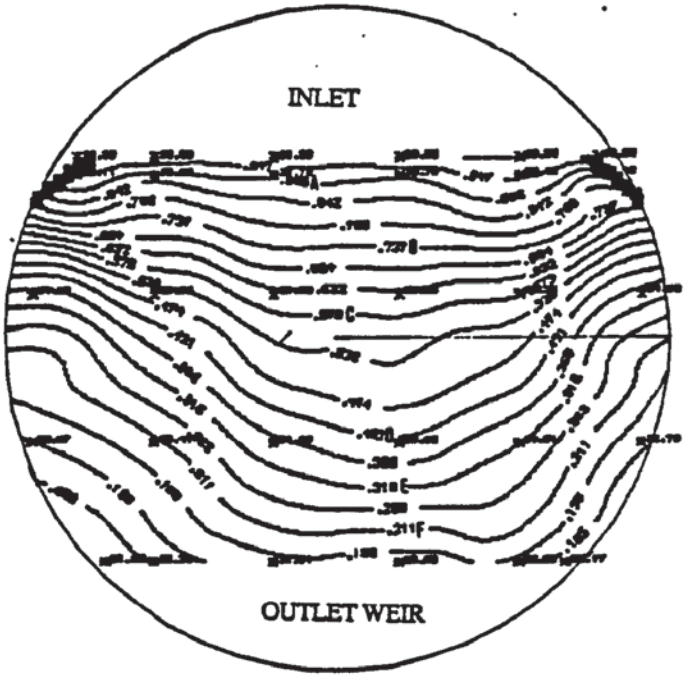

SYMBOL		TR
A	=	0.895
B	=	0.737
C	=	0.579
D	=	0.421
E	=	0.358
F	=	0.211

Figure (7.5.1e) Temperature profile for 12.5 mm diameter hole tray

Capacity factor (C_{sb}) = 0.0851 m/s

Weir load (q/b) = 0.004 m^3/s m

Flow regime : Spray

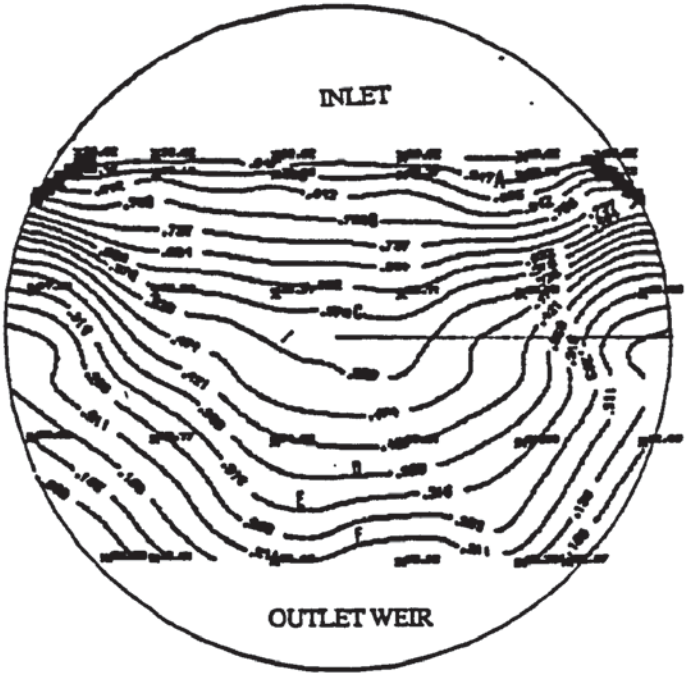

SYMBOL		TR
A	=	0.947
B	=	0.788
C	=	0.578
D	=	0.388
E	=	0.316
F	=	0.211

Figure (7.5.1f) Temperature profile for 12.5 mm diameter hole tray

Capacity factor (C_{sb}) = 0.0851 m/s

Weir load (q/b) = 0.0056 m^3/s m

Flow regime : Mixed

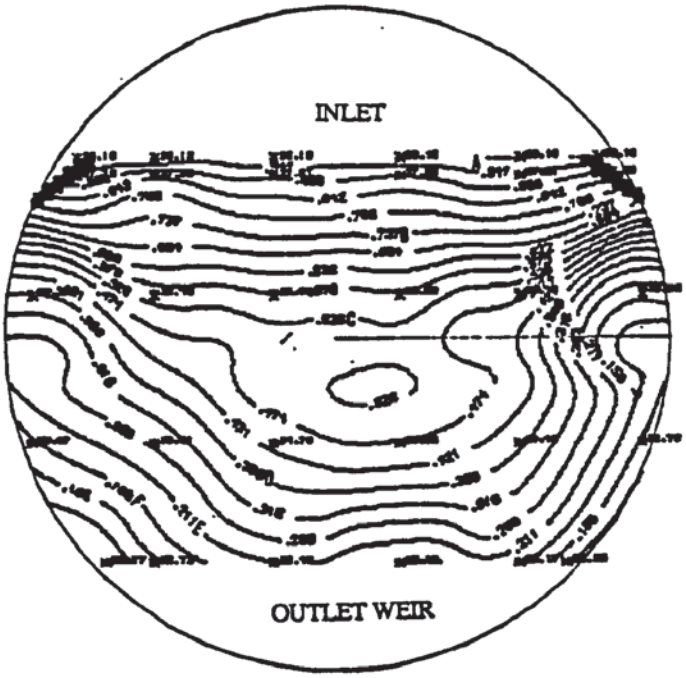

SYMBOL		TR
A	=	0.947
B	=	0.737
C	=	0.526
D	=	0.358
E	=	0.211
F	=	0.158

Figure (7.5.1g) Temperature profile for 12.5 mm diameter hole tray

Capacity factor (C_{sb}) = 0.0851 m/s

Weir load (q/b) = 0.0064 m^3/s m

Flow regime : Mixed

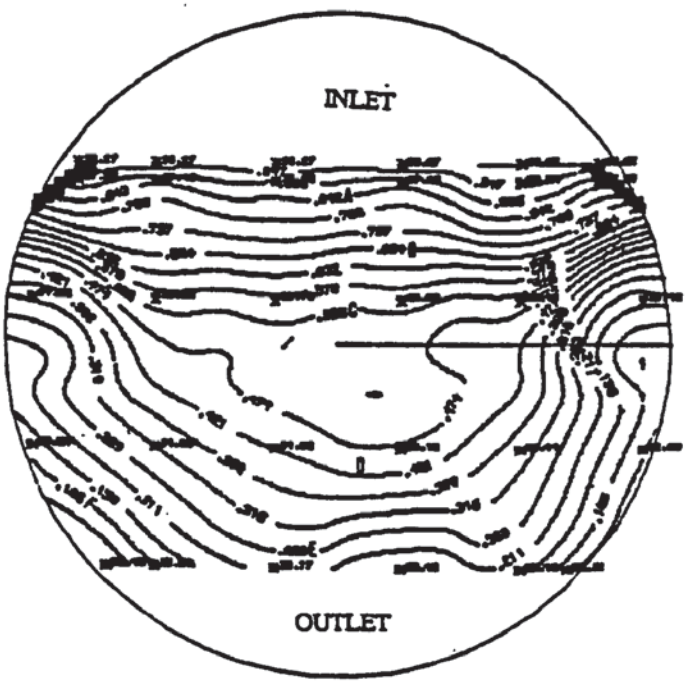

SYMBOL		TR
A	=	0.842
B	=	0.684
C	=	0.526
D	=	0.421
E	=	0.283
F	=	0.105

Figure (7.5.1h) Temperature profile for 12.5 mm diameter hole tray

Capacity factor (C_{sb}) = 0.0851 m/s

Weir load (q/b) = 0.0072 m^3/s m

Flow regime : Mixed

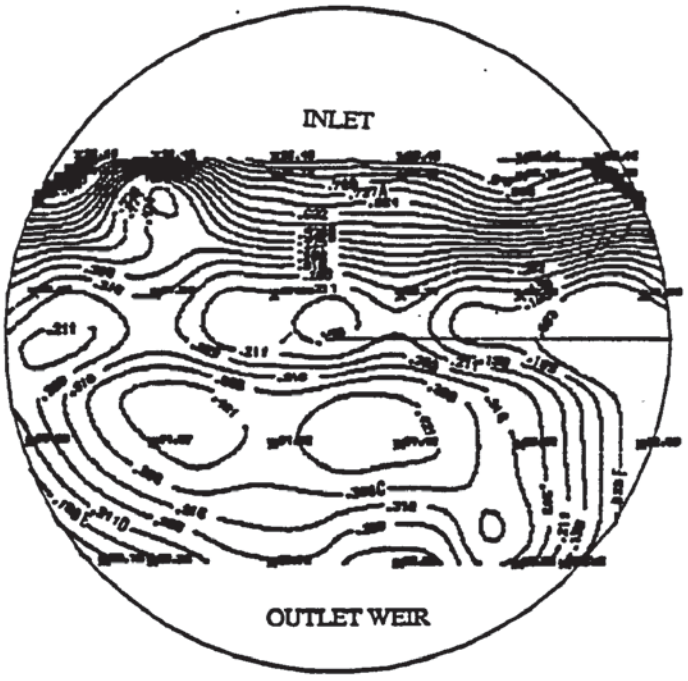

SYMBOL		TR
A	=	0.737
B	=	0.526
C	=	0.368
D	=	0.211
E	=	0.158
F	=	0.033

Figure (7.5.1i) Temperature profile for 12.5 mm diameter hole tray

Capacity factor (C_{sb}) = 0.0851 m/s

Weir load (q/b) = 0.015 m^3/s m

Flow regime : Emulsified

SYMBOL		TR
A	=	0.895
B	=	0.789
C	=	0.632
D	=	0.421
E	=	0.211
F	=	0.159

Figure (7.5.1j) Temperature profile for 12.5 mm diameter hole tray

Capacity factor (C_{sb}) = 0.0851 m/s

Weir load (q/b) = 0.016 m^3/s m

Flow regime : Emulsified

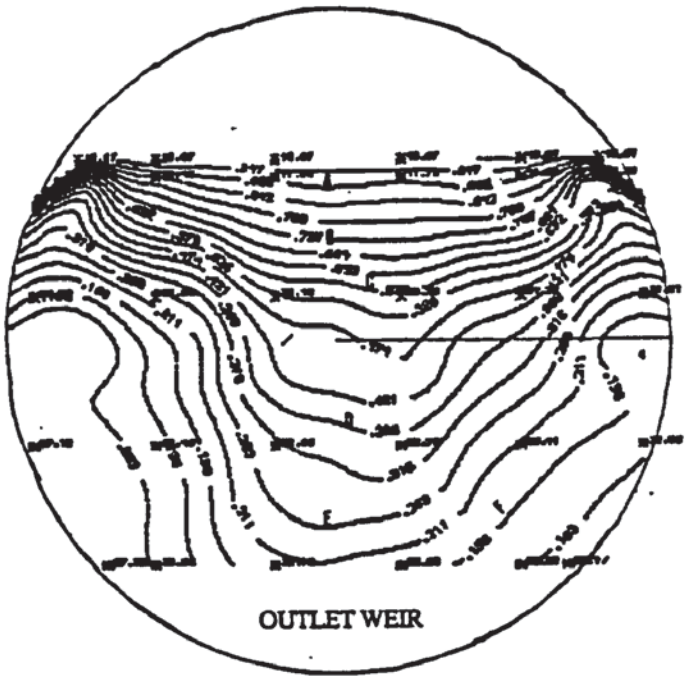

SYMBOL		TR
A	=	0.885
B	=	0.737
C	=	0.532
D	=	0.368
E	=	0.263
F	=	0.158

Figure (7.5.2a) Temperature profile for 12.5 mm diameter hole tray

Capacity factor (C_{sb}) = 0.0775 m/s

Weir load (q/b) = 0.0016 m^3/s m

Flow regime : Spray

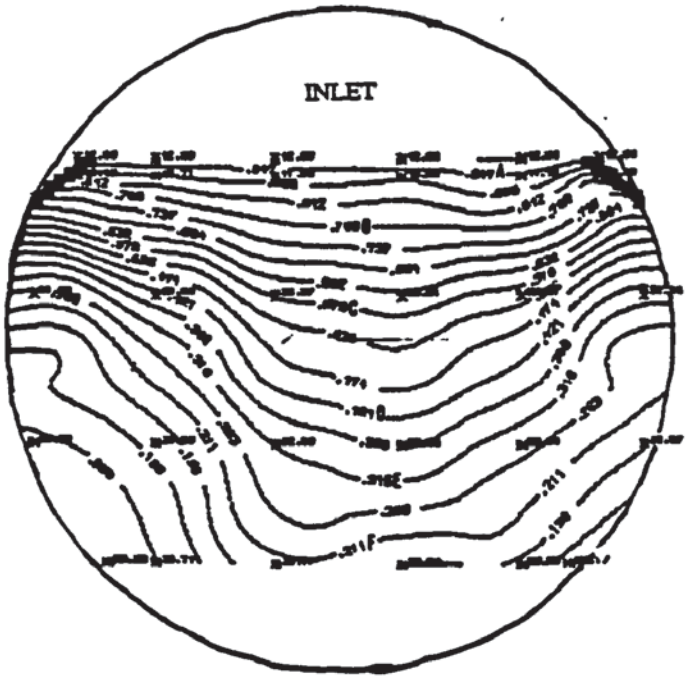

SYMBOL		TR
A	=	0.947
B	=	0.788
C	=	0.579
D	=	0.421
E	=	0.315
F	=	0.211

Figure (7.5.2b) Temperature profile for 12.5 mm diameter hole tray

Capacity factor (C_{sb}) = 0.0775 m/s

Weir load (q/b) = 0.0024 m^3/s m

Flow regime : Spray

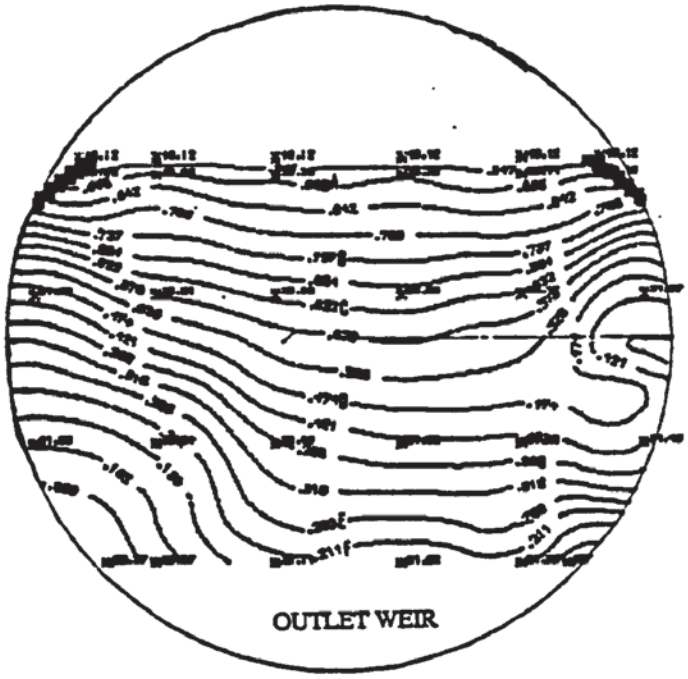

SYMBOL		TR
A	=	0.885
B	=	0.737
C	=	0.632
D	=	0.474
E	=	0.263
F	=	0.211

Figure (7.5.2c) Temperature profile for 12.5 mm diameter hole tray

Capacity factor (C_{sb}) = 0.0775 m/s

Weir load (q/b) = 0.004 m^3/s m

Flow regime : spray

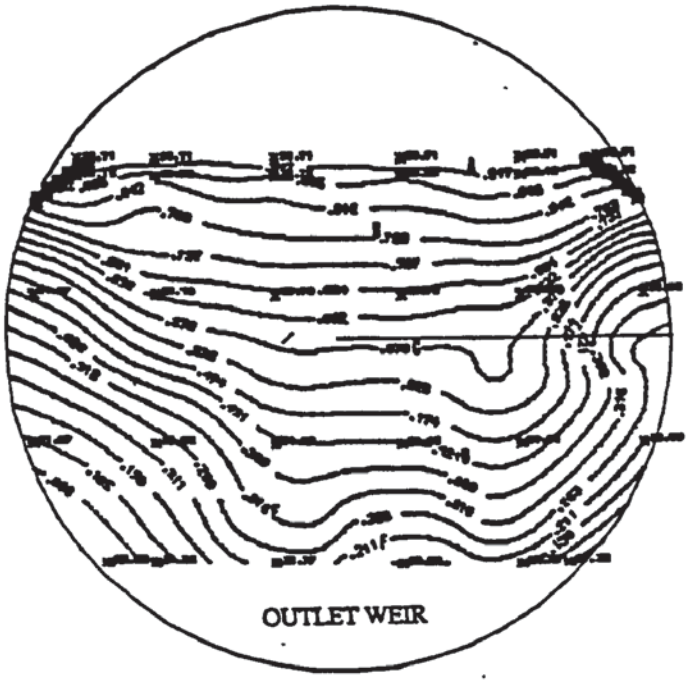

SYMBOL		TR
A	=	0.947
B	=	0.789
C	=	0.578
D	=	0.421
E	=	0.316
F	=	0.211

Figure (7.5.2d) Temperature profile for 12.5 mm diameter hole tray

Capacity factor (C_{sb}) = 0.0775 m/s

Weir load (q/b) = 0.0056 m^3/s m

Flow regime : Mixed

SYMBOL		TR
A	=	0.842
B	=	0.737
C	=	0.526
D	=	0.421
E	=	0.316
F	=	0.059

Figure (7.5.2e) Temperature profile for 12.5 mm diameter hole tray

Capacity factor (C_{sb}) = 0.0775 m/s

Weir load (q/b) = 0.0064 m^3/s m

Flow regime : Mixed

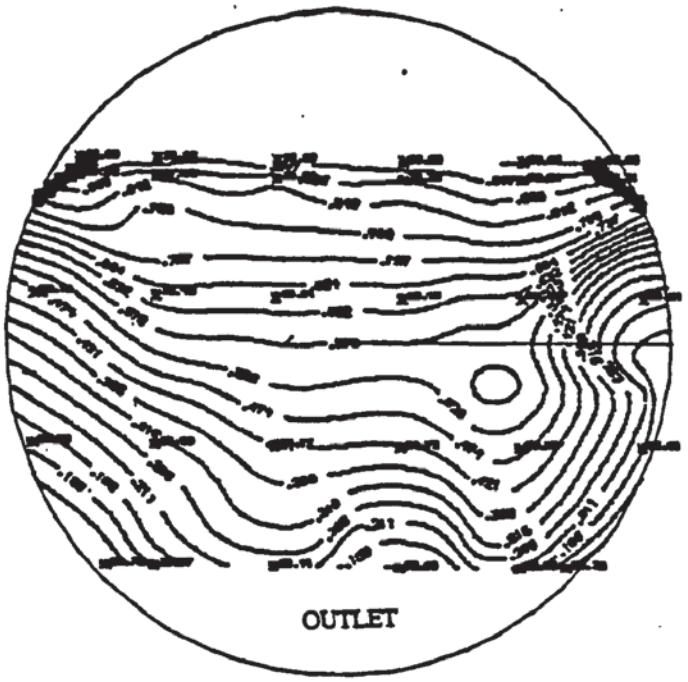

SYMBOL		TR
A	=	0.947
B	=	0.789
C	=	0.526
D	=	0.368
E	=	0.263
F	=	0.185

Figure (7.5.2f) Temperature profile for 12.5 mm diameter hole tray

Capacity factor (C_{sb}) = 0.0775 m/s

Weir load (q/b) = 0.0072 m^3/s m

Flow regime : Mixed

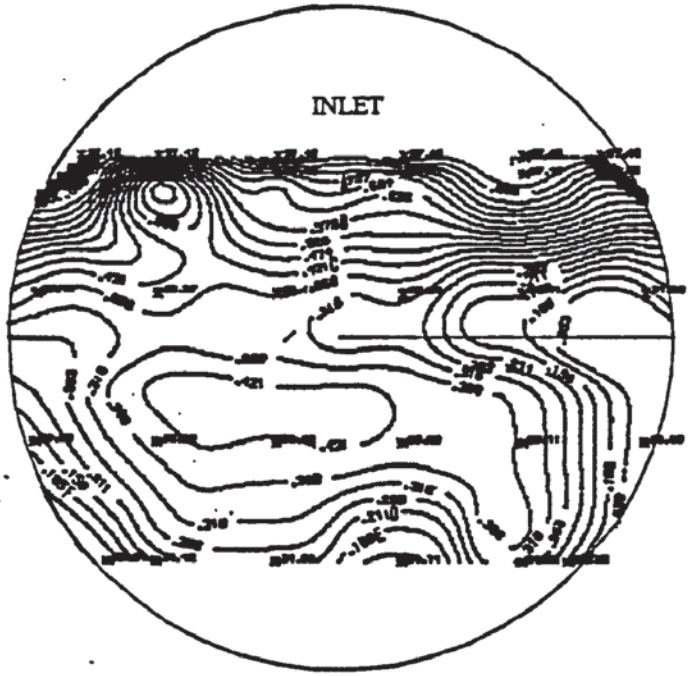

SYMBOL		TR
A	=	0.737
B	=	0.575
C	=	0.421
D	=	0.211
E	=	0.158
F	=	0.105

Figure (7.5.2g) Temperature profile for 12.5 mm diameter hole tray

Capacity factor (C_{sb}) = 0.0775 m/s

Weir load (q/b) = 0.015 m^3/s m

Flow regime : Emulsified.

SYMBOL		TR
A	=	0.474
B	=	0.316
C	=	0.252
D	=	0.211
E	=	0.158
F	=	0.058

Figure (7.5.2h) Temperature profile for 12.5 mm diameter hole tray

Capacity factor (C_{sb}) = 0.0775 m/s

Weir load (q/b) = 0.016 m^3/s m

Flow regime : Emulsified

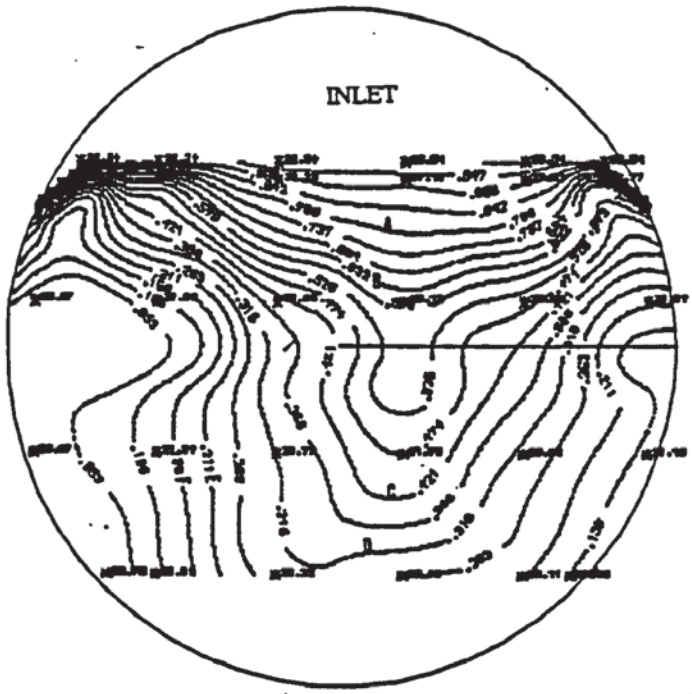

SYMBOL		TR
A	=	0.788
B	=	0.532
C	=	0.421
D	=	0.318
E	=	0.211
F	=	0.158

Figure (7.5.3a) Temperature profile for 12.5 mm diameter hole tray

Capacity factor (C_{sb}) = 0.0605 m/s

Weir load (q/b) = 0.0008 m^3/s m

Flow regime : Intense spray

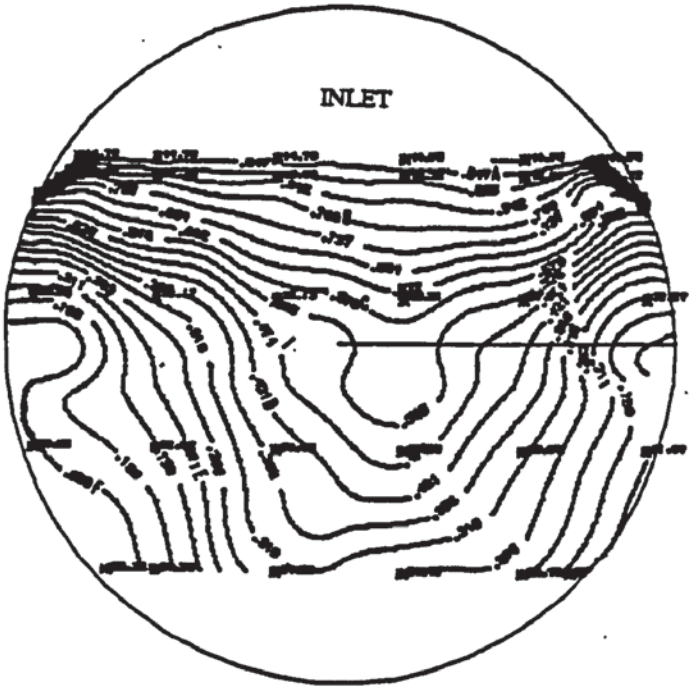

SYMBOL		TR
A	=	0.947
B	=	0.788
C	=	0.598
D	=	0.421
E	=	0.211
F	=	0.053

Figure (7.5.3b) Temperature profile for 12.5 mm diameter hole tray

Capacity factor (C_{sb}) = 0.0605 m/s

Weir load (q/b) = 0.0016 m^3/s m

Flow regime : Spray

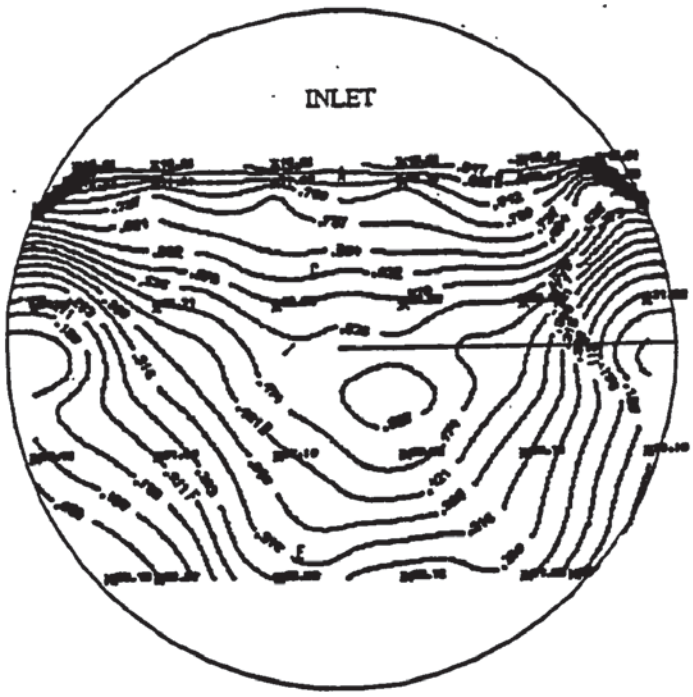

SYMBOL		TR
A	=	0.947
B	=	0.842
C	=	0.582
D	=	0.421
E	=	0.318
F	=	0.211

Figure (7.5.3c) Temperature profile for 12.5 mm diameter hole tray

Capacity factor (C_{sb}) = 0.0605 m/s

Weir load (q/b) = 0.002 m^3/s m

Flow regime : Spray

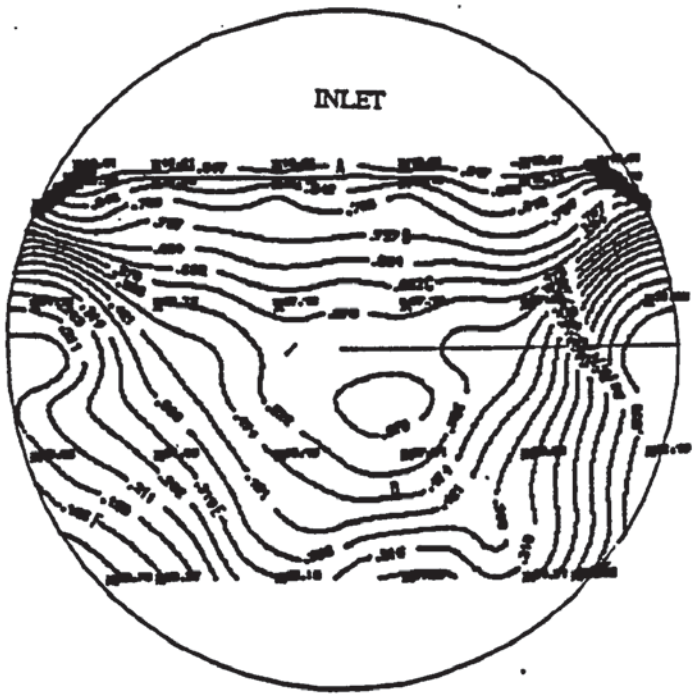

SYMBOL		TR
A	=	0.885
B	=	0.737
C	=	0.582
D	=	0.474
E	=	0.318
F	=	0.105

Figure (7.5.3d) Temperature profile for 12.5 mm diameter hole tray

Capacity factor (C_{sb}) = 0.0605 m/s

Weir load (q/b) = 0.0032 m^3/s m

Flow regime : Spray

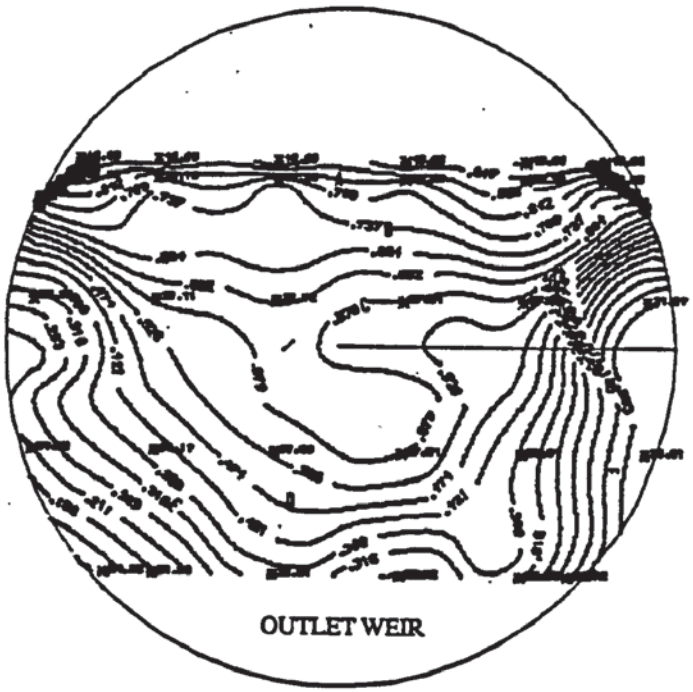

SYMBOL		TR
A	=	0.842
B	=	0.737
C	=	0.578
D	=	0.474
E	=	0.318
F	=	0.105

Figure (7.5.3e) Temperature profile for 12.5 mm diameter hole tray

Capacity factor (C_{sb}) = 0.0605 m/s

Weir load (q/b) = 0.004 m^3/s m

Flow regime : Spray

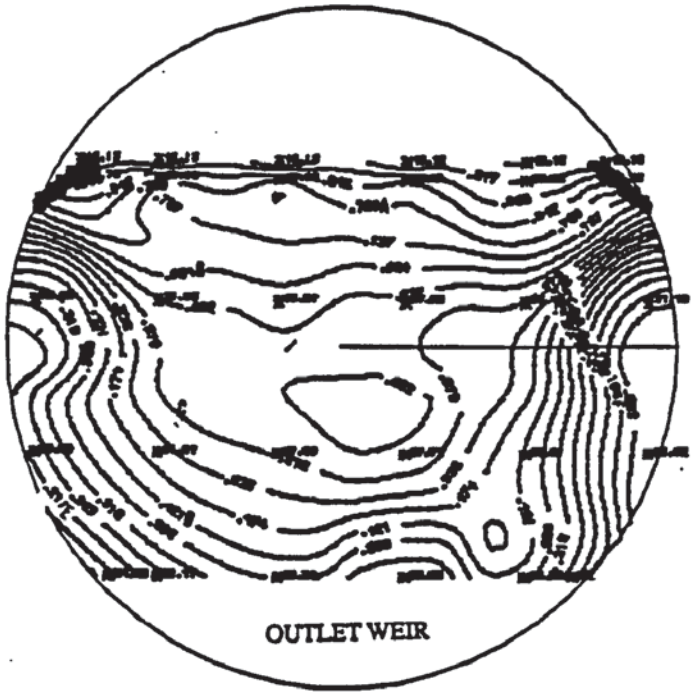

SYMBOL		TR
A	=	0.788
B	=	0.684
C	=	0.578
D	=	0.421
E	=	0.211
F	=	0.105

Figure (7.5.3f) Temperature profile for 12.5 mm diameter hole tray

Capacity factor (C_{sb}) = 0.0605 m/s

Weir load (q/b) = 0.0056m^3/s m

Flow regime : Mixed

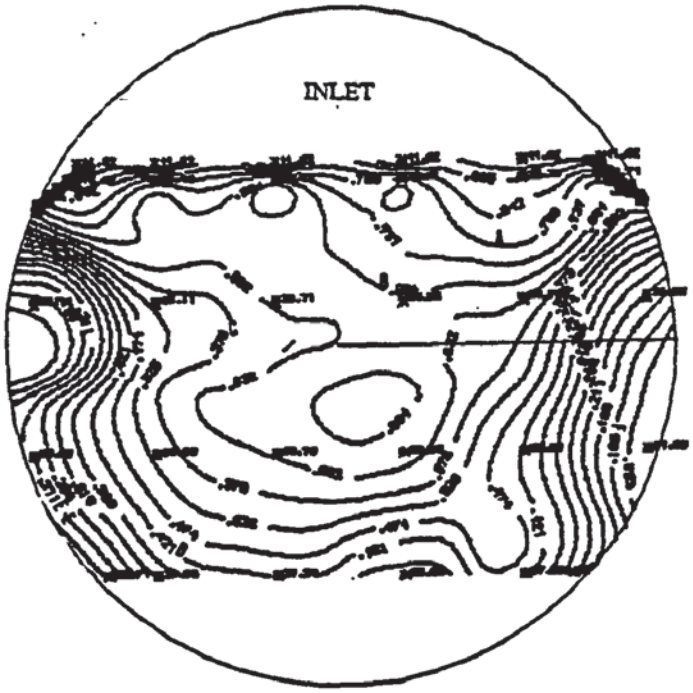

SYMBOL		TR
A	=	0.788
B	=	0.684
C	=	0.578
D	=	0.421
E	=	0.211
F	=	0.105

Figure (7.5.3g) Temperature profile for 12.5 mm diameter hole tray

Capacity factor (C_{sb}) = 0.0605 m/s

Weir load (q/b) = 0.0064 m^3/s m

Flow regime : Mixed

SYMBOL		TR
A	=	0.788
B	=	0.684
C	=	0.578
D	=	0.421
E	=	0.211
F	=	0.105

Figure (7.5.3h) Temperature profile for 12.5 mm diameter hole tray

Capacity factor (C_{sb}) = 0.0605 m/s

Weir load (q/b) = 0.015 m^3/s m

Flow regime : Emulsified

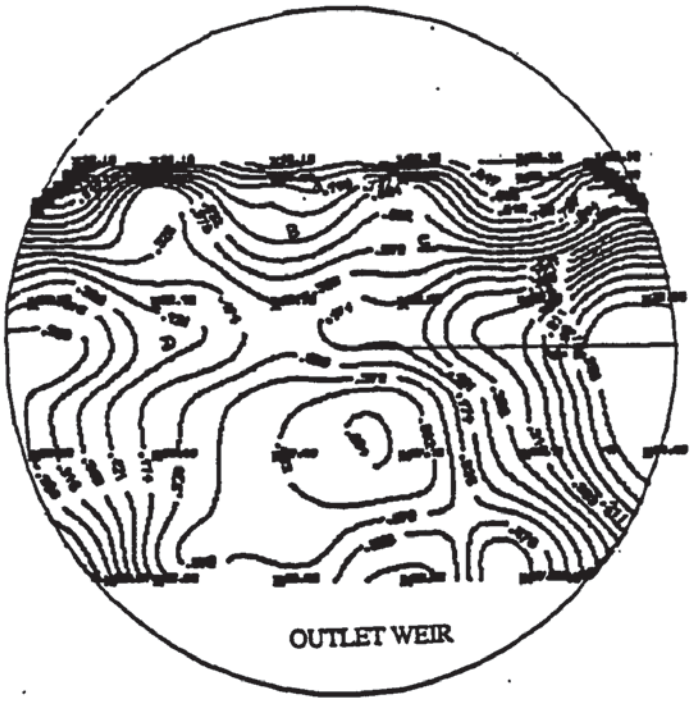

SYMBOL		TR
A	=	0.788
B	=	0.684
C	=	0.578
D	=	0.421
E	=	0.211
F	=	0.105

Figure (7.5.3i) Temperature profile for 12.5 mm diameter hole tray

Capacity factor (C_{sb}) = 0.0605 m/s

Weir load (q/b) = 0.016 m^3/s m

Flow regime : Emulsified

Figure (7.8a): Point Efficiency versus liquid loading for 1mm dia holes

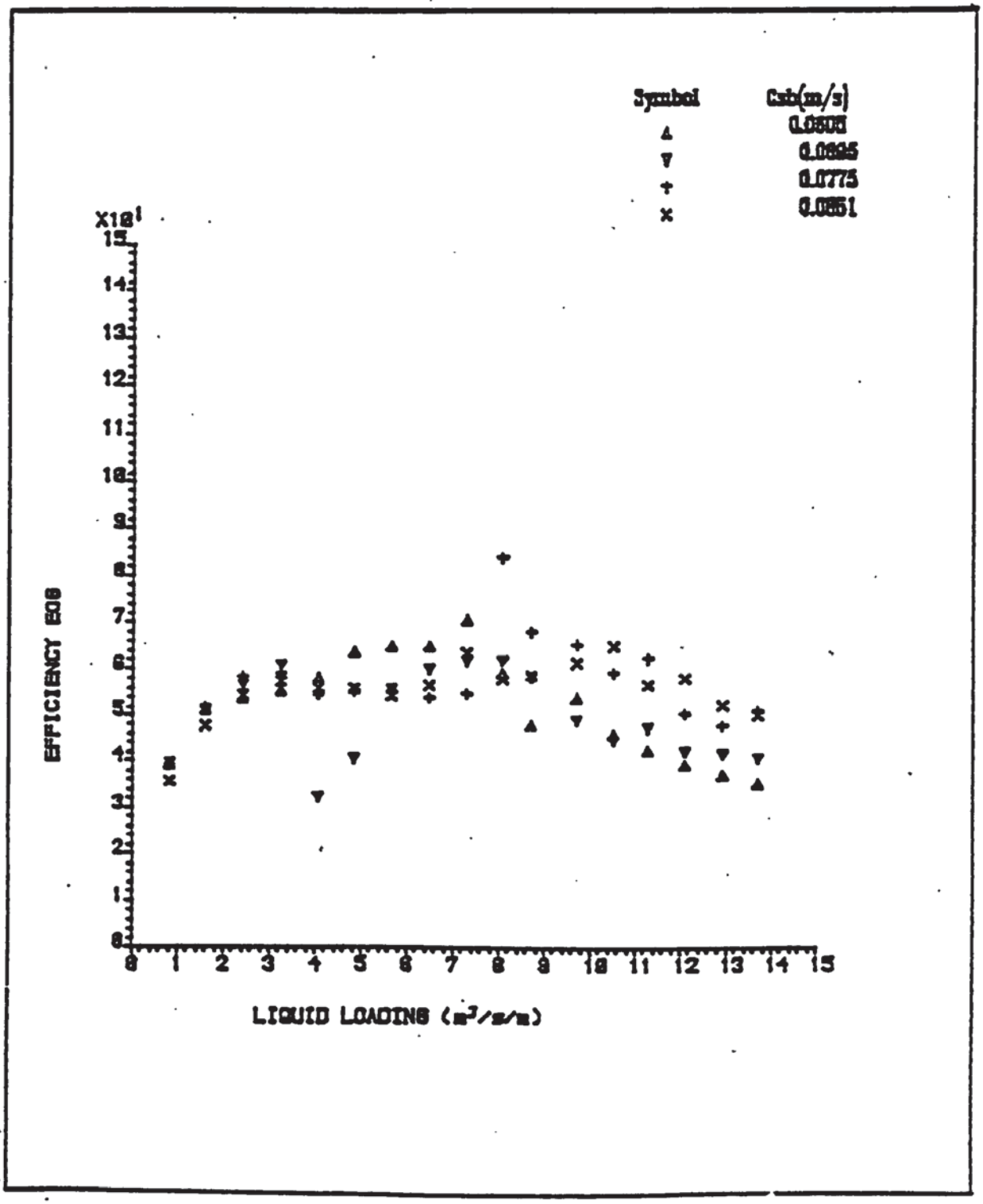

Figure (7.8b) Murphree Vapour Efficiency versus liquid loading for 1mm dia holes

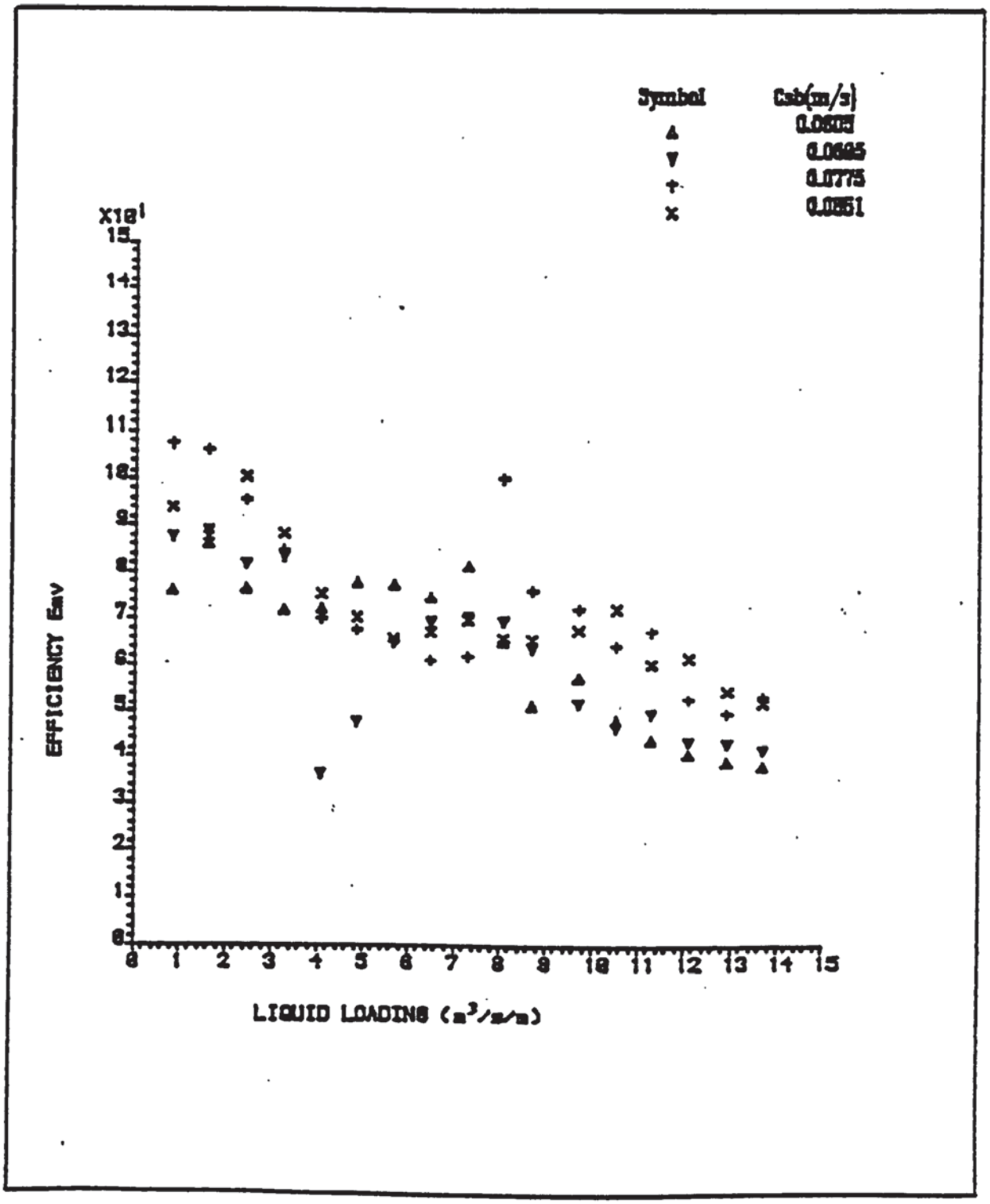

Figure (7.8c): The Ratio of the Murphree Vapour Efficiency to the Point Efficiency versus liquid loading for 1mm dia holes

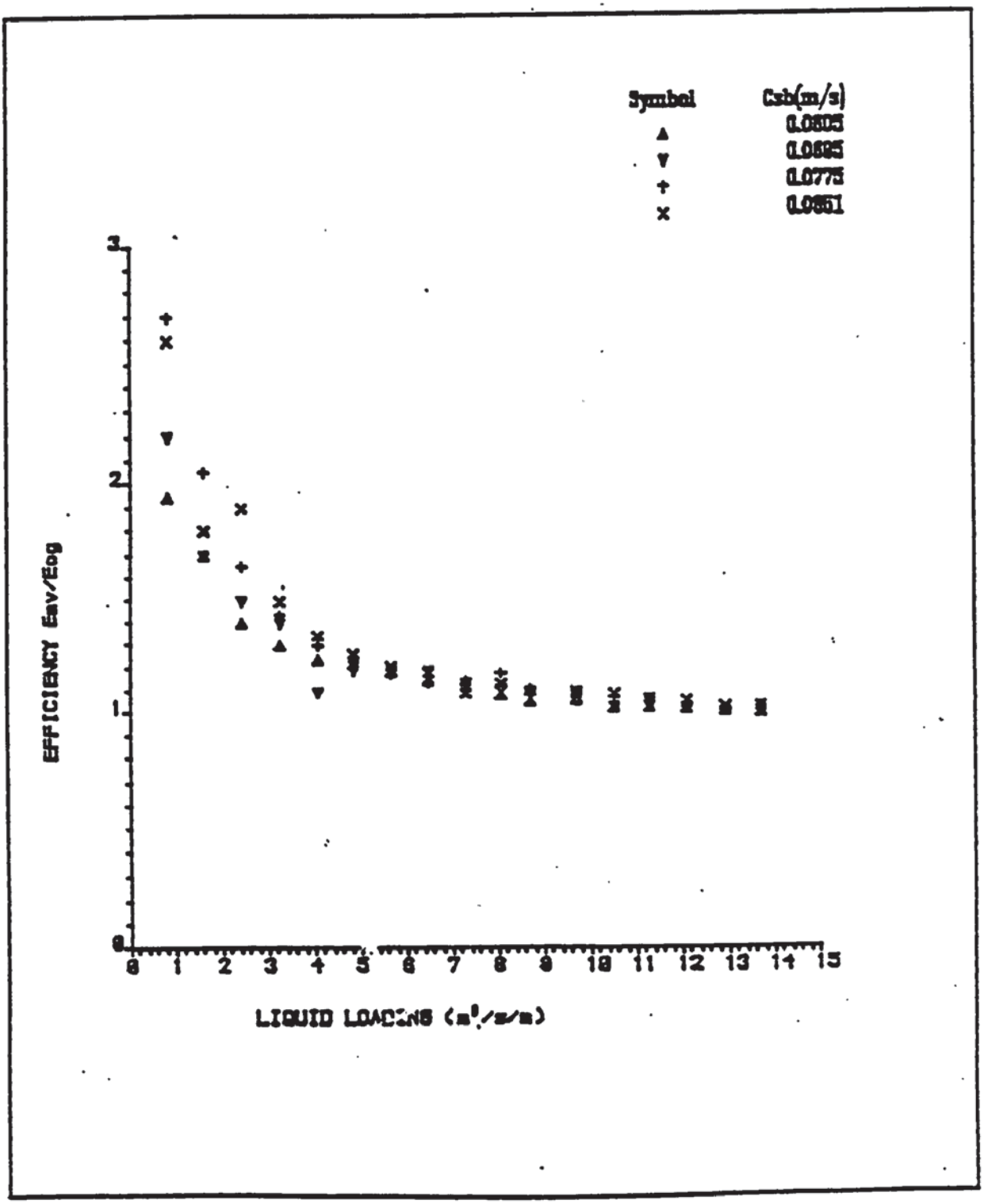

Figure (7.8d) : Point Efficiency versus liquid loading for 12.5 mm dia holes

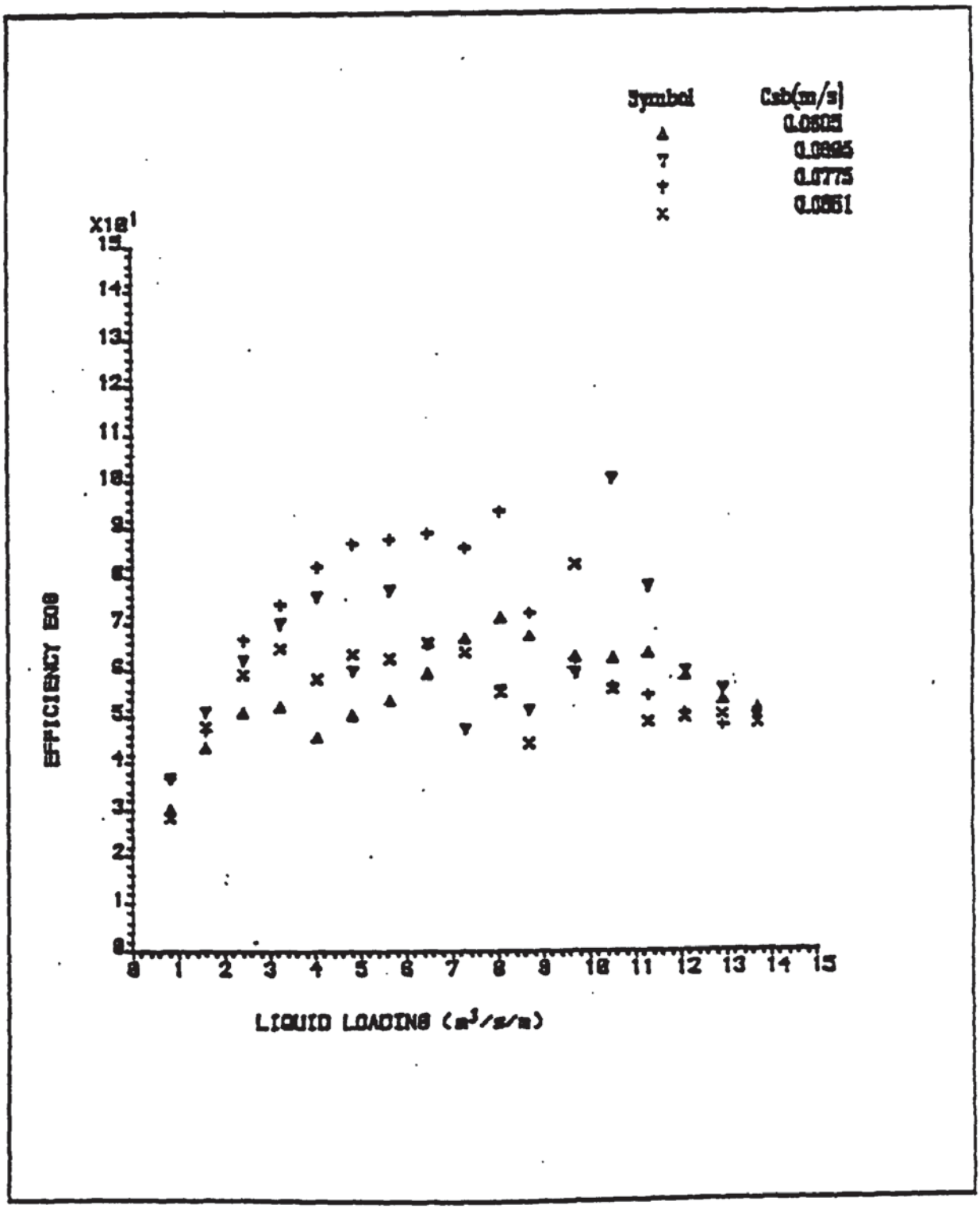

Figure (7.8e): Murphree Vapour Efficiency versus liquid loading for 12.5 mm dia holes

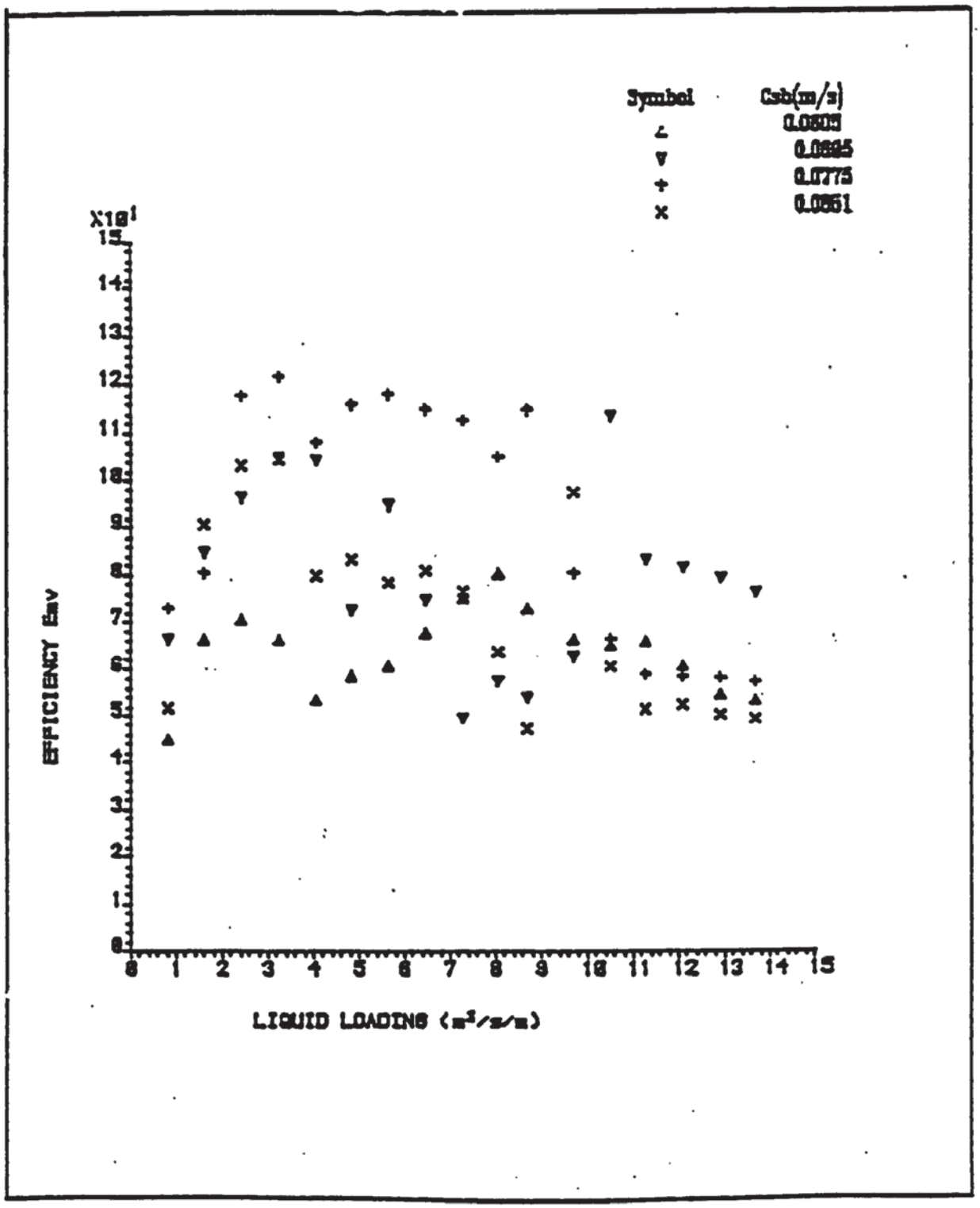

Figure (7.8) : The Ratio of the Murphree Vapour Efficiency to the Point Efficiency versus liquid loading for 12.5 mm dia holes

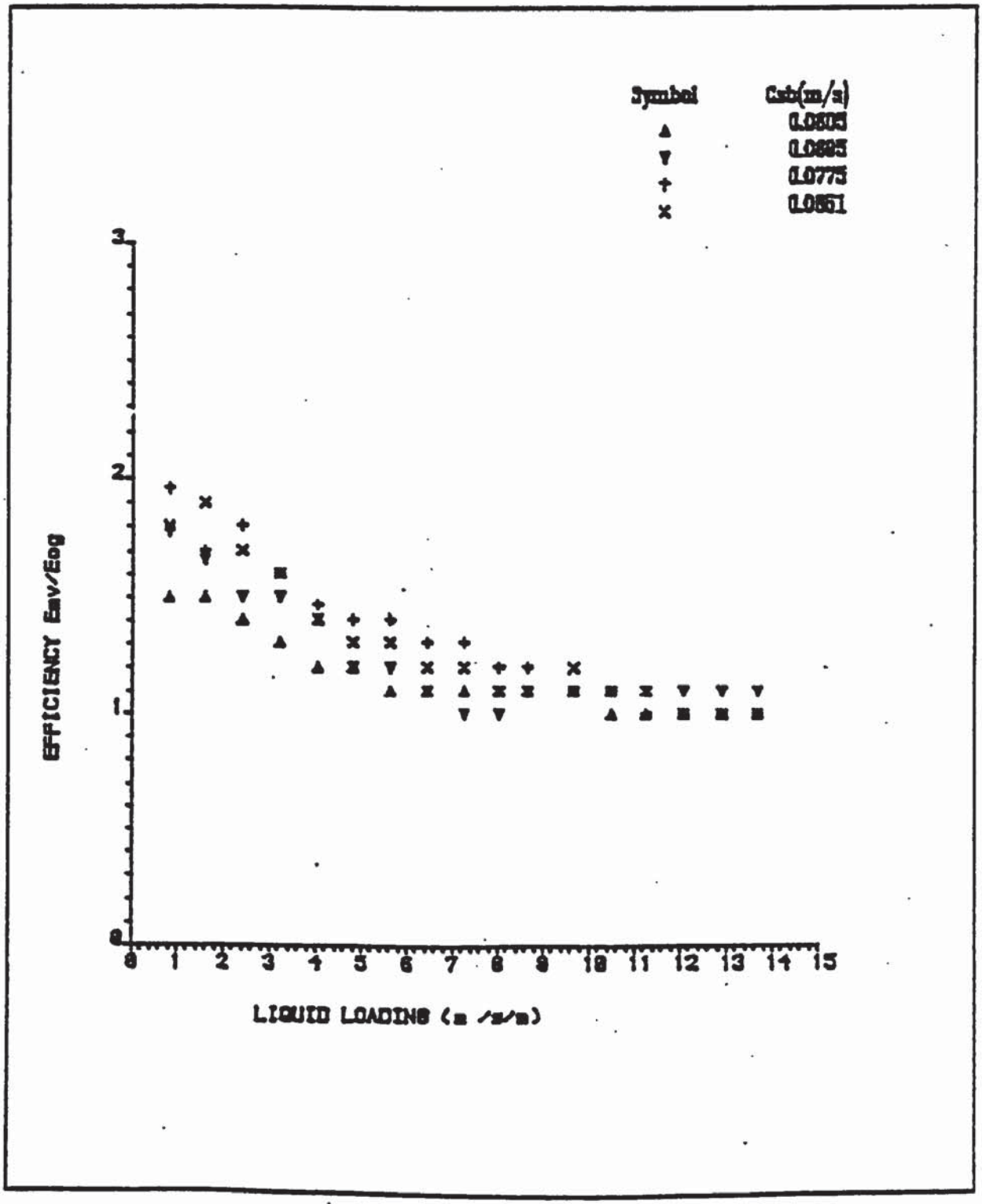

Chapter 8

MEASUREMENT OF OPERATING VARIABLES ON THE TEST TRAYS

8.1 MEASUREMENT OF CLEAR LIQUID HOLD-UP ON TEST TRAYS (SEIVE)

It is known that mass transfer (Point Efficiency) depends on the vapour residence time which in itself depends on the liquid hold-up on the tray. The value must not vary so much across the tray. If the point efficiency does vary across the tray, the decision on where and when to sample the liquid in the tray would be very difficult.

This part of the experimental programme was designed to investigate the commonly used assumption that the point efficiency is constant over all of the tray. If this assumption is found to be invalid then the calculation methods will not be adequate.

Liquid hold up on a tray may be defined as the height of the clear liquid on the tray when the vapour supply is cut off to eliminate the foaming vapour and liquid droplets above it. This boundary can not be clearly defined, especially at very high liquid flowrates.

The standard method of measuring the clear liquid height on an operating tray has been to connect a manometer filled with liquid, to a pressure tapping welded to the tray floor , with the assumption that:

The measured froth pressure drop = The liquid hold-up (h_f)

However this method gives an approximate result and the error associated with it can be significant depending on the flow conditions on the tray. The error involved can be reduced by introducing a correction factor for the momentum head.

$$h_f = Z_l - h_m \qquad (8.1)$$

The error is likely to persist if the froth is not uniform. It has been shown (15) that for froth densities (ρ_f) less than 0.4 the froth may be considered uniform and hence :

$$h_f = Z_f \rho_f = Z_l \qquad (8.2)$$

8.2 EXPERIMENTAL PROCEDURE AND APPARATUS

The trays used for this investigation were the same as those used for the temperature profile measurements (4.5mm and 12.5 mm diameter hole circular trays). 20 stainless steel pressure tappings were welded flush with the tray floor (see figure 5.2a). The stainless steel pipes were connected through PVC tubing to 20 separate glass manometer tubes of 4mm bore. The manometer tubes were placed on a wooden board fixed to a panel close to the simulator column so that the tubes could be levelled with the tray position in the column.

8.2.1 EXPERIMENTAL PROCEDURE

The PVC tubing connecting the sample points on the tray to the manometers were filled with water to bring the level of liquid manometer to the same level as the dry tray. The lines were then cleared of air bubbles by purging then with water under pressure.The position of the liquid level in the manometer tubings was recorded as the static zero position. These readings were recorded before the experimental results were read starting from the static position. Three fixed air capacity factors of (C_{sb} = 0.0605, 0.0775 and 0.0915 m/s for the 12.5 mm hole tray and 0.049, 0.0605 and 0.0695 m/s for the 4.5 mm hole tray) were used and the weir load was increased starting from 0.0008 m^3/s m to 0.008 m^3/s m.

8.2.2 LIQUID HOLD-UP RESULT

The results for the 4.5mm diameter hole tray (figures 8a - 8u) and for 12.5 mm diameter hole tray (figure 8.1a - 8.1u) show the height of liquid at different points on the tray. The results from both trays have shown that significant liquid holdup occurs at the low temperature areas of the tray while the high temperature areas of the tray have less liquid hold-up. Thus there is a similarity in the trend of the height of liquid on a distillation tray with the temperature or concentration profiles. Point measured clear liquid heights are given for the 4.5 mm and 12.5 mm diameter hole trays in Appendix (7.1 and 7.2) respectively.

The results so far have shown that a calculation method not requiring estimates of N_{og} and N_{ol} must be found if full account for the performance of an operating tray is to be made with greater accuracy. The 4.5mm diameter hole tray was found to have a significant area of non uniform liquid hold-up on the tray. The lower temperature areas at the sides of the

tray represented areas on the tray where the liquid had spent more time on the tray without being replenished by fresh liquid flowing onto the tray from the inlet downcomer.

The dip area along the outlet weir in figure 8b can be explained as part of the process of vapour being constantly entraped into the manometer tube due to the violent behaviour of the bi-phase on the tray.

8.3 VIDEO AND STILL PHOTOGRAPHIC STUDIES OF LIQUID FLOW PATTERN

8.3.1 INTRODUCTION

The liquid flow patterns were also studied visually using a dye tracer of potassium permanganate. An equivalent set of experiments were made using the same condition as in the temperature profile experiments. Dye solution was injected on to the tray at the inlet downcomer and video recordings were taken of the movement of the dye as it was thrown about on the active area of the tray from the inlet to the outlet downcomer. Still photographs of the movement of the coloured dye were also taken at the same time.

Still photographs showing the movement of the coloured dye (figure 8.3a - 8.3d) for the 4.5 mm diameter hole tray and Figure (8.3e - 8.3h) for the 12.5 mm diameter hole tray.

8.3.2 EXPERIMENTAL PROCEDURE

Different flow regimes were created on the sieve tray by careful choice of the vapour (air) and liquid loadings. A dye injection apparatus was designed and used to introduce dye tracer onto the tray at the inlet downcomer. The liquid holdups on the tray were also measured using the same method as described in section 8.2 .

The top of the air-water simulator was removed and the appropriate air and water loadings were set . The dye injection system was activated to inject dye tracer onto the tray at the inlet downcomer. A video recording of the movement of the dye tracer was made as the liquid passed from the inlet to the outlet downcomer. Still photographs were also taken at one second intervals as the dye moved across the tray. After the dye study was completed the top of the column was replaced and the temperature of the liquid in cross flow with the air at the preset loadings was measured by the thermocouples and the data was recorded by the computer system. The temperatures were used to create the liquid flow pattern across the tray and the tray efficiency was estimated from the temperature profile

data.

8.3.3 RESULTS OF THE VIDEO AND STILL PHOTOGRAPHIC STUDIES

Interesting results of the movement of the dye were obtained from both the video and the still photographs which were taken under the same operating conditions.The width of the mixing zone and the extent of liquid recirculation on the bubbling area of the tray were easily identified and measured. The frame to frame still photograph showing the injection of the dye tracer and the movement of the tracer across the tray are given in figures (8.3a to 8.3d) for the 4.5 mm diameter hole tray and figure (8.3e to 8.3h) for the 12.5 mm diameter hole tray. Each figure represents 6 photographic frames corresponding to 6 seconds in real time of the dye tracer movement from the inlet downcomer to the outlet weir.

4.5 mm diameter hole tray

At low liquid rate of 0.0016 m^3/s m and constant capacity factor of 0.0605 m/s (figure 8.3a frame 1) a uniform progression of the dye immediately leaving the inlet downcomer can be seen. As the dye progressed half way between the inlet and the outlet weir a significant movement of the dye was observed at the central region of the tray while the dye at both end of the inlet downcomer remained almost stagnant (figure 8.3a frames 2 and 3). Frame 4 and 5 of figure 8.3a showed that the dye at the circular sides of the tray persisted whilst the dye on the central region of the tray was completely replenished by non coloured liquid coming into the tray. Frame 6 showed less coloured liquid at the circular sides of the tray , signifying a gradual replenishment of the liquid at both circular sides by the liquid flowing across the tray.

As the weir load was increased to 0.0064 m^3/s m (figure 8.3b frame 1 to 6) the same dye movement was observed.

When the weir load was increased to 0.008 m^3/s m bringing the dispersion towards the emulsified flow regime the velocity of the dye tracer at the central region of the tray increased significantly (figure 8.3c frames 1, 2, and 3). Although some of the dye tracer stayed longer on the circular side of the tray there was an increased mixing of the liquid on the tray thus reducing significantly the area at the circular side where the dye persisted (figure 8.3c frame 4 and 5). It was observed that (frame 6) only a very small area of the column wall was still occupied by the dye tracer while the central region of the tray was completely free of the dye tracer.

As the weir load was increased to 0.015 m^3/s m (figure 8.3d) the progress of the dye tracer was observed to be very swift across the central region of the tray with little amount of dye still present at the circular sides of the tray (see figure 8.3d frame 1, 2, and 3). Frame 4 and 5 showed that the dye at the circular side was persistent while the central

region was completely free of the dye. Frame 6 showed that the entire tray active area was free of the dye tracer.

12.5 mm hole tray

At low weir load of 0.0016 m^3/s m the progress of the dye across the tray was observed to be the same as that for the 4.5 mm diameter hole tray (see figure 8.3e frames 1 to 6).

As the weir load was increased to 0.0064 m^3/s m a significant increase in the violent action of the dispersion on the tray was observed with an increased dye travelling velocity from the inlet downcomer to the outlet weir . The dye at the central region of the tray was observed to reach the outlet weir in frame 3 (figure 8.3f) whilst a small amount of dye stayed longer at the circular side of the tray towards the outlet weir. Frames 4, 5 and 6 showed some dye present at the exit weir ends and no dye present at the central region.

At a weir load of 0.008 m^3/s m the same dye movement was observed for frame 1 to 5 figure 8.3g. Frame 6 showed that the entire tray active area was free of the dye tracer.

As the weir load was increased to 0.015 m^3/s m the dye tracer was observed to have channelled straight across the central region of the tray leaving very little dye at the outlet weir ends of tray (see figure 8.3h frame 1 to 4) . Frame 5 showed that the whole of the tray active area was free of the dye tracer.

A well defined agreement of the dye tracer studies with the temperature profiles was obtained and good visual information concerning the extent of liquid maldistribution on the tray when in cross flow with air was obtained from these experiments (see figure 8.3a - 8.3d and 8.3e - 8.3h).

However, the movement of the froth is indicated by the movement of the dye and this pattern of movement may be slightly different from the underlying liquid movement below the surface which was indicated by the temperature profile and clear liquid holdup.

8.4 A COMPARISON OF EXPERIMENTAL TEMPERATURE PROFILES WITH PROFILES PREDICTED FROM THE PORTER AND LOCKETT CHANNELLING THEORY

8.4.1 INTRODUCTION

The channelling model was used to compare the experimental data because this model compared well with the experimental data obtained from the (F.R.I) 1.2 m diameter column. The equations for the model were transformed to predict temperature profiles. The point efficiencies estimated using the water cooling technique were substituted into the channelling model for single pass trays to calculate the temperature flow patterns and the Murphree tray efficiency.

8.4.2 THEORY AND METHOD

The analogy between the processes of heat and mass transfer enables a conclusion to be made that the temperature profiles derived from a water cooling experiment will be similar to the concentration profiles of a mass transfer experiment.

In the mass transfer equations liquid phase concentration , x , is replaced by T the temperature of the liquid at a point on the tray and the vapour phase concentration, y , is replaced by H the enthalpy of the air stream passing through that point respectively.

Water cooling theory as applied to trays

The enthalpy of the air (H) is analogous to the vapour concentration (y) and the temperature of the water (T) is analogous to the liquid concentration (x).

The enthalpy of air saturated with water, H^* , in equilibrium with liquid of temperature, T , is given by the equilibrium line and the point efficiency can be rewritten as:

$$E_{og} = (H_2 - H_1) / (H^* - H_1) \qquad (8.4.1)$$

Water cooling analogy to Porter and Lockett channelling theory (Distillation)

Active Region 1

$$D_e[\, d^2x/dw^2 + d^2x/dz^2] - L/h_f\rho_l\rho_f\, dx/dz + (y_2-y_1)\, G/h_f\rho_f\rho_l = 0 \qquad (8.4.2)$$

Stagnant Region 2

$$D_e[\, d^2x/dw^2 + d^2x/dz^2] + (y_2-y_1)\, G/h_f\rho_f\rho_l = 0 \qquad (8.4.3)$$

Equation 8.4.2 and 8.4.3 can now be rewritten in terms of the water cooling analogy:

Water Cooling

Active Region 1

$$D_e[\, d^2T/dw^2 + d^2T/dz^2] - L/h_f\rho_l\rho_f\, dT/dz + (H_1-H_2)\, G/h_f\rho_f\rho_l = 0 \qquad (8.4.4)$$

Stagnant Region 2

$$D_e[\, d^2T/dw^2 + d^2T/dz^2] + (H_1-H_2)\, G/h_f\rho_f\rho_l = 0 \qquad (8.4.5)$$

Equations 8.4.4 & 8.4.5 were solved numerically by the finite difference method. The predicted temperature profiles are shown in figure(8.4a - 8.4d) using E_{og} calculated from 1 mm diameter hole tray data and in figure (8.4e - 8.4h) using E_{og} calculated from the 12.5 mm diameter hole tray data. A computer program written by **Lim et al** (44) was used to predict the temperature profiles and estimate the tray efficiencies.

8.4.3 DISCUSSION OF RESULTS

The experimental conditions and results from the 1mm and the 12.5 mm diameter hole trays were used in the prediction of temperature profiles using the **Porter** and **Lockett** model (54) as given by equations 8.4.4 and 8.4.5. In the model the concentration of the more volatile component in the liquid phase (x) had been replaced by the liquid temperature (T) and the concentration of the more volatile component in the vapour phase had been replaced by the vapour enthalpy (H). The **Porter** and **Lockett** model (54) is based on a large rectangular active area occupying a space equal to the width of the weir by the flow path length. The model also assumes a very much smaller stagnant zone where it is also assumed that no liquid flow occurs.

At the lowest liquid flowrate very flat parallel profiles in the transverse direction for all the active area of the tray were predicted by the model (see figures 8.4a and 8.4e).

At the edge of the tray, the temperature profiles became more "U"-shaped indicating very slow or zero movement of the liquid. As the liquid loading was increased (Figs (8.4b - 8.4d) and Figs (8.4f - 8.4h)), the profiles predicted by the model for the central active region of the tray were very similar with very flat parallel profiles in the transverse direction.

The **Porter** and **Lockett** model is based on the assumption that the active area and the recirculation areas are constant whilst the experimental data in Figures (7.4.3a - 7.4.3d) clearly indicated that the width, shape and position of both the mixing and recirculation zones were constantly changing. Also there were significant differences in the shape of the "U-shaped" profiles and this in some way was due to the fact that the model oversimplified the behaviour of the dispersion on the tray.

8.4.4 EFFICIENCY RESULTS

The experimental Murphree vapour efficiencies have been compared with efficiencies calculated from the plug flow model and the Porter & Lockett model (see Figs (8.4i & 8.4j) for plug flow using E_{og} from 1 mm hole tray and figure (8.4k & 8.4l) for plug flow using E_{og} from 12.5 mm hole tray and (see figures (8.4m & 8.4n) for **Porter** and **Lockett** model using E_{og} from the 1mm hole tray and figures (8.4o & 8.4p) for **Porter** and **Lockett** model using E_{og} from the 12.5 mm hole tray). The plotted results are given in Appendix (8), tables

(8.1 and 8.2) for the 12.5 mm and 1 mm diameter hole trays respectively.

At high liquid loadings the value of λ decreased towards zero and thus the process became gas film controlling. Thus in the plug flow model, the point efficiency tended to unity and also to the value of the Murphree vapour efficiency. In all cases a similar trend of decreasing Murphree vapour efficiency with increasing weir loading has been observed.

One important parameter in the air -water simulation technique is (λ), the ratio of the equilibrium line gradient to the operating line gradient. In conventional distillation, λ lies between 0.7 and 1.3 and often is assumed to be approximately equal to one. However in air water simulation, the value of λ can be varied over a very large range and in these experiments, λ was varied between 15 (corresponding to the spray regime) and approximately 1.0 (corresponding to the emulsified flow regime). Such variations of λ are due entirely to changes in the L/G ratio because for water cooling, the gradient of the saturation line (the "equilibrium line") remains almost constant. Hence, the very high E_{MV}/E_{OG} values which were obtained at very low weir loads and thus very high λ values, can be attributed to the effect of λ in the models.

8.5 REPEATABILITY OF TEMPERATURE MEASUREMENTS

Although the thermocouples were calibrated aganist a platinum resistance thermometer , errors in all the parameters being measured could occur and therefore an analysis was carried out to evaluate the significance of the error and repeatability on the temperature profiles.

Possible causes for non reproducibility of the experimental results are as follows:

(1) Faulty air and water measurement techniques.

(2) Errors in the measurements of the relative humidity (wet and dry bulb temperatures), and

(3) Movement of the tray deck which in effect will cause out of levelness.

It is assumed that all other errors associated with the devices are similar in magnitude for all the repeated experiments over a broad range of flow conditions covering all the flow regimes.

The experiments were repeated after the the tray was removed and later replaced again. Each of the experiments were repeated by choosing randomly the flow conditions covering the flow regimes. The procedure used was the same as that described in section 7.3 .

8.5.1 Interpretation of repeated experimental result

In section 7.3 , it has been mentioned that whilst it was possible to keep the inlet water temperature approximately constant during a particular experiment, it was not possible to set the inlet water temperature to the same repeated value for each experiment . Also the inlet air condition could be different for each experiment due to variations in the condition of the ambient air.

To over come these problems the temperature measurement results were normalised by the use of a reduced temperature T_R:

$$T_R = (T - T_{out})/(T_{in} - T_{out}) \qquad (8.5.1)$$

Thus in all the experiments, the reduced temperature at the inlet was automatically set to unity and all temperature measurements on the remainder of the tray were represented as a fraction. Thus the effect of the neighbouring points on the temperatures at any point would be the same over a repeated experiment.

The experiments were carried out under the same air capacity factors as in the main experiments (0.0605,0.0695 and 0.0851 m/s) with the weir loads chosen at random between 0.08×10^{-2} m^3/s m to 1.8×10^{-2} m^3/s m.

8.5.2 DISCUSSION OF RESULTS

Capacity factor (C_{sb}) of 0.0851m/s

At low liquid rates Figure(8.5.1a - 8.5.1d) the temperature profiles were similar to those in the main experiment (figure 7.5.6g). Generally there was good agreement between the profiles for the capacity factor of 0.0851 m^3/s m . The width of the central channelling region of the tray was slightly less in the repeated temperature profiles than in the main experiment.

Capacity factor (C_{sb}) of 0.0695 m/s

The repeated weir loads were 0.002 ,0.0048,0.0073 and 0.008 m^3/s m. The resulted temperature profiles are shown in figure (8.5.2a - 8.5.2d) and were predominantly U-shaped indicating the channelling of liquid through the central region of the tray. The repeated profiles have more defined axial constant temperature lines at the lower half of the tray emanating from the central sides of the tray to the inlet weir. There was better agreement between the profiles in the intense spray to the mixed flow regimes. In the emulsified regime the deviation was more significant and problems were encountered in preventing liquid drops from entering the air hygrometer. Any form of liquid weeping at the high weir load would affect the effective heat transfer rate on the tray because of the change in the inlet air humidity and therefore create a reduced driving force.

Capacity factor (C_{sb}) of 0.0605 m/s

The repeated experiments at this capacity factor were performed using weir loads of 0.0008 , 0.003 , 0.006 and 0.0128 m^3/s m. The temperature profiles in the repeated experiment (figure 8.5.3a - 8.5.3d) were found to be generally similar to those reported in chapter 7.5 . In the intense spray regime the severe U-shaped profiles were similar and as higher weir loads were investigated the profiles became more transverse in the inlet downcomer section of the tray with less channelling in the central region of the tray.

In the emulsified flow regime the same confused profiles were obtained showing the possible high percentage of temperature repeatability if the parameter recording device could be improved to a high degree of accuracy .

8.5.3 Point and Tray Efficiencies

The Point and Tray efficiencies calculated form the repeated experiments are shown in tables (8.5a , 8.5b and 8.5c). The computed Point and Tray Efficiencies for the repeated experiments lie within the same range as those reported for the initial experiments under the same operating conditions.

There is a minimum of 2% difference between the results and a maximum of about 25% difference for some of the results mostly in the emulsified flow regime. This is very much

lower tray due to the vibration caused by the pressure drop across the tray at such a high weir load. The difficulties in maintaining constant inlet water and inlet air temperatures constant for the initial and the repeated experiments explains the difference between the calculated point and tray efficiencies.

Table (8.5a) Reported(E_{og},E_{mv}) and Repeated(E_{og},E_{mv})$_{re}$ Point and Tray efficiencies.

Capacity Factor of 0.0605 m/s

Weir Load	E_{og}	$(E_{og})_{re}$	E_{mv}	$(E_{mv})_{re}$
0.0008	30.35	31.3	45.0	60.2
0.0024	51.2	63.3	70.9	82.4
0.004	46.1	57.1	70.7	70.2
0.00725	59.7	65.3	68.2	71.7
0.01128	63.0	46.3	46.4	65.8
0.0137	53.5	55.1	61.9	61.9

Table (8.5b) Capacity Factor of 0.0695 m/s

Weir load	E_{og}	$(E_{og})_{re}$	E_{mv}	$(E_{mv})_{re}$
0.0016	51.3	44.6	85.2	68.1
0.0032	70.4	55.9	105.4	73.5
0.006448	66.2	44.7	75.3	52.5
0.00806	56.4	67.4	58.0	76.0
0.0104	100.8	40.6	114.27	42.3
0.0137	78.0	59.4	84.1	60.2

Table (8.5c) Capacity Factor of 0.0851 m/s

Weir load	E_{og}	$(E_{og})_{re}$	E_{mv}	$(E_{mv})_{re}$
0.0008	28.4	28.8	51.7	60.2
0.0024	59.5	52.2	103.4	82.4
0.004	58.3	54.1	80.2	70.2
0.0056	63.7	53.5	84.0	62.1
0.008	64.3	46.9	77.4	47.9
0.00967	44.6	83.7	47.8	88.4
0.012	48.9	53.4	51.6	51.9

8.6 INVESTIGATION OF THE CONDUCTIVE HEAT TRANSFERRED THROUGH THE METAL TEST TRAYS AND THE COLUMN WALL

8.6.1 INTRODUCTION

One important assumption made in the development of this technique has been that heat losses through the column wall and the metal tray would be negligible as the wall and the metal tray will come to a state of equilibrium after steady state has been reached.

Heat transfer through the wall has been proved by **Enjugu** (18) to depend significantly on the material of construction, Thus, using a perspex column should minimise heat losses through the column wall.

To assess the effect of heat losses , a hypothetical elemental strip of froth was considered through which the heat transferred by the vapour passage is equivalent to the total quantity of heat transferred through the colum wall.

The fraction of the tray occupied by the "strip" was considered to be directly proportional to the fraction of heat loss from the strip compared to the tray. A heat balance by **Enjugu** (18) over an element of the froth including the section of the column wall adjacent to the froth showed that under the worst and least probable conditions, the heat transferred through the

wall was less than 10 % (see figure 8.6).

The parameters used in the calculations by **Enjugu** (18) were all assumed and thus a further examination of this phenomena will be carried out to assess the importance or otherwise of the phenomena.

8.6.2 Calculations and Estimation of Parameters

Basic Assumptions

(1) Uniform temperature throughout the froth within the strip.

(2) Negligible heat transfer to the column wall by conduction through the edge of the tray.

(3) Uniform enthalpy of the air entering the tray and

(4) Heat loss in the direction of the plane.

Model equation for air

$$Q_{air} = A_s G\, dH \qquad (8.6.1)$$

Where G = Flow per unit area of tray $kg/m^2 s$
Overall heat balance through the element yields:

$$L_1 C\, \theta = G\, dH \qquad (8.6.2)$$

L_1 = Liquid flow rate per unit area of the tray ($kg/m^2.s$)
For a unit length the area of the strip is given as:

$$A_s = 1.0 * X \qquad (8.6.3)$$

Where X is the thickness of the strip

Heat transfer through column wall is given as

$$q_{wall} = k / t_{wall} (\theta_w - \theta_{air}) \qquad (8.6.4)$$

t_{wall} = wall thickness m

k = thermal conductivity kJ / s m K

Combining equation (8.6.1) and (8.6.4)

$$k\,[(\theta_w - \theta_{air})] / t_{wall} = A_s\, G\, d\, H \qquad (8.6.5)$$

$$A_s = k/(G.dH) * [(\theta_w - \theta_{air})/ t_{wall}]$$

Limiting solution

The maximum value of X is evaluated by considering the highest possible difference in the value of $(\theta_w - \theta_{air})$ and the lowest values of L, C,and T possible in this work.

The air temperature outside the column wall is minimum at the room temperature (θ_{air} = 23°C).

A maximum of 12°C temperature drop was achieved across the trays during the experiments.The temperature gradient varied from point to point on the tray. The inlet water temperature was approximately constant at 40°C,but due to liquid recirculation and stagnant regions near to the column wall, the liquid temperature around the column wall was considerably less than the inlet water temperature.

The average wall temperature at low liquid rate was (θ_w = 29°C) and this is equivalent to the water temperature in the immediate vicinity of the wall. For the spray and mixed flow regimes the value of θ_w can drop to about 25°C.

Hence the highest possible temperature difference is given by:

$$\theta_w - \theta_{air} = 29 - 23 = 6^oC$$

For the mixed regime:

$$L_1 .C = (\text{low flow rate kg/m}^2\text{ s}) \qquad (8.6.6)$$

$$= 0.005 * 4.2 = 0.021$$

consider an average case:

t_{wall} =wall thickness = 0.003m (1/8")

k_{pers} = 7.5 E-8 kJ/s m K

$$X = [k_{pers}/G.H] * [(\theta_w - \theta_{air})/ t_{wall}$$

$$= [(k_{pers}/L C_p \theta) * (q_w - q_{air}) / t_{wall}$$

$$= [(7.5 \times 10\text{-}8 /0.021 *2) * (6/0.003)$$

$$= 0.0035 \text{ m}$$

$$= 3.5 \text{ mm}$$

Under the worst and least probable operating conditions heat transferred through the column wall (perspex) is under 5 % of the total heat loss through the vapour.

8.7 Comparison of temperature profiles for the perspex tray and that of the metal tray.

The investigation was carried out under the highest capacity factor used in this work (0.0851 m/s) with an increasing weir load of 0.0008 to 0.008 m^3/s m with incremental changes of 0.0008 m^3/s m for each run. The individual temperature measurements are given in Appendix (10) .

The temperature profiles (Figures(8.6.1a - 8.6.1d)) were found to be predominantly in the transverse direction without any liquid recirculation regions on the tray. Although some U-shaped profiles are indicated, constant temperature lines run across the tray width for most of the tray.

At low liquid rates the temperature profiles were slightly U-shaped but in the transverse direction and these were different from the severe U-shaped profiles obtained for the metal tray (figure (7.5.2a)). The developed profiles were similar to those obtained for the metal tray whilst operating in the mixed flow regime.

Visually the perspex tray floor was covered by a liquid film while for the same operating conditions the liquid was completely blown of the tray floor into the space above the tray in form of fine spray of liquid. The perspex tray was operated at conditions below the weeping curve but no weeping was observed. This observation could be explained by the effect of wetting of water on the polished surface of the perspex.

As the weir load was increased to the operating conditions for a mixed regime (figure 8.6.1c) the profiles remained in the transverse direction with less U-shaped profiles . The profiles were completely in agreement with the metal tray temperature profiles. The general agreement in the temperature profiles support the assumption that heat losses were not important in the develoment of the water cooling theory, thus at steady state the temperature of the tray will reach an equilibrium state with the liquid and at this state the temperature of the tray will be the same as that of the water on it at any vicinity within the tray active area.

The result for the operating conditions figure (8.6.1d) show irregular U-shaped temperature profiles at both sides of the tray , with liquid retrograde flow at the central region of the tray. The only explanation for the developed constant temperature lines could be the deflection of the relatively weaker perspex tray at the high liquid loading since the the perspex tray was the same thickness as the metal trays.

8.7.1 CONCLUSION

The perspex tray temperature profiles are similar to those obtained for the 12.5mm diameter hole metal tray (figure(7.5.2a - 7.5.6i)). However the different wetting effect of water on perspex resulted in different profiles being obtained for the intense spray regime and the emulsified flow regime. Similar calculated efficiencies for the metal tray and the perspex tray were obtained. Therefore in the development of the water cooling technique, the problem of heat losses can be neglected.

8.8 ERRORS ANALYSIS IN THE EFFICIENCY MODEL

8.8.1 INTRODUCTION

The objective of this part of the research programme is to assess the errors in the point efficiency associated with the collection and processing of the experimental data.

8.8.2 Point Efficiency Model

The point efficiency E_{og} is defined as :

$$\text{Point Efficiency, } E_{og} = (H_{out} - H_{in}) / (H^* - H_{in}) \qquad (8.8.1)$$

The point efficiency is calculated using the intermediate values, H_{out}, H_{in} and H^*. These values are shown in their more fundamental form.

$$H_{out} = [L C_p / G] (T_{in} - T_{out}) + H_{in} \qquad (8.8.2)$$

$$H^* = (C_A * T_{av}) + H_{av} ((C_w * T_{av}) + \lambda) \qquad (8.8.3)$$

$$H_{in} = (C_A * T_{wb}) + H_{wb} ((C_w * T_{wb}) + \lambda) \qquad (8.8.4)$$

Note : 0^oC is the datum temperature.

λ is the Latent heat of vaporisation kJ/kg

Basis of Error Analysis

An associated error, e, should always be equated with a value E because there is already a degree of uncertainty about the value due to the scale not having an infinite number of markings. These errors can be combined in the calculation as follows :

Let

$Q = f(x)$ and $Z = g(a,b,c)$

Suppose x is a measured quantity and Q is the quantity calculated from the formula, $Q = f(x)$.

If the error in x is dx, the corresponding error in y is dy where.

$$\lim_{dx \to 0} \; dy/dx = dy/dx \quad \text{or} \quad dy/dx = dy/dx \text{ for small } dx$$

From this definition, clearly the error in y, dy, can be computed. Expanding this idea, the following relationship appears.

$$dx = (dz/da)\, da + (dz/db)\, db + (dz/dc)\, dc \qquad (8.8.5)$$

The first term is the error in Z due to an error in x only.
This is known as the Principle of Superposition of Errors. If da , db and dc are independent random errors in the ranges , -a to a , -b to b and -c to c respectively then the most probable error ,dz in z is given by.

$$(dz)^2 = \left(\frac{dz}{da}\, da\right)^2 + \left(\frac{dz}{db}\, db\right)^2 + \left(\frac{dz}{dc}\, dc\right)^2 \qquad (8.8.6)$$

This is the basis of all the error analyses carried out in this study and has been used in the development of the computer program used to solve for errors in the efficiency.

Fundamental Measurements And Errors

There are three main measurements to be made: (a) liquid flow, (b) gas flow and (c) temperature.

Temperature

Thermocouples were used to measure the water inlet and outlet temperatures and a thermocouple grid gave the temperatures on the tray, which were used to generate an average tray temperature and associated error. The accuracy of the thermocouples were stated to be + $0.1^{o}C$ at the operating temperature of 30 - $40^{o}C$. Another thermocouple was used to determine the wet bulb temperature of the entering air, but the technique was not reliable and so the error associated with the air inlet enthalpy was assigned manually.

Liquid Flow

Three rotameters were used to measure the liquid flow over the operating range. The ranges measured were 0 - 40, 40 - 200 and 200 - 1000 gallons/min. The error in reading a rotameter is quarter the difference between two adjacent markings, if it can be seen that a middle point exists between the two markings.

The reading errors are therefore, ± 0.5 ,± 2.5 and ± 12.5 gal/min for the rotameters, respectively.

Gas Flow

A correlation was made between the gas superficial velocity(based on the bubbling area) and the pressure drop measured by a water manometer connected to a pitot tube. The reading error in the manometer could be assigned on to the gas superficial velocity by use of the gradient of the correlation equation. The error in the manometer reading was ± 0.005 inches of water.

Non-Variable Values And Errors

The diameter of the tray, although non-variable, was measured to an accuracy of ± 0.001 m, this affects the bubbling area computed value. All other non-variable values and errors are given in table 8.8a.

Table (8.8a) Errors asigned to non-variable values

Parameter	Value	Error
Tray Diameter (m)	1.2	± 0.001
Water Density (kg/m^3)	1000	± 3
Air Density (kg/m^3)	1.22	± 0.05
Specific Heat of Water(kJ/kg K)	4.18	± 0.005
Specific Heat Of Water Vapour (kJ/kg K)	2.006	± 0.0005
Specific Heat Of Air (kJ / kg K)	1.003	± 0.0005
Latent Heat Of Water (kJ / kg)	2495	± 0.5

Source Data

The raw data was taken from the results of experimental runs which had been stored in a data file.

Discussion Of Results

The results (table 8.8b) show that the mean average, expressed as a percentage of the mean average point efficiency is, 6.27%. The error was inherrent from the accuracy of the flow measuring equipment and the thermocouples.

Columns 1,2,3 and 4 give mean average errors for changed accuracies of the different measured variables. Both flows were measured to $\pm$ 0.5 % and the temperature measurement accuracy was increased to $\pm$ 0.05^{o}C , $\pm$ 0.02^{o}C and $\pm$ 0.01^{o}C

The mean average errors, which are comparable to the above result, decreased from $\pm$4.3 % , $\pm$ 4.21 % and $\pm$ 4.19 % as the accuracy of temperature measurement increased.

Superficially, these improved accuracy measurements give only a marginal decrease in the associated point efficiency error. The most interesting point is with the standard deviations of the four results- see table (8.8b). The standard deviations of the average error in the point efficiency, are 0.638 , 0.104, 0.018 and 0.003.

This shows that the error in the average point efficiency converges as the temperature measurement accuracy increases.

Conclusions

The error in the average point efficiency , expressed as a percentage, was approximately 6.3%. In order to reduce this error, it is suggested that the following accuracies in measurement be achieved.

Water Flow	$\pm$ 0.5%
Gas Flow	$\pm$ 0.5%
Temperature Measurement	$\pm$ 0.02%

This should reduce the calculated error to an experimentally acceptable level of 4.2%.

Table (8.8b) Computed results

Parameter	Error	Error	Error	Error
Water flowrate(gal/min)	± 0.5,3.0,15.5	± 0.5	± 0.5	± 0.5
Air flowrate (m/s)	As seen	± 0.5	± 0.5	± 0.5
Air inlet Enthalpy(kJ/kg)	± 0.1	± 0.1	± 0.1	± 0.1
Temperature (^{o}C)	± 0.1	± 0.05	± 0.02	± 0.01
Average Point Efficiency %	± 6.27	± 4.34	± 4.21	± 4.19
Standard Deviation	0.638	0.104	0.018	0.003
Column	1	2	3	4

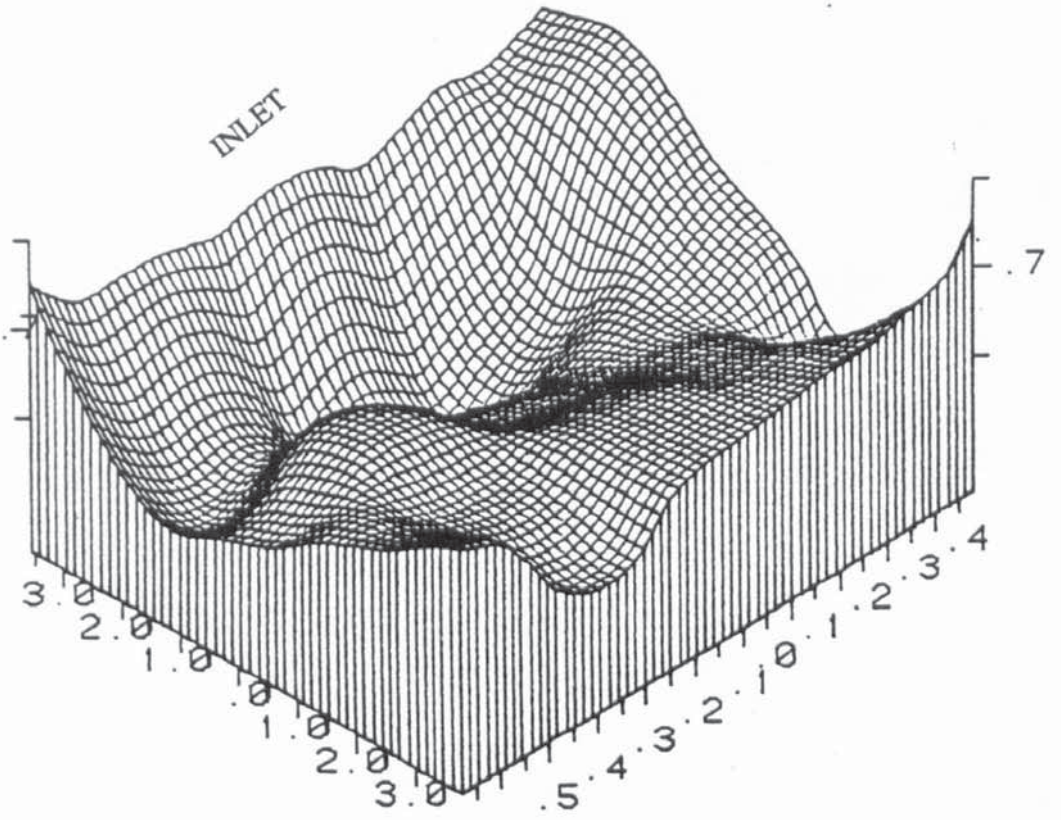

Figure (8a) Best surface of Clear Liquid Hold-Up on 4.5 mm diameter holes tray
weir load (q/b) = 0.0016 m^3/s.m : C_{sb} = 0.049 m/s

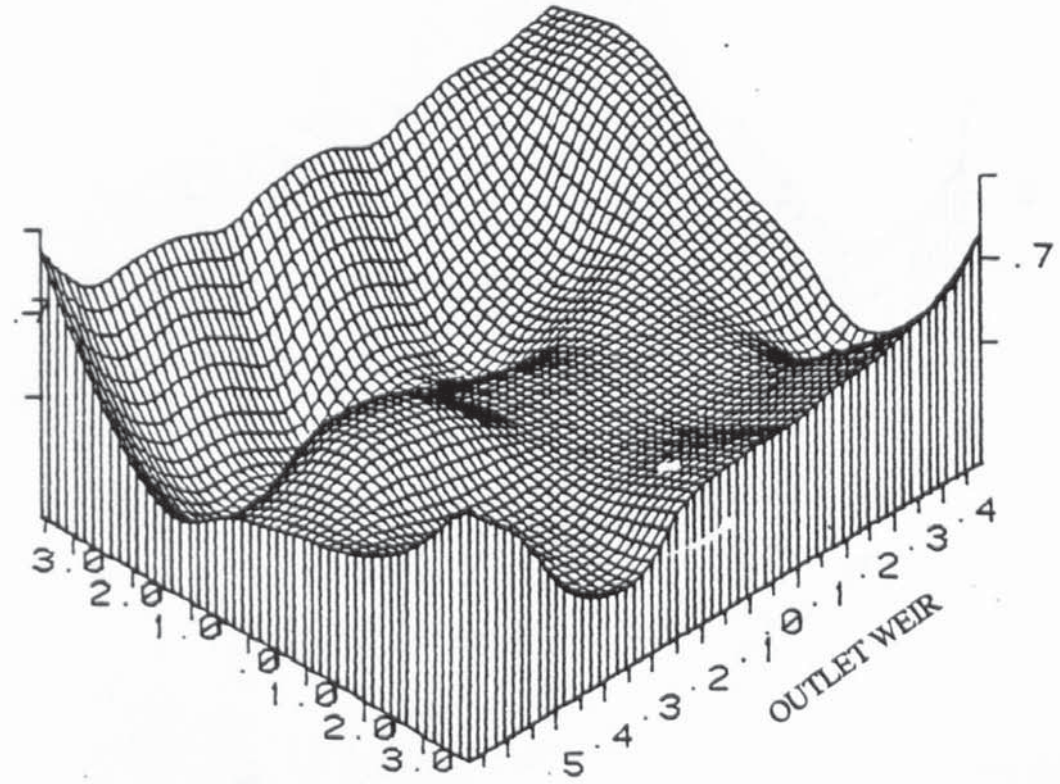

Figure (8b) Best surface of Clear Liquid Hold-Up on 4.5 mm diameter holes tray
weir load (q/b) = 0.0024m^3/s.m : C_{sb} = 0.049 m/s

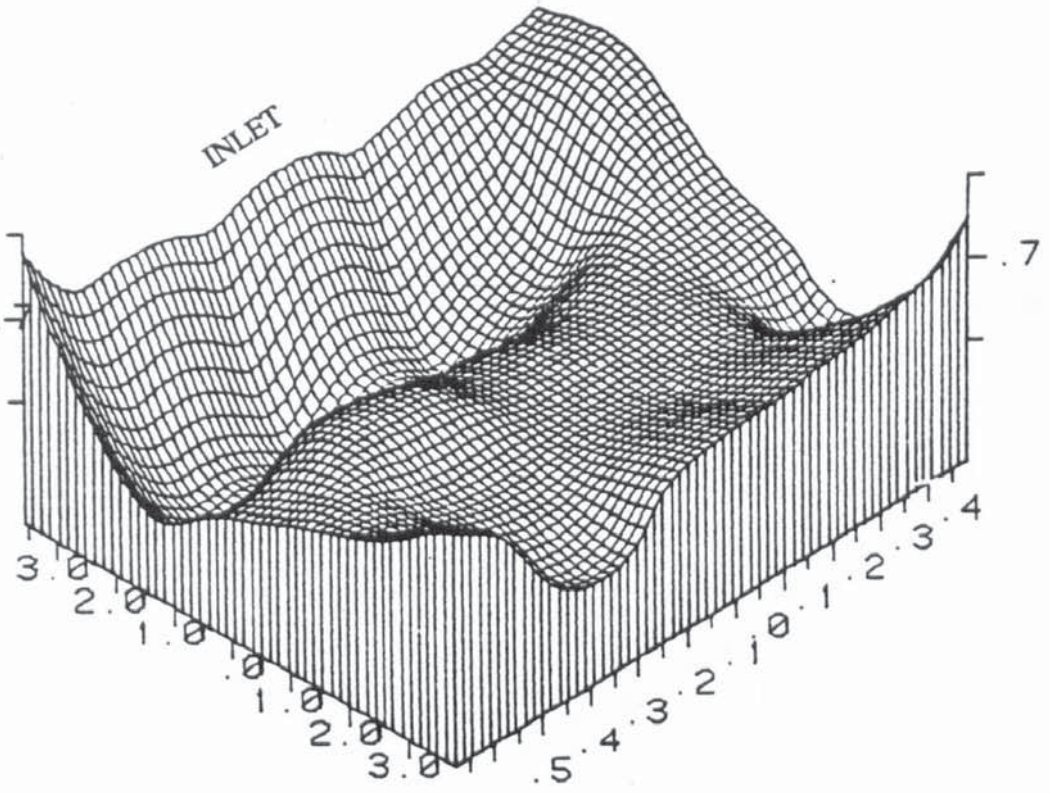

Figure (8c) Best surface of Clear Liquid Hold-Up on 4.5 mm diameter holes tray
weir load (q/b) = 0.0032 m^3/s.m : C_{sb} = 0.049 m/s

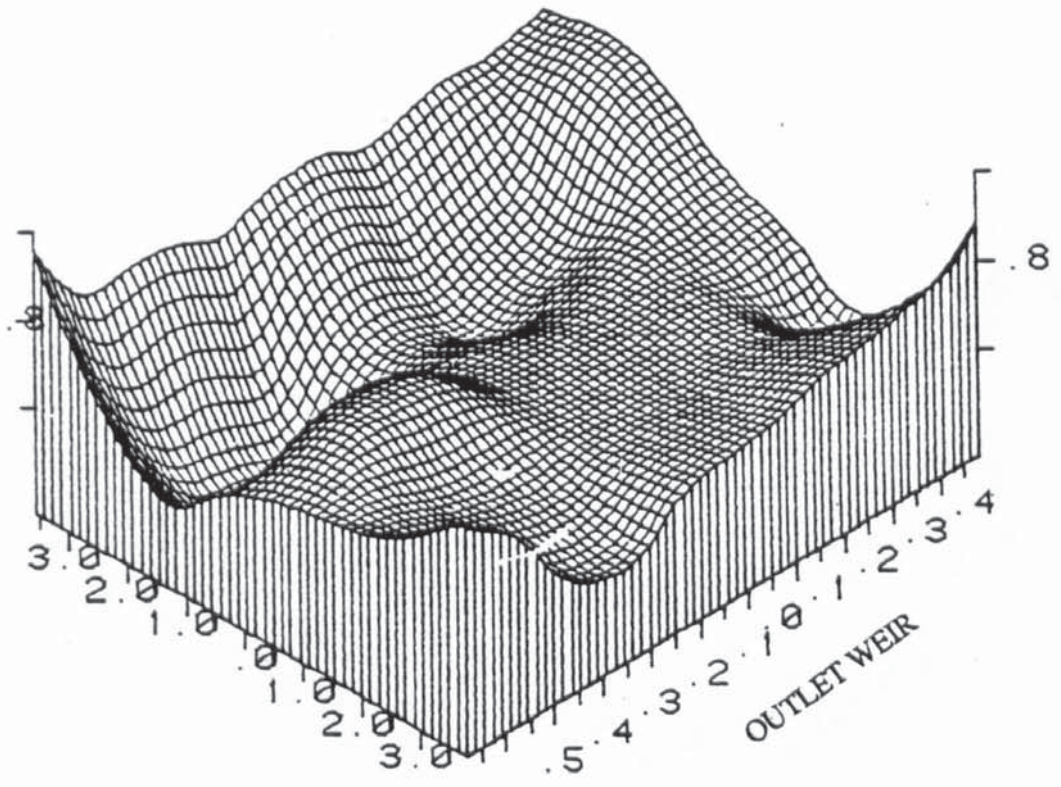

Figure (8d) Best surface of Clear Liquid Hold-Up on 4.5 mm diameter holes tray
weir load (q/b) = 0.0048 m^3/s.m : C_{sb} = 0.049 m/s

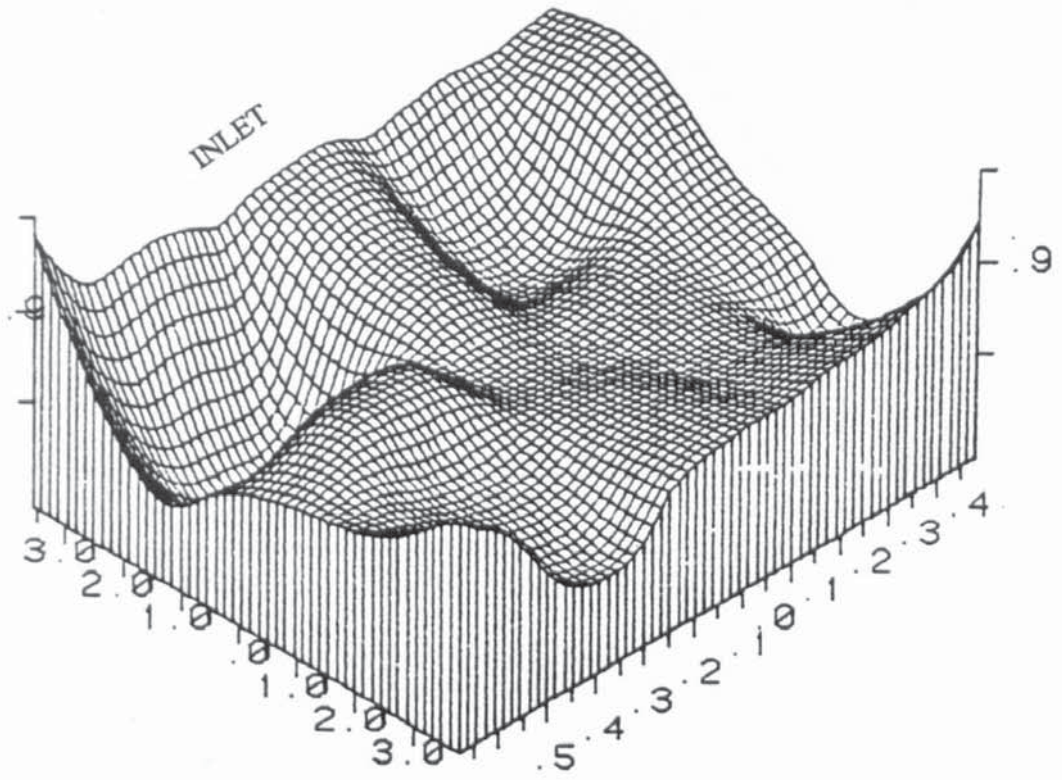

Figure (8e) Best surface of Clear Liquid Hold-Up on 4.5 mm diameter holes tray
weir load (q/b) = 0.0056 m^3/s.m : C_{sb} = 0.049 m/s

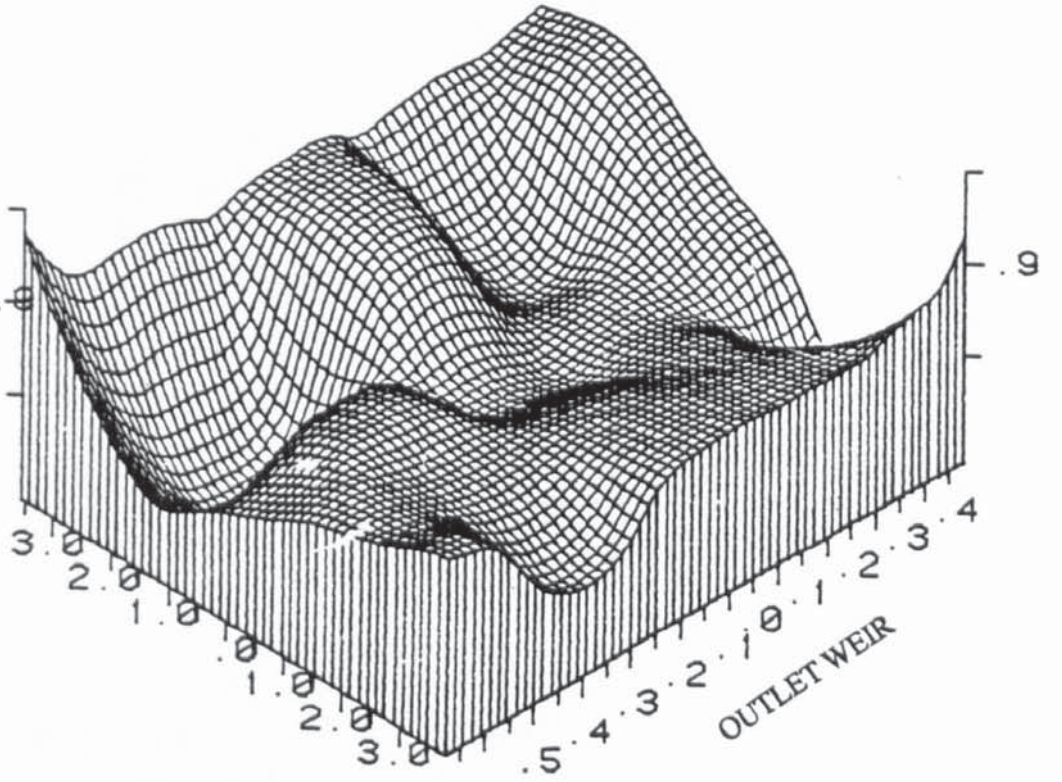

Figure (8f) Best surface of Clear Liquid Hold-Up on 4.5 mm diameter holes tray
weir load (q/b) = 0.0064 m^3/s.m : C_{sb} = 0.049 m/s

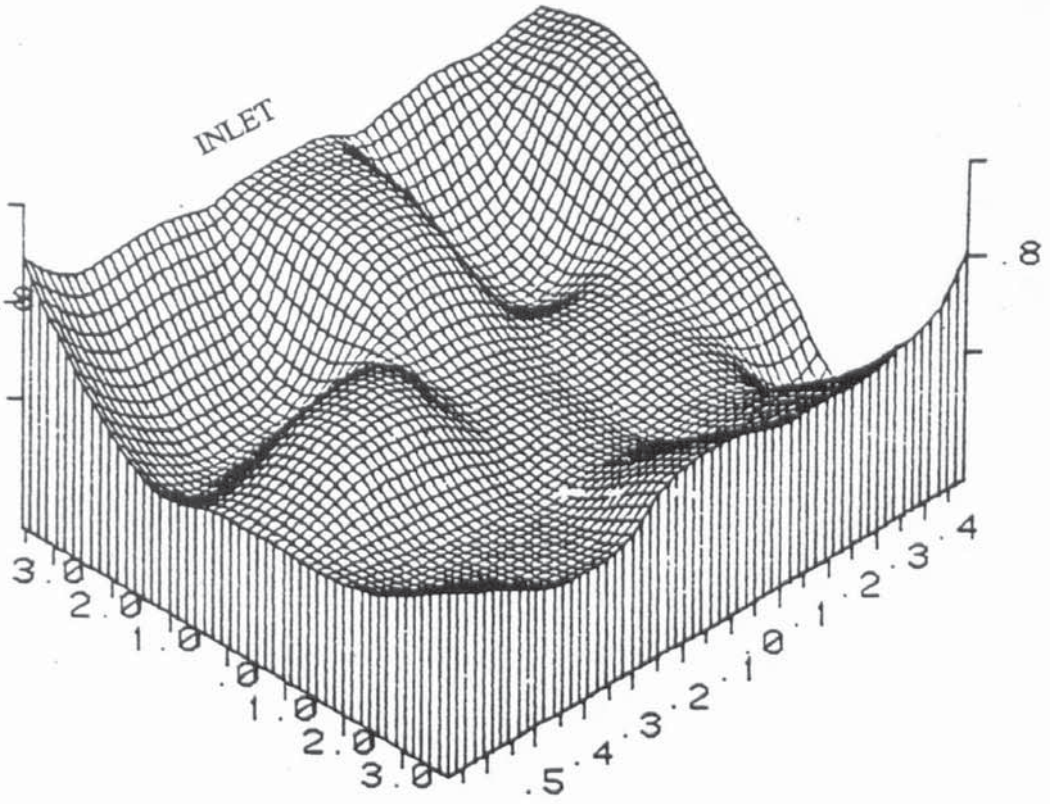

Figure (8g) Best surface of Clear Liquid Hold-Up on 4.5 mm diameter holes tray weir load (q/b) = 0.008 m^3/s.m : C_{sb} = 0.049 m/s

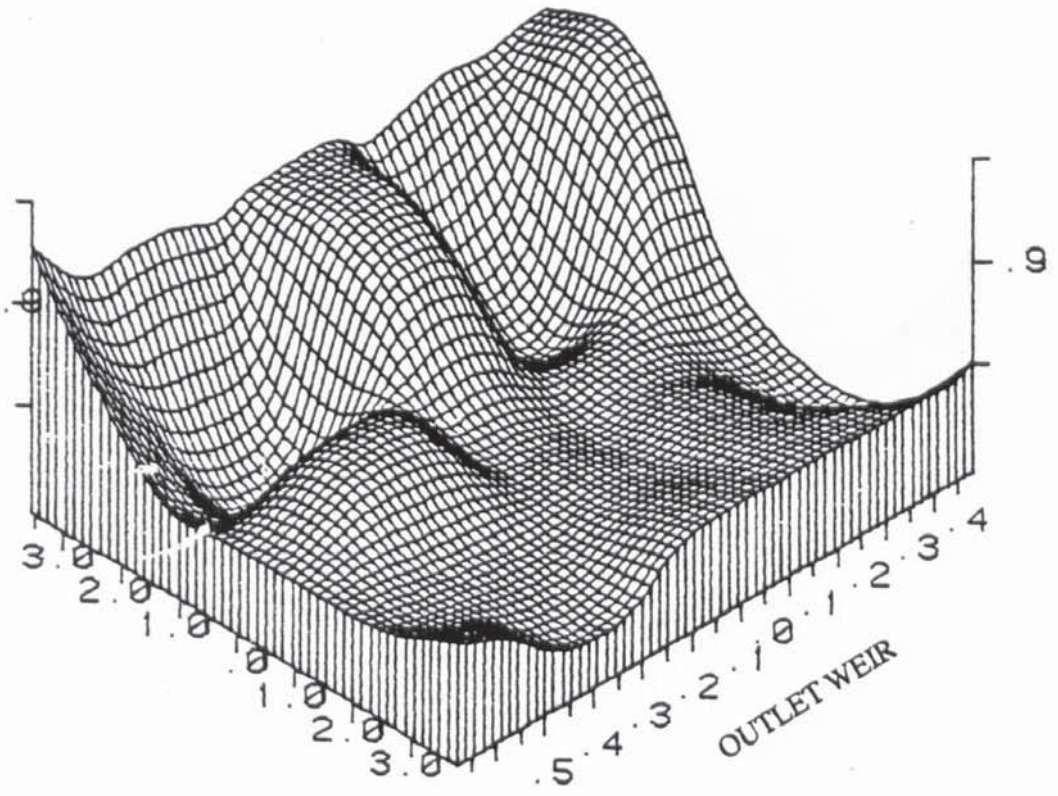

Figure (8h) Best surface of Clear Liquid Hold-Up on 4.5 mm diameter holes tray weir load (q/b) = 0.0016 m^3/s.m : C_{sb} = 0.0605 m/s

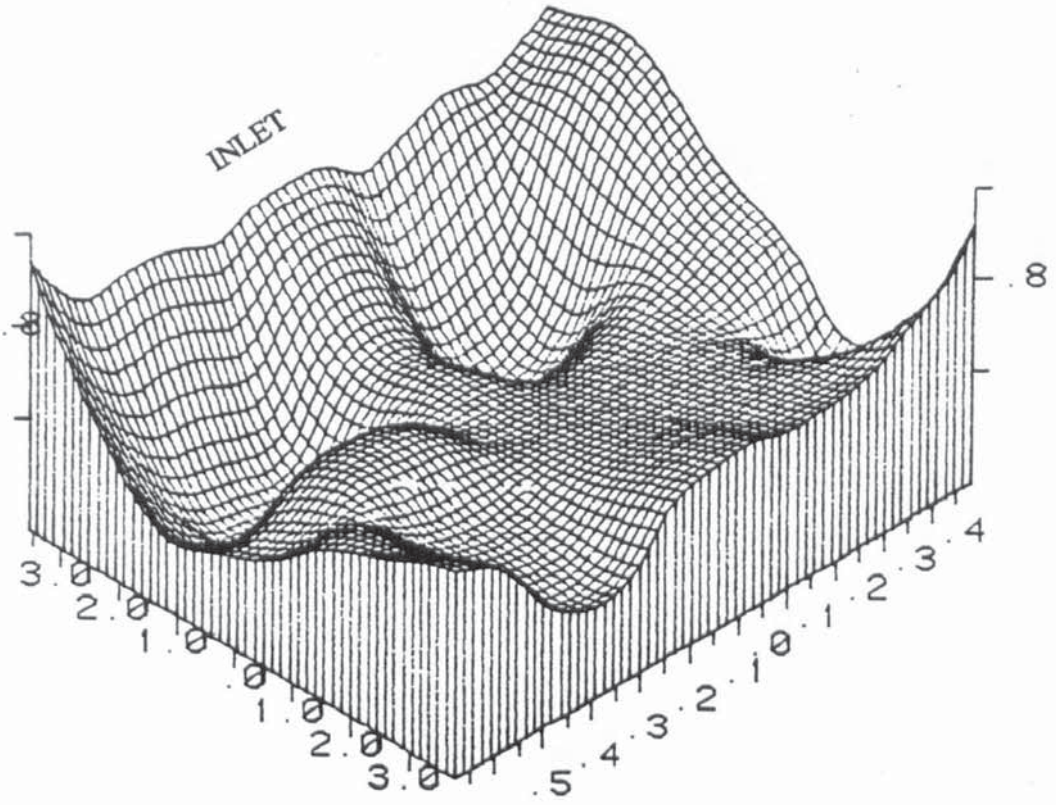

Figure (8i) Best surface of Clear Liquid Hold-Up on 4.5 mm diameter holes tray
weir load (q/b) = 0.0024m^3/s.m : C_{sb} = 0.0605 m/s

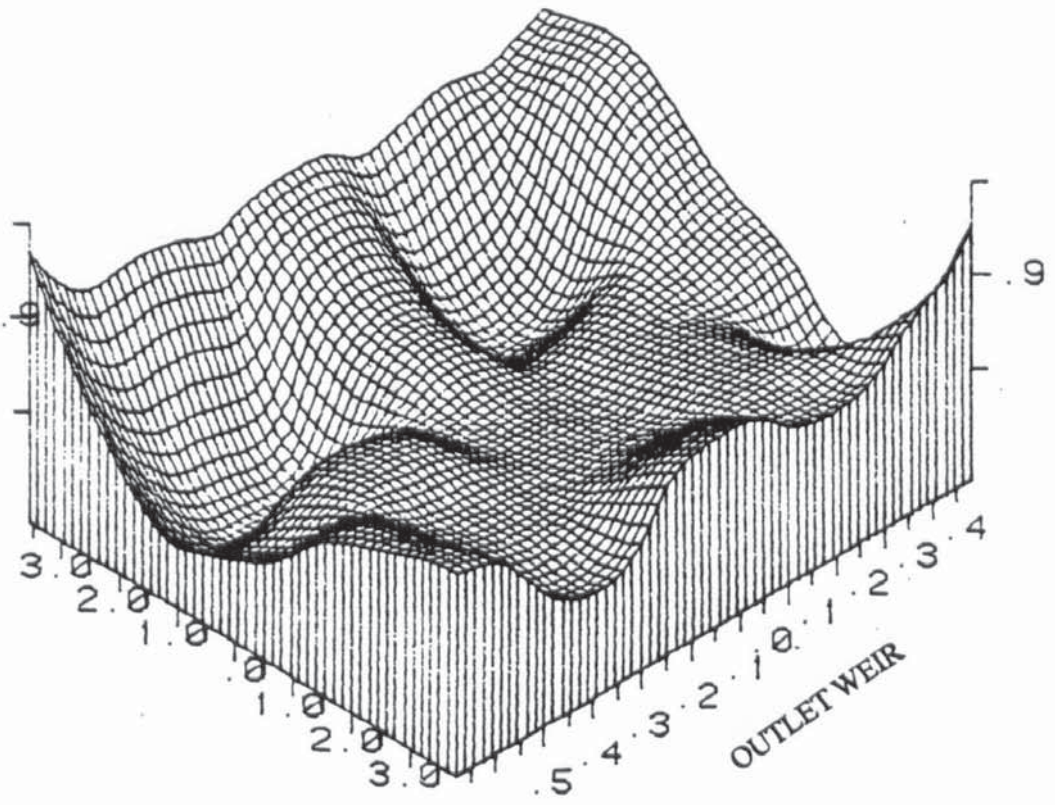

Figure (8j) Best surface of Clear Liquid Hold-Up on 4.5 mm diameter holes tray
weir load (q/b) = 0.0032 m^3/s.m : C_{sb} = 0.0605 m/s

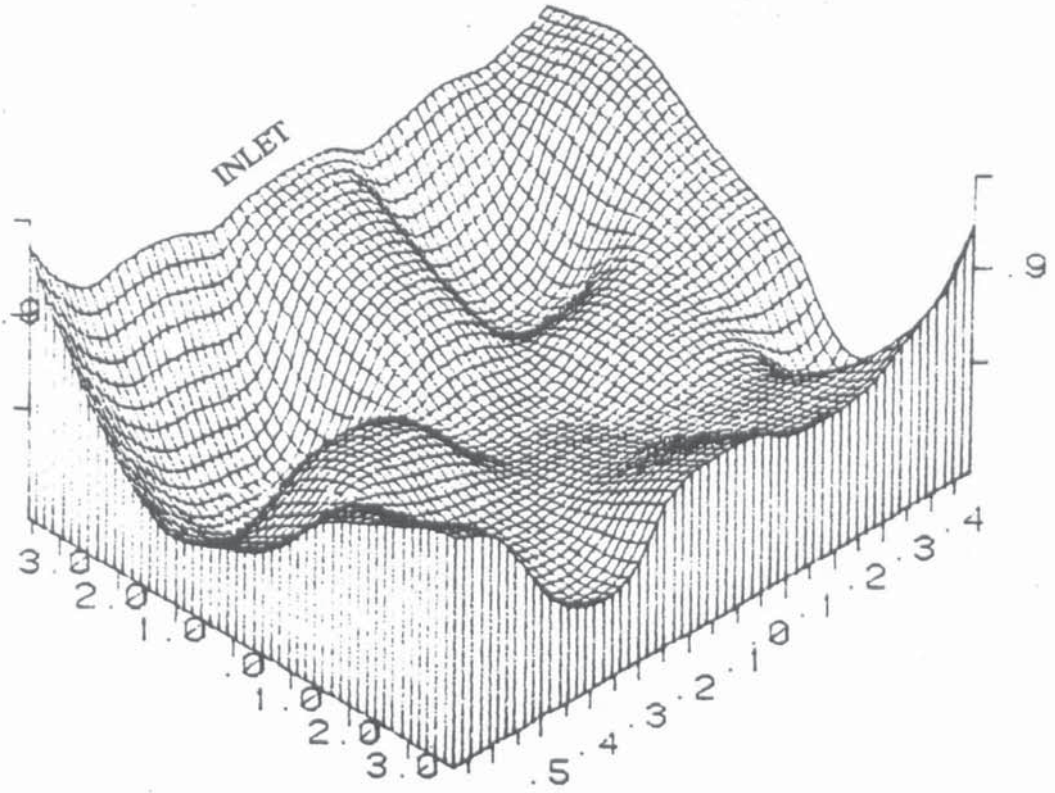

Figure (8k) Best surface of Clear Liquid Hold-Up on 4.5 mm diameter holes tray
weir load (q/b) = 0.0040 m^3/s.m : C_{sb} = 0.0605 m/s

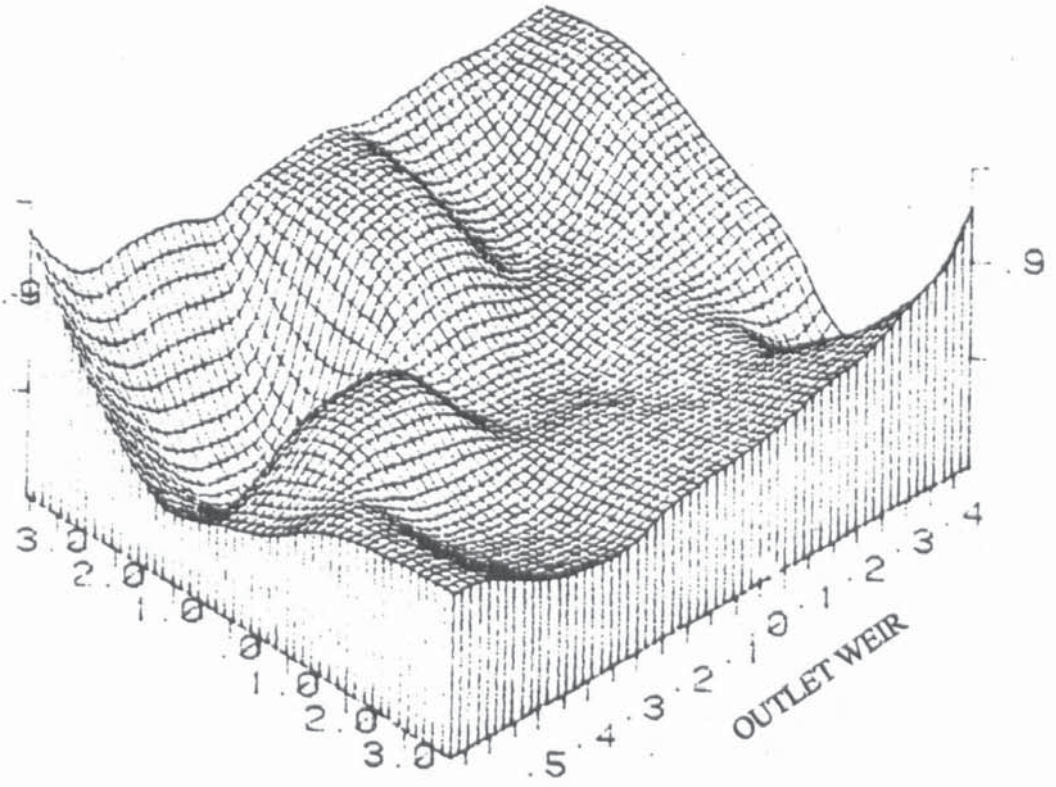

Figure (8l) Best surface of Clear Liquid Hold-Up on 4.5 mm diameter holes tray
weir load (q/b) = 0.0048m^3/s.m : C_{sb} = 0.0605 m/s

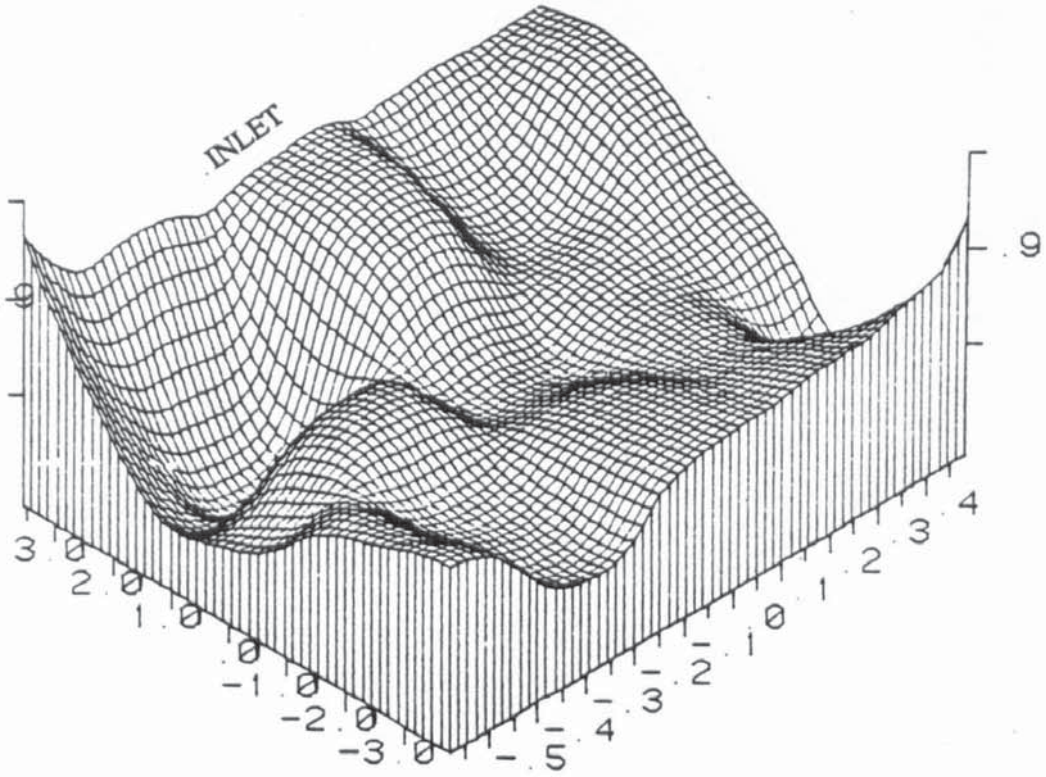

Figure (8m) Best surface of Clear Liquid Hold-Up on 4.5 mm diameter holes tray
weir load (q/b) = 0.0056 m^3/s.m : C_{sb} = 0.0605 m/s

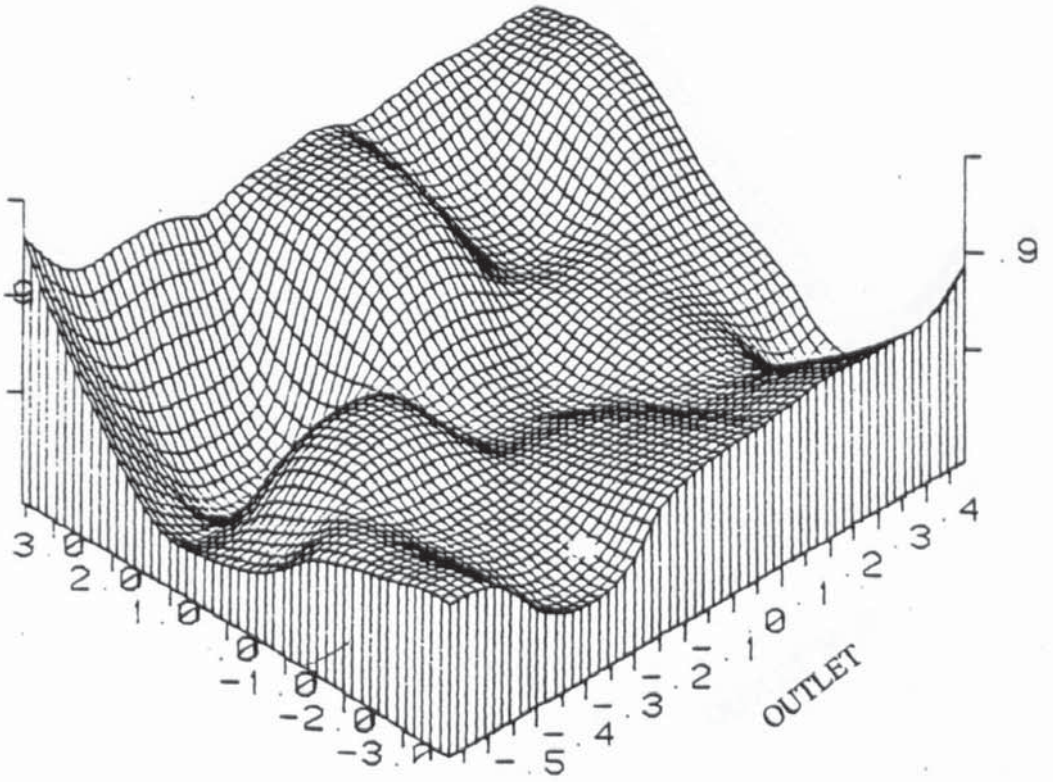

Figure (8n) Best surface of Clear Liquid Hold-Up on 4.5 mm diameter holes tray
weir load (q/b) = 0.0072 m^3/s.m : C_{sb} = 0.0605 m/s

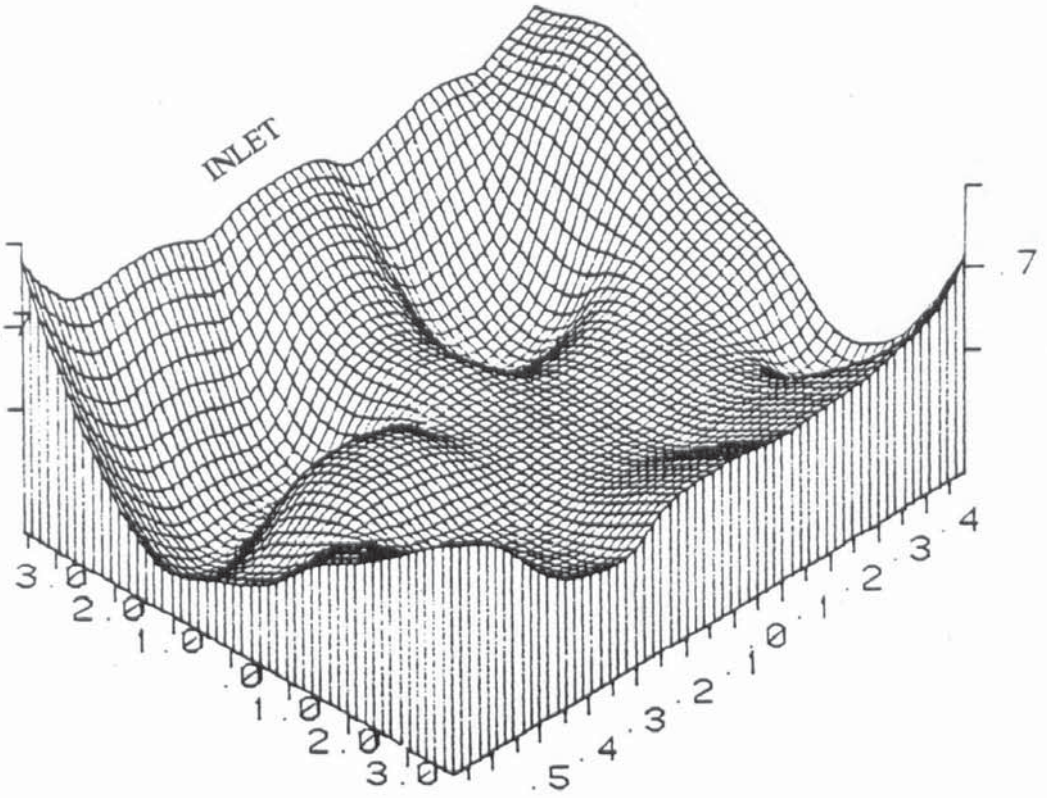

Figure (8o) Best surface of Clear Liquid Hold-Up on 4.5 mm diameter holes tray
weir load (q/b) = 0.0016 m^3/s.m : C_{sb} = 0.0695 m/s

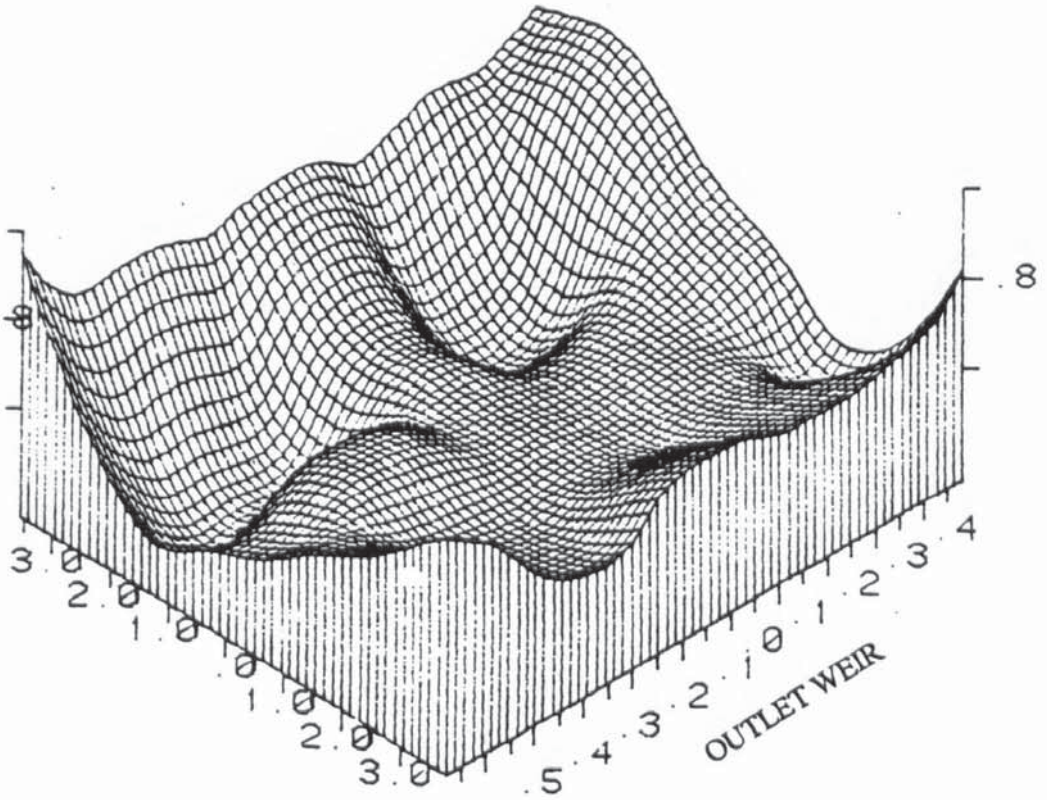

Figure (8p) Best surface of Clear Liquid Hold-Up on 4.5 mm diameter holes tray
weir load (q/b) = 0.0024m^3/s.m : C_{sb} = 0.0695 m/s

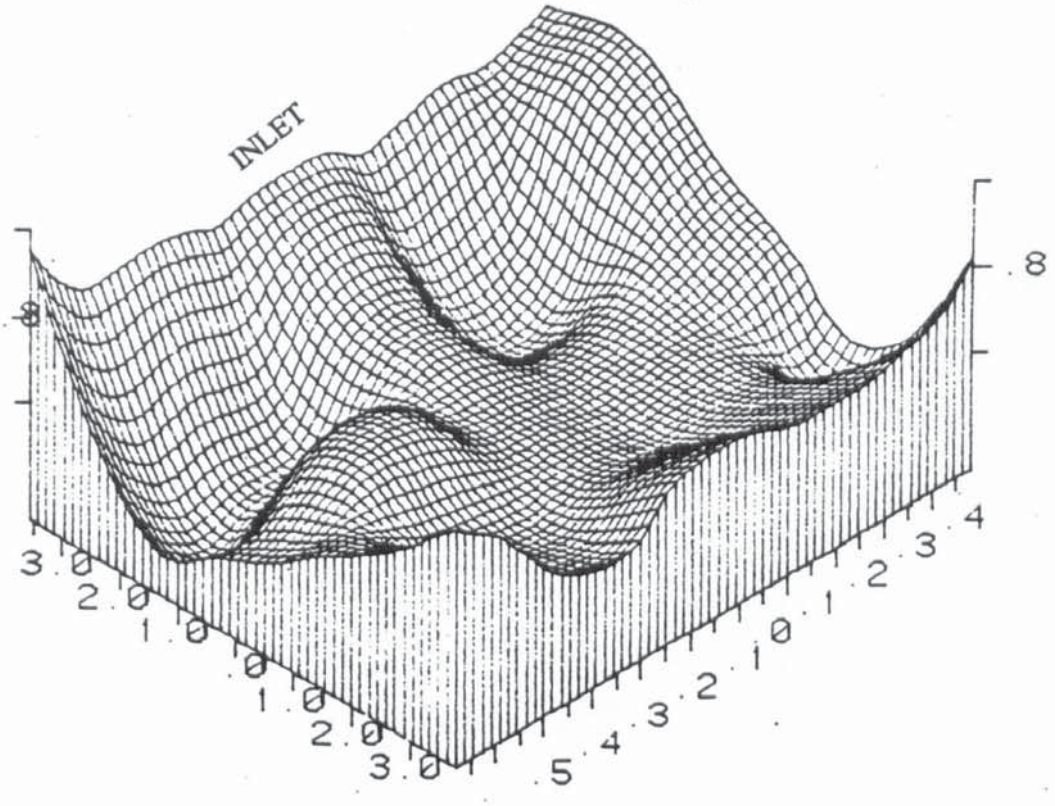

Figure (8q) Best surface of Clear Liquid Hold-Up on 4.5 mm diameter holes tray
weir load (q/b) = 0.0032 m^3/s.m : C_{sb} = 0.0695 m/s

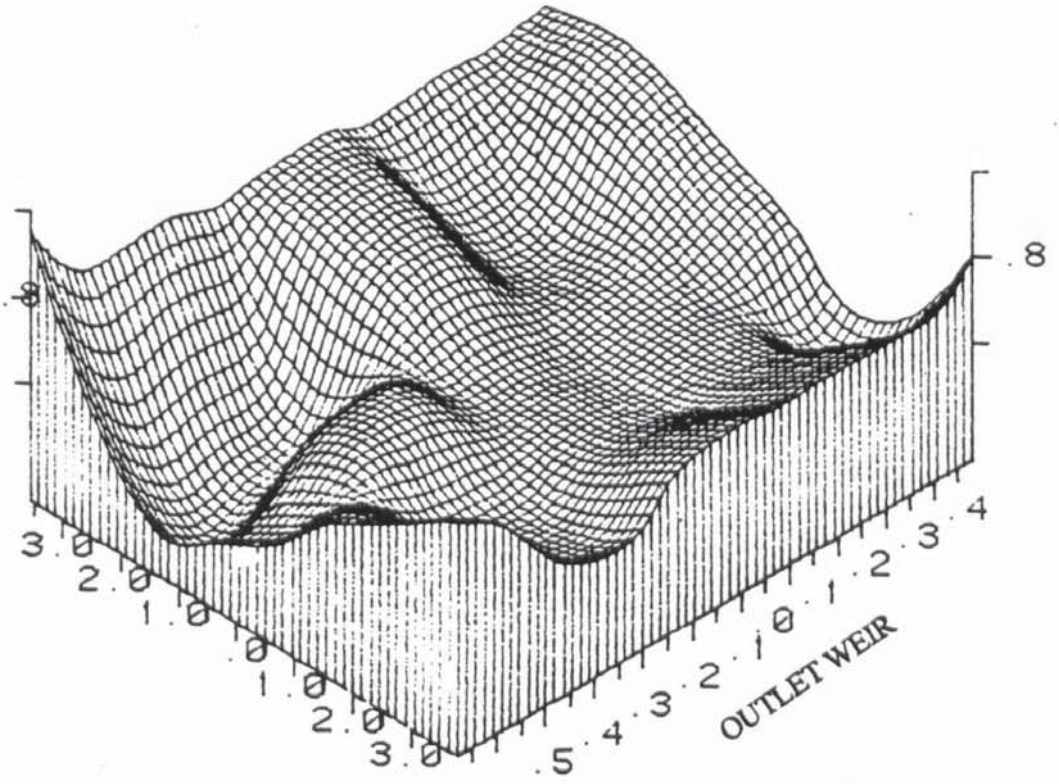

Figure (8r) Best surface of Clear Liquid Hold-Up on 4.5 mm diameter holes tray
weir load (q/b) = 0.0048 m^3/s.m : C_{sb} = 0.0695 m/s

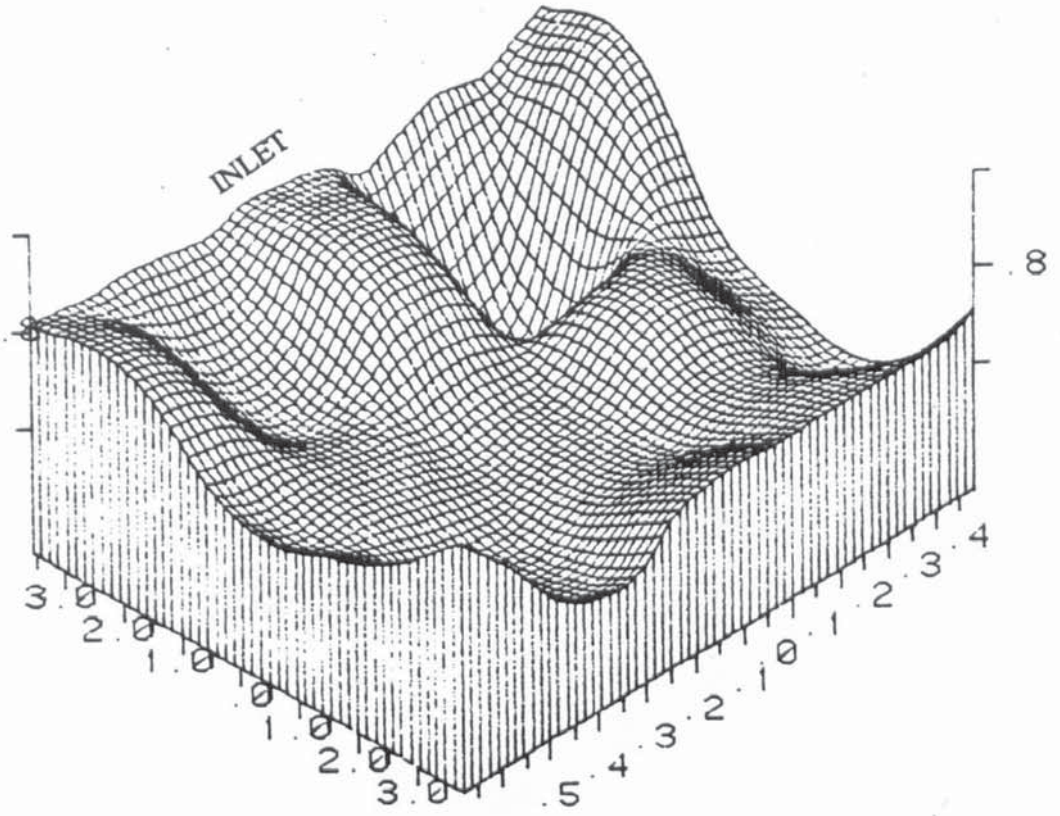

Figure (8s) Best surface of Clear Liquid Hold-Up on 4.5 mm diameter holes tray
weir load (q/b) = 0.0056 m^3/s.m : C_{sb} = 0.0695 m/s

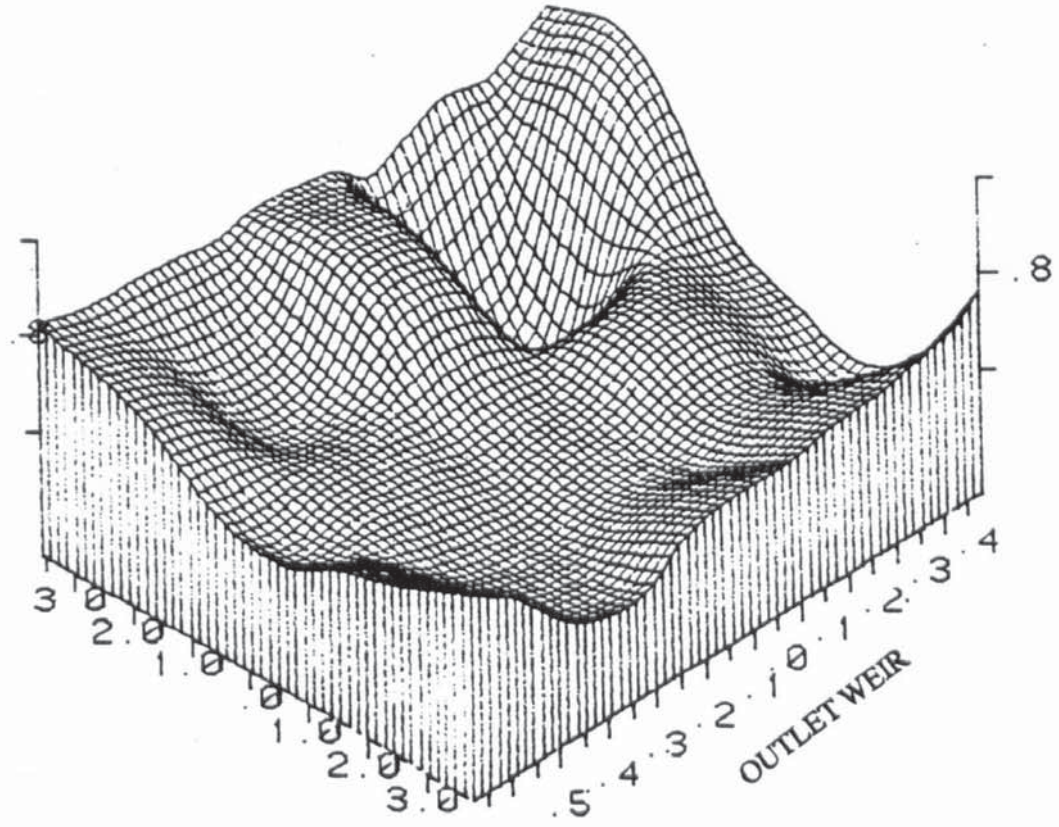

Figure (8t) Best surface of Clear Liquid Hold-Up on 4.5 mm diameter holes tray
weir load (q/b) = 0.0064 m^3/s.m : C_{sb} = 0.0695 m/s

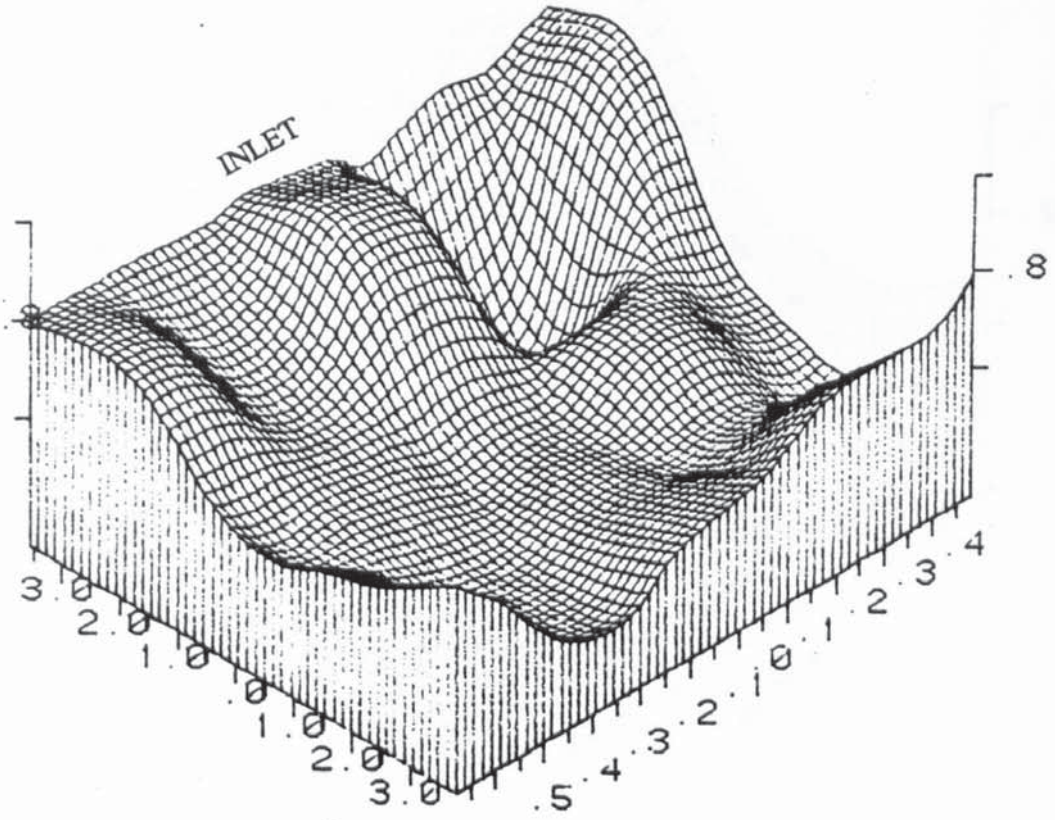

Figure (8u) Best surface of Clear Liquid Hold-Up on 4.5 mm diameter holes tray
weir load (q/b) = 0.008 m^3/s.m : C_{sb} = 0.0695 m/s

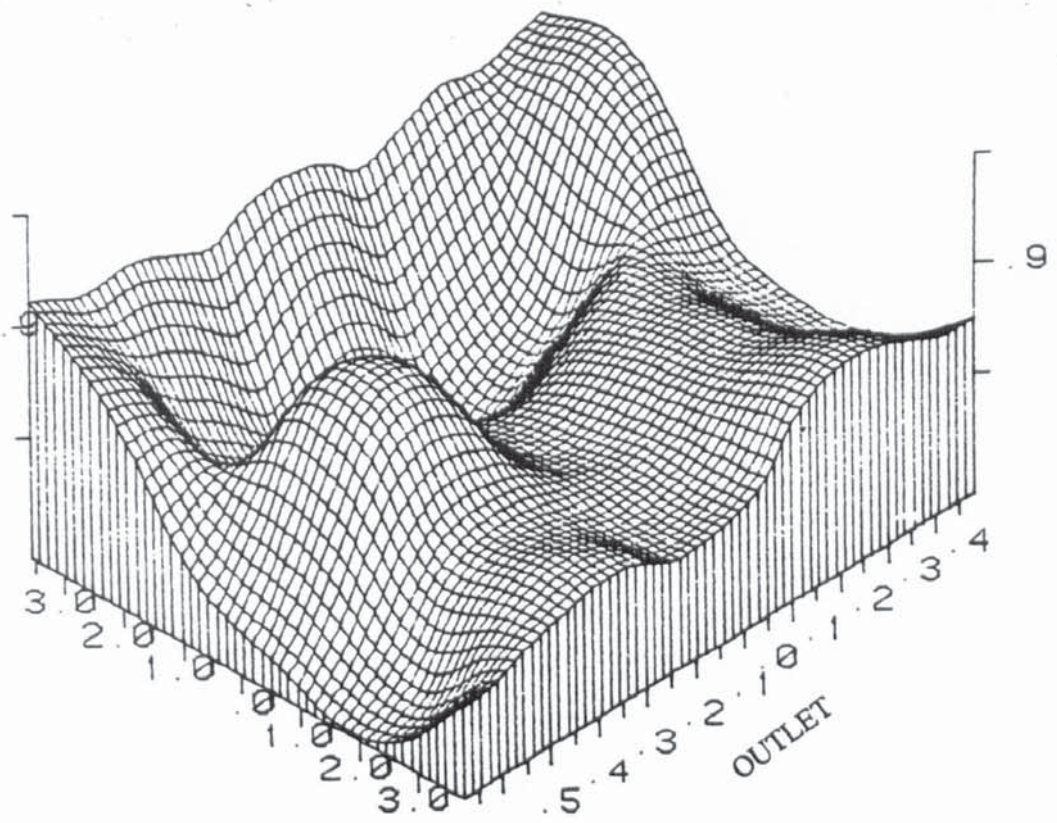

Figure (8.1b) Best surface of Clear Liquid Hold-Up on 12.5 mm diameter holes tray
weir load (q/b) = 0.0032m^3/s.m : C_{sb} = 0.0605 m/s

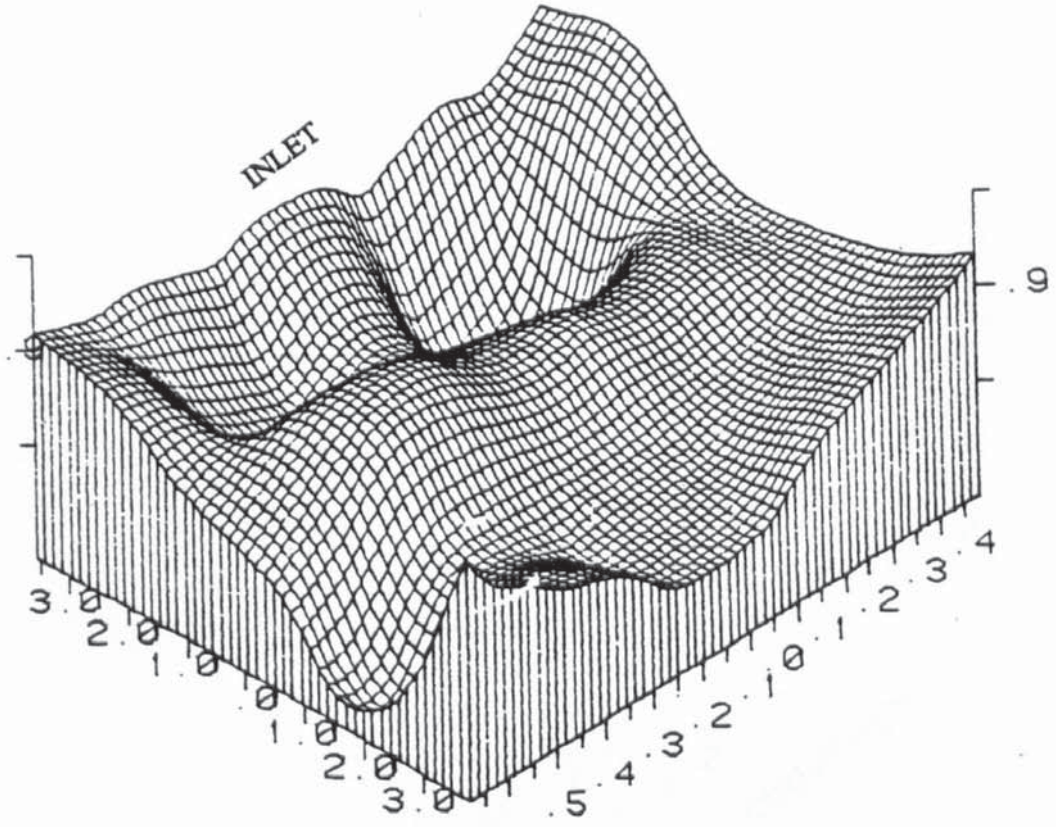

Figure (8.1a) Best surface of Clear Liquid Hold-Up on 12.5 mm diameter holes tray
weir load (q/b) = 0.0016 m^3/s.m : C_{sb} = 0.0605 m/s

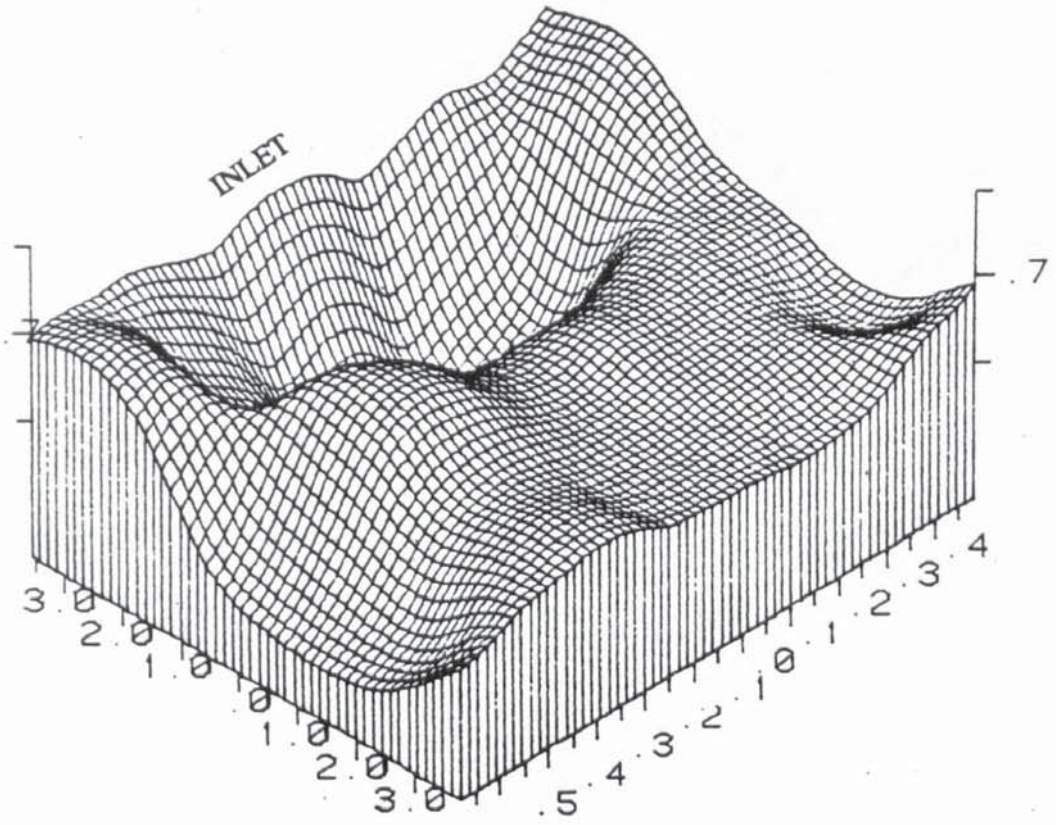

Figure (8.1c) Best surface of Clear Liquid Hold-Up on 12.5 mm diameter holes tray
weir load (q/b) = 0.0048 m^3/s.m : C_{sb} = 0.0605 m/s

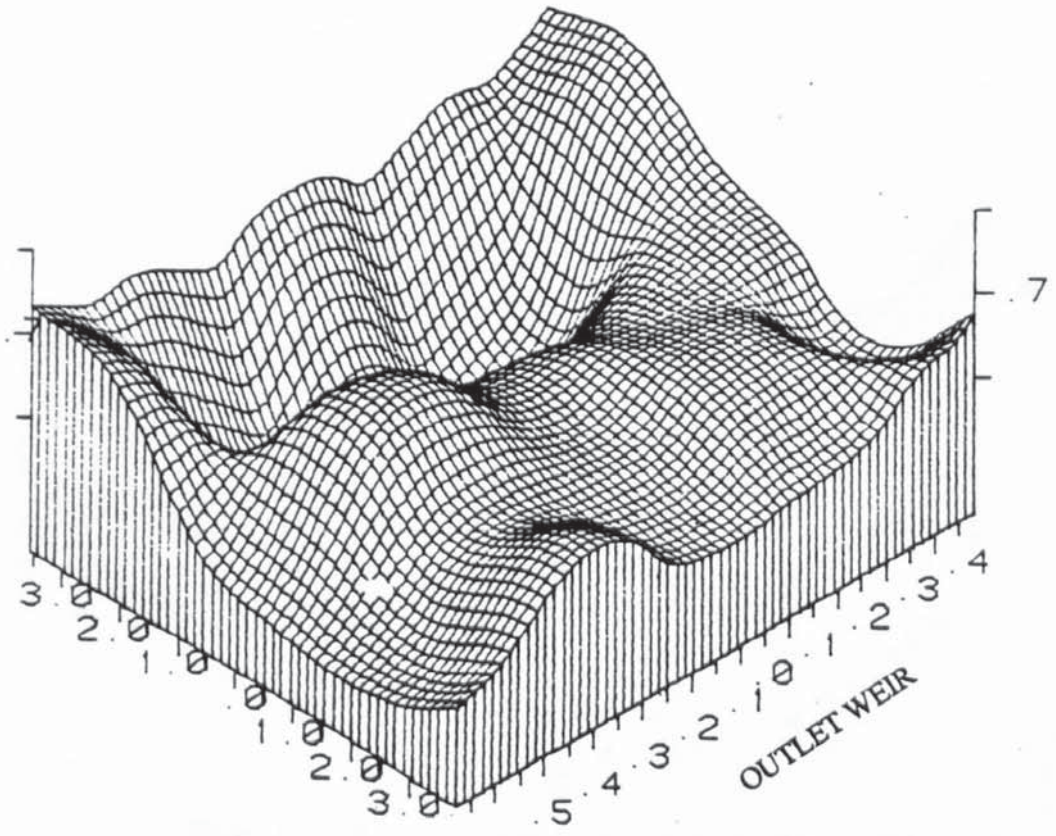

Figure (8.1d) Best surface of Clear Liquid Hold-Up on 12.5 mm diameter holes tray
weir load (q/b) = 0.0048 m^3/s.m : C_{sb} = 0.0605 m/s

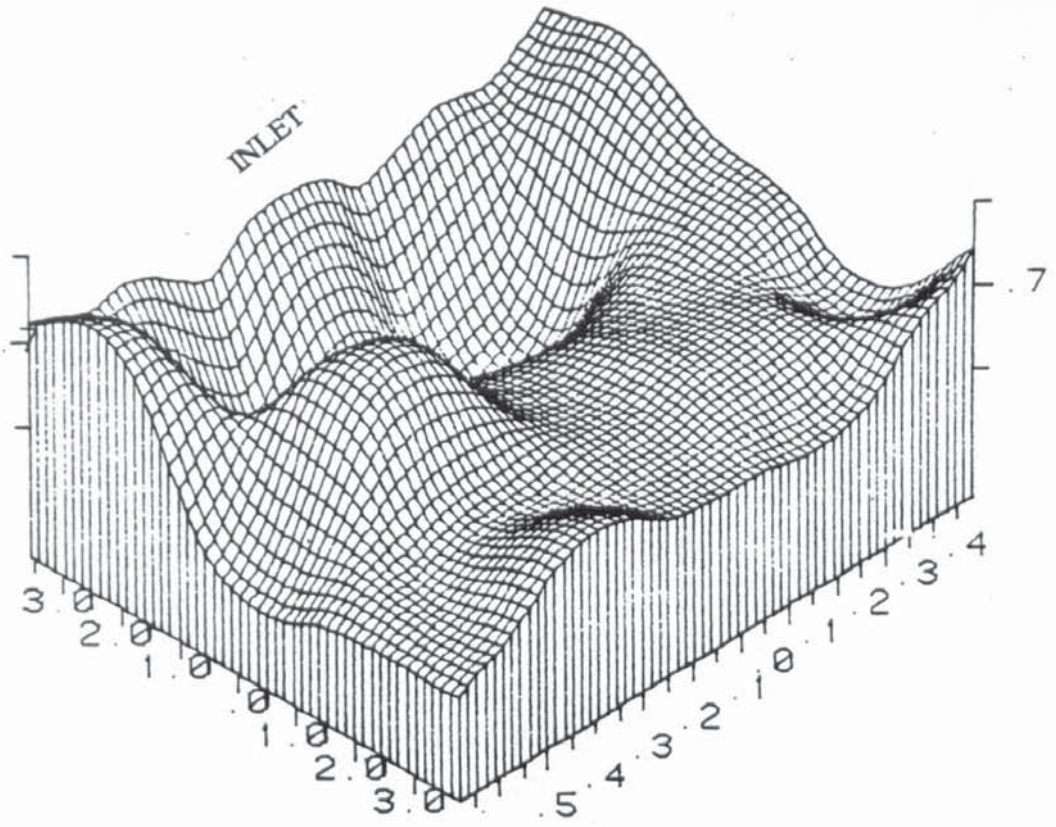

Figure (8.1e) Best surface of Clear Liquid Hold-Up on 12.5 mm diameter holes tray
weir load (q/b) = 0.0064 m^3/s.m : C_{sb} = 0.0605 m/s

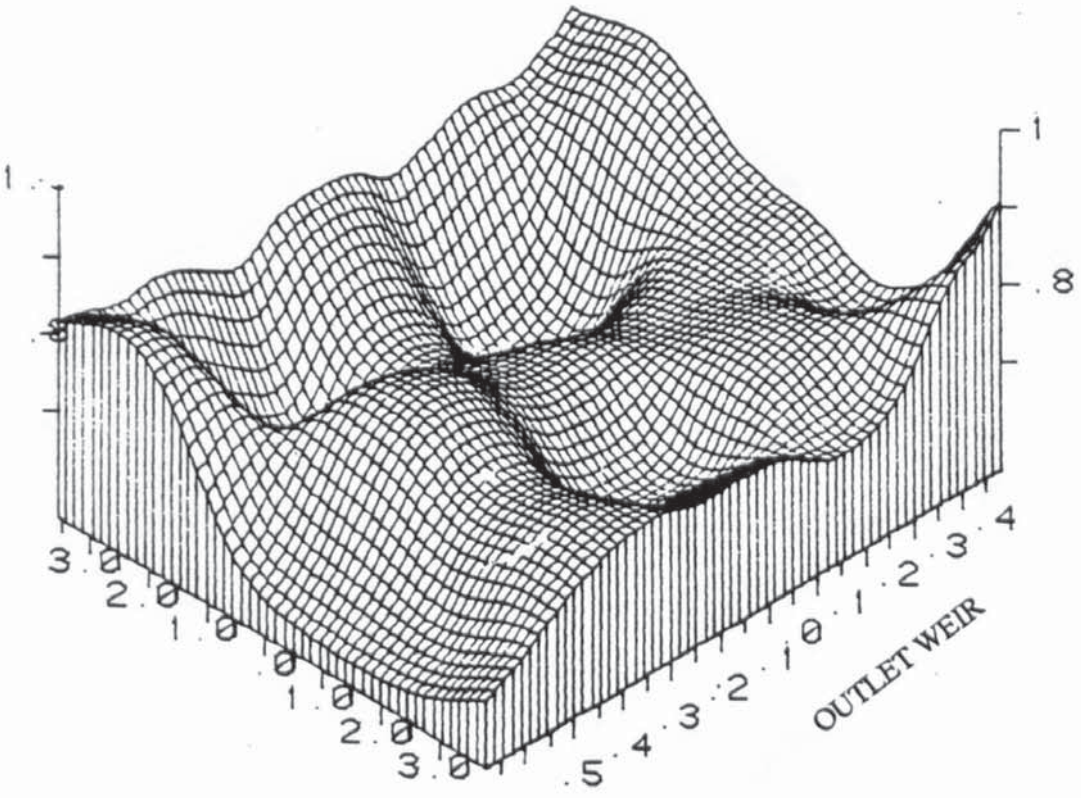

Figure (8.1f) Best surface of Clear Liquid Hold-Up on 12.5 mm diameter holes t
weir load (q/b) = 0.008 m^3/s.m : C_{sb} = 0.0605 m/s

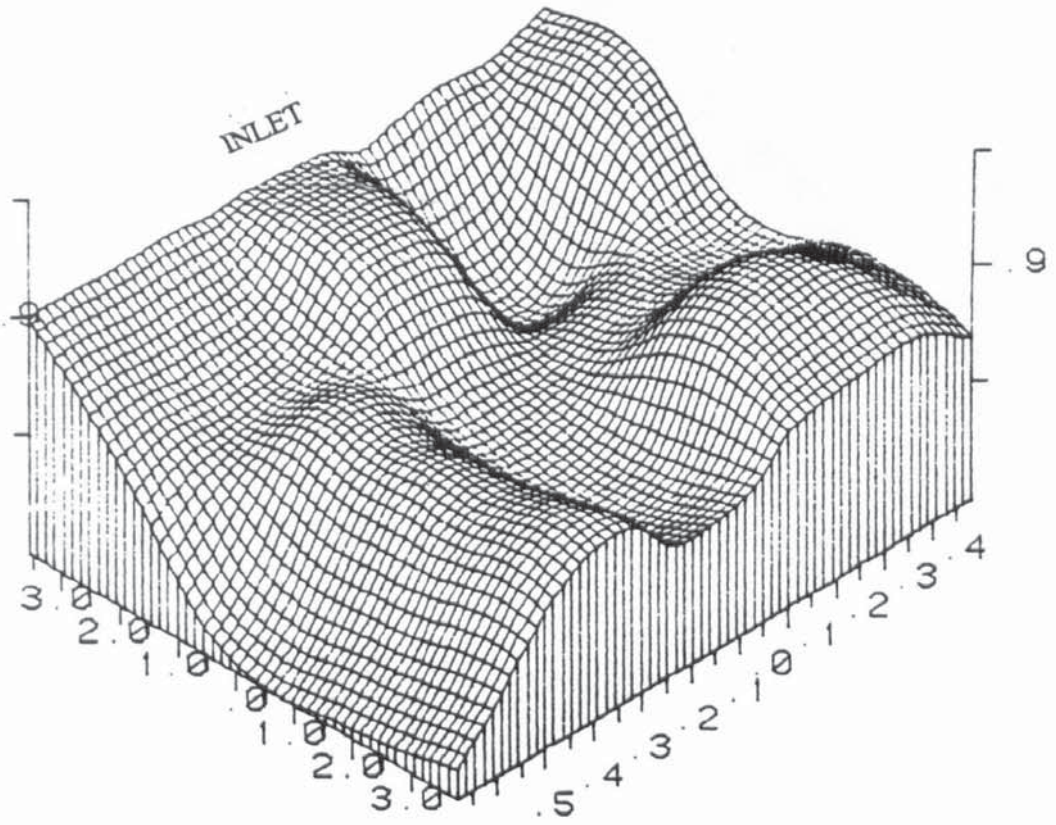

Figure (8.1h) Best surface of Clear Liquid Hold-Up on 12.5 mm diameter holes tray
weir load (q/b) = 0.0016 m^3/s.m : C_{sb} = 0.0775 m/s

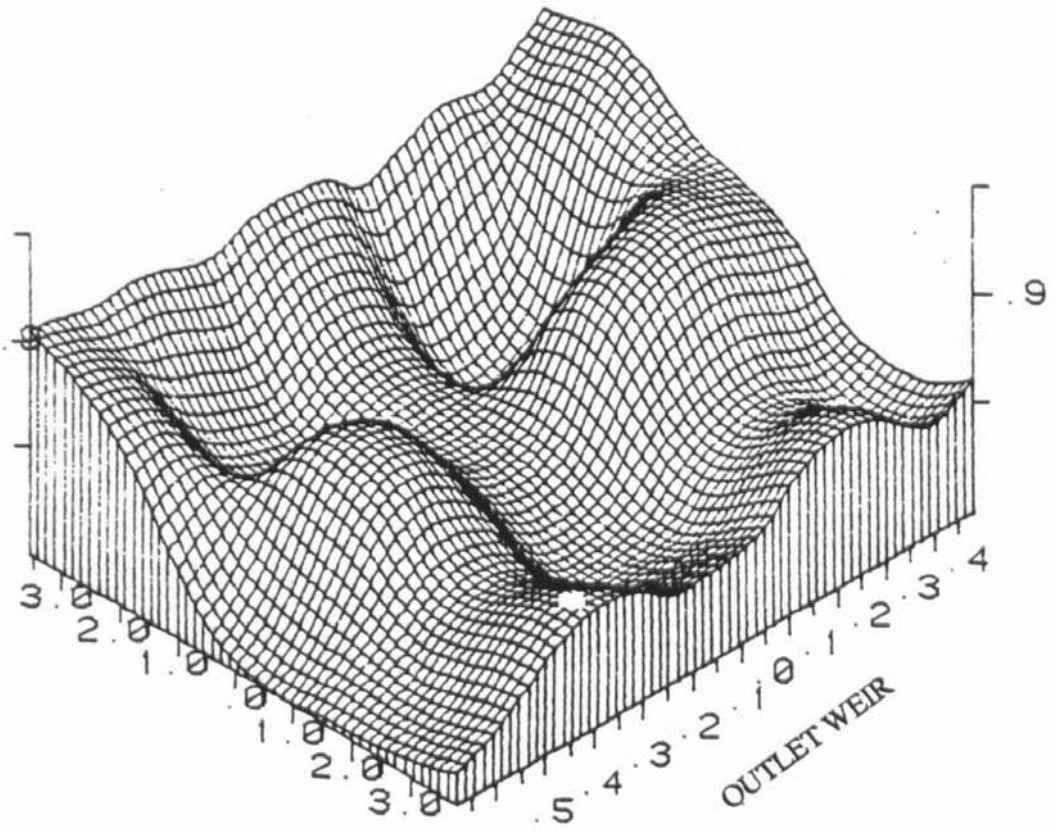

Figure (8.1i) Best surface of Clear Liquid Hold-Up on 12.5 mm diameter holes tra
weir load (q/b) = 0.0032m^3/s.m : C_{sb} = 0.0775 m/s

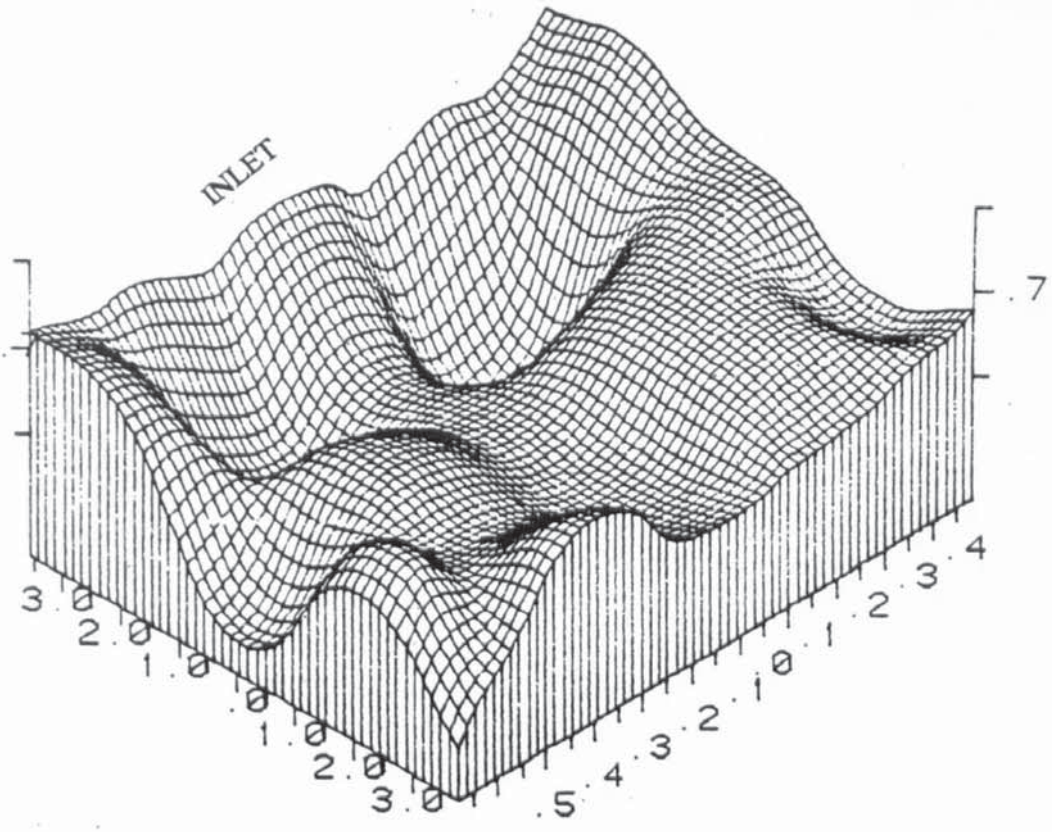

Figure (8.1j) Best surface of Clear Liquid Hold-Up on 12.5 mm diameter holes tray

weir load (q/b) = 0.0048 m^3/s.m : C_{sb} = 0.0775 m/s

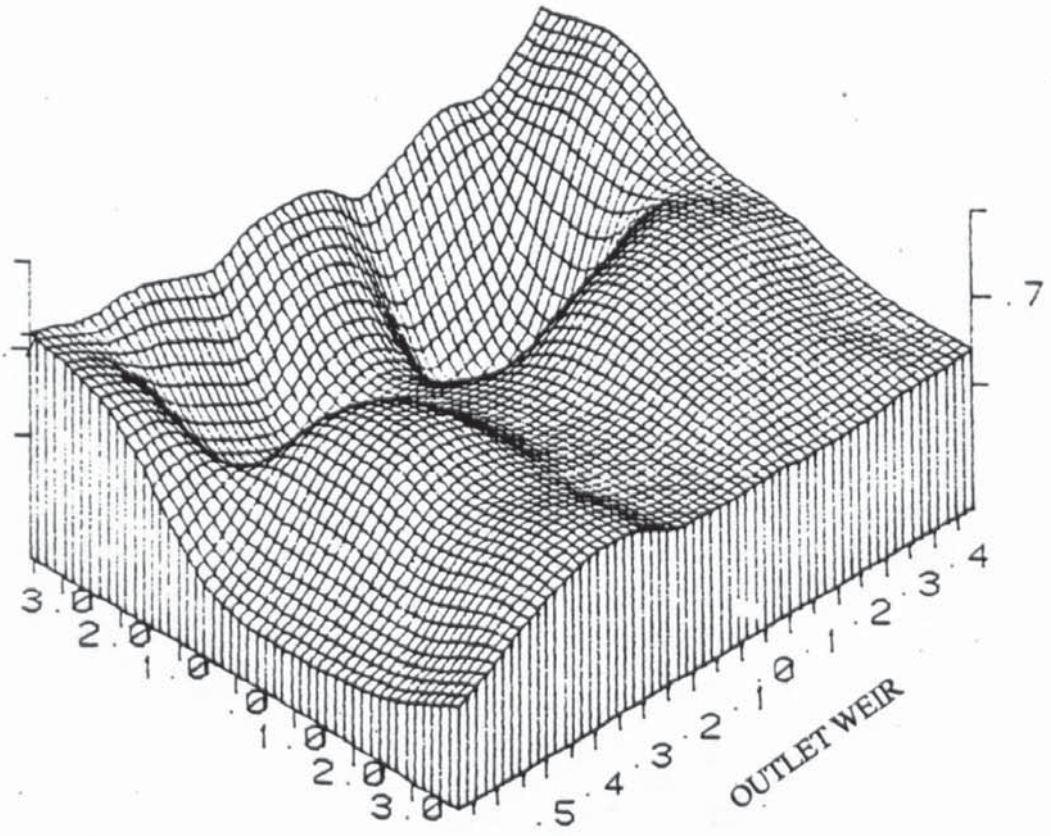

Figure (8.1k) Best surface of Clear Liquid Hold-Up on 12.5 mm diameter holes tray

weir load (q/b) = 0.0048 m^3/s.m : C_{sb} = 0.0775 m/s

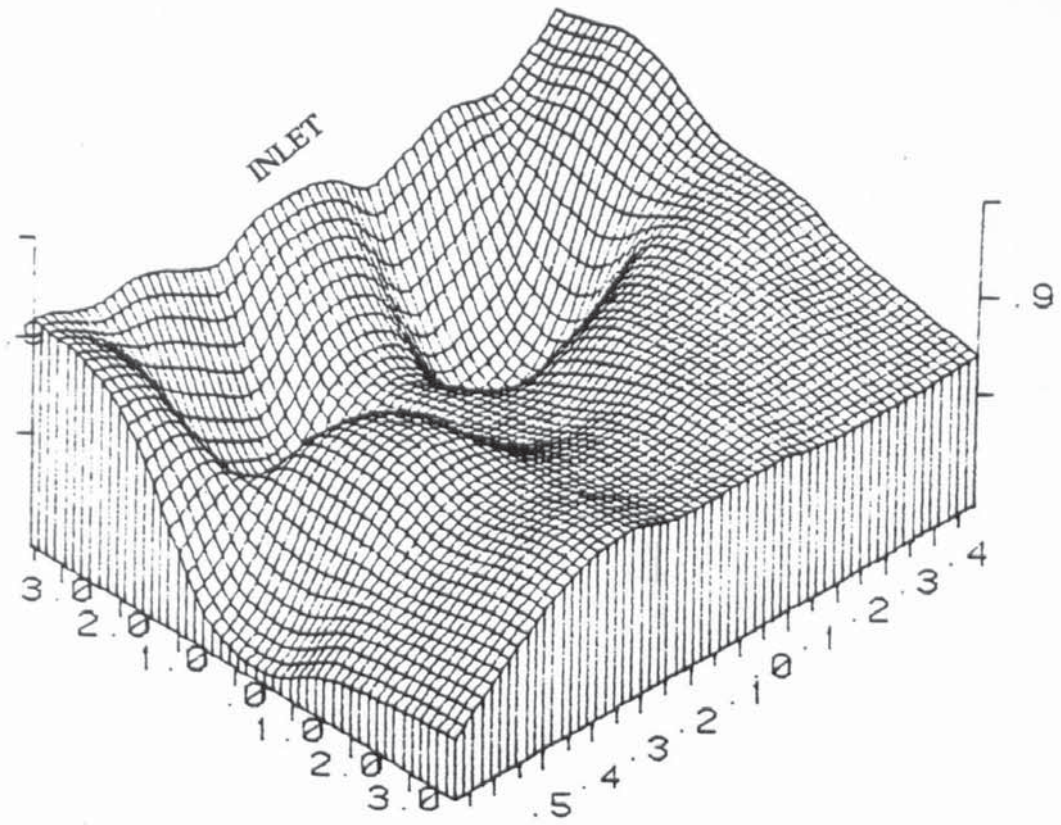

Figure (8.11) Best surface of Clear Liquid Hold-Up on 12.5 mm diameter holes tray
weir load (q/b) = 0.0064 m^3/s.m : C_{sb} = 0.0775 m/s

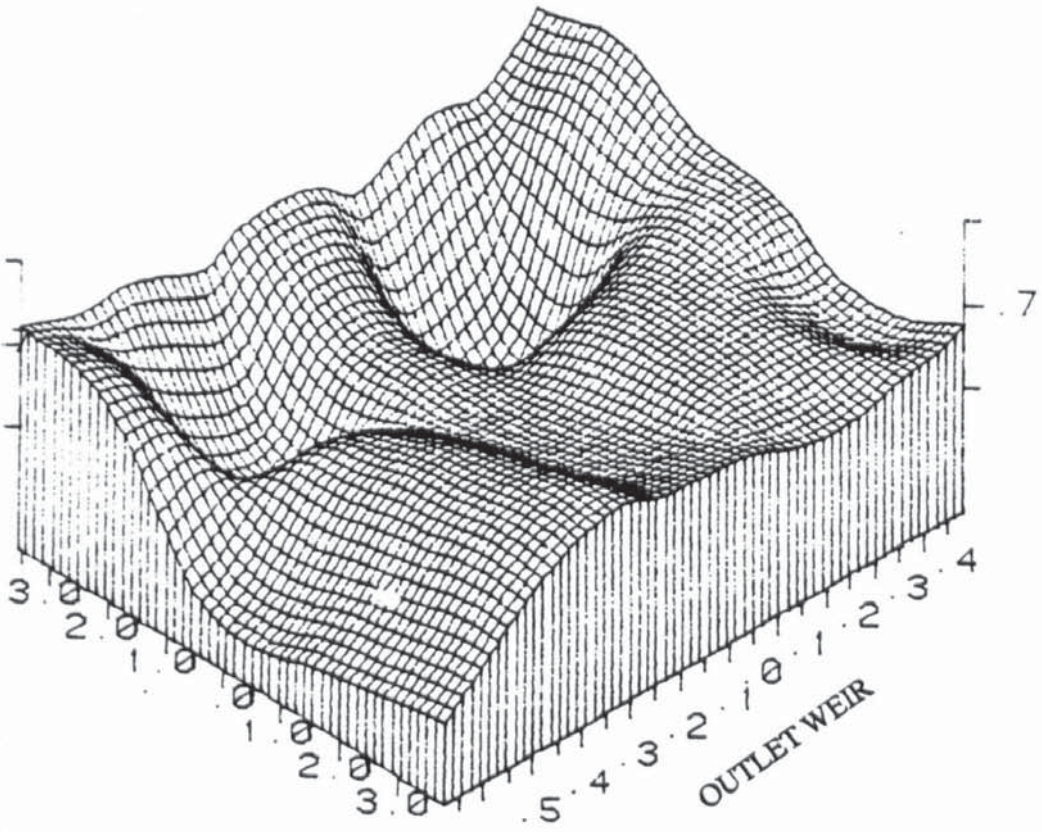

Figure (8.1m) Best surface of Clear Liquid Hold-Up on 12.5 mm diameter holes tray
weir load (q/b) = 0.008 m^3/s.m : C_{sb} = 0.0775m/s

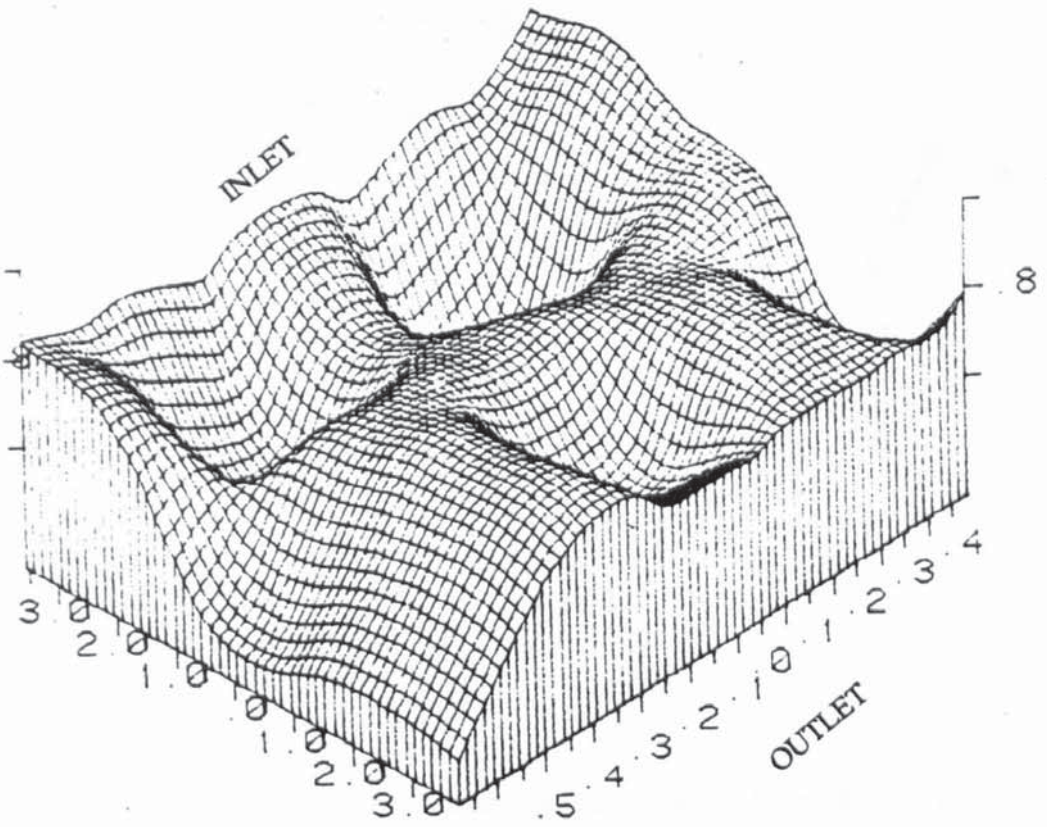

Figure (8.1n) Best surface of Clear Liquid Hold-Up on 12.5 mm diameter holes tray
weir load (q/b) = 0.00967 m^3/s.m : C_{sb} = 0.0775 m/s

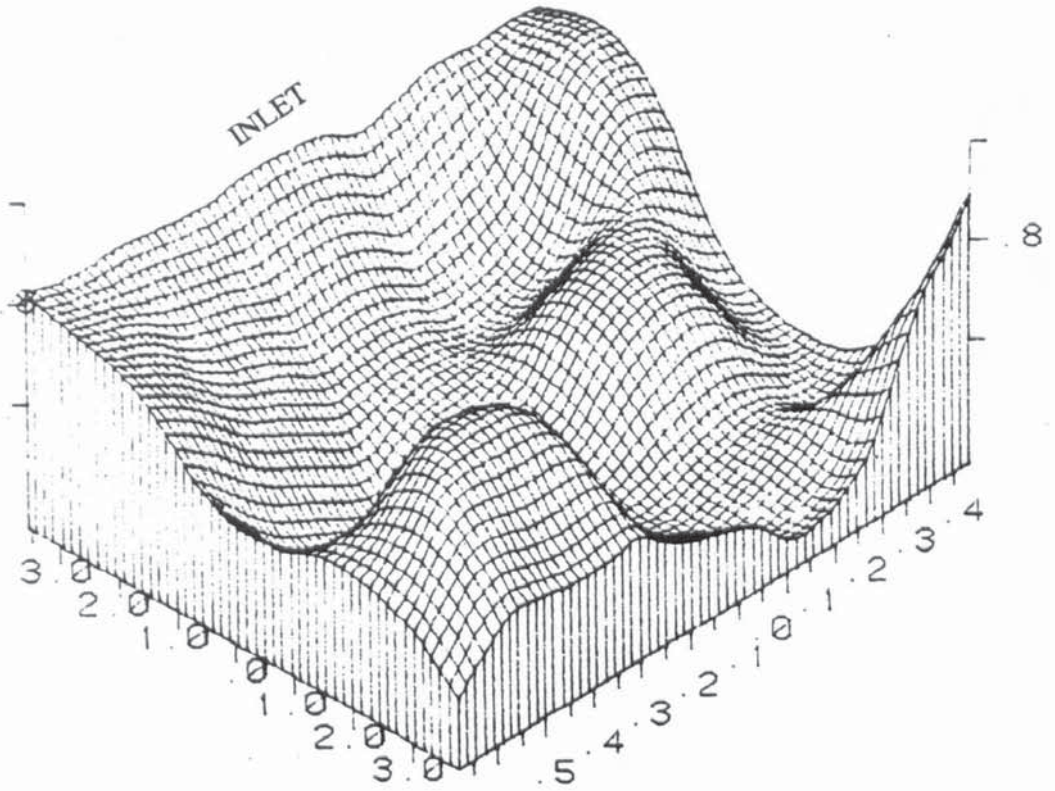

Figure (8.1o) Best surface of Clear Liquid Hold-Up on 12.5 mm diameter holes tray
weir load (q/b) = 0.0016 m^3/s.m : C_{sb} = 0.0775m/s

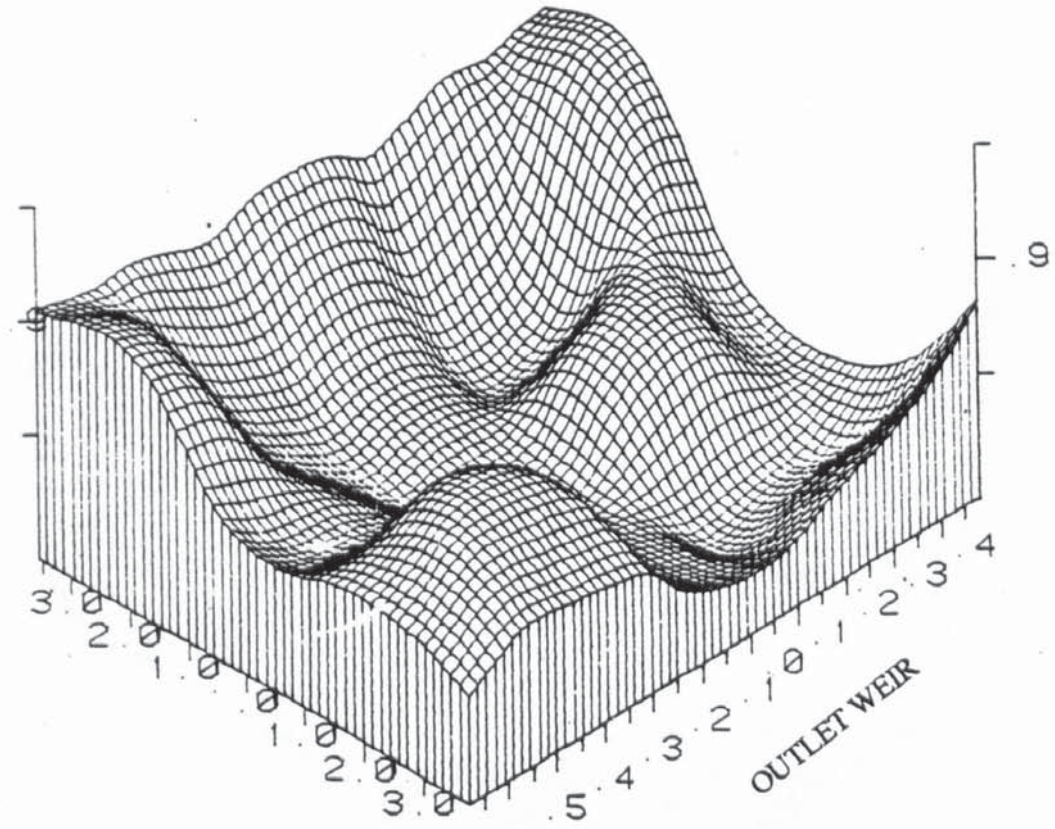

Figure (8.1p) Best surface of Clear Liquid Hold-Up on 12.5 mm diameter holes tray
weir load (q/b) = 0.0032m^3/s.m : C_{sb} = 0.0915 m/s

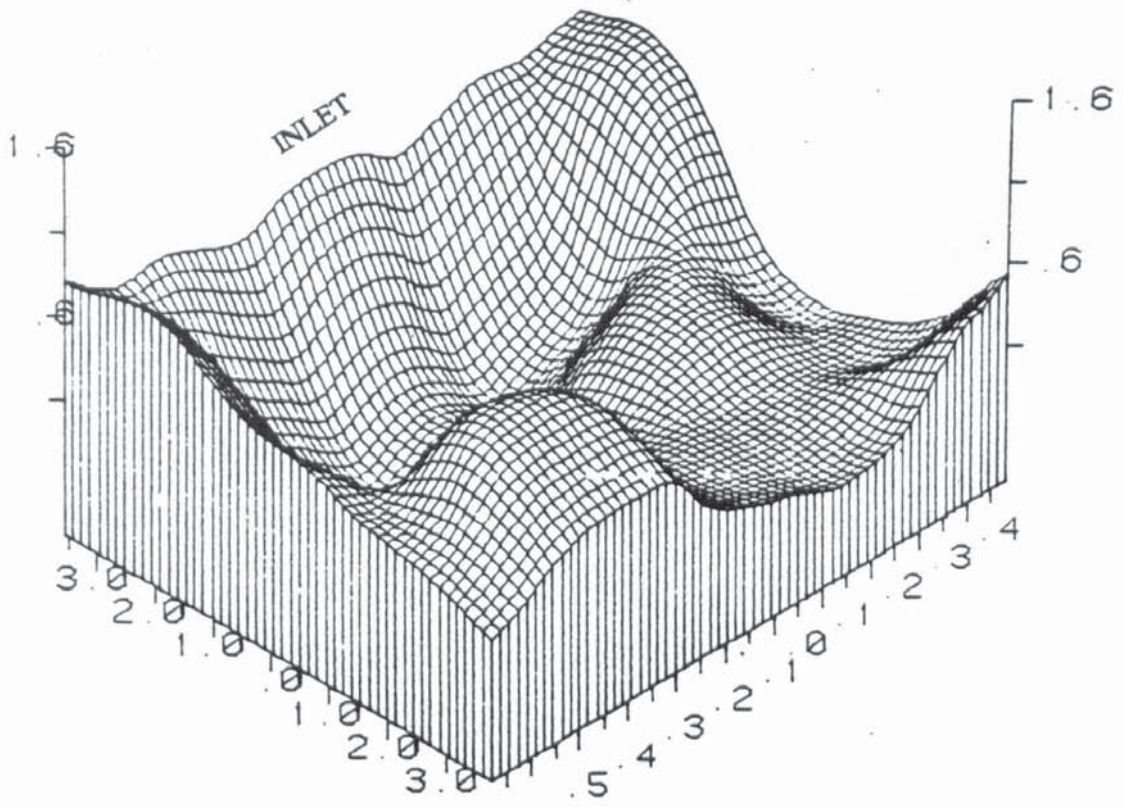

Figure (8.1q) Best surface of Clear Liquid Hold-Up on 12.5 mm diameter holes tray
weir load (q/b) = 0.0048 m^3/s.m : C_{sb} = 0.0915 m/s

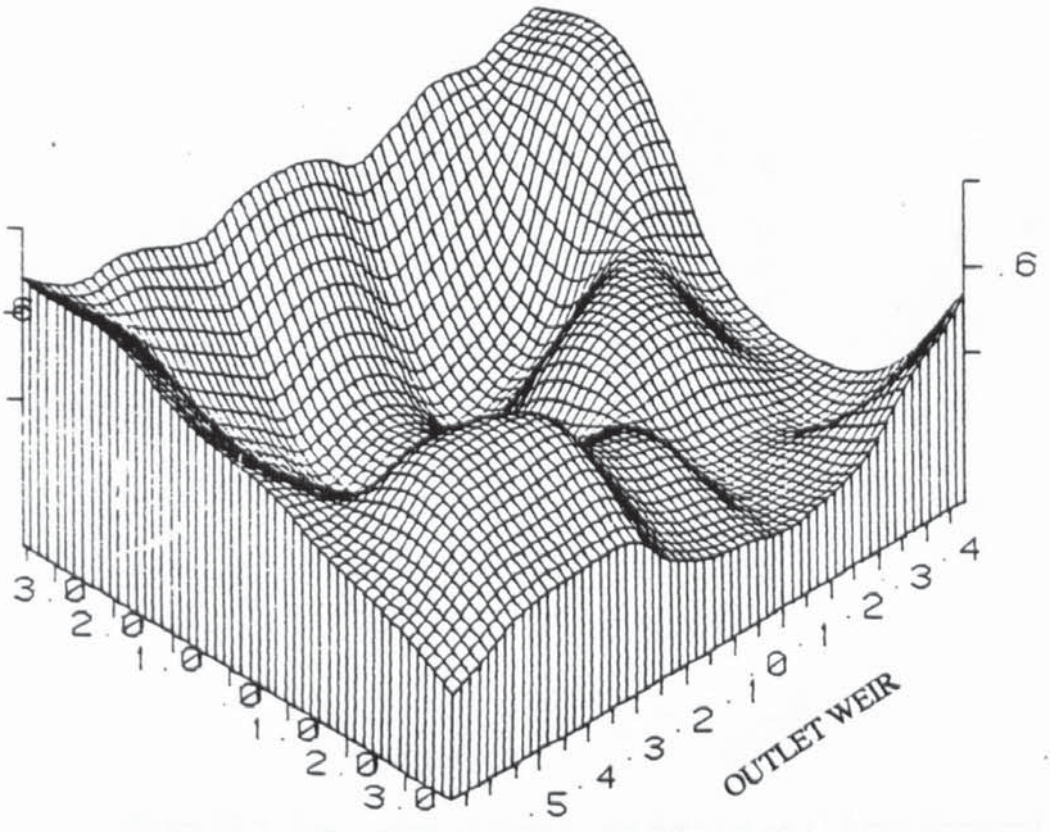

Figure (8.1r) Best surface of Clear Liquid Hold-Up on 12.5 mm diameter holes tray
weir load (q/b) = 0.0064 m^3/s.m : C_{sb} = 0.0915m/s

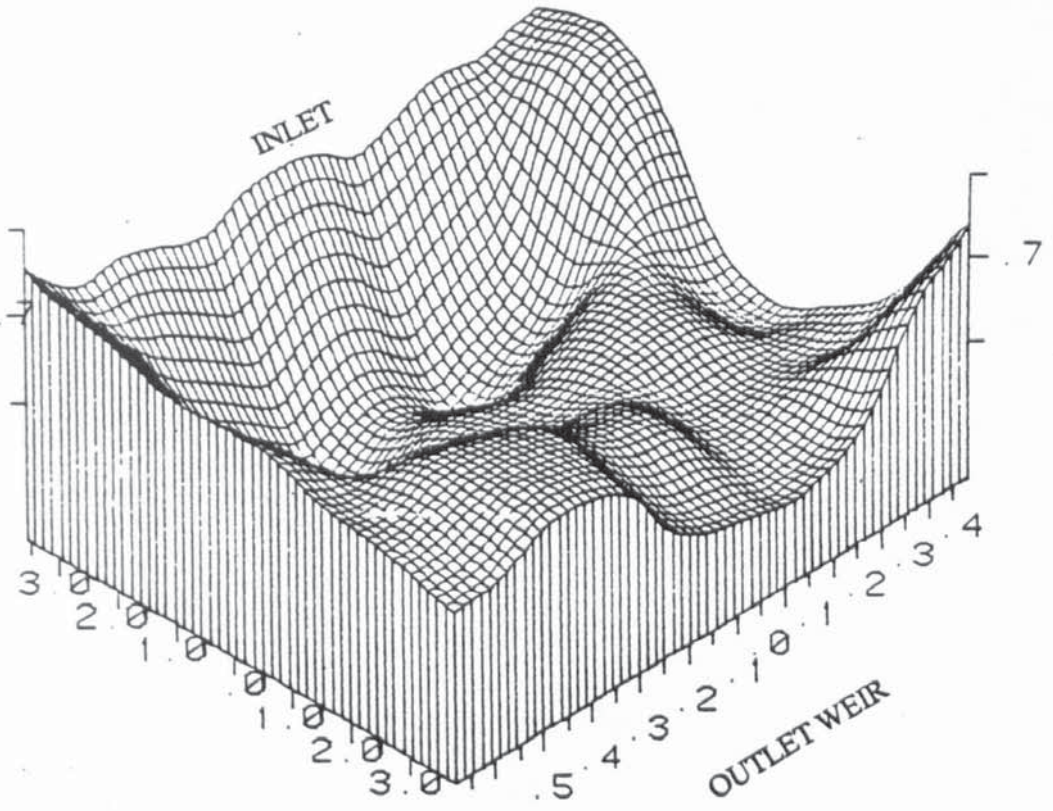

Figure (8.1s) Best surface of Clear Liquid Hold-Up on 12.5 mm diameter holes tray
weir load (q/b) = 0.008 m^3/s.m : C_{sb} = 0.0915 m/s

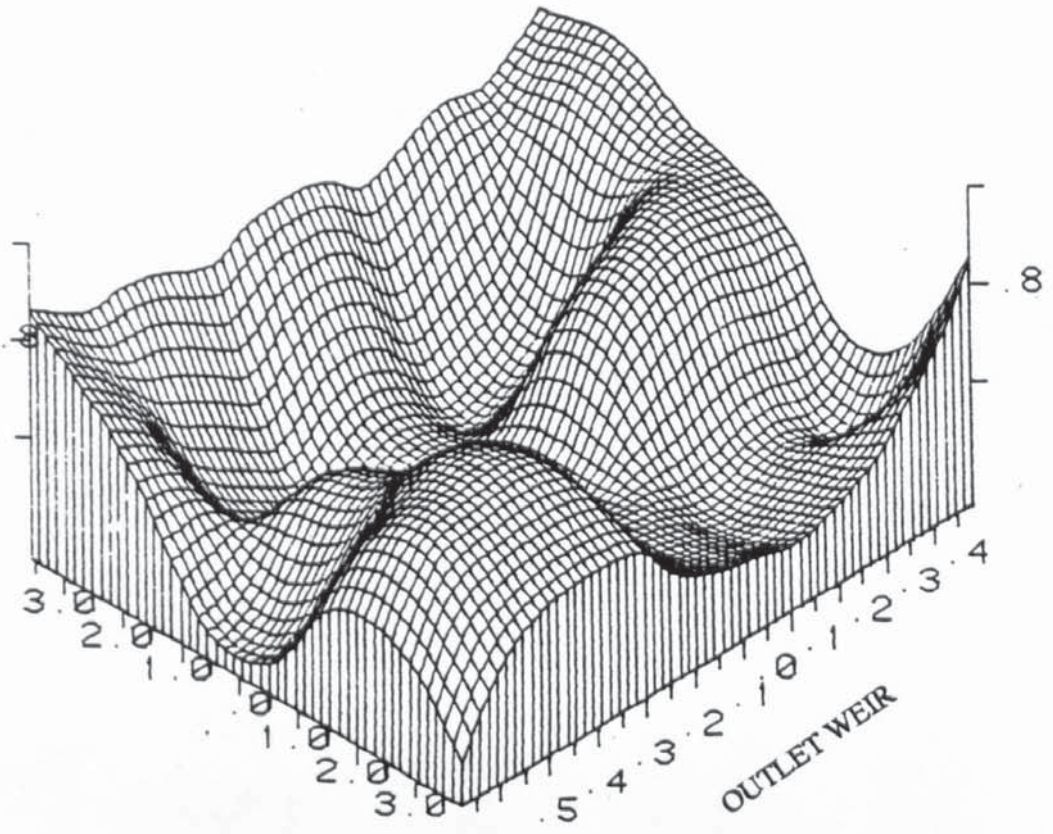

Figure (8.1t) Best surface of Clear Liquid Hold-Up on 12.5 mm diameter holes tray
weir load (q/b) = 0.00967 m^3/s.m : C_{sb} = 0.0915m/s

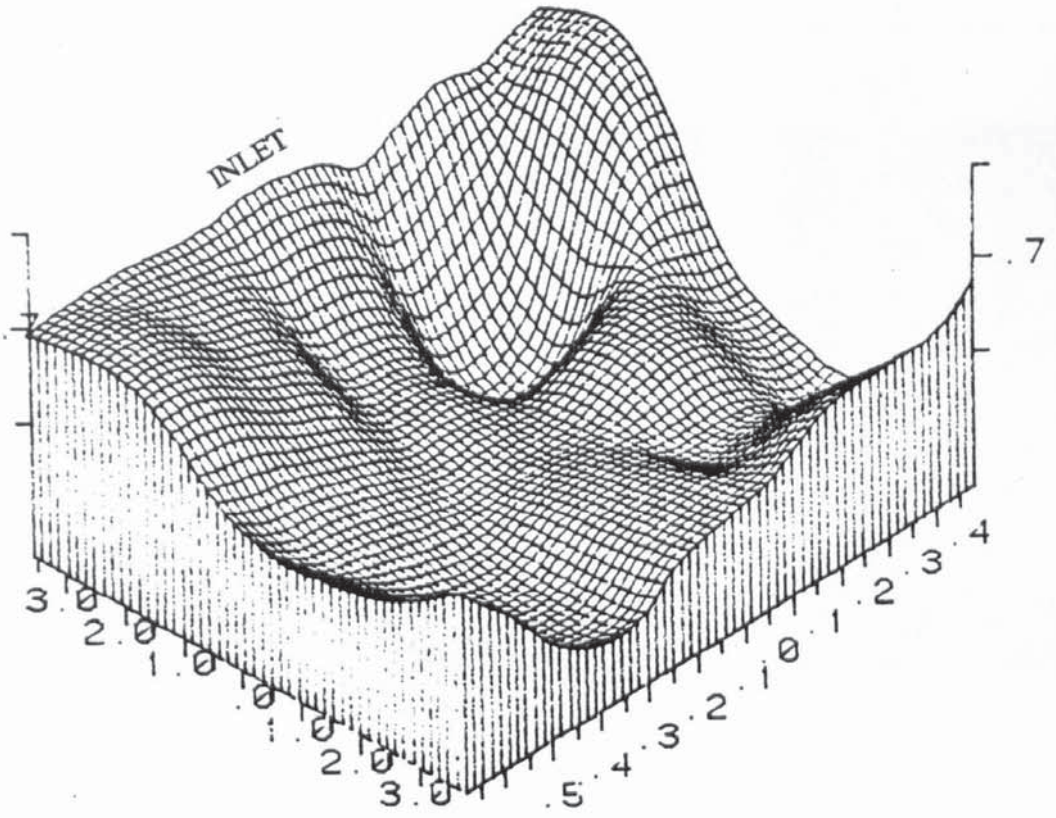

Figure (8.1u) Best surface of Clear Liquid Hold-Up on 12.5 mm diameter holes tray
weir load (q/b) = 0.0116 m^3/s.m : C_{sb} = 0.0915 m/s

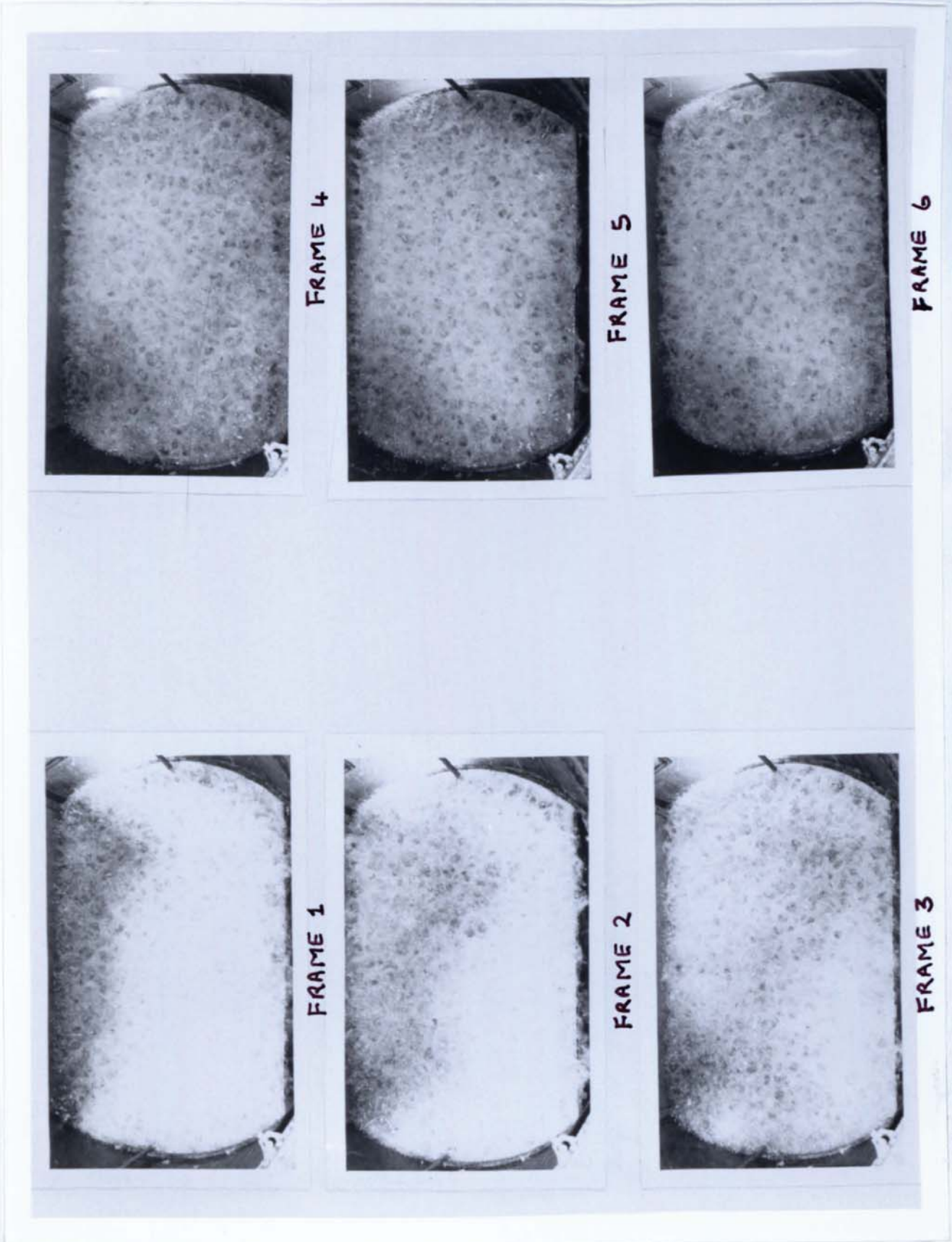

Figure (8.3a) Still photographic Frames of Dye tracer movement on the 4.5mm diameter hole tray. Weir Load (q/b) = 0.0016 m^3/s.m : C_{sb} = 0.0605 m/s : Flow regime = Spray

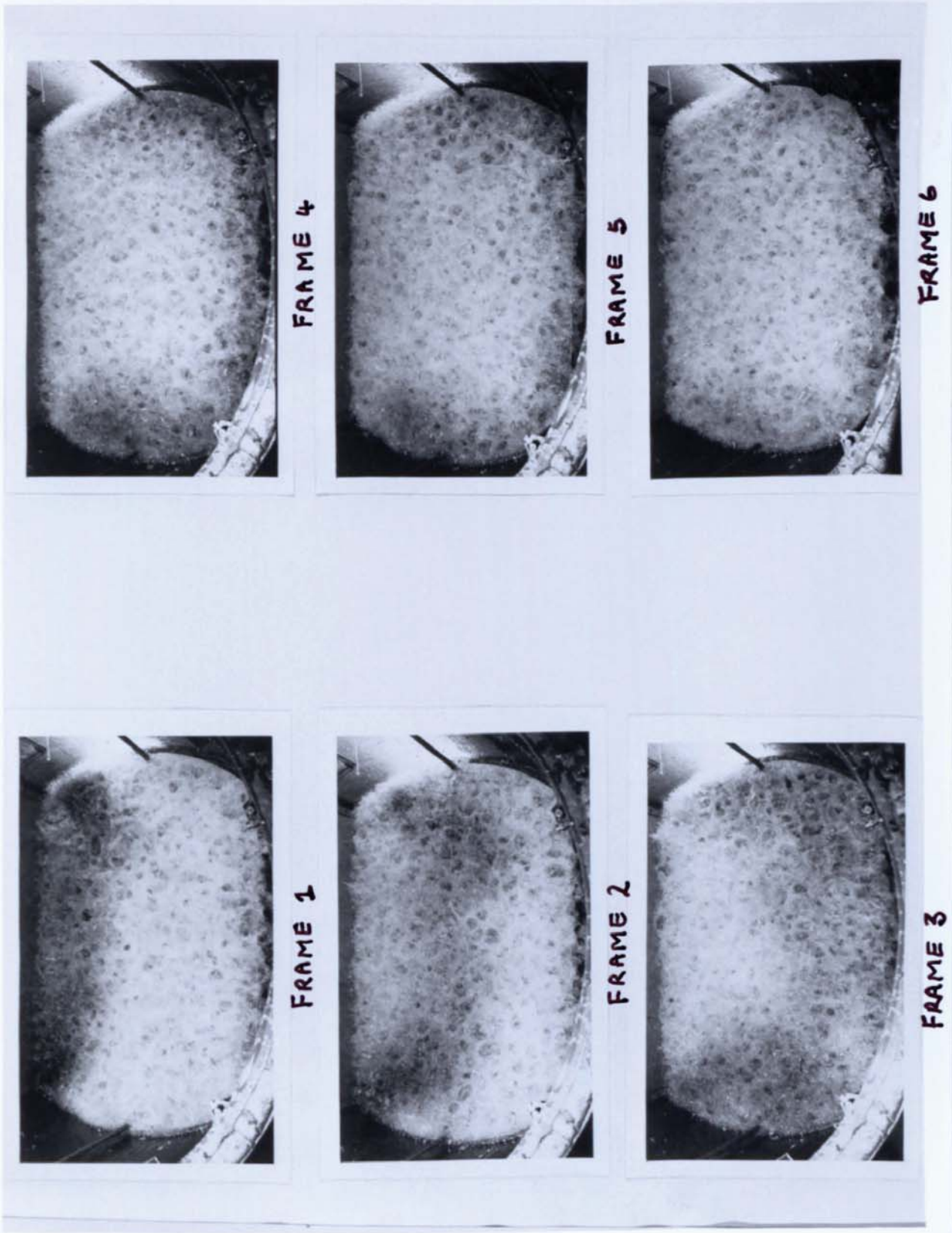

Figure (8.3b) Still photographic Frames of Dye tracer movement on the 4.5mm diameter hole tray. Weir Load (q/b) = 0.0064 m^3/s.m : C_{sb} = 0.0605 m/s : Flow regime = Mixed

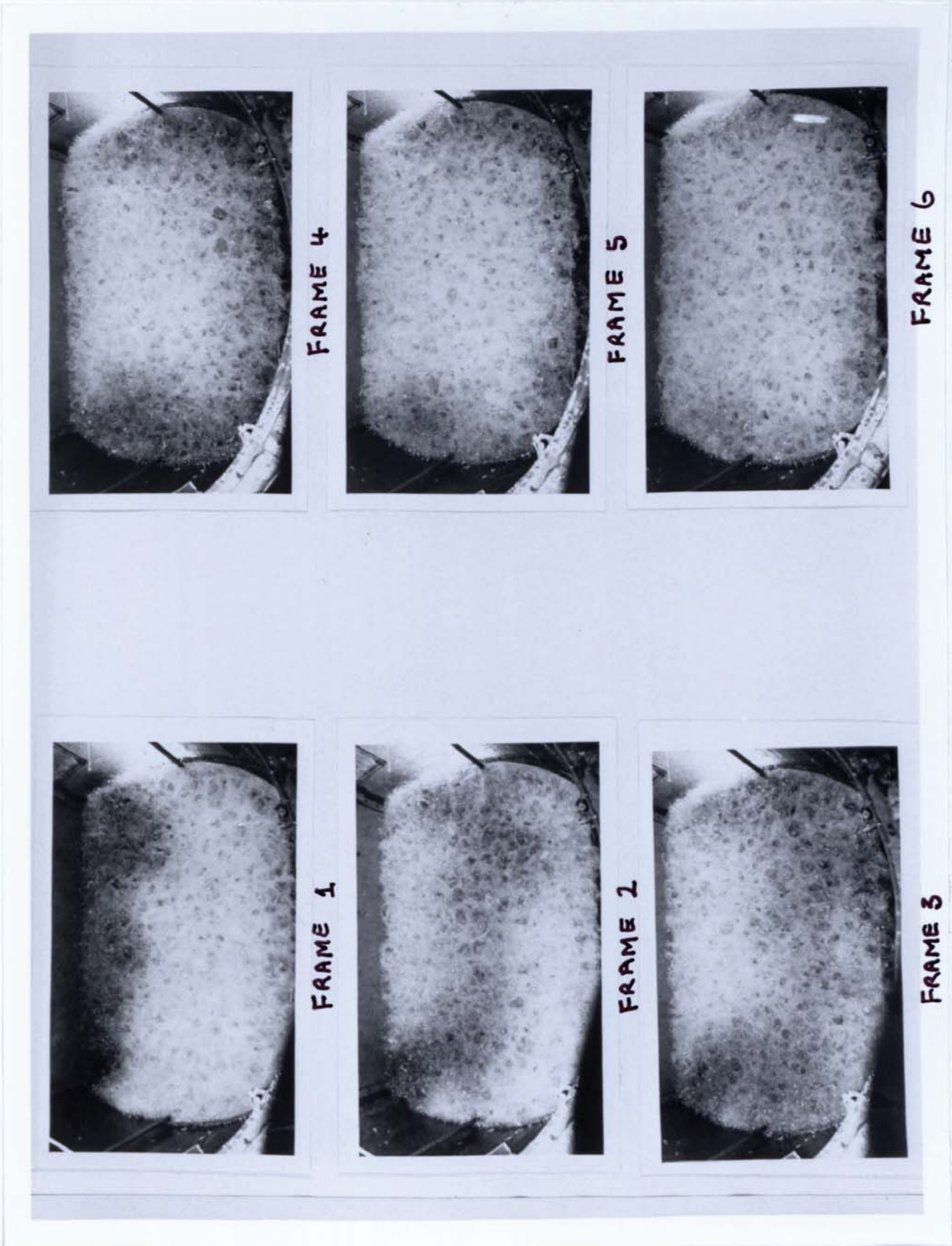

Figure (8.3c) Still photographic Frames of Dye tracer movement on the 4.5mm diameter hole tray. Weir Load (q/b) = 0.008 m^3/s.m : C_{sb} = 0.0605 m/s : Flow regime = Mixed

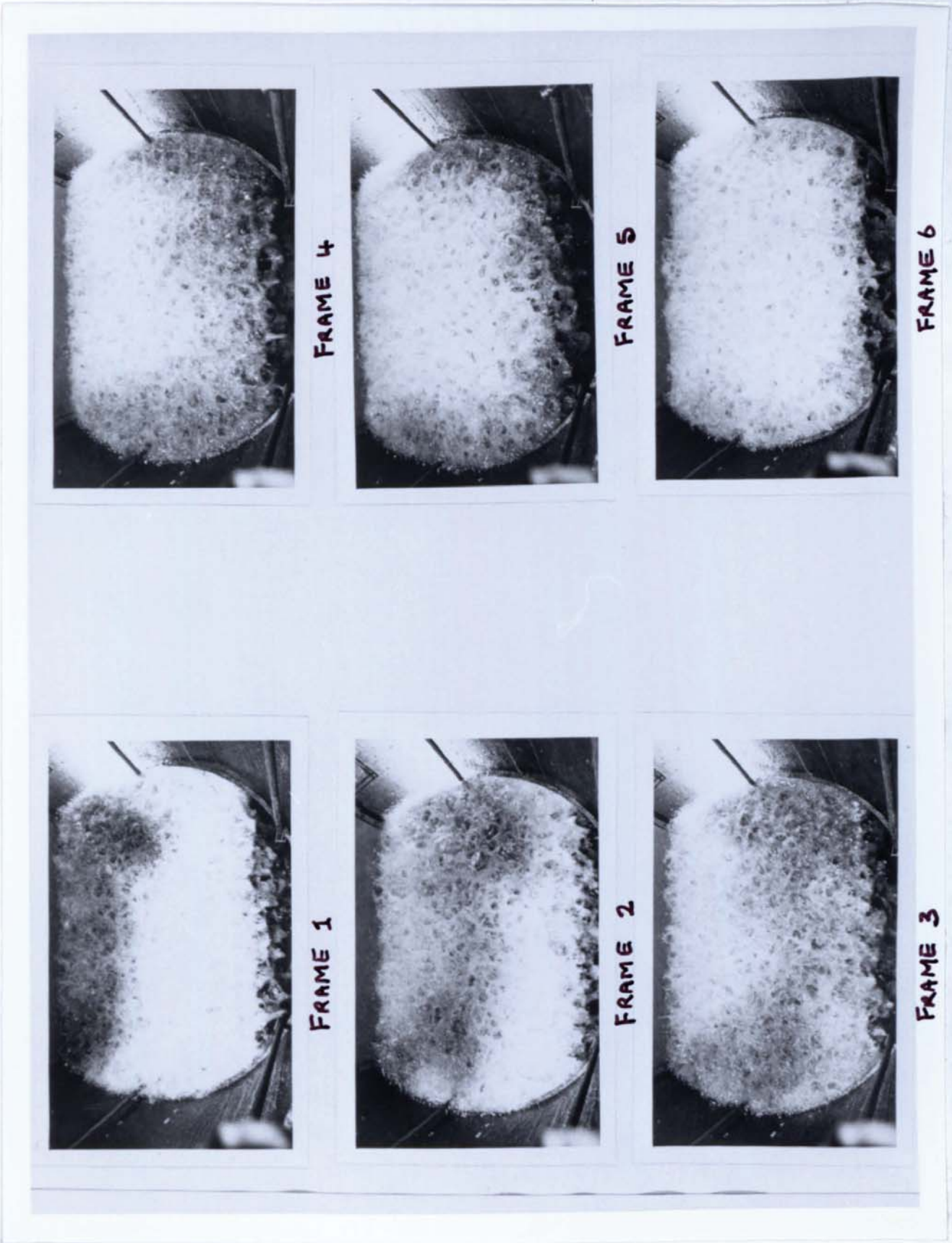

Figure (8.3d) still photographic Frames of Dye tracer movement on the 4.5mm diameter hole tray. Weir Load (q/b) = 0.015 m^3/s.m : C_{sb} = 0.0605 m/s: Flow regime = Emulsified

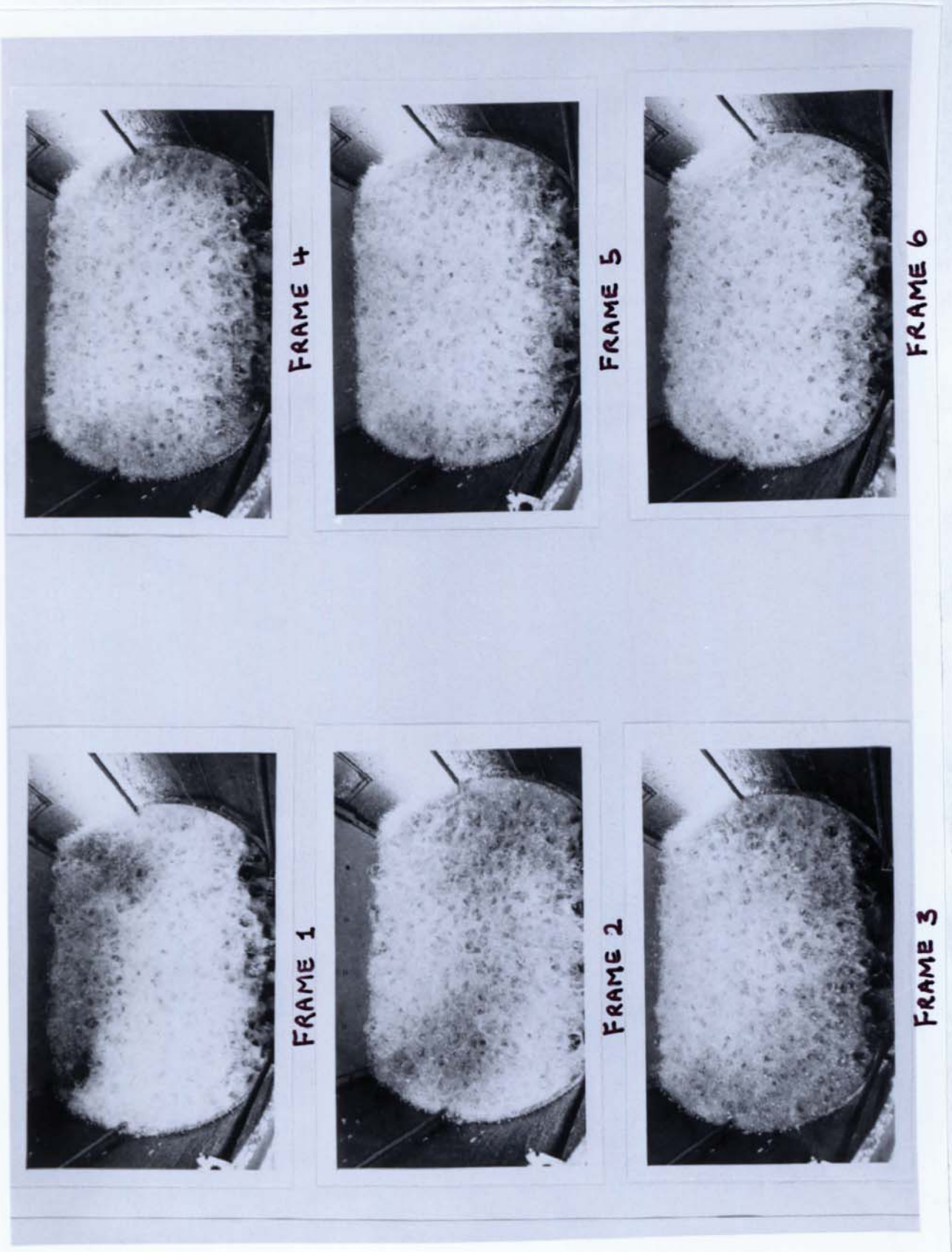

Figure (8.3e) Still photographic Frames of Dye tracer movement on the 12.5 mm diameter hole tray. Weir Load (q/b) = 0.0016 m^3/s.m : C_{sb} = 0.0605 m/s: Flow regime = Spray

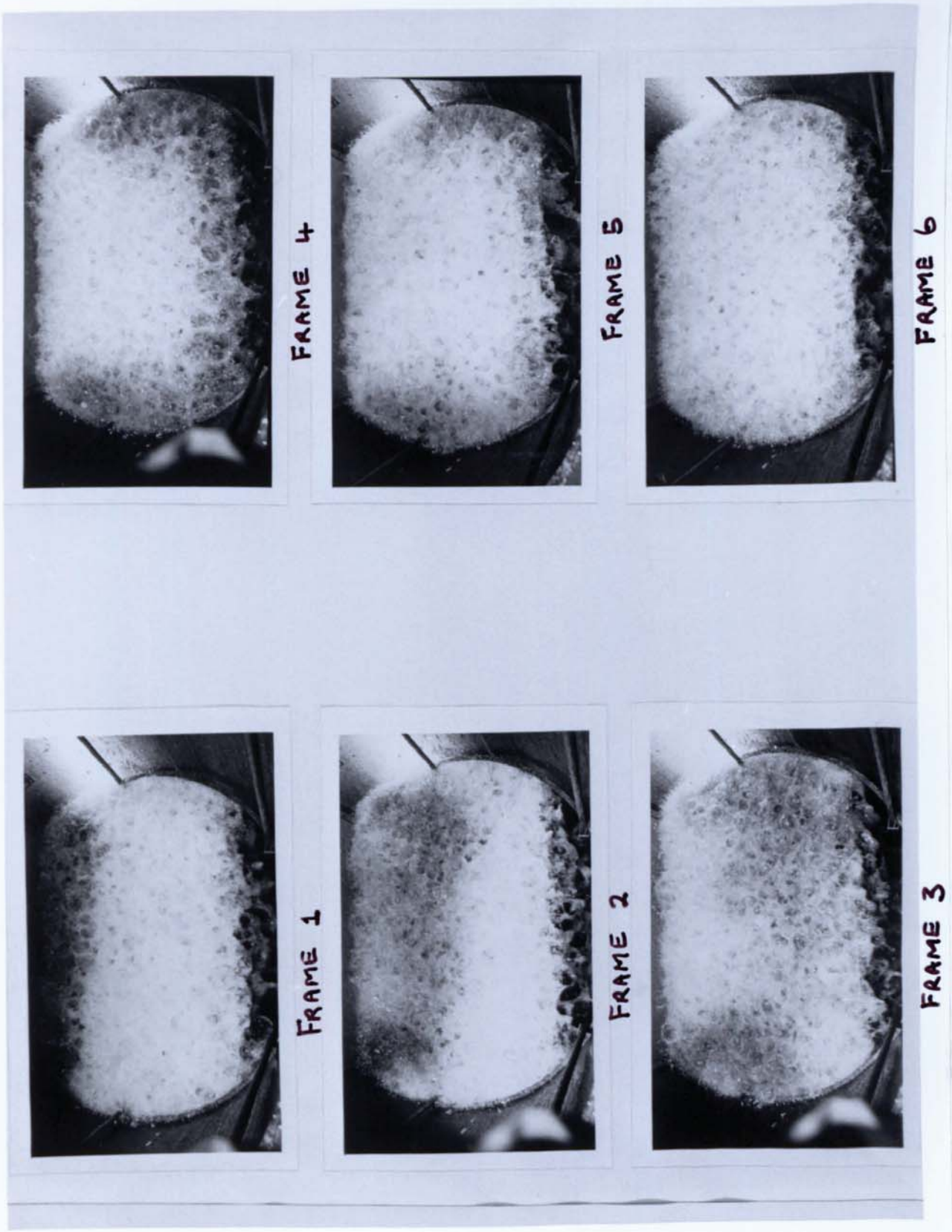

Figure (8.3f) Still photographic Frames of Dye tracer movement on the 12.5 mm diameter hole tray. Weir Load (q/b) = 0.0064 m^3/s.m : C_{sb} = 0.0605 m/s: Flow regime = Mixed

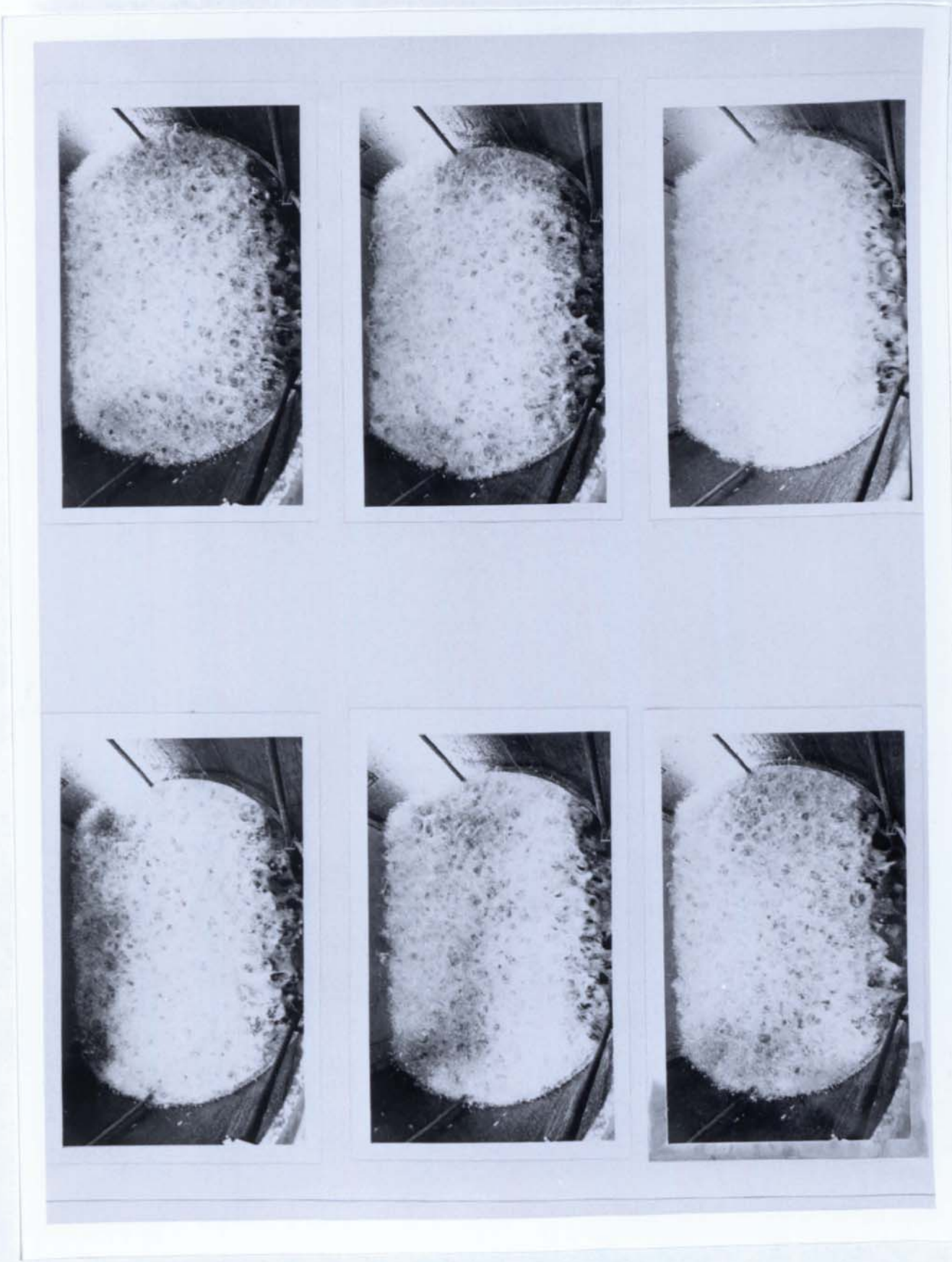

Figure (8.3g) Still photographic Frames of Dye tracer movement on the 12.5 mm diameter hole tray. Weir Load (q/b) = 0.008 m^3/s.m : C_{sb} = 0.0605 m/s: Flow regime = Mixed

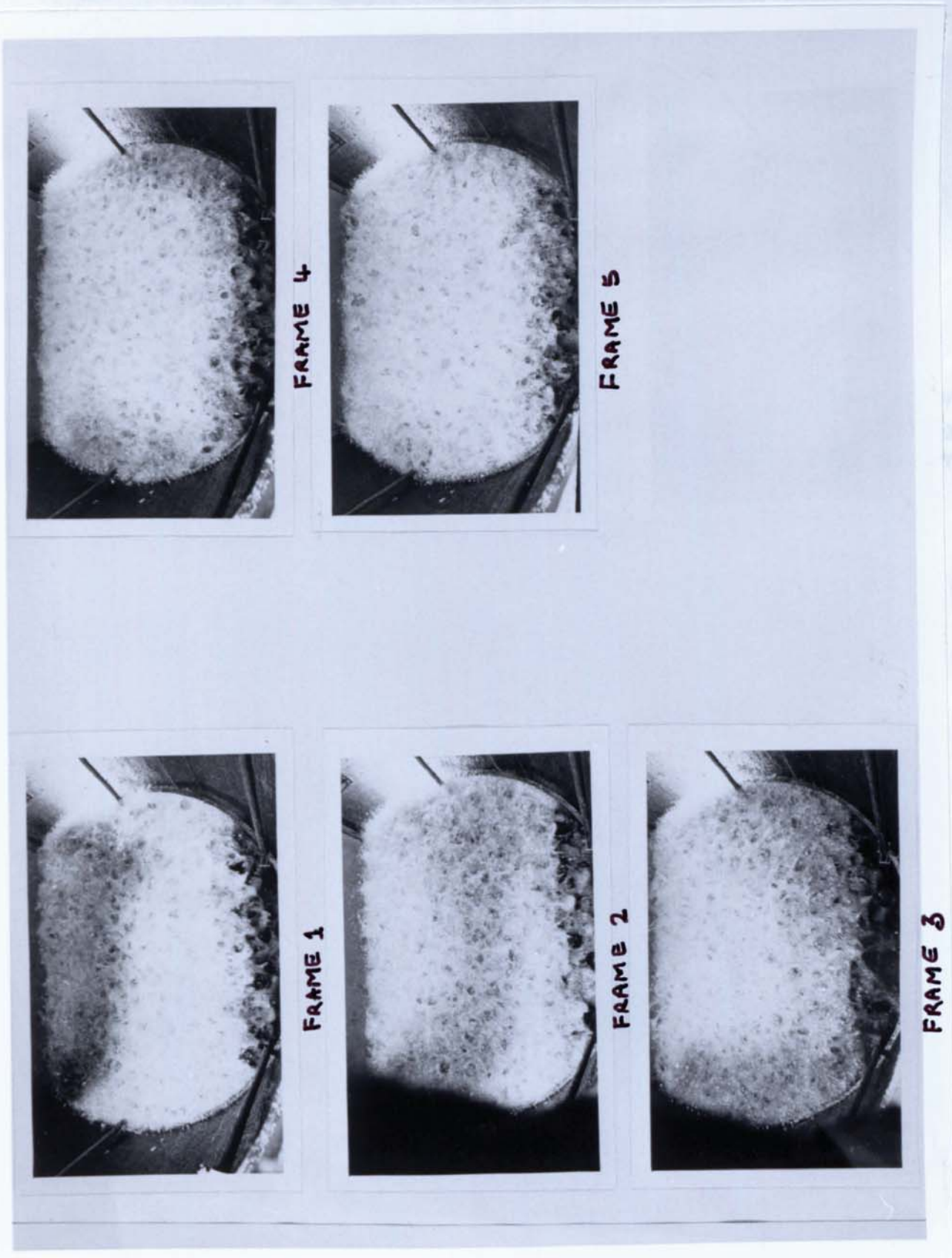

Figure (8.3h) Still photographic Frames of Dye tracer movement on the 12.5 mm diameter hole tray. Weir Load (q/b) = 0.015 m^3/s.m : C_{sb} = 0.0605 m/s: Flow regime = Emulsified

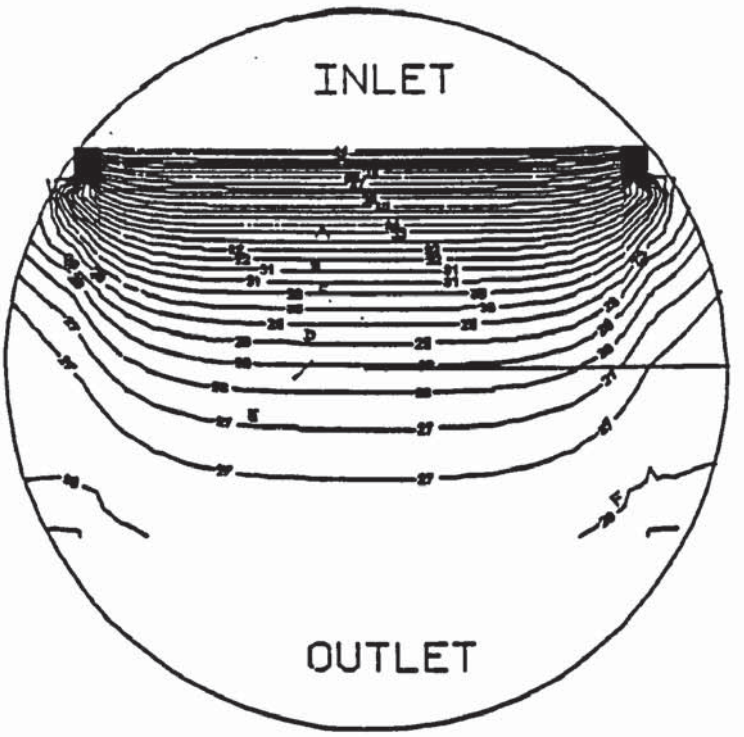

SYMBOL		T°C
A	=	33
B	=	31
C	=	30
D	=	28
E	=	27
F	=	28

CAPACITY FACTOR (C_{sb}) = 0.0695m/s
WEIR LOAD (q/b) = 0.0008 m^3/s.
FLOW REGIME : INTENSE SPRAY

Figure (8.4a) Temperature Profiles predicted from Porter and Lockett Model for 1mm dia holes.

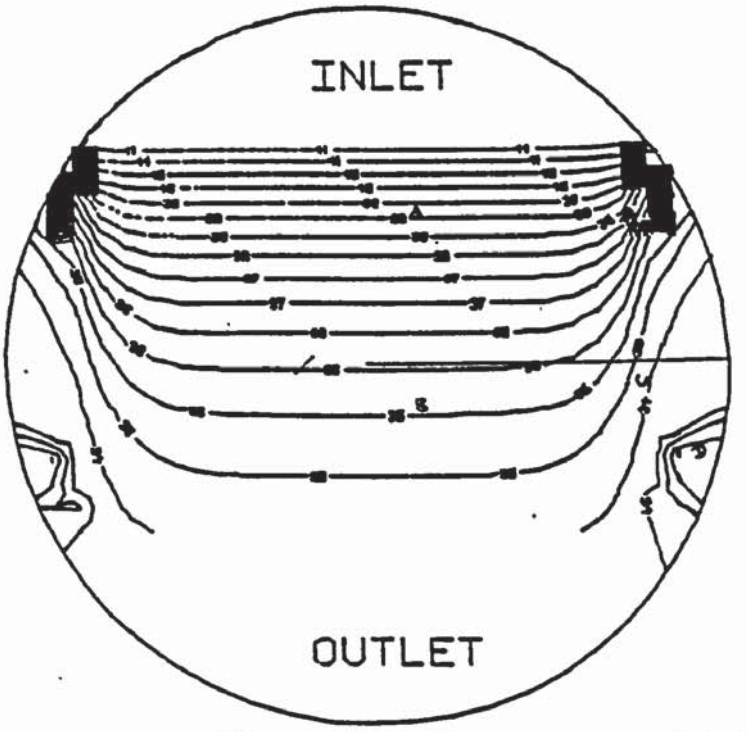

SYMBOL		T°C
A	=	38
B	=	35
C	=	34
D	=	33

CAPACITY FACTOR (C_{sb}) = 0.0695 m/s
WEIR LOAD (q/b) = 0.002 m^3/s.
FLOW REGIME : SPRAY

Figure (8.4b) Temperature Profiles predicted from Porter and Lockett Model for 1mm dia holes

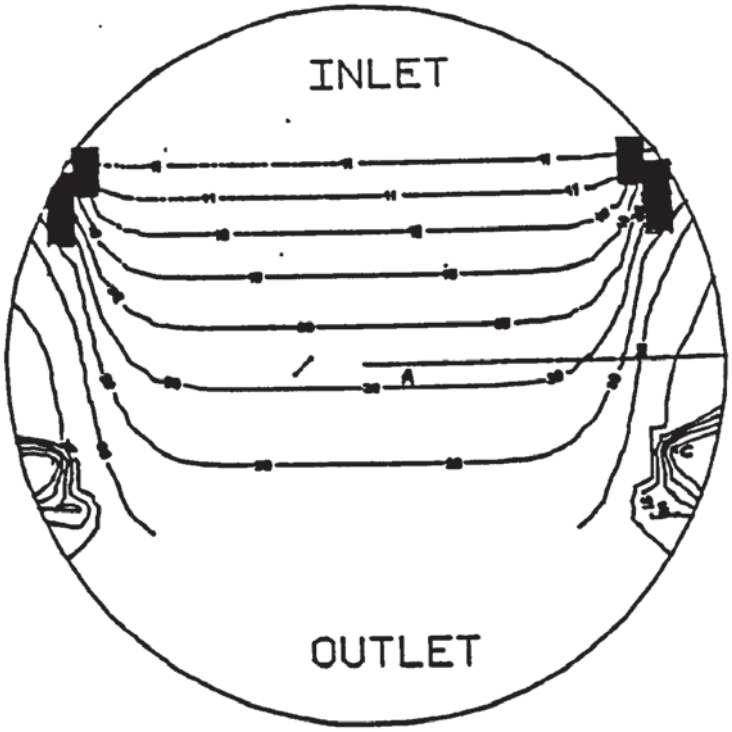

SYMBOL		T°C
A	=	38
B	=	37
C	=	36

CAPACITY FACTOR (C_{sb}) = 0.0695m/s
WEIR LOAD (q/b) = 0.008m^3/s.m
FLOW REGIME : MIXED

Figure (8.4c) Temperature Profiles predicted from Porter and Lockett Model for 1 mm dia holes

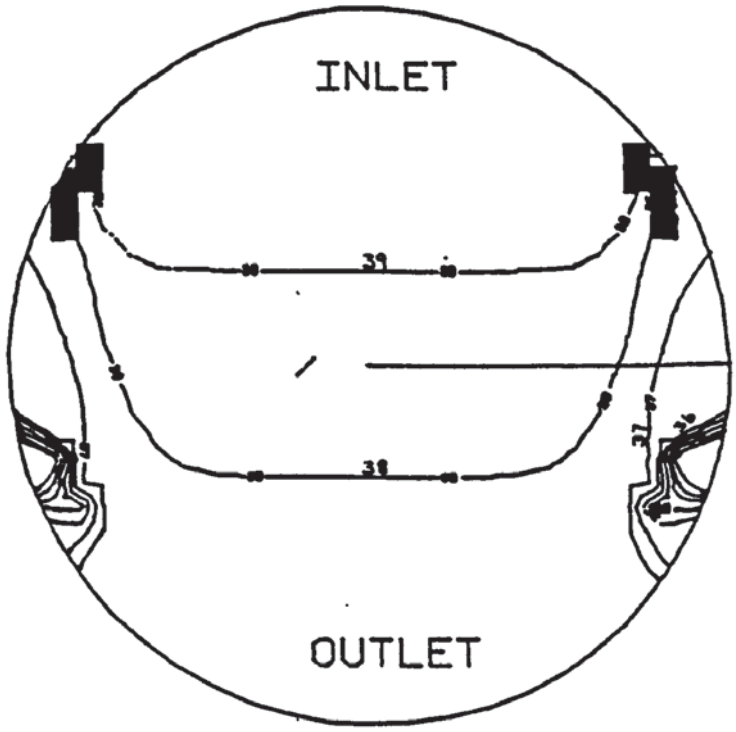

Figure (8.4d) Temperature Profiles predicted from Porter andLockett Model for 1mm dia holes

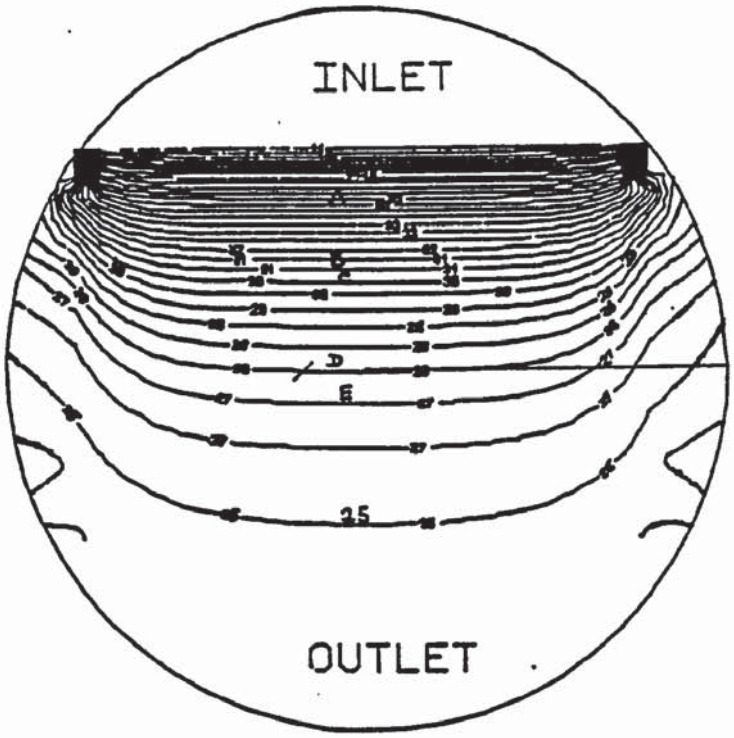

SYMBOL		T°C
A	=	33
B	=	31
C	=	30
D	=	28
E	=	27

CAPACITY FACTOR (C_{sb}) = 0.0695m/s
WEIR LOAD (q/b) = 0.0008 m^3/s.m
FLOW REGIME : INTENSE SPRAY

Figure (8.4e) Temperature Profiles predicted from Porter and Lockett for 12.5mm dia holes

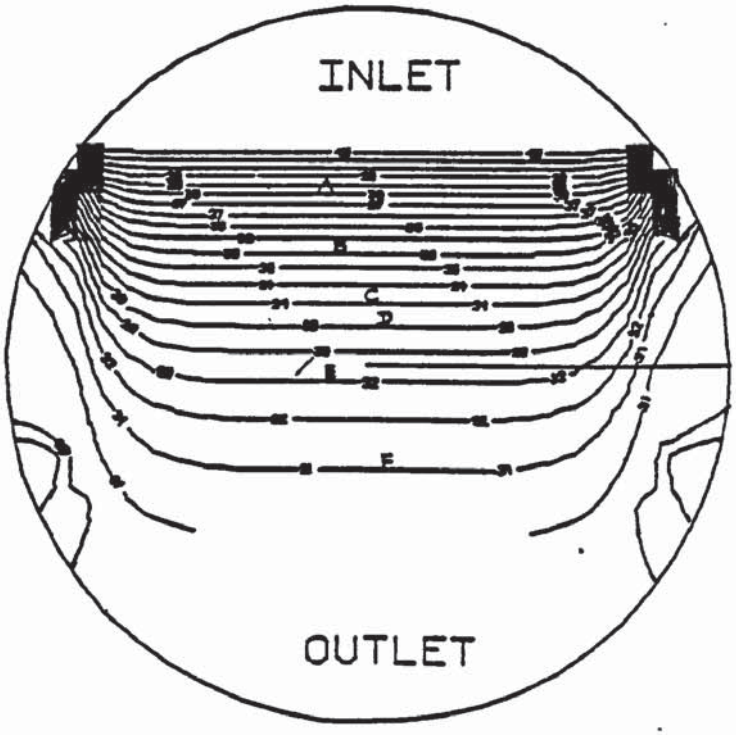

SYMBOL		T°C
A	=	38
B	=	35
C	=	34
D	=	33
E	=	32
F	=	31

CAPACITY FACTOR (C_{sb}) = 0.0695 m/s
WEIR LOAD (q/b) = 0.002 m^3/s.m
FLOW REGIME : SPRAY

Figure (8.4f) Temperature Profiles predicted from Porter and Lockett Model for 12.5 mm dia holes

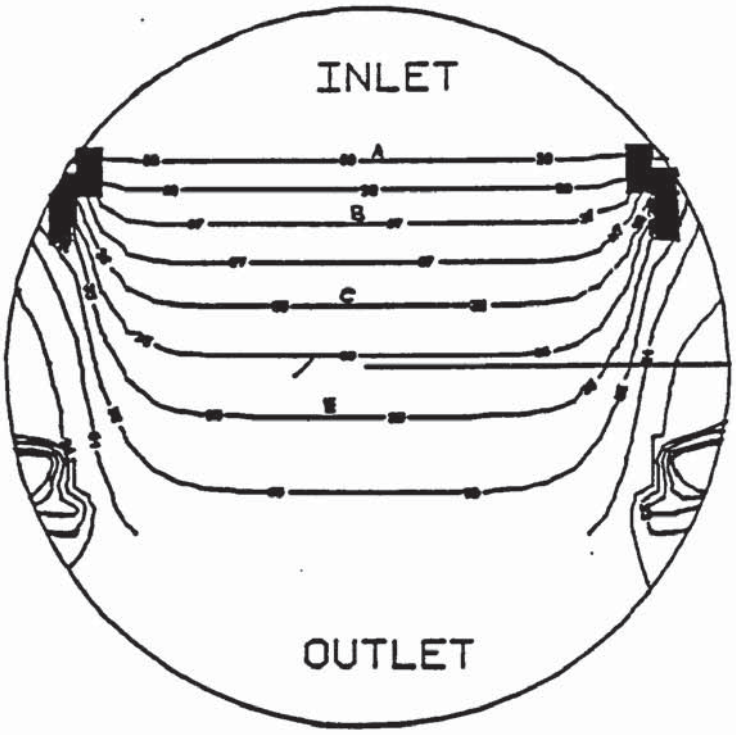

SYMBOL		T°C
A	=	38
B	=	37
C	=	36
D	=	35
E	=	35

CAPACITY FACTOR (C_{sb}) = 0.0695m/s

WEIR LOAD (q/b) = 0.008m^3/s m

FLOW REGIME : MIXED

Figure (8.4g): Temperature Profiles predicted from Porter and lockett Model for 12.5 mm dia holes

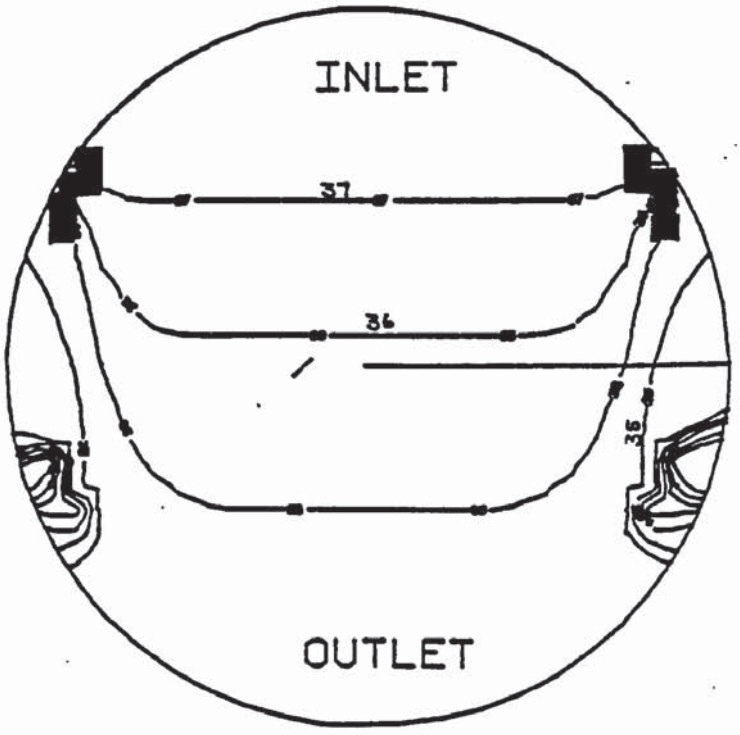

Figure (8.4h) Temperature Profiles predicted from Porter and Lockett Model for 12.5 mm dia holes

Figure (8.4i) : Murphree Vapour Efficiency - predicted by the Plug Flow Model - versus liquid loading for 1mm dia holes

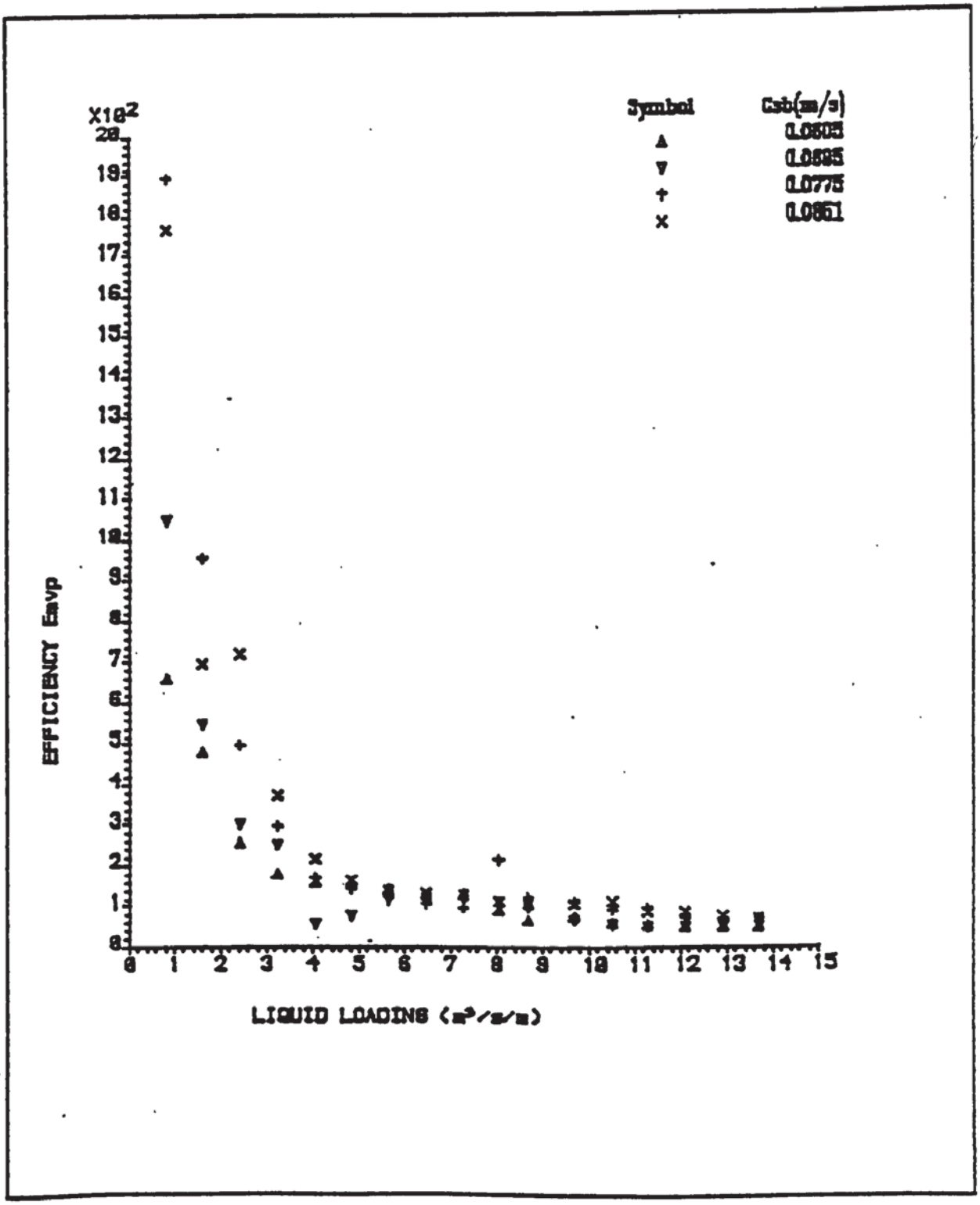

Figure (8.4j) : The Ratio of the Murphree Vapour Efficiency to the Point Efficiency - as predicted by the Plug Flow Model - versus liquid loading for 1mm dia holes

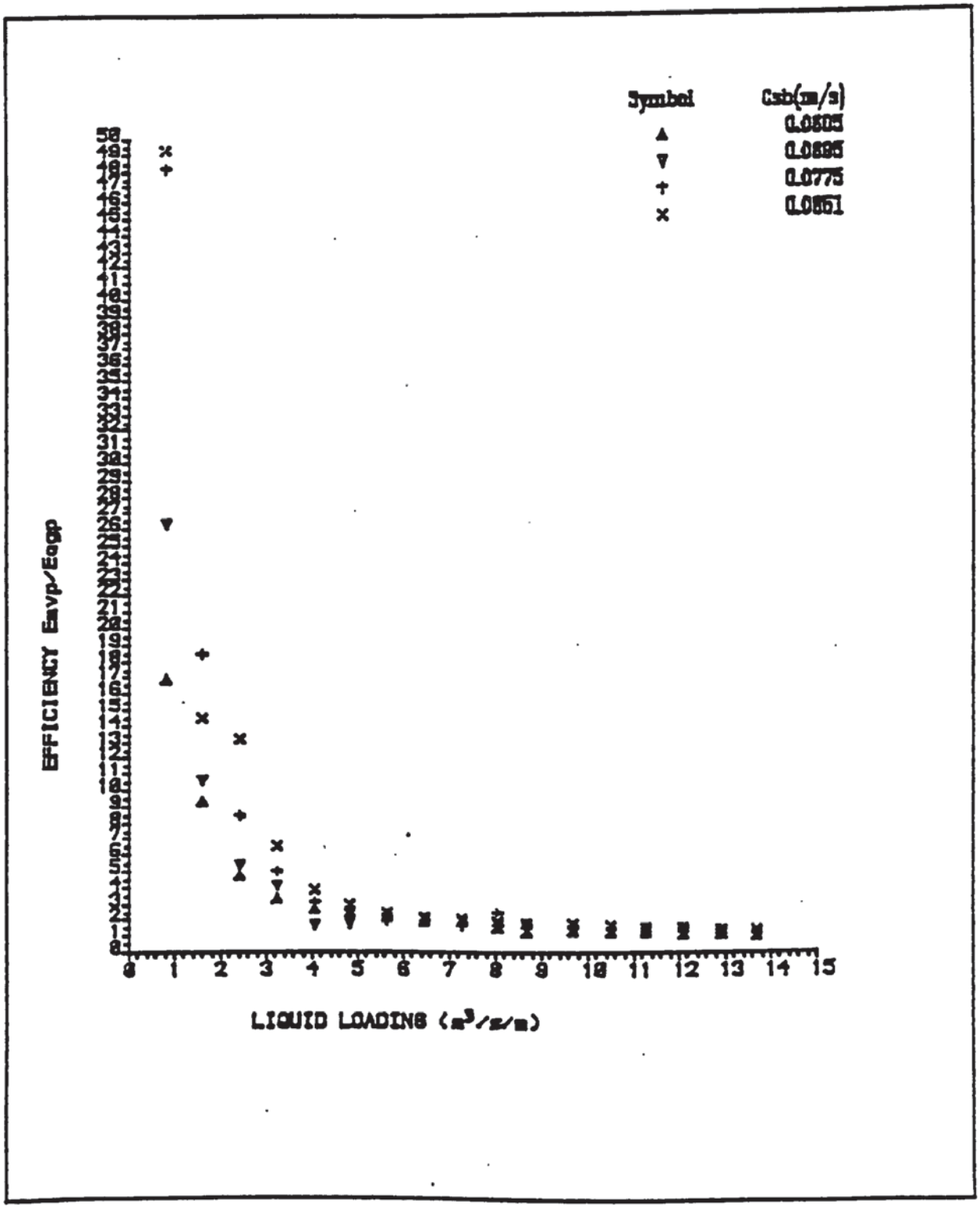

Figure (8.4k): Murphree Vapour Efficiency - predicted by the Plug Flow Model - versus liquid loading for 12.5 mm dia holes

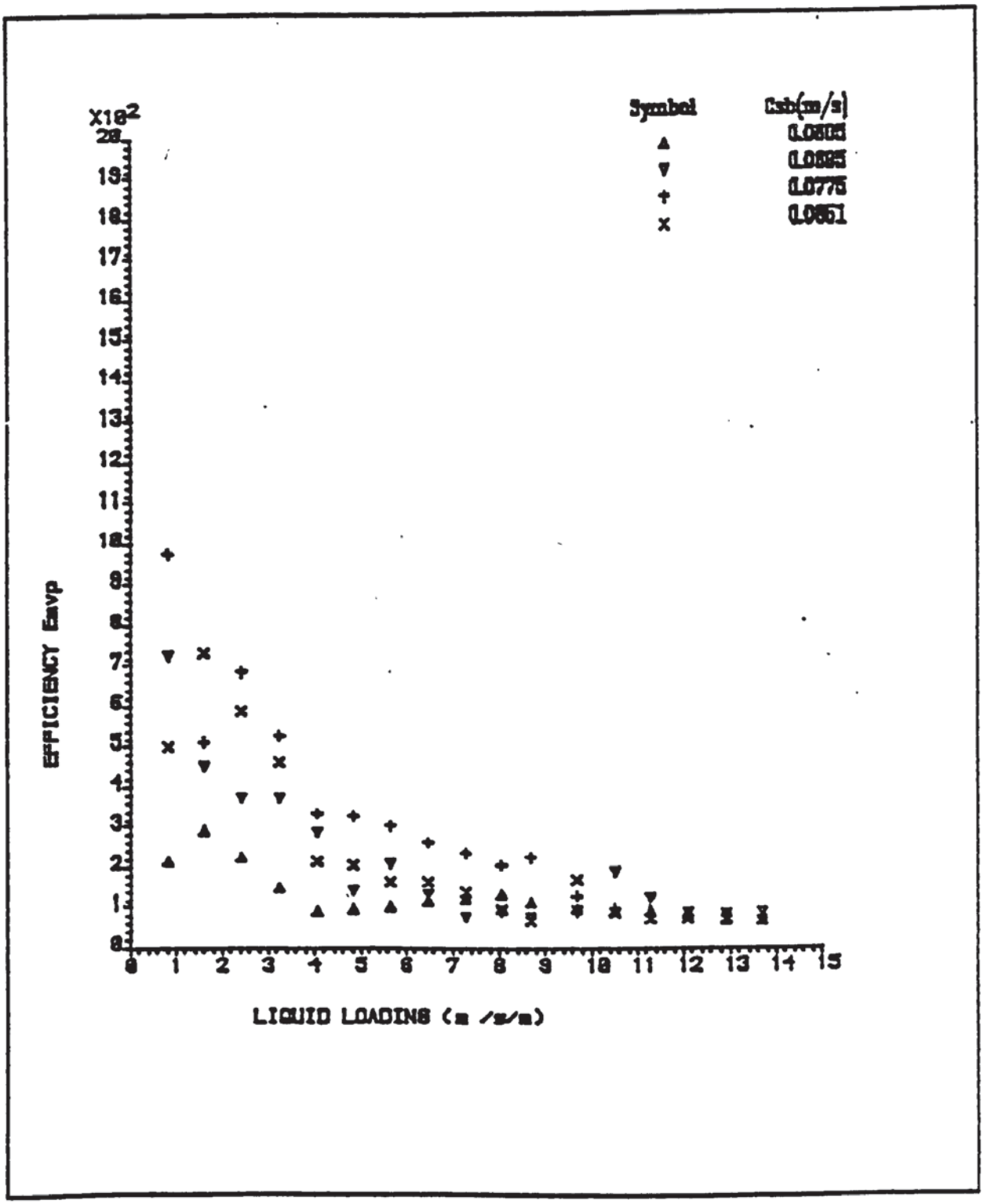

Figure (8.41) : The Ratio of the Murphree Vapour efficiency to the Point Efficiency - as predicte- by the Plug Flow Model - versus liquid loading for 12.5 mm dia holes

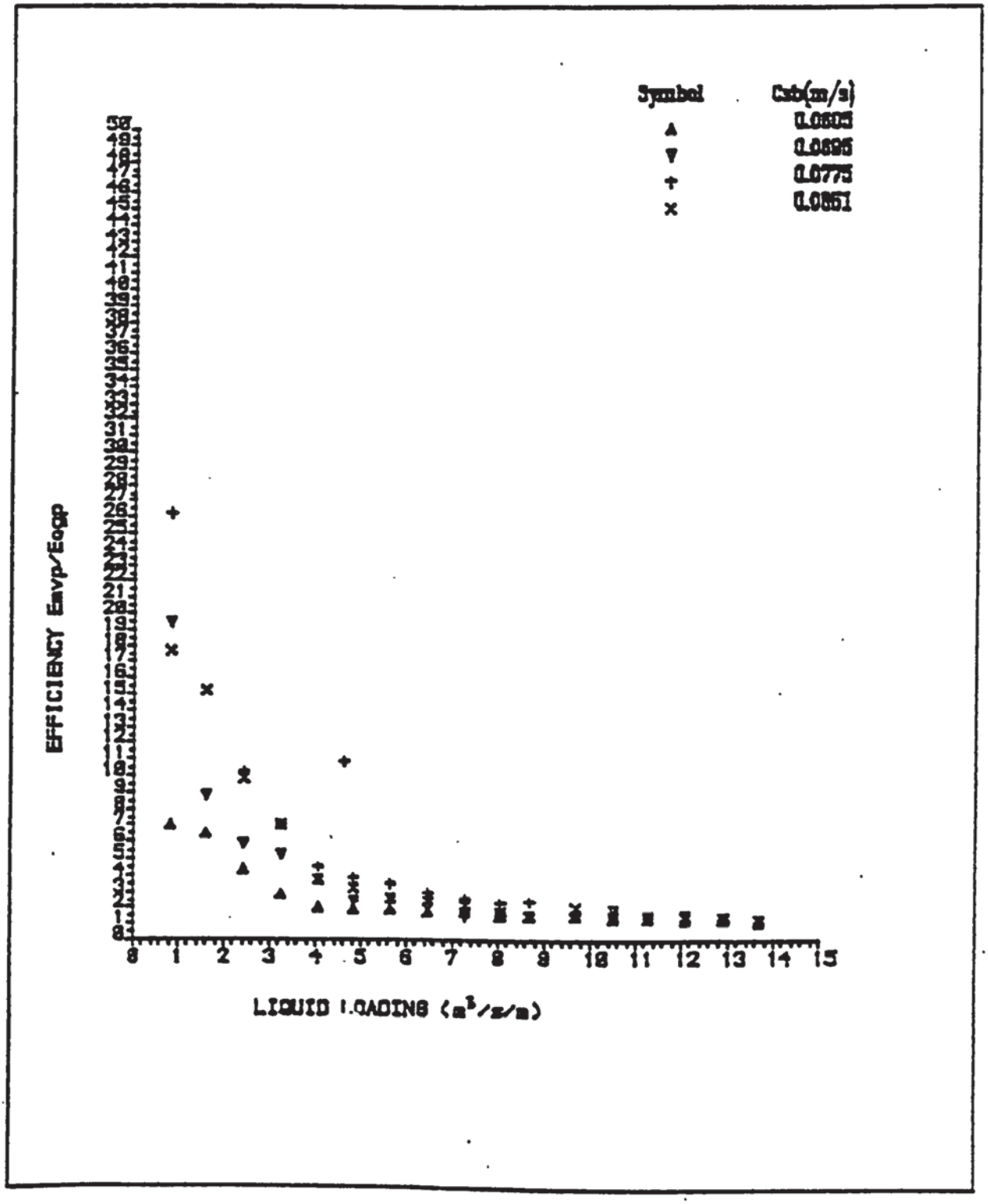

Figure (8.4m): Murphree Vapour Efficiency - predicted by the Porter and Lockett Model - versus liquid loading for 1 mm dia holes

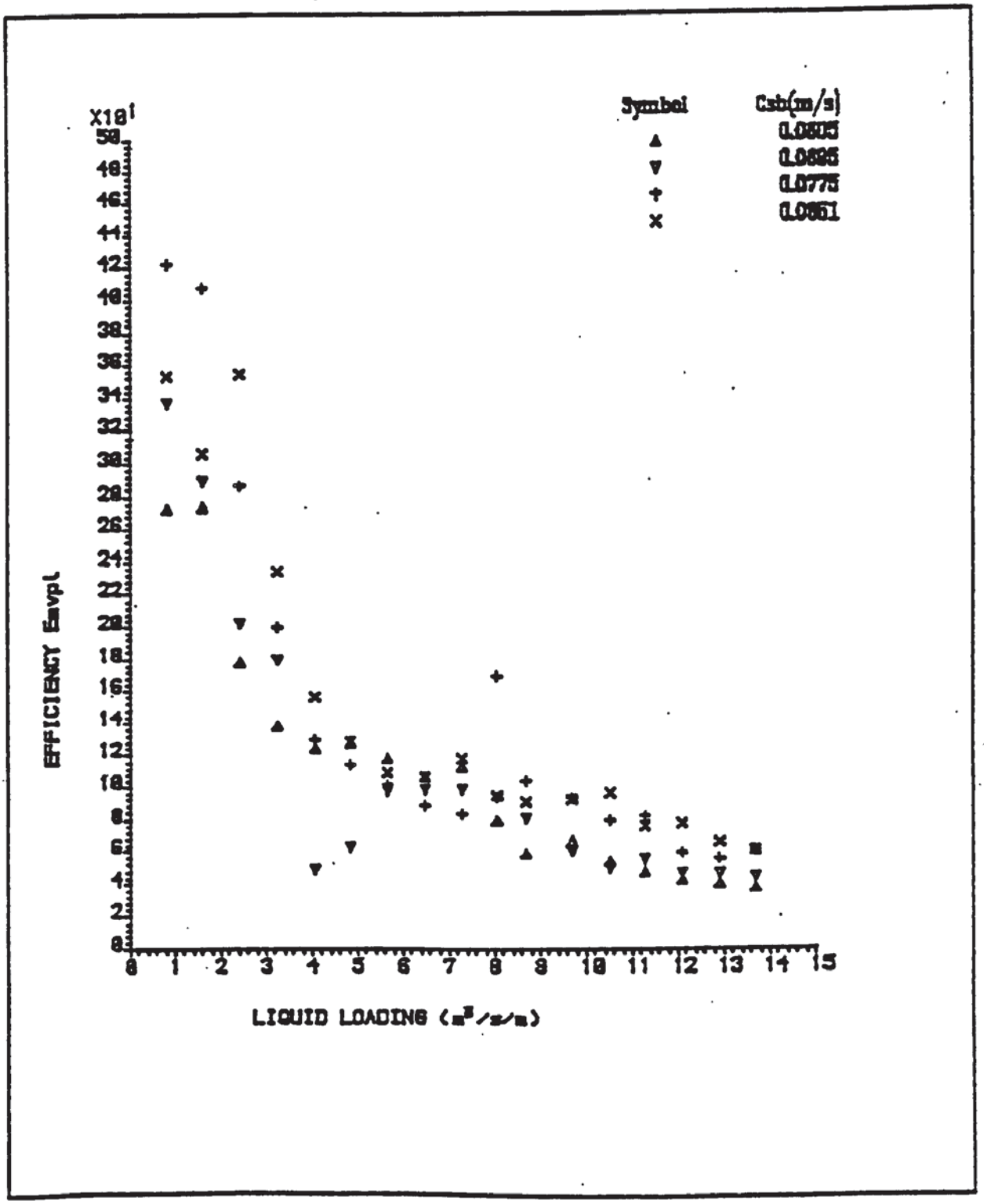

Figure (8.4n) : The Ratio of The Murphree Vapour Efficiency to the Point Efficiency - as predicted by the Porter and Lockett Model - versus liquid loading for 1mm dia holes

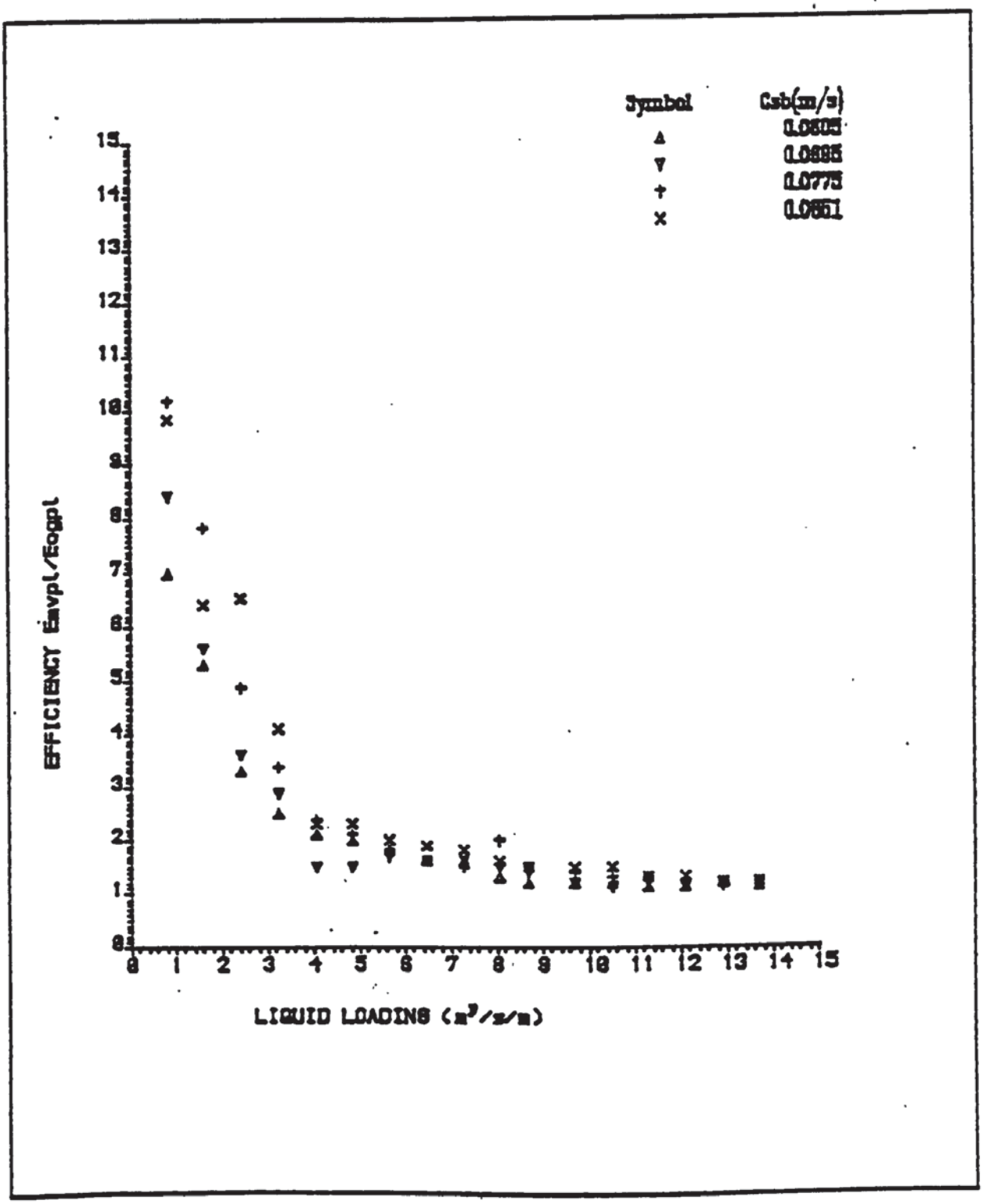

Figure (8.4o) : Murphree Vapour Efficiency - as predicted by the Porter and Lockett Model - versus liquid loading for 12.5 mm dia holes

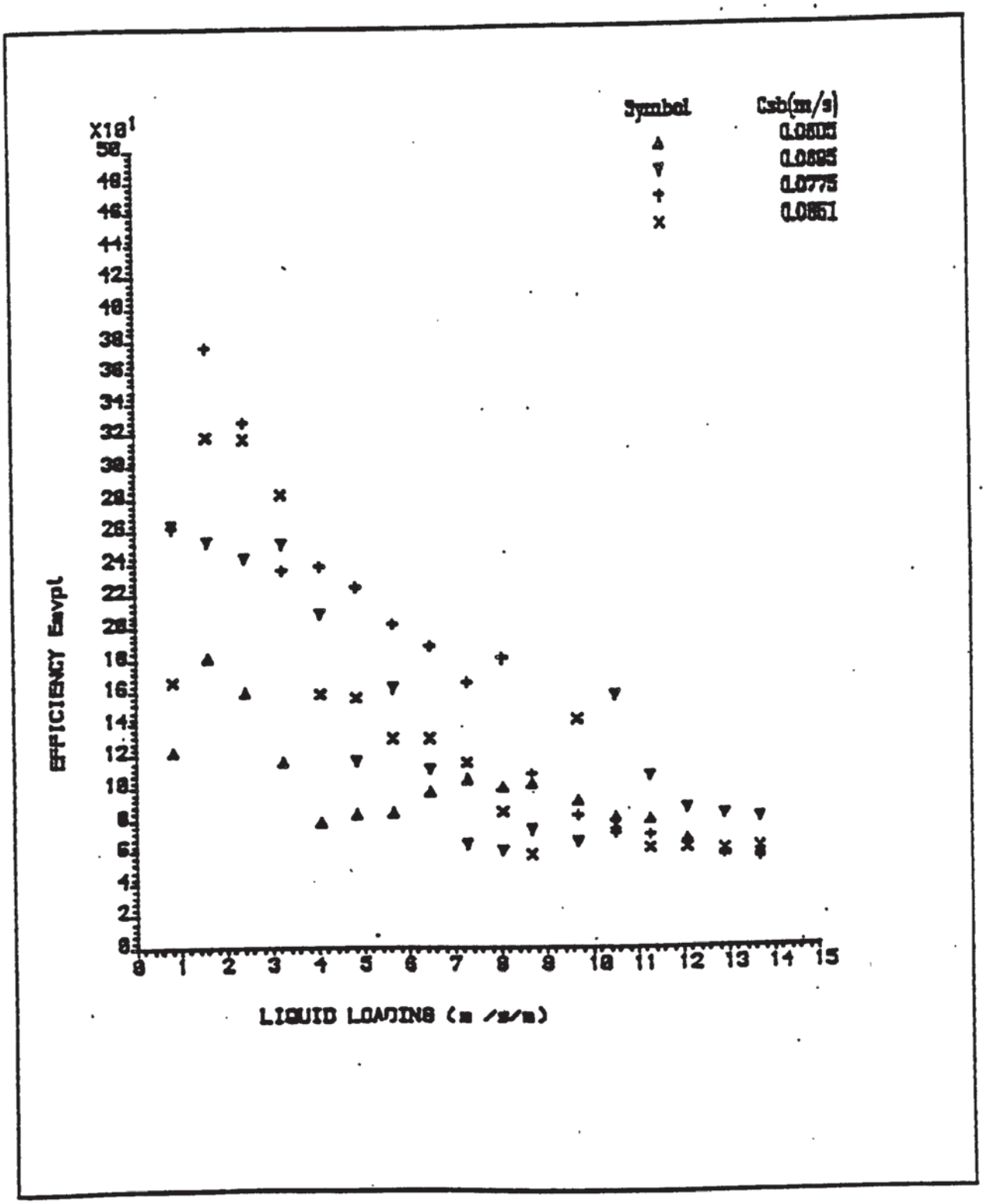

Figure (8.4p): The Ratio of the Murphree Vapour Efficiency to the Point Efficiency - as predicted by the Porter and Lockett Model - versus liquid loading for 12.5 mm dia holes.

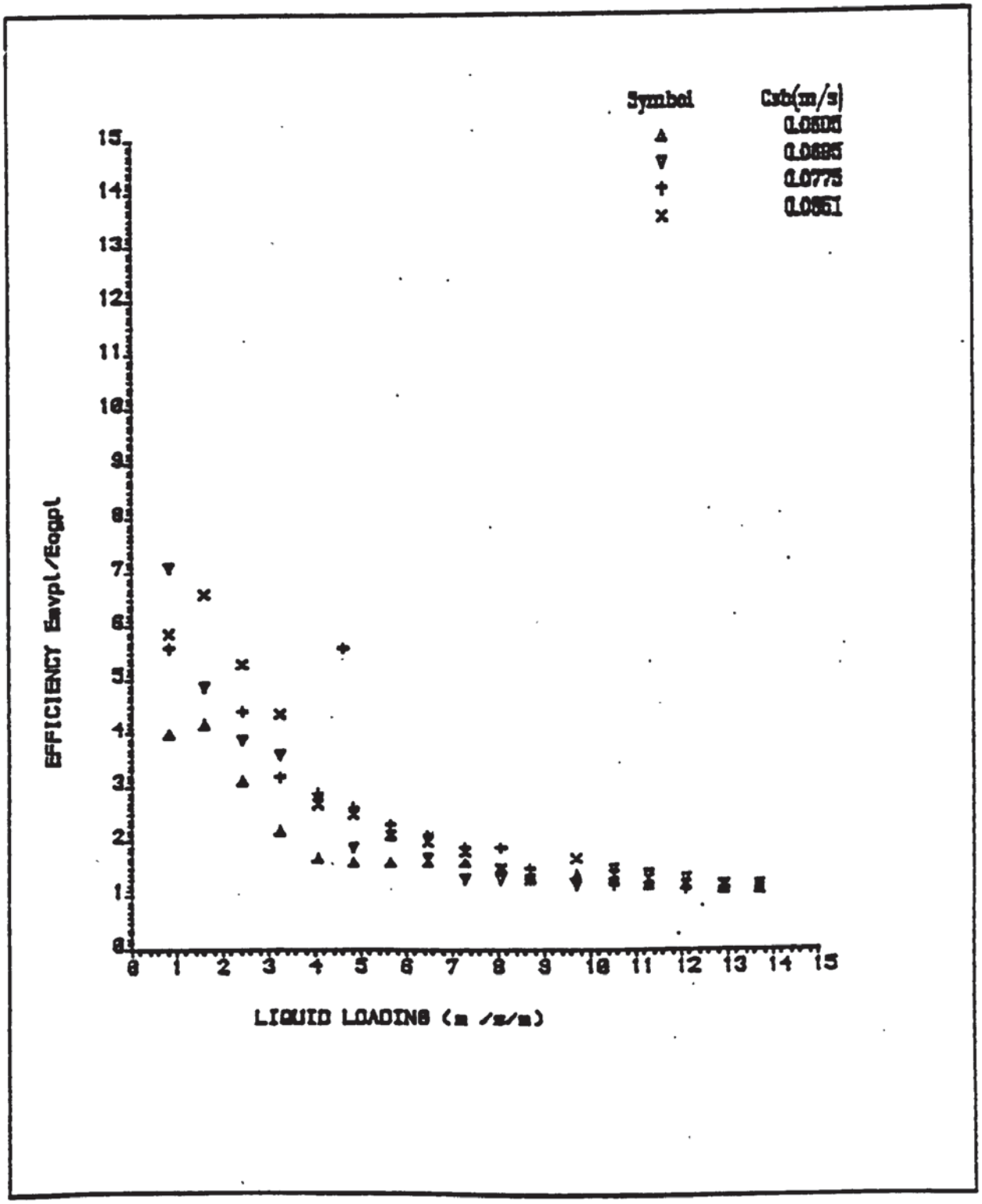

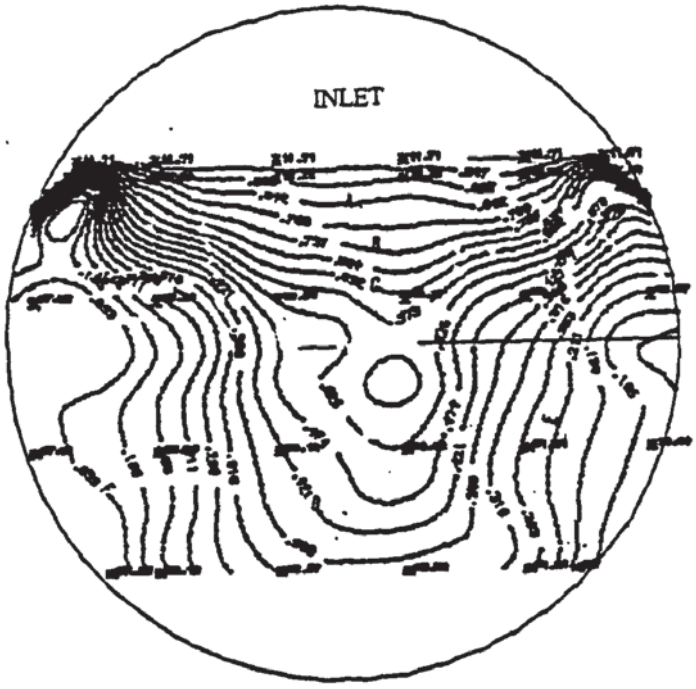

SYMBOL		TR
A	=	0.842
B	=	0.737
C	=	0.532
D	=	0.421
E	=	0.211
F	=	0.053

Figure (8.5.1a) Repeated experiment temperature profiles for 12.5 mm diameter hole tray

Capacity factor (C_{sb}) = 0.0851 m/s

Weir load (q/b) = 0.0008 m^3/s m

Flow regime : Intense spray

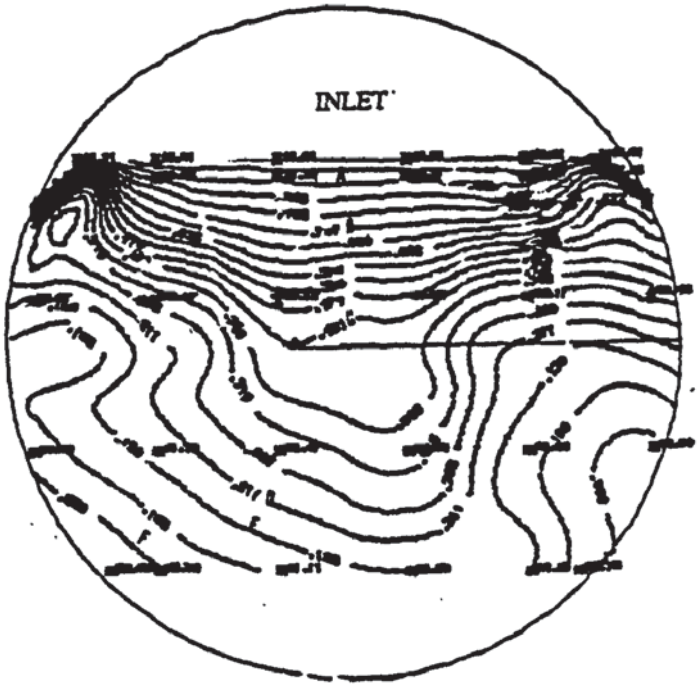

SYMBOL		TR
A	=	0.947
B	=	0.737
C	=	0.421
D	=	0.211
E	=	0.158
F	=	0.053

Figure (8.51b) Repeated experiment temperature profiles for 12.5 mm diameter hole tray

Capacity factor (C_{sb}) = 0.0851 m/s

Weir load (q/b) = 0.0032 m^3/s m

Flow regime : Spray

SYMBOL		TR
A	=	0.885
B	=	0.737
C	=	0.579
D	=	0.421
E	=	0.211
F	=	0.053

Figure (8.5.1c) Repeated experiment temperature profiles for 12.5 mm diameter hole tray

Capacity factor (C_{sb}) = 0.0851 m/s

Weir load (q/b) = 0.006 m^3/s m

Flow regime : Mixed

SYMBOL		TR
A	=	0.842
B	=	0.788
C	=	0.423
D	=	0.474
E	=	0.314
F	=	0.053

Figure (8.5.1d) Repeated experiment temperature profiles for 12.5 mm diameter hole tray

Capacity factor (C_{sb}) = 0.0851 m/s

Weir load (q/b) = 0.0104 m^3/s m

Flow regime : Emulsified

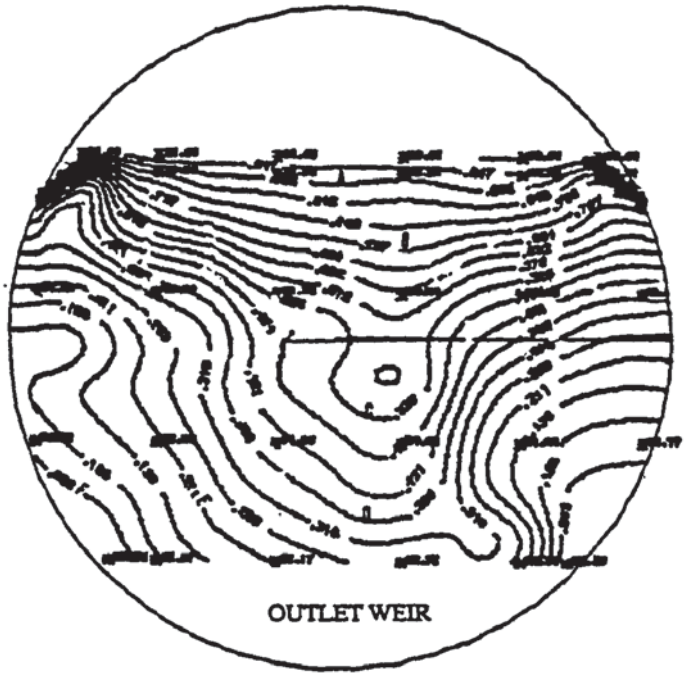

SYMBOL		TR
A	=	0.947
B	=	0.737
C	=	0.525
D	=	0.388
E	=	0.211
F	=	0.053

Figure (8.5.2a) Repeated experiment temperature profiles for 12.5 mm diameter hole tray

Capacity factor (C_{sb}) = 0.0695 m/s

Weir load (q/b) = 0.0008 m^3/s m

Flow regime : Intense spray

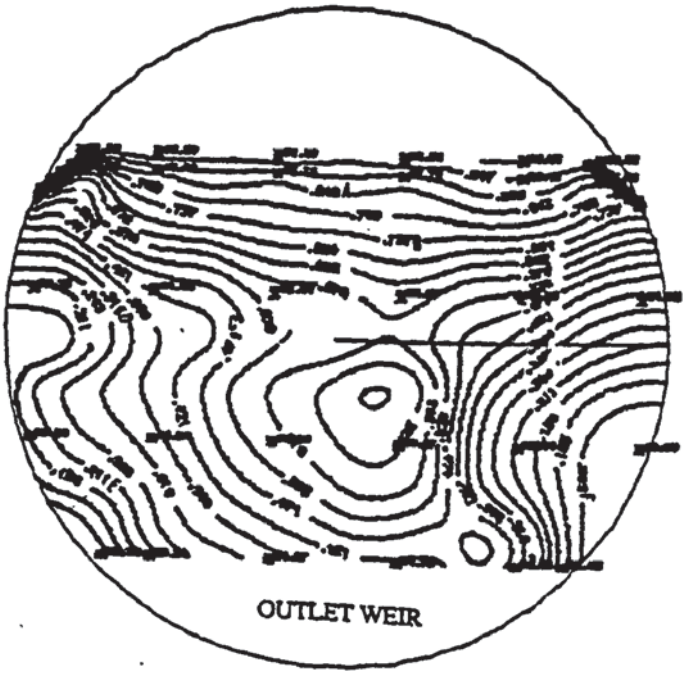

SYMBOL		TR
A	=	0.943
B	=	0.737
C	=	0.471
D	=	0.318
E	=	0.211
F	=	0.053

Figure (8.5.2b) Repeated experiment temperature profiles for 12.5 mm diameter hole tray

Capacity factor (C_{sb}) = 0.0695 m/s

Weir load (q/b) = 0.0056 m^3/s m

Flow regime : Spray

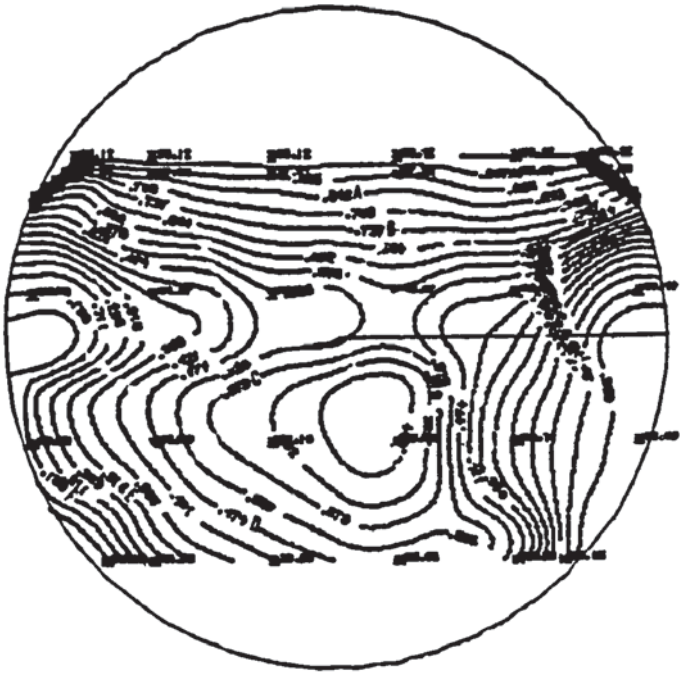

SYMBOL		TR
A	=	0.848
B	=	0.737
C	=	0.579
D	=	0.474
E	=	0.318
F	=	0.158

Figure (8.5.2c) Repeated experiment temperature profiles for 12.5 mm diameter hole tray

Capacity factor (C_{sb}) = 0.0695 m/s

Weir load (q/b) = 0.008 m^3/s m

Flow regime : Mixed

SYMBOL		TR
A	=	0.941
B	=	0.842
C	=	0.758
D	=	0.105
E	=	0.532
F	=	0.751

Figure (8.5.2d) Repeated experiment temperature profiles for 12.5 mm diameter hole tray

Capacity factor (C_{sb}) = 0.0695 m/s

Weir load (q/b) = 0.0128 m^3/s m

Flow regime : Emulsified

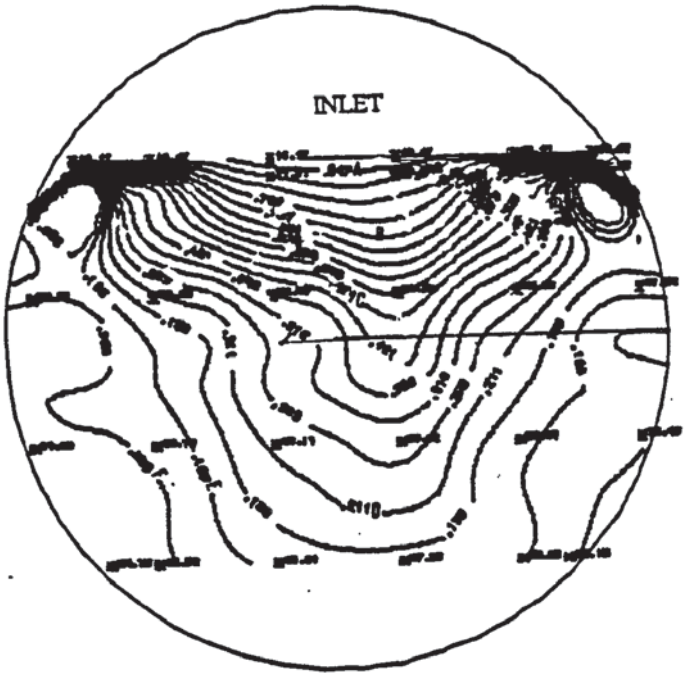

SYMBOL		TR
A	=	0.947
B	=	0.737
C	=	0.474
D	=	0.211
E	=	0.158
F	=	0.053

Figure (8.5.3a) Repeated experiment temperature profiles for 12.5 mm diameter hole tray

Capacity factor (C_{sb}) = 0.0605 m/s

Weir load (q/b) = 0.0008 m^3/s m

Flow regime : Intense spray

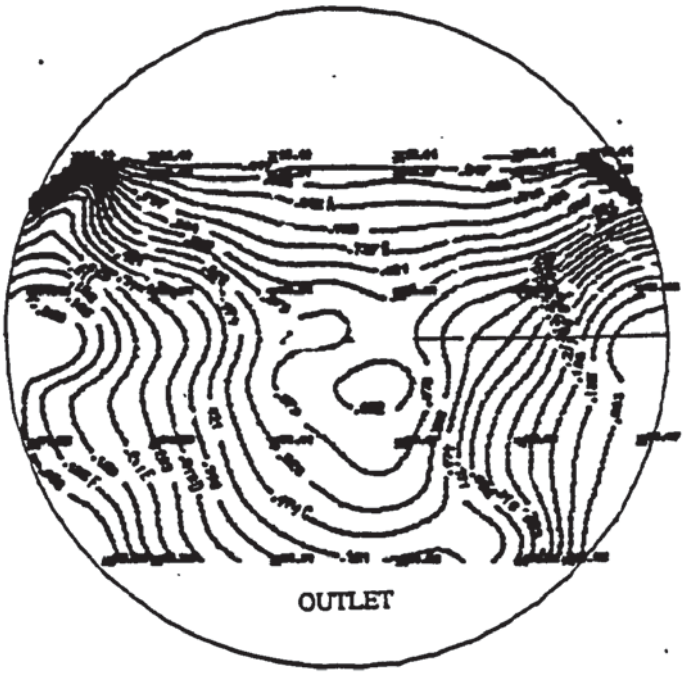

SYMBOL		TR
A	=	0.842
B	=	0.737
C	=	0.526
D	=	0.318
E	=	0.211
F	=	0.105

Figure (8.5.3b) Repeated experiment temperature profiles for 12.5 mm diameter hole tray

Capacity factor (C_{sb}) = 0.0605 m/s

Weir load (q/b) = 0.0032 m^3/s m

Flow regime : Spray

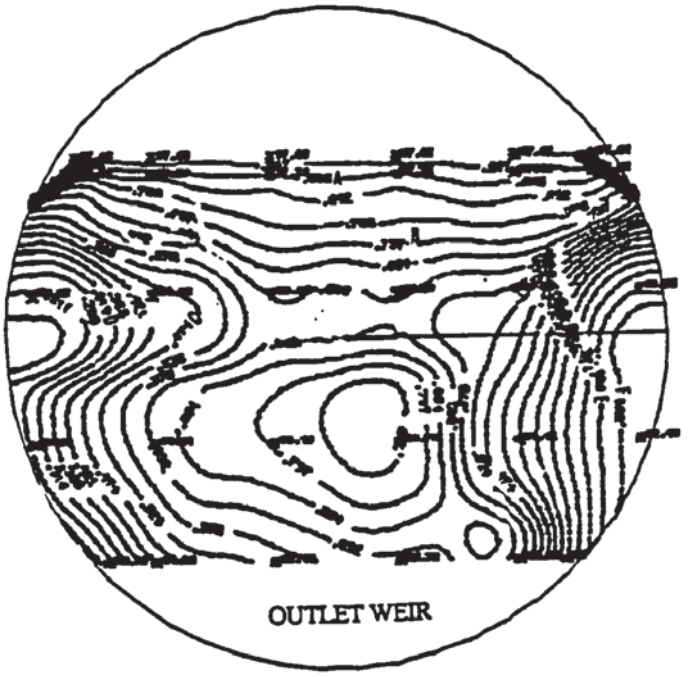

SYMBOL		TR
A	=	0.885
B	=	0.737
C	=	0.474
D	=	0.318
E	=	0.105
F	=	0.053

Figure (8.5.3c) Repeated experiment temperature profiles for 12.5 mm diameter hole tray

Capacity factor (C_{sb}) = 0.0605 m/s

Weir load (q/b) = 0.008 m^3/s m

Flow regime : Mixed

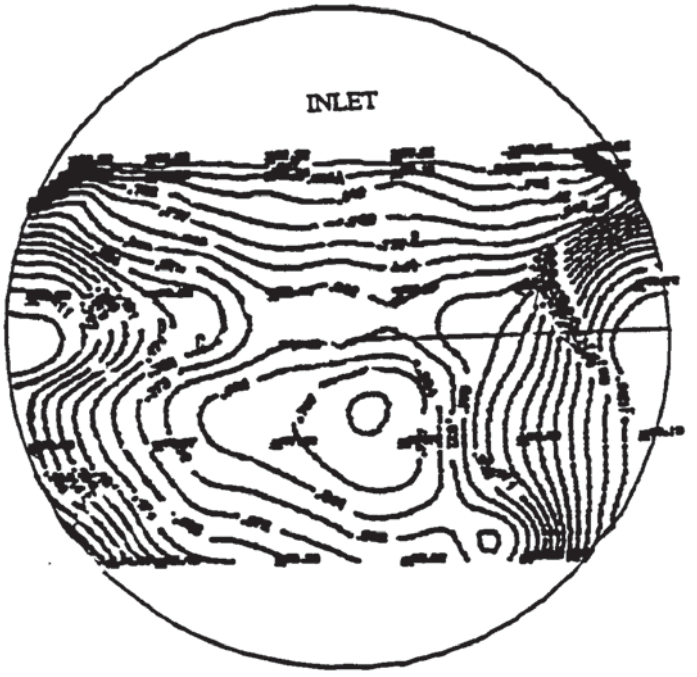

SYMBOL		TR
A	=	0.885
B	=	0.737
C	=	0.584
D	=	0.474
E	=	0.318
F	=	0.053

Figure (8.5.3d) Repeated experiment temperature profiles for 12.5 mm diameter hole tray

Capacity factor (C_{sb}) = 0.0605 m/s

Weir load (q/b) = 0.012 m^3/s m

Flow regime : Emulsified

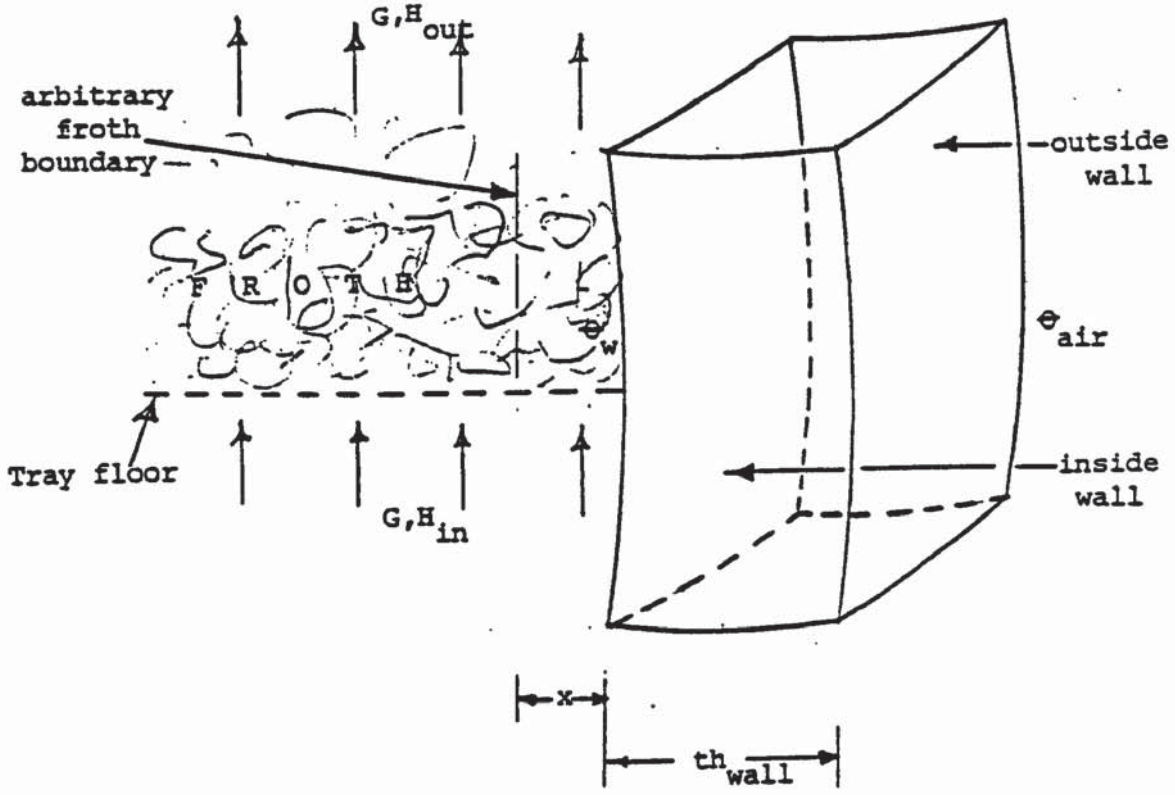

Figure (8.6) Differential element of froth and column wall used in heat balance equations

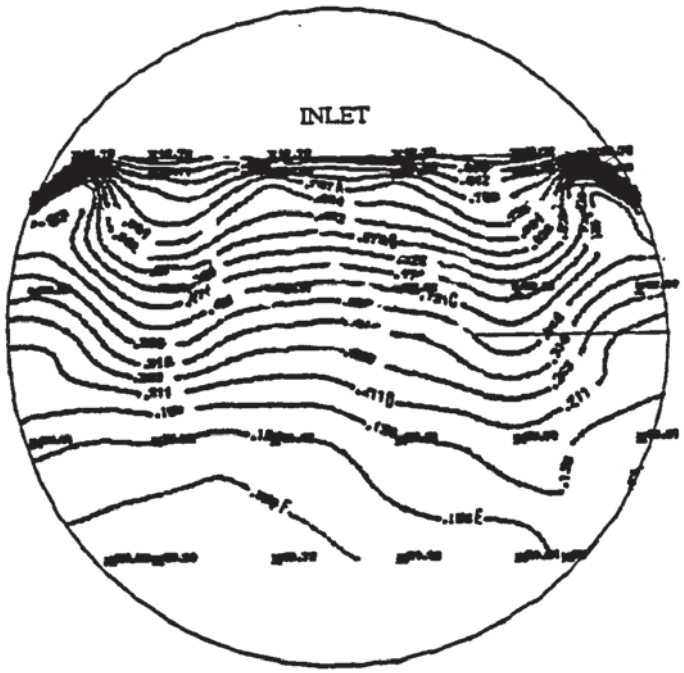

SYMBOL		T°C
A	=	0.787
B	=	0.578
C	=	0.421
D	=	0.211
E	=	0.105
F	=	0.05

Figure (8.6.1a) Perspex tray (12.5 mm diameter hole) temperature profiles

Capacity factor (Csb) = 0.0851 m/s

Weir load (q/b) = 0.0008 m^3/s m

Flow regime : Intense spray

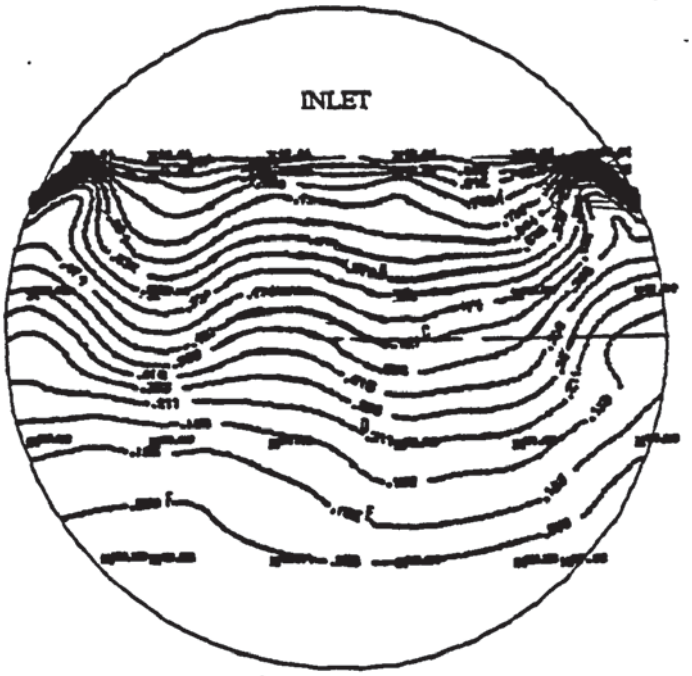

SYMBOL		T°C
A	=	0.788
B	=	0.578
C	=	0.421
D	=	0.211
E	=	0.105
F	=	0.058

Figure (8.6.1b) Perspex tray (12.5 mm diameter hole) temperature profiles

Capacity factor (Csb) = 0.0851 m/s

Weir load (q/b) = 0.004 m^3/s m

Flow regime : Spray

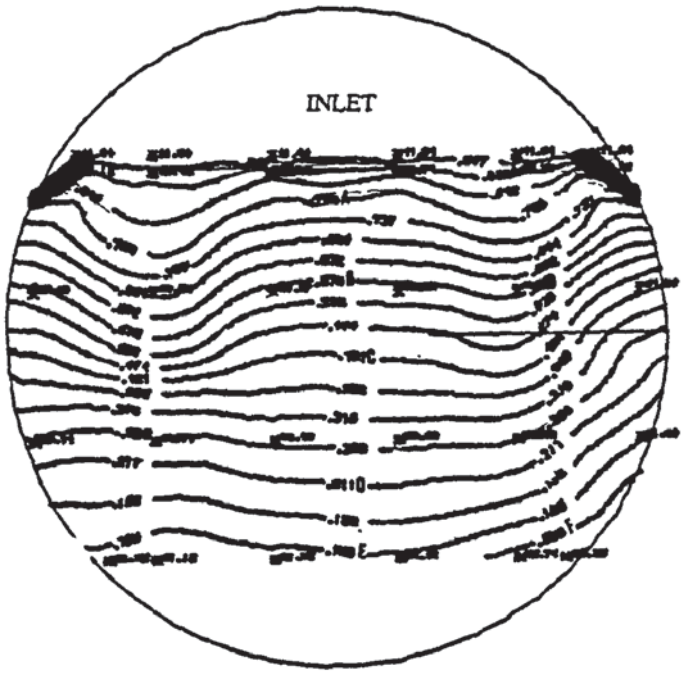

SYMBOL		T°C
A	=	0.788
B	=	0.578
C	=	0.421
D	=	0.211
E	=	0.105
F	=	0.058

Figure (8.6.1c) Perspex tray (12.5 mm diameter hole) temperature profiles

Capacity factor (Csb) = 0.0851 m/s

Weir load (q/b) = 0.006 m^3/s m

Flow regime : Mixed

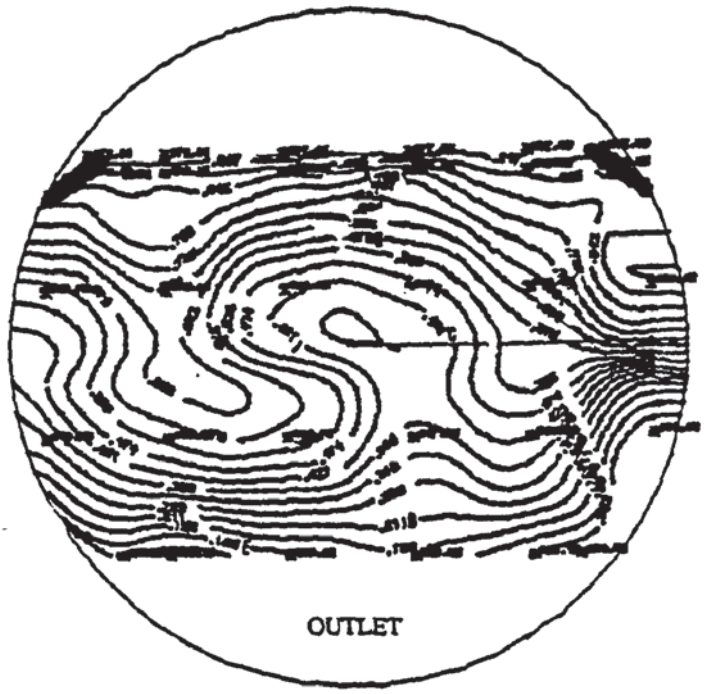

SYMBOL		T°C
A	=	0.788
B	=	0.578
C	=	0.421
D	=	0.211
E	=	0.105

Figure (8.6.1d) Perspex tray (12.5 mm diameter hole) temperature profiles

Capacity factor (Csb) = 0.0851 m/s

Weir load (q/b) = 0.008 m^3/s m

Flow regime : Emulsified

Chapter 9

EXPERIMENT TO STUDY THE EFFECT OF NON UNIFORM LIQUID FLOW OVER THE WEIR ON TRAY EFFICIENCY

9.1 INTRODUCTION

The column efficiency, E_o , is used as the criteria for assessing the performance of a distillation column and an understanding of the point and plate efficiencies on each of the operating trays is required in order to obtain a method which will enable the prediction of column efficiency to be achieved. In practice the outlet concentration of the liquid leaving the tray has always been taken from the mixed contents of the outlet downcomer with the assumption that the weir flow has a uniform concentration. However , there is no work in the open literature concerning possible variations of liquid flow over the outlet weir . The type of flow over the exit weir has always been assumed to be that represented by the Francis weir equation. **Zuiderweg** (74) reported that the flow across the outlet weir in the emulsified flow regime can be represented by the Francis weir equation anticipating the flow to be uniform across the weir based on the expected high liquid hold up in this operating regime. However, in some cases it is known that the liquid does flow over the outlet weir in the form of a spray of drops rather than a continuous stream of liquid. Thus to obtain an accurate estimate of the performance of an individual tray and to give a proper understanding to the calculated efficiencies, consideration should be given to the possible variation of the liquid flow per unit length of the outlet weir. The variation of the liquid flow over the outlet weir may also be related to the flow patterns on the tray and thus to the overall performance and efficiency of the tray.

With the new water cooling technique a method can be developed to calculate the point efficiency on the tray from the temperatures obtained without an exact knowledge of the flow pattern on the tray.With the development of the new water cooling technique, temperature measurements of water in cross flow with air can be made at any point on the tray and with the gas phase enthalpy measurements, the plate efficiency can be estimated based on enthalpy calculations. Thus the equilibrium enthalpy of the air saturated with water is given by :

$$H^* = mT_o + b \qquad (9.1)$$

Assuming average liquid flow across the weir, the equilibrium H^* can be estimated at an

average temperature of the liquid leaving the tray from a suitable enthalpy - temperature correlation. The average temperature (T) is given by :

$$T = (T_1x_1 + T_2x_2 + T_3x_3 + \text{-------} + T_nx_n) / (X) \qquad (9.2)$$

Where X is the total length of the weir and T_1, T_2, T_3 ---- T_n are the temperatures of the liquid measured at intervals of x_1, x_2, x_3, ---- x_n along the weir length.

For a situation where the flow of liquid over the weir length is not uniform , a different method must be used for estimating the temperature or concentration across the weir length.

From a heat balance, it can be established that for a unit length of the weir.

$$Q = M\ C_p \Delta\ T \qquad (9.3)$$

or $$= \rho_l\ C_p\ V \Delta T$$

where Q is the total heat , M is the mass flow rate (liquid kg/s) and V is the volumetric flow rate (m^3/s m). Assuming uniform flow the equation for the entire length will becomes :-

$$Q = M C_p \frac{\Sigma\ \Delta T \Delta X}{X} \qquad (9.4)$$

For non uniform flow the equation becomes:-

$$Q = \rho_l\ C_p \int_0^W V\ T\ dT \qquad (9.5)$$

For the water cooling technique the variation in flow will mean the same variation in the calculated enthalpy of the vapour H^*_{out} in equilibrium with the liquid leaving the tray.

To account for the variation the Tray efficiency model will have to be restructured to accommodate the expected changes in H^*_{out} along the outlet weir length.

$$E_{mv} = [(H_2 - H_1) / (H^*_{out} - H_1)] \qquad (9.6)$$

For uniform flow H^*_{out} is given by:

$$H^*_{out} = C_{air}(T_{out} - T_0) + H_o[C_{pw}(T_{out} - T_0) + \lambda] \quad (9.7)$$

where H_o is the humidity of the saturated air .

For non uniform flow the equation becomes:

$$H^*_{out} = C_{air}(1/A\int_0^W T_{out}\,dT - T_0) + H_o[C_{pw}(1/A\int_0^W T_{out}\,dT - T_0) + \lambda] \quad (9.8)$$

Where

T_0 = Datum Temperature = 273 K

W = Out let weir length m.

λ = Latent heat of vaporisation (kJ/kg)

A computer program was written and used to solve the above equation for H^*_{out} and the tray efficiencies were calculated without the need for the evaluation of the Point efficiency of the vapour and liquid mass transfer coefficients (N_g and N_l).

Since E_{mv} was observed to depend on the assumption of uniform liquid flow (or lack of it) along the outlet weir, an experiment would be necessary to determine whether the liquid flow over the outlet weir was uniform or non-uniform.

9.2 EXPERIMENTAL APPARATUS

The apparatus, which was used to determine the flow over the outlet weir , was designed such that the liquid leaving the tray flowed over the weir into a number of compartments. Thus the length of the outlet weir had been divided into 8 sections, each section containing a perspex compartment. At a particular section of the weir, the liquid would flow over and into one of the compartments and out through a hole in the base of the compartment. At steady state the depth of liquid above the hole in each compartment was set by the flow rate. Thus the flowrate was measured by estimating the liquid depth in each compartment.

The apparatus was designed so that six of the eight compartments had the same width and depth whilst the remaining two comparments were made to fit at the circular column walls. A hard rubber sheet was fitted around the top edge of the box and held to the column wall with a metal ring to prevent loss of liquid between the box and the column walls.

To overcome frothing of the liquid in the downcomer compartments, the clear liquid height was recorded in each compartment using a water manometer.

To allow for a range of liquid flowrates adjustable disharge holes were incorporated in the base of each compartment. Hence the hole diameter for each of the compartments could be increased or decreased to increase or lower the liquid height in the compartment. The compartment dimensions are shown in Figure 9b & 9.1.

The apparatus was carefully lowered into the downcomer and the investigation were carried out at the same weir loads and capacity factors as described in chapter 7 .

9.3 CALIBRATION OF THE COMPARTMENTS

Since the weir flow measuring device contained three different compartment shapes, each of the same depth, it became necessary to calibrate each different type of compartment. Liquid (water) of known flow rates was passed through the individual compartment and the head of liquid in each compartment was recorded.

A calibration of liquid flow rate against the height of liquid in each compartment was plotted (see figure 9a) and this was used to determine the actual liquid flow rate in each compartment during the experiment. The flow rate per unit length of the weir was calculated by dividing the flow rate corresponding to that compartment by the width of the compartment..

9.4 DISCUSSION OF RESULTS

One interesting observation in this experimental programme was that the distribution of the liquid flow over the outlet weir changed with increasing weir load. This experiment was only performed using the 12.5 mm diameter hole tray at three different C_{sb} values (0.0605, 0.0775 and 0.092) and with increasing values of the weir load. The calculated results are given in Appendix (11), tables (9.1a to 9.1t).

Capacity factor of 0.0605 m/s

At low liquid loading (0.0016 m^3/s m), figure (9.1a - 9.1b) it was found that the liquid flow across the outlet weir length was uniform without any liquid channelling across the weir as was the case for the temperature profiles on the tray. This could be explained by the suggestion that the liquid flow across the exit weir for a tray operating in the spray regime is controlled by the liquid drop velocities (77). At the weir the fine spray of liquid atomised by the gas jetting through the hole was thrown across the tray outlet .

However it has been suggested by **Zuiderweg** (77) that the flow across the outlet weir in the emulsified flow regime can be represented by the Francis weir equation and that was with the assumption that the liquid flow across the weir in the emulsified regime would be uniform as a result of a reduction in the resistance to flow by the gas as the liquid hold-up increased.

The present results have shown that the expected channel (uniform flow) across the weir only occurred while operating conditions were limited to the spray and mixed flow regimes at a low capacity factor (0.0605 m/s) figure (9.1c - 9.1d). Although in the mixed regime there is evidence of more liquid flow at the central section of the tray .

It was found that as the operating conditions were changed to operate in the emulsified flow regime figure (9.1e - 9.1f), the developed flow was found to change with more liquid channelling at the central section of the tray leaving the flow at the ends of the weir relatively very low, with a peak at an area slightly more than half way to the edge of the weir starting from figure 9.1d. The peak may be explained as the boundary of the central mixing zone. Figure (9.1f).

Capacity factor of 0.0775 m/s

As shown in figure (9.1g & 9.1h) the flow across the weir in the spray regime (weir loads of 0.0016 to 0.003 m^3/s m) was found to be uniform with less evidence of low velocity liquid at both ends of the weir. As the weir load was further increased to above 0.003 m^3/s m, thereby changing from the spray to mixed flow regime, the flow over the weir was found to show more liquid channelling in the central section of the tray leaving the sides with relatively low velocity liquid. The peak was also identified in this flow regime. Figure (9.1i and 9.1j). On increasing the weir load to conditions identified with the emulsified flow regime , the observed flow across the weir was similar to those obtained for the mixed flow regime with less liquid flow on the both

ends of the weir (figure (9.1k & 9.1l).

Capacity factor of 0.0851 m/s.

The observed flow across the weir (figure (9.1m & 9.1n)) show a uniform liquid channel across the weir at low liquid loadings of (0.0016 m^3/s m).

As the weir load was increased towards the mixed flow operating conditions (0.003 m^3/s m) the liquid flow increased at the central region of the tray with much slower liquid at the ends of the outlet weir.figure (9.1o & 9.1p). With further increases in the weir load to the emulsified flow regime, it was found that there was an increase in the liquid channelling through the central section of the weir, with much lower rate liquid flowing at the areas next to the column wall (figure 9.1q).

9.4.1 Efficiencies result

The calculated tray efficiencies(see table 9.2) were found to show good agreement with those estimated without taken in to account the flow across the outlet weir for low capacity factor of 0.0605 m/s. This supports the observed uniform flow patterns obtained for the increasing liquid loadings for low capacity factors.

The efficiencies for the experiments with a high capacity factor of 0.0775 m/s were found to be under 100 % with a maximum tray efficiency $(E_{mv})_w$ value of 96 % in the mixed flow regime while for those under the same operating conditions for which the nature of liquid flow over the outlet weir was not considered were found to have tray efficiency $(E_{mv})_{nw}$ values of more than 100 % over the mixed flow regime operating conditions. The high efficiency values associated with the experiments for which the temperature of the liquid leaving the tray was measured at a point along the outlet weir can be explained by the non-uniform liquid flow across the outlet weir.

9.4.2 Conclusions

Generally more liquid was flowing across the central region of the tray for the three sets of capacity factors. However, maximum liquid flow was observed at approximately each end of the weir for a number of experiments with high liquid flowrates. These `peaks` could be interpreted as the boundary of the central mixing zone.

The flow of the liquid across the outlet weir is controlled by the magnitude of the resistance to flow by the gas jet passing through the hole.

At high capacity factors and high weir loads the flow of liquid across the outlet weir follows the same flow pattern as that developed on the active area of the tray.

The combined effect of the flow across the weir and the underlying liquid flow patterns on the tray can lead to over estimation of the tray performance.

Similar Tray efficiencies were computed for the experiments performed at low gas rate with the flow across the weir considered and the calculated results for when flow across the outlet weir was not considered.

The discrepancy in the results at high gas rates indicated the extent of the effect of liquid flow over the weir on the estimated tray efficiencies.

Table (9.2) Calculated tray efficiencies from the efficiency model with flow across the weir considered for the 12.5mm diameter hole tray.

weir load m^3/s m	C_{sb}=0.0605 m/s		C_{sb}=0.0775 m/s	
	$(E_{mv})_{nw}$	$(E_{mv})_w$	$(E_{mv})_{nw}$	$(E_{mv})_w$
0.0008	45.0	41.5	73.3	50.7
0.0016	66.6	61.4	80.9	89.8
0.0024	70.9	67.6	118.1	93.3
0.0032	66.3	64.4	122.4	96.1
0.004	53.5	56.9	108.5	82.1
0.0048	59.0	60.2	116.6	84.5
0.0056	61.0	61.5	118.9	79.5
0.0064	68.2	67.3	115.5	82.6
0.0072	76.1	77.0	113.6	79.2
0.008	81.2	85.3	105.8	66.8
0.0087	73.5	78.5	115.8	54.8
0.00967	67.0	74.2	81.1	69.4
0.0104	65.8	63.4	66.9	66.3
0.01128	66.3	63.5	59.3	58.5
0.01209	55.1	56.4	52.6	54.6

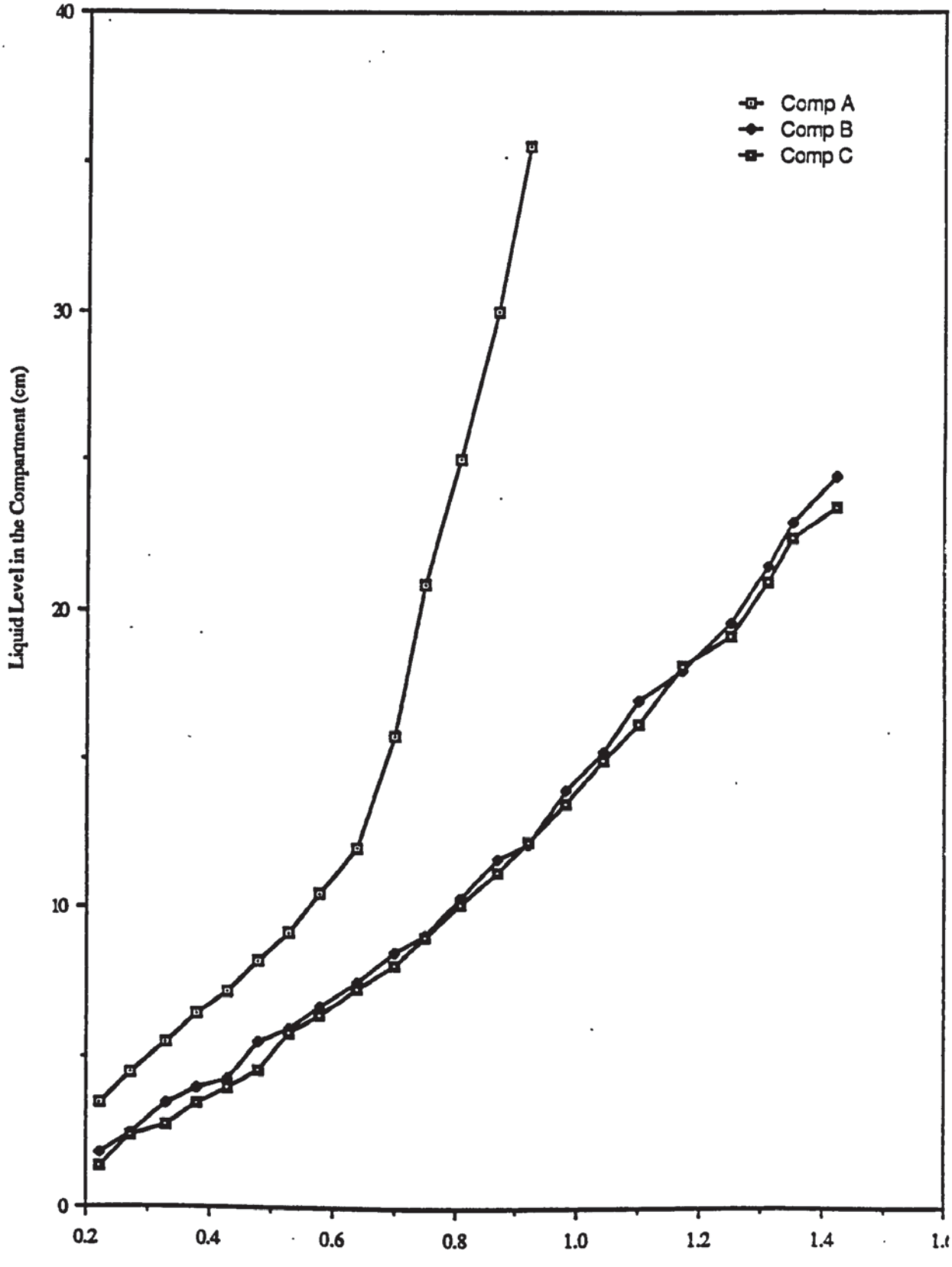

Figure (9a) Compartments Calibration Graph

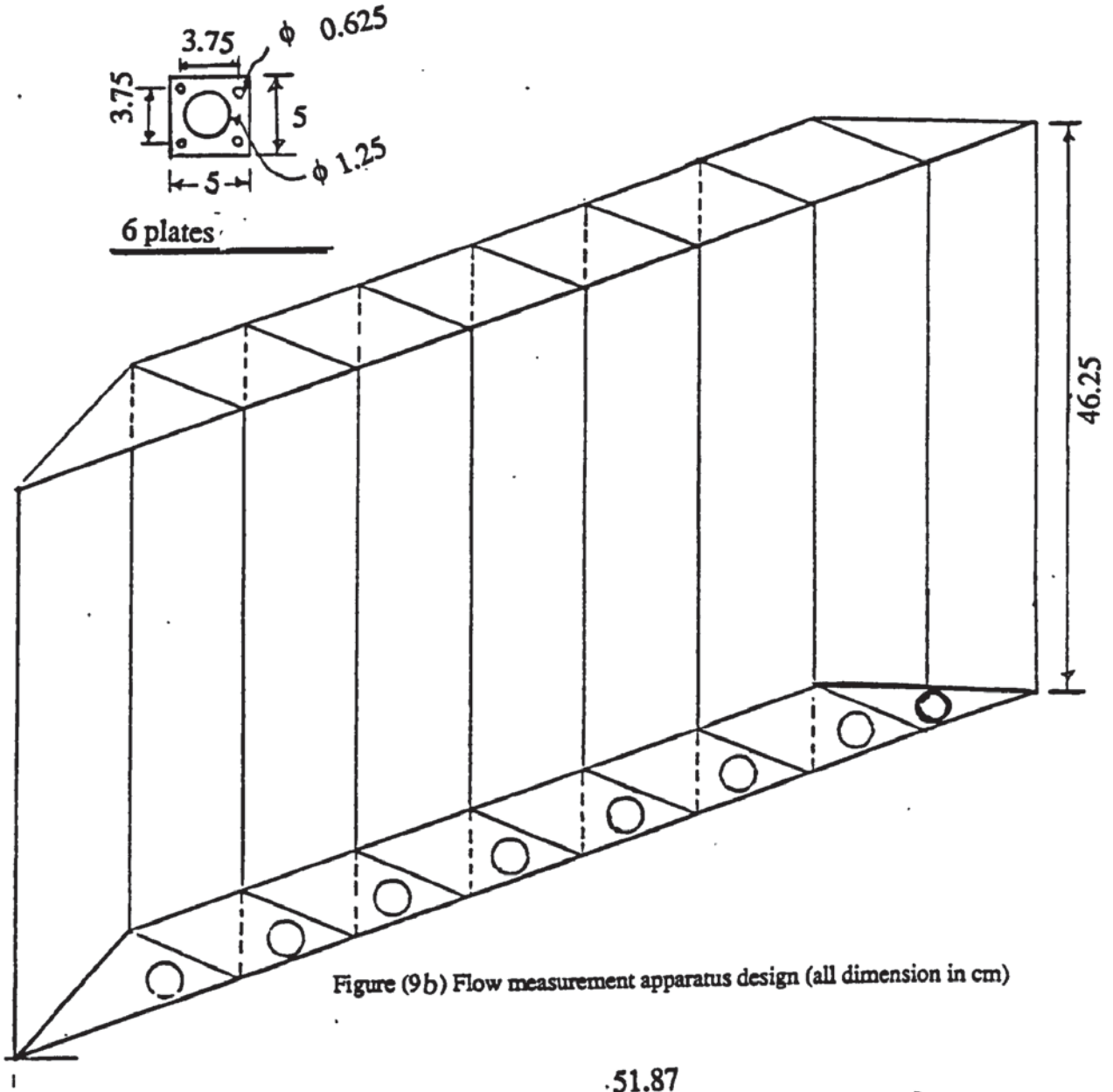

Figure (9b) Flow measurement apparatus design (all dimension in cm)

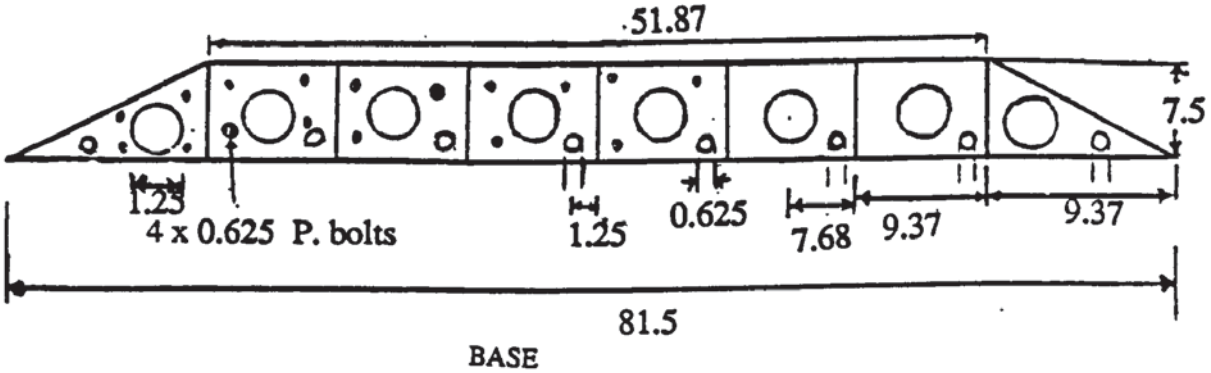

BASE

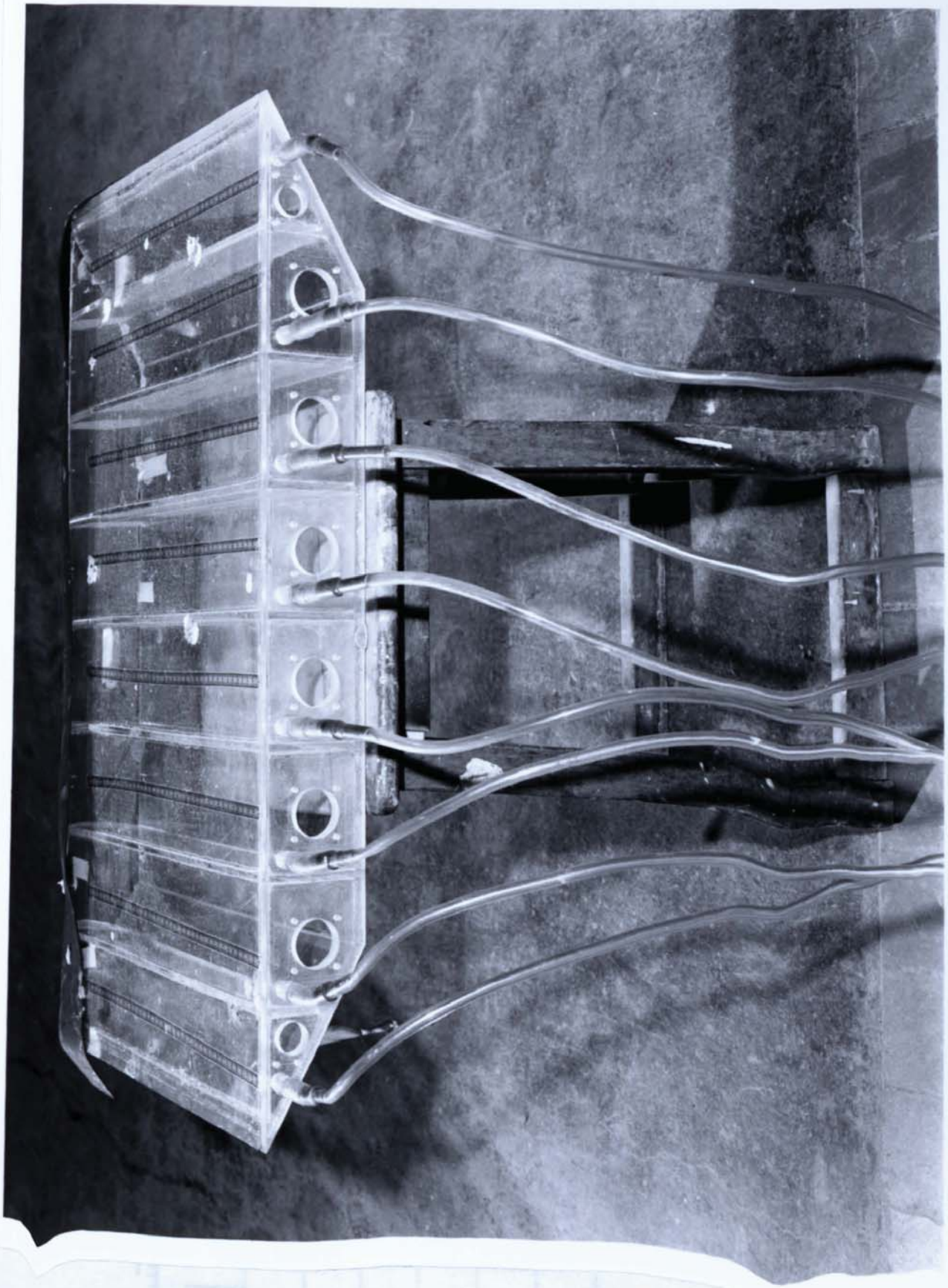

Figure (9.1) Typical apparatus used

Figure (9.1a) Graph of flow-per unit length vs weir length : weir load = 0.0016 $m^3/s.m$

C_{sb} = 0.0605 m/s

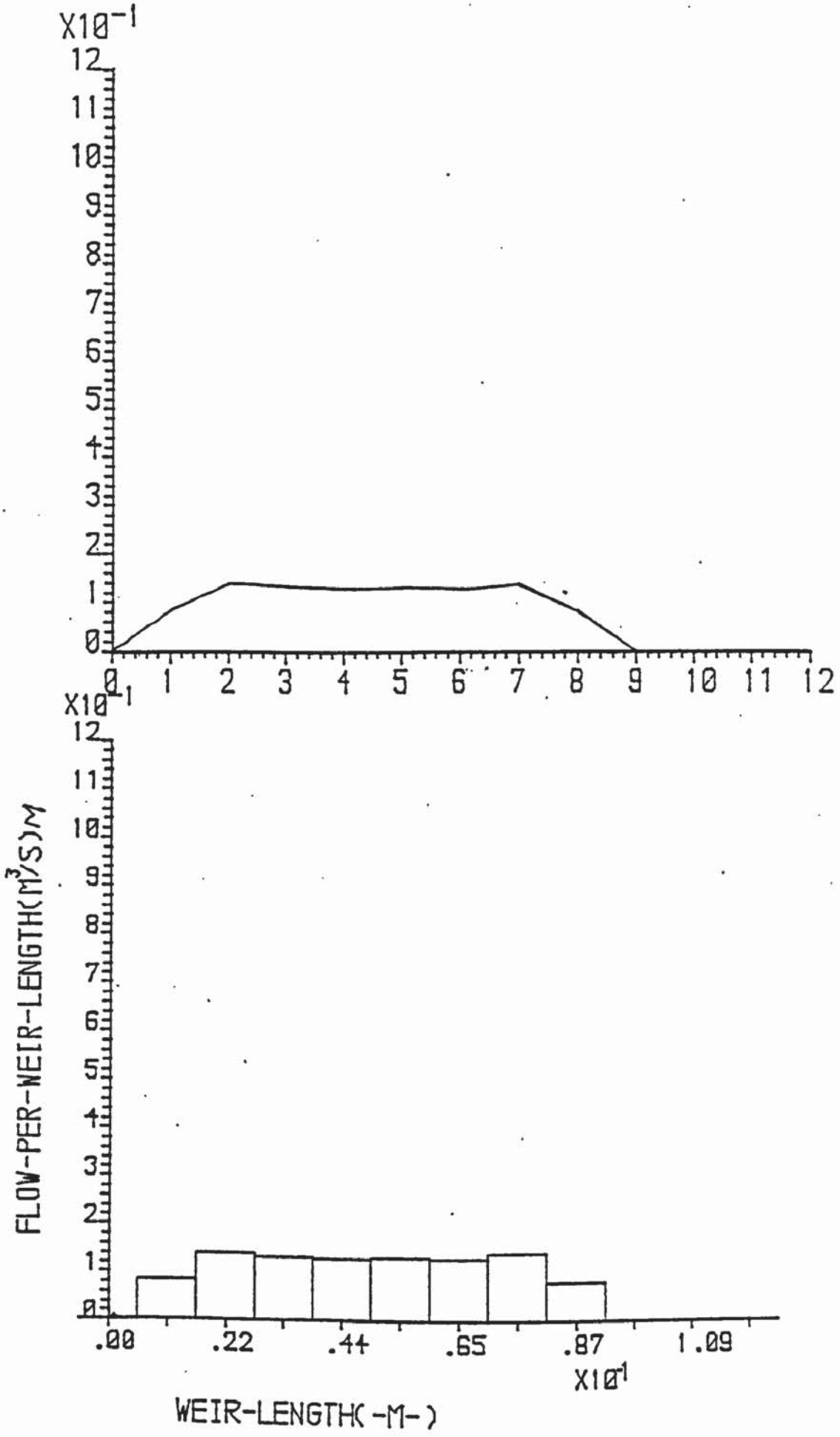

Figure (9.1b) Graph of flow-per unit length vs weir length : weir load = 0.0032 m^3/s.

C_{sb} = 0.0605 m/s

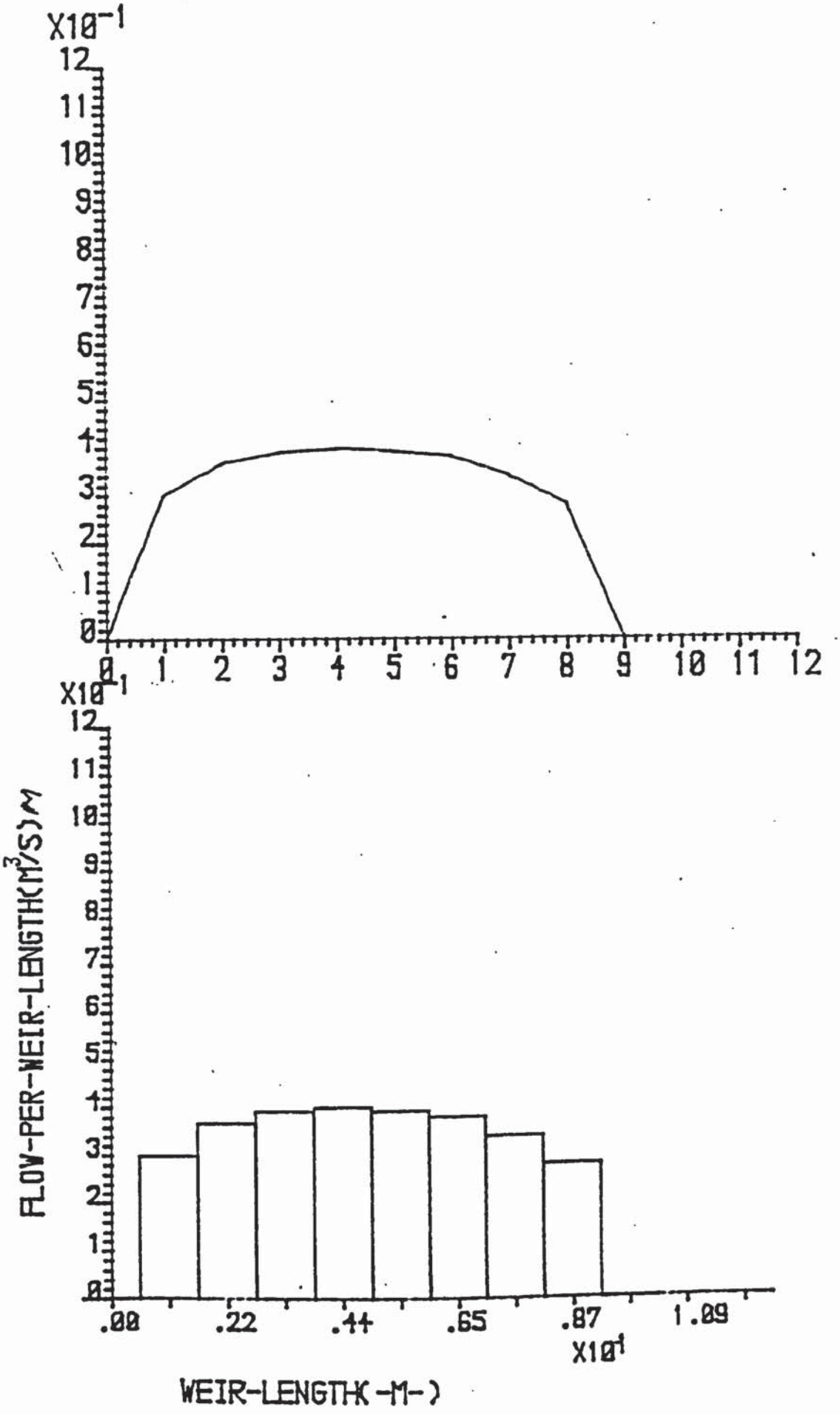

Figure (9.1c) Graph of flow-per unit length vs weir length : weir load = 0.0048 m^3/s.m

C_{sh} = 0.0605 m/s

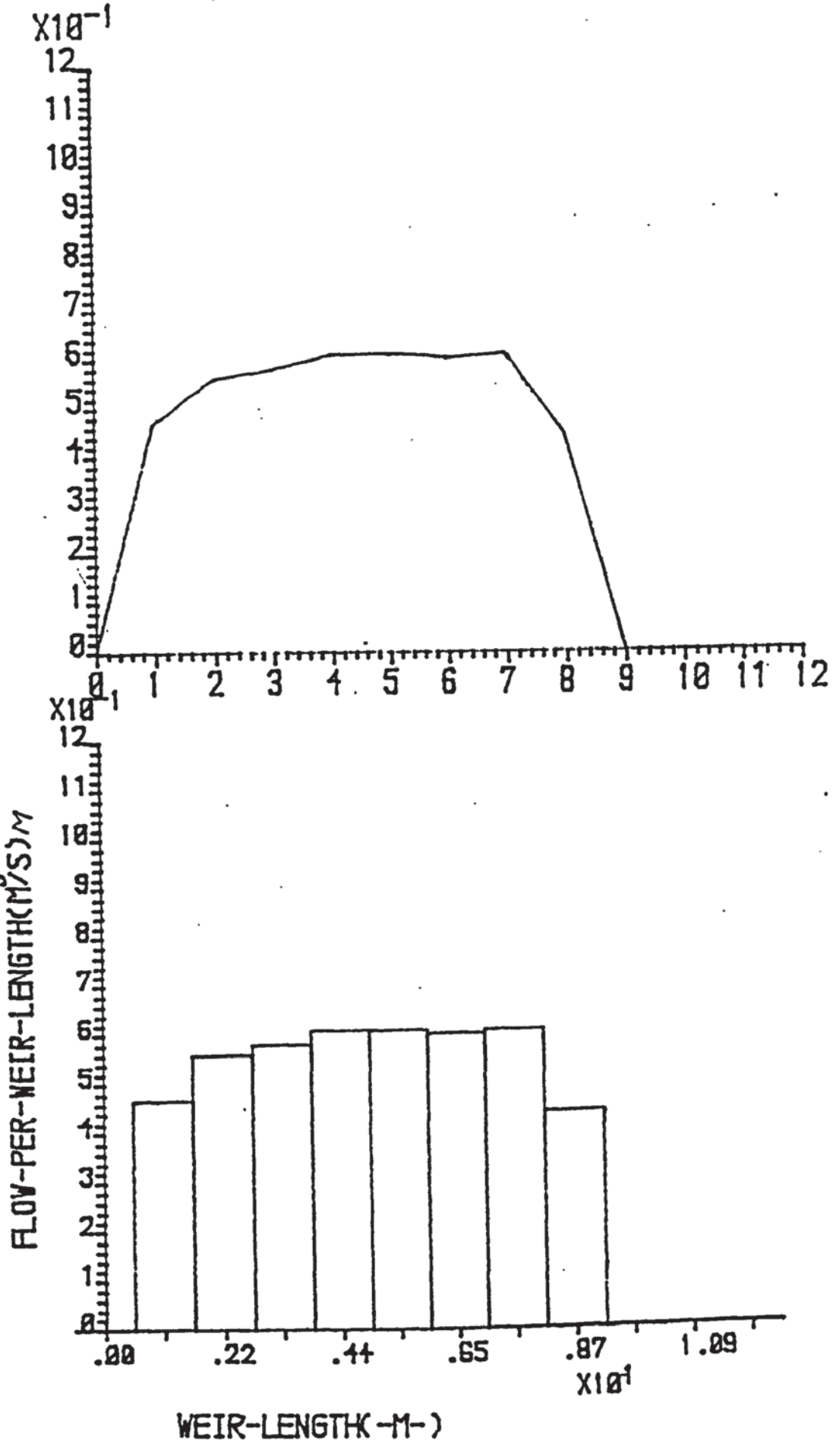

Figure (9.1d) Graph of flow-per unit length vs weir length : weir load = 0.0064 m^3/s

C_{sb} = 0.0605 m/s

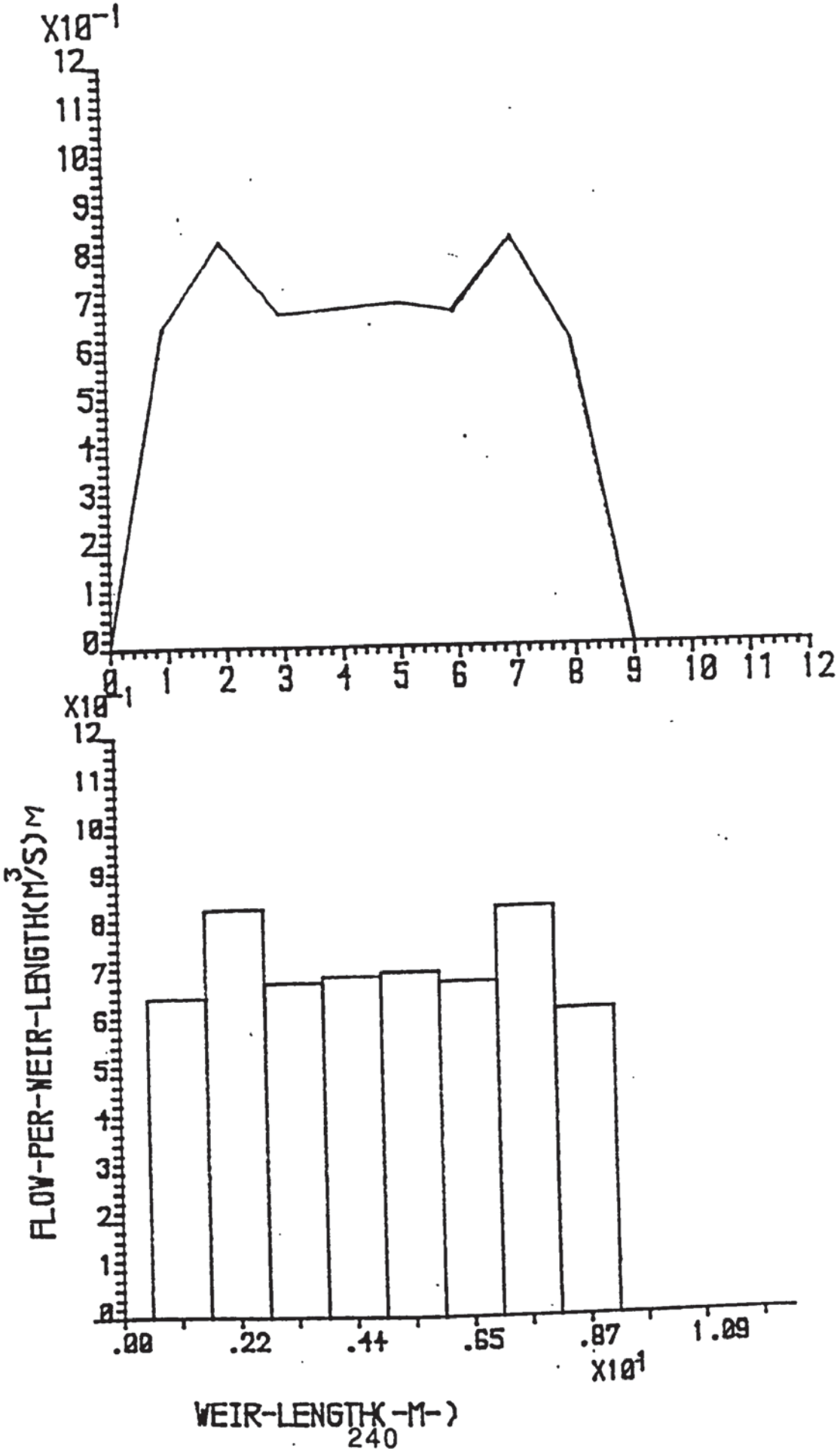

Figure (9.1e) Graph of flow-per unit length vs weir length : weir load = 0.008 $m^3/s.m$

C_{Sb} = 0.0605 m/s

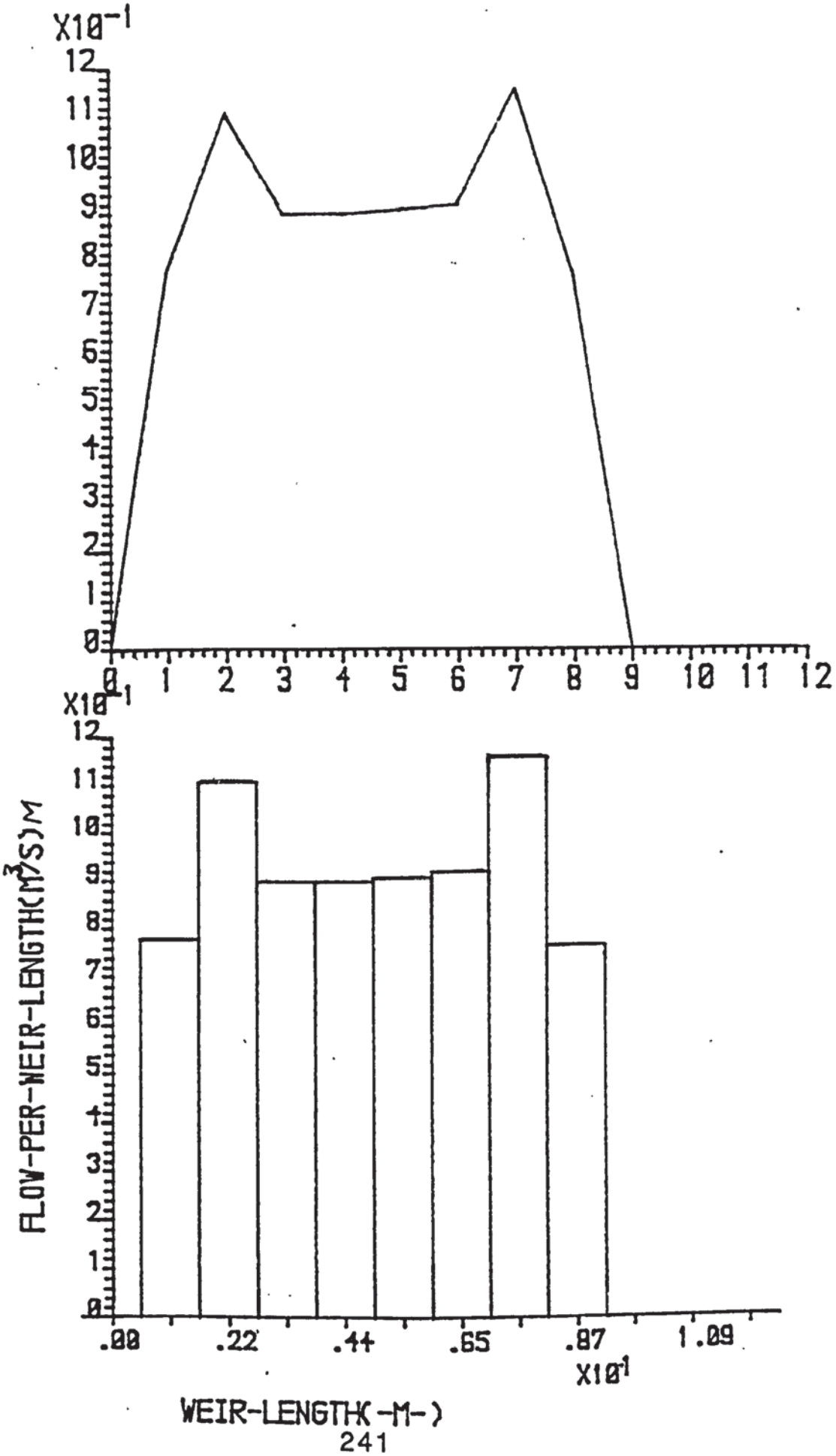

Figure (9.1f) Graph of flow-per unit length vs weir length : weir load = 0.00967 m^3/s

C_{sb} = 0.0605 m/s

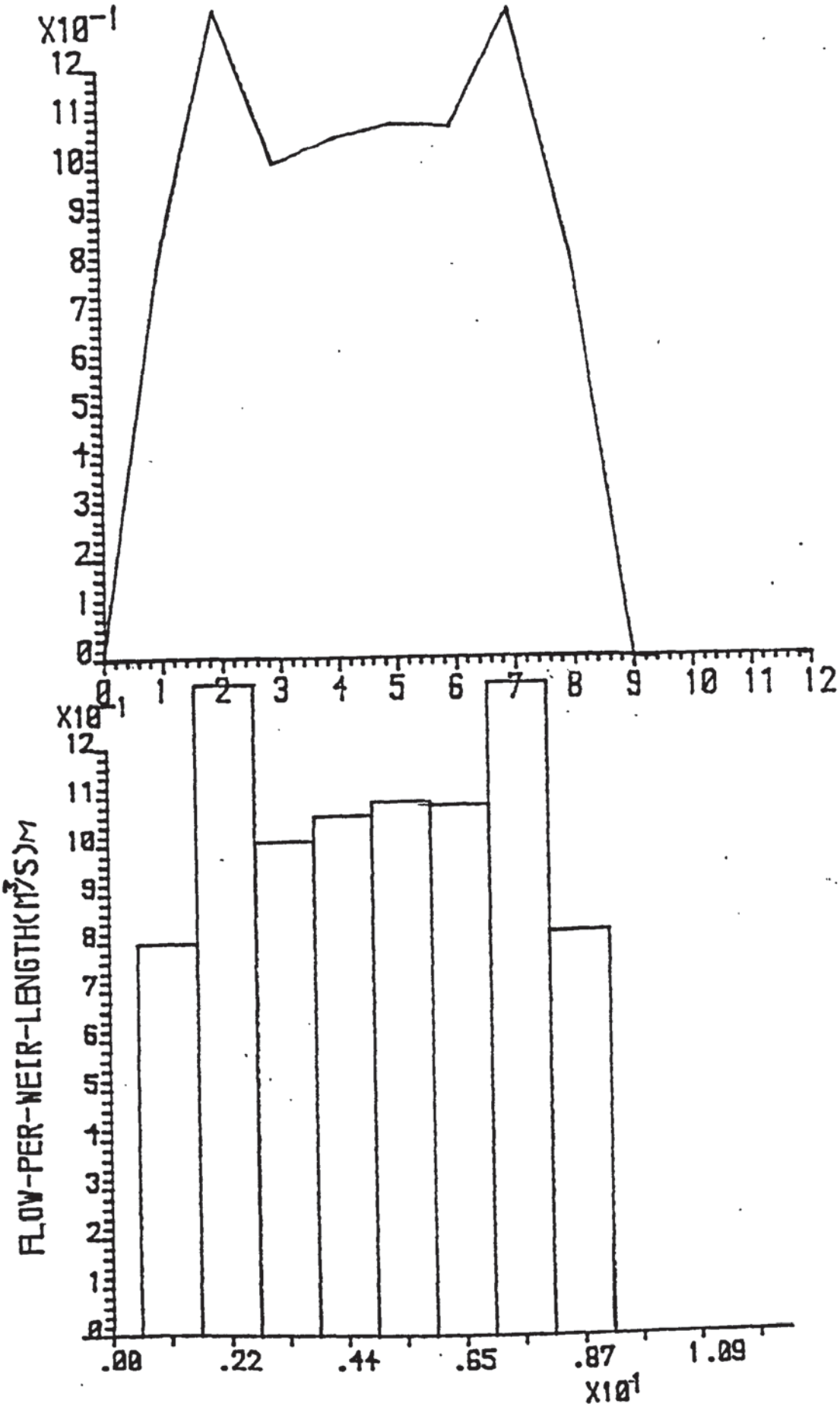

Figure (9.1g) Graph of flow-per unit length vs weir length : weir load = 0.0016 $m^3/s.m$

C_{sb} = 0.0775 m/s

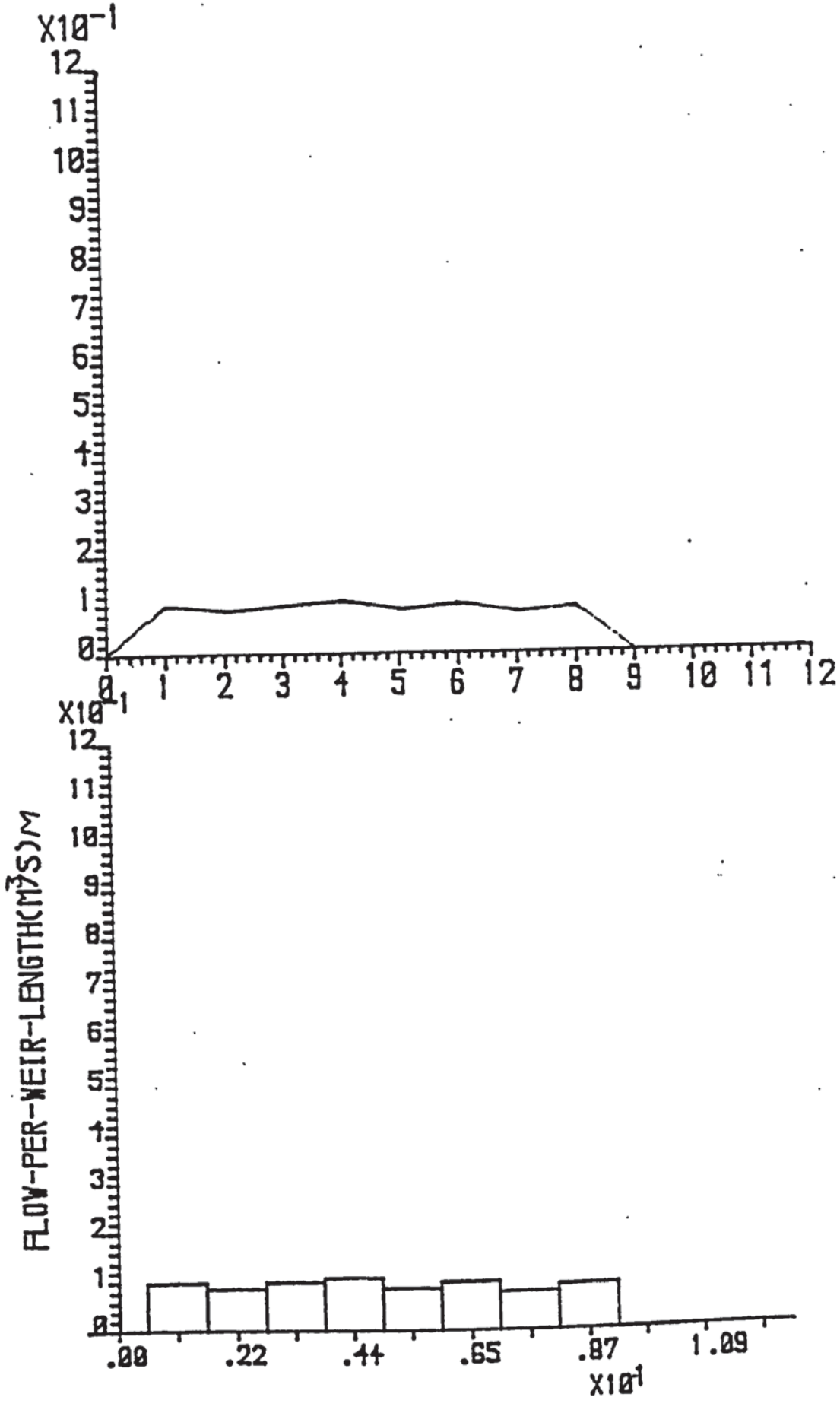

Figure (9.1h) Graph of flow-per unit length vs weir length : weir load = 0.0032 $m^3/s.m$

C_{sb} = 0.0775 m/s

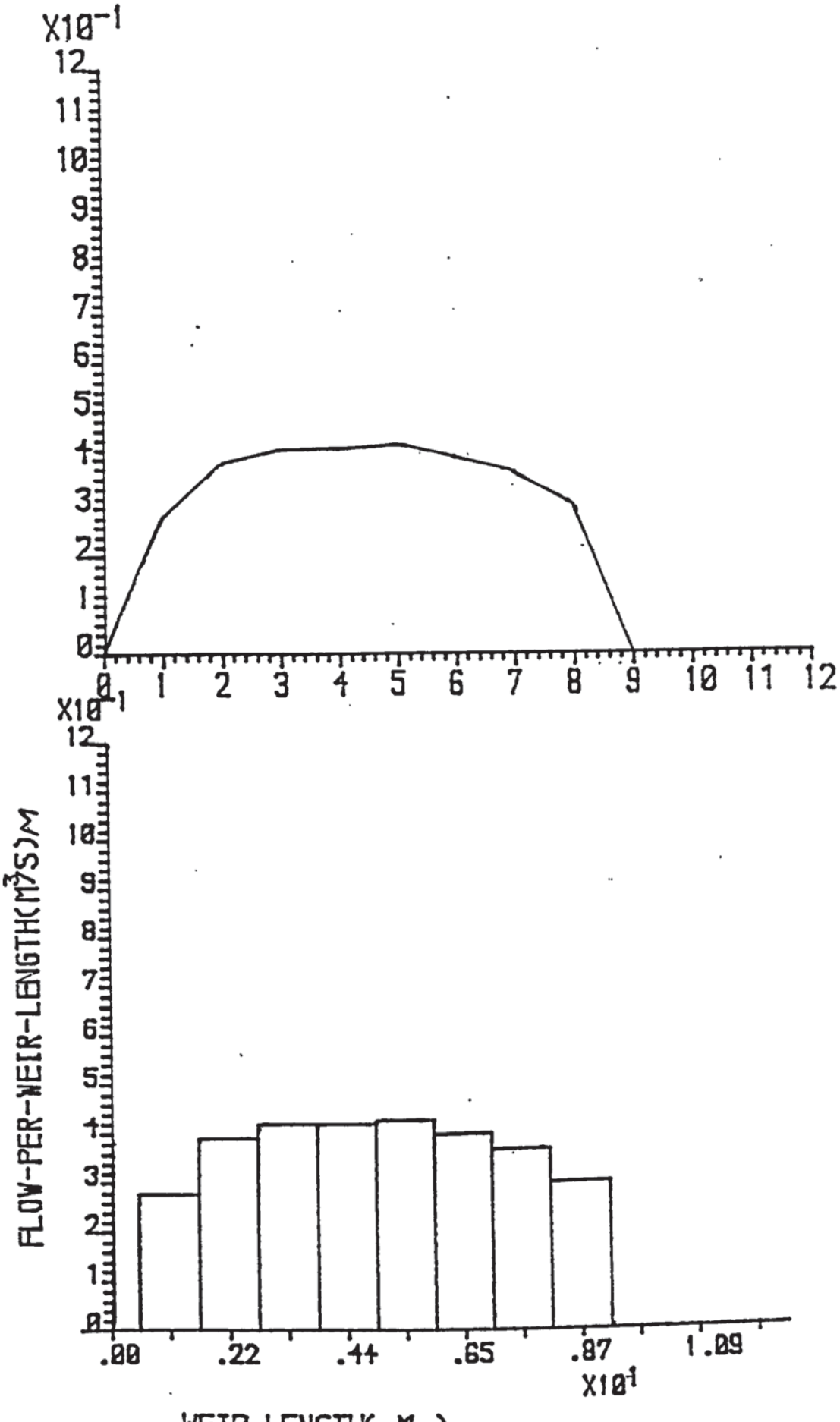

Figure (9.1i) Graph of flow-per unit length vs weir length : weir load = 0.0048 $m^3/s.m$

C_{sb} = 0.0775 m/s

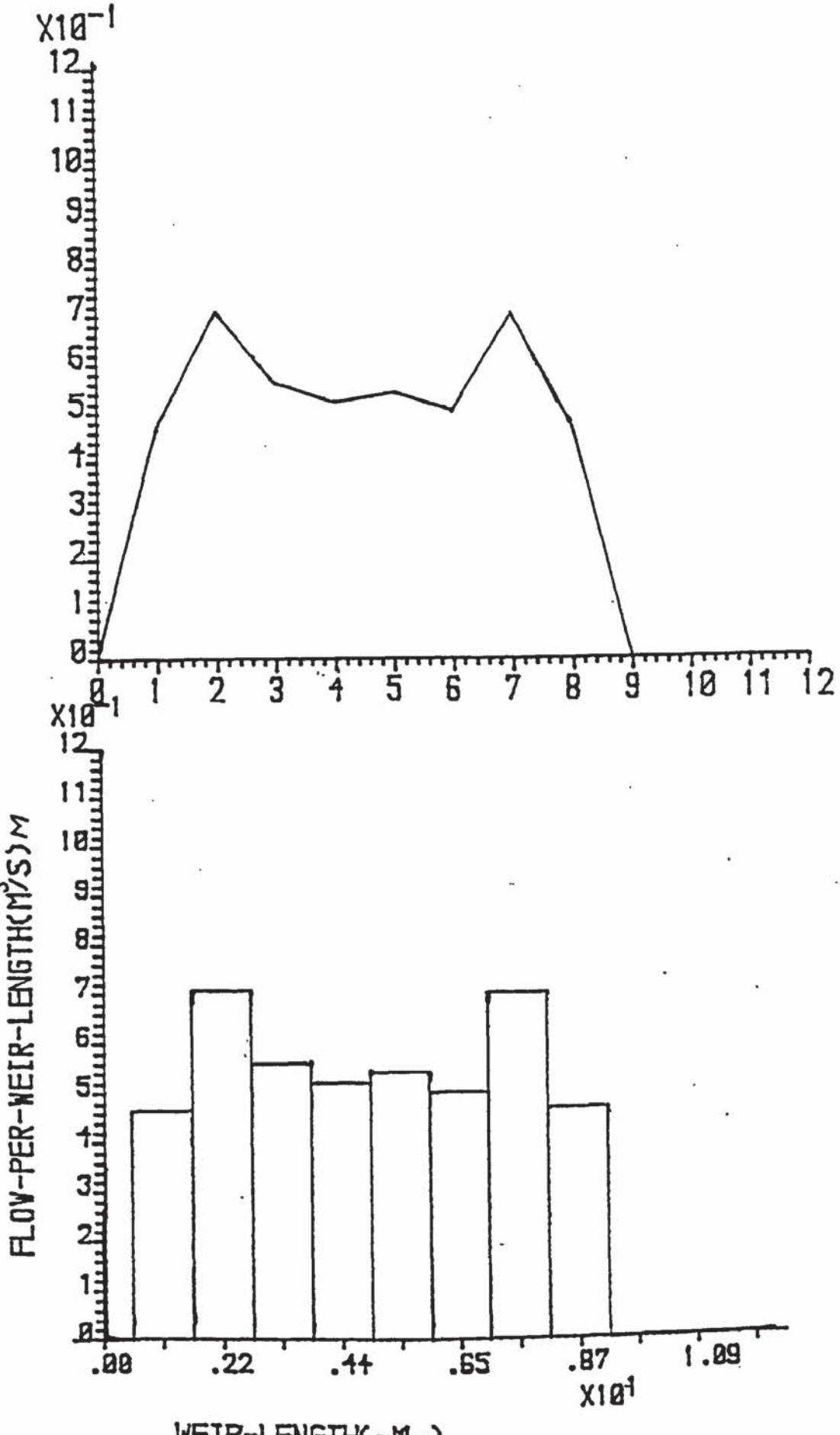

Figure (9.1j) Graph of flow-per unit length vs weir length : weir load = 0.0064 $m^3/s.m$

C_{sb} = 0.0775 m/s

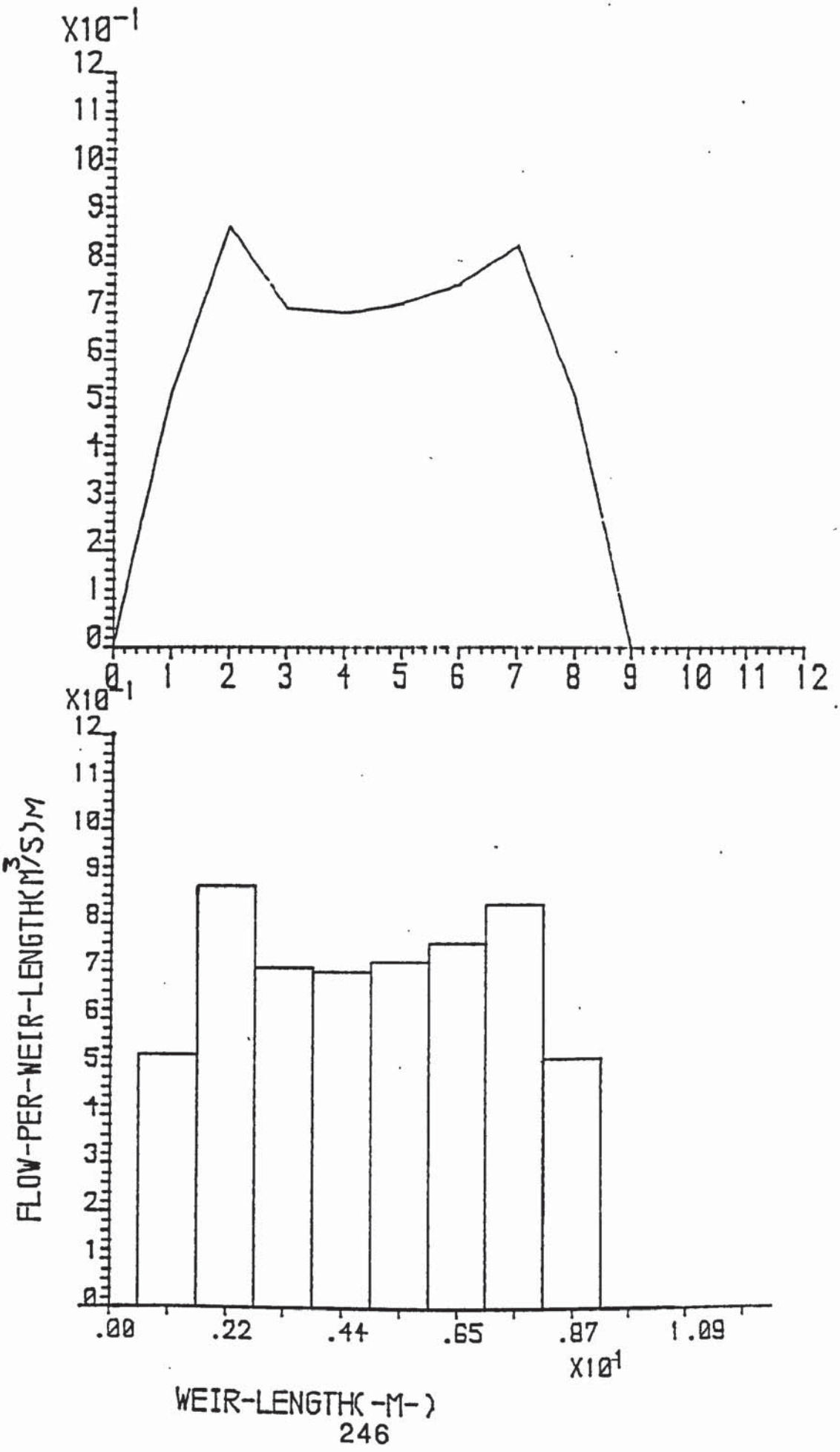

Figure (9.1k) Graph of flow-per unit length vs weir length : weir load = 0.008 $m^3/s.m$

C_{sb} = 0.0775 m/s

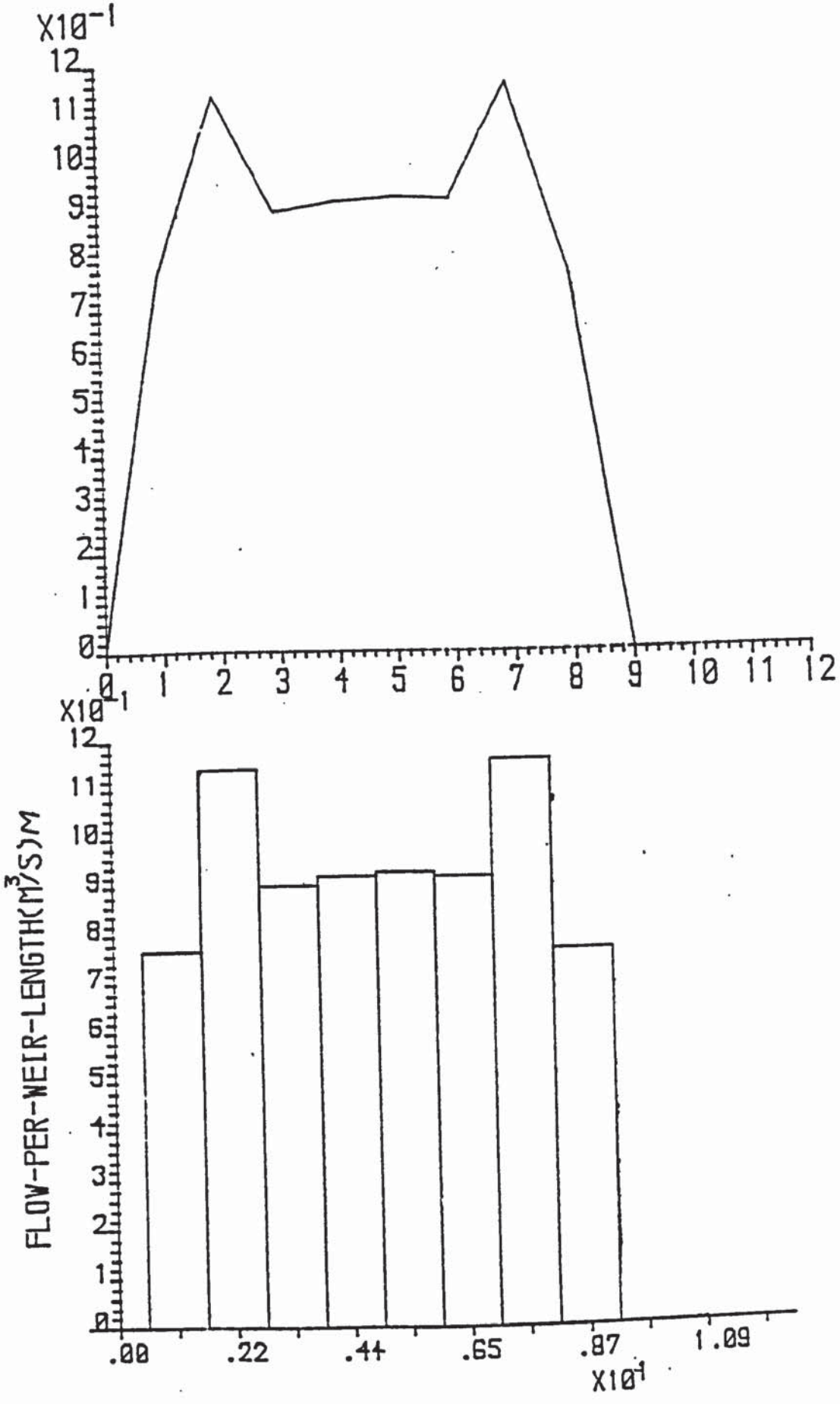

Figure (9.11) Graph of flow-per unit length vs weir length : weir load = 0.00967 $m^3/s.m$

C_{sb} = 0.0775 m/s

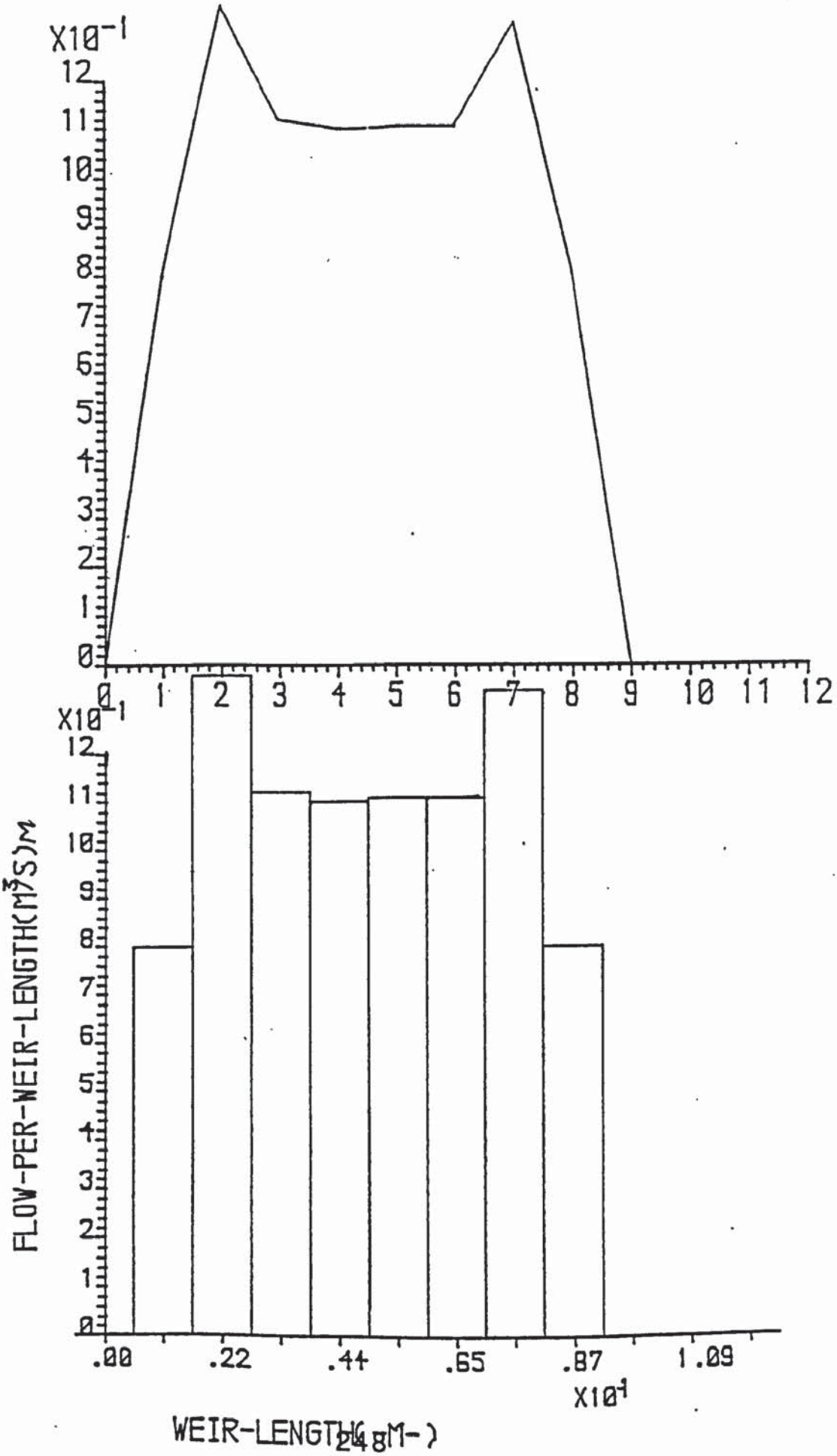

Figure (9.1m) Graph of flow-per unit length vs weir length : weir load = 0.0016 $m^3/s.m$

C_{sb} = 0.0851 m/s

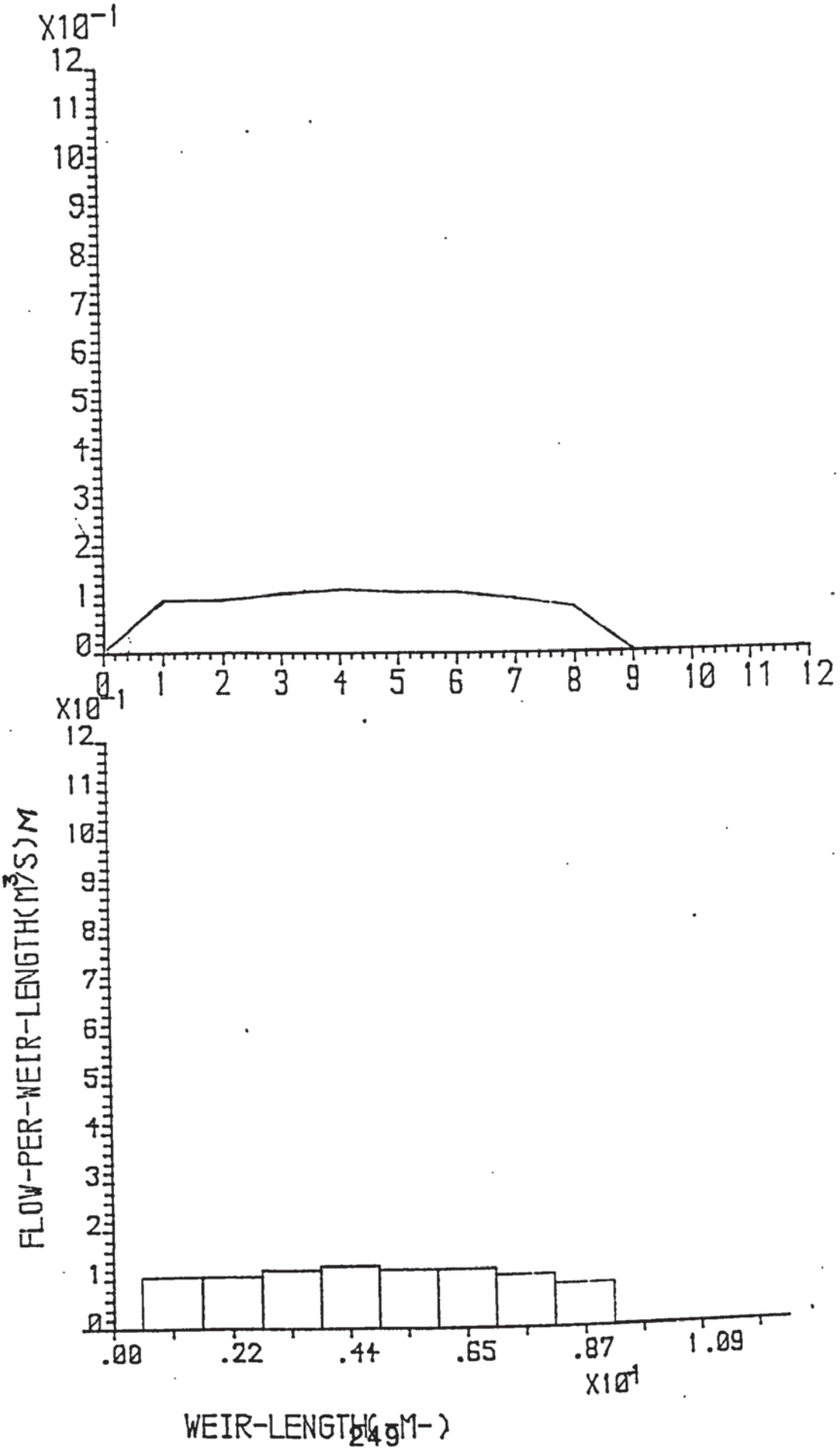

Figure (9.1n) Graph of flow-per unit length vs weir length : weir load = 0.0032 $m^3/s.m$

C_{sb} = 0.0851 m/s

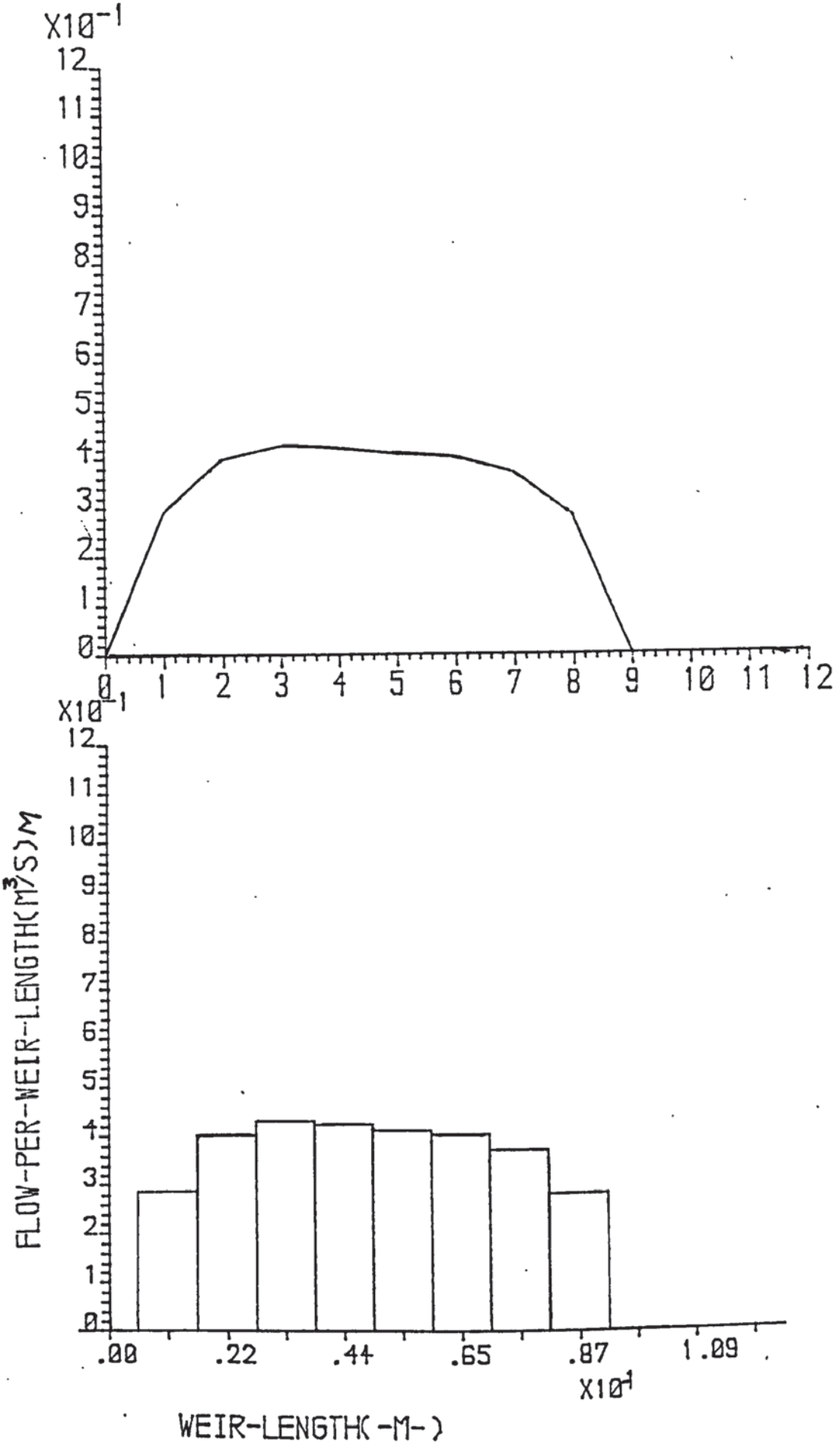

Figure (9.1o) Graph of flow-per unit length vs weir length : weir load = 0.0048 $m^3/s.m$

C_{sb} = 0.0851 m/s

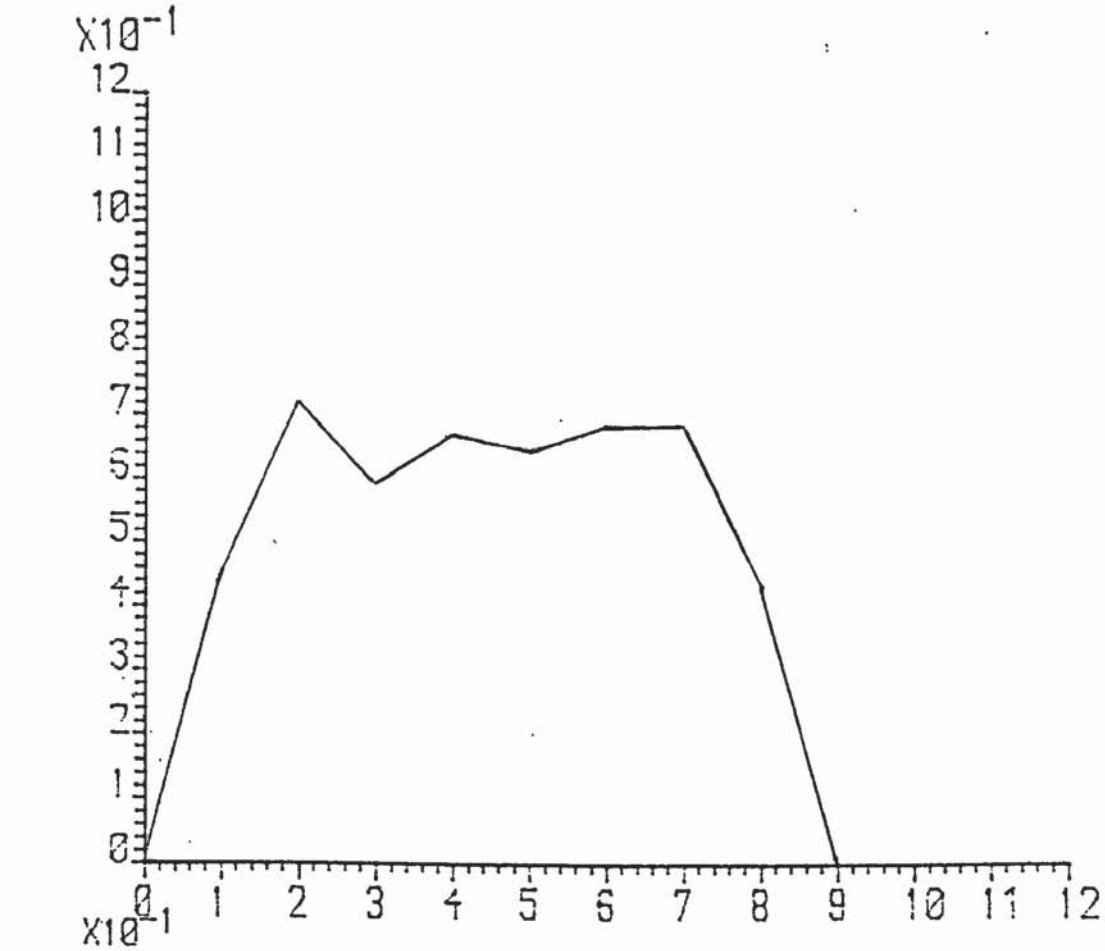

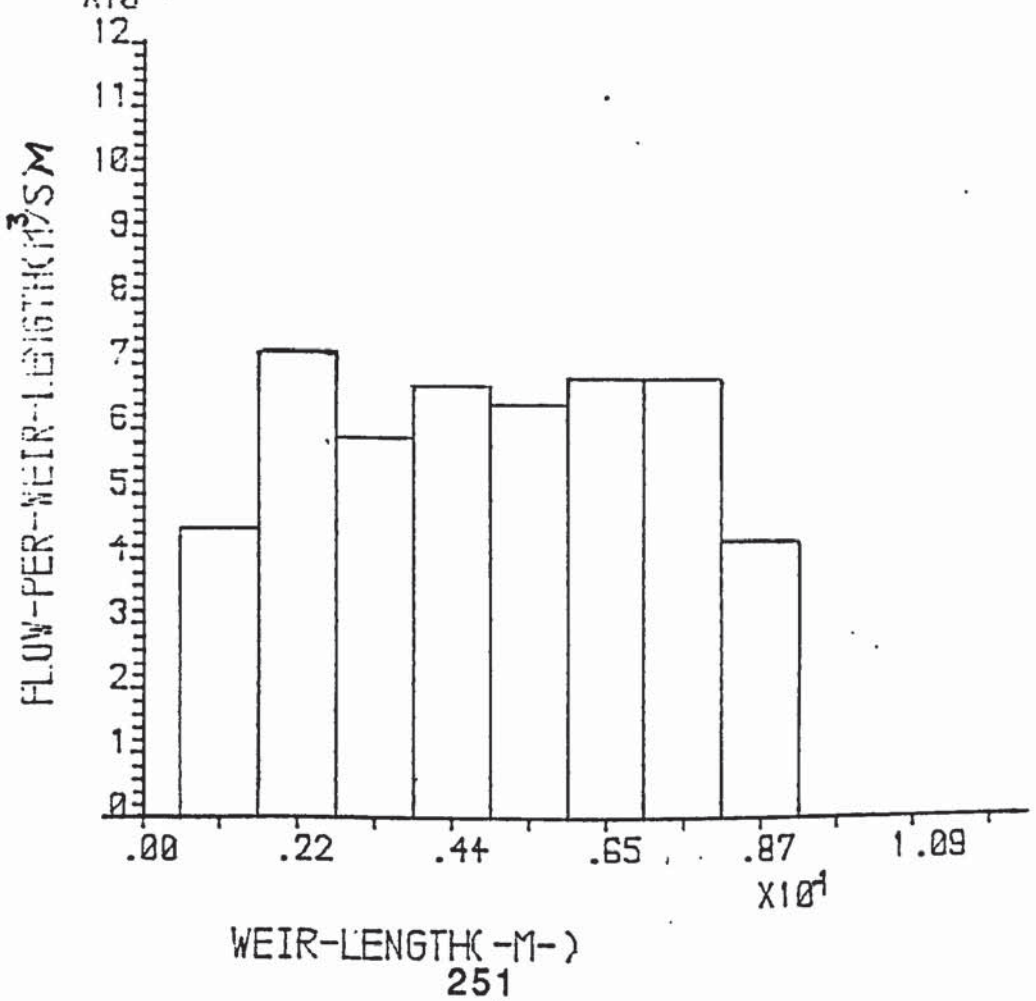

Figure (9.1p) Graph of flow-per unit length vs weir length : weir load = 0.0064 $m^3/s.m$

C_{sb} = 0.0851 m/s

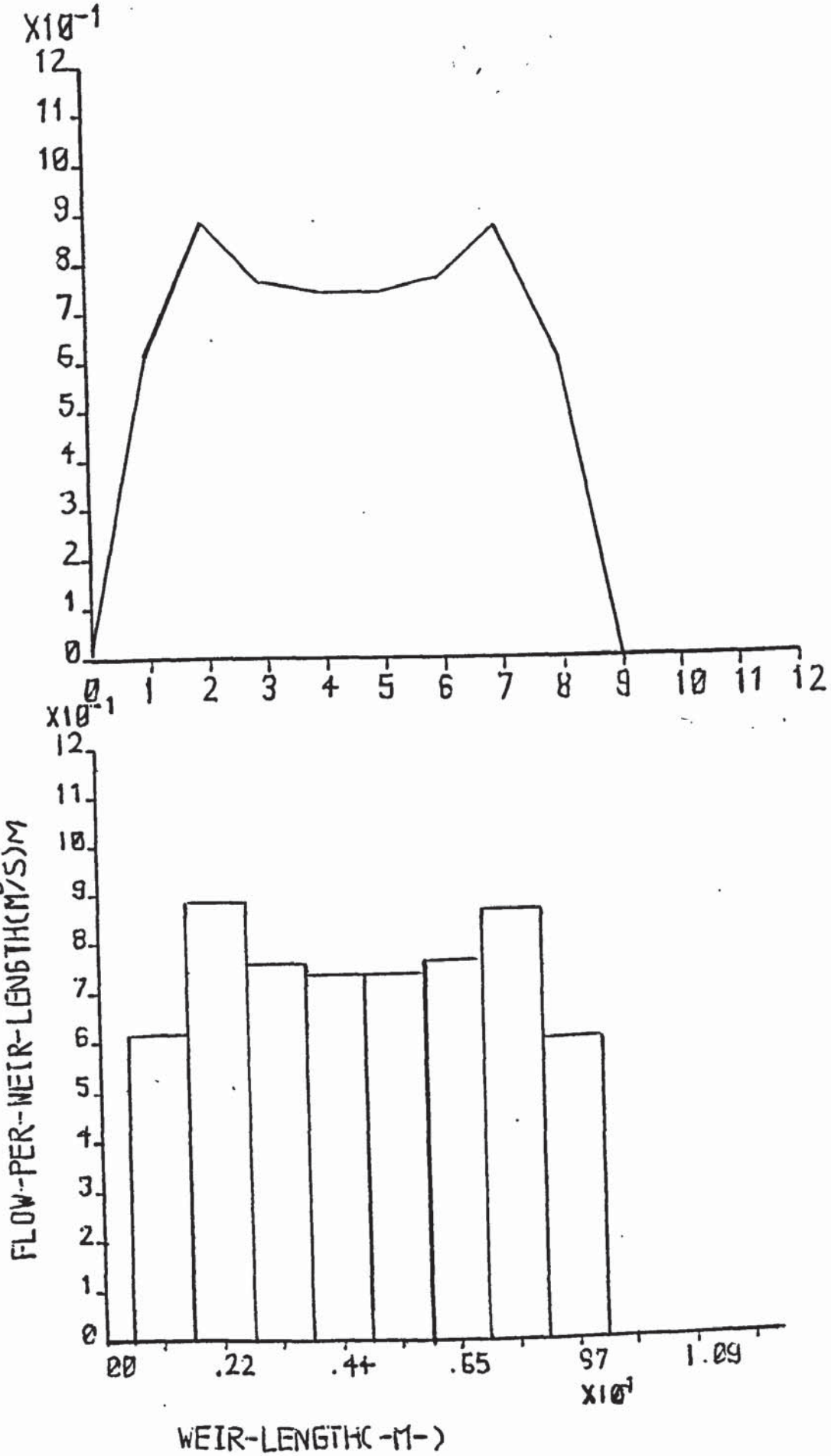

Figure (9.1q) Graph of flow-per unit length vs weir length : weir load = 0.008 $m^3/s.m$

C_{sb} = 0.0851 m/s

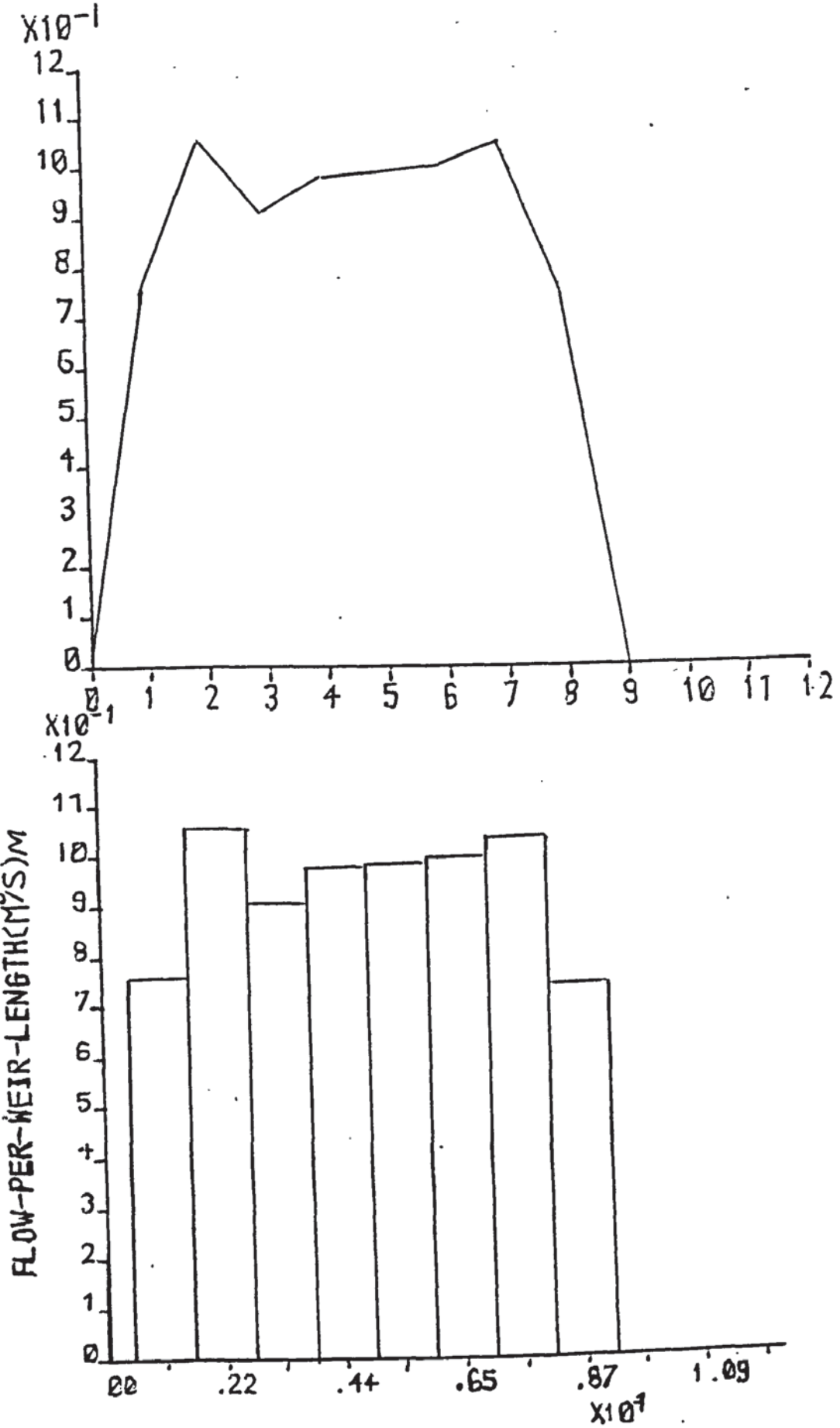

Chapter 10

MEASUREMENTS OF THE EDDY DIFFUSION COEFFICIENT (D_e) ON THE EXPERIMENTAL SIEVE TRAYS

10.1 INTRODUCTION

The performance of the individual tray in a distillation column has been described in section (7) to be dependent on the nature of the bi-phase flow across the tray from the inlet weir to the outlet downcomer. The mixing of the liquid on the tray takes place by two main mechanisms :

1. Transportation across the tray due to the bulk flow of the liquid, and
2. Transportation from one position to another in the direction of flow at a rate proportional to the concentration gradient.

The first mechanism was treated in sections (6 and 7).

When a liquid flows through a bubbly dispersion on a plate from the inlet to the outlet weir, a concentration gradient exists in the liquid in the direction of flow. The concept of eddy diffusion supposes that the existing concentration gradient on the tray can be interpreted by the law of diffusion. It is known that when turbulent conditions exist in a fluid, mass transfer by eddies can be considered to be analogous to molecular diffusion.

The advantage of this principle is that experiments can be set up separately to measure the effective diffusivity which is a quantitative measurement of the extent of liquid mixing in a bubbly dispersion on a tray.

This phenomena of liquid mixing was first recognised in the early 1930s and it was used in most of the early ideas and models to build up the analysis of point to tray efficiencies . However, it was **Danckwerts** (15) who first pointed out that the longitudinal mixing of fluids in a continuous flow system channel could be treated like molecular diffusion.

Barker and Self (7) used a rectangular sieve tray 5ft 8ins long,and13.5in wide with 3/16in diameter holes in order to evaluate liquid mixing effects in sieve tray columns.

Longitudinal eddy coefficients were measured using an unsteady-state on a static tray and steady state on dynamic tray tracer techniques. Using an air-water simulation column,

Barker and Self (7) correlated the Eddy diffusivity value (D_e) they obtained by the

unsteady-state tracer experiments, in terms of the liquid hold-up and the superficial velocity. The range of variables studied was for superficial air velocities between 1 to 4.8 ft/s and liquid holdup between 2 to 3.5 inches.

$$D_e = 0.01298\ U^{1.44} + 0.0324h_l - 0.0605 \qquad (10.1)$$

where U_s = superficial air velocity ft/s

h_l = clear liquid holdup

The results from the correlation of **Barker** and **Self** (7) were compared with those obtained from a study of reported correlated results in the A.I.Ch.E. There was a significant difference in the results.

Biddulph and **Ashton** (84) studied liquid back mixing effect on bi-phase local efficiency on a knoch flexitray of o.69 m in diameter using thesame salt tracer injection technique as in **Barker** and **Self.** Their experiment was carried out on a circular tray in an air- water simulator column using two liquid flow rates (460 and 317 l/min m) respectively.

From their results, they concluded that the eddy diffusivity of a sieve tray is independent of the air flow rates and of the physical properties of the system. **Biddulph** and **Ashton** (84) pointed out that the obtained results were much greater than that expected for a sieve tray. This might be explained by the expected nature of liquid flow across a circular tray, this may have introduced some element of recirculation zones into the system reducing or increasing the effect of the eddy diffusion mechanism.

Shore and **Haselden** (66) studied liquid mixing for the ethanol-methanol system using a column containing three rectangular plates 2 ft (0.16 m) long and (1ft) 0.305m wide with 1/8 inches (0.318 cm) holes on a triangular pitch and 6.4% free area. They proposed a liquid mixing mechanism where the mixing effect was produced by the rising vapour stream from each row of holes and they suggested that the characteristics of this mixing were essentially unchanged. Using data obtained by **Foss** (25), **Shore** and **Haselden** (66) derived a new correlation for the eddy diffusivity.

$$D_e = 0.48\ h_f\ \ k_s^{0.63} \qquad (10.2)$$

where

h_f = froth height

$k_s = U_s\,[(\rho_v/\rho_l - \rho_v)]^{0.5}$

U_s = superficial velocity

ρ_l , ρ_v = liquid and vapour densities respectively.

The model has only been used for the case of a completely mixed inlet vapour. Since Eddy-diffusion mechanism accounts for only one of the factors that cause liquid mixing on the tray, the results of the previous experiments have failed to indicate at what operating conditions this phenomena can be ignored or when the phenomena is very important in column design.Hence the object of this part of the research programme is to study the mixing effect at different operating conditions and to determine whether the operating conditions have any impact on the mixing process.

10.2 THE EDDY DIFFUSION MODEL

Consider a small vertical section of aerated liquid on a sieve tray.

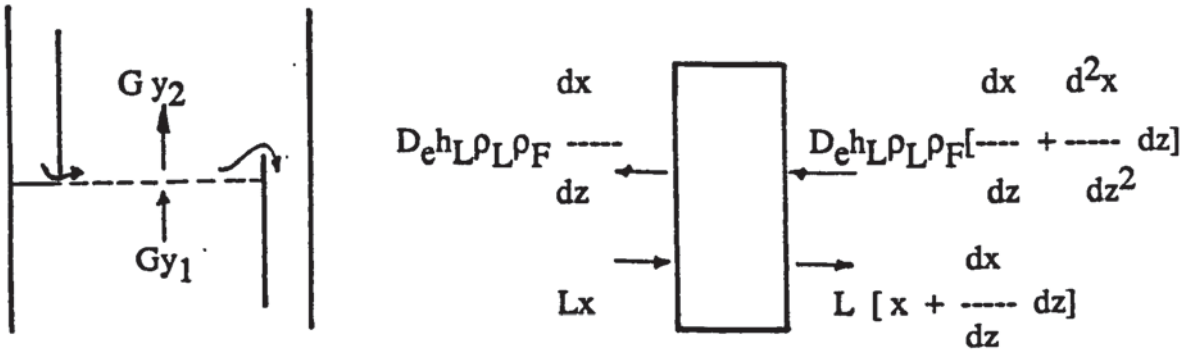

Assuming steady state operating conditions, any change in concentration or concentration gradient on the tray can only occur if there is a difference between the rate of removal of volatile component by the stripping gas and the rate of replenishment of the inflowing liquid and a redistributing effect due to liquid momentum.

Carrying out of a material balance on a section of an aerated liquid.

$$D_e \frac{d^2x}{dz^2} - \frac{L}{h_L \rho_L \rho_F} \frac{dx}{dz} + \frac{G}{h_L \rho_L \rho_F}(y_2 - y_1) = 0 \qquad (10.2.1)$$

dividing through by:

$$\frac{L}{h_L \rho_L \rho_F}$$

and rearranging:

$$\frac{\rho_L \rho_F h_L D_e}{L} \frac{d^2x}{dz^2} - \frac{dx}{dz} + \frac{G}{L}(y_2 - y_1) = 0 \qquad (10.2.2)$$

but $$\frac{\rho_L \rho_F h_L D_e}{L} = \frac{1}{P_e}$$

$$E_{mv} = \frac{y_2 - y_1}{y^* - y_1}$$

but if the operating line is straight

$$y^* = mx + b$$

$$E_{mv} = \frac{y_2 - y_1}{mx + b - y_1} \qquad (10.2.3)$$

and $$y_1 = mx^* + b$$

$$E_{mv} = \frac{y_2 - y_1}{m(x - x^*)} \qquad (10.2.4)$$

$$y_2 - y_1 = E_{mv}\, m\, (x - x^*)$$

$$\frac{1}{P_e} \frac{d^2x}{dz^2} - \frac{dx}{dz} + \frac{Gm}{L} E_{mv}(x - x^*) = 0 \qquad (10.2.4)$$

$$\text{Let} \quad w = \frac{z}{z_1} \quad \text{therefore} \quad \frac{dw}{dz} = \frac{1}{z_1}$$

Where z = distance of the sampling point to the tray, z_1 = operating length of tray hence

$$\frac{dx}{dz} = \frac{dx}{dw}\,\frac{dw}{dz} = \frac{1}{z_1}\,\frac{dx}{dw}$$

$$\text{therefore} \quad \frac{d^2x}{dz^2} = \frac{dx}{dw}\,\frac{d^2w}{dz^2} = \frac{dw}{dz}\,\frac{d^2x}{dw^2}\,\frac{dw}{dz} = \frac{1}{z^2}\,\frac{d^2x}{dw^2}$$

Substituting in the above:

$$\frac{1}{P_e z_1^2}\,\frac{d^2x}{dw^2} - \frac{1}{z_1}\,\frac{dx}{dw} + \frac{Gm}{L} E_{mv}(x - x^*) = 0 \qquad (10.2.5)$$

For a plate with no mass transfer between the liquid and vapour phase equation above reduces to:

$$\frac{1}{P_e z_1}\,\frac{d^2x}{dw^2} - \frac{dx}{dw} = 0 \qquad (10.2.6)$$

Where $z_1 = Z_L$ = operating length of the tray

$$W = w = \frac{\text{distance along the plate from inlet weir to sample point}}{\text{operating length of the tray}}$$

If the tray has a sufficient length such that none of the tracer reaches the tray inlet weir, the solution of the above equations becomes:

$$\frac{x - x_o}{x_q - x_o} = \frac{\exp(P_e Z_L W) - 1}{\exp(P_e Z_L) - 1} \qquad (10.2.7)$$

If $PeZ_L >> 1$

$$\frac{x - x_o}{x_q - x_o} = -\exp[P_e Z_L (W-1)] \qquad (10.2.8)$$

$$\log \frac{x - x_o}{x_q - x_o} = [P_e Z_L (1-W)] \qquad (10.2.9)$$

A plot of

$\log \frac{x - x_o}{x_q - x_o}$ vesus (1-W) on a semi log paper will give a slope of $P_e Z_L$

$$\text{but } P_e Z_L = \frac{LZ_L}{h_L \rho_L \rho_F D_e} = \frac{VZ_L}{D_e} \qquad (10.2.10)$$

$V = \frac{L}{h_L \rho_L}$ = Liquid velocity across the tray

L = Liquid flowrate $m^3/s\ m$

Note : $\frac{L}{h_L \rho_L \rho_F D_e}$ = the ratio of material transferred by direct transport and by diffusion.

10.3 EXPERIMENTAL PROCEDURE

The technique employed for the measurement of the Eddy diffusion coefficient (coefficient of mixing) on the test trays was the steady-state tracer technique. In order to eliminate the effect of the bi-phase recirculation at the sides of the tray, a rectangular tray was used. The main principle of the experiment was to continuously and uniformly inject a salt solution (NaCl) across the width of the tray approximately six inches from the outlet weir and to measure the extent of the tracer diffusion upstream. Sampling holes were connected to

sampling glass tubes using P.V.C. tubings.

The tracer solutions were made up by mixing 1 to 5 kg of common salt with 50 litres of water. To inject the tracer uniformly across the tray an injection grid was made from a copper tube with a number of identical diameter holes. The liquid flowing through each hole was measured and the variation of flow along the grid was found to be negligible. To avoid weeping, the air blower was started first in all the experiments and set to the required dry tray air velocity. The water flow was started by turning on the centrifugal pump. The flow rate was controlled by adjusting the control valve on the supply line to the required value. The bi-phase flowed for five minutes to allow the test condition to stabilise. The tracer pump was switched on and the tracer solution recirculated to achieve good mixing of the tracer in the storage tank. The flowrate to the injection grid was controlled by a rotameter which had been previously calibrated.

The salt concentration on the tray was limited to 1 g/l. A series of sample points were fixed from below the tray floor and on the centre line of the tray. Samples from the tray floor flowed by gravity and the rate of sampling was controlled by screw-clips on each of the sample P.V.C.tubes. The samples were removed at a constant rate and collected into 50ml sample bottles. The contents of each sample bottle were throughly mixed before a small sample was drawn for analysis. A sample of the inlet water was taken from the inlet downcomer for each experiment at the same time. The liquid hold-up for each of the runs were measured by means of external water manometers.

10.4 LIQUID HOLD UP MEASUREMENTS

The liquid hold up measurements were made by means of sample taps contained in tubes welded to the floor of the test trays. These tubes were connected by means of P.V.C tubing to external glass manometers.The manometer reading gave the equivalent clear liquid height of the bubbly dispersion on the tray. The liquid level in the manometers ocsillated slightly and therefore mean values were used. An average value of the clear liquid height (h_L) values collected over the operating length of the tray was used for estimating the foam velocity (V_f) (operating length being the distance from the inlet weir to the tracer injection point on the tray).

10.5 CONDUCTIVITY CELL CALIBRATION

The conductivity cell was calibrated by measuring, at 25 ^{o}C , the specific conductivities of standard samples whose concentrations ranged from 0.0025 g/l to 1 g/l. The raw data (see table 10.1) was then used to create a calibration curve (see figure 10.1).
Note : 1.08 is the correction factor for the conductivity cell meter used and c is the constant in the equation of a straight line plot of conductivity versus salt concentration.

Table (10.1) Conductivity cell calibration table

NO	g salt/l	cond cell measure	cond x 1.08	salt con + c
1	1.0	1.94	2.095	1.06
2	0.8	1.60	1.728	0.86
3	0.5	1.03	1.112	0.56
4	0.2	0.48	0.518	0.26
5	0.1	0.28	0.302	0.16
6	0.05	0.16	0.173	0.11
7	0.02	0.10	0.108	0.08
8	0.01	0.09	0.097	0.07
9	0.005	0.08	0.086	0.65
10	0.0025	0.07	0.076	0.0625

conductivity of the main water supply = 0.0972

and the concentration of water = 0.07

10.5.1 Analysis of the samples

The salt concentration of each liquid sample was measured by the specific conductivitiy cell. All samples were analysed at a constant temperature of 25^{o}C, and all the samples were placed in a constant temperature water bath.

10.5.2 Foam velocity (V_f)

In calculating the eddy diffusion coefficient(D_e) it was necessary to know the values of the froth velocity (V_f) for each experiment and these were calculated from the relationship.

$$V_f = Q_l/Z_{av} \qquad (10.5.1)$$

Where Q_l is expressed in (m^3/s m) and Z_{av} (m) is defined as the height of clear liquid to which the froth would collapse if all the air were removed from it.

10.5.3 SAMPLE CALCULATION

Table (10.2) OPERATING CONDITIONS

Liquid Loading (m^3/s m)	0.00124
Capacity factor (m/s)	0.08766
Outlet weir height (mm)	24.5
Operating length of Tray (cm) (measured from inlet weir to the tracer injection position)	55
Clear liquid height (mm)	22
Temperature (^oC)	25
Atmospheric Pressure (atms)	1

Samples were taken along the tray length starting upstream of 6 inches away from the outlet weir and at 2.5 inches intervals upstream to the inlet weir, that is at positions 22.0, 19.5, 17.0, 14.5, 12.0, 9.5, 7.0, 4.5, and 2.0 inches from the inlet weir.

A sample of calculated results are given in table(10.3) below.

Table (10.3) Sample of calculated results for $\log(x-x_o/x_g-x_o)$ vs 1-w plot

sample	specific conductivity	concentration	$x-x_o/x_g-x_o$	1-W
	mS	g /l		
1 (at grid)	1.242	0.6	1.0	0
2	0.4428	0.26	0.39	0.11
3	0.2268	0.14	0.13	0.23
4	0.1512	0.102	0.06	0.34
5	0.1188	0.084	0.026	0.45
6 (extent of diff)	0.108	0.078	0.01	0.57
7 (no tracer)	0.0972 (as main water)	0.07	–	–

Where, x = salt concentration of sample at 25°C (g /l)

x_o = salt concentration of main water suplied to the tray (sample from inlet weir) g /l

x_g = Salt concentration at tracer injection position (g/l)

s = Distance along the plate from the inlet weir to the sample point (cm)

ε = Operating length of the tray (cm)

$W = s/\varepsilon$

A plot of $\log((x-x_o)/(x_g-x_o))$ versus (1-W) is shown in figures(10.5.3a - 10.5.3h) for the 1 mm diameter hole tray and in figures (10.5.3i - 10.5.3t) for the 12.5 mm diameter hole tray. The graghs are linear when $P_e >> 1$. The gradient of the line on semi-log graph paper gives the value of the Peclet number (P_e). For the case chosen for sample calculation (Figure (10.5.3i)).

P_e = (18.57562).

But

$$P_e = V_f * Z_{av} / D_e$$

V_f as stated above is given by,

V_f = (liquid rate per unit weir length)/(average liquid hold-up)

Therefore:

$$V_f = 0.00124/22.5 * 0.001$$
$$= 0.0551 \text{ m/s}$$

and

$$D_e = (V_f * Z_{av})/ P_e$$

$$= 0.5588 * 0.0551/ 18.57562$$

$$= 0.00166 \text{ m}^2/\text{s}$$

The experimental results are given in Appendix((12) tables (10.4 for the 12.5 mm diameter holes tray and 10.5 for the 1 mm diameter hole tray) and the graphical plots of D_e versus liquid loading in figures(10.6a to 10.6h) for the 1 mm diameter hole and in figures (10.6i to 10.6t) for the 12.5 mm diameter hole tray.

10.6 INTERPRETATION OF THE EXPERIMENTAL RESULTS

In this work , measurements of liquid hold-up were made across the whole length of the tray,with the knowledge that the operating condition on the tray should be such that none of the tracer reaches the tray inlet weir. It was found that the variations in the clear liquid heights measured in the manometers were much smaller than those which have been reported by other workers (7,12 & 24).

There was a small increase in the value of the clear liquid height near to the out let weir, while the hold-up remained approximately constant fot the rest of the tray. The tray levelness was checked at a number of positions before starting the experiment. The increase of the clear liquid height at the locations near the outlet weir could be explained by the outlet weir effect which in itself will not have any effect on the estimated results of the coefficient of mixing (D_e) since the tracer injection grid and the sampling points were located 147mm away from

this area.

The slight fluctuation of the clear liquid height in the manometer can be attributed to the bubbling behaviour of the bi-phase on the tray. As bubbling takes place on the tray, bubbles are being formed and some are collapsing causing a series of "reactions" both along the tray and also the manometer connections.

1 mm hole experimental (D_e) results

Experiments on the 1mm hole tray were started with the tray installed without an outlet weir before an initial outlet weir height of 12.5mm was fitted. The same experimental conditions were repeated as in the 12.5mm hole tray experiments (i.e capacity factors of 0.06196, 0.08766 and 0.1073m/s and weir loads of 0.00124, 0.00249, 0.00373 and 0.00497 m^3/s m). The interesting result for both experiments was that no tracer concentration was detected in the liquid up-stream beyond the tracer injection position on the tray for the increasing liquid loadings. This apparently underlines the influence of the outlet weir on the extent of liquid mixing by eddy diffusional mechanism. On increasing the weir height to 25mm under the same capacity factor and liquid loadings , tracer concentrations were then detected up-stream. The D_e values (of 0.0018m^2/s) (figure 10.6a) estimated for runs at capacity factor of 0.08766m/s remained constant over the increasing weir loads of 0.00124, 0.00249 and 0.00373 m^3/s m. There was a sharp increase in D_e value(of 0.004 m^2/s) when the weir load was increased up to 0.00497 m^3/s m.

As the capacity factor was increased to 0.1073 m/s at increasing weir load, the estimated D_e values (figure (10.6b)) increased from 0.002 to 0.0048 m^2/s for weir load of 0.00124 and 0.00249 m^3/s m respectively and then increased to 0.004 and 0.0032 m^2/s for the increasing weir load of 0.00373 and 0.00497 m^3/s m.

37.5mm weir height

For the air capacity factor of 0.06196m/s there was a slight increase in the D_e value (figure 10.6c) from 0.0025 to 0.0029 m^2/s for the liquid loading of 0.00124, 0.00249 and 0.00373 m^3/s m and then decrease to 0.0026 m^2/s for a weir load of 0.00497 m^3/s m. On increasing the capacity factor up to 0.08766 and 0.1073 m/s the estimated values of the eddy diffusion coefficient decreased from 0.0042 to 0.0019 m^2/s and from 0.112 to 0.015 m^2/s with increasing weir load respectively (figure 10.6d & 10.6e).

50.0 mm weir height

For an air capacity factor of 0.06196 m/s the estimated D_e values (figure 10.6f) increased with increasing liquid loading of (0.00124, 0.00249 and 0.00373 m^3/s m) from 0.0011 to 0.00118 m^2/s and decreased to 0.0012 m^2/s for 0.00497 m^3/s m weir load. On increasing the weir load to 0.08766 and 0.1073 m/s the D_e values (figure 10.6g & 10.6h) decreased with increasing liquid loading from a higher value at the lowest weir load to a lower value at the highest weir load.The estimated values for both capacity factors were 0.0044 to 0.0026 m^2/s and 0.054 to 0.0068 m^2/s respectively.

12.5mm hole tray

37.5mm weir height

It was found that for a constant capacity factor of 0.06196 m/s the D_e value (figure (10.6i)) increased slightly from 0.00166 m^2/s to 0.0019 m^2/s with increasing liquid loading from (0.00124 to 0.00497 m^3 / s m). As the capacity factor was increased to 0.0876 m/s and the same liquid rates repeated, the D_e values decreased (figure 10.6j) from 0.0032 m^2/s at low liquid loading of 0.0025 m^2/s m to a high liquid loading of 0.00497 m^3/s m.

The capacity factor was increased to 0.1073 m/s and D_e values decreased from 0.1088 to 0.02 m^2/s with increasing liquid loading figure (10.6k).

50mm weir height

The same trend of a slight increase in the estimated D_e values (figure 10.6l) was obtained for the low capacity factor of 0.06196m/s with increasing weir load from 0.001 to 0.0013 m^2/s. As the capacity factor was increased to 0.08766 and 0.1073 m/s respectively the D_e values decreased (figures (10.6m & 10.6n) with increase in the weir load from 0.0027 to 0.00165 m^2/s and 0.026 to 0.0073 m^2/s .

62.5mm weir height

At the low capacity factor of 0.06196m/s the D_e values (figure (10.6o)) remained constant at 0.0013 m^2/s for the four weir loads respectively. As the capacity factor was increased to 0.08766 m/s the D_e values (figure (10.6p)) were also constant at 0.0018 m^2/s for the four liquid loadings. As the capacity factor was increased up to 0.1073 m/s there was a marked increase in the eddy diffusivity value for the lowest liquid capacity factor of 0.037 m^2/s and a sharp decrease (figure (10.6q)) to 0.0045 m^2/s for the highest weir load of 0.00497 m^3/s .

75.0mm weir height

The D_e values increased slightly (figure 10.6r) from 0.0012 to 0.0031 m^2/s at a low capacity factor of 0.06196 m/s with the increasing weir load. As the capacity factors were increased to 0.08766 and 0.1073 m/s respectively the D_e values (figure (10.6s & 10.6t)) decreased from 0.0025 to 0.0018 m^2/s and 0.044 to 0.037 m^2/s with increasing liquid loading of 0.00124, 0.00249, 0.00373 and 0.00497 m^3/s m.

10.7 DISCUSSION OF RESULTS

In all the experiments the calculated Peclet number values (P_e) increased with an increase in the liquid loading as well as increasing capacity factor. One remarkable feature of the present results has been represented on the graphs of $\text{Log}((x - x_o)/(x_g - x_o))$ versus 1 - W (see figures 10.3i to 10.3t). The results clearly indicated the extent to which the tracer concentration travelled up-stream towards the inlet weir. As the liquid weir load was increased the extent of tracer diffusion from the grid point rapidly falls to zero. This can only be explained by the suggestion that at different stage on the tray during the formation of the flow regimes, the liquid entering the tray under goes multiple atomisation and most of the liquid elements spent a considerable part of their passage time as droplets and part under going transformation on the tray floor. Since the process of atomisation decreases with increase in the weir load as well as the clear liquid hold-up on the tray , this increases the underlying liquid flow momentum and hence reducing the process of tracer diffusion up stream.

The decrease in the estimated D_e values at high weir loads could be explained as being the case of the liquid momentum dominating the bulk flow of liquid on the tray and hence controls

the movement of the bi-phase on the tray. A visual observation also indicated a more forward liquid trajectory with increasing liquid loading.

The increase observed in D_e values at low weir loads may be explained as the effect of entrained liquid droplets which under spray situations reaches a free height and falls back in to the froth randomly. Since the rate at which the drops fall back to the froth is the same as the rate at which they are replenished the resultant effect increases the rate of mixing on the tray.

For the two different hole size trays the estimated coefficient of mixing was generally higher for the 1mm hole tray . This may be explained by the less resistance to flow caused by the vapour jets through the holes observed in the small hole tray experiments.

10.8 CONCLUSION

When the air capacity factor were less or equal to 0.06196 m/s the estimated eddy diffusion coefficients remained constant with increasing weir load for both trays.

The estimated D_e values for all the tested weir heights generally increased with increasing capacity factor, but generally decreased with increasing weir load.This trend was not typical of the A.I.Ch.E report and the result reported by **Barker** and **Self** (7).

A comparison of the D_e values obtained on the 1mm hole tray and that of the 12.5 mm hole tray indicates that the degree of mixing by eddy diffusion on small hole trays are higher than for big hole trays under the same operating conditions and outlet weir height.

The results obtained here could not be compared with the published results because it is important that the plate characteristics such as, tray levelness and the liquid hold-up, be measured by a standard procedure and the clamping arrangment of the tray to avoid much tray deck movement in the lateral direction,which presumably was termed sinusoidal effect by **Barker** and **Self** (7).

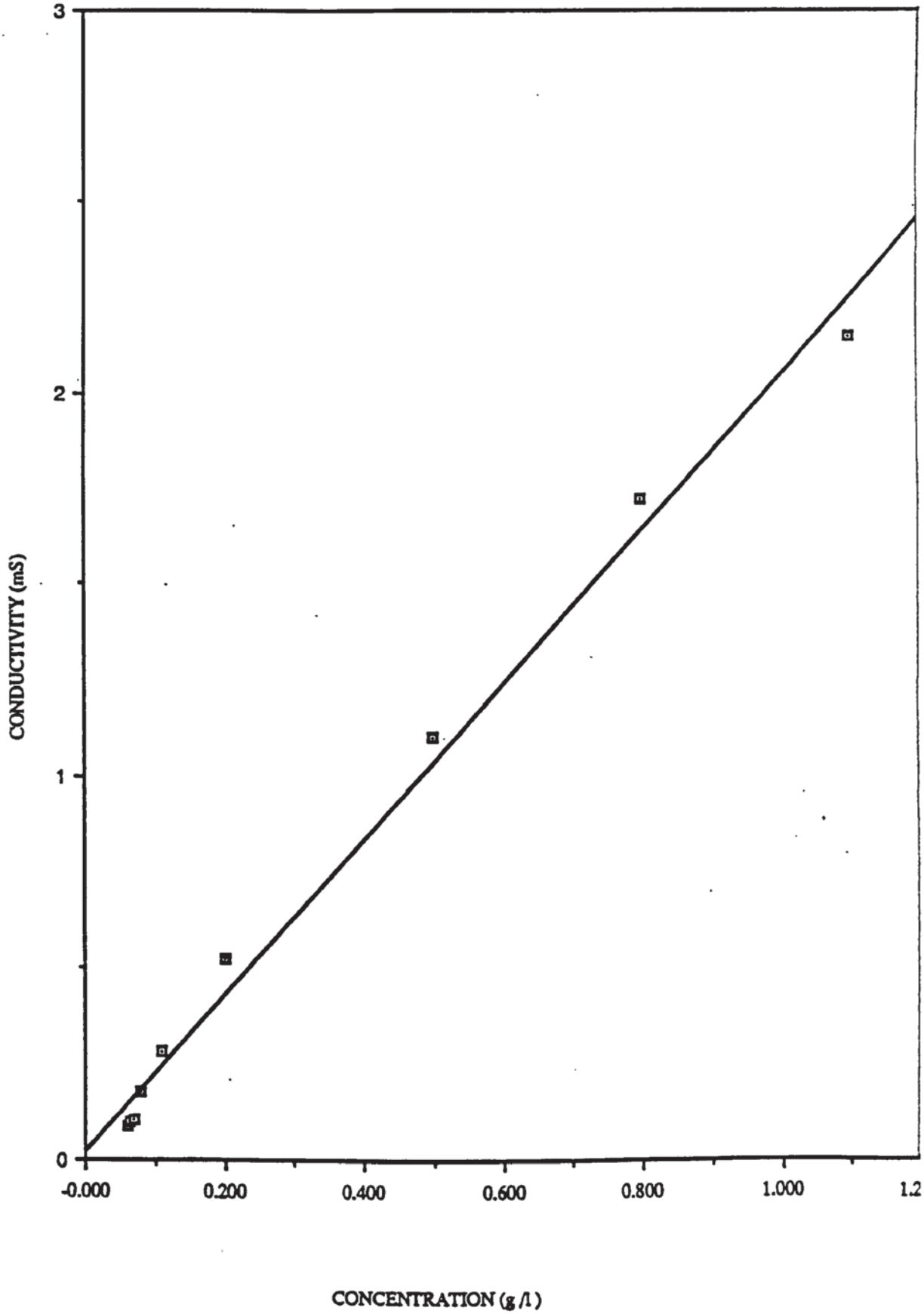

Figure (10.1) Conductivity versus concentration graph

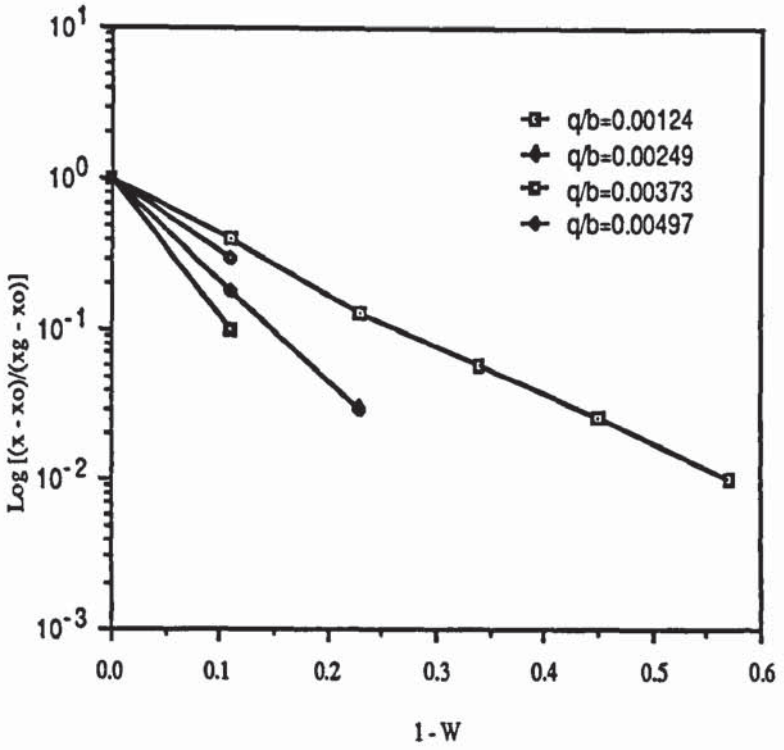

Figure (10.5.3a) graph of Log(x-xo/xg-xo) vs 1-W for1mm holes tray weir height 12.5mm

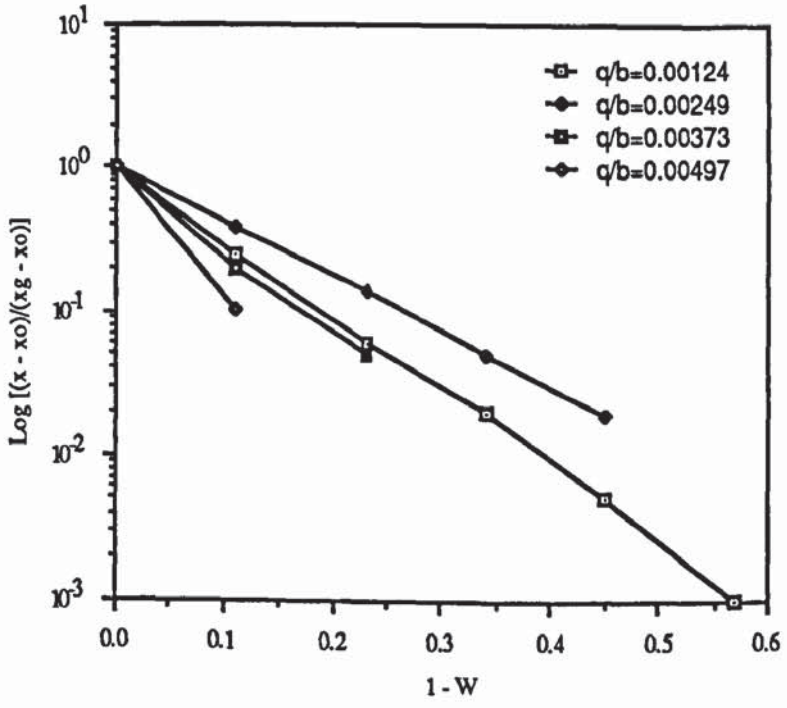

Figure (10.5.3b) graph of Log (x-xo/xg-xo) vs 1-W for 1mm holes tray weir height 12.5 mm

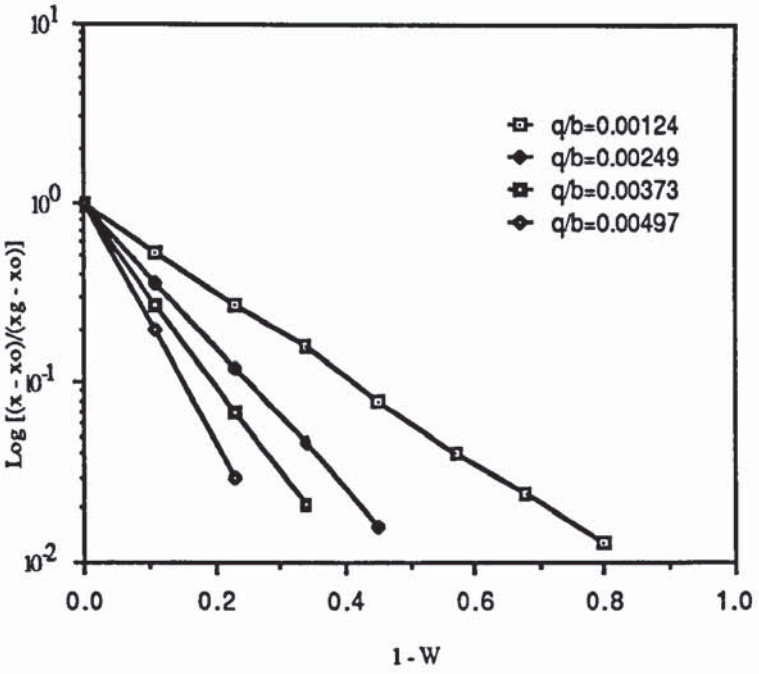

Figure (10.5.3c) graph of Log(x-xo/xg-xo) vs 1-W for 1 mm holes tray weir height 37.5

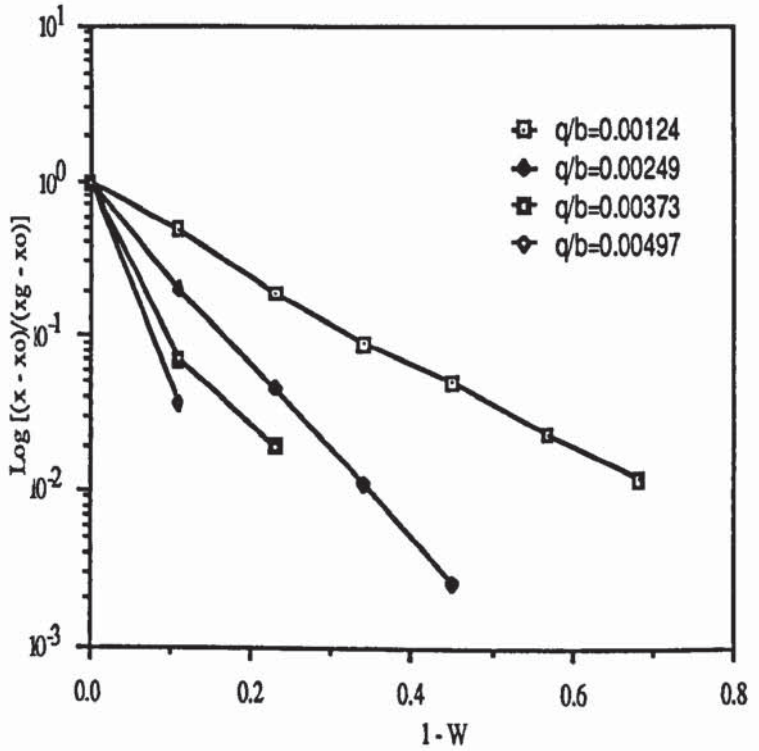

Figure (10.5.3d) graph of Log(x-xo/xg-xo) vs 1-W for 1 mm holes tray weir height 37.5 mm

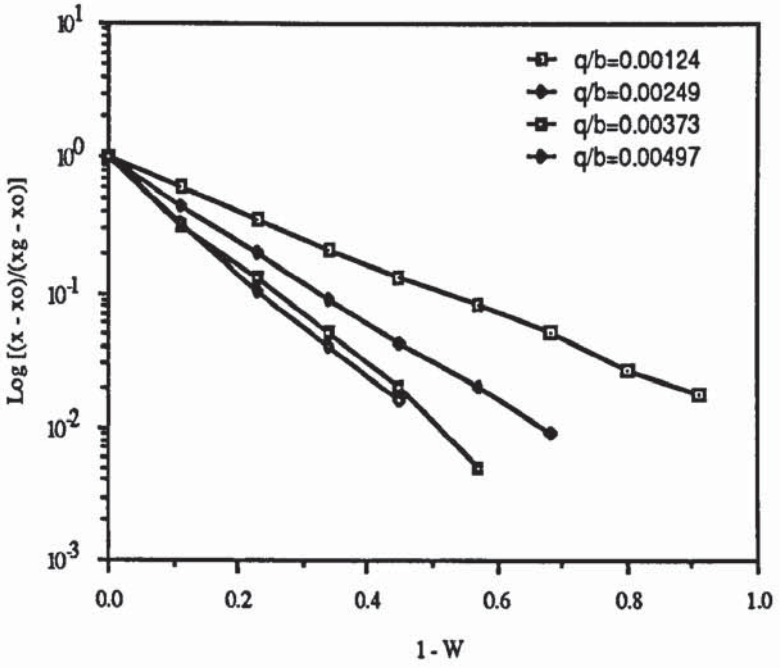

Figure (10.5.3e) graph of Log(x-xo/xg-xo) vs 1-W for 1mm holes tray weir height 37.5 :Csb=0.1070 m/s

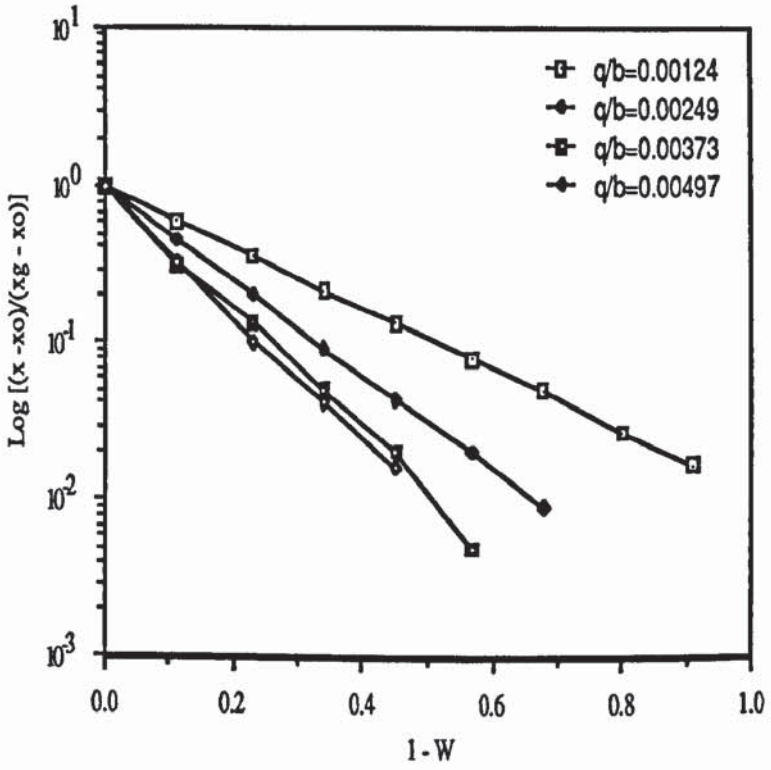

Figure (10.5.3f) graph of Log(x-xo/xg-xo) vs 1-W for 1 mm holes tray weir height 50.0 mm : Csb=0.06196 m/s

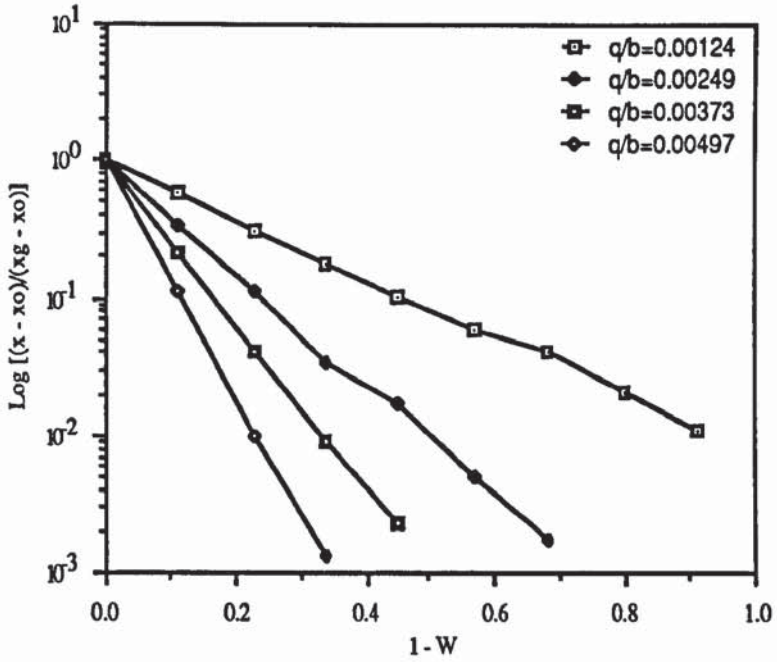

Figure (10.5.3g) graph of Log(x-xo/xg-xo) vs 1-W for 1mm holes tray weir height 50.0 mm : Csb = 0.08766 m/s

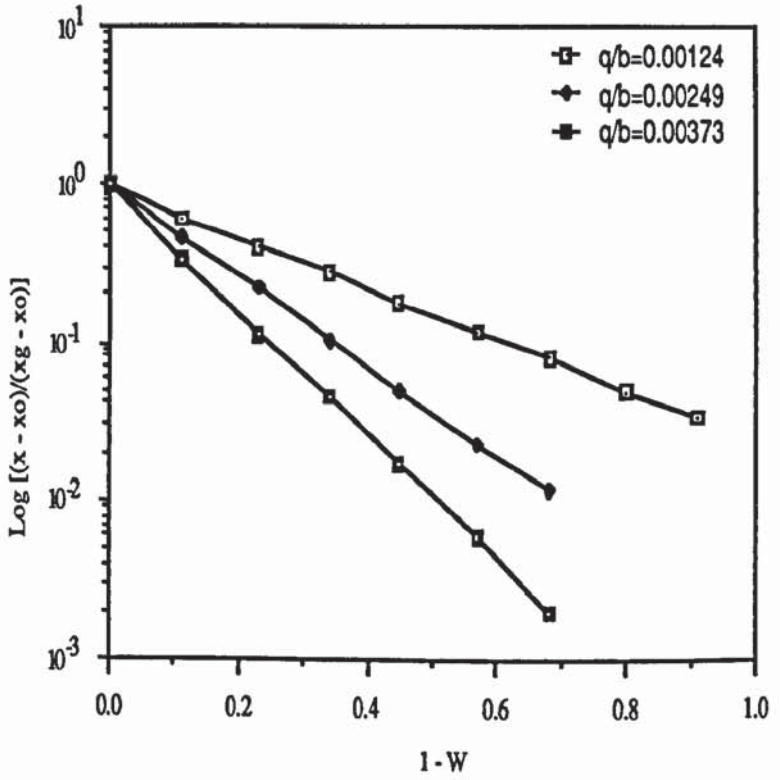

Figure (10.5.3h) graph of Log(x-xo/xg-xo) vs 1-w for imm holes tray weir height 50.0mm : Csb =0.1073 mm

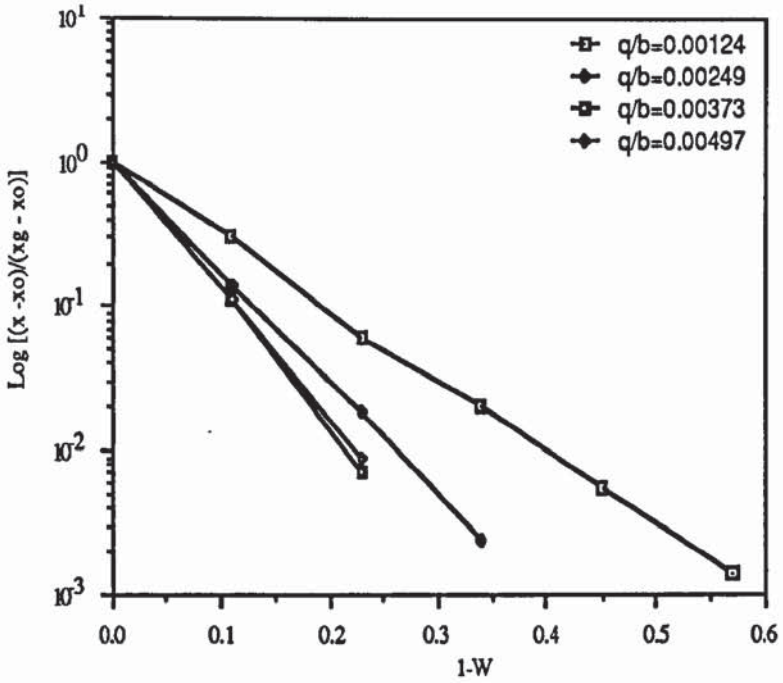

Figure (10.5.3i) graph of Log(x-xo/xg-xo) vs 1-W for 12.5 mm holes tray weir height 37.5 mm : Csb + 0.06196 m/s

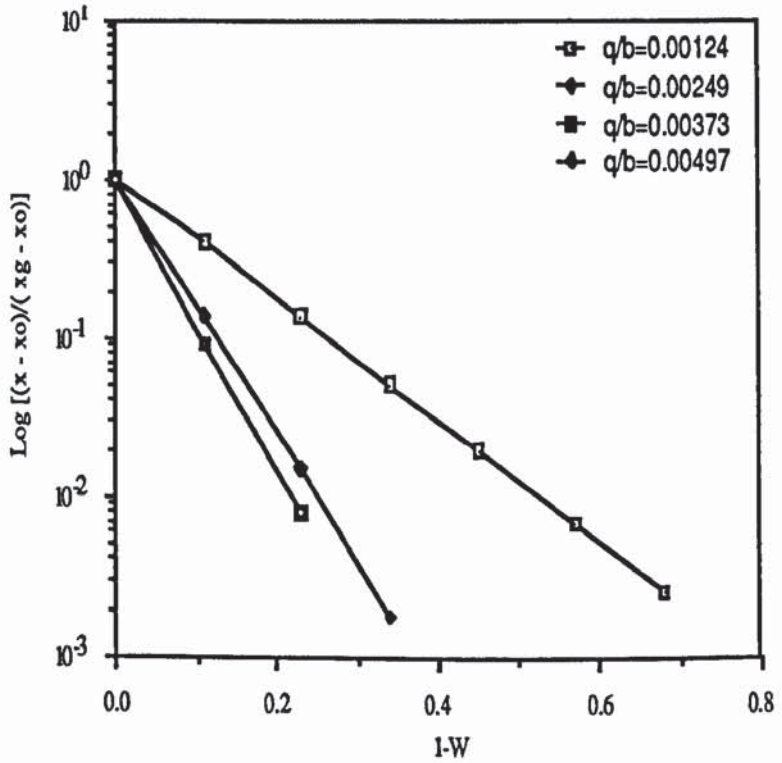

Figure (10.5.3j) graph of Log(x-xo/xg-xo) vs 1-W for 12.5 mm holes tray weir height 37.5 mm : Csb =0.0876 m/s

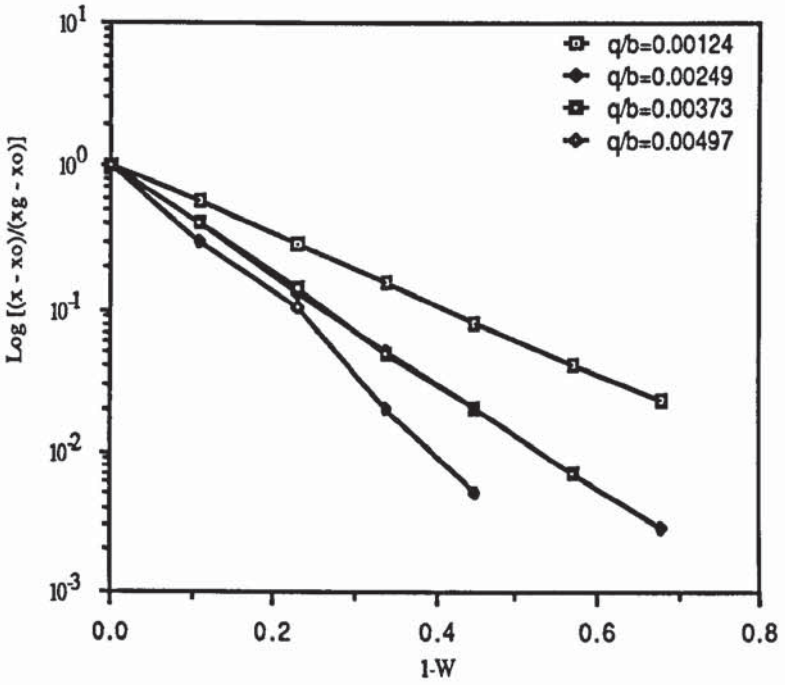

Figure (10.5.3k) graph of Log(x-xo/xg-xo) vs 1-W for 12.5 mm holes tray weir height 37.5 mm : Csb = 0.1073 m/s

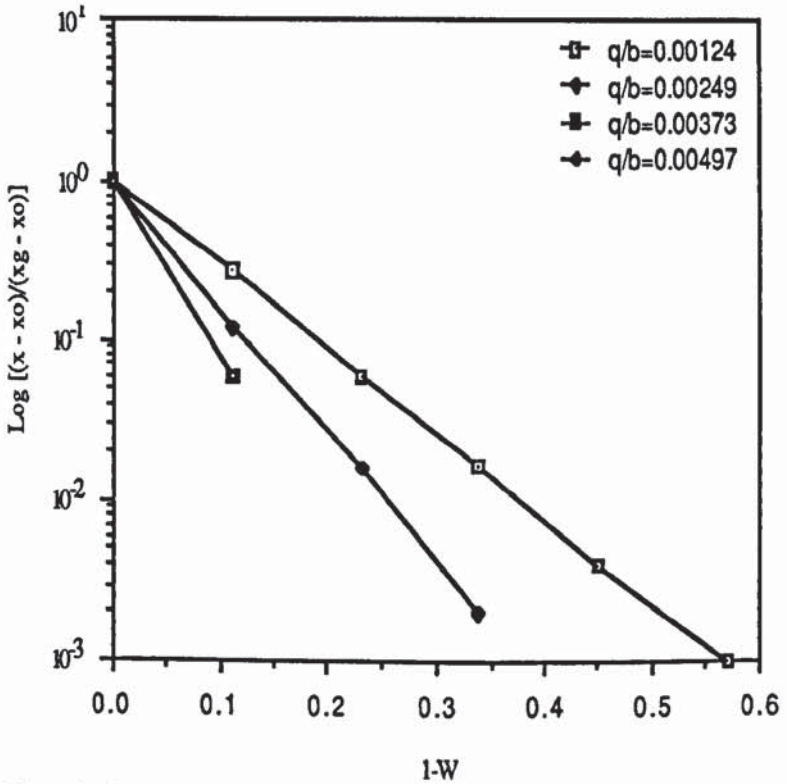

Figure (10.5.3l) graph of Log(x-xo/xg-xo) vs 1-W for 12.5 mm holes tray weir height 50.0 mm : Csb = 0.06196 m/s

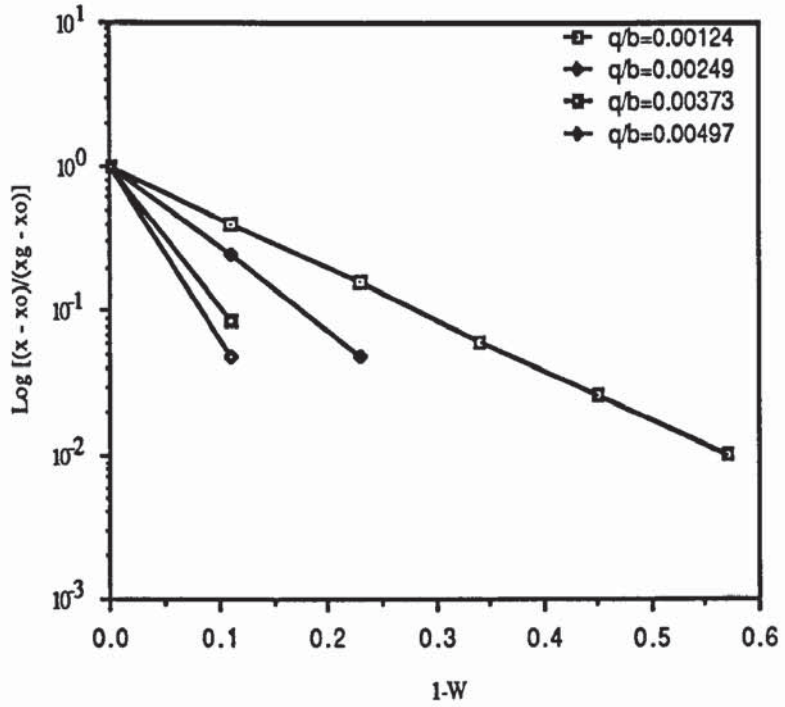

Figure (10.5.3m) graph of Log(x-xo/xg-xo) vs 1-W for 12.5 mm holes tray weir height 50.0 mm : Csb =0.08766 m/s

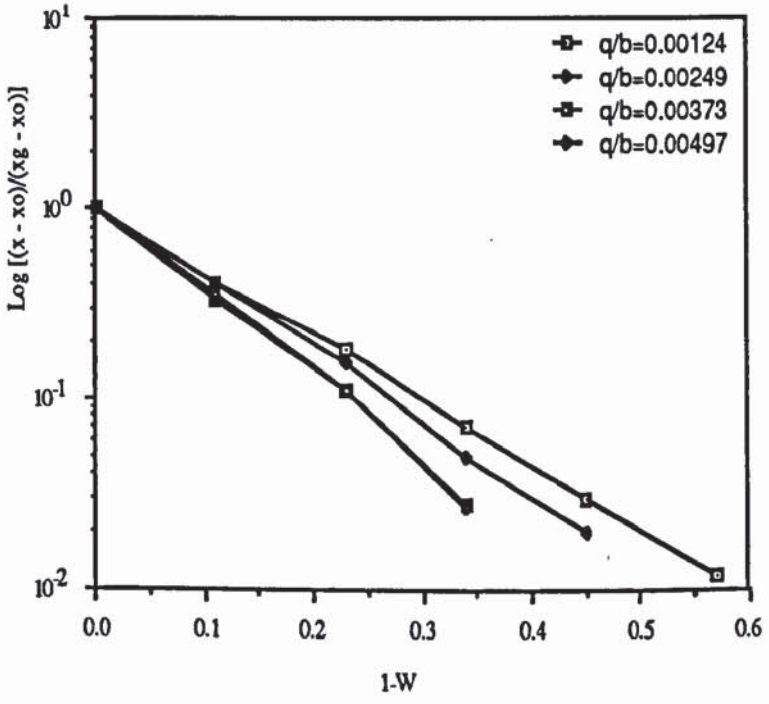

Figure(10.5.3n) graph of Log(x-xo/xg-xo) vs 1-W for 12.5 mm holes tray weir height 50.0 mm : Csb = 0.1073 m/s

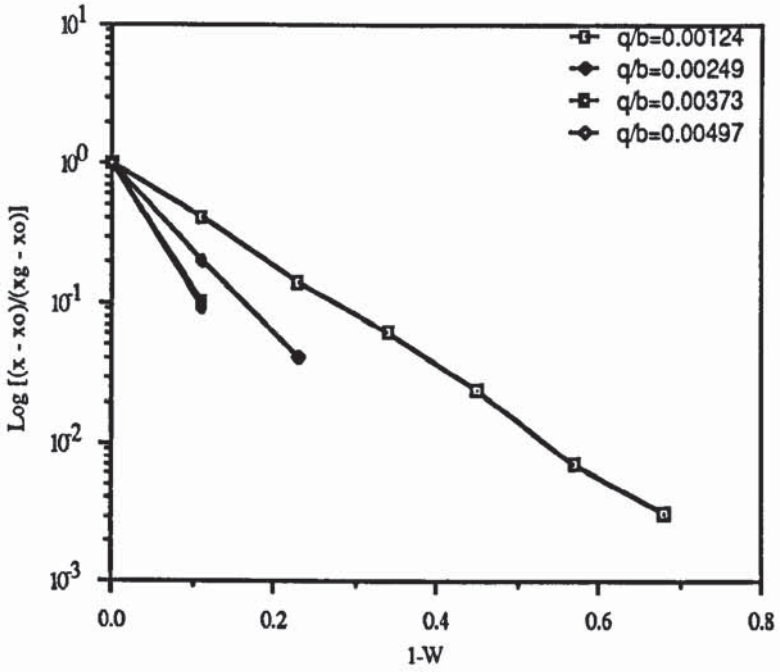

Figure (10.5.3o) graph of Log(x-xo/xg-xo) vs 1-W for 12.5 mm holes tray weir height 62.5 mm :Csb =0.06196 m/s

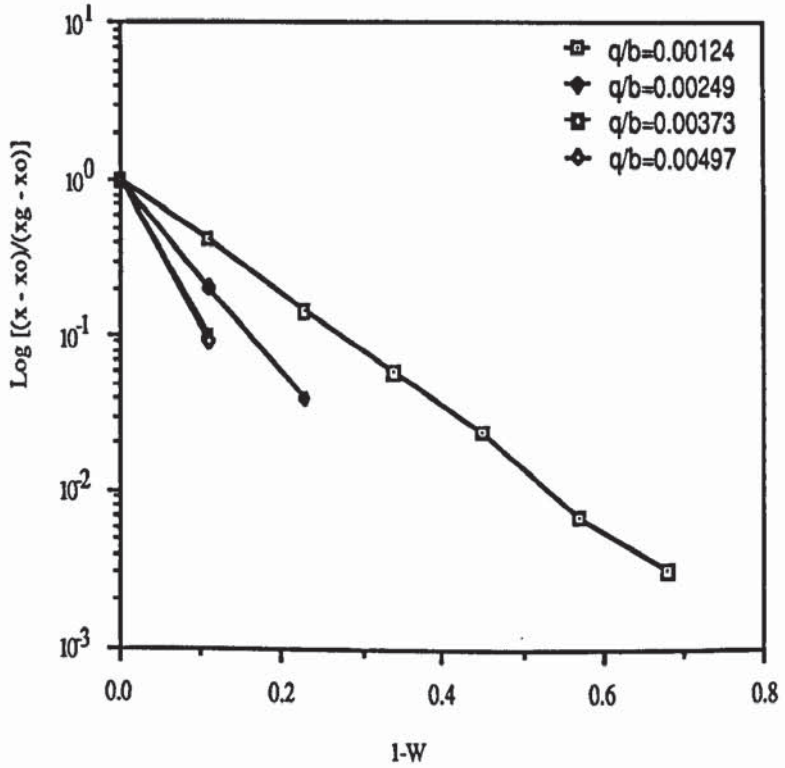

Figure(10.5.3p) graph of Log(x-xo/xg-xo) vs 1-W for 12.5 mm holes tray weir height 62.5 mm : Csb= 0.08766 m/s

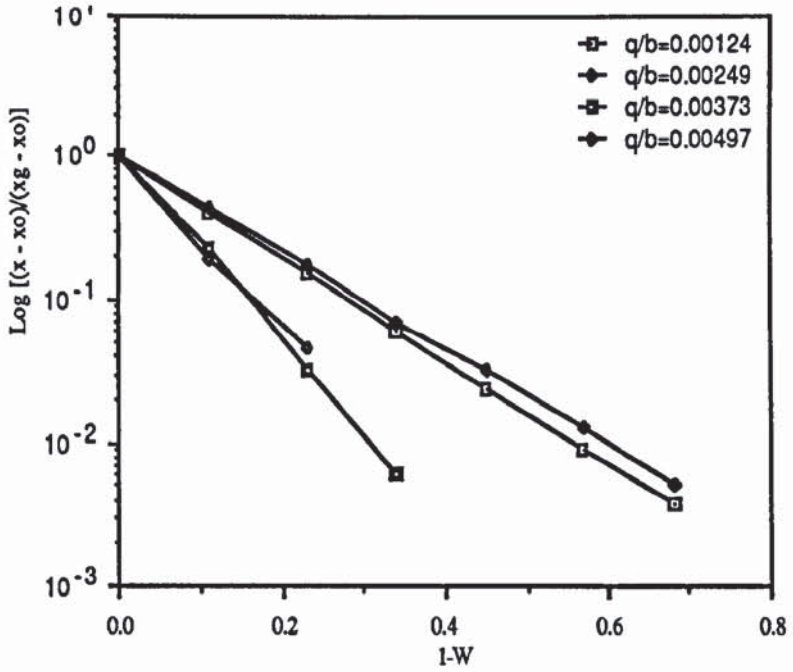

Figure(10.5.3q) graph of Log(x-xo/xg-xo) vs 1-W for 12.5 mm holes tray weir height 62.5 mm : Csb = 0.1073 m/s

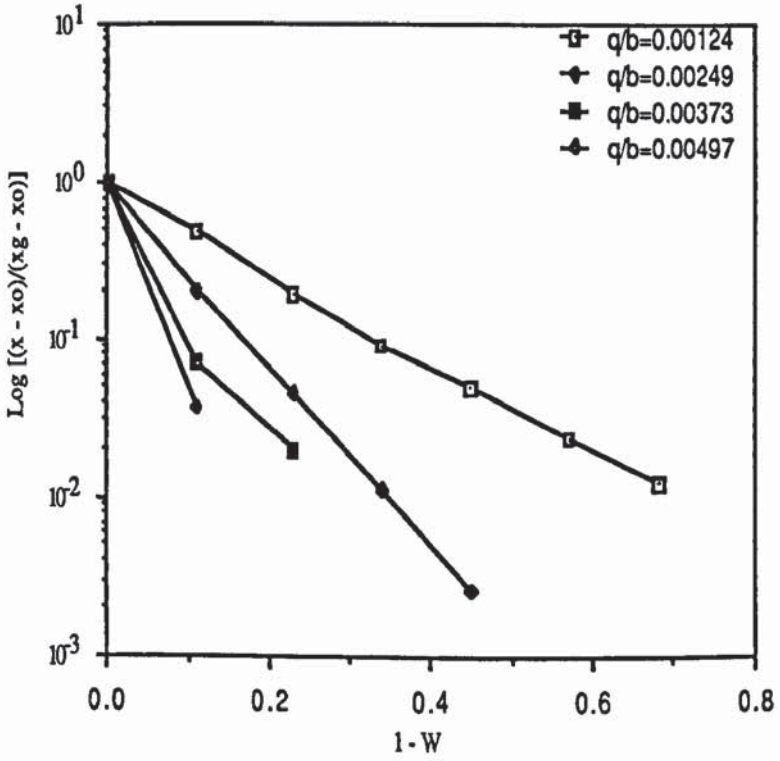

Figure (10.5.3r) graph of Log(x-xo/xg-xo) vs 1-W for 12.5 mm holes tray weir height 75.0 mm : Csb = 0.06196 m/s

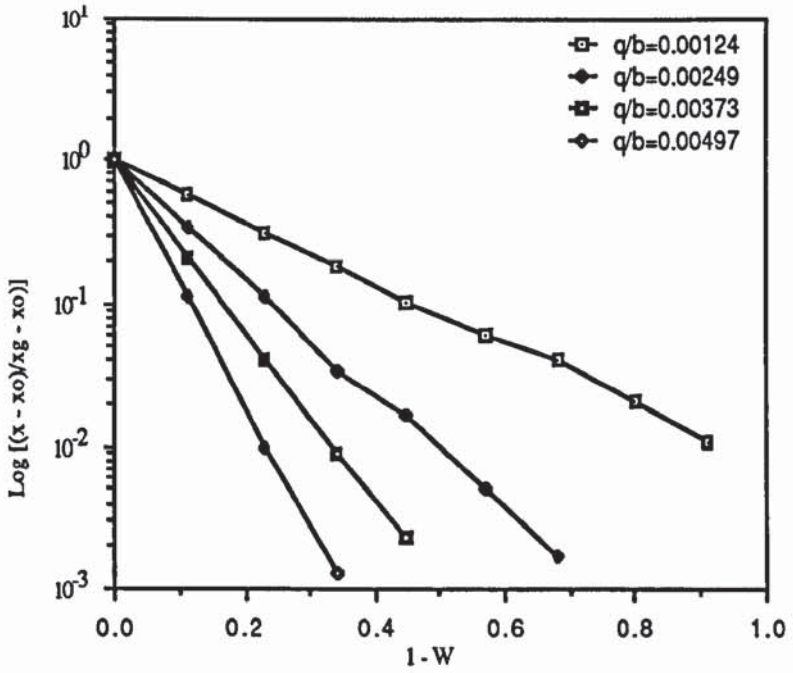

Figure (10.5.3s) graph of Log(x-xo/xg-xo) vs 1-W for 12.5 mm holes tray weir height 75.0 mm : Csb = 0.08766 m/s

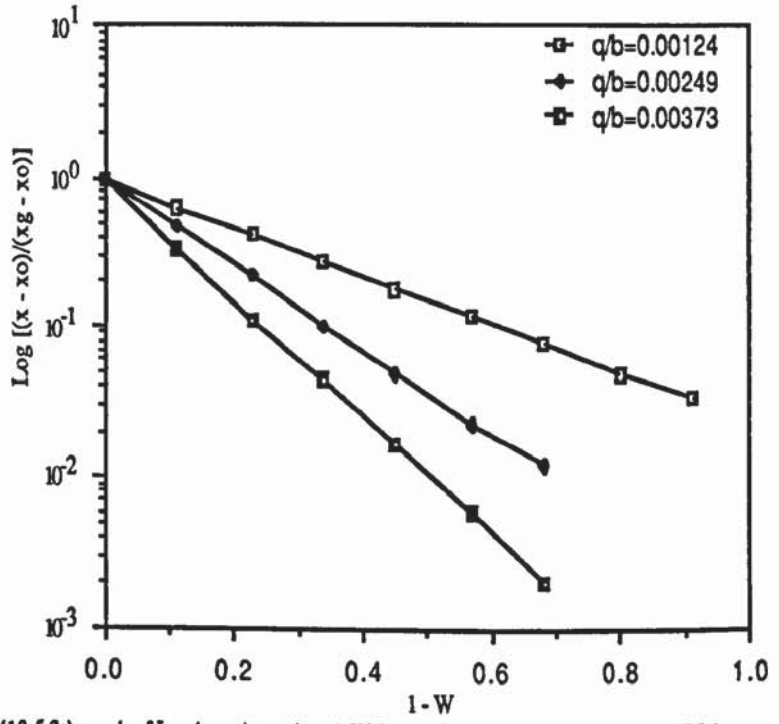

Figure (10.5.3t) graph of Log(x-xo/xg-xo) vs 1-W for 12.5 mm holes tray weir height 75.0 mm : Csb =0.1073 m/s

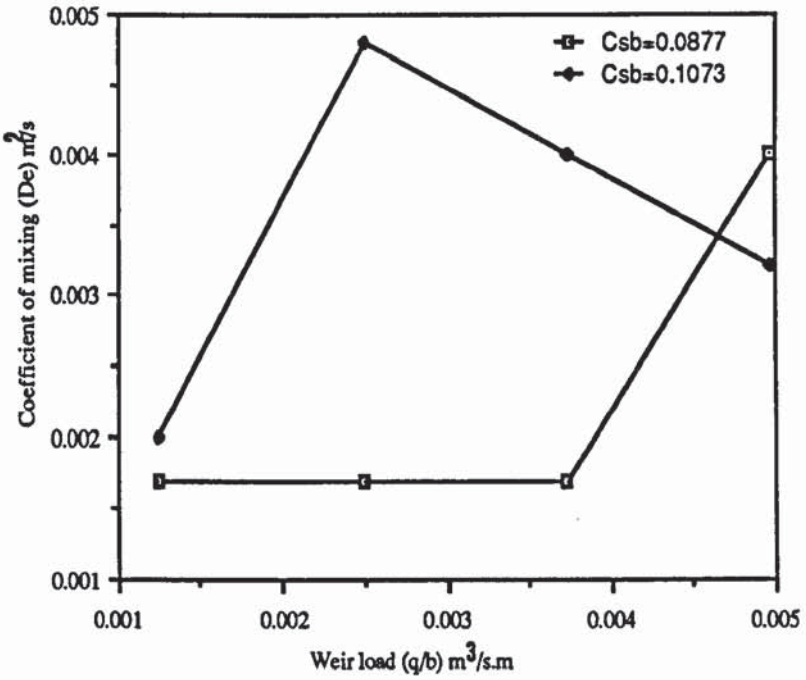

Figure (10.6a) Graph of De vs weir load for 1mm holes tray weir height 12.5 mm

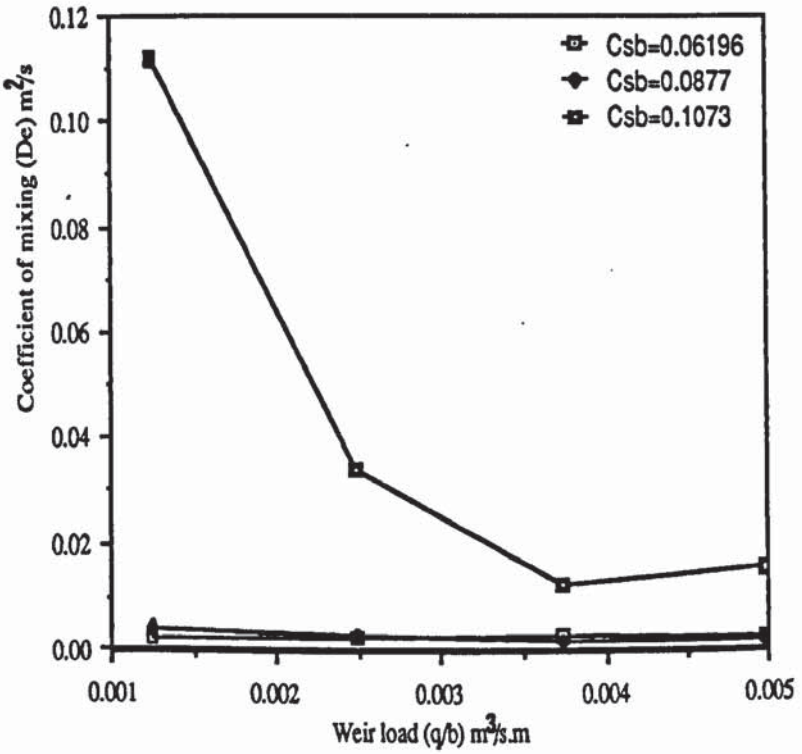

Figuire(10.6b) Graph of De vs weir load for 1 mm holes tray weir height 37.5 mm

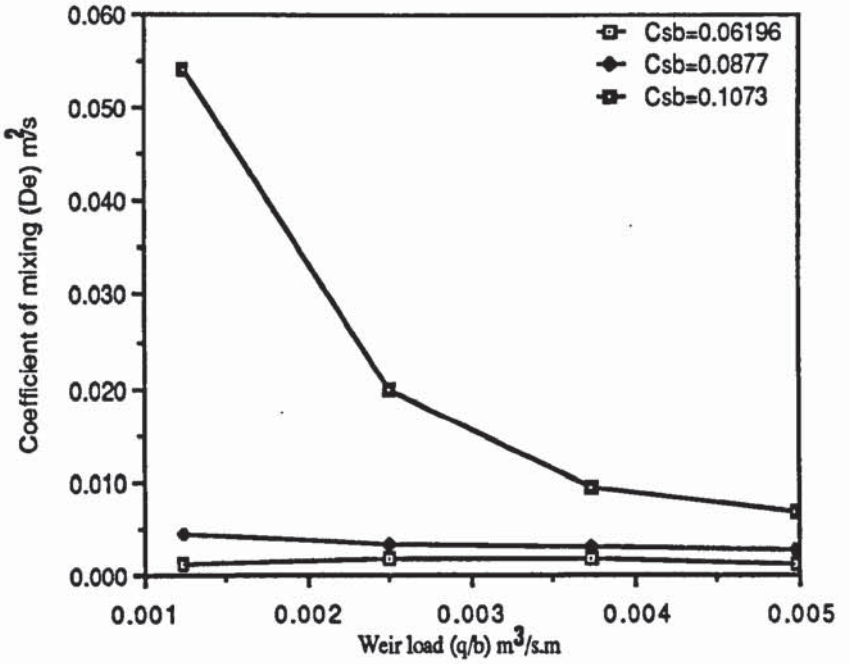

Figure (10.6c) Graph of De vs weir load for 1 mm holes tray weir height 50.0 mm

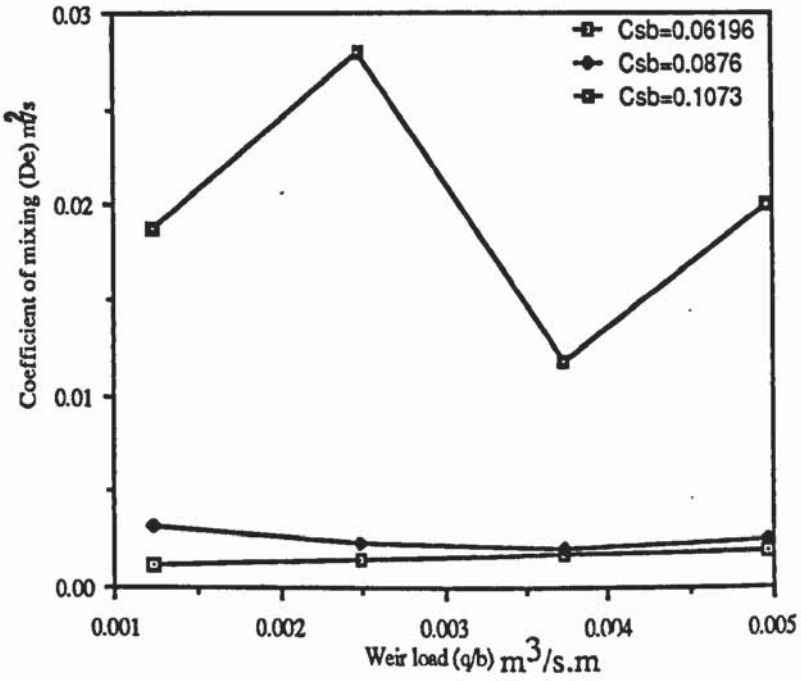

Figure (10.6d) Graph of De vs weir load for 12.5mm holes tray weir height 37.5 mm

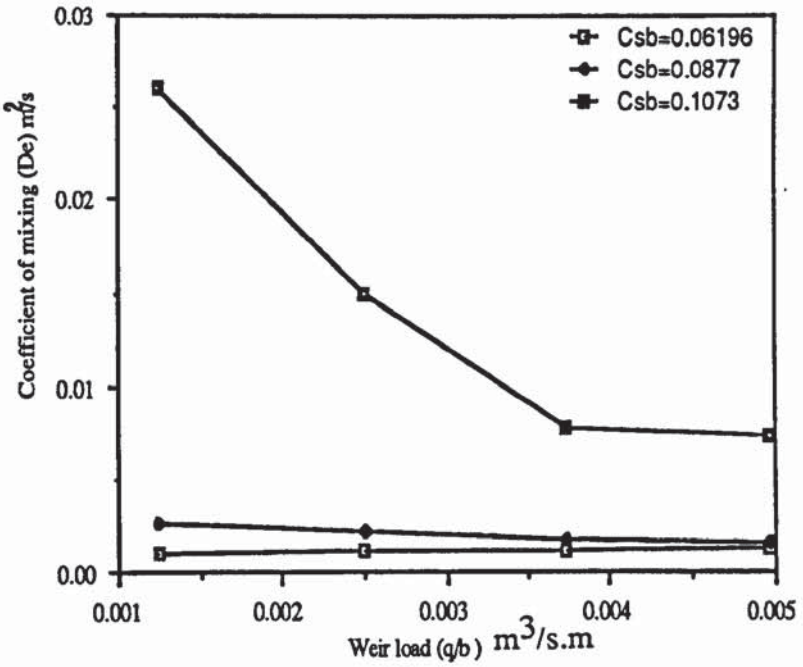

Figure (10.6e) Graph of De vs weir load for 12.5 mm holes tray weir height 50.0mm

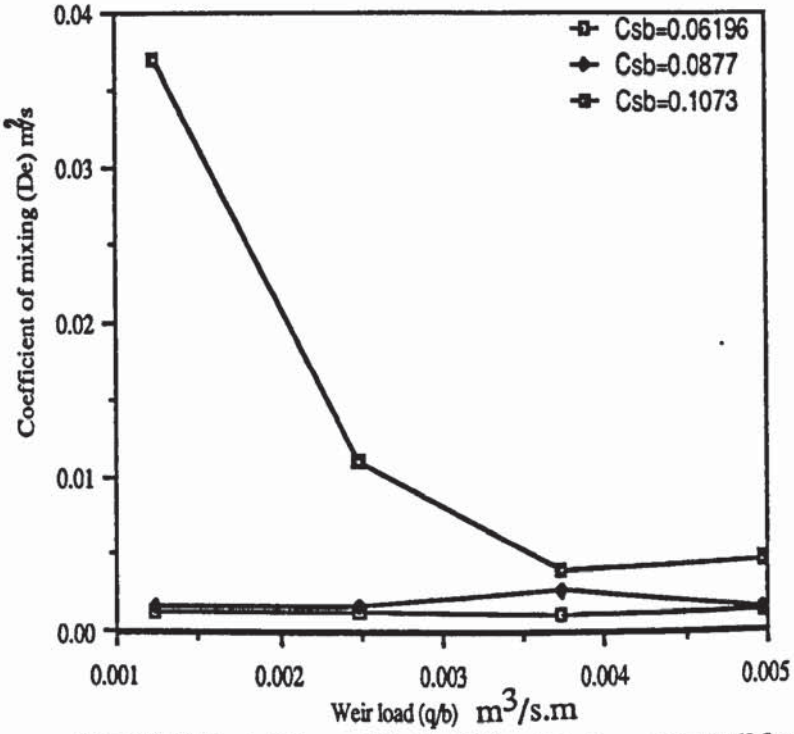

Figure (10.6f) Graph of De vs weir load for 12.5 mm holes tray weir height 62.5 mm

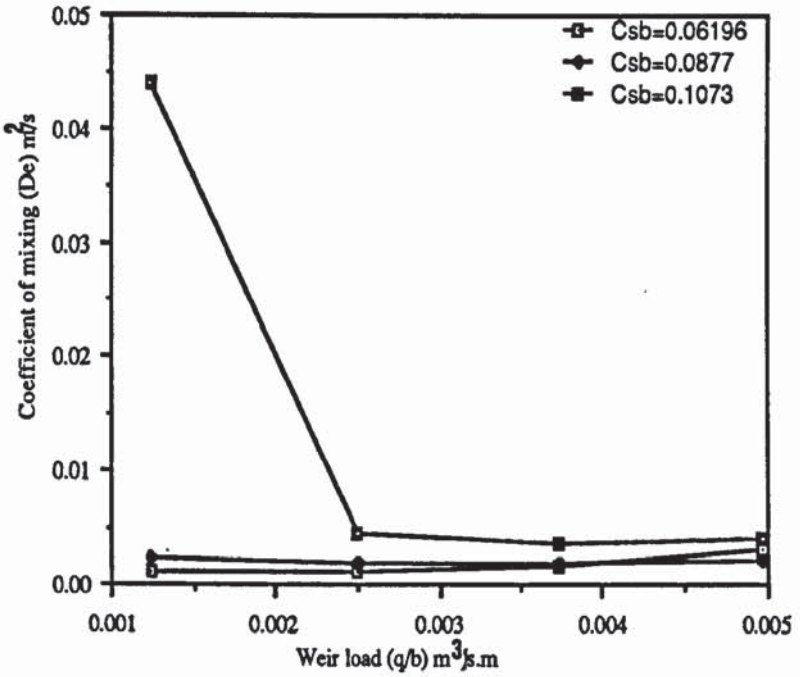

Figure (10.6g) Graph of De vs weir load for 12.5 mm holes tray weir height 75.0 mm

Chapter 11

11.1 DISCUSSION OF EXPERIMENTAL RESULTS

The experimental FRI data from a 1.2 m diameter distillation column separating cyclohexane and n-butane, was used to test the accuracy for predicting tray efficiency from a range of theoretical models. However all the theoretical models calculated tray efficiency from a point efficiency, which in turn was calculated from an emperical correlation. A comparison between the tray efficiency values predicted from the models and the results from the FRI experimental plant show a significant difference.Tables (4.5 and 4.6). It is evident that there was close agreement between the FRI experimental data and the results calculated from the Porter and Lockett model although their model did allow for back mixing on the tray and did not use the simple plug flow as was the case for some of the models. The point efficiencies could have been easily calculated if the liquid and vapour mass transfer resistances were known. Since the tray efficiencies obtained from the theoretical models depend on the point efficiency and hence the liquid and vapour mass transfer resistances, an improved method for predicting tray efficiency can only be obtained if an improved method is available for calculating the mass transfer resistance.

Such an improvement is made difficult by the results obtained from the liquid hold-up experiments which showed that the liquid hold-up on an operating tray varied from point to point over the active area of the tray. The process of calculating point efficiency becomes a weak one and the results are known to follow the same trend as the clear liquid seal on the tray. Thus, there is a need to develop a theoretical model based on the understanding of the physics of the liquid flow across the tray and which will enable design engineers to estimate the performance of a particular tray design without the need to calculate liquid and vapour mass transfer coefficients. This has been the object of the present investigations.

Many previous research workers have represented the flow on an operating tray in the form of a rectangular flow path (plug flow). In order to overcome the practical problem of obtaining many liquid and vapour samples from a large tray on which a real separation is being carried out, a new technique has been developed which enabled the separations to be simulated by blowing unsaturated air through hot water and to measure the temperature, at many points, of the water as it flowed across the tray. Temperature profiles (analogous to concentration profiles) could then be built up over the tray. This "water-cooling technique" was then applied to the problem of evaluating the performance of different sized sieve trays.

It has been observed from this work that when the liquid flow patterns were examined for different hole size trays, the flow patterns (temperature profiles) which were developed were found to be dependent on the tray hole diameter. For many of the operating conditions, the temperature profiles for the 4.5 mm diameter hole tray had very significant recirculation zones at the circular corners of the tray emanating from the inlet down-comer to the outlet weir. However, the temperature profiles for the tray with 12.5 mm diameter hole had recirculation zones which were situated towards the outlet weir while operating in the spray regime and a predominantly flat tranverse profiles from the region of the inlet downcomer to the middle half of the tray active area. The profiles were further improved when operating at high capacity factors at the increasing weir loads. Under these conditions the profiles were found to be flat in the transverse direction without axial temperature profiles when operating in the mixed flow regime.

The poorer mixing associated with the 4.5 mm diameter hole tray may be explained by the way in which the gas emerged from the tray hole. The extent of jetting varied for different hole sizes and for the case of the small hole it was observed that the gas tended to emerge in the form of a jet with a smaller cone angle which limited the mixing length (which is the local distance the wave created by the resistance to flow by the gas jet velocity going through the hole and the hold-up liquid on the tray) can travel before interacting into similar waves from another hole in the same vicinity. In the case of the larger hole the gas was observed to diverge with a larger cone angle which would give the gas a more side ways directional effect thus improving the mixing characteristics of the tray and hence an increased mixing length.

The temperature profiles were examined in terms of the different flow regimes and it was found that the tray temperature profiles were severely U-shaped at very low weir load. The resulting froth dispersion was defined by **Enjugu** (18) as an intense spray. At this operating condition visual observation indicated that the liquid was dispersed into a cloud of fine droplets above the tray leaving the tray floor clearly visible and liquid was observed to flow over the outlet weir in the form of a cloud of liquid droplets rather than in the conventional way as indicated by the Francis weir equation. In commercial columns, such operating conditions have been controlled by the introduction of a baffled or blocked weir.

Generally, as the weir load was increased, the shape of the profile changed from a severe U-shape to a flat profile especially in the areas towards the inlet downcomer with U-shaped profiles at the section near the outlet weir while operating in the spray regime. In the mixed flow regime, the temperature profiles were observed to be predominantly in the transverse direction. As the weir load was increased further to bring the operating condition into the emulsified flow regime, a more confused flow pattern was observed with liquid recirculation zones and some U-shaped profiles scattered over the central region of the tray. It could be that different parts of the tray could be operating in different flow regimes. The relatively high

momentum of the liquid in some parts of the tray could be opposed by the equally high momentum of the retrograde flow(increased liquid hold-up hence increased weir effect).

These opposing flows may over come each other in some part of the tray, creating regions on the tray where the resistance to flow by the gas might be over come by the liquid momentum and hence the gas will in such situations be entrained by the liquid onto the tray below. The regions where the gas resistance is high (low liquid hold-up) gas by passing might be induced resulting in areas of constant low temperature profiles.

The hydrodynamic conditions on the trays were examined by injecting a dye tracer (potassium permanganate) at the inlet down-comer and the movement of the dye from the inlet to the outlet weir was recorded by the use of a video or still photographic technique.

The movement of the froth , the width of the liquid channelling region and the extent of the liquid recirculation zones(stagnant region) were clearly indicated by the movement and intensity of the dye in the experiments for both the small and large hole diameter trays. The extent of the stagnant regions shown in the still photographic pictures was related to the flow patterns obtained from the temperature profiles.

The mass transfer efficiencies have been shown to increase at any capacity factor above the incipent weeping point and below the flood line with increasing weir load from the spray to the mixed flow regimes. When the tray operating conditions were in the intense spray condition (low weir load), the gas jetting effect dominated the bi-phase mixing on the tray. The liquid on reaching the tray was completely atomised into a fine dispersed phase, thus leaving little or no liquid hold-up on the tray floor. Since the performance of an operating tray and the rate of mass transfer depends on the residence time of the vapour in the liquid, the efficiencies were found to be very low.

As the weir load was increased (the clear liquid seal increased) the calculated point and tray efficiencies increased up to a maximum value in the mixed flow regime operating condition. It has been suggested by **Raper et al** (61) that tray operations be limited to the spray regime because of the observed increase in the tray efficiencies while operating in the spray regime.

In the emulsified flow condition a decrease occurred in the tray efficiency . The decrease in the efficiency values can be explained by the way the liquid momentum at the high weir loads dominates the underlying movement of the liquid and the froth. The liquid on the tray was observed to form the continuous phase. Due to a fixed gap at the inlet weir, liquid jetting occurred from the gap under the apron. In real operation in single pass tray columns vapour could be entrained onto the next tray below as suggested by **Zuiderweg** (78). However in this work the construction of the inlet downcomer was such that the gap under the apron was permanently fixed(25 mm). The fixed clearance under the apron meant that at very high weir loads corresponding to the emulsified flow regime and with significant liquid back up in the

inlet down-comer for any of the capacity factors, liquid was observed to jet from the inlet across to the middle of the tray causing some of the liquid to effectively by pass the active area of the tray with a subsequent reduction in the contact time of the froth with the vapour .

The value of λ (mG/L) was found to change over a wide range in the air-water simulation technique. In the conventional distillation, λ lies between 0.7 to 1.3 and often is assumed to be approximately equal to 1.0 . For this work, the value was observed to vary between 15.0 corresponding to the spray regime and approximately to 1.0 for the emulsified flow regime.

Such variation of λ was due entirely to changes in the value of the L/G ratio because the gradient of the equilibrium line (saturation line) remains almost constant for water cooling. This explains the high E_{mv}/E_{og} values which were obtained at very low weir loads and thus very high λ values.

The distribution of liquid over the exit weir was measured. This work showed that liquid flow across the outlet weir at low weir loads, for any given capacity factor between the incipient weeping line and the 80 % flood curve, was uniform and can be considered to be channel flow across the weir length for spray and intense spray conditions. This result can be explained by the way liquid is atomised into clouds of spray leaving the tray floor clearly visible. The atomised liquid elements will spend most of their time as droplets and when the drops reach a free height, the drops will fall back to the tray floor only to be reatomised. The dispersion of liquid from one location to another by the jetting effect of the vapour is believed to be responsible for the way in which the liquid flows across the weir while operating in the intense spray regime and the spray regime. As the weir load was increased, the flow patterns were found to change with more liquid channelling through the central region of the weir, with a peak at each end at high weir loads.

The computed tray efficiencies show reasonable agreement with the values calculated when the flow of liquid across the exit weir was not considered in the calculation of the efficiencies at low capacity factor. At high capacity factor of 0.0775 m/s there was a discrepancy in the results while operating in the mixed and the emulsified flow regimes. The discrepancy can be explained by the way liquid temperature was measured at the central position along the way length assuming plug flow and the $(E_{mv})_{nw}$ values were observed to be well over 100 % in the spray and the mixed flow regimes. Those computed with the flow across the weir considered by integrating the enthalpy along the exit weir show efficiency values of less than 100 % in the spray and the mixed flow regimes.

The extent of liquid back mixing by eddy diffusion mechanism was studied under the same operating conditions as in the flow pattern experiments, an observation was made that the tracer could not be detected upstream away from the injection grid above certain weir loads. Thus, the limit of the experimental conditions were set below this maximum weir load of (0.005 m^3/s m).

For all the experiments, the computed Peclect number(P_e) increased with increasing liquid loading for each capacity factor investigated for both the 1 mm and 12.5 mm diameter hole trays. The resulted graphs of $\log[(x - x_o)/(x_g - x_o)]$ versus (1 - W) indicated that as the liquid loading was increased, the distance up stream to which the tracer concentration was detectable decreased. These observations may help in trying to understand which part of the back mixing mechanism should be associated with the atomised liquid droplets and that due to the liquid passage along the tray floor. The decrease in the extent of back mixing of liquid on the tray suggests that during the intense spray situation, the movement of the froth could solely be by droplets movement, which might explain the increased D_e values computed at low weir loads. The calculated coefficient of mixing (D_e) was generally greater for the small hole tray. This supports the suggested weir effect and the diffusivity wave send back as the liquid flow is restricted by the outlet weir, such waves in the case of large hole trays are pushed forward by the jetting vapour through the hole.

Chapter 12

CONCLUSIONS

The following conclusions can be drawn from this work, that

[1] The existing efficiency models over simplify the nature of liquid flow across the tray from the inlet down-comer to the outlet weir on single pass trays. From their results, it follows that an operating tray is not well described by the existing models and the efficiencies calculated from the models do not agree well with the plant data.

[2] The liquid flow pattern depends on hole diameter. The extent of liquid channelling and recirculation was most severe for the sieve plate with 4.5 mm holes than for the larger 12.5 mm holes tray.

[3] The water cooling technique is an effective technique for determining the effect of the liquid flow pattern on tray efficiency and the effect of tray design modification on liquid flow pattern. It is suitable for large diameter tray columns. Their information may then be used to develop improved theoretical models of tray efficiency.

[4] The video and still photographic recordings of dye tracer movement over the tray showed the same flow patterns as the temperature profiles. The video and the still photographic recording technique were powerful ways of demonstrating the nature of the froth dispersion.

[5] The presence on the tray of liquid channelling (i.e liquid cross flow between downcomers and the slowly moving or recirculating liquid at the sides) is often accompanied by compremental variations in the liquid holdup (i.e. liquid holdup at the sides of the tray is significantly higher than that in the centre. There was a higher clear liquid hold-up at the low temperature areas on the tray while the high temperature areas have less liquid hold-up, demonstrating that the height of the clear liquid seal followed the same trend as the temperature profiles.

[6] The temperature profiles for the 12.5 mm diameter holes had recirculation zones which were situated towards the outlet weir and very flat, transverse profiles from the region of the inlet weir to the central region of the tray and moderate U-shaped profiles between the central region and the outlet weir.

[7] The temperature profiles for the 4.5 mm diameter holes tray had very significant recirculation zones at the circular edge of the tray emanating from the inlet weir to the outlet down-comer, while the remaining central region of the tray contained very severe U-shaped profiles.

[8] For the 1mm hole tray with a calming zone channelling was also observed for all the flow rates tested and the recirculation zones were less than that observed for the 4.5 mm hole tray. This might be the effect of the calming zone.

[9] While operating in the emulsified flow regime the temperature profiles were confused with recirculation zones and severe U-shaped profiles scattered on the tray suggesting the tray might be operating under different localised flow regimes.

[10] For all the capacity factors the computed point efficiencies increased with increasing weir load for the spray and the mixed flow regimes, with the maximum efficiency values in the mixed regime .

[11] The expected trend of increase in efficiency values with increasing weir load was not observed for the emulsified flow regime condition due to jetting of the liquid from the fixed inlet weir gap.

[12] The calculated tray efficiencies increased in value when there was a reduction in the U-shaped profiles and the size of the recirculation regions at the circular edge of the tray.

[13] A uniform flow of liquid across the exit weir in the intense spray condition was observed in the form of liquid droplets and of uniform flow across the weir.

[14] Liquid flow across the outlet weir in the mixed and emulsified flow regimes had more liquid channelling through the central section of the weir with less liquid flow over both ends of the weir.

[15] The tray efficiencies calculated for integrated temperature variation along the weir length was of maximum value of 96 % while those computed with the outlet temperature assumed uniform across the weir of value well over 100 %.

[16] The eddy diffusion coefficients (D_e) values for all the examined weir heights generally increased with increase in the capacity factor and generally decreased with increasing weir loads.

[17] The calculated eddy diffusion coefficient (D_e) values are higher for the small hole trays than the large diameter hole trays.

[18] The extent of back mixing by eddy diffusion mechanism is limited by the underlying momentum of the liquid flowing across the outlet weir and this is dependent on the weir load.

Chapter 13

RECOMMENDATIONS FOR FUTURE WORK

[1] To develop a theory of fundamental two phase flow which explains observations described above in the conclusion.

[2] To use this as a basis for improved models of tray efficiency.

[3] To use this as a mean of avoiding those tray designs in danger of failing in practice.

[4] To experiment further on larger diameter tray and investigate if the 4.5 mm diameter hole tray will still give significant channelling.

[5] To explain the changes in back mixing with hole size and the flow regime effects.

[6] To try and develop trays which will reduce non-uniformity or the recirculation zones and can be more predictable and efficient.

NOMENCLATURE

Symbols defined and used locally are not included here.

a =	Interfacial mass transfer area (m^2/m^3)
A =	Bubbling area of tray (m^2)
A_f=	Fractional free area (m^2)
b =	Weir length (m)
C_{air}=	Specific heat of air (kJ/kg K)
C_W=	Specific heat of water (kJ/kg K)
C_p=	Specific heat of moist air (kJ/(kgdry air)K)
C_{sb}=	Capacity factor $C_F = U_{sb}/[\rho_V/(\rho_L - \rho_V)]^{0.5}$
D_e=	Eddy diffusivity (m^2/s)
d_n=	Hole diameter (m)
d_p=	Diameter of liquid particles formed (m)
E_{mV}=	Murphree tray efficiency, (vapour phase).
E_{og}=	Point efficiency (vapour phase)
E_o=	Overall column efficiency
F =	F - factor
G =	Vapour rate (kmol/s) or ($m^3/s/m^2$)
h_f =	Height of froth (mm)
h_L=	Clear liquid hold-up (cm)
H =	Enthalpy of vapour (kJ/kg)
H^*=	Saturation enthalpy of vapour (kJ/kg)
H_{fg}=	Latent heat of vaporisation (kJ/kg)
H_{air}=	Humidity of unsaturated air (kg moisture/kg dry air)
H^*=	Humidity of saturated air (kg moisture/kg dry air)
k_y=	Film mass transfer coefficient in vapour phase (kmol/s/m)
Kg=	Overall mass transfer coefficient air kmol/m^2 s bar
Kg'=	Overall mass transfer coefficient based on humidity difference as the driving force, kg/m2s (kgw.v/kg air)
L =	Liquid rate (kmol/s) or (m^3/s m)

m =	In mass transfer =slope of the equilibrium Line in heat transfer = slope of saturation enthalpy line
N =	Mass transfer rate of the more volatile component (kmol/s m^2)
P_e=	Peclet number
Q =	Heat transfer rate (kJ/s m^2)
q =	Volumetric liquid flowrate (m^3/s m)
q/b=	Weir load (m^3/s m)
T =	Temperature (^oC)
T_R=	Reduced temperature
t_{wall} =	Wall thickness (mm)
t =	Time (s)
U_g or V=	vapour flowrate (m^3/s) or velocity (m/s)
w =	Width of channelling section (m)
x or X=	Liquid phase concentration (mole fraction)
x^* or X^*=	Liquid concentration in equilibrium with vapour (mole fraction)
y or Y=	Vapour phase concentration (mole fraction)
y_i or Yi=	Vapour phase concentration leaving plate i (mole fraction)
y^* or Y^*=	Vapour phase concentration in equilibrium with liquid (mole fraction)
z or Z=	Distance between downcomers (m)
λ =	Slope of equilibrium line/slope of operating line (mG/L)
ρ_F=	Froth density (m^3 of liquid/m^3 of froth)
ρ_L=	Liquid density (kg/m^3)

Subscripts

in =	Inlet
f =	Final or Froth
R or r =	Reduced
re =	repeated
o or out =	Outlet
G =	Gas or Vapour
L =	Liquid
OG =	Overall Gas
pl =	Porter and Lockett model
p =	Plug flow model
W=	Water

w =	Nonuniform flow across the outlet weir considered
nw=	Assumed uniform liquid flow over the outlet weir

REFERENCES

[1] AIChE "Bubble Tray Design Manual : Prediction of Fractionation Efficiency" 1958 (New York : American Institution of Chemical engineers)

[2] Akebe,W. T. University of Aston in Birmingham (MSc Thesis) 1984 .

[3] Ani , C.C. University of Aston in Birmingham (M.Sc Thesis) 1984.

[4] Ani,C.C. 18th Annual Chem . Engng . Dept . Symp., 1987.

[5] Ani,C.C , and Davies,B. IChE Annual Research Meeting Uni. Nottingham 1987.

[6] Barber,A.D., and Wijn,E.F. Instn.Chem.Engrs Symp.Ser.,

[7] Barker,P.E., and Self,M.F . Chem.Engng.Sci.,1962,17,541

[8] Bell ,R.L. AIChE Journal, 1972,18,No.3,491.

[9] Bell ,R.L. AIChE Journal, 1972,18,No.3,498

[10] Bell ,R.L. , and Solari,R.B. AIChE Journal, 1974,20,688.

[11] Biddulph,M.W., and Stephens ,D.J. AIChE Journal ,1974, 20. No.1, 60.

[12] Biddulph,M.W. AIChE Journal ,1975,21,41.

[13] Brambilla,A., Gianolio,E., and Nencetti,G.F.,Inst.Chem. Eng. Symp. Series, No 56, 1979,3.2/1 - 3.2/20.

[14] Burgess,R.G., and Robinson,K.Instn.Chem.Engrs.Symp Ser., 1969,32,2:34.

[15] Danckwerts, P. V. Chem. Engng. Sci 1953 ,2 No . 1,1.

[16] Danckwerts, P. V. Gas-Liquid Reactions . 1970 (ed)

[17] Diener,D.A Ind.& Eng. Chem.,Process Des .& Dev.,1967 ,6 , 499.

[18] Enjugu,B.A. Ph.D Thesis,1986,Uni. of Aston in Birmingham.

[19] Fair ,J.R. Petro/Chem Engr.,1961 ,33 ,Part 10, Sept, 45.

[20] Fair ,J.R. , and Smith,B.D ., Design of Equilibrium Stage, Proceses, 1963,pp.551 ,McGraw Hill , New York.

[21] Fair,J.R. , and Bolles,W.L. Chem Engng. 1968 ,75, April , 167.

[22] Fane,A.G., Sawistowski,H. , Instn.Chem. Engr . Symp.Ser. , 1969,1969,32,1:8.

[23] Fenske, M.R. Ind .Eng . Chem .1932 ,24 , 482.

[24] Foss ,A.S., Gerster,J.A., and Pigford,R.L. AIChE Journal, 1958, 4, 231.

[25] Foss ,A.S., and Gerster,J.A. Chem.Eng.Prog. 1956,vol 52,No 1,28.

[26] Gautreaux,M.F., and O`Connell,H.E. Chem . Eng. Progr., 1955, 51, 232.

[27] Gerald,C.F Applied Numerical Analysis ,1978,2nd Ed.,

[28] Gerster,J.A., Hill,A.B., Hochgraf,N.N, and Robinson,N.G."Tray Efficiencies in Distillation Column" Final Report From University Of Delware, 1958. (New York : American Institions of Chemical Engineers.

[29] Heap,B.R. and Pink,M.G., Three Contouring Algor Mathematics Report No 81, 1969.

[30] Hofhuis,P.A.M., and Zuiderweg,F.J. Instn.Chem .Engrs Symp. 1979,56,2.2/1.

[31] Johnson,A.I., and Marangozis,.J. Can. J . Chem . Engrs., 1958, 36, 161.

[32] Kafarov, V.V,Shestopalov,V.V., Komissarov,Y.A. Instn.Chem.Engrs. Symp. Ser. 1979, 562.3/79

[33] Kastanek,F., and Standart,G. Separation Science, 1967,2,439.

[34] Kirschbaum,E. Destillier und Rektifier Technik,4^{e} Auflage Springer, Verlag, Berlin, 1969.

[35] Kirschbaum,E. Distillation and Rectification 1948,p.276, Chemical Publishing co ., New York.

[36] Kirschbaum,E., and Forsch. Gebiete.Ingenieurer , 1934 ,5 , 245.

[37] Kler,S., Lavin,J.T., Ani,C.C. and Davies,B. IChemE. Symp. Series, 1987, No 104,B471 - B477.

[38] Kouri, R.J., and Sohlo,J. 1981,Paper 44e, AIChE 90th National Meeting, Houston.

[39] Kouri, R.J., and Sohlo,J. 1982, " The Effect of Developing Liquid Patterns on Distillation Plate Efficiency," Paper Presented at EFCE Working Party on Distillation, Absorption & Extraction , Helsinki.

[40] Kouri, R.J., and Sohlo,J. "The Effect of Developing Liquid Flow Patterns on Distillation Plate Efficiency" .1983.

[41] Lewis,W.J. Jr. Ind. Eng. Chem.,1936,28,399.

[42] Lewis,W.J. Jr. Trans ASME 1922,44,325.

[43] Lim, C.T., Ph.D Thesis , 1973, University of Manchester Institute of Technology.

[44] Lim, C.T.,Porter, K. E ., and Lockett,M.J Trans.Instn .Chem . Engrs., 1974,52,193.

[45] Lockett, M. Trans . Instn.Chem .Engrs., 1981,59,26.

[46] Lockett,M., Porter,K.E., and Bassoon,K. Trans. Instn. Chem. Engrs. 1975, 53, 125.

[47] Lockett,M., Spiller,G.T., Porter,K.E.,Trans. Instn . Chem .Engrs. 1976,54 ,202.

[48] Microlink Users Manual, 1983, Biodata Limited England.

[49] Muller ,R.L., and Prince,R.G.H. Chem . Eng. Sci. ,1972 , 27 , 1583.

[50] Murphree,E.V.J. Ind. Eng. Chem., 1925 ,17, 747.

[51] Numerical Algorithm Group Ltd ,Oxford, U.K, NagF Lib: 1476/o: MK10, Curve & Surface Fitting.

[52] Perry,R.H., and Green,D. Perry Chemical engineering Hand Book, 1984 , 6th ed.

[53] Pinckzewski, W.V., Fell,C.J.D. Trans . Instn . Chem Engrs., 1972, 50, 102.

[54] Pinckzewski, W.V., Fell,C.J.D. Trans . Instn . Chem Engrs., 1977, 55, 46.

[55] Porter,K.E., Davies,B., Enjugu,B.A. and Ani,C.C., IChemE. Symp. Series. 1987, No 104, A569 - A588.

[56] Porter,K.E., Lockett,M.J., and Lim,C.T. Trans. Instn. Chem.Engrs. 1973,50,91.

[57] Porter,K.E., and Jenkins,J.D. Instn . Chem. Engr. Symp. Ser., 1979, 56, 75.

[58] Porter,K.E., Safekourdi,A., and Lockett,M.J. Trans Instn .Chem. Engrs. 1977, 55, 190.

[59] Porter,K.E., and Wong,P.F.Y. Instn . Chem . Engrs. Symp. Ser., 1977, 32, 2:22.

[60] Raper,J.A. Ph.D Thesis, 1979, University of New South Walses.

[61] Raper,J.A., Hai,N.T., Pinczewski, W.V., and Fell,C.J.D. Chem. Engng. Sci., 1984, 62, 111.

[62] Raper,J.A., Kearney,M.S., Burgess,J.M., and Fell,C.J.D. Chem. Engng. Sci., 1982, 37, No.4., 501.

[63] Raper,J.A., Pinczewski,W.V., and Fell,C.J.D. Chem. Eng. Res. Des., 1984, 62,111.

[64] Sakata,M., and Yanagi,T. Instn. Chem. Engrs. Symp. Ser., 1979, 56, 3.2/21.

[65] Sakata,M., and Yanagi,T. Data Presented at The Instn.Chem. Engrs. Symp.Ser., 1979,56.

[66] Shore,D. and Haselden,G.G. IChemE. Symp. Ser., 1969.No 32, 2:54

[67] Sohlo,J., and Kinnunen,S. Trans.Instn.Chem . Engrs., 1977,55,71.

[68] Sohlo,J., and Kouri,R.J. 71st AIChE Annual Meeting , Miami,1978, No 73b.

[69] Sohlo,J., and Kouri,R.J. Chem.Engng.Sci. 1982 ,37 ,193

[70] Solari,R.B., and Bell,R.L. "The Effects of Transverse Eddy Dispersion on Distillation Efficiency", March 1978, ,Paper No 46f Presented

to The Annual Meeting AIChE Atlanta.

[71] Solari,R.B., and Bell,R.L. " Liquid Flow Patterns and Velocity distribution on Commercial Scale Sieve Trays. 1982.

[72] Taylor,J.R. An Introduction to Error Analysis, 1982, pp 40-74, University Science books: Mill Valley ,CA,USA.

[73] The Properties of gases and liquid, by Robert,C.Reid, John, M.Prraushitz, and Sherwood,T.K.

[74] The TPRC DATA Series : Thermodynamics of Matter,1970,vol 2, P 960, IFI/ Plenum Data Corporation ,New York.

[75] Topping J.R Errors of Observation and their treatment, 1955 ed ,Union Brothers limited : London.

[76] Weiler,D.W., Deeinicki,W.V., England , and B.L. Chem.Engng.Progr. 1971, 69, 67.

[77] Wilkinson,J.H., and REeinsch,C., Hand book for Automatic Computation II, Linear Algebra , Berlin Springer-Verlag.

[78] Zuiderweg,F.J , Chem.Engng.Sci. 1982, 37, No.10, 1441.

[79] Zuiderweg,F.J., and Groot,J.H. de , Meeboer,B.,Meer ,D.Van der, Instn.Chem.Engr.Symp.Ser.,1969,31(5),78.

[80] Zuiderweg,F.J., and Harmens, A Chem .Engng.Sci.,158,9,89.

[81] Zuiderweg,F.J., Hofhuis,P.A.M., and Kuzniar,J. Anaheim Meeting, AIChE.

[82] Stichlmair, J., and Weisshuhun, E., Chem. Ing. Tech., No. 5, pp 242 - 247, (1973)

[83] Stichlmair, J., and Ulbrich, s. I.Chem.E symposium series, No. 104, A555. 1987.

[84] Biddulph, M.W., and Ashton, N., Chem.E. journal, No 14, (1977), pp 7 - 15.

APPENDICES

Appendix 1

ESTIMATE OF PHYSICO-CHEMICAL PROPERTIES OF THE COMPONENTS USED IN EFFICIENCY STUDIES

COMPONENTS

(1) Cyclo-Hexane

A = 15.7527 B = 2766.63 C = -50.50

H_V = 7160 (Heat of vaporization at boiling point)

(2) Normal - Heptane

A = 15.8737 B = 2911.32 C = -15.57

H_V = 7576

(3) n-Butane

A = 15.6782 B = 2154.9 C = -34.42

H_V = 5352

(4) Iso-Butane

A = 15.538 B = 2032.73 C = 33.15

H_V = 5090

ESTIMATE FOR ANTOINE CONSTANTS

The Antoine constants for the above components are given in the following literature:

(1) The properties of gases and liquid, Robert C. Reid,

John M. Praushitz and Thomas K. Sherwood

(2) Physical properties of chemical compounds I, II and III

The estimate method for compounds not included in the literature are given below

(b)(1) ESTIMATE OF THE HEAT OF VAPORIZATION

The Chen equation (36) is recommended,

The values in the literature have been calculated at normal boiling points. Hence for the present analysis the ΔH_v values at standard Temp 100 ^oC have to be calculated.

$$H_v = T(7.90T_r - 7.82 - 7.11\log P_{vr})/1.07 - T_r$$

Where $T_{bv} = T_b/T_c$ $T_r = T/R$

T_c = critical temperature K

T_b = normal boiling point Temp K

T = standard normal temperature $100^oC = 373.15K$

R = 1.987 cal / g mole K

(B2) At normal boiling point

$$H_{vb} = RT_cT_{br}[3.978Tbr - 3.938 + 1.555LnP_c/1.07 - T_{br}]$$

(B3) from the law of corressponding states the correlation by PITZER et al (36)

$$H_v/T = S_v \quad W \quad S_v$$

multiplying by T_r/R gives

$$H_v/RT_c = 7.08(1-T_r)^{0.354} + 10.95w(1-T_r)^{0.456}$$

where $W = 3/7(\theta / 1-\theta) \log P_c - 1$

$\theta = T_b/T_c$ (given in the literature)

$P_c =$ (critical pressure given in the literature)

$T_r = T/T_c$

T = working Temp or standard temp 100 ^oC = 373.15K

FOR CYCLOHEXANE

$T_b = 353.9$ $T_c = 553,4$, $P_c = 40.2$, $W = 0.213$

$T_r = 373.15/553.4 = 0.674286$

$(1-T_r)^{0.354} = 0.6722704$

$(1-T_r)^{0.456} = 0.5995885$

$\theta = T_b/T_c = 353.9/553.4 = 0.6395013$

$W = 3/7(\theta/1-\theta)(\log 40.2)-1 = 0.2196$

$H_V = R\, T_c\, [7.08(1-T_r)^{0.354} + 10.95W(1-T_r)^{0.456}]$

1.987 553.4[(7.08 0.6722704) + (10.95 0.2196 0.5995885)]
= 6819.158

FOR NORMAL HEPTANE

T_b = 371.6, T_c = 540.2, P_c = 27, W = 0.351

T_r = 373.15/540.2 = 0.69076

$(1-T_r)^{0.354}$ = 0.66003

$(1-T_r)^{0.456}$ = 0.58556

$\theta = T_b/T_c$ = 371.6/540.2 = 0.6878934

W = 3/7(θ/1-θ)(log 27) - = 0.3520

H_v = 1.987 540.2[7.08 0.66003 + 10.95 0.352 0.58556]
= 7438.42

N-BUTANE

T_b = 272.2, T_c = 425.2, P_c = 37.5, W = 0.193

$T_r = T/T_c$ = 373.15/425.2 = 0.877587

$(1-T_r)^{0.354}$ = 0.4754348

$(1-T_r)^{0.456}$ = 0.3837508

H_v = 1.987 425.2[7.08 0.475438 + 10.95 0.193 0.3837508]
= 3529.1172

ISO BUTANE

T_b = 261.3, T_c = 408.1, P_c = 36, W 0.176

$T_r = T/T_c$ = 373.15/408.1 = 0.9143592

$(1-T_r)^{0.354}$ = 0.4189565

$(1-T_r)^{0.456}$ = 0.3260636

H_v = 1.987 408.1[7.08 0.4189565 + 10.95 0.176 0.3260636]

= 2914.8436

N-HEPTANE

T_b = 371.6, T_c = 540.2, P_c = 27, W = 0.351

T_r = 373.15/540.2 = 0.6907627

0.354 $(1-T_r)0.354$ = 0.6600295

0.456 $(1-T_r)0.456$ = 0.5855623

ΔH = 1.987 540.2[7.08 0.66002957 + 10.95 0.351 0.5855623]

= 7431.6232

ESTIMATE OF HEAT CAPACITY (C_p)

for vapour C_p or C_v

$$C_{pv} = A + BT + CT^2 + DT^3$$

where A,B,C, and D are constants given in the literature

CYCLOHEXANE

$$C_p = -13.027 + 0.1460\ 373.15 + (-6.027\ 10^{-6}\ 373.15^2) + (3.156\ 10^{-9}\ 373.15^3)$$

= 40.778 cal/mol K

N-HEPTANE

$$C_p = -1.229 + 0.1615\ 373.15 + (-8.720\ 10^{-5}\ 373.15^2) + (1.829\ 10^{-8}\ 373.15^3)$$

= 47.843 cal/mol K

N-BUTANE

$$Cp = 2.266 + 7.913\ 10^{-2}\ 373.15 + (2.647\ 10^{-5}\ 373.15^2) + (-0.674\ 10^{-9}\ 373.15^3)$$
$$= 28.0726 \text{ cal/mol K}$$

ISO-BUTANE

$$Cp = -0.332 + 9.18\ 10^{-2}\ 373.15\ (-4.409\ 10^{-5}\ 373.15^2) + (6.915\ 10^{-9}\ 373.15^3)$$
$$= 28.177 \text{ cal/mol K}$$

HEAT CAPACITY for liquid (Cp)

Using Missenard method (Thermodynamic properties Robert C. Reid)

CYCLOHEXANE

C6H12 = 6 CH2

C_{pl} = 7.4 x 6 = 44.4 cal/ mol K

N-BUTANE

C_4H_{10} CH_3-CH_2-CH_2-CH_3

2 CH_3 = 2 x 11.55 = 23.1

2*CH_2 = 2 x 7.4 = 14.8

C_{Pl} = 37.9 cal/mol K

ISO-BUTANE

CH_3 -CH_3-CH-CH_3

3 CH_3 = 3 x 11.55 = 34.65

1 CH = 1 x 6.7 = 6.7

C_{pl} = 41.35 cal/g mol K

N-HEPTANE

CH_3- CH_3 - CH_3-CH -CH -CH_2-CH_3

4 CH_3 = 4 x 11.55 = 46.2

2 CH = 2 x 6.7 = 13.4

1 CH_2 = 1 x 7.4 = 7.4

Cp_l = 67.0 cal/g mol K

Gas Or Vapour

K_3 to K_4 $K_3=H_o$ $K_1 = C_v$

$H_o = H_v - C_{pv} T_o$

where the value of To is the operating temperature or standard temp (as in this case 373.15K) or 100 ^oC

Cyclohexane

H_o = 681.158 - 40.778*100 = 2741.358

$= H_v - C_v T_o$

N-BUTANE

H_o = 3529.12-2807.26 = 721.86

ISO-BUTANE

H_o = 2914.843 - 2817.7 = 97.14

N-HEPTANE = 7431.62 - 4784.3 = 2647.32

LIQUID K_1 to K_3 $K_1 = h_o$ $K_2 = Cp_l$

$ho = -Cp_l T_o$

cyclohexane = 44.4 x 100 = 4440

n-Butane = -3790
Iso-Butane = -4135
n-Heptane = -6700

Appendix 2

AIR CALIBRATION(Transverse air measurement at the top of the column) Inclined manometer setting $h_m = 0.01$

Table (5.2) Grid points Air flow rate measurement on top of the column

1	3	3	4	5	6	7	8	9	10	11	12
0.01	0.01	0.01	0.01	0.01	0.01	0.011	0.012	0.01	0.01	0.01	0.01
0.01	0.011	0.01	0.01	0.011	0.011	0.012	0.012	0.011	0.01	0.01	0.01
0.009	0.01	0.011	0.01	0.011	0.011	0.012	0.012	0.012	0.012	0.009	.008
0.009	0.009	0.011	0.012	0.012	0.013	0.012	0.012	0.011	0.01	0.008	.008
0.009	0.01	0.011	0.01	0.011	0.012	0.011	0.011	0.011	0.011	0.01	.009

Total h = 0.63

Average h value = 0.63/60 = 0.0105

The average transverse value was used to calculate the dry tray air flow rates and the calculated values were plotted against the the inclined manometer readings.

Table (5.3)

Plotted values of h_m and the calculated superficial air velocity based on the tray active area.

h_m	superficial air velocity U_s	Capacity factor C_{sb}
0.025	0.7	0.02
0.05	1.0	0.0325
0.1	1.4	0.048
0.15	1.7	0.0605
0.2	1.96	0.0695
0.25	2.2	0.0775
0.3	2.4	0.0851
0.35	2.6	0.0925

Appendix 3

Average Point Temperature Measurements on 1 mm diameter holes Rectangular tray

Point Measured Temperatures on the 1 mm diameter holes Rectangular Tray
Capacity Factor (C_{sb}=0.0605 m/s)

The first number of the presented data represents the measured system properties as shown below

Number of Runs for each capacity factor (C_{sb}) = 9

The first row represents the following:-

Lowest point temperature on the tray = 33.43 ^oC

Relative Humidity of the inlet Air = 0.009

Dry bulb temperature of the inlet Air = 34.44 ^oC

Inlet Water Temperature Measured at the down-comer = 45.58 ^oC

Mean outlet Water temperature Measured along the exit Weir = 34.34 ^oC

Liquid flowrate (in gal/min) or (cm^3/s cm) = 10.0

Air superficial flow rate (in m/s) = 1.7

The six columns after the " outlet weir" represent the point measured temperatures on the trays starting from the outlet weir to the inlet downcomer in rows of five.

9

33.43	0.009	34.44	45.58	34.34	10.0	1.70
			outlet weir			
	33.44	34.55	35.18	35.20	34.50	33.43
	35.13	36.61	37.16	37.19	36.74	35.15
	39.48	39.67	39.74	39.72	39.67	39.45
	43.54	43.65	43.75	43.38	43.38	43.26
	45.58	45.58	45.58	45.58	45.58	45.58
			inlet down-comer			
40.63	0.0390	35.39	47.48	41.13	20.0	1.70
	40.63	40.99	42.00	42.09	40.96	40.66
	40.85	42.05	42.74	42.72	42.01	40.98
	43.66	44.07	44.20	43.27	43.21	43.91
	46.53	46.15	46.33	45.18	45.91	45.85
	47.48	47.48	47.48	47.48	47.48	47.48
43.06	0.049	34.94	48.42	43.42	30.0	1.70
	43.06	43.33	43.53	43.28	43.34	43.06
	44.10	44.02	44.96	44.37	44.09	44.01
	45.43	45.53	45.76	45.69	45.51	45.57
	47.09	47.22	47.38	47.15	47.35	47.08
	48.42	48.42	48.42	48.42	48.42	48.42
43.00	0.049	34.27	47.52	44.14	40.0	1.70
	43.00	43.24	43.52	43.49	43.33	43.06
	44.44	44.50	45.18	45.21	44.38	44.49
	45.03	45.16	45.55	45.53	45.14	45.06
	46.34	46.56	46.70	46.88	46.45	46.37
	47.52	47.52	47.52	47.52	47.52	47.52
44.32	0.0489	34.17	47.41	44.71	50.0	1.70
	44.30	44.41	45.01	45.13	44.33	44.32
	44.49	44.43	45.34	45.33	44.48	44.41
	45.40	45.30	45.51	45.46	45.23	45.98
	46.51	46.57	46.79	46.73	46.58	46.48
	47.41	47.41	47.41	47.41	47.41	47.41
44.00	0.049	33.07	45.99	43.85	60.0	1.70
	44.01	44.02	44.04	44.06	44.01	44.00
	44.07	44.19	44.46	44.35	44.16	44.08
	44.48	44.79	44.86	44.87	44.85	44.52
	45.31	45.52	45.91	45.96	45.47	45.32
	45.99	45.99	45.99	45.99	45.99	45.99
43.30	0.0487	31.13	45.50	43.69	70.0	1.70
	43.34	43.48	43.95	43.89	43.41	43.30
	44.56	44.59	44.95	44.94	44.56	44.53
	44.59	44.62	44.98	44.97	44.66	44.56
	45.22	45.20	45.19	45.24	45.18	45.24
	45.50	45.50	45.50	45.50	45.50	45.50
43.37	0.0492	25.83	45.38	43.75	80.0	1.70

	43.37	43.52	44.05	43.93	43.62	43.40
	44.61	44.84	44.97	44.78	44.80	44.66
	44.72	44.92	44.90	44.98	44.91	44.76
	45.11	45.19	45.09	45.15	45.16	45.16
	45.38	45.38	45.38	45.38	45.38	45.38
43.16	0.049	23.95	45.23	43.80	90.0	1.70
	44.02	43.61	44.00	43.93	43.14	43.12
	43.79	43.82	44.02	44.01	43.38	43.16
	43.89	43.88	43.80	43.91	43.56	43.85
	44.97	44.85	44.96	44.90	45.04	44.97
	45.23	45.23	45.23	45.23	45.23	45.23

Appendix 3.1 Calculated Point and Tray Efficiencies for the Rectangular Tray.

Table (6.2) Capacity factor of 0.0605 m/s

Weir Load $m^3/s\ m$	E_{og}	E_{mv}	E_{mv}/E_{og}
0.001233	19.8	33.1	1.68
0.002486	37.3	66.4	1.78
0.003729	51.5	87.4	1.7
0.004972	46.5	64.0	1.38
0.006215	44.6	55.7	1.25
0.007458	51.6	63.0	1.22
0.0087	51.0	60.0	1.17
0.00994	47.9	54.11	1.13
0.01118	45.3	49.9	1.1

Table(6.3) Capacity factor of 0.0695 m/s

Weir Load $m^3/s\ m$	E_{og}	E_{mv}	E_{mv}/E_{og}
0.001233	29.2	54.6	1.87
0.002486	38.9	61.9	1.59
0.003729	51.8	83.5	1.6
0.004972	55.5	78.1	1.4
0.006215	52.5	64.9	1.2
0.007458	54.5	64.0	1.17
0.0087	50.9	57.2	1.12
0.00994	58.4	64.2	1.09
0.01118	62.5	67.4	1.07
0.01243	54.4	57.2	1.05
0.01367	45.6	47.5	1.04
0.0149	28.5	26.1	1.0

Table (6.4) Capacity foctor of 0.0851 m/s

Weir Load $m^3/s\ m$	E_{og}	E_{mv}	E_{mv}/E_{og}
0.001233	27.6	64.9	2.34
0.002486	38.8	72.8	1.88
0.003729	51.9	88.0	1.69
0.004972	53.8	79.4	1.48
0.006215	50.9	63.7	1.25

0.007458	53.4	63.1	1.18
0.0087	55.5	64.0	1.15
0.00994	50.2	53.6	1.06
0.01118	50.8	53.3	1.04
0.01243	46.3	48.5	1.05
0.01367	43.5	44.3	1.02
0.0149	43.5	43.6	1.0

Appendix 4

AVERAGE POINT TEMPERATURE MEASUREMENTS ON THE 1mm DIAMETER HOLES TRAY

C_{sb} = 0.0605 m/s

15

26.38	0.005	33.28	41.88	27.79	10.0	1.70
	26.38	27.39	29.13	29.33	28.03	26.46
	27.65	30.06	31.67	31.65	29.38	27.10
	28.15	32.15	34.46	34.50	33.74	29.22
	37.81	39.18	40.22	39.54	39.51	38.90
	41.88	41.88	41.88	41.88	41.88	41.88
30.77	0.005	34.00	45.33	32.63	20.0	1.70
	30.77	32.31	34.36	34.60	32.81	30.93
	32.57	35.55	37.25	36.88	33.87	31.31
	33.75	36.98	39.15	38.60	38.04	33.76
	43.25	43.25	44.02	42.84	43.02	42.74
	45.33	45.33	45.33	45.33	45.33	45.33
33.08	0.005	34.02	43.99	34.91	30.0	1.70
	33.08	34.63	36.44	36.82	35.25	33.21
	34.69	37.39	38.58	37.76	35.43	32.92
	35.88	37.65	39.60	38.88	38.37	35.86
	42.73	42.71	43.01	41.88	42.09	42.08
	43.99	43.99	43.99	43.99	43.99	43.99
33.92	0.0048	33.83	43.00	35.95	40.0	1.70
	33.92	35.77	37.32	37.57	36.61	34.52
	35.62	38.14	39.22	38.73	36.19	34.21
	36.79	37.97	39.49	39.02	38.61	37.13
	42.06	41.88	42.15	40.91	41.47	41.26
	43.00	43.00	43.00	43.00	43.00	43.00
34.69	0.0048	33.43	42.67	36.63	50.0	1.70
	34.69	36.47	37.76	38.14	37.24	35.49
	36.23	38.69	39.11	38.62	36.74	35.33
	37.64	38.66	40.00	39.41	38.77	38.00
	41.86	41.66	41.86	40.68	41.26	41.26
	42.67	42.67	42.67	42.67	42.67	42.67
35.39	0.005	33.47	42.48	36.95	60.0	1.70
	35.39	36.67	37.93	38.30	37.45	35.95

	36.70	38.75	39.39	38.42	37.12	35.95
	38.29	38.77	39.87	39.74	39.07	38.51
	41.80	41.51	41.77	40.72	41.12	41.08
	42.48	42.48	42.48	42.48	42.48	42.48
36.01	0.0048	33.39	42.26	37.37	70.0	1.70
	36.01	37.14	38.01	38.39	37.86	36.78
	37.28	38.86	39.09	38.73	37.53	36.73
	38.74	38.84	40.20	39.41	39.18	38.62
	41.66	41.30	41.50	40.63	41.08	40.85
	42.26	42.26	42.26	42.26	42.26	42.26
36.08	0.0048	33.29	41.39	37.27	80.0	1.70
	36.08	37.18	37.68	38.32	37.69	36.69
	37.36	38.77	38.70	38.44	37.17	36.53
	38.26	38.16	39.30	39.15	38.68	38.24
	40.83	40.51	40.70	39.98	40.32	40.25
	41.39	41.39	41.39	41.39	41.39	41.39
35.96	0.0048	32.31	40.89	36.95	90.0	1.70
	35.96	36.80	37.23	37.74	37.43	36.59
	37.27	38.15	37.82	37.49	37.21	37.03
	38.71	38.44	39.09	38.93	38.45	38.12
	40.46	40.27	40.30	39.48	40.12	39.68
	40.89	40.89	40.89	40.89	40.89	40.89
35.27	0.0045	32.18	38.63	35.98	100.0	1.70
	35.27	35.79	36.09	36.58	36.39	35.74
	36.29	36.91	36.75	36.04	35.83	35.55
	36.98	36.81	37.21	36.71	36.81	36.44
	38.33	38.17	38.25	37.56	38.06	37.73
	38.63	38.63	38.63	38.63	38.63	38.63
35.45	0.005	27.15	38.65	36.55	110.0	1.70
	35.83	36.30	36.67	37.07	37.07	36.33
	36.65	37.15	37.18	36.70	35.96	35.45
	37.24	36.86	37.45	36.72	36.86	36.67
	38.36	38.22	38.32	37.80	38.16	37.86
	38.65	38.65	38.65	38.65	38.65	38.65
36.40	0.004	28.42	39.67	37.35	120.0	1.70
	36.66	37.17	37.45	37.97	37.84	37.02
	37.59	38.12	38.06	37.72	36.72	36.40
	38.07	37.80	38.27	37.61	37.85	37.37
	39.36	39.18	39.27	38.83	39.14	38.69
	39.67	39.67	39.67	39.67	39.67	39.67
36.26	0.004	21.95	39.46	37.50	130.0	1.70
	36.84	37.27	37.61	38.04	38.07	37.16
	37.59	38.23	38.33	37.66	36.84	36.26
	37.91	37.52	38.11	37.29	37.82	37.45
	39.11	39.04	39.10	38.72	38.97	38.62
	39.46	39.46	39.46	39.46	39.46	39.46
36.24	0.007	20.12	39.42	37.81	140.0	1.70
	37.20	37.62	37.92	38.18	38.39	37.55

	37.93	38.63	38.46	37.98	37.17	36.24
	38.01	37.54	37.96	37.61	37.81	37.56
	39.17	39.06	39.06	38.80	39.04	38.65
	39.42	39.42	39.42	39.42	39.42	39.42
36.18	0.006	19.60	39.50	38.04	150.0	1.70
	37.39	37.81	38.23	38.39	38.71	37.72
	38.14	38.70	38.69	38.08	37.26	36.18
	38.21	37.50	38.21	37.56	37.98	37.71
	39.21	39.09	39.24	38.99	39.15	38.79
	39.50	39.50	39.50	39.50	39.50	39.50

C_{sb} = 0.0695 m/s

17

24.47	0.004	33.36	42.37	25.95	10.0	1.9
	24.47	25.23	26.93	27.49	26.37	25.27
	25.86	27.62	29.73	30.29	27.67	25.80
	27.10	29.52	32.62	33.34	32.47	28.29
	36.63	38.99	39.83	39.31	39.10	38.67
	42.37	42.37	42.37	42.37	42.37	42.37
28.90	0.005	34.01	42.97	30.47	20.0	1.9
	28.90	29.90	31.69	32.08	30.93	29.30
	30.65	32.48	34.06	34.12	31.93	29.83
	32.44	33.93	35.76	36.29	35.67	32.46
	40.72	41.28	41.25	40.33	40.52	40.55
	42.97	42.97	42.97	42.97	42.97	42.97
30.69	0.005	34.28	41.26	32.23	30.0	1.9
	30.69	31.71	33.35	33.80	32.74	31.10
	32.30	34.05	35.35	35.10	32.98	31.04
	34.06	34.80	36.38	36.83	33.06	33.91
	40.02	40.11	40.06	39.35	39.52	39.56
	41.26	41.26	41.26	41.26	41.26	41.26
32.24	0.006	34.55	41.49	33.85	40.0	1.9
	32.24	33.35	35.07	35.49	34.29	32.67
	34.00	35.85	36.51	36.14	34.29	32.62
	35.82	36.25	37.56	37.53	36.89	35.51
	40.53	40.57	40.38	39.56	40.01	39.97
	41.49	41.49	41.49	41.49	41.49	41.49
34.38	0.006	34.56	38.63	35.56	50.0	1.9
	34.83	35.39	35.87	36.32	35.98	34.98
	35.85	36.63	36.53	36.10	34.75	34.38
	36.62	35.95	36.41	36.33	36.04	35.96
	38.09	38.08	38.03	37.37	37.68	37.49
	38.63	38.63	38.63	38.63	38.63	38.63
35.06	0.0058	33.66	38.96	35.52	60.0	1.9
	35.85	36.39	36.55	37.17	37.00	36.15

	36.91	37.50	37.27	37.15	35.66	35.06
	37.37	36.70	37.04	36.54	36.79	36.48
	38.53	38.50	38.56	37.64	38.20	37.90
	38.96	38.96	38.96	38.96	38.96	38.96
35.38	0.006	34.30	40.75	36.47	70.0	1.9
	35.38	36.18	37.02	37.50	36.89	35.87
	36.71	37.96	37.98	37.89	36.28	35.51
	37.97	37.62	38.16	37.81	37.81	37.44
	40.08	40.06	40.04	39.20	39.66	39.42
	40.75	40.75	40.75	40.75	40.75	40.75
35.57	0.0068	34.05	40.76	36.76	80.0	1.9
	35.73	36.63	37.24	37.69	37.26	35.99
	37.13	38.21	38.01	37.57	36.36	35.57
	38.23	37.67	38.13	37.74	37.91	37.68
	40.15	40.10	40.09	39.25	39.65	39.43
	40.76	40.76	40.76	40.76	40.76	40.76
35.75	0.0065	33.85	40.54	36.86	90.0	1.9
	35.99	36.72	37.12	37.73	37.39	36.23
	37.32	38.21	37.92	37.62	36.44	35.75
	38.23	37.96	38.05	37.99	37.96	37.39
	39.95	39.95	39.87	39.00	39.52	39.37
	40.54	40.54	40.54	40.54	40.54	40.54
35.90	0.0065	33.53	40.26	36.94	100.0	1.9
	36.31	37.04	37.26	37.63	37.56	36.50
	37.37	37.97	38.18	37.69	36.36	35.87
	38.19	37.76	38.11	37.67	37.59	37.39
	39.70	39.65	39.64	38.82	39.29	39.09
	40.26	40.26	40.26	40.26	40.26	40.26
35.87	0.0065	33.48	39.96	37.15	110.0	1.9
	36.48	36.94	37.29	37.82	37.68	36.70
	37.55	38.10	37.97	37.79	36.58	35.87
	38.19	37.43	37.77	37.18	37.68	37.41
	39.48	39.44	39.45	38.56	39.13	38.88
	39.96	39.96	39.96	39.96	39.96	39.96
34.05	0.0045	30.71	37.47	35.44	120.0	1.9
	34.85	35.17	35.59	35.83	36.17	35.04
	35.54	35.90	39.06	35.59	35.04	34.05
	36.24	34.98	35.70	35.43	35.79	35.64
	37.12	37.03	37.02	36.68	36.94	36.63
	37.47	37.47	37.47	37.47	37.47	34.47
33.08	0.0045	32.64	36.32	34.78	130.0	1.9
	34.24	34.37	34.92	35.23	35.41	34.49
	34.88	35.25	35.25	35.02	34.26	33.08
	35.26	34.46	34.68	34.61	34.66	34.65
	36.07	35.95	35.85	35.64	35.91	35.49
	36.32	36.32	36.32	36.32	36.32	36.32
34.50	0.006	31.20	37.79	36.13	140.0	1.9
	35.69	35.82	36.06	36.59	36.84	35.76

	36.32	36.72	36.64	35.79	35.72	34.50
	36.72	35.63	35.73	36.12	35.82	35.95
	37.48	37.40	37.30	37.25	37.41	37.08
	37.79	37.79	37.79	37.79	37.79	37.79
34.42	0.006	26.68	37.90	36.42	150.0	1.9
	35.99	36.22	36.52	36.74	37.11	35.91
	36.50	37.04	36.90	36.61	35.78	34.42
	36.75	35.89	36.37	35.93	36.13	36.03
	37.61	37.52	37.63	37.40	37.52	37.17
	37.90	37.90	37.90	37.90	37.90	37.90
34.44	0.005	22.66	37.92	36.43	160.0	1.9
	35.90	36.27	36.55	36.71	37.19	35.94
	36.41	36.89	36.86	36.37	35.60	34.44
	36.75	35.14	36.55	36.10	35.84	35.99
	37.58	37.47	37.62	37.41	37.54	37.22
	37.92	37.92	37.92	37.92	37.92	37.92
34.45	0.005	21.19	37.78	36.39	170.0	1.9
	35.89	36.23	36.55	36.63	37.11	35.93
	36.39	36.91	36.86	36.15	35.61	34.45
	36.65	35.26	36.53	35.73	36.15	35.94
	37.45	37.37	37.52	37.31	37.43	37.19
	37.78	37.78	37.78	37.78	37.78	37.78

C_{sb} = 0.0775 m/s

17

24.90	0.008	32.57	43.21	26.05	10.0	2.18
	24.90	25.47	26.86	27.21	26.47	25.41
	26.12	27.64	29.27	30.17	28.23	26.71
	28.11	30.08	32.75	33.91	32.16	29.02
	37.80	40.40	40.78	40.33	40.31	38.96
	43.21	43.21	43.21	43.21	43.21	43.21
29.26	0.009	33.14	44.54	30.47	20.0	2.18
	29.26	29.76	31.45	31.96	30.91	29.50
	30.93	32.66	33.82	34.07	32.26	30.86
	33.94	35.12	36.33	37.37	36.34	33.15
	42.41	42.84	42.55	41.96	41.85	41.78
	44.54	44.54	44.54	44.54	44.54	44.54
31.04	0.009	33.34	42.90	32.42	30.0	2.18
	31.10	31.97	33.73	34.12	32.58	31.04
	32.49	34.61	35.49	35.46	33.56	32.04
	34.73	35.89	37.53	37.50	36.36	34.16
	41.52	41.70	41.46	40.73	41.08	40.94
	42.90	42.90	42.90	42.90	42.90	42.90
32.46	0.0085	33.50	41.92	33.76	40.0	2.18
	32.46	33.56	34.80	35.04	34.13	32.56
	33.69	35.76	36.18	35.93	34.65	33.49
	35.83	36.39	37.85	37.57	37.41	35.68
	40.81	41.01	40.73	40.02	40.46	40.39
	41.92	41.92	41.92	41.92	41.92	41.92
33.49	0.009	33.51	40.19	34.51	50.0	2.18

	33.49	34.41	35.04	35.47	35.09	33.58
	34.53	36.09	36.25	35.81	34.86	34.45
	36.74	36.57	37.25	37.05	36.98	36.31
	39.40	39.44	39.27	38.52	38.97	38.96
	40.19	40.19	40.19	40.19	40.19	40.19
34.10	0.009	33.59	39.97	35.12	60.0	2.18
	34.10	34.85	35.66	35.95	35.78	34.40
	35.26	36.46	36.04	35.87	35.25	35.25
	37.11	36.83	37.20	37.14	36.75	36.55
	39.25	39.27	39.11	38.36	38.87	38.72
	39.97	39.97	39.97	39.97	39.97	39.97
34.77	0.0085	33.65	40.02	35.72	70.0	2.18
	34.77	35.59	36.10	36.34	36.45	35.09
	35.86	36.60	36.80	36.24	35.55	35.88
	37.68	37.09	37.22	37.05	37.30	36.85
	39.38	39.35	39.26	38.54	39.01	38.95
	39.89	39.89	39.89	39.89	39.89	39.89
35.22	0.0085	33.60	39.89	36.20	80.0	2.18
	35.22	35.91	36.12	36.70	36.75	36.38
	36.30	36.68	37.19	36.40	35.76	36.15
	37.72	36.65	37.52	36.92	36.82	37.08
	39.23	39.28	39.11	38.50	39.00	38.67
	39.89	39.89	39.89	39.89	39.89	39.89
34.63	0.0085	33.56	38.24	35.21	90.0	2.18
	34.66	35.15	35.33	35.66	35.81	34.63
	35.59	36.00	36.08	35.86	34.89	35.11
	36.68	35.13	36.16	35.88	35.68	35.87
	37.72	37.73	37.61	37.04	37.45	37.26
	38.24	38.24	38.24	38.24	38.24	38.24
36.18	0.009	34.26	41.89	36.90	100.0	2.18
	36.23	36.74	37.09	37.57	37.61	36.18
	37.16	37.90	37.93	37.53	37.60	37.98
	39.72	38.66	39.09	39.31	38.86	38.77
	39.72	38.66	39.09	39.31	38.86	38.77
	41.89	41.89	41.89	41.89	41.89	41.89
34.70	0.01	35.12	38.47	35.56	110.0	2.18
	34.70	35.12	35.36	35.74	35.99	34.94
	35.43	36.12	35.71	35.25	35.65	35.72
	37.16	35.61	36.45	36.26	36.12	36.41
	38.02	38.05	37.86	37.32	37.77	37.45
	38.47	38.47	38.47	38.47	38.47	38.47
35.21	0.01	35.37	38.26	35.71	120.0	2.18
	35.21	35.47	35.80	36.18	36.37	35.24
	35.72	36.39	36.34	35.91	35.79	35.59
	37.07	35.58	35.88	36.12	36.03	36.24
	37.90	37.92	37.73	37.32	37.66	37.39
	38.26	38.26	38.26	38.26	38.26	38.26
35.78	0.01	35.46	38.55	36.33	130.0	2.18
	35.85	36.20	36.36	36.73	37.08	35.78

	36.44	37.30	36.81	36.53	36.07	36.08
	37.29	36.06	36.36	36.59	35.99	36.73
	38.22	38.21	38.06	37.71	38.00	37.67
	38.55	38.55	38.55	38.55	38.55	38.55
35.83	0.01	35.59	38.79	36.59	140.0	2.18
	36.07	36.38	36.71	36.99	37.43	35.93
	36.62	37.46	37.06	36.64	36.32	36.20
	37.51	35.83	36.20	36.77	36.53	36.86
	38.48	38.44	38.33	37.90	38.15	37.84
	38.79	38.79	38.79	38.79	38.79	38.79
33.92	0.01	35.09	37.89	36.31	150.0	2.18
	35.91	36.11	36.30	36.56	37.11	35.89
	36.35	36.94	36.69	36.09	35.84	35.85
	36.80	33.92	36.23	36.34	35.43	36.10
	37.59	37.57	37.52	37.23	37.42	37.22
	37.89	37.89	37.89	37.89	37.89	37.89
33.75	0.009	33.61	37.72	36.25	160.0	2.18
	35.82	36.17	36.22	36.53	36.92	35.84
	36.27	36.67	36.62	36.09	35.71	35.55
	36.65	33.75	35.90	36.16	35.02	35.69
	37.41	37.44	37.37	37.10	37.26	37.07
	37.72	37.72	37.72	37.72	37.72	37.72
35.52	0.01	30.26	39.14	37.46	170.0	2.18
	37.04	37.49	37.44	37.89	38.22	36.68
	37.61	38.01	37.63	36.75	37.26	36.83
	37.91	35.52	37.44	37.53	36.54	37.01
	38.86	38.84	38.76	38.44	38.71	38.46
	39.14	39.14	39.14	39.14	39.14	39.14

C_{sb} = 0.0851 m/s

17

25.67	0.008	34.84	42.94	26.46	10.0	2.4
	25.67	26.01	27.22	27.47	26.61	25.76
	26.77	28.02	29.59	29.36	26.91	26.02
	27.87	29.20	32.26	31.51	30.88	28.42
	39.05	38.96	40.80	39.73	39.28	38.47
	42.94	42.94	42.94	42.94	42.94	42.94
28.73	0.0085	35.22	41.29	29.68	20.0	2.4
	28.73	29.08	30.52	31.06	29.92	28.78
	29.86	31.40	32.50	32.37	30.25	29.22
	31.27	32.33	33.98	33.33	33.97	31.19
	39.41	39.28	39.54	38.97	38.92	38.95
	41.29	41.29	41.29	41.29	41.29	41.29
31.44	0.005	35.08	47.82	32.85	30.0	2.4
	31.55	32.35	34.12	34.42	33.23	31.44

	32.97	35.82	35.66	35.63	34.83	33.13
	36.44	37.91	39.64	38.37	38.69	35.67
	46.14	45.82	45.66	44.93	45.30	45.26
	47.82	47.82	47.82	47.82	47.82	47.82
32.28	0.0048	34.93	44.06	33.49	40.0	2.4
	32.28	33.18	34.36	34.79	33.99	32.34
	33.44	36.00	35.75	35.78	34.90	33.54
	36.79	38.56	38.30	37.18	38.91	36.57
	42.92	42.93	42.51	41.71	42.37	42.44
	44.06	44.06	44.06	44.06	44.06	44.06
32.77	0.0048	34.33	41.51	33.93	50.0	2.4
	32.77	33.82	34.85	34.82	34.50	32.81
	33.76	35.89	35.58	35.05	34.75	33.62
	37.15	37.28	37.12	36.54	37.52	36.59
	40.60	40.64	40.43	39.50	40.08	40.12
	41.51	41.51	41.51	41.51	41.51	41.51
33.17	0.0047	33.96	40.54	34.35	60.0	2.4
	33.17	34.36	34.98	35.32	34.94	33.30
	34.43	35.99	35.63	34.77	34.87	34.11
	37.51	36.19	36.61	36.27	36.71	36.47
	39.66	39.74	39.49	38.76	39.50	39.23
	40.54	40.54	40.54	40.54	40.54	40.54
33.99	0.004	32.94	40.39	34.96	70.0	2.4
	34.09	35.06	35.42	35.63	35.58	33.99
	35.12	36.05	35.78	35.56	35.23	34.83
	38.04	35.45	36.75	36.59	36.39	37.11
	39.65	39.65	38.58	39.75	39.27	39.19
	40.39	40.39	40.39	40.39	40.39	40.39
34.68	0.004	33.46	40.48	35.48	80.0	2.4
	34.89	35.34	35.79	36.02	36.18	34.68
	36.03	37.05	36.76	35.86	35.74	35.37
	38.49	35.17	36.87	37.09	36.69	37.05
	39.70	39.83	39.58	39.83	39.41	39.21
	40.48	40.48	40.48	40.48	40.48	40.48
34.88	0.004	36.18	40.04	35.57	90.0	2.4
	35.05	35.43	35.72	36.07	36.28	34.88
	35.73	37.43	36.26	35.69	35.88	35.35
	37.95	35.93	36.20	36.78	35.87	37.00
	39.26	39.41	39.20	38.46	38.02	38.79
	40.04	40.04	40.04	40.04	40.04	40.04
34.64	0.004	32.85	39.46	35.50	100.0	2.4
	34.99	35.31	35.58	35.99	36.29	34.86
	35.49	37.11	35.90	35.79	35.85	35.36
	37.69	34.64	35.30	36.60	35.28	36.84
	38.83	38.88	38.73	38.04	38.51	38.38
	39.46	39.46	39.46	39.46	39.46	39.46
34.34	0.0038	33.11	39.21	35.60	110.0	2.4
	35.10	35.52	35.74	36.13	36.54	34.55

	35.71	37.05	35.83	35.73	35.90	35.21
	37.63	34.34	35.38	36.48	35.10	36.61
	38.66	38.71	38.56	37.78	38.31	38.02
	39.21	39.21	39.21	39.21	39.21	39.21
34.39	0.0038	32.85	38.91	35.50	120.0	2.4
	34.95	35.33	35.64	36.02	36.46	34.61
	35.55	36.95	36.03	35.66	35.97	35.07
	37.39	34.39	34.88	36.32	34.94	36.24
	38.35	35.43	38.19	37.65	38.05	37.87
	38.91	38.91	38.91	38.91	38.91	38.91
34.43	0.0038	32.95	38.64	35.34	130.0	2.4
	34.97	35.50	35.45	35.01	36.69	34.43
	35.70	36.60	35.91	35.00	36.15	35.25
	37.10	34.58	34.83	36.16	34.91	36.16
	38.10	38.13	37.99	37.51	37.86	37.69
	38.64	38.64	38.64	38.64	38.64	38.64
31.70	0.0038	32.92	38.39	35.74	140.0	2.4
	35.33	35.86	35.65	36.05	36.74	34.83
	35.88	36.67	35.88	35.58	35.92	35.43
	37.06	31.70	35.12	36.03	33.29	36.13
	37.96	37.93	37.92	37.55	37.73	37.51
	38.39	38.39	38.39	38.39	38.39	38.39
31.34	0.0038	33.06	38.38	35.84	150.0	2.4
	35.44	35.95	35.80	36.09	36.77	34.96
	36.06	36.63	35.95	35.64	35.95	35.32
	37.10	31.34	34.89	35.94	33.76	35.81
	37.90	37.99	37.88	37.44	37.70	37.60
	38.38	38.38	38.38	38.38	38.38	38.38
33.16	0.0038	32.71	38.32	36.15	160.0	2.4
	35.99	36.22	35.94	36.49	36.90	35.33
	36.69	36.84	35.82	34.67	36.17	35.73
	37.13	33.16	35.65	36.31	34.00	35.77
	37.97	37.95	37.93	37.40	37.82	37.63
	38.32	38.32	38.32	38.32	38.32	38.32
32.88	0.0038	32.72	38.38	36.40	170.0	2.4
	36.33	36.49	36.36	36.79	37.04	35.39
	36.74	36.81	36.18	35.17	36.47	35.87
	37.22	32.88	36.11	36.40	33.54	35.70
	38.07	38.00	38.01	37.74	37.90	37.69
	38.38	38.38	38.38	38.38	38.38	38.38

Appendix 4.1 Tray & Point Efficiency results for 1mm diameter hole tray.

Table (7.2) Capacity factor of 0.0605 m/s

Weir Load $m^3/s\ m$	E_{og}	E_{mv}	E_{mv}/E_{og}
0.000806	39.1	76.4	1.95
0.00161	51.4	86.7	1.7
0.00241	54.2	76.6	1.4
0.00322	55.8	72.2	1.3
0.00403	58.7	72.9	1.24
0.0056	64.4	78.6	1.22
0.00644	65.7	78.0	1.18
0.00725	65.6	75.6	1.15
0.00806	71.4	82.2	1.15
0.00866	59.9	65.5	1.09
0.00967	48.7	51.7	1.06
0.0104	54.5	58.2	1.07
0.01128	46.3	48.6	1.o4
0.0209	42.7	44.3	1.04
0.02896	39.9	41.1	1.03
0.0137	53.5	55.1	1.0

Table (7.3) Capacity factor of 0.0695 m/s

Weir Load $m^3/s\ m$	E_{og}	E_{mv}	E_{mv}/E_{og}
0.000806	39.9	87.8	2.2
0.00161	51.5	89.1	1.7
0.00241	56.6	82.2	1.5
0.00322	61.1	83.9	1.4
0.00403	32.8	36.4	1.1
0.0056	41.2	48.1	1.2
0.00644	56.2	65.6	1.2
0.00725	60.6	69.9	1.2
0.00806	62.3	70.9	1.14
0.00866	62.7	70.3	1.12
0.00967	58.8	64.3	1.09
0.0104	49.5	52.4	1.06
0.01128	44.9	46.7	1.04
0.0209	47.9	49.9	1.04
0.02896	42.3	43.7	1.03
0.0137	42.0	43.2	1.02

Table (7.4) Capacity factor of 0.0775 m/s

Weir Load $m^3/s\ m$	E_{og}	E_{mv}	E_{mv}/E_{og}
0.000806	39.3	107.7	2.7
0.00161	51.9	106.3	2.05
0.00241	58.3	96.01	1.65
0.00322	59.2	85.4	1.44
0.00403	54.8	70.6	1.3
0.0056	55.7	68.4	1.23
0.00644	55.6	65.8	1.18
0.00725	54.1	61.8	1.14
0.00806	55.5	62.4	1.12

0.00866	84.6	100.9	1.19
0.00967	68.9	77.0	1.12
0.0104	65.9	72.9	1.11
0.01128	59.9	64.9	1.08
0.0209	62.9	67.7	1.07
0.02896	50.9	53.1	1.04
0.0137	48.3	49.9	1.03

Table (7.5) Capacity factor of 0.0851 m/s

Weir Load $m^3/s\ m$	E_{og}	E_{mv}	E_{mv}/E_{og}
0.000806	35.9	94.3	2.6
0.00161	47.9	87.9	1.8
0.00241	54.5	101.1	1.9
0.00322	57.5	89.0	1.5
0.00403	56.1	76.1	1.35
0.0056	56.2	71.2	1.27
0.00644	55.0	66.7	1.21
0.00725	57.1	67.9	1.19
0.00806	64.2	70.7	1.1
0.00866	58.6	66.6	1.14
0.00967	59.2	66.1	1.11
0.0104	62.1	68.4	1.1
0.01128	65.5	72.7	1.1
0.0209	57.1	60.9	1.07
0.02896	58.7	62.2	1.08
0.0137	52.6	55.1	1.04

Appendix 5

AVERAGE TEMPERATURE VALUES FOR 3/16 INCH HOLE DIAMETER TRAY

C_{sb} = 0.049 m/s

L = 20 Gal/min

inlet temp 40.99 °C

27.05	34.75	38.98	38.98	39.41	37.63
27.99	30.90	35.57	36.94	35.49	27.08
31.24	34.06	35.64	36.57	30.93	25.69
30.88	31.68	33.36	34.66	34.10	31.41

outlet weir temp 32.32 ° C

L = 30 Gal/min

inlet temp 39.56°C

32.29	38.41	39.18	38.50	38.75	38.77
29.24	33.39	36.77	37.30	36.42	29.67
32.35	35.99	36.92	37.29	34.27	28.23
32.71	34.09	35.31	36.03	35.57	32.51

outlet weir temp 36.45°C

L = 40 Gal/min

inlet temp 39.56° C

34.35	38.44	38.36	38.50	38.54	38.67
31.16	35.17	37.73	37.66	37.40	32.65
34.11	37.34	37.98	38.03	35.98	31.63
34.77	36.29	36.96	37.34	37.04	35.09

outlet weir temp 36.50 ° C

L = 60 Gal/min

inlet temp 42.36 °C

37.29	41.38	40.90	41.08	41.22	41.31
32.95	37.38	40.38	40.21	40.05	34.87
36.21	40.05	40.95	40.65	38.51	33.87
37.09	38.87	39.59	39.86	39.63	37.57

outlet weir temp 38.72 °C

L = 70 Gal/min

inlet temp 41.75 °C

38.88	40.31	38.85	39.61	39.94	39.91
33.32	37.84	39.81	39.63	39.30	36.20
37.03	40.38	41.12	40.74	38.37	34.33
37.79	39.69	40.31	40.33	40.10	38.72

outlet weir temp 38.45 ° C

L = 80 Gal/min

inlet temp 40.20 ° C

38.85	39.87	38.70	39.06	39.31	39.52
34.27	38.21	39.47	39.43	39.15	37.17
37.19	40.04	40.61	40.09	38.43	35.23
37.86	39.33	39.90	40.18	40.03	38.91

outlet weir temp 38.43 ° C

C_{sb} = 0.0605 m/s

L = 20 Gal/min

inlet temp 45.66 °C

26.18	29.95	38.51	42.08	41.98	32.15
28.50	29.81	36.70	37.52	28.54	26.15
30.76	33.13	35.62	33.63	27.91	26.37
29.70	30.64	32.36	32.80	31.86	30.26

outlet weir temp 31.98 °C

L = 30 Gal/min

inlet temp 40.95 °C

29.74	36.61	39.45	38.96	39.01	34.71
28.40	30.51	36.73	36.86	33.22	27.40
30.95	34.65	36.14	36.13	30.78	27.31
30.89	33.30	34.25	34.56	33.82	31.85

outlet weir temp 34.00 °C

L = 40 Gal/min

inlet temp 40.97 °C

32.74	39.07	40.04	39.29	39.42	39.05
29.54	33.18	37.98	38.00	36.33	29.48
32.38	36.34	38.09	38.17	34.11	28.86
33.10	35.92	36.63	36.76	36.30	33.86

outlet weir temp 36.25 °C

L = 50 Gal/min

inlet temp 39.68 °C

34.32	38.43	38.75	38.60	38.47	38.85
30.10	34.31	37.64	37.55	37.22	31.12
32.70	36.32	37.90	37.86	35.43	29.77
33.40	36.16	36.70	36.82	36.52	34.29

outlet weir temp 36.46 °C

L = 60 Gal/min

inlet temp 41.06 °C

38.92	40.40	39.20	40.01	40.28	40.20
31.90	37.43	39.55	39.44	39.48	35.88
34.65	38.70	40.47	40.37	38.65	32.58
36.21	38.98	39.50	39.63	39.39	37.29

outlet weir temp 39.00 °C

L = 70 Gal/min

inlet temp 40.99 °C

38.62	39.64	38.01	38.98	39.28	39.22
32.58	37.56	38.63	38.71	38.68	36.38
35.20	38.94	40.03	40.16	38.22	33.04
36.44	38.77	39.27	39.53	39.36	37.62

outlet weir temp 38.96 °C

L = 80 Gal/min

inlet temp 41.65 °C

39.98	40.83	38.77	40.18	40.42	40.47
34.21	38.81	39.76	39.95	39.97	38.68
36.49	40.12	41.27	41.44	39.75	34.54
37.51	39.89	40.46	40.82	40.58	38.85

outlet weir temp 39.80 °C

L = 90 Gal/min

inlet temp 41.99 °C

39.74	40.79	38.92	40.10	40.31	40.61
35.77	39.19	39.69	39.84	40.05	39.28
37.39	40.77	41.49	41.77	40.02	34.99
38.21	40.37	40.89	41.29	41.12	39.74

outlet weir temp 40.00 ° C

For C_{sb} = 0.0695 m/s

L = 20 Gal/min

inlet temp 42.11 ° C

32.90	38.95	40.38	40.05	39.72	36.35
27.79	30.24	37.50	37.69	33.23	27.59
30.76	35.09	37.22	36.84	30.84	27.34
31.90	34.59	35.23	35.30	34.50	37.46

outlet weir temp 34.98 ° C

L = 30 Gal/min

inlet temp 40.33 °C

34.72	38.58	39.28	38.88	38.69	38.29
28.16	31.98	37.21	37.25	35.24	28.70
31.58	35.95	38.02	37.91	32.68	27.95
32.92	35.87	36.49	36.48	35.91	33.53

outlet weir temp 36.12 °C

L = 40 Gal/min

inlet temp 40.95 °C

37.34	39.91	39.74	39.52	39.50	39.66
29.22	34.07	38.26	37.98	37.11	30.76
32.62	37.19	39.30	39.25	34.80	29.30
34.37	37.27	37.90	37.88	37.42	34.98

outlet weir temp 37.32 ° C

L = 50 Gal/min

inlet temp 40.14 °C

38.30	39.67	38.59	39.16	39.38	40.14
29.93	35.31	38.07	38.13	38.08	33.38
32.57	37.27	39.03	39.16	36.60	31.29
34.64	37.40	38.00	38.08	37.89	35.60

outlet weir temp 37.43 °C

L = 60 Gal/min

inlet temp 40.76 ° C

39.36	40.35	38.64	39.78	40.07	39.94
31.16	36.68	38.65	38.67	38.82	35.23
33.30	37.85	39.94	40.23	37.68	32.11
35.40	38.45	39.03	39.25	39.12	36.78

outlet weir temp 38.69 °C

L = 70 Gal/min

inlet temp 40.44 °C

38.37	39.96	38.43	39.66	39.84	39.72
31.99	37.02	38.30	38.47	38.79	36.49
33.83	38.28	39.96	40.35	38.17	33.02
35.81	38.58	39.10	39.46	39.21	37.22

outlet weir temp 39.99 °C

L = 80 Gal/min

inlet temp 40.44 °C

38.37	39.96	38.43	39.66	39.84	39.72
31.99	37.02	38.30	38.47	38.79	36.49
33.83	38.28	39.96	40.35	38.17	33.02
35.81	38.58	39.10	39.46	39.21	37.22

outlet weir temp 38.64 °C

L = 80 Gal/min

inlet temp 40.70 °C

39.29	40.29	38.40	39.72	39.87	39.98
32.57	37.04	38.55	38.65	38.96	36.76
33.76	38.60	40.18	40.67	38.42	33.44
36.04	38.78	39.44	39.78	39.63	37.46

outlet weir temp 39.12 °C

L = 90 Gal/min

inlet temp 41.56 °C

39.08	40.37	38.06	39.67	39.70	39.91
36.25	38.22	38.57	38.54	39.18	38.37
36.90	40.54	41.47	42.02	39.06	34.72
38.00	40.46	40.85	41.24	41.19	39.62

outlet weir temp 40.58 °C

Appendix 6

AVERAGE TEMPERATURE MEASUREMENTS USED FOR PROFILES FOR 1/2 INCH HOLE DIAMETER TRAY(STANDARD TRAY)

14

25.67	0.006	21.22	38.54	27.84	10.0	1.70
	25.70	26.84	29.32	29.13	28.41	27.63
	25.67	27.34	29.77	31.76	29.56	27.48
	25.87	27.05	30.88	33.43	32.05	28.54
	32.28	33.73	36.90	37.46	37.37	34.77
	38.54	38.54	38.54	38.54	38.54	38.54
30.32	0.0054	21.66	44.70	32.70	20.0	1.70
	30.32	31.38	34.56	34.10	33.48	32.36
	30.98	32.52	35.85	37.38	35.00	31.94
	32.20	35.17	38.13	39.21	37.74	33.24
	42.07	42.36	42.72	43.32	43.61	41.72
	44.70	44.70	44.70	44.70	44.70	44.70
32.45	0.005	20.59	43.91	34.15	30.0	1.70
	32.45	33.04	35.55	35.12	34.93	33.80
	33.40	34.89	37.10	38.08	36.15	33.18
	34.47	37.71	39.03	38.98	38.32	34.09
	42.52	41.64	41.58	41.91	42.77	41.03
	43.91	43.91	43.91	43.91	43.91	43.91
32.45	0.005	20.46	40.81	34.02	40.0	1.70
	32.76	33.27	35.10	34.57	34.77	33.66
	33.63	34.85	36.46	37.04	35.28	32.49
	34.40	36.75	37.48	37.45	37.09	33.28
	40.28	39.56	39.48	39.46	40.13	39.49
	40.81	40.81	40.81	40.81	40.81	40.81
33.61	0.0049	20.20	40.06	35.25	50.0	1.70
	34.09	34.58	35.81	35.27	35.68	34.72
	34.93	36.14	37.05	37.34	35.94	33.61
	35.55	37.41	37.72	37.34	37.20	34.04
	39.56	38.78	38.56	39.00	39.59	39.03
	40.06	40.06	40.06	40.06	40.06	40.06

33.92	0.005	20.37	40.15	35.63	60.0	1.70
	34.80	35.44	36.24	35.65	36.29	35.36
	35.35	37.04	37.55	37.74	36.51	33.92
	35.69	37.85	38.04	37.80	37.49	34.43
	39.73	38.88	38.85	39.21	39.82	39.32
	40.15	40.15	40.15	40.15	40.15	40.15
34.63	0.0052	20.75	41.02	36.74	70.0	1.70
	35.74	36.68	37.34	36.85	37.39	36.42
	35.96	38.09	38.70	38.80	37.27	34.63
	35.14	38.11	38.71	38.96	38.70	35.95
	40.54	39.45	38.85	39.61	40.39	39.74
	41.02	41.02	41.02	41.02	41.02	41.02
35.95	0.0042	19.19	42.79	38.03	80.0	1.70
	36.88	38.21	38.80	37.92	38.95	38.03
	36.88	39.46	40.09	40.26	38.87	35.95
	37.19	40.12	40.54	40.48	39.38	36.41
	42.29	41.19	40.33	41.06	42.51	41.54
	42.79	42.79	42.79	42.79	42.79	42.79
34.86	0.004	18.95	41.13	36.75	90.0	1.70
	35.66	36.74	37.41	36.64	37.53	36.60
	35.83	38.11	38.68	38.78	38.52	34.86
	36.06	38.75	39.03	38.62	37.98	35.24
	40.65	39.91	38.83	39.52	40.70	40.02
	41.13	41.13	41.13	41.13	41.13	41.13
35.68	0.003	17.37	41.43	36.97	100.0	1.70
	35.96	36.93	37.40	36.70	37.79	37.06
	35.68	37.89	38.43	38.44	38.38	35.97
	36.83	39.05	39.68	39.48	38.01	35.99
	41.32	39.90	38.40	40.01	41.36	40.46
	41.43	41.43	41.43	41.43	41.43	41.43
35.57	0.0034	19.08	40.43	36.89	110.0	1.70
	35.98	37.01	37.22	36.67	37.45	37.06
	35.72	37.59	37.96	38.02	37.73	35.69
	36.57	37.72	38.52	38.47	36.97	35.57
	40.27	38.33	36.52	38.39	40.35	38.47
	40.43	40.43	40.43	40.43	40.43	40.43
35.08	0.0058	20.20	40.79	37.86	120.0	1.70
	36.99	37.96	38.09	37.50	38.53	38.08
	36.86	38.50	38.74	39.02	38.29	36.27
	37.42	38.18	38.86	38.73	37.29	36.31
	40.67	38.87	35.08	38.68	40.79	38.54
	40.79	40.79	40.79	40.79	40.79	40.79
36.54	0.008	20.51	40.83	38.25	130.0	1.70
	37.31	38.35	38.50	37.98	38.84	38.51
	37.35	38.78	39.01	39.26	38.33	36.54
	37.82	38.30	38.84	38.80	37.60	36.69
	40.65	38.61	36.64	37.65	40.84	38.46
	40.83	40.83	40.83	40.83	40.83	40.83

36.15	0.008	19.76	40.44	38.04	140.0	1.70
	37.00	38.08	38.32	37.85	38.67	38.29
	37.19	38.46	38.91	38.94	37.93	36.15
	37.63	38.20	38.47	38.36	37.25	36.39
	40.19	38.23	37.34	37.99	40.32	37.57
	40.44	40.44	40.44	40.44	40.44	40.44
36.63	0.008	20.24	40.31	38.23	150.0	1.70
	37.27	38.33	38.52	37.96	38.86	38.41
	37.35	38.45	38.86	39.07	37.94	36.63
	37.73	38.31	38.48	38.35	37.56	36.77
	40.10	38.52	38.86	38.28	40.21	38.64
	40.31	40.31	40.31	40.31	40.31	40.31
35.06	0.007	19.98	38.18	36.57	160.0	1.70
	35.84	36.58	36.80	36.50	37.05	36.62
	35.89	36.60	37.03	37.16	36.17	35.06
	36.06	36.42	36.70	36.53	36.08	35.26
	37.99	37.01	37.58	37.27	38.12	37.58
	38.18	38.18	38.18	38.18	38.18	38.18

C_{sb} = 0.0695 m/s

14

25.13	0.005	32.00	43.21	27.97	10.0	1.9
	25.59	26.80	29.89	29.43	28.37	27.75
	25.31	27.07	30.61	32.56	29.17	27.09
	25.13	26.83	32.25	35.32	32.24	28.21
	31.47	34.76	41.30	41.61	40.12	25.87
	43.21	43.21	43.21	43.21	43.21	43.21
27.03	0.0045	32.73	40.63	29.33	20.0	1.9
	27.03	28.24	31.30	30.79	29.80	28.83
	27.17	28.99	32.40	33.58	30.97	38.15
	28.23	30.58	34.36	35.44	33.44	29.50
	37.36	39.04	39.68	39.72	39.73	37.69
	40.63	40.63	40.63	40.63	40.63	40.63
28.67	0.005	32.73	39.85	30.51	30.0	1.9
	28.67	29.71	32.02	31.51	31.10	31.02
	29.09	30.77	33.37	34.07	33.30	30.52
	31.61	34.39	36.16	36.38	35.38	31.62
	39.19	38.84	38.85	38.94	39.46	38.49
	39.85	39.85	39.85	39.85	39.85	39.85
31.01	0.005	32.90	41.99	32.70	40.0	1.9
	31.01	32.00	34.14	33.53	33.39	32.15
	31.61	33.43	35.64	36.25	35.61	32.50
	34.25	37.12	38.43	38.55	37.85	33.66
	41.47	40.89	41.06	40.94	41.53	40.78
	41.99	41.99	41.99	41.99	41.99	41.99

32.74	0.015	33.01	38.98	33.79	50.0	1.9
	32.74	33.54	34.66	33.89	34.49	33.43
	33.47	34.82	35.86	35.92	35.45	32.91
	34.94	36.74	36.94	36.81	36.30	33.46
	38.68	38.02	37.95	38.12	38.65	38.31
	38.98	38.98	38.98	38.98	39.98	38.98
33.47	0.01	30.01	39.50	34.94	60.0	1.9
	33.91	34.81	35.76	34.83	35.65	34.70
	34.43	36.32	36.82	36.99	36.10	33.47
	33.89	36.60	37.27	37.37	37.39	35.38
	39.15	38.14	38.41	38.36	39.20	38.76
	39.50	39.50	39.50	39.50	39.50	39.50
33.94	0.015	33.01	39.76	35.57	70.0	1.9
	34.58	35.61	36.23	35.47	36.32	35.35
	34.95	36.85	37.38	37.44	36.50	33.94
	35.91	37.63	37.78	37.65	36.81	34.49
	39.36	38.22	38.48	38.80	39.46	39.00
	39.76	39.76	39.76	39.76	39.76	39.76
34.23	0.014	30.01	39.28	35.95	80.0	1.9
	35.02	36.10	36.41	35.66	36.63	35.90
	35.54	36.93	37.34	37.45	36.33	34.23
	36.12	36.83	37.07	37.04	35.77	34.64
	39.02	37.17	37.23	38.25	39.11	38.44
	39.28	39.28	39.28	39.28	39.28	39.28
35.02	0.013	28.20	38.94	36.67	90.0	1.9
	36.02	36.79	36.91	36.36	37.23	36.72
	36.41	37.02	37.19	37.39	36.42	35.30
	36.77	36.76	36.58	36.34	35.92	35.92
	38.69	36.83	35.02	37.12	38.75	36.81
	38.94	38.94	38.94	38.94	38.94	39.94
33.63	0.015	33.02	38.90	36.85	100.0	1.9
	33.25	36.85	37.03	36.58	37.41	37.00
	36.74	37.09	37.26	37.39	36.37	35.60
	36.94	36.92	36.44	36.26	36.22	36.09
	38.64	37.01	33.63	36.16	38.75	37.01
	38.90	38.90	38.90	38.90	38.90	38.90
34.78	0.01	23.09	38.58	36.25	110.0	1.9
	35.63	36.31	36.48	36.02	36.78	36.30
	36.10	36.62	36.97	36.98	35.08	36.04
	36.56	36.35	36.24	36.07	35.55	35.53
	38.37	36.79	34.78	36.83	38.41	36.98
	38.58	38.58	38.58	38.58	38.58	38.58
34.21	0.01	20.07	38.42	35.89	120.0	1.9
	35.23	35.93	36.20	35.63	36.47	35.87
	35.57	36.64	36.93	37.04	35.87	34.21
	35.82	36.07	36.41	36.20	35.31	34.56
	38.23	36.27	36.52	37.15	38.33	37.56
	38.42	38.42	38.42	38.42	38.42	38.42

34.17	0.0055	33.82	38.11	34.59	130.0	1.9
	33.91	34.58	34.87	34.17	35.28	34.72
	34.23	35.22	35.30	35.49	35.90	34.49
	35.76	36.03	36.05	35.84	35.27	35.01
	38.07	35.87	35.80	36.10	38.21	36.98
	38.11	38.11	38.11	38.11	38.11	38.11
34.66	0.006	28.16	38.21	35.44	140.0	1.9
	34.91	35.52	35.70	35.08	36.00	35.43
	35.27	35.92	36.06	36.08	35.96	34.90
	36.29	36.27	36.03	35.82	35.42	35.46
	38.12	36.05	34.66	36.22	38.18	36.62
	38.21	38.21	38.21	38.21	38.21	38.21
C_{sb} =0.0775 m/s						
14						
23.85	0.004	30.50	43.23	25.99	10.0	2.18
	24.19	25.05	27.16	27.22	26.35	25.94
	23.85	24.90	28.78	30.26	27.02	25.86
	23.95	26.17	32.07	34.09	31.39	27.25
	27.59	30.89	40.63	40.90	37.38	33.16
	43.23	43.23	43.23	43.23	43.23	43.23
27.12	0.003	27.25	43.07	28.81	20.0	2.18
	27.20	28.08	30.18	30.03	28.92	28.47
	27.12	28.49	32.00	32.73	30.41	29.00
	28.75	30.98	35.42	36.26	34.39	30.51
	37.56	40.46	41.68	41.72	41.62	38.36
	43.07	43.07	43.07	43.07	43.07	43.07
28.02	0.0045	30.59	42.30	29.51	30.0	2.18
	28.02	28.74	30.77	30.29	30.05	29.17
	28.59	29.83	32.58	33.35	32.05	30.37
	31.68	33.85	36.37	36.91	35.91	32.96
	40.47	40.71	41.05	40.96	41.43	39.99
	42.30	42.30	42.30	42.30	42.30	42.30
28.96	0.0035	30.37	41.38	30.22	40.0	2.18
	28.96	29.76	31.13	30.77	30.83	29.90
	29.85	30.72	33.26	33.85	33.23	31.60
	33.58	35.08	36.76	36.76	36.99	36.51
	40.61	40.14	40.27	40.30	40.78	39.90
	41.38	41.38	41.38	41.38	41.38	41.38
30.27	0.0035	30.23	40.12	31.37	50.0	2.18
	30.27	30.97	32.14	31.92	31.95	30.99
	31.36	32.04	33.85	34.32	34.26	34.46
	34.69	36.01	36.65	36.86	36.47	34.57
	39.55	38.98	39.29	39.20	39.44	39.19
	40.12	40.12	40.12	40.12	40.12	40.12
30.68	0.0035	30.72	39.71	31.72	60.0	2.18
	30.68	31.36	32.77	32.08	32.20	31.22
	31.57	32.82	34.38	34.46	34.80	32.59
	34.67	36.43	36.78	36.79	36.54	33.88
	39.16	38.53	38.76	38.88	39.18	38.92
	39.71	39.71	39.71	39.71	39.71	39.71

31.21	0.004	30.55	39.36	32.21	70.0	2.18
	31.21	32.02	33.10	32.37	32.76	31.79
	32.15	33.26	34.53	34.52	35.09	32.68
	34.92	36.72	36.81	36.69	36.37	33.78
	38.94	38.22	38.47	38.65	39.05	38.52
	39.36	39.36	39.36	39.36	39.36	39.36
31.76	0.004	30.20	38.93	32.61	80.0	2.18
	31.76	32.57	33.41	32.49	33.20	32.25
	32.65	33.89	34.77	34.72	35.25	32.93
	35.13	36.49	36.51	36.48	36.15	33.51
	38.56	37.88	38.03	38.20	38.54	38.31
	38.93	38.93	38.93	38.93	38.93	38.93
32.25	0.0045	28.46	38.84	33.05	90.0	2.18
	32.25	32.92	33.74	33.10	33.60	32.68
	33.09	34.35	35.00	35.00	35.36	33.04
	35.22	36.40	36.57	36.41	35.89	33.69
	38.45	37.54	37.86	38.25	38.50	38.16
	38.84	38.84	38.84	38.84	38.84	38.84
32.45	0.0035	22.55	38.80	33.21	100.0	2.18
	32.45	33.07	33.94	33.32	33.77	32.72
	33.20	34.61	35.10	35.07	35.34	33.01
	35.22	36.42	36.54	36.34	35.74	33.61
	38.45	37.41	37.86	38.03	38.49	38.12
	38.80	38.80	38.80	38.80	38.80	38.80
33.04	0.0065	22.94	39.15	33.88	110.0	2.18
	33.04	33.74	34.59	33.95	34.39	33.58
	33.76	34.99	35.75	35.75	35.78	33.67
	35.49	37.20	37.15	36.93	36.24	34.04
	38.94	37.87	38.15	38.53	39.02	38.57
	39.15	39.15	39.15	39.15	39.15	39.15
33.80	0.0064	31.50	37.45	34.38	120.0	2.18
	33.84	34.42	34.65	34.14	34.92	34.32
	34.29	35.23	35.32	35.28	35.11	33.80
	35.19	35.27	35.17	35.02	34.41	34.09
	37.34	35.27	36.40	36.41	37.43	36.85
	37.45	37.45	37.45	37.45	37.45	37.45
33.96	0.0065	31.80	37.01	34.64	130.0	2.18
	34.15	34.60	34.78	34.45	35.19	34.69
	34.66	35.02	35.09	35.27	34.77	33.96
	35.08	35.08	34.48	34.47	34.52	34.48
	36.14	37.00	35.72	35.49	34.62	36.85
	37.01	37.01	37.01	37.01	37.01	37.10
34.35	0.0068	32.81	37.25	35.25	140.0	2.18
	34.91	35.15	35.41	34.99	35.73	35.35
	35.34	35.27	35.44	35.46	34.73	34.35
	35.58	35.57	34.55	34.37	35.07	35.15
	37.05	35.61	35.21	35.23	37.15	35.60
	37.25	37.25	37.25	37.25	37.25	37.25

C_{sb} = 0.0851 m/s

15

24.29	0.005	19.44	42.90	25.80	10.0	2.4
	24.29	24.78	26.48	27.26	26.27	25.70
	24.57	25.47	28.49	30.00	27.06	25.84
	25.60	28.08	32.53	34.30	29.89	26.74
	27.68	32.35	40.57	41.53	37.62	31.10
	42.90	42.90	42.90	42.90	42.90	42.90
27.49	0.007	31.00	41.95	28.70	20.0	2.4
	27.49	27.82	29.42	29.55	29.21	28.68
	28.14	28.65	30.77	31.84	30.30	29.36
	29.90	32.37	35.14	35.54	34.10	31.38
	35.87	39.70	40.77	41.09	40.82	37.13
	41.95	41.95	41.95	41.95	41.95	41.95
28.78	0.0065	31.18	41.46	29.84	30.0	2.4
	28.78	29.37	30.45	30.33	30.26	29.87
	29.38	30.37	32.49	32.71	31.91	31.03
	32.24	34.04	35.88	36.40	35.14	33.15
	38.93	40.01	40.51	40.64	40.75	38.79
	41.46	41.46	41.46	41.46	41.46	41.46
30.51	0.0065	31.03	41.75	31.40	40.0	2.4
	30.51	31.07	31.82	31.78	31.88	31.36
	31.14	31.90	33.73	34.33	33.56	32.17
	34.15	35.80	37.06	37.39	36.41	34.31
	40.76	40.72	40.78	40.87	41.01	40.02
	41.75	41.75	41.75	41.75	41.75	41.75
31.88	0.007	30.94	39.50	32.58	50.0	2.4
	31.88	32.35	32.94	32.88	32.96	32.47
	32.67	33.41	34.59	35.00	34.31	32.79
	34.59	35.69	36.60	36.65	36.35	34.59
	39.11	38.55	38.78	38.78	39.19	38.46
	39.50	39.50	39.50	39.50	39.50	39.50
32.04	0.007	31.15	39.02	32.85	60.0	2.4
	32.05	32.61	33.45	33.16	33.23	32.57
	32.80	33.77	34.90	35.01	34.39	32.85
	34.30	35.99	36.31	36.41	35.70	33.90
	38.48	38.13	38.20	38.27	38.76	38.12
	39.02	39.02	39.02	39.02	39.02	39.02
32.17	0.006	29.46	38.19	32.86	70.0	2.4
	32.17	32.73	33.42	33.12	33.17	32.55
	33.07	33.81	34.78	35.00	34.45	32.75
	34.37	35.49	35.65	35.63	35.13	33.26
	37.78	37.29	37.61	37.55	37.81	37.55
	38.19	38.19	38.19	38.19	38.19	38.19
32.46	0.006	28.15	38.27	33.18	80.0	2.4
	32.46	33.04	33.77	33.43	33.48	32.91
	33.24	34.30	34.92	35.16	34.44	32.83
	34.38	35.69	35.78	35.66	35.40	33.48
	37.86	37.45	37.66	37.49	38.04	37.57
	38.27	38.27	38.27	38.27	38.27	38.27

31.81	0.003	17.49	37.69	32.38	90.0	2.4
	31.81	32.24	32.91	32.37	32.85	32.10
	32.69	33.46	34.09	34.31	34.42	32.73
	34.31	35.30	35.13	35.25	34.67	33.21
	37.45	36.41	37.04	36.99	37.58	37.05
	37.69	37.69	37.69	37.69	37.69	37.69
31.97	0.0035	18.20	36.49	32.57	100.0	2.4
	31.97	32.49	33.01	32.56	33.01	32.37
	32.56	33.64	33.86	34.06	34.10	32.60
	33.90	34.66	34.08	34.50	33.94	32.85
	36.75	35.41	36.12	36.15	36.84	36.49
	36.49	36.49	36.49	36.49	36.49	36.49
32.91	0.0035	18.27	36.02	33.25	110.0	2.4
	32.91	33.05	33.31	33.14	33.52	33.25
	33.29	33.38	33.25	33.31	33.35	33.68
	33.96	34.14	32.50	33.05	33.58	33.53
	35.84	33.98	35.01	35.14	35.89	35.10
	36.02	36.02	36.02	36.02	36.02	36.02
31.91	0.0042	21.49	37.23	32.60	120.0	2.4
	31.91	32.44	33.17	32.71	33.09	32.30
	32.77	33.57	34.30	34.37	33.78	32.24
	33.82	34.87	34.76	34.79	34.38	32.86
	36.99	36.13	36.58	36.56	36.97	36.35
	37.23	37.23	37.23	37.23	37.23	37.23
32.83	0.004	19.34	36.46	33.51	130.0	2.4
	33.16	33.36	33.76	33.50	33.90	33.38
	33.58	34.37	34.32	34.43	33.95	32.83
	33.96	34.00	33.58	33.71	33.35	33.00
	36.34	34.69	35.78	35.81	36.42	36.05
	36.46	36.46	36.46	36.46	36.46	36.46
33.07	0.004	19.54	36.39	34.00	140.0	2.4
	33.60	33.96	34.17	33.78	34.44	34.05
	34.00	34.32	34.44	34.43	33.86	33.12
	34.28	34.43	33.07	33.09	33.63	33.32
	36.25	34.16	35.58	35.66	36.35	35.88
	36.39	36.39	36.39	36.39	36.39	36.39
33.14	0.004	19.24	36.34	34.05	150.0	2.4
	33.68	33.86	34.16	33.97	34.44	34.16
	34.09	34.15	34.05	34.19	33.73	33.30
	34.26	34.17	33.14	33.17	33.90	33.72
	36.18	34.10	35.32	35.49	36.37	35.64
	36.34	36.34	36.34	36.34	36.34	36.34

Appendix 6.1 Computed Point & Tray efficiency values for 12.5 mm Diameter hole Tray.

Table (7.6) Capacity factor of 0.0605 m/s

Weir Load $m^3/s\ m$	E_{og}	E_{mv}	E_{mv}/E_{og}
0.000806	30.5	45.0	1.5
0.00161	43.7	66.6	1.5
0.00241	51.2	70.9	1.4
0.00322	52.7	66.3	1.3
0.00403	46.1	53.5	1.2
0.0056	51.1	59.0	1.2
0.00644	54.0	61.0	1.1
0.00725	59.7	68.2	1.1
0.00806	67.2	76.1	1.1
0.00866	71.8	81.2	1.1
0.00967	67.8	73.5	1.1
0.0104	63.3	67.0	1.1
0.01128	63.0	65.8	1.0
0.0209	63.8	66.3	1.0
0.02896	59.0	61.1	1.0
0.0137	53.5	55.1	1.0

Table (7.7) Capacity factor of 0.0695 m/s

Weir Load $m^3/s\ m$	E_{og}	E_{mv}	E_{mv}/E_{og}
0.000806	37.2	66.7	1.8
0.00161	51.3	85.2	1.7
0.00241	62.7	96.7	1.5
0.00322	70.4	105.4	1.5
0.00403	76.3	104.8	1.4
0.0056	60.3	73.1	1.2
0.00644	77.5	95.5	1.2
0.00725	66.2	75.3	1.1
0.00806	47.7	50.2	1.0
0.00866	56.4	58.0	1.0
0.00967	52.0	54.6	1.1
0.0104	59.6	63.6	1.1
0.01128	100.8	114.27	1.1
0.0209	78.0	84.1	1.1
0.02896	59.0	61.1	1.0
0.0137	53.5	55.1	1.0

Table (7.8) Capacity factor of 0.0775 m/s

Weir Load $m^3/s\ m$	E_{og}	E_{mv}	E_{mv}/E_{og}
0.000806	37.2	73.3	2.0
0.00161	47.2	80.9	1.7
0.00241	66.9	118.1	1.8
0.00322	74.7	122.4	1.6
0.00403	74.1	108.5	1.64
0.0056	82.6	116.6	1.4
0.00644	87.3	118.9	1.4
0.00725	88.4	115.5	1.3
0.00806	89.7	113.6	1.3
0.00866	86.4	105.8	1.2
0.00967	94.2	115.8	1.2
0.0104	72.8	81.1	1.1
0.01128	62.5	66.9	1.1
0.0209	56.9	59.3	1.1
0.02896	59.0	61.1	1.0
0.0137	53.5	55.1	1.0

Table (7.9) Capacity factor of 0.0851 m/s

Weir Load $m^3/s\ m$	E_{og}	E_{mv}	E_{mv}/E_{og}
0.000806	28.4	51.7	1.8
0.00161	48.4	91.0	1.9
0.00241	59.5	103.4	1.7
0.00322	65.27	104.9	1.6
0.00403	58.3	80.2	1.4
0.0056	63.7	84.0	1.3
0.00644	62.8	78.8	1.3
0.00725	66.4	81.8	1.2
0.00806	64.3	77.4	1.2
0.00866	56.0	64.4	1.1
0.00967	44.6	47.8	1.1
0.0104	83.1	98.0	1.2
0.01128	56.2	61.0	1.1
0.0209	48.9	51.6	1.1
0.02896	50.1	52.6	1.0
0.0137	53.5	55.1	1.0

Appendix 7

Appendix (7.1) LIQUID HOLD-UP ON THE TRAY (4.5 mm HOLE DIAMETER SIEVE TRAY) (cm)

C_{sb} = 0.049 m/s

q/b = 0.161E-2 m^3/s m

outlet

2.6	2.6	2.3	2.5	3.0
2.8	3.1	2.7	2.7	2.9
3.1	2.9	3.0	2.9	2.4
3.3	3.2	3.1	2.8	3.3

inlet

q/b = 0.242E-2 m^3/s m

1.8	1.7	1.8	2.0	1.7
2.1	2.3	2.0	2.0	2.1
2.2	2.0	2.0	2.0	1.8
2.4	2.3	2.2	2.0	2.5

q/b = 0.3224E-2 m^3/s m

1.8	1.7	1.8	2.0	1.7
2.2	2.4	2.2	2.2	2.2
2.4	2.2	2.2	2.2	1.9
2.6	2.5	2.4	2.1	2.6

q/b = 0.484E-2 m^3/s m

1.9	1.7	2.1	2.2	1.9
2.4	2.6	2.3	2.3	2.3
2.5	2.3	2.3	2.3	2.0
2.7	2.6	2.4	2.2	2.7

q/b = 0.564E-2 m^3/s m

2.1	1.9	2.7	2.4	2.4
2.6	2.8	2.5	2.5	2.5
2.7	2.5	2.6	2.5	2.2
2.9	2.8	2.7	2.4	2.9

q/b = 0.645E-2 m^3/s m

2.6	2.4	3.3	2.8	3.2
2.9	3.1	2.8	2.8	2.9
3.1	3.0	3.0	2.9	2.4
3.2	3.1	3.1	2.8	3.2

q/b = 0.806E-2 m^3/s m

3.0	2.9	3.7	3.0	3.4
3.1	3.4	3.1	3.0	3.0
3.2	3.1	3.1	3.0	2.5
3.4	3.3	3.4	3.1	3.3

C_{sb} = 0.0605 m/s

q/b = 0.161E-2 m^3/s m

1.7	1.5	1.9	1.6	2.1
1.9	2.1	1.9	1.9	2.1
2.2	1.9	2.0	2.0	1.7
2.4	2.2	2.2	1.9	2.3

q/b = 0.242E-2 m^3/s m

1.8	1.6	2.2	1.9	2.3
2.0	2.2	2.0	2.1	2.2
2.4	2.1	2.1	2.2	1.8
2.6	2.3	2.5	2.1	2.5

q/b = 0.3224E-2 m^3/s m

2.0	1.8	2.5	2.1	2.5
2.2	2.4	2.1	2.3	2.4
2.6	2.2	2.2	2.2	1.9
2.6	2.4	2.5	2.2	2.7

q/b = 0.4030E-2 m^3/s m

2.2	1.9	3.0	2.6	3.0
2.4	2.8	2.4	2.5	2.6
2.7	2.4	2.5	2.5	2.1
3.0	2.8	2.6	2.5	2.7

q/b = 0.484E-2 $m^3/s.m$

2.4	2.1	3.2	2.8	3.2
2.5	2.9	2.6	2.7	2.7
2.9	2.6	2.8	2.7	2.2
3.1	3.0	2.9	2.6	3.0

q/b = 0.564E-2 m^3/s m

2.6	2.3	3.5	3.0	3.4
2.6	3.1	2.7	2.9	2.8
3.0	2.8	2.9	2.8	2.4
3.2	3.2	3.1	2.7	3.1

q/b = 0.7254E-2 m^3/s m

2.8	2.7	4.0	3.3	3.7
2.7	3.2	2.9	3.0	2.9
3.1	2.9	3.0	3.0	2.5
3.3	3.3	3.2	2.9	3.2

C_{sb} = 0.0695 m/s

q/b = 0.161E-2 m^3/s m

1.5	1.4	1.9	1.6	2.0
1.7	2.0	1.8	1.8	2.0
2.1	1.8	1.8	1.8	1.6
2.2	2.1	2.1	2.0	2.4

q/b = 0.242E-2 m^3/s m

1.6	1.5	2.0	1.7	2.2
1.9	2.1	1.9	1.9	2.1
2.2	1.9	1.9	1.9	1.7
2.3	2.2	2.3	2.1	2.5

q/b = 0.3224E-2 m^3/s m

1.7	1.7	2.2	1.9	2.4
2.2	2.3	2.0	2.0	2.2
2.3	2.0	2.0	2.0	1.8
2.4	2.3	2.4	2.2	2.6

q/b = 0.4030E-2 m^3/s m

1.8	1.8	2.6	2.3	2.7
2.1	2.4	2.2	2.2	2.4
2.5	2.1	2.2	2.2	2.0
2.5	2.5	2.5	2.3	2.7

q/b = 0.484E-2 m^3/s m

1.9	1.9	2.9	2.5	2.9
2.5	2.4	2.3	2.6	2.2
2.6	2.2	2.3	2.4	2.1
2.6	2.6	2.6	2.4	2.8

q/b = 0.564E-2 m^3/s m

3.0	2.7	3.2	2.0	2.1
2.6	2.6	2.5	2.7	2.4
2.8	2.4	2.4	2.5	2.2
2.9	2.5	2.7	2.8	2.9

q/b = 0.6448E-2 m^3/s m

3.3	3.0	3.4	2.3	2.3
2.8	2.7	2.6	2.8	2.5
2.9	2.5	2.6	2.6	2.4
3.1	3.1	2.8	2.6	3.0

q/b = 0.7254E-2 m^3/s m

3.5	3.2	3.6	2.5	2.6
3.0	2.8	2.7	2.9	2.6
3.0	2.6	2.8	2.7	2.5
3.2	3.2	2.9	2.7	3.1

q/b 0.806E-2 m^3/s m

3.1	2.9	2.8	3.0	2.7
3.1	2.7	2.9	2.8	2.6
3.3	3.3 3	3.0	2.8	3.2

Appendix (7.2) LIQUID HOLD-UP ON THE 12.5 mm DIAMETER HOLES TRAY (cm)

For C_{sb} = 0.0605 m/s

q/b = 0.0.161E-2 m^3/s m

3.8	3.5	3.0	2.7	4.0
3.8	3.4	3.2	3.2	2.5
3.7	3.7	3.7	4.0	3.2
3.8	3.2	3.3	2.6	3.6

q/b = 0.3224E-2 m^3/s m

3.3	3.5	3.4	4.1	3.9
3.3	3.8	3.4	3.5	2.6
3.3	3.7	3.3	4.3	2.8
3.8	3.1	2.9	3.1	3.6

q/b = 0.484E-2 m^3/s m

3.8	4.0	3.8	3.8	4.2
3.8	4.0	3.9	4.0	3.0
4.1	4.1	4.0	4.5	3.0
4.5	3.7	2.9	3.1	3.9

q/b = 0.645E-2 m^3/s m

4.5	4.0	3.8	4.5	3.9
3.8	4.5	4.1	4.2	3.3
4.5	4.3	4.3	5.0	3.4
4.7	3.2	3.3	3.3	4.2

q/b = 0.806E-2 m^3/s m

5.1	4.5	4.5	4.8	4.3
4.5	4.8	4.6	4.5	4.1
5.0	4.6	4.5	5.5	3.8
5.3	3.5	3.8	3.6	4.5

q/b = 0.967E-2 m^3/s m

5.9	4.8	5.0	5.0	4.5
4.7	5.1	4.1	5.0	3.8
5.1	4.8	4.8	5.5	3.8
5.6	3.8	4.4	3.9	5.1

C_{sb} = 0.0775 m/s
q/b = 0.161E-2 m^3/s m

2.5	3.0	2.8	3.2	3.2
3.2	3.5	2.6	3.0	2.1
3.0	3.0	2.7	3.0	2.0
3.0	3.0	3.5	2.7	3.3

q/b = 0.3224E-2 m^3/s m

3.0	3.5	3.3	3.9	3.5
3.4	3.5	2.8	3.3	2.6
4.2	4.5	3.1	4.0	2.5
4.0	3.3	3.5	3.0	3.6

q/b = 0.484E-2 m^3/s m

3.4	4.1	3.5	3.7	3.9
3.7	4.0	3.3	3.6	2.8
4.2	4.0	3.4	3.8	2.8
4.0	3.0	3.3	2.8	3.8

q/b = 0.645E-2 m^3/s m

3.6	4.0	3.8	3.8	3.9
4.0	4.2	3.8	4.0	2.9
4.3	4.5	3.7	4.3	2.8
4.1	3.1	3.3	2.6	3.9

q/b = 0.806E-2 m^3/s m

3.7	4.3	4.3	4.2	4.2
4.5	4.5	4.2	4.2	3.2
4.9	4.5	3.8	4.5	2.7
4.5	3.1	3.6	3.0	3.8

q/b = 0.967E-2 m^3/s m

3.9	4.5	4.5	4.2	4.4
4.2	4.5	4.1	4.5	3.3
4.8	4.5	3.9	4.3	3.0
4.5	3.2	4.0	2.9	4.0

q/b = 1.169E-2 m^3/s m

4.0	4.8	4.6	4.7	4.7
3.8	5.0	3.8	5.0	3.6
5.0	4.8	4.7	4.8	3.2
4.7	3.5	4.3	3.2	4.1

C_{sb} = 0.0915 m/s

q/b = 0.322E-2 m^3/s m

2.1	2.1	1.8	1.6	2.8
2.3	3.0	1.3	1.5	1.5
2.1	1.3	1.5	2.3	1.5
2.7	2.3	2.0	2.0	2.0

q/b = 0.484E-2 m^3/s m

2.7	2.7	2.0	2.4	2.8
2.8	3.3	1.8	1.5	2.0
2.6	2.3	1.7	2.6	2.0
3.7	2.6	2.4	2.2	2.7

q/b = 0.645E-2 m^3/s m

2.7	2.9	2.3	2.3	3.0
3.0	3.7	2.8	2.0	2.0
3.4	2.5	2.0	2.8	2.0
3.5	2.4	2.0	2.0	2.7

q/b = 0.806E-2 m^3/s m

3.2	3.5	2.8	2.6	3.3
3.3	4.0	2.6	2.5	2.5
3.6	2.4	2.2	2.8	2.3
3.7	2.4	2.1	2.3	3.5

q/b = 0.967E-2 m^3/s m

3.4	3.7	2.6	2.7	3.8
3.6	3.7	3.0	2.5	2.7
3.9	2.8	2.5	2.8	2.3
3.5	2.4	2.1	2.3	3.6

q/b = 1.169E-2 m^3/s m

3.5	3.9	3.0	3.1	4.0
3.8	4.7	2.8	2.7	3.0
4.3	4.5	2.5	3.8	2.3
3.7	2.8	2.7	2.6	3.7

Appendix 8

Computed Tray Efficiency results for Porter & Lockett Model Using Point Efficiency Values calculated for the 12.5 mm diameter hole tray.
Table (8.1) Capacity factor of 0.0605, 0.0695, 0.0775 and 0.0851 m/s

Weir Load $m^3/s\ m$	E_{mvpl} C_{sb}=0.0605	E_{mvpl} C_{sb}=0.0695	E_{mvpl} C_{sb}=0.0775	E_{mvpl} C_{sb}=0.0851
0.000806	123.3	264.7	262.2	166.5
0.00161	181.6	253.9	375.8	319.5
0.00241	160.1	243.1	328.5	317.9
0.00322	116.9	252.1	235.4	283.7
0.00403	78.5	209.5	238.6	158.6
0.0056	83.7	116.9	226.0	155.8
0.00644	85.2	162.2	202.3	130.2
0.00725	96.9	111.1	188.5	130.5
0.00806	104.9	63.5	164.9	114.8
0.00866	99.5	60.7	181.1	85.1
0.00967	103.0	73.7	107.2	58.3
0.0104	91.6	65.1	82.3	142.3
0.01128	80.3	158	70.5	75.7
0.0209	79.2	105	---	60.9
0.02896	67.0	---	---	61.5
0.0137	53.5	----	----	------

Table (8.2) Tray Efficiency calculated from Porter & Lockett Model using Computed Point Efficiency for the 1 mm diameter hole tray.

Weir Load $m^3/s\ m$	E_{mvpl} C_{sb}=0.0605	E_{mvpl} C_{sb}=0.0695	E_{mvpl} C_{sb}=0.0775	E_{mvpl} C_{sb}=0.0851
0.000806	273.1	336.8	423.0	354.1
0.00161	274.2	289.6	407.2	306.8
0.00241	178.8	202.6	286.9	355.6
0.00322	137.9	179.8	200.4	234.4
0.00403	124.9	48.1	128.9	156.1
0.0056	127.6	63.6	113.6	128.2
0.00644	118.1	96.8	101.7	109.3
0.00725	106.4	99.3	89.0	106.6
0.00806	112.8	98.1	83.6	117.6
0.00866	79.3	93.3	169.6	94.4
0.00967	58.5	80.8	104.4	90.6
0.0104	67.0	59.9	93.5	92.4
0.01128	53.3	50.6	79.24	96.1
0.0209	47.0	54.8	82.6	76.0
0.02896	42.6	46.36	59.6	64.8
0.0137	----	45.6	54.7	60.4

Appendix 9

REPEATED EXPERIMENTAL POINT TEMPERATURES FOR THE 12.5 mm DIAMETER HOLES TRAY

C_{sb} = 0.0605 m/s

6

24.24	0.007	25.45	39.48	28.15	10.0	1.70
	25.63	27.53	29.55	29.94	29.07	27.21
	25.17	27.55	30.20	32.20	28.50	26.48
	24.24	25.39	29.57	33.69	31.19	27.16
	25.46	29.88	36.90	37.50	36.35	33.90
	39.48	39.48	39.48	39.48	39.48	39.48
32.45	0.0140	34.41	44.69	34.98	30.0	1.70
	32.46	33.88	36.31	37.05	36.34	33.88
	32.90	35.23	37.97	39.23	36.01	33.36
	33.16	36.44	39.27	40.34	38.55	33.93
	39.07	42.49	43.46	43.15	43.42	42.47
	44.69	44.69	44.69	44.69	44.69	44.69
34.40	0.013	33.35	41.39	36.31	50.0	1.70
	34.86	35.66	37.01	37.62	37.33	35.41
	35.23	37.48	38.33	38.86	36.54	34.40
	34.73	37.25	38.68	38.85	38.09	34.72
	39.23	40.20	40.44	40.30	41.00	40.69
	41.39	41.39	41.39	41.39	41.39	41.39
34.87	0.018	33.05	40.35	37.63	90.0	1.70
	36.31	37.58	38.06	38.42	38.65	36.80
	36.16	38.51	38.96	39.29	37.19	34.87
	35.48	37.33	38.50	38.44	37.55	35.18
	39.38	38.85	39.79	39.65	39.48	39.91
	40.35	40.35	40.35	40.35	40.35	40.35
36.90	0.0190	33.89	40.42	39.15	140.0	1.70
	38.54	39.11	39.25	39.60	39.90	38.53
	38.26	39.82	39.71	39.97	38.15	36.90
	37.43	37.11	38.49	38.44	38.08	37.62
	40.13	37.50	40.09	39.20	39.44	40.40
	40.42	40.42	40.42	40.42	40.42	40.42
35.74	0.015	33.39	39.68	38.21	170.0	1.70
	37.97	38.29	38.40	38.46	38.51	37.67
	37.93	38.60	38.69	39.61	36.14	35.74
	36.76	36.59	37.30	37.21	36.85	36.56
	38.29	36.52	38.88	38.75	39.06	38.81
	39.68	39.68	39.68	39.68	39.68	39.68

C_{sb} = 0.0851 m/s

7

24.15	0.001	30.60	46.47	25.83	10.0	2.4
	24.15	25.02	26.84	27.26	26.55	25.46
	24.83	25.70	29.11	30.52	26.87	25.46
	25.48	28.55	32.27	36.01	30.89	27.02
	28.00	37.10	44.01	44.55	38.45	31.59
	46.47	46.47	46.47	46.47	46.47	46.47
29.89	0.010	30.54	40.31	30.86	30.0	2.4
	29.89	30.39	31.11	31.53	31.51	30.76
	30.66	31.73	32.87	33.39	31.16	30.34
	31.67	32.87	35.10	34.74	33.11	33.42
	35.71	38.69	39.35	39.36	39.60	37.96
	40.31	40.31	40.31	40.31	40.31	40.31
31.07	0.0115	30.45	37.62	32.34	50.0	2.4
	31.58	32.06	32.53	32.85	32.89	32.14
	32.24	33.13	34.15	34.54	32.16	31.07
	32.30	33.36	34.19	34.86	34.03	33.36
	35.60	36.91	37.15	37.05	37.36	36.71
	37.62	37.62	37.62	37.62	37.62	37.62
31.17	0.0149	29.37	35.85	32.83	70.0	2.4
	32.01	32.61	33.26	33.42	33.37	32.32
	32.65	33.49	34.29	34.42	32.39	31.17
	32.15	33.03	33.37	33.53	33.24	32.14
	34.96	35.06	35.34	35.59	35.69	35.28
	35.85	35.85	35.85	35.85	35.85	35.85
31.35	0.0200	29.30	34.78	33.48	100.0	2.4
	33.11	33.35	33.55	33.73	33.87	33.28
	33.35	33.87	33.82	33.58	32.40	32.00
	32.48	32.24	31.35	31.75	32.29	32.61
	34.51	33.72	34.51	34.24	34.64	34.68
	34.78	34.78	34.78	34.78	34.78	34.78
31.40	0.023	29.94	34.74	33.27	120.0	2.4
	32.98	33.08	33.25	33.41	33.58	33.37
	33.13	33.15	32.97	33.06	32.31	32.55
	32.80	32.50	31.40	31.57	32.65	33.49
	34.51	33.50	34.34	34.01	34.40	34.66
	34.74	34.74	34.74	34.74	34.74	34.74
30.82	0.0208	29.72	34.63	33.72	150.0	2.4
	33.43	33.49	33.58	33.74	34.01	34.09
	33.60	33.34	33.12	33.13	32.33	32.82
	32.88	32.36	30.82	31.11	32.86	33.90
	34.32	32.56	34.00	33.51	34.11	34.63
	34.63	34.63	34.63	34.63	34.63	34.63

Appendix 10

12.5 mm DIAMETER HOLE PERSPEX TRAY POINT TEMPERATURES

C_{sb} = 0.0605 m/s

13

25.25	0.011	29.40	39.98	26.92	10.0	1.70
	25.25	25.68	27.53	28.58	27.45	27.02
	26.21	25.84	28.87	30.92	29.09	26.76
	27.55	31.32	31.49	31.95	30.87	26.93
	31.39	37.34	36.61	36.02	35.42	29.29
	39.98	39.98	39.98	39.98	39.98	39.98
32.44	0.010	29.82	46.30	33.40	20.0	1.70
	32.44	31.97	33.56	35.13	33.96	33.36
	34.24	35.27	35.89	37.52	36.34	32.46
	35.89	40.52	38.85	38.35	39.28	32.91
	43.17	44.69	43.46	43.06	43.96	41.75
	46.30	46.30	46.30	46.30	46.30	46.30
33.35	0.009	30.09	44.41	35.05	30.0	1.70
	34.60	34.30	34.86	36.28	36.56	34.74
	35.68	37.88	36.78	37.95	37.47	33.35
	37.27	40.71	39.03	38.74	39.85	34.37
	42.86	43.25	43.04	42.01	43.13	42.89
	44.41	44.41	44.41	44.41	44.41	44.41
33.34	0.009	33.74	43.30	35.50	40.0	1.70
	35.11	35.11	35.48	36.61	35.86	34.86
	36.16	38.51	37.21	38.31	37.33	33.34
	37.92	40.45	38.90	39.22	39.70	34.93
	42.31	42.52	42.29	41.55	42.41	42.37
	43.30	43.31	43.31	43.31	43.31	43.31
33.48	0.0085	34.25	41.01	35.74	50.0	1.70
	35.33	35.46	35.74	36.74	36.18	35.04
	36.02	38.15	37.30	37.85	36.94	33.48
	37.31	39.11	38.22	38.27	38.63	35.98
	40.29	40.44	40.37	39.88	40.63	40.50
	41.01	41.01	41.01	41.01	41.01	41.01
34.63	0.0075	34.52	41.23	36.68	60.0	1.70
	36.14	36.54	36.80	37.64	37.12	35.88
	36.75	38.83	38.11	38.74	37.85	34.63
	37.89	39.62	38.96	38.79	38.94	37.02
	40.76	40.65	40.56	40.03	40.56	40.80
	41.23	41.23	41.23	41.23	41.23	41.23
33.89	0.011	32.11	38.91	34.82	70.0	1.70
	34.40	34.61	34.84	35.60	35.33	34.17
	36.46	36.50	35.96	36.29	36.48	33.89
	36.46	37.73	37.15	37.06	37.29	35.67
	38.53	38.42	38.38	37.95	38.48	38.71
	38.91	38.91	38.91	38.91	38.91	38.91

33.95	0.011	33.81	38.72	35.33	80.0	1.70
	34.90	35.22	35.34	36.07	35.75	34.70
	35.20	36.93	36.41	36.79	36.56	33.95
	36.37	37.61	36.96	36.85	37.29	35.94
	38.35	38.27	38.24	37.52	38.12	38.50
	38.72	38.72	38.72	38.72	38.72	38.72
34.42	0.011	33.39	38.93	35.95	90.0	1.70
	35.39	35.79	35.81	36.45	36.30	35.20
	35.77	37.44	36.80	37.20	36.84	34.42
	36.70	37.89	37.26	37.08	37.29	35.94
	38.52	38.54	38.39	37.59	38.29	38.73
	38.93	38.93	38.93	38.93	38.93	38.93
34.47	0.011	33.89	38.70	35.95	100.0	1.70
	35.56	35.95	35.99	36.51	36.41	35.31
	35.94	37.44	36.89	37.29	36.73	34.47
	36.78	37.77	37.16	36.96	37.17	35.85
	38.34	38.42	38.17	37.08	38.01	38.58
	38.70	38.70	38.70	38.70	38.70	38.70
34.64	0.0125	33.34	38.45	36.01	110.0	1.70
	35.60	35.98	36.09	36.51	36.54	35.38
	35.96	37.37	36.92	37.09	36.76	34.64
	36.73	37.67	37.02	36.84	37.15	36.00
	38.19	38.20	37.84	36.69	37.74	38.38
	38.45	38.45	38.45	38.45	38.45	38.45
34.70	0.013	30.73	38.37	36.01	120.0	1.70
	35.55	35.99	36.10	36.50	36.53	35.40
	35.93	37.27	36.94	37.10	36.66	34.70
	36.66	37.60	36.96	36.83	37.07	36.04
	38.10	38.12	37.71	36.26	37.63	38.34
	38.37	38.37	38.37	38.37	38.37	38.3
35.05	0.014	29.82	38.12	36.07	130.0	1.70
	35.61	36.04	36.14	36.49	36.58	35.60
	36.00	37.10	36.86	37.03	36.66	35.05
	36.57	37.41	36.68	36.57	37.01	36.32
	37.87	37.89	37.40	36.03	36.94	38.11
	38.12	38.12	38.12	38.12	38.12	38.12

C_{sb} = 0.0851 m/s

13

23.34	0.007	30.70	40.70	23.98	10.0	2.4
	23.62	23.34	23.75	24.49	24.64	25.51
	25.51	25.22	25.07	26.01	26.73	25.51
	28.93	32.31	30.41	30.62	32.01	28.34
	34.70	38.11	36.43	37.06	38.36	34.38
	40.70	40.70	40.70	40.70	40.70	40.70
28.03	0.009	25.21	43.94	28.35	20.0	2.4
	28.23	28.03	28.71	28.84	28.33	27.98
	30.09	30.00	30.28	31.39	31.03	29.20
	33.62	37.27	35.35	36.59	35.68	31.64
	39.20	41.83	41.02	40.89	41.74	38.10
	43.94	43.94	43.94	43.94	43.94	43.94

28.89	0.010	30.60	41.65	29.51	30.0	2.4
	29.82	29.52	29.73	29.92	29.21	28.89
	31.69	31.72	31.29	31.29	31.66	30.15
	35.51	36.99	35.96	36.17	35.80	32.49
	39.27	40.37	39.76	39.40	40.09	38.13
	41.65	41.65	41.65	41.65	41.65	41.65
30.39	0.010	31.56	41.34	31.04	40.0	2.4
	31.30	31.10	31.30	31.41	30.74	30.39
	33.14	33.14	33.40	33.48	33.32	31.64
	36.51	38.05	36.57	36.53	36.93	34.64
	40.10	40.49	39.88	39.74	40.22	39.49
	41.34	41.34	41.34	41.34	41.34	41.34
31.59	0.010	32.77	38.91	32.03	50.0	2.4
	32.11	31.95	32.25	32.36	31.94	31.59
	33.59	34.25	33.71	34.06	33.58	32.36
	35.75	36.69	35.95	35.76	36.26	35.04
	35.05	38.35	37.96	37.74	38.22	38.06
	38.91	38.91	38.91	38.91	38.91	38.91
32.19	0.010	33.04	38.38	32.62	60.0	2.4
	32.75	32.53	32.76	33.04	32.45	32.19
	34.05	34.67	33.73	34.37	33.92	32.68
	35.69	36.42	35.80	35.65	36.12	35.11
	37.66	37.86	37.68	37.47	37.83	37.74
	38.38	38.38	38.38	38.38	38.38	38.38
32.42	0.0096	33.27	38.05	32.92	70.0	2.4
	32.96	32.87	33.14	33.39	32.77	32.42
	34.17	34.99	34.04	34.46	34.16	32.77
	35.76	36.48	35.60	35.78	36.06	35.11
	37.41	37.51	37.32	37.17	37.58	37.54
	38.05	38.05	38.05	38.05	38.05	38.05
33.12	0.009	33.58	37.73	33.41	80.0	2.4
	33.38	33.22	33.51	33.82	33.38	33.17
	34.46	35.44	34.45	34.96	34.88	33.12
	35.57	36.33	35.52	35.42	36.17	35.19
	37.29	37.29	37.18	36.87	37.14	37.42
	37.73	37.73	37.73	37.73	37.73	37.73
33.45	0.011	33.71	37.26	33.68	90.0	2.4
	33.68	33.54	33.79	33.98	33.64	33.46
	34.67	35.52	35.57	34.79	35.06	33.45
	35.37	36.08	35.13	35.18	35.95	36.99
	36.86	36.83	36.73	36.49	36.95	36.99
	37.26	37.26	37.26	37.26	37.26	37.26
33.62	0.0109	33.51	37.11	33.84	100.0	2.4
	33.82	33.74	33.88	34.13	33.87	33.62
	34.78	35.50	34.70	34.95	35.24	33.74
	35.46	36.17	35.12	35.32	35.92	35.33
	36.81	36.81	36.70	36.50	36.82	36.91
	37.11	37.11	37.11	37.11	37.11	37.11

33.33	0.0109	33.07	36.49	33.61	110.0	2.4
	33.63	33.49	33.61	33.97	33.65	33.33
	34.49	35.09	34.47	34.62	35.00	33.38
	34.95	35.55	34.68	34.81	35.37	34.74
	36.22	36.18	36.14	35.88	36.13	36.28
	36.49	36.49	36.49	36.49	36.49	36.49
33.58	0.0109	32.78	37.90	33.78	120.0	2.4
	33.74	33.62	33.75	34.17	33.83	33.58
	34.81	35.29	34.71	34.95	36.00	34.28
	36.21	36.88	35.92	36.15	36.69	35.92
	37.61	37.55	37.45	37.26	37.62	37.63
	37.90	37.90	37.90	37.90	37.90	37.90
34.00	0.011	32.26	36.88	34.10	130.0	2.4
	34.02	33.96	34.00	34.28	34.30	34.09
	34.76	35.20	34.61	34.70	35.53	34.57
	35.63	36.21	35.13	35.49	36.02	35.58
	36.68	36.65	36.53	36.28	36.61	36.78
	36.88	36.88	36.88	36.88	36.88	36.88

APPENDIX 11 FLOW ACROSS THE OUTLET WEIR

Table(9.1a) Compartment Flow per unit length of weir q/b =0.0032 m^3/s m
C_{sb} =0.0605 m/s

compartment	Level(cm)in Compartment	Total Flow in to comp $x10^{-3}m^3/min$	Flow per unit weir length m^3/s m
1	4.4	0.27	0.3
2	3.3	0.33	0.37
3	3.1	0.35	0.39
4	3.2	0.36	0.40
5	3.1	0.35	0.39
6	3.0	0.34	0.38
7	3.1	0.31	0.34
8	4.0	0.25	0.28

Table (9.1b) weir load(0.0048m^3/s m)

compartment	Level(cm)in Compartment	Total Flow in to comp x$10^{-3}m^3$/min	Flow per unit weir length m^3/s m
1	7.0	0.42	0.47
2	5.5	0.5	0.56
3	5.5	0.52	0.58
4	6.0	0.55	0.61
5	6.0	0.55	0.61
6	5.8	0.54	0.6
7	6.2	0.55	0.61
8	6.8	0.40	0.44

Table (9.1c) weir load(0.0064m^3/s m)

compartment	Level(cm)in Compartment	Total Flow in to comp x$10^{-3}m^3$/min	Flow per unit weir length m^3/s m (10^{-3})
1	11	0.59	0.66
2	9.5	0.76	0.84
3	7.0	0.62	0.69
4	7.2	0.63	0.7
5	7.4	0.64	0.71
6	7.1	0.62	0.69
7	9.5	0.76	0.84
8	10.5	0.57	0.63

Table (9.1d) weir load(0.008m^3/s m)

compartment	Level(cm)in Compartment	Total Flow in to comp x$10^{-3}m^3$/min	Flow per unit weir length m^3/s m (10^{-3})
1	16.0	0.7	0.78
2	14.0	1.0	1.11
3	10.0	0.81	0.9
4	10.0	0.81	0.9
5	10.1	0.82	0.91
6	10.2	0.83	0.92

7	15.0	1.04	1.16
8	15.0	0.69	0.77

Table (9.1e) weir load(0.00967m^3/s m)

compartment	Level(cm)in Compartment	Total Flow in to comp x$10^{-3}m^3$/min	Flow per unit weir length m^3/s m (10^{-3})
1	19.0	0.74	0.82
2	19.0	1.2	1.33
3	13.1	0.96	1.01
4	13.0	0.95	1.06
5	13.6	0.98	1.09
6	13.4	0.97	1.08
7	19.0	1.2	1.33
8	19.0	0.74	0.82

Table (9.1f) weir load(0.01128m^3/s m)

compartment	Level(cm)in Compartment	Total Flow in to comp x$10^{-3}m^3$/min	Flow per unit weir length m^3/s m (10^{-3})
1	22	0.77	0.86
2	20.4	1.26	0.14
3	17.0	1.13	0.126
4	17.6	1.15	1.128
5	17.8	1.17	1.13
6	17.6	1.15	1.128
7	20.2	1.25	1.138
8	21.2	0.76	0.84

Table (9.1g) weir load(0.0016m^3/s m) C_{sb} = 0.0775 m/s

compartment	Level(cm)in Compartment	Total Flow in to comp x$10^{-3}m^3$/min	Flow per unit weir length m^3/s m (10^{-3})
1	1.6	0.09	0.1
2	0.8	0.08	0.09
3	0.5	0.09	0.1
4	0.6	0.1	0.11
5	0.4	0.08	0.09
6	0.5	0.09	0.1
7	0.7	0.075	0.08
8	1.5	0.085	0.094

Table (9.1h) weir load(0.0032 m^3/s m) C_{sb} = 0.0775 m/s

compartment	Level(cm)in Compartment	Total Flow in to comp x$10^{-3}m^3$/min	Flow per unit weir length m^3/s m (10^{-3})
1	4.0	0.25	0.28
2	3.6	0.35	0.39
3	3.5	0.38	0.42
4	3.4	0.38	0.42
5	3.6	0.39	0.43
6	3.2	0.36	0.4
7	3.3	0.33	0.37
8	4.3	0.27	0.3

Table (9.1i) weir load(0.0048 m^3/s m) C_{sb} = 0.0775 m/s

compartment	Level(cm)in Compartment	Total Flow in to comp x$10^{-3}m^3$/min	Flow per unit weir length m^3/s m (10^{-3})
1	7.0	0.42	0.47
2	7.5	0.64	0.71
3	5.1	0.51	0.56
4	6.3	0.47	0.52
5	6.6	0.49	0.54
6	6.0	0.45	0.5
7	7.4	0.63	0.7
8	7.0	0.42	0.47

Table (9.1j) weir load(0.0064 m^3/s m) C_{sb} = 0.0775 m/s

compartment	Level(cm)in Compartment	Total Flow in to comp $x10^{-3}m^3/min$	Flow per unit weir length m^3/s m
1	10.5	0.48	0.53
2	10.0	0.79	0.88
3	7.4	0.64	0.71
4	7.3	0.63	0.7
5	7.5	0.65	0.72
6	7.6	0.68	0.76
7	9.6	0.76	0.84
8	10.3	0.47	0.52

Table (9.1k) weir load(0.008 m^3/s m) C_{sb} = 0.0775 m/s

compartment	Level(cm)in Compartment	Total Flow in to comp $x10^{-3}m^3/min$	Flow per unit weir length m^3/s m (10^{-3})
1	15.0	0.69	0.77
2	14.8	1.03	1.14
3	10.2	0.81	0.9
4	10.6	0.83	0.92
5	10.7	0.835	0.93
6	10.5	0.83	0.92
7	15.0	1.04	1.16
8	15.1	0.69	0.77

Table (9.1l) weir load(0.00967 m^3/s m) C_{sb} = 0.0775 m/s

compartment	Level(cm)in Compartment	Total Flow in to comp $x10^{-3}m^3/min$	Flow per unit weir length m^3/s m (10^{-3})
1	17.0	0.72	0.8
2	19.4	1.2	1.36
3	14.1	1.01	1.12
4	13.8	0.99	1.1
5	13.9	1.0	1.11
6	13.9	1.0	1.11
7	19.2	1.2	1.33

8	17.0	0.72	0.8

Table (9.1m) weir load(0.0113 m^3/s m) C_{sb} = 0.0775 m/s

compartment	Level(cm)in Compartment	Total Flow in to comp $x10^{-3}m^3/min$	Flow per unit weir length m^3/s m(10^{-3})
1	20.0	0.75	0.83
2	20.0	1.24	1.38
3	18.1	1.18	1.31
4	17.9	1.17	1.3
5	18.2	1.19	1.32
6	17.8	1.17	1.3
7	20.0	1.24	1.38
8	19.6	0.74	0.82

Table (9.1n) weir load(0.0016 m^3/s m) C_{sb} = 0.0851 m/s

compartment	Level(cm)in Compartment	Total Flow in to comp $x10^{-3}m^3/min$	Flow per unit weir length m^3/s m(10^{-3})
1	1.8	0.1	0.11
2	0.85	0.1	0.11
3	0.7	0.11	0.12
4	0.8	0.12	0.13
5	0.7	0.11	0.12
6	0.7	0.11	0.12
7	0.9	0.1	0.11
8	1.7	0.08	0.09

Table (9.1o) weir load(0.0032 m^3/s m) C_{sb} = 0.0851 m/s

compartment	Level(cm)in Compartment	Total Flow in to comp $x10^{-3}m^3/min$	Flow per unit weir length m^3/s m(10^{-3})
1	4.2	0.26	0.29
2	3.7	0.36	0.4
3	3.6	0.39	0.43
4	3.5	0.38	0.42
5	3.4	0.37	0.41

6	3.3	0.36	0.4
7	3.4	0.34	0.37
8	4.1	0.25	0.28

Table (9.1p) weir load(0.0048 m^3/s m) C_{sb} = 0.0851m/s

compartment	Level(cm)in Compartment	Total Flow in to comp $x10^{-3}m^3/min$	Flow per unit weir length m^3/s m(10^{-3})
1	6.7	0.41	0.45
2	7.8	0.65	0.72
3	5.6	0.53	0.59
4	6.8	0.60	0.67
5	6.4	0.58	0.64
6	6.9	0.61	0.68
7	7.0	0.61	0.68
8	6.3	0.39	0.43

Table (9.1q) weir load(0.0064 m^3/s m) C_{sb} = 0.0851 m/s

compartment	Level(cm)in Compartment	Total Flow in to comp $x10^{-3}m^3/min$	Flow per unit weir length m^3/s m(10^{-3})
1	10.1	0.56	0.62
2	10.3	0.8	0.89
3	7.9	0.68	0.76
4	7.7	0.665	0.74
5	7.8	0.67	0.74
6	8.0	0.69	0.77
7	9.9	0.78	0.87
8	9.6	0.55	0.61

Table (9.1r) weir load(0.008 m^3/s m) C_{sb} = 0.0851 m/s

compartment	Level(cm)in Compartment	Total Flow in to comp $x10^{-3}m^3/min$	Flow per unit weir length m^3/s m(10^{-3})
1	14.4	0.68	0.76
2	13.0	0.95	1.06
3	11.2	0.82	0.91

4	11.5	0.88	0.98
5	11.7	0.89	0.99
6	11.9	0.9	1.0
7	12.9	0.94	1.04
8	14.1	0.67	0.74

Table (9.1s) weir load(0.00967 m^3/s m) C_{sb} = 0.0851 m/s

compartment	Level(cm)in Compartment	Total Flow in to comp $x10^{-3}m^3/min$	Flow per unit weir length m^3/s m(10^{-3})
1	16.5	0.72	0.8
2	19.5	1.22	1.35
3	15.0	1.04	1.16
4	14.6	1.03	1.14
5	15.0	1.04	1.16
6	14.9	1.02	1.13
7	18.0	1.17	1.3
8	16.2	0.71	0.79

Table (9.1t) weir load(0.01128 m^3/s m) C_{sb} = 0.0851 m/s

compartment	Level(cm)in Compartment	Total Flow in to comp $x10^{-3}m^3/min$	Flow per unit weir length m^3/s m(10^{-3})
1	19.0	0.74	0.82
2	20.0	1.24	1.34
3	18.8	1.21	1.34
4	18.8	1.21	1.34
5	18.9	1.215	1.35
6	18.8	1.21	1.34
7	20.0	1.24	1.38
8	18.7	0.73	0.81

APPENDIX 12 EDDY DIFFUSION COEFFICIENT (De)

Appendix (12.1) 1 mm Hole Diameter Tray Results

RUN 1 Sample calculation table for plots of $Log(x - x_o)/(x_g - x_o)$ versus 1-W

SAMPLE POINT	CONCN	$(x - x_o/x_g - x_o)$	1 - W
1	0.6	1	1
2	0.26	0.39	0.11
3	0.14	0.13	0.23
4	0.102	0.06	0.34
5	0.084	0.026	0.45
6	0.078	0.01	0.57

SAMPLE POINTS	WEIR LOAD (q/b) m^3/s m			
	0.00124	0.00249	0.00373	0.00497
1 (inlet grid)	1	1	1	1
2	0.39	0.18	0.1	0.3
3	0.13	0.03		
4	0.06			
5	0.026			
6	0.01			

RUN 2

SAMPLE POINTS	WEIR LOAD (q/b) m^3/s m			
	0.00124	0.00249	0.00373	0.00497
		$Log[(x - x_o)/(x_g - x_o)]$		
1 (inlet grid)	1	1	1	1
2	0.52	0.26	0.27	0.2
3	0.27	0.12	0.07	0.03
4	0.16	0.046	0.021	
5	0.08	0.016		
6	0.04			
7	0.024			
8	0.013			

RUN 3

SAMPLE POINTS	WEIR LOAD (q/b) m^3/s m			
	0.00124	0.00249	0.00373	0.00497
		$Log[(x - x_o)/(x_g - x_o)]$		
1 (inlet grid)	1	1	1	1
2	0.25	0.39	0.2	0.1
3	0.06	0.14	0.05	
4	0.02	0.05		
5	0.005	0.019		
6	0.001			

RUN 4

SAMPLE POINTS	0.00124	WEIR LOAD (q/b) m^3/s m 0.00249	0.00373	0.00497
		$Log[(x - x_o)/(x_g - x_o)]$		
1 (inlet grid)	1	1	1	1
2	0.48	0.2	0.07	0.036
3	0.19	0.046	0.02	
4	0.09	0.011		
5	0.05	0.0026		
6	0.024			
7	0.012			

RUN 5

SAMPLE POINTS	0.00124	WEIR LOAD (q/b) m^3/s m 0.00249	0.00373	0.00497
		$Log[(x - x_o)/(x_g - x_o)]$		
1 (inlet grid)	1	1	1	1
2	0.6	0.44	0.31	0.33
3	0.35	0.2	0.13	0.1
4	0.21	0.091	0.05	0.04
5	0.013	0.043	0.02	0.016
6	0.08	0.02	0.005	
7	0.05	0.009		
8	0.027			
9	0.017			

RUN 6

SAMPLE POINTS	0.00124	WEIR LOAD (q/b) m^3/s m 0.00249	0.00373	0.00497
		$Log[(x - x_o)/(x_g - x_o)]$		
1 (inlet grid)	1	1	1	1
2	0.25	0.26	0.16	0.06
3	0.056	0.06	0.03	
4	0.022	0.015		
5	0.006			
6	0.0014			

RUN 7

SAMPLE POINTS	0.00124	WEIR LOAD (q/b) m^3/s m 0.00249	0.00373	0.00497
		$Log[(x - x_o)/(x_g - x_o)]$		
1 (inlet grid)	1	1	1	1
2	0.58	0.34	0.21	0.11
3	0.31	0.11	0.04	0.01
4	0.18	0.034	0.009	0.0013
5	0.1	0.017	0.0023	
6	0.06	0.005		
7	0.04	0.0017		
8	0.021			
9	0.011			

RUN 8

SAMPLE POINTS	WEIR LOAD (q/b) m^3/s m			
	0.00124	0.00249	0.00373	0.00497
		$Log[(x - x_o)/(x_g - x_o)]$		
1 (inlet grid)	1	1	1	1
2	0.62	0.47	0.34	0.27
3	0.41	0.22	0.11	0.1
4	0.28	0.1	0.044	0.026
5	0.18	0.05	0.017	0.06
6	0.12	0.023	0.006	
7	0.08	0.012	0.002	
8	0.05			
9	0.034			

Appendix (12.2) Results for 12.5mm diameter hole Tray (Values of Log (x-xo)/(xg-xo) at increasing weir load and constant air capacity factors (C_{sb})

RUN 1

SAMPLE POINTS	WEIR LOAD (q/b) m^3/s m			
	0.00124	0.00249	0.00373	0.00497
		$Log[(x - x_o)/(x_g - x_o)]$		
1 (inlet grid)	1	1	1	1
2	0.3	0.14	0.11	0.11
3	0.06	0.019	0.007	0.009
4	0.02	0.0024		
5	0.0056			
6	0.0014			

RUN 2

SAMPLE POINTS	WEIR LOAD (q/b) m^3/s m			
	0.00124	0.00249	0.00373	0.00497
		$Log[(x - x_o)/(x_g - x_o)]$		
1 (inlet grid)	1	1	1	1
2	0.41	0.14	0.09	0.09
3	0.14	0.015	0.008	0.008
4	0.02	0.0018		
5	0.007			
6	0.0026			

RUN 3

SAMPLE POINTS	WEIR LOAD (q/b) m^3/s m			
	0.00124	0.00249	0.00373	0.00497
		$Log[(x - x_o)/(x_g - x_o)]$		
1 (inlet grid)	1	1	1	1
2	0.56	0.4	0.4	0.30
3	0.28	0.13	0.14	0.1
4	0.15	0.05	0.049	0.02
5	0.08	0.02	0.02	0.005
6	0.04	0.007	0.007	
7	0.023	0.0029		

RUN 4

SAMPLE POINTS	WEIR LOAD (q/b) m^3/s m			
	0.00124	0.00249	0.00373	0.00497
		$Log[(x - x_o)/(x_g - x_o)]$		
1 (inlet grid)	1	1	1	1
2	0.27	0.12	0.06	0.06
3	0.06	0.016		
4	0.017	0.002		
5	0.004			
6	0.001			

RUN 5

SAMPLE POINTS	WEIR LOAD (q/b) m^3/s m			
	0.00124	0.00249	0.00373	0.00497
		$Log[(x - x_o)/(x_g - x_o)]$		
1 (inlet grid)	1	1	1	1
2	0.4	0.24	0.086	0.048
3	0.016	0.049		
4	0.026			
5	0.01			

RUN 6

SAMPLE POINTS	WEIR LOAD (q/b) m^3/s m			
	0.00124	0.00249	0.00373	0.00497
		$Log[(x - x_o)/(x_g - x_o)]$		
1 (inlet grid)	1	1	1	1
2	0.4	0.4	0.33	0.35
3	0.18	0.15	0.11	0.11
4	0.07	0.05	0.028	0.027
5	0.03	0.02		
6	0.012			

RUN 7

SAMPLE POINTS	WEIR LOAD (q/b) m^3/s m			
	0.00124	0.00249	0.00373	0.00497
		$Log[(x - x_o)/(x_g - x_o)]$		
1 (inlet grid)	1	1	1	1
2	0.41	0.2	0.1	0.09
3	0.06	0.04		
4	0.024			
5	0.007			
6	0.0031			

RUN 8

SAMPLE POINTS	WEIR LOAD (q/b) m^3/s m			
	0.00124	0.00249	0.00373	0.00497
		$Log[(x - x_o)/(x_g - x_o)]$		
1 (inlet grid)	1	1	1	1
2	0.38	0.2	0.13	0.066
3	0.12	0.047	0.08	
4	0.045			
5	0.016			
6	0.0046			

RUN 9

SAMPLE POINTS	WEIR LOAD (q/b) m^3/s m			
	0.00124	0.00249	0.00373	0.00497
		Log[(x - x_o)/(x_g - x_o)]		
1 (inlet grid)	1	1	1	1
2	0.4	0.44	0.23	0.19
3	0.15	0.17	0.032	0.046
4	0.06	0.07	0.006	
5	0.024	0.032		
6	0.009	0.013		
7	0.0037	0.005		

RUN 10

SAMPLE POINTS	WEIR LOAD (q/b) m^3/s m			
	0.00124	0.00249	0.00373	0.00497
		Log[(x - x_o)/(x_g - x_o)]		
1 (inlet grid)	1	1	1	1
2	0.45	0.24	0.19	0.19
3	0.18	0.03	0.04	0.022
4	0.07	0.006		
5	0.032			
6	0.013			
7	0.005			

RUN 11

SAMPLE POINTS	WEIR LOAD (q/b) m^3/s m			
	0.00124	0.00249	0.00373	0.00497
		Log[(x - x_o)/(x_g - x_o)]		
1 (inlet grid)	1	1	1	1
2	0.51	0.26	0.16	0.13
3	0.28	0.07	0.03	0.018
4	0.15	0.02		
5	0.08	0.004		
6	0.04			
7	0.02			
8	0.011			

RUN 12

SAMPLE POINTS	WEIR LOAD (q/b) m^3/s m			
	0.00124	0.00249	0.00373	0.00497
		Log[(x - x_o)/(x_g - x_o)]		
1 (inlet grid)	1	1	1	1
2	0.48	0.38	0.35	0.33
3	0.21	0.13	0.1	0.08
4	0.09	0.05	0.028	0.02
5	0.04	0.018	0.007	
6	0.019	0.005		
7	0.009			

Table(10.4)

12.5 mm Hole Tray Results of Eddy Diffusion Coeff(De) , Peclet number(Pe) & Liquid Hold-Up on the Trays

Weir mm	C_{sb} m/s	Hold-up mm	weir load $m^3/s\ m$	NPE P_e	D_e m^2/s
37.5	0.06196	22	0.00124	26.99	0.00117
		25.0	0.00249	39.77	0.0014
		27.5	0.00373	45.65	0.00166
		31.0	0.00497	47.105	0.0019
37.5	0.0876	11.0	0.00124	20.0049	0.0032
		14.5	0.00249	41.54	0.0023
		19.5	0.00373	52.96	0.002
		21.0	0.00497	52.96	0.002
37.5	0.1073	0.5	0.00124	12.76	0.1088
		2.5	0.00249	19.76	0.028
		7.5	0.00373	23.58	0.01178
		9.0	0.00497	15.11	0.020
50.0	0.06196	24.0	0.00124	27.87	0.0010
		29.0	0.00249	42.04	0.00114
		32.5	0.00373	58.83	0.0011
		36.5	0.00497	58.82	0.0013
50.0	0.08766	14.0	0.00124	18.58	0.0027
		20.5	0.00249	30.57	0.0022
		23.0	0.00373	51.30	0.0018
		26.5	0.00497	63.49	0.00165
50.0	0.1073	1.5	0.00124	17.84	0.026
		4.5	0.00249	19.99	0.015
		11.0	0.00373	24.19	0.0078
		15.5	0.00497	24.43	0.0073
65.5	0.06196	27.5	0.00124	19.54	0.0013
		32.5	0.00249	32.19	0.0013
		36.0	0.00373	48.14	0.0012
		41.5	0.00497	50.35	0.0013
62.5	0.08766	18.0	0.00124	21.72	0.0018
		25.5	0.00249	30.58	0.0018
		30.0	0.00373	25.26	0.0027
		56.21	0.00497	56.21	0.0016
62.5	0.1073	1.0	0.00124	18.94	0.037
		7.0	0.00249	17.92	0.011
		15.0	0.00373	34.61	0.004
		20.0	0.00497	30.79	0.0045

75.0	0.06196	32.0	0.00124	17.92	0.0012
		36.0	0.00249	34.61	0.0011
		40.0	0.00373	32.19	0.0016
		45.0	0.00497	25.82	0.0031
75	0.08766	21.5	0.00124	12.97	0.0025
		28.0	0.00249	28.22	0.0018
		31.0	0.00373	35.07	0.0019
		33.0	0.00497	40.17	0.0021
75.0	0.1073	1.0	0.00124	15.93	0.044
		14.0	0.00249	21.38	0.0046
		22.0	0.00373	25.36	0.0037
		25.5	0.00497	26.46	0.0041

Table (10.5) Results for the 1mm diameter holes tray.

Weir mm	C_{sb} m/s	Hold-up mm	Weir load $m^3/s\ m$	NPE P_e	D_e m^2/s
25.0	0.08766	22.0	0.00124	18.58	0.0017
		23.0	0.00249	35.25	0.0017
		25.3	0.00373	48.14	0.0017
		27.5	0.00497	25.17	0.004
25.0	0.1073	12.7	0.00124	27.56	0.002
		14.5	0.00249	19.94	0.0048
		16.7	0.00373	31.32	0.004
		18.0	0.00497	48.14	0.0032
37.5	0.06196	22.3	0.00124	12.59	0.0025
		25.0	0.00249	21.025	0.0026
		27.0	0.00373	26.93	0.0029
		31.0	0.00497	35.07	0.0026
37.5	0.08766	11.0	0.00124	14.92	0.0042
		14.5	0.00249	31.38	0.003
		19.5	0.00373	42.85	0.002
		21.0	0.00497	70.1	0.0019
37.5	0.1073	0.6	0.00124	10.30	0.112
		2.6	0.00249	15.93	0.034
		7.5	0.00373	22.49	0.012
		9.0	0.00497	21.01	0.015
50.0	0.06196	24.0	0.00124	26.24	0.0011
		29.0	0.00249	27.97	0.0017
		32.5	0.00373	35.07	0.0018
		36.5	0.00497	62.64	0.0012

50.0	0.08766	14.0	0.00124	11.30	0.0044
		20.5	0.00249	21.57	0.0031
		22.9	0.00373	31.99	0.0028
		26.5	0.00497	40.62	0.0026
50.0	0.1073	1.5	0.00124	8.51	0.054
		4.5	0.00249	15.25	0.02
		10.8	0.00373	20.85	0.0095
		15.6	0.00497	26.15	0.0068

APPENDIX 13 CALIBRATION GRAPHS FOR THE THERMOCOUPLES

(See next page)

LaserShare™ Print Server

User: CHRIS

Application: MacWrite

Document: list of figures

Date: 24/1/89

Time: 6:45:35 pm

Pages: 0

LaserWriter: LaserWriter

Spooler: LaserWriter Spooler

Status: Deleted

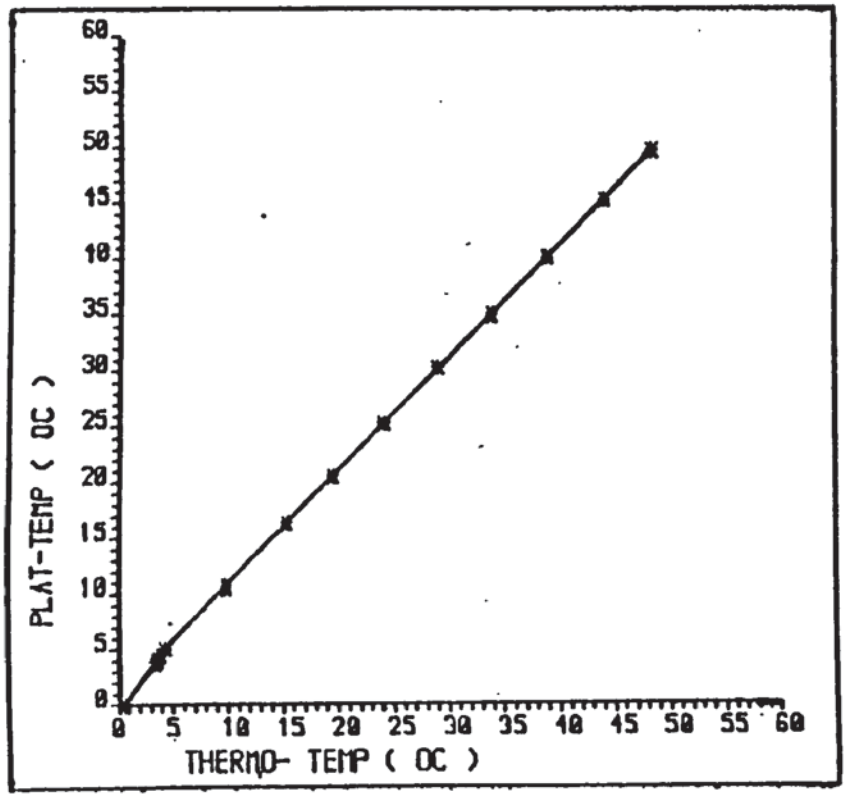

THERMO-CALIBRATION-GRAPH(-2-)

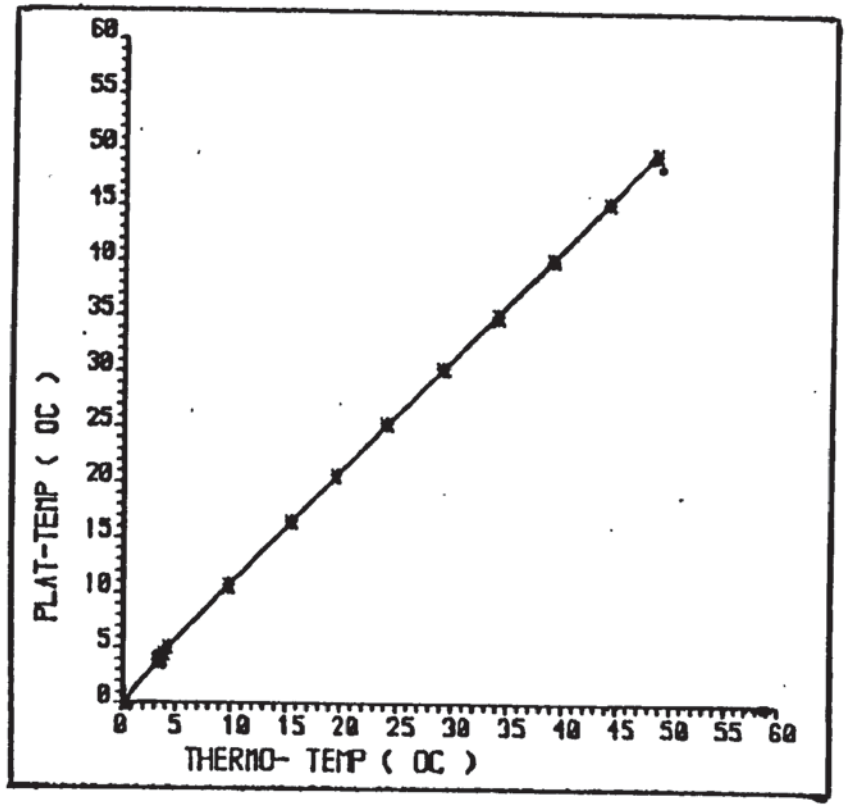

THERMO-CALIBRATION-GRAPH(-1-)

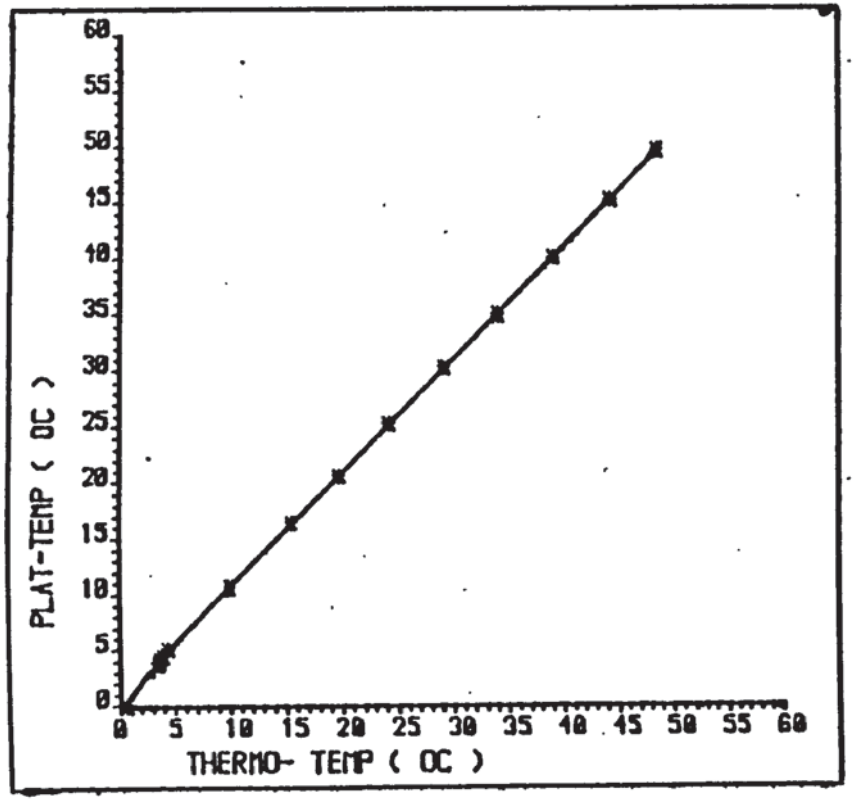

THERMO-CALIBRATION-GRAPH(-4-)

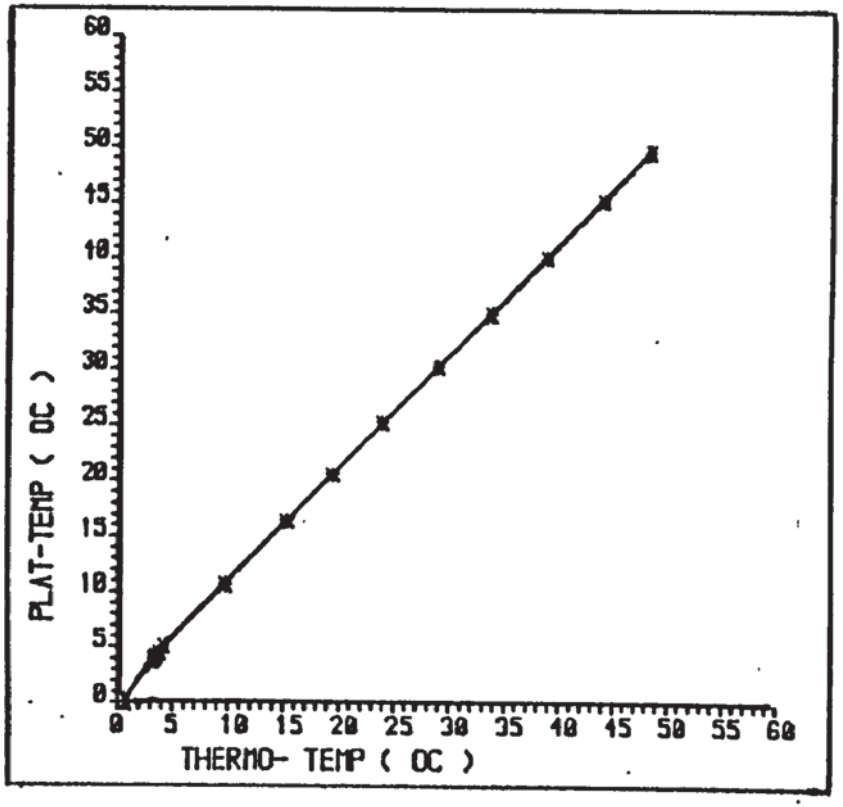

THERMO-CALIBRATION-GRAPH(-3-)

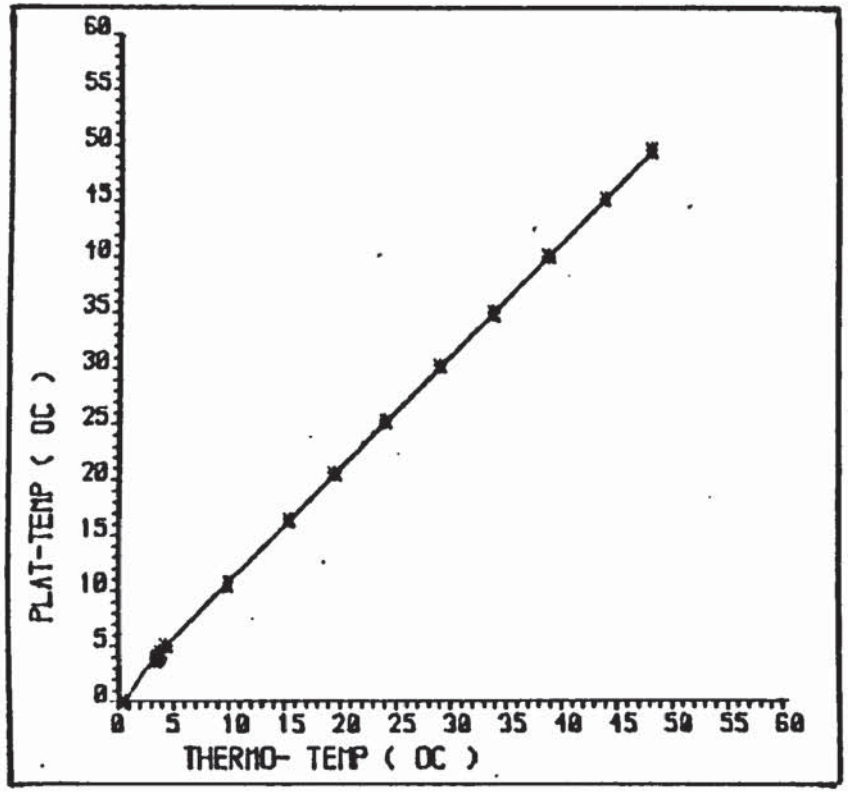

THERMO-CALIBRATION-GRAPH(- 6 -)

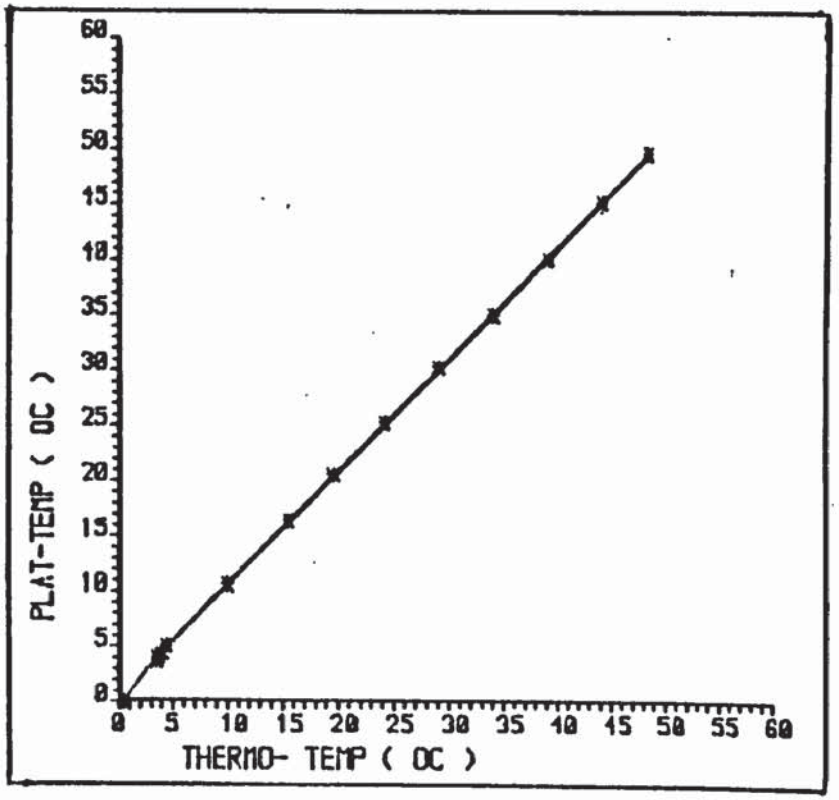

THERMO-CALIBRATION-GRAPH(- 5 -)

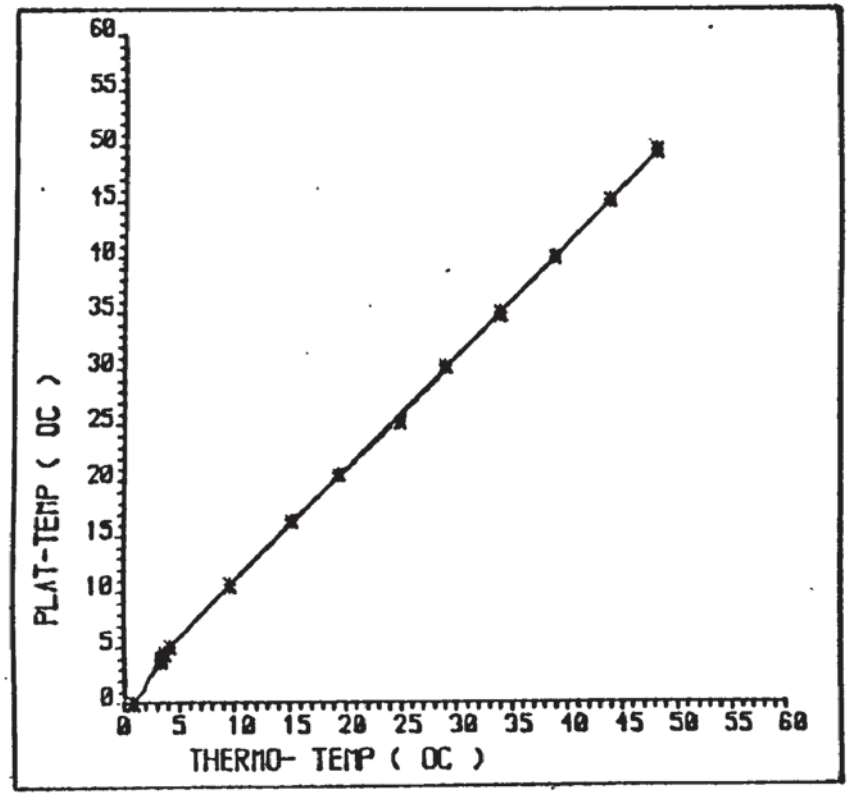

THERMO-CALIBRATION-GRAPH(- 7 -)

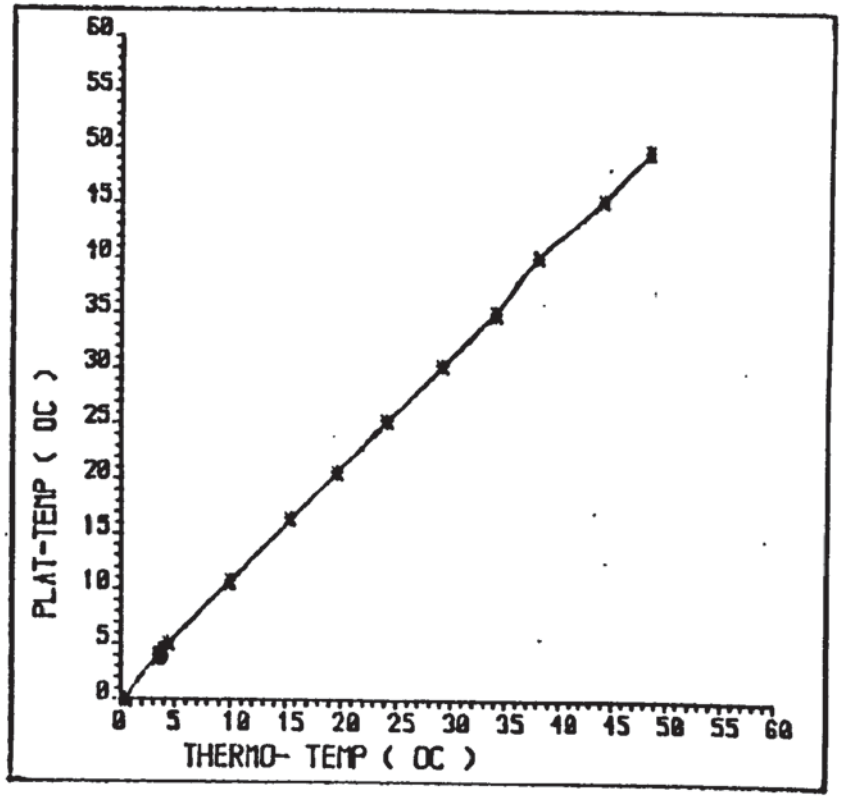

THERMO-CALIBRATION-GRAPH(- 8 -)

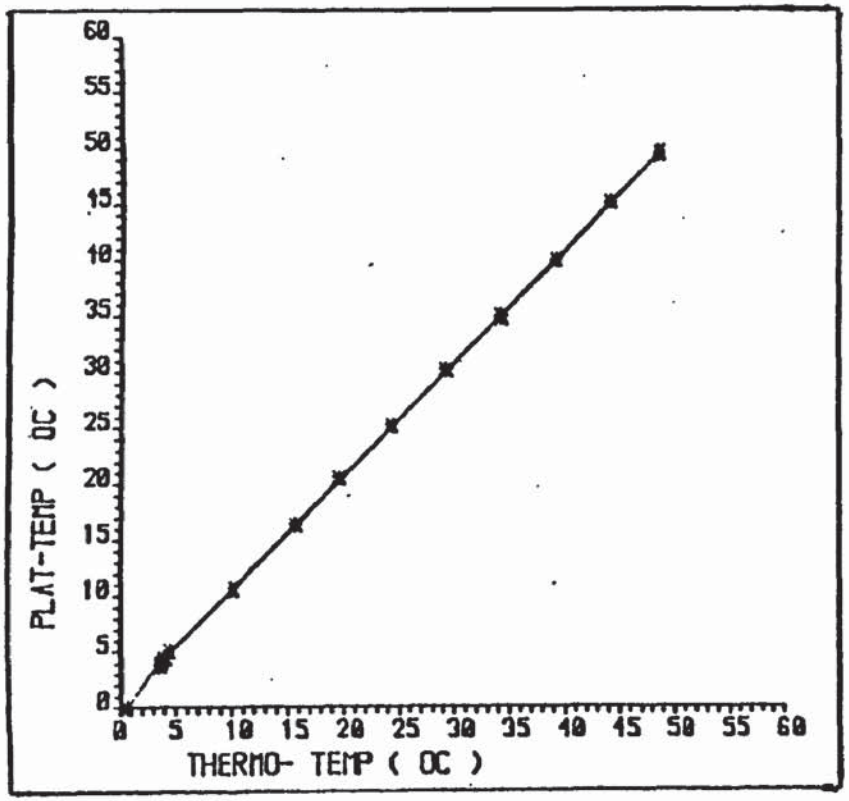

THERMO-CALIBRATION-GRAPH(-9-)

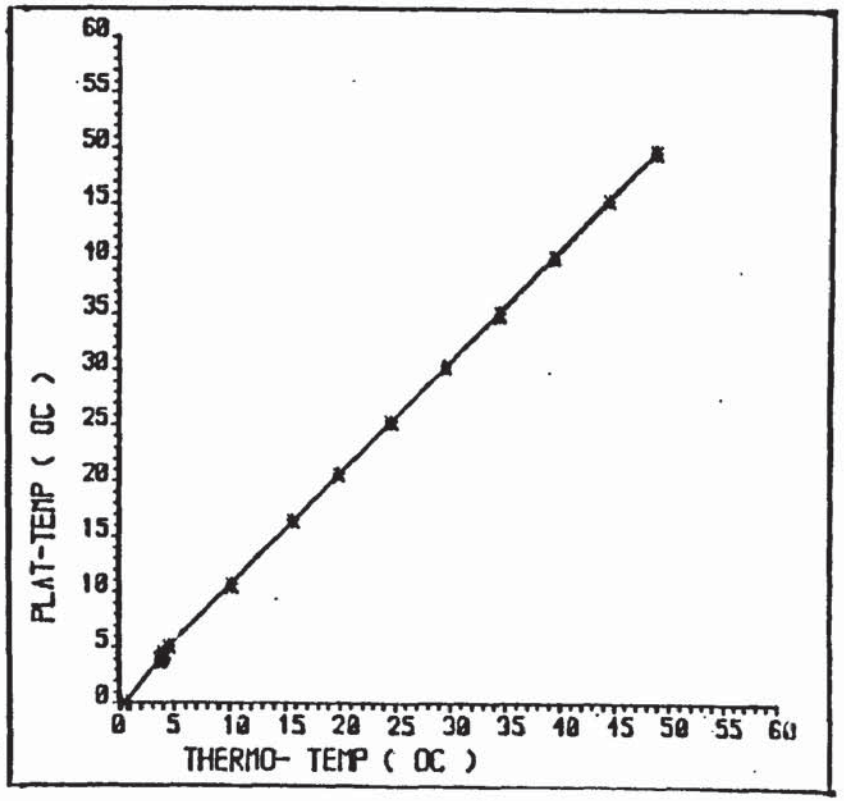

THERMO-CALIBRATION-GRAPH(-10-)

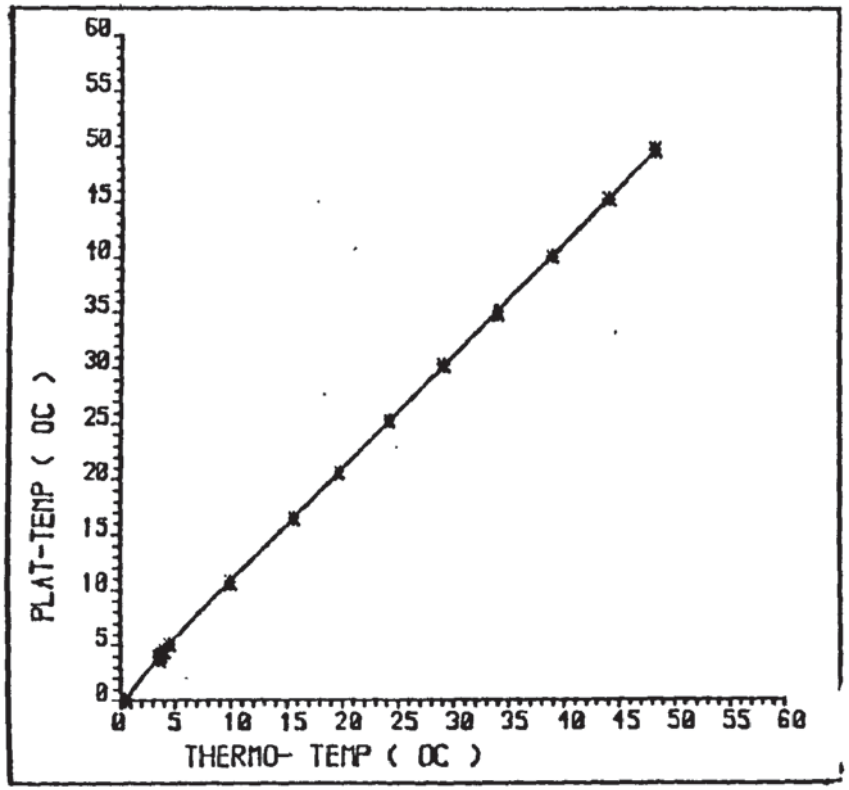

THERMO-CALIBRATION-GRAPH(-12-)

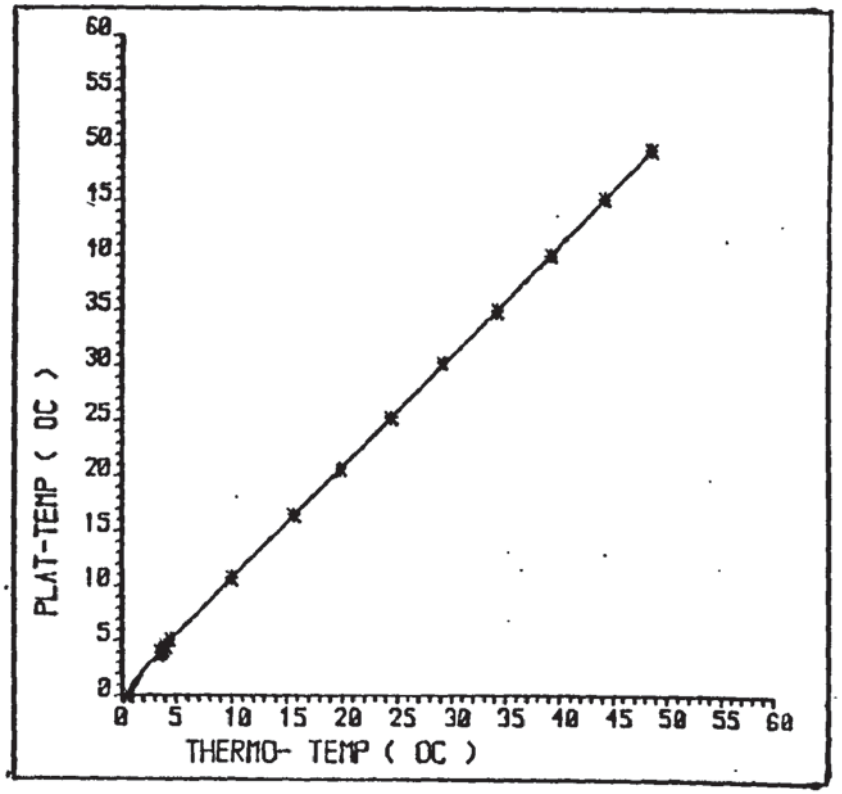

THERMO-CALIBRATION-GRAPH(-11-)

APPENDIX 14 COMPUTER PROGRAMS

```
CCCC PROGRAM TO DRAW LINES OF CONSTANT TEMPS USING EACH SCAN
                              VALUE
CCCC          ALSO PLOT THE AVERAGE VALUES
CCCC           DY CHRISTIAN CHIKODILI ANI.
      COMMON/AA/AT(60,50),BT(60,50),ZT(60,50)
      COMMON/AAA/ W(7000)
      COMMON/PPP/ XP(30),YP(30)
      DIMENSION TTOU(30),TTH(30),TTA(30),TTIN(30)
      DIMENSION TTOUT(30),TTL(30),TTG(30),X(30),Y(30),Z(30)
      DIMENSION ZZ(540),ZN(30),HF(30),ZIM(5,6),EOG2(30)
      REAL  A,B,G,L,GF,TI,TT,HF2,TIN,TOUT,LL,V,JI,LAMDA,LAMDAEOG,G1,
       L1,ZZZ
      REAL  MOP,H1,H2,TA,EOG,EMV,HFN,HFNA,G11,G12,G13,CL,HF3,AA,
       RUN,CSB
      REAL LLOAD,EOG1,EVEO
      INTEGER I,J,IV,NAMU,CHIME,S
      COMMON/NUM/NIN,NDATA,NSCR,NRESULT,NNRESULT,LLRESULT
      CHARACTER CHOICE*5
      SPECIAL COMMON AA
      SPECIAL COMMON AAA
C     ************************************************************
      NIN=0
      NDATA=101
      NZDATA=21
      NSCR=3
      NRESULT=102
      NNRESULT=103
      LLRESULT=104
C     ************************************************************
C     CALL FOPEN(NRESULT)
      CALL FOPEN(NDATA)
C     ************************************************************
C     SET up arrays X,Y,Z of 30 data points
C     ************************************************
C     READ THE DATA FROM CHENNEL 7
C     ************************************************
```

```
      WRITE(3,'(" INPUT THE VALUE OF NZSET1")')
      READ *, NZSET1
      READ(NDATA,*) NZSET
      IM=0
      DO 559 J=1,NZSET1
      READ(NDATA,*) TTOU(J),TTH(J),TTA(J),TTIN(J),TTOUT(J),TTL(J),TTG(J)
      DO 664 K=1,5
      READ (NDATA,*) (ZIM(K,I),I=1,6)
  664 CONTINUE
  559 CONTINUE
      DO 555 J=1,NZSET-NZSET1
      READ(NDATA,*) TTOU(J),TTH(J),TTA(J),TTIN(J),TTOUT(J),TTL(J),TTG(J)
      DO 554 K=1,5
      READ (NDATA,*) (ZIM(K,I),I=1,6)
  554 CONTINUE
      DO 553 K=1,5
      DO 553 I=1,6
      IM=IM+1
      ZZ(IM)=ZIM(K,I)
  553 CONTINUE
  555 CONTINUE
      CALL FOPEN(NRESULT)
       WRITE(NRESULT,290)
  290   FORMAT('RESULT OF TEMP FIELD AND CALCULATED EFFICIENCY'/)
C     PUT THE INLET TEMPERATURE OF LIQUID IN DCM 37.08 DEG.C
       ND=30
       RUN = 0.0
      NJ=0
      NCOUNT=0
      NCC=0
       PRINT*,"INPUT THE VALUE OF Csb "
       READ*,CSB
       DO 99 JJ1=1,NZSET
       II=0
      TOU=TTOU(NCOUNT+1)
      H=TTH(NCOUNT+1)
      TA=TTA(NCOUNT+1)
      TIN=TTIN(NCOUNT+1)
```

```
      TOUT=TTOUT(NCOUNT+1)
      L=TTL(NCOUNT+1)
      G=TTG(NCOUNT+1)
CC      PRINT*,"INPUT THE VALUE OF Z(I) FOR I=25,30 "
      RUN = RUN + 1.0
      WRITE(NRESULT,300)RUN
300   FORMAT("RUN NO ",5X,F10.0/)
      WRITE(NRESULT,301)CSB
301   FORMAT("Csb =",10X,F10.7)
      LLOAD =L * 8.0603E-5
      WRITE(NRESULT,302)LLOAD
302   FORMAT("LIQUID LOADING (Q/b)=",10X,F10.8/)
      WRITE(NRESULT,5556)
      WRITE(NRESULT,5555) TOU,H,TA,TIN,TOUT,L,G
 5556 FORMAT(' TOU . H . TA . TIN . TOUT .
     * L . G .')
 5555 FORMAT(7F10.5/)
      WRITE(NRESULT,5557)
5557   FORMAT(/'MEASURED POINT TEMPERATURES ON THE TRAY')
C
      DO 88 I=1+NJ,30+NJ
      II=II+1
      Z(II)=ZZ(I)
   88 CONTINUE
      N = 1
      DO 111 I=1,5
      WRITE(NRESULT,222)(Z(II),II=N,N+5)
      N = N + 6
111   CONTINUE
222   FORMAT(6F8.2)
C
CC   NCOUNT=NCOUNT+1
C
CCCC  CHOICE OF EITHER CONTOURS(2-D)OR ISOMETRIC(3-D) DRAWING
      PRINT*
      WRITE(NSCR,220)
 220  FORMAT(/"DO YOU WANT A 2-D OR 3-D PLOT OF TEMP. PROFILES?")
1000  PRINT*,"ENTER ""2"" FOR 2-D OR ""3"" FOR 3-D"
```

```
      READ*,NAMU
        IF (NAMU.NE.2.AND.NAMU.NE.3) GOTO 1000
      IF (NAMU.EQ.3) THEN
CCCC  choose viewpoint for 3-d plot
       PRINT*
       PRINT*,"FROM WHICH ANGLE DO YOU WISH TO VIEW THE PLOT?"
       PRINT*,"INPUT VALUE OF ""IV"" AS FOLLOWS:"
       PRINT*,"(INLET AT TOP OF PLOT, OUTLET AT BOTTOM)"
       PRINT*,"VALUE OF IV   CORNER VIEWED FROM"
       PRINT*,"   0        BOTTOM LEFT"
       PRINT*,"   1        BOTTOM RIGHT"
       PRINT*,"   2        TOP RIGHT"
       PRINT*,"   3        TOP LEFT"
2000  READ*,IV
       IF (IV.NE.0.AND.IV.NE.1.AND.IV.NE.2.AND.IV.NE.3) THEN
        PRINT*,"PLEASE ENTER ONLY 0,1,2, OR 3"
        GOTO 2000
       END IF
      END IF
CCCC  CHOICE OF PLOTTING DEVICE EITHER TERMINALOR GRAPHIC PLOTTER
      PRINT*
      PRINT*,"GRAPHICAL OUTPUT TO TERMINAL OR GRAPH PLOTTER?"
3000  PRINT*,"ENTER ""T"" FOR TERMINAL OR ""G"" FOR PLOTTER"
      READ "(A)",CHOICE
      IF (CHOICE.NE."T".AND.CHOICE.NE."G") GOTO 3000
      PRINT*
         IF (CHOICE.EQ."T") THEN
CC
        CL = 4.18
        ML = 18.0
        MG = 29.0
        PL = 1000.0
        JI = 2495.0
        CA = 1.003
        CW = 2.006
        TAIR = TA + 273.0
CC
        TT = TOUT + 273.0
```

```
      TI = TIN + 273.0
CC
      H1 = CA*(TAIR-273.0) + H*(CW*(TAIR-273.0) + JI)
      PRINT*,"H1=",H1
CC
      G11 = (H/18.0)/(1.0/29.0)
      G12 =(1-G11)*G
      G13 = (29.0/22.4)*(273.0/TAIR)
      G1 = G12 * G13
       PRINT*,"G1=",G1
        WRITE(NRESULT,30)G1
30       FORMAT(/"G1 =",10X,F10.6)
      L1 = (L*PL*7.577E-5)/(8554.0/1.0E4)
      PRINT*,"L1=",L1
       WRITE(NRESULT,40)L1
40      FORMAT("L1 =",10X,F10.6/)
CCCC  CALCULATION OF THE SLOPE FOR THE OPERATING LINE
      MOP = (L1*CL)/G1
CC
       H2 = (MOP*(TI-TT)) + H1
       PRINT*,"H2=",H2
CC
       HFN =0.0
       DO 5 I=1,ND
       NCC= NCC+1
         ZN(I) = ZZ(NCC) + 273.0
   HO=-25.556+(ZN(I)*0.26465)-((ZN(I)**2)*9.16147E-4)+((ZN(I)**3)*1.
  *06061E-6)
        HF(I)=(CA*(ZN(I)-273.0))+(HO*(CW*(ZN(I)-273.0) + JI))
        HFN = HFN + HF(I)
    H3 = (MOP*(TI-ZN(I))) + H1
       EOG2(I) = (H3 - H1)/(HF(I) - H1)
CCC
CC       WRITE(NRESULT,2222)EOG1
5        CONTINUE
       WRITE(NRESULT,2222)
```

```
2222      FORMAT('   ZN(I) *     EOG1    ')
      DO 2 I=1,ND
        WRITE(NRESULT,2223)ZN(I)-273,EOG2(I)
2     CONTINUE
2223      FORMAT(2(F10.5))
      CALL MAINTEMP(30,ZN,HF,5,5,L1,G1,TIN,TOUT,AVSLOPE,AVLAMDA)
         HFNA = HFN/(30.0)
         PRINT*,HFN,HFNA
CC
CCC  CALCULATE THE POINT EFFICIENCY(EOG)
          EOG = (H2 - H1)/(HFNA - H1)
          PRINT*,"EOG=",EOG
       WRITE(NRESULT,44)EOG
44     FORMAT(/"EOG =",10X,F10.5)
CC CALCULATE PLUG FLOW EMV AND USE IT TO ESTIMATE EMV/EOG PLUG
FLOW
       EMVPLUG =(1.0/AVLAMDA)*((EXP(EOG*AVLAMDA)) - 1.0)
       EMVEOGP = EMVPLUG/EOG
       WRITE(NRESULT,*) 'EMVPLUG =',EMVPLUG
       WRITE(NRESULT,*) 'EMVEOGP =',EMVEOGP
CC CALCULATE THE HUMIDITY AT TEMP OF OUTLET LIQUID
CC
    HO1=-25.556+(TT*0.26465)-((TT**2)*9.16147E-4)+((TT**3)*1.06061E-6)
    HO2=-25.556+(TI*0.26465)-((TI**2)*9.16147E-4)+((TI**3)*1.06061E-6)
          HF2 =CA*(TT-273.0)+ HO1*(CW*(TT-273.0)+JI)
      PRINT*,"HF2=",HF2
      HF3 = (CA*(TI-273.0))+(HO2*(CW*(TI-273.0))+JI)
          EMV =(H2 - H1)/(HF2 - H1)
          PRINT*,"EMV=",EMV
      WRITE(NRESULT,45)EMV
45     FORMAT("EMV =",10X,F10.5///)
      EVEO = EMV/EOG
      WRITE(NRESULT,46)EVEO
46     FORMAT("EVEO =",10X,F10.5//)
      PRINT*,"EVEO=",EVEO
CC
CC
    IF(JJ1.EQ.1.0) CALL GINO
```

```
    ELSE
      IF(JJ1.EQ.1.0) CALL GINO
    END IF
CCCC  SUPRIMPOSE 30 DATA POINTS ON 2-D PLOT
      CALL RANPTS(-8)
      DO 217 I=1,ND
      ZD = ZN(I)-273.0
217    CONTINUE
       Z(I)=ZD
CC     DO 216 I=1,ND
C
     DO 8888 I=1,30
     X(I)=XP(I)
     Y(I)=YP(I)
 8888 CONTINUE
C
    CALL RANGRD(30,X,Y,Z,60,-51.0,51.0,50,-32.5,35.5,AT,7000,W)
CC6   CONTINUE
CCCC interpolate from data points to give temps. at the nodes
CCCC of a regular 60 by 50 grid called AT
CC   CALL RANGRD(30,X,Y,Z,60,-51.0,51.0,50,-32.5,35.5,AT,7000,W)
CC
     DO 10 I=1,60
     DO 10 J=1,50
      ZT(I,J) = (AT(I,J)-TOU)/(TIN-TOU)
       IF(AT(I,J).LE.TOU) ZT(I,J)=0.0
       IF(AT(I,J).GE.TIN) ZT(I,J)=1.0
CC      TZ(I,J) = (AT(I,J) - TOUT)/(TIN - TOUT)
10      CONTINUE
       DO 909 I=1,3
       DO 909 J=36,50
        ZT(I,J) = ZT(4,J)
909     CONTINUE
       DO 949 I=57,60
       DO 949 J=36,50
        ZT(I,J) = ZT(56,J)
949    CONTINUE
C       IF(NAMU.EQ.3)THEN
```

```
      IF (NAMU.EQ.3) THEN
CCCC  choose between full or partial plots
      PRINT*
      PRINT*,"DO YOU WANT A COMPLETE 3-D PLOT OR A PLOT OF JUST"
      PRINT*,"            1 OF THE 4 TEMPERATURE SUB-RANGES?"
4000  PRINT*,"ENTER 0 FOR COMPLETE PLOT, 1 FOR LOWEST SUB-RANGE,"
      PRINT*,"         2 FOR 2ND, 3 FOR 3RD OR 4 FOR HIGHEST"
      READ*,S
      IF (S.NE.0.AND.S.NE.1.AND.S.NE.2.AND.S.NE.3.AND.S.NE.4) GOTO 4000
      IF (S.EQ.0) THEN
CCCC  draw full plot in only 1 colour (black)
CC    CALL LEVELS(32.83,41.71)
CC    CALL ISOFRA(2)
       IF(NCOUNT.EQ.0) CALL SHIFT2(45.0,30.0)
       CALL PICCLE
      CALL SCALE(0.6)
      CALL ISOSCA(5.0,5.0,0.5)
      CALL ISOPRJ(60,-51.0,51.0,50,-32.5,35.5,ZT,IV,7000,W)
      CALL SCALE(1.667)
       NJ = NJ + 30
       NCOUNT = NCOUNT + 1
       IF (NCOUNT.GE.NZSET) GO TO 999
       GO TO 99
     ELSE
CCCC  set variables for 1 of the 4 partial 3-d plots
C
C
      A=0.0+0.125*(S-1)
      B=1.0+0.125*S
CCCC  if highest range selected set upper limit B to slightly higher
CCCC  value so that a smooth upper edge is drawn
      IF (S.EQ.4) B=1.6
      FOR I=1,60
       FOR J=1,50
CCCC    set each value in auxiliary array BT to base (lowest) temp.
CCCC    INPUT THE VALUE OF THE LOWEST TEMPERATURE (E.G 32.68)
      BT(I,J)=0.0
CCCC    for each T value in AT: if it lies within range chosen copy
```

```
CCCC    it into its corresponding position in BT
        IF (ZT(I,J).GT.A.AND.ZT(I,J).LE.B) BT(I,J)=ZT(I,J)
       END FOR
      END FOR
CCCC   select pen colour and max. height of plot (depends on range selected)
      CALL PENSEL(5-S,0.0,0)
      CALL HEIRAT(0.125*S)
CCCC   alter default scaling on temp. axis so that markings do not overlap
      CALL ISOSCA(5.0,5.0,0.5)
CCCC   draw the partial 3-d plot in the appropriate colour
      CALL ISOPRJ(60,-51.0,51.0,50,-32.5,35.5,ZT,IV,7000,W)
     END IF
    ELSE
CCCC  initialise variables in DO loop for the complete 2-d plot
     CHIME=4
     G=0.125
C
      A=0.01
     B=1.0+0.125
     DO
      FOR I=1,60
       FOR J=1,50
CCCC    for 2-d plot: set all T values in AT which are below current
CCCC    range (1/4 of total range) to lower value of current range,and
CCCC    set all values above range to upper value of range
        IF (ZT(I,J).LT.A) BT(I,J)=A
        IF (ZT(I,J).GT.B) BT(I,J)=B
CCCC    for each T value in AT: if it lies within current range copy
CCCC    it into its corresponding position in array BT
        IF (ZT(I,J).GT.A.AND.ZT(I,J).LE.B) BT(I,J)=ZT(I,J)
       END FOR
      END FOR
cc set all the temperature values outside the tray circular edge to zero
      DO 26 I=1,60
      DO 26 J=1,50
      IF(BT(I,J).GT.1.0) BT(I,J)=1.0
      IF(BT(I,J).LT.0.0) BT(I,J)=0.0
26     CONTINUE
```

```
      DO 3 I=1,6
      BT(I,1)=0.0
      BT(I,50)=0.0
3     CONTINUE
      DO 4 I=55,60
      BT(I,1)=0.0
      BT(I,50)=0.0
4     CONTINUE
      DO 27 I=1,5
      BT(I,2)=0.0
      BT(I,49)=0.0
27    CONTINUE
      DO 28 I=56,60
      BT(I,2)=0.0
      BT(I,49)=0.0
28    CONTINUE
      DO 29 I=1,4
      BT(I,3)=0.0
      BT(I,48)=0.0
29    CONTINUE
      DO 6 I=57,60
      BT(I,3)=0.0
      BT(I,48)=0.0
6     CONTINUE
      DO 7 I=1,3
      BT(I,4)=0.0
      BT(I,47)=0.0
7     CONTINUE
      DO 8 I=58,60
      BT(I,4)=0.0
      BT(I,47)=0.0
8     CONTINUE
      DO 9 I=1,2
      BT(I,5)=0.0
      BT(I,46)=0.0
9     CONTINUE
      DO 12 I=59,60
      BT(I,5)=0.0
```

```
      BT(I,46)=0.0
12     CONTINUE
      BT(1,6)=0.0
      BT(1,45)=0.0
      BT(60,6)=0.0
      BT(60,45)=0.0
CCCC   select plotting pen colour for current temp. range
      CALL PENSEL(CHIME,0.0,0)
CCCC   SELECTION OF TYPE OF FRAME TO BE DRAWN ( CIRCULAR TRAY )
      CALL SETFRA(2)
      GO TO 399
      CALL PIEPAP(66.0,96.0,66.5)
      CALL PIECHA(1.0,1,0,1,1,0)
CCCC   DRAW CONTOURS ON 2-D PLOT
      CALL LEVELS(0.0,1.0)
       CALL LABCON(0,1,0.0,0)
      CALL DRACON(60,-51.0,51.0,50,-32.5,35.5,BT,20,0,7000,W)
CCCC   TO DRAW THE CONTOURS IN (COLOURS) IF TEMP RANGE ABOVE
MINIMUM TEMP
C 399 CONTINUE
399      IF (CHIME.EQ.4.AND.CHOICE.EQ."T")THEN
       CALL PICCLE
      CALL LEVELS(0.0,1.0)
      CALL LABCON(0,1,0.0,1)
C      CALL PIEPAP(90.0,110.0,100.5)
C      CALL PIECHA(1.0,1,0,1,1,0)
      CALL RANPTS(-8)
C      DO 1111 JJ2=1,NZSET
C       IF(JJ2.EQ.1.0)  CALL SCALE(0.5)
CC       ELSE
CC     IF (JJ1.GT.1.0) CALL SCALE(0.5)
CC      CALL SHIFT2(70.0,90.0)
CCC    IF (JJ1.GT.1.0) CALL SCALE(2.0)
      IF(JJ1.EQ.1.0) CALL SHIFT2(50.0,50.0)
CC      IF(JJ1.EQ.1.0) CALL SCALE(0.5)
      CALL DRACON(60,-51.0,51.0,50,-32.5,35.5,BT,20,0,7000,W)
      CALL CONSPA(-0.0,5.0,XSP,YSP)
C
```

```
      CALL PIEPAP(120.0,XSP,YSP-5.0)
      CALL PIECHA(1.0,1,1,1,1,0)
C     CALL SCALE(2.0)
CC     END IF
CC      IF(JJ2.EQ.1.0) CALL SCALE(2.0)
CC         END IF
       END IF
1111   CONTINUE
CCCC   increment/decrement variables for next run through DO loop
C      CHIME=CHIME-1
      CHIME=CHIME-3
CC     G=G+0.125
CC     A=A+0.125
CC     B=B+0.125
       UNTIL(CHIME.LE.1)
CC     END IF
CC      CALL DEVEND
C991      CONTINUE
        NJ = NJ + 30
     NCOUNT = NCOUNT + 1
     IF(NCOUNT.GE.NZSET) GO TO 999
CC     GO TO 3333
      END IF
99      CONTINUE
     CALL MOVTO2(-30.0,-30.0)
     CALL LINBY2(230.0,0.0)
     CALL LINBY2(0.0,175.0)
     CALL LINBY2(-230.0,0.0)
     CALL LINBY2(0.0,-175.0)
C99     CONTINUE
      CALL DEVEND
 999 STOP
     END
C    ************************************************************
C    DATA INPUT FROM SCREEN BY ASS. 0=*
C    DATA INPUT FROM DATA FILE BY NDATA=7 (NO ASS. NEEDED)
C    ************************************************************
C
```

```
      SUBROUTINE FOPEN (NFILE)
C
      CHARACTER*8 FILENAME
C
      NSCR=0
      WRITE (NSCR,202) NFILE
  202 FORMAT(/" ** ENTER FILE NAME OF DATA FOR CHANNEL",I4," **")
      READ (NSCR,204) FILENAME
  204 FORMAT (A8)
      OPEN (UNIT=NFILE,FILE='       '//FILENAME)
      RETURN
      END
C     ****************************************************************
      SUBROUTINE
MAINTEMP(ND,ZN,HF,MS,MF,L1,G1,TIN,TOUT,AVSLOPE,AVLAMDA)
C
C
      DIMENSION X(30),Y(30),ZN(30),HF(30)
      DIMENSION XX(30),YY(30),CC(10)
      DIMENSION F(30),FD(30),SLOPE(30)
      REAL L1,LAMD,LAMDA(30),EMV1,EMV2(30),TIN,TOUT,BETA
      COMMON/NUM/NIN,NDATA,NSCR,NRESULT,NNRESULT,LLRESULT
C
C     DATA X/0.0,0.1,0.2,0.3,0.4,0.5,0.6,0.7,0.8,0.9/
C     DATA Y/0.0,0.56,0.86,1.06,1.23,1.40,1.48,1.61,1.66,1.76/
C
      NSCR=0
      DO 10 I=1,ND
      XX(I)=ZN(I)-273.0
      YY(I)=HF(I)
   10 CONTINUE
      CALL POLY(ND,XX,YY,MS,MF,CC)
      NG=5
      DO 15 J=1,ND
      SUM=CC(1)
      DO 20 I=1,NG
      SUM=SUM+CC(I+1)*(XX(J)**I)
   20 CONTINUE
```

```
      F(J)=SUM
   15 CONTINUE
         SUMD1 = 0.0
      DO 45 J=1,ND
      SUMD=CC(2)
      DO 40 I=2,NG
      SUMD=SUMD+I*CC(I+1)*(XX(J)**(I-1))
       LAMD = SUMD   * (G1/L1)
CC       SUMD1 = SUMD1 + SUMD
CC       EMV1 = ((1/LAMD)*((TIN/TOUT)-1))
CC    WRITE(NSCR,*) G1,L1,SUMD,LAMD
   40 CONTINUE
CC       AVSLOPE = SUMD1/30.0
      SLOPE(J)=SUMD
CC       AVLAMDA = AVSLOPE * ( G1/L1)
         LAMDA(J) = LAMD
CC    EMV2(J) = EMV1
   45 CONTINUE
CC     AVSLOPE = SUMD1/30.0
CC     AVLAMDA = AVSLOPE * ( G1/L1)
      WRITE(NRESULT,100)
  100 FORMAT(//'    ZN     HF     POLY     SLOPE     LAMDA ')
      DO 50 I=1,24
       SUMD1 = SUMD1 + SLOPE(I)
   50    CONTINUE
        DO 51 I=1,ND
      WRITE(NRESULT,200) XX(I),YY(I),F(I),SLOPE(I),LAMDA(I)
   51    CONTINUE
       AVSLOPE = SUMD1/24.0
       AVLAMDA = AVSLOPE*(G1/L1)
C50    CONTINUE
C      DO 51 I=1,ND
200    FORMAT(5(1X,F10.5))
       WRITE(NRESULT,288)
288    FORMAT(//'CALCULATED EMV BASED ON PLUG FLOW')
      WRITE(NRESULT,299)
299    FORMAT('    AVSLOPE       AVLAMDA ')
C      DO 51 I=1,ND
```

```
      WRITE(NRESULT,297)AVSLOPE,AVLAMDA
C1     CONTINUE
297    FORMAT(1X,2F10.5)
C 200 FORMAT(5(1X,F10.5))
C
    RETURN
    END
C
CCC  PROGRAM TO FIT A POLYNOMIAL TO A SET OF DATA AND COMPUTE
CCC  THE COEFF OF THE NORMAL EQUATION FOR LEAST SQUER
CCC  PARAMETERS ARE
CCCCC  X,Y, ARRAY OF X,Y VALUES
CCCCC  N  NUMBER OF DATA PAIRS
CCCCC  MS,MF,  THE RANGE OF DEGREE OF POLYNOMIALS
CCCCC  C  ARRAY OF COEFFS  OF LEAST SQUARE POLYNOMIALS
C
    SUBROUTINE POLY(N,X,Y,MS,MF,C)
C
    DIMENSION X(100),Y(100),C(10),A(10,11),XN(100)
    COMMON/NUM/NIN,NDATA,NSCR,NRESULT,NNRESULT,LLRESULT
CCC
CCCC  READ IN MS,MF,THE PROGRAM WILL FIND COEFFS FOR EACH DEGREE
OF
CCCC  POLYNOMIAL FROM MS TO MF
CCCC  TO CHECK IF MAXIMUM DEGREE REQUESTED EXCEEDS N-1 IF
REDUCE TO
CCCC  N-1 AND PRINT MESSAGE
    IF(MF.LE.(N-1)) GOTO 5
    MF = N - 1
5   MFP1=MF+1
    MFP2=MF+2
CCC  PUT ONE IN TO A NEW ARRAY THIS WILL HOLD POWERS OF THE X
VALUES
CCCC  AS IT PROCEEDS
     DO 10 I = 1,N
10    XN(I)=1
CC   COMPUTE FIRST COLUMN AND N+1 ST COLUMN OF A,I MOVES DOWN
THE
```

```
CC    ROWS,J SUMS OVER THE N VALUES
      DO 30 I=1,MFP1
      A(I,1) = 0.0
      A(I,MFP2)=0.0
      DO 20 J = 1,N
      A(I,1) = A(I,1) + XN(J)
      A(I,MFP2) =A(I,MFP2)+Y(J)*XN(J)
20     XN(J)=XN(J)*X(J)
30     CONTINUE
CCCC COMPUTTHE LAST ROW OF A I MOVE DOWN THE ROWS ,J SUM OVER
CCC  THE   N VALUES
       DO 50 I=2,MFP1
      A(MFP1,I)=0.0
      DO 40 J = 1,N
      A(MFP1,I)=A(MFP1,I)+XN(J)
40     XN(J) = XN(J)*X(J)
50     CONTINUE
C    FILL THE REST OF THE MATRIX
     DO  70 J=2,MFP1
      DO 60 I=1,MF
60     A(I,J)=A(I+1,J-1)
70     CONTINUE
CCC   CALLSUBROUTINE TO SOLVE THE SYSTEM FOR DEGREE MS TO MF
CCC    GET THE LU DECOMPOSITION OF A
      CALL ANI(A,MFP1,10)
CCCC    RESET THE R.HS INTO C
      MSP1 = MS + 1
      DO 95 I=MSP1,MFP1
      DO 90 J =1,I
90     C(J)= A(J,MFP2)
    CALL AMI(A,C,I,10)
      IM1=I-1
CCCC   WRITE OUT THE COEFF OF THE LEAST SQUARE
CCC          POLYNOMIAL
      WRITE(NRESULT,201)
201    FORMAT(//' COEFFICIENTS OF POLY ')
      WRITE (NRESULT,202)IM1, (C(J), J=1,I)
202    FORMAT(3X,I5,4X,8(G16.7,2X))
```

```
CCCC    COMPUT AND PRINT VALUES OF BETA=SUM OF DEV
SQUARED/(N-M-1)
        BETA =0.0
        DO 94 IPT = 1,N
        SUM=0.0
        DO 93 ICOEF = 2,I
        JCOEF=I-ICOEF+2
        SUM = (SUM + C(JCOEF))*X(IPT)
93       CONTINUE
        SUM=SUM+C(1)
        BETA=BETA+(Y(IPT)-SUM)**2
94       CONTINUE
        BETA = BETA/(N-I)
        WRITE (NRESULT,203) BETA
203      FORMAT(/"BETA =",3X,F10.5)
95       CONTINUE
        RETURN
        END
CCCCC
CCCC
      SUBROUTINE ANI(A,N,NDIM)
      DIMENSION A(NDIM,NDIM)
     COMMON/NUM/NIN,NDATA,NSCR,NRESULT,NNRESULT,LLRESULT
CCC     THIS ROUTINE FORMS LU EQUIVALENT OF SQUARE
CCC       THE VALUES ARE NOT INCLUDED IN THE RESULT
        DO 30 I = 1,N
        DO 30 J = 2,N
        SUM=0.0
        IF (J.GT.I)GOTO 15
        JM1=J-1
        DO 10 K=1,JM1
10       SUM=SUM+A(I,K)*A(K,J)
        A(I,J)=A(I,J)-SUM
        GO TO 30
15       IM1=I-1
        IF (IM1.EQ.0.0)GO TO 25
        DO 20 K=1,IM1
20       SUM = SUM +A(I,K)*A(K,J)
```

```
CCCC   TEST FOR SMALL VALUE ON DIAGONAL
25      IF(ABS(A(I,I)).LT.1.E-10)GOTO 99
        A(I,J)=(A(I,J)-SUM)/A(I,I)
30       CONTINUE
        RETURN
99       WRITE (*,100) I
100   FORMAT(5X,I10.5,'REDUCTION NOT COMPLETED SMALL DIVISOR')
        RETURN
        END
CCCCC
CCCC
      SUBROUTINE AMI (A,B,N,NDIM)
      DIMENSION  A(NDIM,NDIM), B(NDIM)
   COMMON/NUM/NIN,NDATA,NSCR,NRESULT,NNRESULT,LLRESULT
CCC   THIS SUBROUTINE FINDS THE SOLN TO SET OF LINEAR EQUATIONS
CCC    DO THE REDUCTION STEP
       B(1)=B(1)/A(1,1)
       DO 20 I = 2,N
       IM1=I-1
       SUM =0.0
       DO 10 K=1,IM1
10      SUM=SUM+A(I,K)*B(K)
20      B(I)=(B(I)-SUM)/A(I,I)
CCCC   BACK SUBSTITUTION ELEMENT OF U ON DIAGONAL ARE ALL ONES
       DO 40 J = 2,N
       NMJP2 = N - J + 2
       NMJP1=N-J+1
       SUM=0.0
       DO 30 K = NMJP2,N
30      SUM=SUM+A(NMJP1,K)*B(K)
40      B(NMJP1)=B(NMJP1)-SUM
       RETURN
       END
C
C   ***************************************************************
C
   BLOCK DATA
C
```

```
      COMMON/PPP/ X(30),Y(30)
C
      DATA X/-38.5,-30.5,-10.5,10.5,30.5,38.5,-51.0,-30.5,-10.5,10.5,
     *30.5,51.0,-51.0,-30.5,-10.5,10.5,30.5,51.0,-43.5,-30.5,-10.5,10.5,
     *30.5,43.5,-43.5,-30.5,-10.5,10.5,30.5,43.5/
      DATA Y/6*-32.5,6*-12.50,6*12.50,6*32.5,6*35.5/
      END
```

APPENDIX 15 LIST OF PUBLICATIONS (see next page)